University of Southampton

Faculty of Environmental & Life Sciences

School of Biological Sciences

Investigating the impact of alterations in α-synuclein on mitochondrial health, mitochondrial quality control and neuronal differentiation

by

Naomi Jasmin Thorne

ORCID ID: 0000-0001-5364-0253

Thesis for the degree of Doctor of Philosophy

April 2025

University of Southampton

Abstract

Faculty of Environmental & Life Sciences

School of Biological Sciences

Doctor of Philosophy

Investigating the impact of alterations in α-synuclein on mitochondrial health and quality control

by

Naomi Jasmin Thorne

Mitochondrial quality control (mito-QC) co-ordinates dynamic changes in the mitochondrial network that maintain optimal function and cell health. Dysregulated mito-QC has been associated with numerous pathologies, including Parkinson's disease (PD) which is characterised by degeneration of dopaminergic neurons in the substantia nigra pars compacta (SNpc). The mechanisms of neuronal death in PD are still unknown, but have been linked to the aggregation of α-synuclein; a protein which pathologically forms intracellular inclusions, known as Lewy bodies, in PD brains. A relationship between α-synuclein and mito-QC has been established based on the presence of dysfunctional mitochondria in both PD patients and models of α-synuclein pathology. However, exactly how α-synuclein may impact mito-QC mechanisms is not well understood. Recent research has shown that α-synuclein can use mitochondrial membranes to seed aggregation of toxic oligomeric species, resulting in mitochondrial dysfunction and potentiating disease pathogenesis. Though the majority of research has focused on the hypothesis that pathological α-synuclein may exhibit a toxic gain-of-function that disrupts mito-QC, it is also possible that this could occur through α-synuclein loss-of-function. Since α-synuclein associates with and remodels phospholipid membranes, has been suggested to contain a mitochondrial targeting sequence and can be mitochondrially imported, it may have a physiological role in mito-QC that is lost under pathological circumstances.

In an α-synuclein loss-of-function model, I observe that physiological α-synuclein is not required for mitochondrial energy production or co-ordination of mito-QC. I do not find evidence of a direct functional association between endogenous α-synuclein and mitochondria, however I suggest that α-synuclein may modulate autophagy flux and lysosomal morphology through its action as a cytosolic molecular chaperone. This provides novel insight into α-synuclein's physiological function in the context of mito-QC. I also investigated the impact of pathological α-synuclein on mito-QC, where I found that α-synuclein overexpression did not disrupt mitochondrial function or damage-induced whole mitochondrial clearance, but did influence autophagosome number and lysosomal size. Since alterations in these phenotypes were also seen in my loss-of-function model, I consider that physiological α-synuclein may have a role in modulating autophagy that is disrupted in pathological circumstances such as PD. Overexpression of α-synuclein also increased mitochondrial fragmentation and mitochondrial-derived vesicles (MDVs) at steady state, suggesting that excess α-synuclein increases the baseline mito-QC response. I suggest that upregulation of these responses may occur due to an α-synuclein-induced increase in oxidative stress. Together, these data indicate that pathological α-synuclein, rather than a lack of physiological α-synuclein, is primarily responsible for dysregulated mitochondrial function in PD.

Since α-synuclein's pathological impact primarily occurs in dopaminergic neurons of the SNpc, it would be important to further investigate interactions between α-synuclein and mito-QC in a model that better recapitulates this neuronal environment. Accordingly, I generated a neuronal model through differentiation of SH-SY5Y cells that can be used for future work. In this study, I characterised how

perturbations in α-synuclein expression impacted neuronal phenotype in differentiated cells, finding that overexpression of α-synuclein A53T, but not wild-type, reduced neuronal morphology and expression of neuronal markers. Interestingly, α-synuclein knockout cells showed a similar but less exaggerated phenotype, suggesting that defects in neuronal differentiation in both cell lines may be explained by loss of physiological α-synuclein activity. This provides insight into α-synuclein's role in neuronal development.

Table of Contents

Table of Tables

Table of Figures

Table of Figures

Table of Figures

Table of Figures

Table of Figures

Table of Figures

Table of Figures

Research Thesis: Declaration of Authorship

Print name: Naomi Thorne

Title of thesis: Investigating the impact of alterations in α-synuclein on mitochondrial health, mitochondrial quality control and neuronal differentiation

I declare that this thesis and the work presented in it are my own and has been generated by me as the result of my own original research.

I confirm that:

1. This work was done wholly or mainly while in candidature for a research degree at this University;
2. Where any part of this thesis has previously been submitted for a degree or any other qualification at this University or any other institution, this has been clearly stated;
3. Where I have consulted the published work of others, this is always clearly attributed;
4. Where I have quoted from the work of others, the source is always given. With the exception of such quotations, this thesis is entirely my own work;
5. I have acknowledged all main sources of help;
6. Where the thesis is based on work done by myself jointly with others, I have made clear exactly what was done by others and what I have contributed myself;
7. Parts of this work have been published as:
   Thorne, N. J and Tumbarello, D. A. (2022). The relationship of alpha-synuclein to mitochondrial dynamics and quality control. *Front. Mol. Neurosci*. 15: 947191. doi: 10.3389/fnmol.2022.947191
   Parts from this literature review have been repurposed for the Introduction of this thesis.

Signature: ..... Date: 29.04.25

Acknowledgements

Undertaking this PhD has honestly been one of the best decisions I have ever made. I have learned so much and feel I have truly grown, both as a scientist and as a person. My time at the University of Southampton has been amazing, and I have so many people to thank for making my PhD experience so wonderful.

Firstly, this project was funded by the Gerald Kerkut Charitable Trust and the University of Southampton. I am so grateful to Gerald for leaving such a fantastic legacy by founding the trust, which has helped so many PhD students here in Southampton. I feel incredibly lucky that I received funding from this charity as well as help towards conference costs and nominal registration. Thank you to Dr Niall Horn, Dr Alan Thomas and Professor Robert Walker for all your hard work in running the trust and providing support.

Huge thanks go to my project supervisor, Dr David Tumbarello. Thank you so much for offering me this studentship and welcoming me into your lab. You have provided fantastic support over the past 4 years, and I couldn't have asked for a better supervisor. You were patient when teaching me lab skills, gave so much feedback on written work and pushed me to be a better scientist. You have helped to build my confidence by creating the supportive lab environment that others wish they had. I have truly loved my time in the Tumbarello lab, and it has given me the best foundation on which to build my scientific career.

I'd like to mention all the other members of staff who have helped me over the course of this PhD. Thank you to Dr Melissa Andrews for your kindness and your quiet but unwavering support. To Professor Vincent O'Connor, for your supportive chats as you walked past my desk and asked me how I was getting on. To Dr Angus Wann, for your help with outreach activities and for your genuine attitude to improving postgrad life in Southampton. Thank you to Dr Yihua Wang for providing insight into my project at my second progression review, and to Professor Katrin Deinhardt for your input throughout this project and your belief in my abilities.

So many people have provided me with invaluable scientific help and advice over the course of my lab work. Enormous thanks go to Dr Mark Willett from the IMC who taught me to use countless machines and had endless patience when explaining physics concepts to me several times over. Thank you to the wonderful team of technicians who provided so much training and support. Jacob Trend was a genuine lifesaver when it came to image analysis – writing ImageJ® macros and teaching me how to write them myself. I actually don't know what I would have done without you! Thanks to Matt Trimby who also helped with image analysis, saving me so much time and frustration. For advice and help with using the Seahorse bioanalyzer, thank you

to Joshua Green-Jenkinson, Dr Triana Amen and Nick Howe. I was on a tight schedule to get that data, so your help was invaluable. For help with differentiation of SH-SY5Y cells, thank you to Kirstie Williamson who provided great, time-saving advice. Thank you to Dr Charlotte Collier for passing down your knowledge from your experience in the Tumbarello lab. Outside of the lab, I would like to thank Kam Kaur for always being a friendly and supportive face who genuinely cares about every person in this building.

Despite starting this PhD in relative isolation because of COVID-19, I have managed to make some incredible friendships which have made my time here so much more enjoyable. I am forever grateful that Toby Segasby chose a project in the Tumbarello lab that brought us together – you have become one of my very closest friends and I can't thank you enough for all your support both in and out of the lab. Thanks to Lloyd Steele-Nicholson for your friendship and silliness, and to Belle Creith for your unwavering support, love and creativity. To many other friends around the building: Beatriz Valdez-Moreno, Matt Cleary, Matt Davis-Lunn, Jacob Trend, Amber Cooper, Dianne Lopez, Yomna Moqidem, Ryan Lawrence, Miguel Ramirez-Moreno & Naziah Choudhury, thank you for making Building 85 such a lovely environment.

Outside of my PhD, a huge part of my University of Southampton experience has been my time with Southampton Vixens Cheer & Dance. Thank you for being such a fun distraction from the PhD, for giving me wonderful friends and for teaching me so much about myself. I never would have thought I would be coaching a competitive cheer team, but you made me feel like I could and it was one of the best things I have ever done.

Thanks go to my family and friends for their ongoing love and support throughout these past 4 years. To my Cardiff girls, for sticking by me and making life so much fun even though we are rarely in the same place. To my sister, Gemma, thank you for being my best friend now and forever, and always being there for me no matter what. To my Mum and Dad, thank you for always believing in me, never putting any pressure on me and being the most wonderful parents. You guys are the best family I could ask for and I am forever grateful to have you with me. To my grandparents, I know you are all here with me in spirit and I hope I have made you all proud.

And finally, to me. I really did that!!!! Though I have absolutely loved my PhD, things have not been easy: a pandemic, plenty of anxiety, huge life changes and self-doubt. But I got there in the end! I am, and will always be, so proud of myself.

Definitions and Abbreviations

AA..... amino acid

Aβ..... amyloid-beta

Acetyl CoA ..... acetyl coenzyme A

AD ..... Alzheimer's disease

ADP ..... adenosine diphosphate

ALS..... amyotrophic lateral sclerosis

AMPK..... AMP-activated protein kinase

A/O..... antimycin A/oligomycin

APP..... amyloid precursor protein

Atg..... autophagy-related protein

Atg16L ..... Atg16-like protein

ATP ..... adenosine triphosphate

BAD ..... Bcl-2-associated death promoter

BafA1..... bafilomycin A1

BAK..... Bcl-2 antagonist/killer 1

BAX..... Bcl-2-associated X-protein

BCA ..... bicinchoninic acid

BCL-2 ..... B-cell lymphoma 2

BDNF..... brain-derived neurotrophic factor

BNIP ..... BCL-2/adenovirus E1B 19kDa protein-interacting protein 3

BSA..... bovine serum albumin

Btz ..... bortezomib

Ca^{2+} ..... calcium ion

cAMP ..... cyclic adenosine monophosphate

CCCP ..... carbonyl cyanide m-chlorophenyl hydrazone

CL..... cardiolipin

CMA ..... chaperone-mediated autophagy

CO_2 ..... carbon dioxide

CoA ..... coenzyme A

Complex I ..... NADH/ubiquinone oxidoreductase

Complex II..... succinate dehydrogenase

Complex III..... ubiquinone/cytochrome c oxidoreductase

Complex IV ..... cytochrome c oxidase

CoQ..... coenzyme Q

CoxII ..... cytochrome c oxygenase subunit 2

CytC ..... cytochrome C

DAMPs..... damage-associated molecular patterns

DAPI ..... 4', 6-diamidino-2-phenylindole

DAT..... dopamine transporter

DHAP..... dihydroxyacetone phosphate

DMEM..... Dulbecco's modified eagle medium

DMSO ..... dimethyl sulfoxide

DNA..... deoxyribonucleic acid

DPBS ..... Dulbecco's phosphate buffered saline

Drp1 ..... dynamin-related protein 1

e^- ..... electron

E1 ..... ubiquitin activating enzyme

E2 ..... ubiquitin conjugating enzyme

E3 ..... ubiquitin ligase

ETDA..... ethylenediaminetetraacetic acid

ER..... endoplasmic reticulum

ERK..... extracellular-signal-related kinase

ETC..... electron transport chain

EV..... empty vector

FA..... fatty acid

F-actin ..... filamentous actin

FAD(H) ..... flavin adenine dinucleotide (hydrogen)

FBS ..... fetal bovine serum

FIP200 ..... focal adhesion kinase family interacting protein of 200kDa

FKBP8 ..... FK506-binding protein 8

FRET ..... fluorescence resonance energy transfer

FUNDC1 ..... FUN14 domain-containing protein 1

GAP glyceraldehyde-3-phosphate

GAPDH ..... glyceraldehyde 3-phosphate dehydrogenase

GAP43 ..... growth associated protein 43

GDP ..... guanosine diphosphate

GFP ..... green fluorescent protein

gRNA ..... guide RNA

GSK3β ..... glycogen synthase kinase 3β

GTP ..... guanosine triphosphate

GWAS ..... genome-wide association study

H+ ..... proton

H_2O ..... water

H_2O_2 ..... hydrogen peroxide

HCl ..... hydrochloric acid

HD ..... Huntington's disease

HIV ..... human immunodeficiency virus

IMM ..... inner mitochondrial membrane

IMS ..... intermembrane space

iPSC ..... induced pluripotent stem cell

KCl ..... potassium chloride

LAMP1 ..... lysosomal-associated membrane protein 1

LB ..... Lewy body

LC3..... microtubule-associated protein light chain 3

LD..... lipid droplet

L-DOPA..... L-3, 4-dihydroxyphenylalanine

MAGIC ..... mitochondria as guardian in cytosol

MAMs ..... mitochondria-associated membranes

MAPL ..... mitochondrial-anchored protein ligase

mCU ..... mitochondrial Ca^{2+} uniporter

MDV..... mitochondrial-derived vesicle

Mff ..... mitochondrial fission factor

Mfn1 ..... mitofusin 1

Mfn2 ..... mitofusin 2

Miro ..... mitochondrial rho GTPase

Mito-QC ..... mitochondrial quality control

MPTP 1-methyl-4-phenyl-1,2,3,6-tetrahydropyridine

mRNA ..... messenger RNA

mtDNA..... mitochondrial DNA

mTORC1 ..... mechanistic target of rapamycin complex 1

mtPTP ..... mitochondrial permeability transition pore

mtUPR ..... mitochondrial unfolded protein response

NAC..... nascent polypeptide-associated complex

NAD(H) ..... nicotinamide adenine dinucleotide (hydrogen)

NaOH ..... sodium hydroxide

NDP52 ..... nuclear dot protein 52

NEAA ..... non-essential amino acids

NIX ..... NIP3-like protein X

NMR ..... nuclear magnetic resonance

O_2 ..... oxygen

O_2^- ..... superoxide anion

OCR..... oxygen consumption rate

$OH^{\bullet}$..... hydroxyl radical

OMM..... outer mitochondrial membrane

Opa1 ..... optic atrophy 1

OXPHOS ..... oxidative phosphorylation

PAMPs ..... pathogen-associated molecular patterns

PARL..... presenilin-associated rhomboid-like protein

PBS..... phosphate buffered saline

PCR ..... polymerase chain reaction

PD ..... Parkinson's disease

PDH..... pyruvate dehydrogenase

PDL..... poly-D-lysine

PE..... phosphatidylethanolamine

PEI..... polyethylenimine

PFA..... paraformaldehyde

P_i ..... phosphate group

PI3P..... phosphatidylinositol 3-phosphate

PINK1 ..... PTEN-induced kinase 1

PKC ..... protein kinase C

PP2A..... protein phosphatase 2A

P/S..... penicillin/streptomycin

pS129 ..... phospho-serine

PTM ..... post-translational modification

pUb ..... phospho-ubiquitin

pUb S65..... phospho-ubiquitin serine 65

PVDF ..... polyvinylidene difluoride

RA..... retinoic acid

Rab1 ..... Ras-associated binding protein 1

RARs..... retinoic acid receptors

RAREs..... retinoic acid response elements

RLU ..... relative light units

RIPA..... radioimmunoprecipitation assay

RNA ..... ribonucleic acid

ROI ..... region of interest

ROS ..... reactive oxygen species

RXRs..... retinoid X receptors

SDS ..... sodium dodecyl sulfate

SNAP29 ..... synaptosomal-associated protein 29

SNARE ..... soluble N-ethylmaleimide-sensitive factor activating protein receptor

SNCA..... α-synuclein gene

SNCA KO ..... α-synuclein knockout

SNpc ..... substantia nigra pars compacta

Snx3 ..... sorting nexin 3

STORM..... stochastic optical reconstruction microscopy

Succinyl CoA..... succinyl coenzyme A

Tau ..... tubulin-associated unit protein

TAX1BP1 ..... Tax1-binding protein 1

TBE ..... Tris/borate/EDTA buffer

TBS ..... Tris-buffered saline

ThT ..... thioflavin T

TIM ..... translocase of the inner membrane

TMRM ..... tetramethylrhodamine

TOM..... translocase of the outer membrane

Ub ..... ubiquitin

ULK1..... unc-51-like-autophagy-activating kinase 1

UPS ..... ubiquitin/proteasome system

VAMP8 ..... vesicle-associated membrane protein 6

V-ATPase ..... vacuolar H+ ATPase

VDAC ..... voltage-dependent anion channel

VPS ..... vacuolar protein sorting protein

WIPI2 ..... WD repeat domain phosphoinositide-interacting protein 2

WT ..... wild-type

6-OHDA 6-hydroxydopamine/2,4,5-trihydroxyphenethylamine

ΔΨm ..... mitochondrial membrane potential

Chapter 1 Introduction

Disclaimer: parts of this work have been published as Thorne, N. J and Tumbarello, D. A. (2022). The relationship of alpha-synuclein to mitochondrial dynamics and quality control. *Front. Mol. Neurosci*. 15: 947191. doi: 10.3389/fnmol.2022.947191

Cell homeostasis is the dynamic, self-governed process by which cells regulate and maintain efficient function. This is facilitated by the ability of individual organelles to adapt to changes in external conditions and integrate their functions to drive cell survival (Billman, 2020). A key element of cell homeostasis is the regulation of bioenergetics, since energy output must be modulated based on both nutrient input and the cell's metabolic requirements, which are ever-changing. This is controlled by mitochondria; organelles most well-characterised as the "powerhouses" of the cell which are essential for the production of energy in almost all eukaryotic cells (Cooper, 2000). By generating the energy molecule adenosine triphosphate (ATP), mitochondria provide fuel for all metabolic reactions that underpin cellular activity. In addition to their role in energy production, mitochondria act as a central signalling hub, with regulatory roles in lipid transport, calcium (Ca^{2+}) homeostasis, organelle communication and apoptosis (San-Millán, 2023). Accordingly, maintaining mitochondrial function is imperative for cell health and viability.

Alterations in mitochondrial activity have been shown to contribute to the progression of a range of pathologies, including diabetes, cancer, neurodegeneration and cardiovascular disease. Changes in cellular energy production are particularly important in the development of these diseases, with alterations in mitochondrial glucose metabolism linked to both insulin resistance in diabetes and tumorigenesis in cancer (Rhodes, 2005; Rossignol et al., 2004; Warburg, 1956). Oxidative stress also contributes to disease pathogenesis, with excessive production of reactive oxygen species (ROS) by dysfunctional mitochondria known to promote cell death in neurodegenerative diseases such as Alzheimer's disease (AD) and Parkinson's disease (PD) (Balaban et al., 2005; Rangaraju et al., 2019).

1.1 The mitochondrion

1.1.1 Mitochondrial structure

The essential and diverse functions of mitochondria in eukaryotic cells are facilitated by its unique structure. Mitochondria are double-membraned entities, possessing an inner and outer mitochondrial membrane (IMM and OMM, respectively) that are structurally and functionally distinct, separated by the intermembrane space (IMS) (T. Rostovtseva & Colombini, 1997). The OMM is a porous phospholipid membrane that represents a boundary between the mitochondria and the cytoplasm (Cooper, 2000). It enables free movement of ions and small, uncharged molecules through porins and mediates mitochondrial import of larger proteins through complexes such as translocase of the outer membrane (TOM) complexes (Cooper, 2000; Pitt & Buchanan, 2021). In contrast, the IMM is much less permeable, acting as a functional barrier between the IMS and the innermost part of the mitochondria, the matrix. The IMM is a membrane highly folded into structures called cristae, where ATP production occurs through the electron transport chain (ETC); a series of 4 respiratory complexes that generate a mitochondrial membrane potential ($\Delta\Psi m$) across the IMM through oxidative phosphorylation (OXPHOS) (Kühlbrandt, 2015). The selectivity of this membrane is crucial to maintain this electrochemical gradient between the IMS and the matrix, which directly facilitates the generation of ATP. The matrix is a protein-dense compartment where many enzymatic reactions occur alongside regulatory processes like (DNA) replication, translation and protein synthesis (Kühlbrandt, 2015). Initially evolved from the engulfment of proteobacteria by the ancestors of modern eukaryotes, mitochondria possess their own genetic material in the form of mitochondrial DNA (mtDNA) (Lane & Martin, 2010). MtDNA exists as circular chromosomes inside the matrix, encoding 13 mitochondrial proteins that comprise subunits of the respiratory complexes involved in OXPHOS (Taanman, 1999). Together, these mitochondrial compartments enable the production of ATP (**Figure 1**).

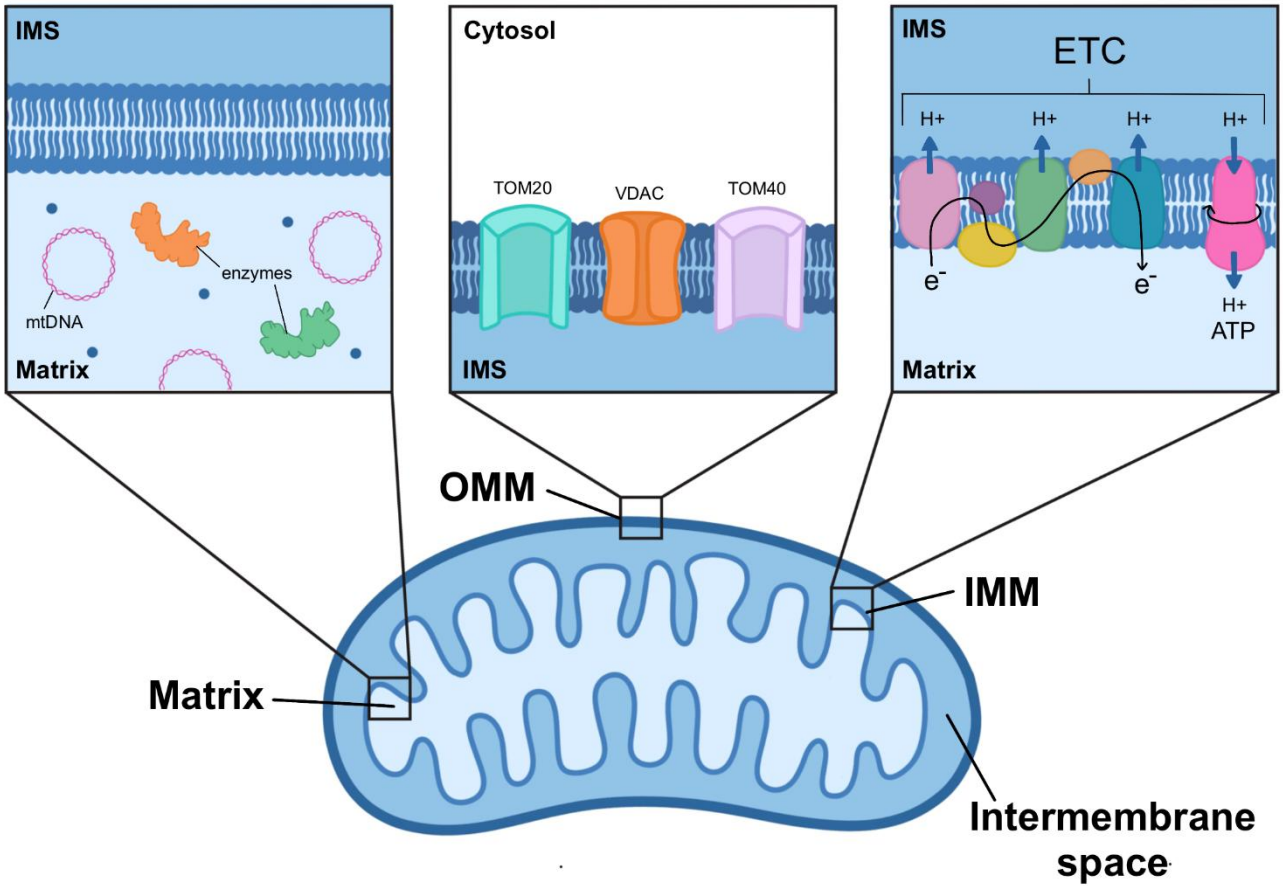

Figure 1: Schematic of the main structural features of mitochondria

The mitochondrion is a double-membraned organelle with distinct structural and functional features. The innermost compartment is the matrix, containing mtDNA, enzymes and ribosomes. This is separated from the intermembrane space (IMS) by the inner mitochondrial membrane (IMM) that forms folded cristae, which are the site of OXPHOS where electron transport chain complexes are embedded. The IMS is separated from the cytoplasm by the outer mitochondrial membrane (OMM) which facilitates mitochondrial import through transporters and ion channels.

1.1.2 Mitochondrial function

1.1.2.1 ATP production

The role of mitochondria as the main energy producers of the cell makes them essential for cell metabolism. The majority of mitochondrial energy production occurs through OXPHOS, responsible for the generating approximately 90% of all cellular ATP (Cooper, 2000). This relies on energy from electron donors that are produced by the processing of acetyl coenzyme A (acetyl CoA) through the Krebs cycle (Krebs & Johnson, 1937, 1980). One of the main substrates for this cycle is pyruvate, a product of glucose metabolism that occurs outside the mitochondria (Cooper, 2000). The co-ordination of these three processes optimises mitochondrial ATP production.

1.1.2.1.1 Glycolysis

Occurring in the cytoplasm, glycolysis is the pathway responsible for the metabolism of glucose through a series of enzymatic reactions (Cooper, 2000; Lenzen, 2014). This process generates 2 molecules of ATP anaerobically, but its primary function is to facilitate aerobic ATP production by forming 2 molecules of pyruvate for the Krebs cycle.

Firstly, the hydroxyl group on carbon-6 of glucose is phosphorylated by hexokinase to generate glucose-6-phosphate, using one molecule of ATP. This is converted to fructose-6-phosphate by phosphoglucose isomerase, which is further phosphorylated at carbon-1 by phosphofructokinase-1 to form fructose-1,6-bisphosphate. Fructose-1,6-bisphosphate is then processed by aldolase into 2 smaller molecules, using another molecule of ATP: glyceraldehyde-3-phosphate (GAP) and dihydroxyacetone phosphate (DHAP). DHAP is further processed into another GAP molecule by triosephosphate isomerase. These GAP molecules are converted into 2 1,3-biphosphoglycerate molecules by glyceraldehyde-3-phosphate dehydrogenase (GAPDH) by oxidation and phosphorylation by inorganic phosphate (P_i). This process reduces 2 molecules of the cofactor nicotinamide adenine dinucleotide (NAD+), generating 2 molecules of NADH which are fed into OXPHOS. The 2 1,3-biphosphoglycerate molecules are converted to 2 molecules of 3-phosphoglycerate by phosphoglycerate kinase, with the removal of a phosphate group from each enabling the generation of 2 molecules of ATP from adenosine diphosphate (ADP). The 3-phosphoglycerate molecules are both isomerised to 2-phosphoglycerate by phosphoglycerate mutase. Reduction of 2-phosphoglycerate molecules by enolase generates 2 molecules of phosphoenolpyruvate. In the final step, 2 molecules of pyruvate are formed by pyruvate kinase, with the removal of phosphate groups enabling the production of 2 more molecules of ATP (**Figure 2**).

The overall outputs from the breakdown of one glucose molecule by glycolysis are 2 molecules of ATP, 2 molecules of pyruvate to be used in the Krebs cycle and 2 molecules of NADH to be used as electron donors in the mitochondrial ETC. Under anaerobic conditions, pyruvate is catalysed to lactate which oxidises a molecule of NADH, providing NAD+ for further glycolytic reactions.

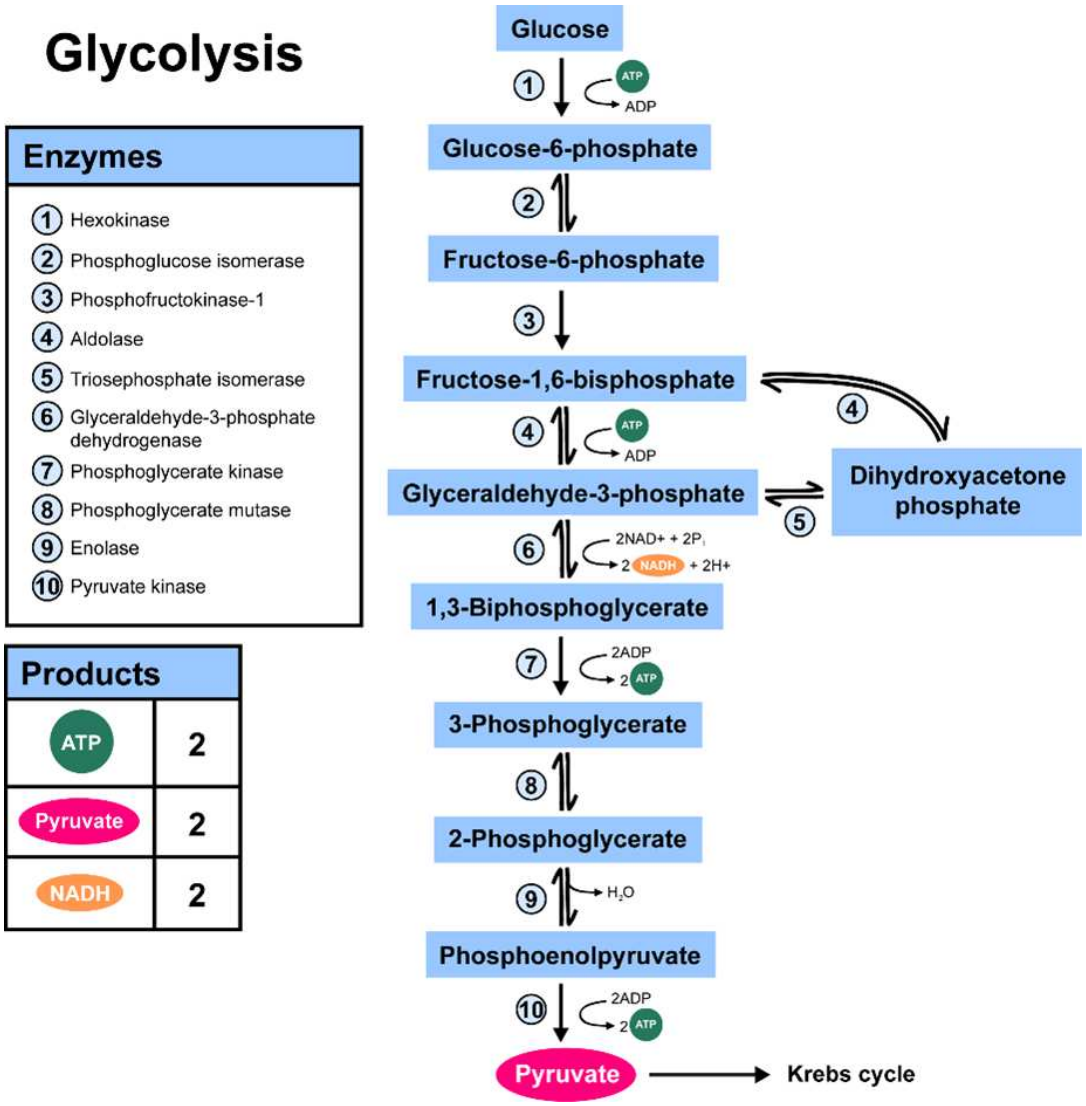

Figure 2: Schematic showing steps of the glycolysis pathway

Glycolysis describes the process of converting glucose into pyruvate which occurs in the cytoplasm. Each glucose molecule generates 2 net molecules of ATP, alongside 2 molecules of pyruvate which enter the Krebs cycle and 2 molecules of NADH which act as electron donors in OXPHOS.

1.1.2.1.2 Krebs cycle

Though glycolysis generates 2 molecules of NADH, the main production of electron donors for OXPHOS occurs through the Krebs cycle (Krebs & Johnson, 1937, 1980). The Krebs cycle occurs in the mitochondrial matrix and starts with the pyruvate molecules generated by glycolysis, which must first be actively transported from the cytoplasm into mitochondria through the pyruvate translocase transporter. Once inside the matrix, pyruvate is first converted to acetyl coenzyme A (acetyl CoA) by the action of enzymes within the pyruvate dehydrogenase complex (PDH). Acetyl CoA represents the main substrate for the Krebs cycle (Alberts et al., 2002).

Firstly, acetyl CoA is reduced by citrate synthase to form citrate, which is isomerised by aconitase to isocitrate. Isocitrate is then decarboxylated to form α-ketoglutarate by the action of isocitrate dehydrogenase, producing carbon dioxide (CO_2) and reducing NAD+ to NADH. Another decarboxylation step occurs by α-ketoglutarate dehydrogenase, again producing CO_2 and NADH alongside succinyl coenzyme A (succinyl CoA). Succinyl CoA is then hydrolysed to form succinate by succinyl CoA synthase, which also phosphorylates ADP to ATP or guanosine diphosphate (GDP) to guanosine triphosphate (GTP), respectively. Succinate is oxidised to fumarate by complex II of the ETC, succinate dehydrogenase, which also results in the reduction of flavin adenine dinucleotide (FAD+) to $FADH_2$. Fumarate is hydrated to malate by fumarate hydratase, which is converted to oxaloacetate by malate dehydrogenase, generating another molecule of NADH. Oxaloacetate is then reduced to citrate by citrate synthase, and then begins the cycle again.

From each molecule of pyruvate, the cycle generates 2 molecules of ATP and 4 molecules of CO_2 alongside 2 molecules of $FADH_2$ and NADH to be fed into the mitochondrial ETC as electron donors (**Figure 3**) (Alberts et al., 2002).

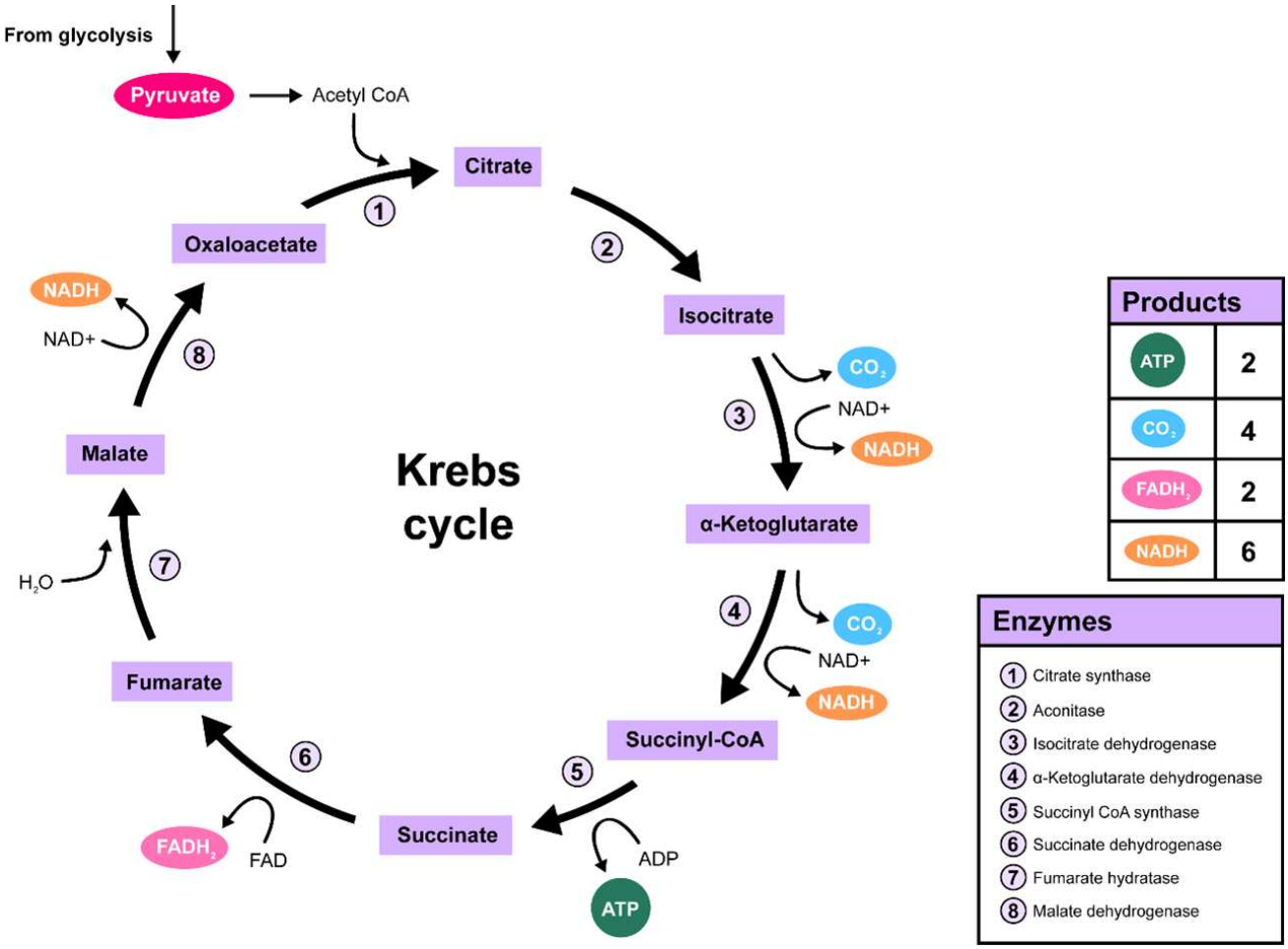

Figure 3: Schematic showing steps of the Krebs cycle

The Krebs cycle is a process that occurs inside the mitochondria and converts pyruvate from glycolysis into electron donors to be used for OXPHOS. Each pyruvate molecule generates 2 ATP molecules and 4 CO_2 molecules alongside electron donors, 2 molecules of $FADH_2$ and 6 molecules of NADH. These go on to participate in OXPHOS.

1.1.2.1.3 The ETC and OXPHOS

A series of respiratory complexes embedded in the IMM comprise the ETC which facilitates OXPHOS, with the transfer of electrons through these proteins generating the electrochemical gradient required for production of ATP by the ATP synthase pump (**Figure 4**). The electrons used in this process originate from electron donors in the matrix generated by glycolysis and the Krebs cycle: NADH and $FADH_2$.

Firstly, NADH/ubiquinone oxidoreductase (complex I) generates NAD+ from NADH molecules and succinate dehydrogenase (complex II) generates FAD+ from $FADH_2$ molecules. Both these processes facilitate the entry of free electrons into the ETC, which are passed to the cofactor protein coenzyme Q (CoQ). CoQ is reduced to ubiquinol, enabling transport of electrons to the next complex, ubiquinone/cytochrome c oxidoreductase (complex III). In this complex, electrons are accepted by the heme group of the peripheral membrane protein cytochrome c, which carries electrons to the final component of the ETC, cytochrome c oxidase (complex IV) (Cooper, 2000).

As well as transporting electrons, respiratory complexes I, III and IV act as H+ ion (proton) pumps that move protons across the IMM from the mitochondrial matrix to the IMS, generating a huge difference in proton concentration between these two compartments that generates a pH difference of approximately 0.75. Movement of protons creates an electrochemical gradient across the IMM that generates $\Delta\Psi m$ with a voltage of approximately 140-180mV (Bagkos et al., 2014; Kühlbrandt, 2015). This gradient drives the generation of ATP through the final protein embedded in the IMM: ATP synthase. The ATP synthase pump is made up of two main components: F_0 and F_1. The F_0 subunit is embedded in the IMM and provides a channel to enable the flow of protons from the high-proton IMS back to the low-proton matrix. This ion movement is coupled to rotation of the F_1 subunit, which is structurally bound to F_0 but resides in the matrix. This rotation induces a conformational change that facilitates binding of ADP and P_i to generate ATP. ATP can then be transported out of the matrix through mitochondrial ADP/ATP carriers, and through the OMM by voltage-gated anion channels (VDAC) into the cell cytoplasm (Ruprecht et al., 2019; Varughese et al., 2021).

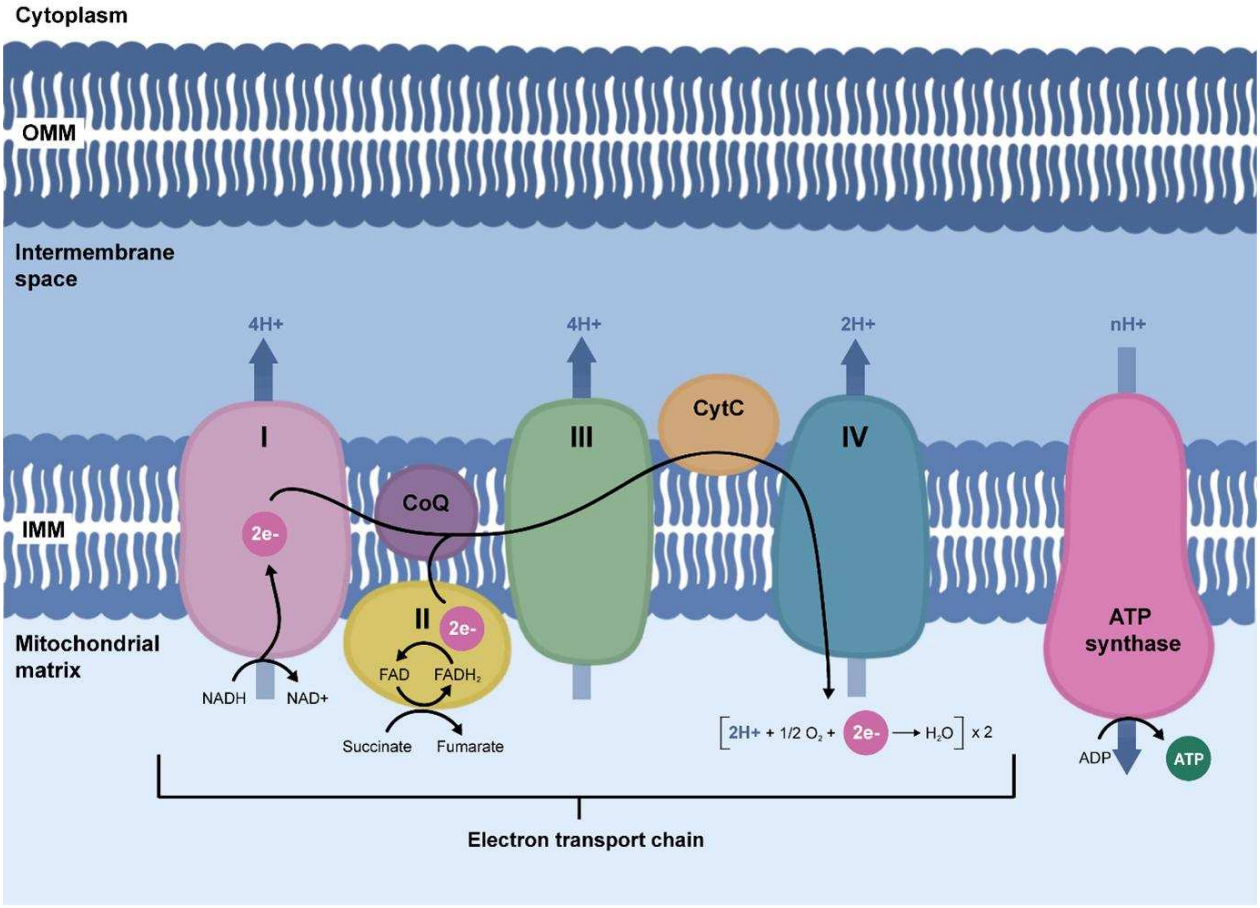

Figure 4: Schematic representation of the electron transport chain

OXPHOS occurs through a series of embedded proteins in the IMM known as the electron transport chain. Electrons from acceptors NADH and $FADH_2$ are transported through these complexes, generating a proton gradient that drives rotation of the ATP synthase pump, which generates ATP

1.1.2.2 Other cellular functions

Alongside the production of energy, mitochondria participate in a range of cellular functions that facilitate homeostasis, as summarised in **Figure 5**.

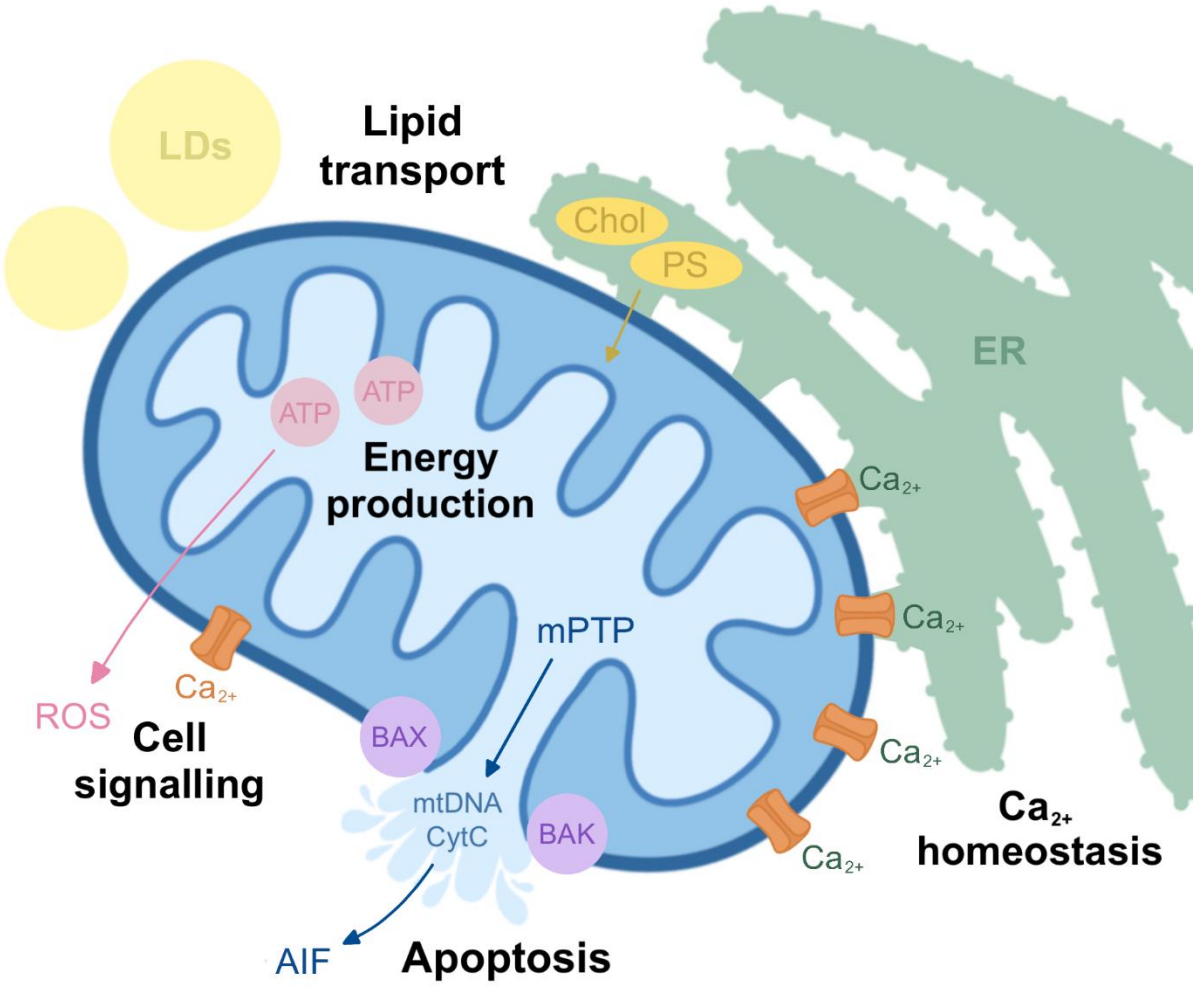

Figure 5: Schematic showing mitochondrial functions across the cell

Mitochondria have a range of cellular functions. This includes energy production inside the mitochondria which produce ATP, but also produce ROS for cell signalling. Signalling can also occur through Ca^{2+}, which can be buffered from the cytosol and taken up from the ER. Lipid transport occurs from the ER to the mitochondria, where phospholipids like cholesterol (chol) and phosphatidylserine (PS) become part of mitochondrial membranes. Mitochondria also take part in lipid storage through lipid droplets (LDs). They can also signal apoptosis triggered by BAX and BAK, leading to release and activation of pro-apoptotic signals.

1.1.2.2.1 Calcium homeostasis

Mitochondria play a crucial role in maintenance of Ca^{2+} homeostasis (Rizzuto et al., 2000). Ca^{2+} is a vital messenger that is involved in a variety of pathways, facilitating extremely fast signals such as synaptic transmission, as well as processes mediated over a longer time period, such as cell proliferation and migration (Santo-Domingo & Demaurex, 2010). In addition to controlling intracellular signalling, Ca^{2+} also enables communication between cells. Ca^{2+}-mediated exocytosis occurs in a range of cells, for example, the secretion of hormones from endocrine cells and of neurotransmitters from neurons (Südhof, 2012). In excitable cells such as neurons and cardiac myocytes, Ca^{2+} is also involved in the generation of action potentials that facilitate neuronal signalling (Catterall, 2011). Given its range of functions, regulation of intracellular Ca^{2+} is vital.

The ability of Ca^{2+} to act as such a versatile messenger is results from differences in Ca^{2+} concentration between cellular compartments, generated by a range of channels able to permit Ca^{2+} transport in both organelle and plasma membranes (Zü & Reiser, 2011). Accordingly, mechanisms to control and regulate levels of cytosolic Ca^{2+} are extremely important. The major site of Ca^{2+} storage is the endoplasmic reticulum (ER), but mitochondria are able to take up Ca^{2+} ions from the cytosol through the mitochondrial Ca^{2+} uniporter (mCU) (Santo-Domingo & Demaurex, 2010). This enables mitochondria to act as a buffer against high intracellular Ca^{2+} levels, helping to shape and regulate Ca^{2+} signalling. An increase in Ca^{2+} concentration in the mitochondrial matrix directly enhances respiration rate by activating a number of Ca^{2+}-dependent enzymes involved in the Krebs cycle as well as the ATPase pump (Maechler & Wollheim, 2001; Santo-Domingo & Demaurex, 2010). As such, mitochondrial Ca^{2+} ensures that synthesis of ATP is tuned to the cell's energetic requirements (McCormack & Denton, 1989).

1.1.2.2.2 Regulation of apoptosis

Intracellular Ca^{2+} levels can also convey life or death signals to mitochondria, which have a role in regulating apoptosis (Tait & Green, 2010). In circumstances of poor cell health, two members of the apoptosis-regulating B-cell lymphoma 2 (BCL-2) family, BCL-2-associated X (BAX) and BCL-2 antagonist/killer 1 (BAK), form pores in the OMM (Singh et al., 2019; Yamazaki & Galluzzi, 2022). This occurs primarily at mitochondrial contacts with the ER known as mitochondrial-associated membranes (MAMs), increasing the mobilisation of Ca^{2+} from its ER stores to mitochondria, causing an overload of mitochondrial Ca^{2+} (Sukumaran et al., 2021). This can result in prolonged opening of the mitochondrial permeability transition pore (mtPTP), meaning the selectivity of the IMM is lost and thus the $\Delta\Psi m$ (Kidd et al., 2002). Subsequent mitochondrial swelling leads to rupture of the OMM, initiating the release of a range of pro-

apoptotic factors into the cytosol, such as cytochrome C and apoptosis-inducing factor (AIF), that activate caspases and result in cell death (Martinou et al., 2000).

1.1.2.2.3 Lipid transfer & storage

Mitochondria also have a regulatory relationship with cellular lipids. Since mitochondrial membranes are constantly being remodelled, mitochondria must import lipids from other cellular compartments such as the ER to facilitate this (Talari et al., 2023). In addition to this, mitochondria have a role in lipid storage. Fatty acids are stored in the cell as triacylglycerol and packaged into dynamic organelles known as lipid droplets (LDs). LDs have been shown to represent an important energy reserve, which is particularly important in cases of nutrient deprivation. Mitochondria are able to bind LDs, where they can utilise these fatty acids through β-oxidation, generating acetyl CoA that can be processed via the Krebs cycle (Olzmann & Carvalho, 2019). In addition, mitochondria have been shown to promote both fatty acid oxidation and synthesis of triacylglycerides, suggesting that they can enhance fatty acid storage (Benador et al., 2018; Talari et al., 2023).

1.1.2.2.4 Organelle communication

Another important aspect of mitochondrial function is communication with other organelles. As discussed, mitochondria have extensive contacts with the ER at MAMs, facilitating lipid transfer, Ca^{2+} signalling and regulation of apoptosis. Alongside this, mitochondria also have crosstalk with a range of other organelles, as summarised in **Table 1**.

Table 1: Summary of communication between mitochondria and other organelles

Organelle	**Mitochondrial function**	**Reference**
ER	Modulation of Ca^{2+} signalling; regulation of apoptosis	(Ronayne & Latorre-Muro, 2024)
Golgi apparatus	Ca^{2+} buffering	(Dolman et al., 2005)
Nucleus	Supply of metabolites for epigenetic modifications; regulation of gene expression	(Shteinfer-Kuzmine et al., 2021)
Lysosomes	Regulation of lysosomal activity; regulation of lysosome and mitochondrial dynamics	(Wong et al., 2019)
LDs	Synthesis of triacylglycerides; oxidation of fatty acids in nutrient deprivation	(Benador et al., 2018; Talari et al., 2023)
Peroxisomes	Peroxisome biogenesis; maintaining lipid balance; maintaining redox balance; immune signalling	(Fransen et al., 2017)

1.2 Mitochondrial quality control

Given that mitochondria are responsible for such a wide range of important cellular processes, they are indispensable for regulating cell homeostasis. Therefore, maintaining effective mitochondrial function is vital. To ensure mitochondria stay healthy, they can assess damage by self-surveillance and have a range of mitochondrial quality control (mito-QC) mechanisms that they can co-ordinate at steady state and can upregulate in response to both localised and accumulated stress (**Figure 6**) (Eisner et al., 2018; Roca-Portoles & Tait, 2021).

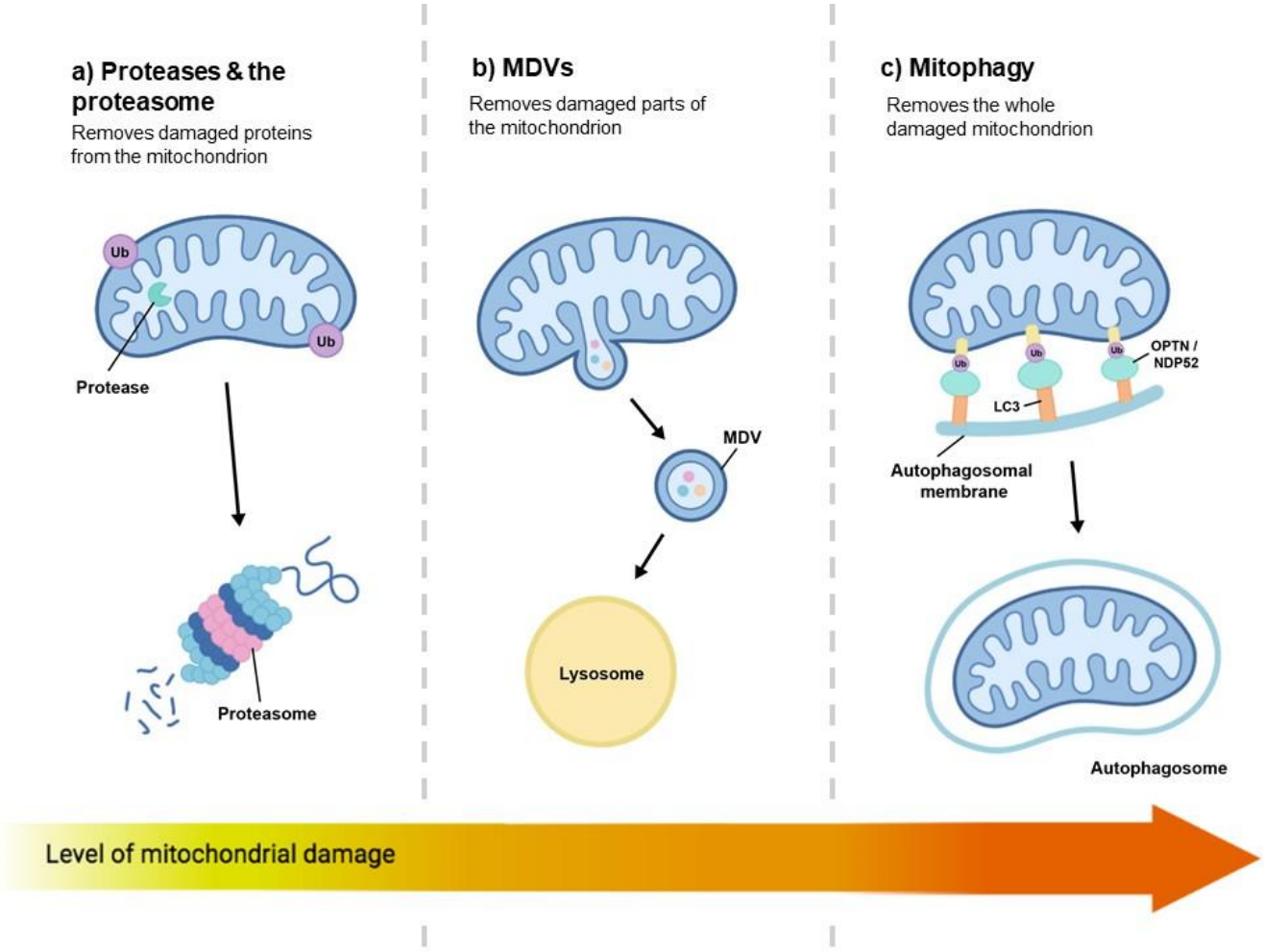

Figure 6: Schematic showing mitochondrial quality control systems

Mitochondrial quality control mechanisms occur at steady state and can be upregulated in response to increasing levels of damage. The first line of defence is degradation of individual damaged proteins by mitochondrial proteases and the proteasome (a). The next level of mito-QC occurs through MDVs, which can encapsulate groups of damaged proteins and fully formed complexes, and can traffic to the lysosome for degradation (b). As a last resort in circumstances of excessive damage, mitophagy can be triggered to degrade the entire organelle (c).

1.2.1 Mitochondrial dynamics

Healthy mitochondria form an interconnected network, and mitochondrial dynamics refers to the constant remodelling of this network by dynamin-like GTPases (Youle & Van Der Bliek, 2012). These morphological changes are driven by mitochondrial function and are co-ordinated by two main processes: fission and fusion (**Figure 7**).

1.2.1.1 Mitochondrial fusion

Mitochondrial fusion is driven by energy demand and enables the unification of several mitochondria into a single organelle (Youle & Van Der Bliek, 2012). This facilitates mitochondrial complementation, often occurring between one defective and one healthy organelle. This fusion event enables damaged organelles to regain functional mitochondrial components, enhancing the oxidative capacity of the resulting organelle (Detmer & Chan, 2007; Youle & Van Der Bliek, 2012). Mitochondria are trafficked towards each other along the cytoskeleton prior to merging of both the IMM and OMM, which occur by mechanistically distinct processes (Huang et al., 2023; Meeusen et al., 2004). At the OMM, this is co-ordinated by the GTPases mitofusin 1 and 2 (Mfn1 and Mfn2) which tether to the membrane and hydrolyse GTP to facilitate fusion (Ryan & Stojanovski, 2012). At the IMM, fusion occurs by another large GTPase, optic atrophy 1 (Opa1), which is dependent on $\Delta\Psi m$ and also regulates the morphology of cristae (Olichon et al., 2003).

1.2.1.2 Mitochondrial fission

Mitochondrial fission is the splitting of a single mitochondrion into 2 daughter organelles and is an important prerequisite for the removal of dysfunctional mitochondria by mitophagy, since it enables sequestration of damaged mitochondrial contents (Westermann, 2012). This process occurs through the GTPase dynamin-related protein 1 (Drp1), which is recruited to mitochondria by a combination of molecules, including mitochondrial fission factor (Mff). Drp1 molecules bind together to form a ring that encircles and constricts mitochondria using energy from the hydrolysis of GTP to cleave them into two (Bleazard et al., 1999; Friedman & Nunnari, 2014; Legesse-Miller et al., 1953).

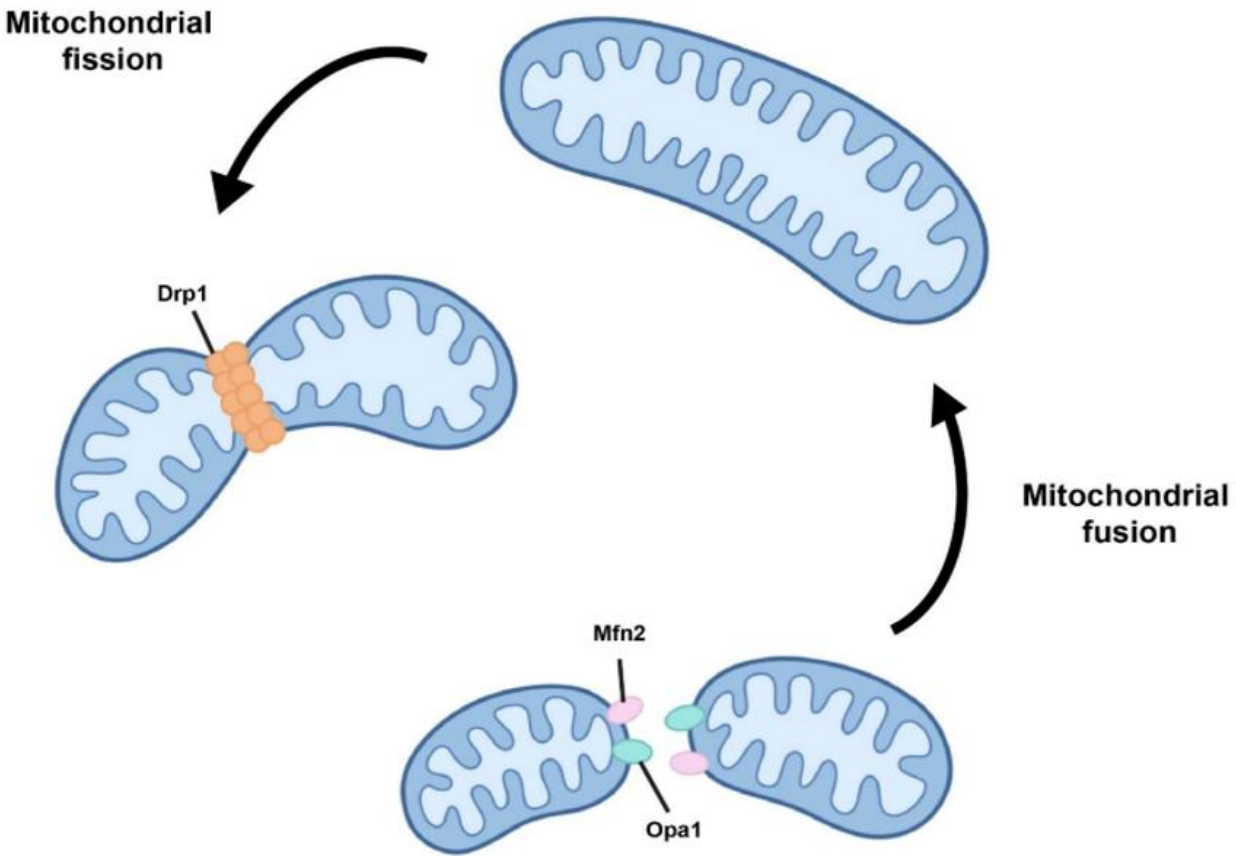

Figure 7: Schematic showing mitochondrial dynamics

Mitochondria are dynamic organelles with constant changes in morphology, controlled by mitochondrial dynamics which refers to fission/fusion events. Mitochondrial fission refers to the splitting of a single organelle into 2 daughter mitochondria by the concentric ring activity of Drp1 that facilitates mitochondrial membrane scission. Mitochondrial fusion refers to the merging of 2 individual mitochondria into a single organelle through the action of fusion regulators Mfn2 at the OMM and Opa1 at the IMM.

1.2.2 Antioxidant enzymes

The role of mitochondria in ATP synthesis increases their exposure to ROS, which form as by-products of OXPHOS due to the partial reduction of molecular oxygen (O_2). This produces high levels of both the superoxide anion (O_2^-) and the hydroxyl radical ($OH^\bullet$), which can cause oxidative stress and mitochondrial damage by disrupting mitochondrial protein structure and mutating mtDNA (Nita & Grzybowski, 2016). To combat this, mitochondria possess various antioxidant enzymes which act as a first line of defence against ROS (Brillo et al., 2021). These include superoxide dismutase, catalase and glutathione peroxidase which scavenge excess

ROS and catalyse their conversion into less reactive species, such as hydrogen peroxide (H_2O_2) (Matés J, 1999; Yang & Lian, 2020). As well as removing mitochondrial ROS, these enzymes provide mitochondria with a redox buffering ability that allows the quenching of cytosolic H_2O_2 to ease cellular oxidative stress (Ježek & Hlavatá, 2005; Mailloux, 2018). When ROS production exceeds antioxidant enzyme capability, damaged lipids and proteins accumulate within the mitochondria, impacting their health and function. At this point, mito-QC systems can be employed at the molecular level, working to ensure the correct stoichiometry and folding of mitochondrial proteins to limit damage (Jin & Youle, 2013).

1.2.3 Proteasomal degradation & the mtUPR

Mitochondria contain a range of proteases that can degrade unfolded, misfolded or oxidised soluble proteins directly within the organelle (Deshwal et al., 2024). Alongside this intramitochondrial mito-QC mechanism, defective proteins can be trafficked out of mitochondria and degraded by the ubiquitin-proteasome system (UPS) (Rödl & Herrmann, 2023). Damaged proteins can be exposed to the cytosol, where they are tagged with ubiquitin (Ub) by the action of 3 enzymes: ubiquitin activating enzyme (E1), ubiquitin conjugating enzyme (E2) and ubiquitin ligase (E3). Ub acts as a degradation signal, triggering targeting of the damaged protein to the 26S proteasome where it is degraded into small peptides (Pickart & Eddins, 2004; Taylor & Rutter, 2011). The UPS is also responsible for removing non-imported fractions of mitochondrial proteins and stalled intermediate proteins from OMM translocases, upholding efficient mitochondrial import mechanisms (Bragoszewski et al., 2013; Mårtensson et al., 2019).

When damaged mitochondrial proteins accumulate, mitochondrial dysfunction can directly trigger the transcription of genes to help alleviate damage (Inigo & Chandra, 2022). This adaptive stress response is known as the mitochondrial unfolded protein response (mtUPR), and enables the upregulation of molecular chaperones to aid correct protein folding and proteases to degrade those that are beyond repair (Pellegrino et al., 2014). These mechanisms are extremely important for the removal of individual damaged mitochondrial proteins.

1.2.4 MDVs

The next level of mito-QC is conducted by mitochondrial-derived vesicles (MDVs); vesicular compartments formed when small regions of mitochondrial membrane bud off from the mitochondria (Sugiura et al., 2014). Approximately 70-150nm in diameter, MDVs have been shown to turnover fully assembled protein complexes as well as sequester damaged mitochondrial components (König et al., 2021; Neuspiel et al., 2008; Sugiura et al., 2014). Once

formed, MDVs are trafficked away from the mitochondrion to a range of cellular targets, with the most well-characterised being the endolysosomal system where MDV contents are digested (McLelland et al., 2016)

MDVs exist as one of two structural subtypes: single-membraned vesicles derived from the OMM, or double-membraned vesicles derived from the IMM (**Figure 8**) (Neuspiel et al., 2008; Soubannier et al., 2012a; Soubannier et al., 2012b). Proteomics analysis of MDVs purified from mouse brain identified MDV cargo proteins, revealing the enrichment of 72 functionally diverse proteins and inciting speculation that any mitochondrial component could become MDV cargo under the right conditions (Robertson et al., 2004). The contents of a given MDV directly influences its end destination, with OMM-derived MDVs containing mitochondria-associated protein ligase (MAPL) shown to target peroxisomes but those containing TOM20 trafficked to lysosomes (Neuspiel et al., 2008; Soubannier et al., 2012a; Soubannier et al., 2012b). This cargo selectivity enables MDVs to sequester damaged proteins, with MDVs shown to be enriched for oxidised mitochondrial components in response to oxidative stress (Soubannier et al., 2012b). Interestingly, trafficking of TOM20-positive vesicles has been shown to be independent of mitochondrial depolarisation, indicating that MDVs act as an early line of defence, removing damaging components and thus reducing the likelihood that mitochondria will require more energy-intensive mito-QC responses such as mitophagy (McLelland et al., 2014; Soubannier et al., 2012b).

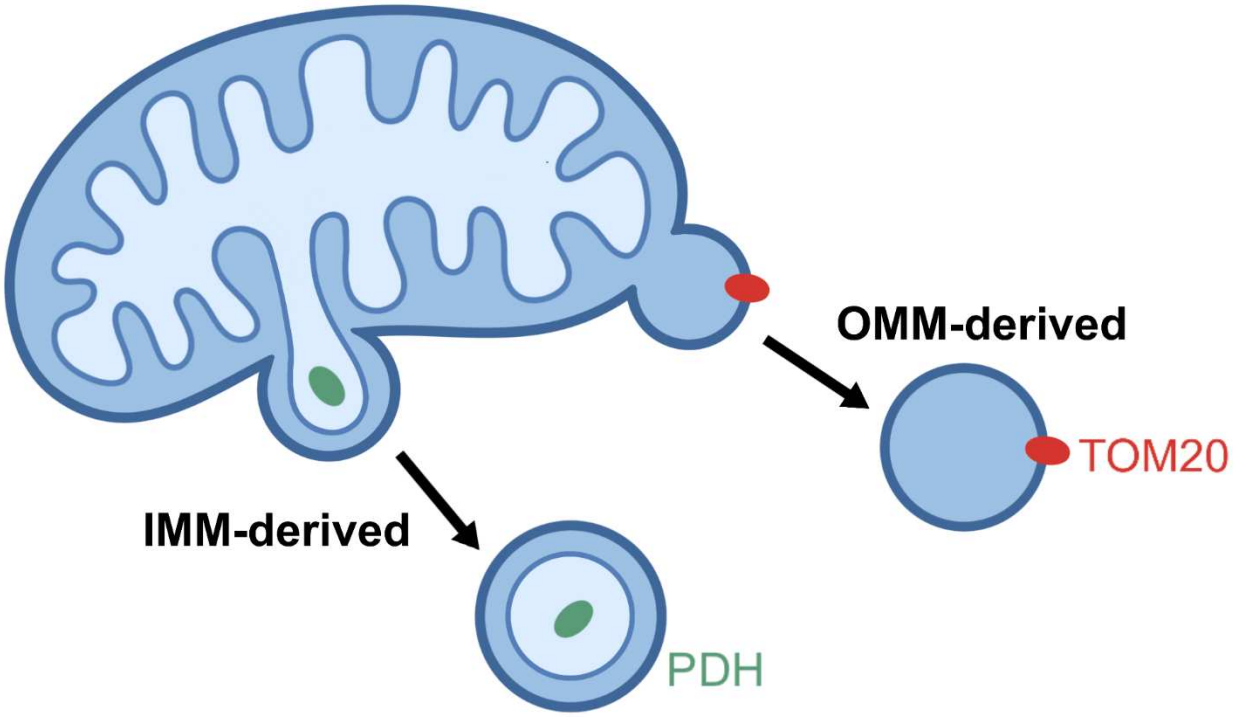

Figure 8: Schematic showing the 2 main structural subtypes of MDVs

2 main structural subtypes of MDVs exist: those from the OMM and those from the IMM. OMM-derived MDVs have a single membrane and often exhibit cargo selectivity for the OMM protein, TOM20 but exclude the matrix marker, PDH. In contrast, IMM-derived MDVs have a double membrane and exhibit cargo selectivity for PDH, but exclude TOM20.

1.2.5 Mitophagy

1.2.5.1 Macroautophagy: an overview

Autophagy refers to the process of delivering damaged cellular components to the lysosome for degradation and recycling, enabling cells to adapt to changing conditions and maintain homeostasis (Z. Yang & Klionsky, 2010). This occurs through several distinct mechanisms, with small debris and specific proteins targeted by microautophagy and chaperone-mediated autophagy (CMA) respectively, while the removal of large cellular components and organelles is directed by the most used pathway: macroautophagy (Z. Yang & Klionsky, 2010).

Initiation of macroautophagy is tightly controlled by the activity of unc-51-like-autophagy-activating kinase 1 (ULK1), which is regulated by nutrient availability (Nakatogawa, 2020; Yin et al., 2016). In nutrient-rich conditions, activity of mechanistic target of rapamycin complex 1

(mTORC1) inhibits ULK1, suppressing autophagy in healthy cells (Hosokawa et al., 2009). However, in response to nutrient deprivation, mTORC1 is downregulated and AMP-activated protein kinase (AMPK) becomes active, phosphorylating ULK1 and initiating autophagy to combat cell stress (Dunlop et al., 2011). Subsequently, a complex formed of ULK1, focal adhesion kinase family interacting protein of 200kDa (FIP200), autophagy-related protein (Atg) 13 (Atg13) and Atg101 translocates to autophagy initiation sites to promote formation of the autophagosome precursor membrane, the phagophore (Zachari & Ganley, 2017). Another protein complex, comprised of vacuolar protein sorting protein (VPS) 34 (VPS34) and Beclin-1, facilitates nucleation of this membrane by producing the phospholipid phosphatidylinositol 3-phosphate (PI3P) (Z. Yang & Klionsky, 2010). PI3P recruits members of the Atg8 protein family that are required for elongation and maturation of autophagosomes, such as microtubule-associated protein light chain 3 (LC3) (Nakatogawa, 2020). In addition, PI3P acts as a lipid signal to bind other autophagy-promoting proteins such as WD repeat domain phosphoinositide-interacting protein 2 (WIPI2) which recruit Atg16-like protein (Atg16L), Atg5 and Atg12 that are responsible for the conjugation of cytosolic LC3-I to phosphatidylethanolamine (PE) in the autophagosome membrane, forming lipidated LC3-II (Kabeya et al., 2000; Zachari & Ganley, 2017). Autophagosomes are trafficked to lysosomes via motor proteins, with autophagosome-lysosome fusion co-ordinated by Rab7 and facilitated by soluble N-ethylmaleimide-sensitive factor activating protein receptor (SNARE) complexes (Wang et al., 2016; Yin et al., 2016).

1.2.5.2 Mitophagy

A type of macroautophagy specific to mitochondria, mitophagy is triggered upon excessive oxidative stress. Mitochondria experience alterations in membrane permeability that induce loss of the $\Delta\Psi m$, disrupting OXPHOS and triggering sequestration of the organelle inside an autophagosome, co-ordinated by a range of autophagy proteins as described in **1.2.5.1** (Zang & Klionsky, 2010). Following autophagosome-lysosome fusion, mitochondrial contents are degraded and recycled back to the cell. Removal of whole damaged mitochondria by mitophagy prevents the expansion of damage to the rest of the cell and is reserved for inordinate levels of stress due to the high energy demand it requires both to co-ordinate mitophagy and to replace the eliminated mitochondria (Cadete et al., 2016). The most well-characterised pathway occurs through Ub-mediated mitophagy, co-ordinated by PTEN-induced putative kinase 1 (PINK1) and Parkin (Allen et al., 2013; Ke, 2020).

1.2.5.3 PINK1/Parkin-dependent mitophagy

PINK1 is a mitochondrial-targeted serine/threonine kinase that is rapidly degraded under physiological conditions, but accumulates on the OMM in response to loss of ΔΨm (Rüb et al., 2017). This accumulation enables PINK1 to phosphorylate Ub on its serine 65 residue (pUb S65), triggering the mitochondrial recruitment of the E3 enzyme, Parkin (Narendra et al., 2010; Rüb et al., 2017). PINK1 can then phosphorylate the serine 65 residue of Parkin's Ub-like domain, activating its enzymatic activity and thus facilitating ubiquitylation of proteins on the OMM (Koyano et al., 2014; Narendra et al., 2008; Narendra et al., 2010). Parkin's activity can be further enhanced by binding pUb S65, which increases the phosphorylation of Parkin's Ub-like domain by PINK1 (Wauer et al., 2015). This combined action of PINK1, Parkin and pUb S65 facilitates the addition of polyubiquitin chains to mitochondrial proteins. Links between these chains on the OMM and Atg8 family proteins on the surface of the autophagosome are directly mediated by autophagy receptors such as nuclear dot protein 52kDa (NDP52), optineurin and Tax1-binding protein 1 (TAX1BP1) (Lazarou et al., 2015; Ryan & Tumbarello, 2018). Tethering of these membranes facilitates engulfment of the mitochondrion by the autophagosome and subsequent degradation by the endolysosomal system (Stolz et al., 2014). This process is summarised in **Figure 9**.

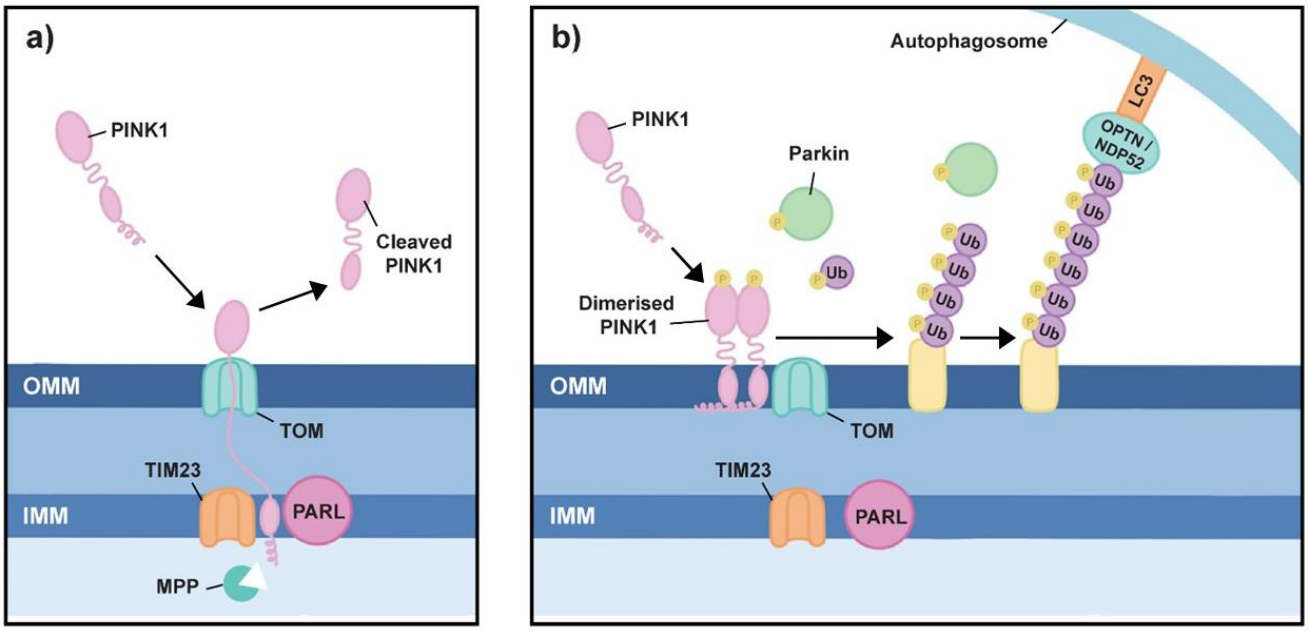

Figure 9: Schematic showing the mechanisms of PINK1/Parkin-dependent mitophagy

PINK1/Parkin-dependent mitophagy can be triggered upon loss of mitochondrial membrane potential (ΔΨm). At steady state (a), PINK1 is recruited to mitochondria. It enters through the TOM complex and its N-terminus is transferred to the IMM where it is cleaved and degraded in the cytosol by the proteasome. Upon depolarisation (b), PINK1 accumulates on the OMM, dimerises and autophosphorylates instead of being degraded. The kinase activity of PINK1 phosphorylates ubiquitin and Parkin at serine 65, activating Parkin's E3 ubiquitin ligase activity. Parkin facilitates the formation of ubiquitin chains, which are further phosphorylated by PINK1. Autophagy receptors such as optineurin (OPTN) contain both ubiquitin- and LC3-binding domains, allowing the mitochondria and autophagosome to be tethered together, facilitating engulfment and degradation of the damaged organelle.

1.2.5.4 PINK1/Parkin-independent mitophagy

Mitochondrial clearance can also be co-ordinated via Ub-independent mechanisms, such as through receptors and lipids. Receptor-mediated mitophagy occurs through autophagy receptors embedded in the OMM that can directly bind autophagosomal GABARAP and LC3, such as FUN14 domain-containing 1 (FUNDC1), FK506-binding protein 8 (FKBP8), BCL-2/adenovirus E1B 19kDa protein-interacting protein 3 (BNIP) and NIP3-like protein X (NIX) (Bunker et al., 2023; Liu et al., 2012). FUNDC1 and BNIP have both been shown to specifically mediate mitophagy induced by hypoxic conditions (Liu et al., 2012; Quinsay et al., 2010).

Lipid-mediated mitophagy can be co-ordinated by the phospholipid, cardiolipin (CL). CL is found in the IMM, forming approximately 20% of its total phospholipid mass (Horvath & Daum, 2013). Due to its unsaturated fatty acyl chains, CL is particularly sensitive to oxidative stress, which underpins its role as a regulator of mitophagy. Oxidised CL is redistributed from the IMM to the OMM, where it is externalised and can be directly recognised by autophagosomal LC3 to initiate mitophagy (Chu et al., 2013). In addition, mitophagy can be further promoted by the autophagy regulator, Beclin1, which preferentially binds CL-rich membranes (Huang et al., 2012).

1.3 Consequences of dysfunctional mito-QC

Mitochondrial dysfunction is a key driver of a range of diseases, including heart failure, diabetes, human immunodeficiency virus (HIV) infection and neurodegenerative disease (Hong et al., 2024). Since mito-QC mechanisms are essential to maintain mitochondrial health, defects in the effectiveness of these pathways have been suggested as factors leading to mitochondrial dysfunction. This is particularly true in age-associated diseases since mitochondrial health and respiratory capacity has been shown to decrease as we age, meaning efficient mito-QC systems are of even more importance (Conley et al., 2000; Santanasto et al., 2015).

1.3.1 Mito-QC in disease

In the case of heart failure, dysregulated mitochondrial dynamics are considered a hallmark of the disease (Hinton et al., 2024). An increase in mitochondrial fragmentation is triggered in cardiomyocytes as a result of an upregulation of the fission protein, Drp1, and a downregulation of the fusion proteins, Mfn2 and Opa1 (Sabbah et al., 2018). Fragmentation of mitochondria as a result of disrupted fission and fusion has been shown to induce a form of dilated cardiomyopathy and death in mouse models (Wai et al., 2015). This is likely due to the reduced respiratory capacity of the mitochondrial network. Dysfunctions in mitochondrial dynamics therefore contribute to the induction of heart failure.

Mitochondrial dynamics are also impacted by HIV, since the virus' envelope protein has been shown to directly interfere with expression of fission/fusion proteins (Fields et al., 2016). In addition, HIV increases the sensitivity of T-lymphocytes to changes in $\Delta\Psi m$, making them prone to mitochondrial-mediated apoptosis (Arnoult et al., 2003). This causes depletion of key cells required for the immune response, such as macrophages and monocytes (Février et al., 2011). In this case, altered mitochondrial dynamics contribute to a weakened immune response.

Imbalances in mito-QC have also been shown to be important for the development of cancer, since cancerous cells exhibit alterations in mitochondrial respiratory capacity (Warburg, 1956). Elevated levels of the mitochondrial chaperone, heat shock protein 70 (HSP70), are associated with many cancers, and it has been shown to promote tumorigenesis through its role in inhibiting BAX in mitochondria-mediated apoptosis (Juhasz et al., 2014; Kondrikov et al., 2015). PINK1/Parkin-dependent mitophagy has been suggested to be protective in cancer, since a correlation has been shown between impaired Parkin activity and development of tumours (Bernardini et al., 2017). Loss of control over the activity of

mitochondrial chaperones and mitophagy proteins causes disruptions to mito-QC, assisting in the development of cancer.

Dysfunctional mito-QC is a key feature of neurodegenerative diseases. In AD, increased expression of mitochondrial fission proteins has been shown to correlate with the accumulation of tubulin-associated unit proteins (Tau), the protein responsible for forming hallmark neurofibrillary tangles (Wang et al., 2008). In turn, Tau and the aggregatory protein amyloid-beta (Aβ), can disrupt mitochondrial transport which may impact mito-QC at all levels (Y. R. Zheng et al., 2019). Further, Aβ can be mitochondrially internalised, with aggregated species shown to impair mitochondrial protein import and induce mitochondrial dysfunction (Cenini et al., 2016). This mitochondrial dysfunction results in oxidative stress, creating a damaging feedback loop that exacerbates Aβ pathology, leading to toxicity and cell death (Cheignon et al., 2018).

1.3.2 Mito-QC in Parkinson's disease

The connection between mitochondrial dysfunction and pathology is particularly strong in PD. PD is characterised by the selective degeneration of dopaminergic neurons in the substantia nigra pars compacta (SNpc) of the striatum that results in a collection of cognitive, psychiatric and motor symptoms (Dauer & Przedborski, 2003; Opara et al., 2017). Interestingly, SNpc neurons have a high metabolic burden due to their copious synaptic connections and elevated ROS production because of their dopamine metabolism, making them particularly vulnerable to oxidative stress (Bolam & Pissadaki, 2012; Pacelli et al., 2015). It has been suggested that this increased vulnerability may explain the selectivity of neuronal degeneration in the early stages of PD, though the mechanisms of cell death responsible for this are not well defined (Bolam & Pissadaki, 2012; Pacelli et al., 2015).

Under physiological and pathological conditions, cell death can occur through a range of controlled and uncontrolled mechanisms. Controlled mechanisms, such as apoptosis, are key for homeostasis and direct specific downstream events to co-ordinate cell death in response to stress signals (Yuan & Ofengeim, 2024). Uncontrolled mechanisms, such as necrosis, can also trigger death in response to unexpected external factors such as infection or trauma (Yuan & Ofengeim, 2024). Increases in a variety of cell death pathways have been reported in PD patients and animal models, but there is no process defined as being primarily responsible for SNpc cell death. The contributions of cell death pathways of neurodegeneration in PD have been well discussed by Pedrão et al. (2024), and a summary of these is shown in

Table 2.

Mechanism	Description	Evidence for a role in PD
Apoptosis	Programmed cell death by caspases	- Elevated caspase activity in PD patients (Mogi et al., 2000) - Caspase inhibitors & anti-apoptotic factors rescue cell death in PD models (Akao et al., 2002; Iaccarino et al., 2007) - Apoptotic bodies observed in PD patients (Tompkins et al., 1997)
Necrosis	Uncontrolled, non-apoptotic inflammatory cell death	- Necrosis observed in PD models (Callizot et al., 2019) - Necrosis inhibitors reduce cell death in PD models (Wu et al., 2015)
Ferroptosis	Programmed iron-dependent cell death	- Interactions between α-synuclein and iron metabolism well-documented (Chen et al., 2019) - Anti-ferroptosis molecules neuroprotective in PD models (Southon et al., 2020) - Anti-ferroptosis molecules shown to slow PD progression and reduce motor symptoms in clinical trials (Devos et al., 2014)
Pyroptosis	Programmed cell death by inflammasome	- Pyroptosis-associated inflammatory factors promote cell death in PD models (Koprich et al., 2008) - Inflammasome inhibitors neuroprotective in PD models (Que et al., 2021) - Drugs inducing pyroptosis can induce PD symptoms in animal models (Wang et al., 2022)
Autophagy-dependent cell death	Programmed cell death by autophagic machinery	- Abnormal expression of autophagy genes can be causative for PD (Paisán-Ruíz et al., 2004; Zimprich et al., 2011) - Antioxidants to manipulate autophagy pathway are neuroprotective in PD models (Q. Yu et al., 2023)

Table 2: Summary of evidence that implicates cell death mechanisms in PD pathology

Mechanism	Description	Evidence for a role in PD
Apoptosis	Programmed cell death by caspases	- Elevated caspase activity in PD patients (Mogi et al., 2000) - Caspase inhibitors & anti-apoptotic factors rescue cell death in PD models (Akao et al., 2002; Iaccarino et al., 2007) - Apoptotic bodies observed in PD patients (Tompkins et al., 1997)
Necrosis	Uncontrolled, non-apoptotic inflammatory cell death	- Necrosis observed in PD models (Callizot et al., 2019) - Necrosis inhibitors reduce cell death in PD models (Wu et al., 2015)
Ferroptosis	Programmed iron-dependent cell death	- Interactions between α-synuclein and iron metabolism well-documented (Chen et al., 2019) - Anti-ferroptosis molecules neuroprotective in PD models (Southon et al., 2020) - Anti-ferroptosis molecules shown to slow PD progression and reduce motor symptoms in clinical trials (Devos et al., 2014)
Pyroptosis	Programmed cell death by inflammasome	- Pyroptosis-associated inflammatory factors promote cell death in PD models (Koprich et al., 2008) - Inflammasome inhibitors neuroprotective in PD models (Que et al., 2021) - Drugs inducing pyroptosis can induce PD symptoms in animal models (Wang et al., 2022)
Autophagy-dependent cell death	Programmed cell death by autophagic machinery	- Abnormal expression of autophagy genes can be causative for PD (Paisán-Ruíz et al., 2004; Zimprich et al., 2011) - Antioxidants to manipulate autophagy pathway are neuroprotective in PD models (Q. Yu et al., 2023)

Interestingly, many of these cell death pathways can be triggered by mitochondrial damage, ROS and oxidative stress. Given the increased susceptibility of SNpc neurons to oxidative stress, mitochondrial dysfunction has been identified as a potential basis for targeted cell degeneration (Ganjam et al., 2019; Martin et al., 2006). Evidence for mitochondrial dysfunction as a driver of PD pathology was first highlighted when synthetic heroin drug users inadvertently ingested the mitochondrial inhibitor, MPTP (1-methyl-4-phenyl-1,2,3,6-tetrahydropyridine), resulting in symptoms with striking comparability to PD (Davis et al., 1979). Post-mortem assessment revealed the degeneration of SNpc neurons and the presence of Lewy bodies (LBs); intracellular inclusions that are a hallmark characteristic of PD pathology (Davis et al., 1979; William Langston et al., 1983). Alongside MPTP, other chemical inhibitors of mitochondrial function such as 6-hydroxydopamine (6-OHDA) and rotenone are now used to generate animal models of PD (Betarbet et al., 2000; Ungerstedt, 1971). Clinical studies have also provided physiological evidence of mitochondrial pathology in the PD brain, with mitochondrial complex I deficiency and increased mtDNA mutations reported in the striatum of post-mortem tissue compared to controls (Bender et al., 2006; Schapira et al., 1989).

This observation that SNpc neurons are especially sensitive to mitochondrial dysfunction suggested that precise damage control by mito-QC would be extremely important to maintain cell health. The relationship between mito-QC and PD pathology was validated by genome-wide association studies (GWAS), which identified a number of PD-associated genetic perturbations in genes with defined roles in co-ordination of mito-QC (Billingsley et al., 2019; Chang et al., 2017). Two of the first mutations to be linked with familial PD pathogenesis were in genes for the mitophagy regulators PINK1 and Parkin (Kitada et al., 1998; Valente et al., 2004). Interestingly, this was followed by the discovery of many more PD-associated mutations in genes with defined roles at mitochondria as well as the downstream endolysosomal compartment implicated in mitophagy (**Table 3**). This provides support for the hypothesis that dysfunctions in mito-QC are intrinsically linked to PD pathology.

Table 3: Mitochondrial and endolysosomal genes linked to Parkinson's disease

Gene	Protein	Function	Reference
ASAH1	N-acylsphingosine amidohydrolase 1	Lysosomal lipid hydrolase	(Aharon-Peretz et al., 2004; Robak et al., 2017)
ATP13A2	ATPase cation transporting 13A2	Late endosomal transporter; lysosomal polyamine exporter	(Ramirez et al., 2006)
ATP6V0A1	ATPase H+ transporting V0 subunit a1	Proton transporter mediating organelle acidification	(Chang et al., 2017; Morel, 2003)
CHCHD2	Coiled-coil-helix-coiled-coil-helix domain-containing protein 2	Biogenesis and regulation of ETC proteins in mitochondria	(Funayama et al., 2015; Kee et al., 2021)
COQ7	Coenzyme Q7 hydroxylase	Mitochondrial enzyme required for coenzyme Q synthesis	(Chang et al., 2017; Freyer et al., 2015)
CTSB	Cathepsin B	Lysosomal protease in autophagy	(Chang et al., 2017; Yadati et al., 2020)
CTSD	Cathepsin D	Lysosomal protease in autophagy	(Benes et al., 2008; Robak et al., 2017)
PARK7	Parkinsonism associated deglycase (DJ1)	Redox-sensitive chaperone and protease	(Bonifati et al., 2002; Hijioka et al., 2017)
FBXO7	F-box only protein 7	Component of E3 ubiquitin ligase; PINK1-Parkin mitophagy	(Burchell et al., 2013; Fonzo et al., 2009)
GALC	Galactosylceramidase	Lysosomal hydrolase	(Chang et al., 2017; Robak et al., 2017)
GBA	Glucosylceramidase β	Lysosomal hydrolase	(Magalhaes et al., 2016; Sidransky et al., 2009)
LRRK2	Leucine rich repeat kinase 2	Serine/threonine kinase regulating Rab GTPase function in endolysosomal system	(Bonet-Ponce et al., 2020; Paisán-Ruíz et al., 2004)
PRKN	Parkin RBR E3 ubiquitin protein ligase	Ubiquitylates mitochondrial proteins; mitophagy regulator	(Kitada et al., 1998; Pickrell & Youle, 2015)
PINK1	PTEN induced kinase 1	Mitochondrial damage sensor; mitophagy regulator	(Pickrell & Youle, 2015; Valente et al., 2004)

Gene	Protein	Function	Reference
RAB7L1	RAB7, member RAS oncogene family-like 1	Recruits LRRK2 to the Golgi to promote Golgi-derived vesicles	(Beilina et al., 2014; Nalls et al., 2014)
SCARB2	Scavenger receptor class B member 2	Endo/lysosomal membrane protein in lipid transport	(Do et al., 2011; Gonzalez et al., 2014)
SMPD1	Sphingomyelin phosphodiesterase 1	Lysosomal lipid hydrolase	(Alcalay et al., 2019; Schuchman, 2010)
TMEM175	Transmembrane protein 175	Potassium channel in late endosomes/lysosomes	(Nalls et al., 2014; Zhang et al., 2020)
VPS35	VPS35 retromer complex component	Subunit of retromer complex for endosomal retrograde transport	(Deng et al., 2013; Zimprich et al., 2011)

1.4 α-synuclein

Aside from mutations in mito-QC genes, the most common PD-associated mutations are in the SNCA gene which codes for α-synuclein: a small, amyloid forming protein that is primarily expressed in the brain (Polymeropoulos et al., 1997). It has a range of physiological functions in neuronal cells, but can aggregate under pathological circumstances to form damaging species that eventually constitute LBs in PD and other synucleinopathies such as LB dementia and multiple systems atrophy (MSA) (Cremades & Dobson, 2018). This α-synuclein aggregation causes cytotoxicity and neuronal degeneration, though the mechanisms behind this are still not well understood. Toxic gain-of-function of α-synuclein is thought to drive pathology, with α-synuclein aggregates shown to disrupt normal functioning of the endolysosomal system, cytoskeleton and mitochondria (Alim et al., 2004; Hashimoto et al., 1999; Hsu et al., 2000). However, loss-of-function of physiological α-synuclein has also been suggested to contribute to PD, since it has a range of regulatory actions that contribute to neuronal function (Kanaan & Manfredsson, 2012). The structure of α-synuclein facilitates its ability to function both physiologically and pathologically.

1.4.1 Synuclein structure and family

1.4.1.1 Protein structure

α-synuclein is an intrinsically disordered protein made of 140 amino acid (AA) residues, comprised of 3 domains: an N-terminal α-helix, a central domain (NAC) and a C-terminal acidic tail (Emamzadeh, 2016) (**Figure 10**). The N-terminal segment (residues 1-60) is a positively charged region with numerous amphipathic 11-mer repetitions that each contain a highly conserved KTKEGV motif (Brontesi et al., 2023; Emamzadeh, 2016). α-synuclein forms a helical structure when bound to lipid membranes, and this ability is directly modulated by these KTKEGV repeats (Braun et al., 2017; Emamzadeh, 2016). The majority of PD-associated mutations in SNCA occur within the N-terminal domain (Emanuele & Chieregatti, 2015). The hydrophobic NAC domain (residues 61-95) is aggregation-prone, able to bind amyloids to generate fibrillar species (Giasson et al., 2001). Finally, the highly acidic C-terminal segment (residues 96-140) exhibits a random coil structure, due to its net negative charge. This domain interacts with small molecules such as Ca^{2+} and is the site for several post-translational modifications (PTMs) that regulate α-synuclein activity (Emamzadeh, 2016). Additionally, the C-terminus can inhibit protein aggregation through electrostatic repulsion, but also appears to be required for α-synuclein oligomerisation (Farzadfard et al., 2022).

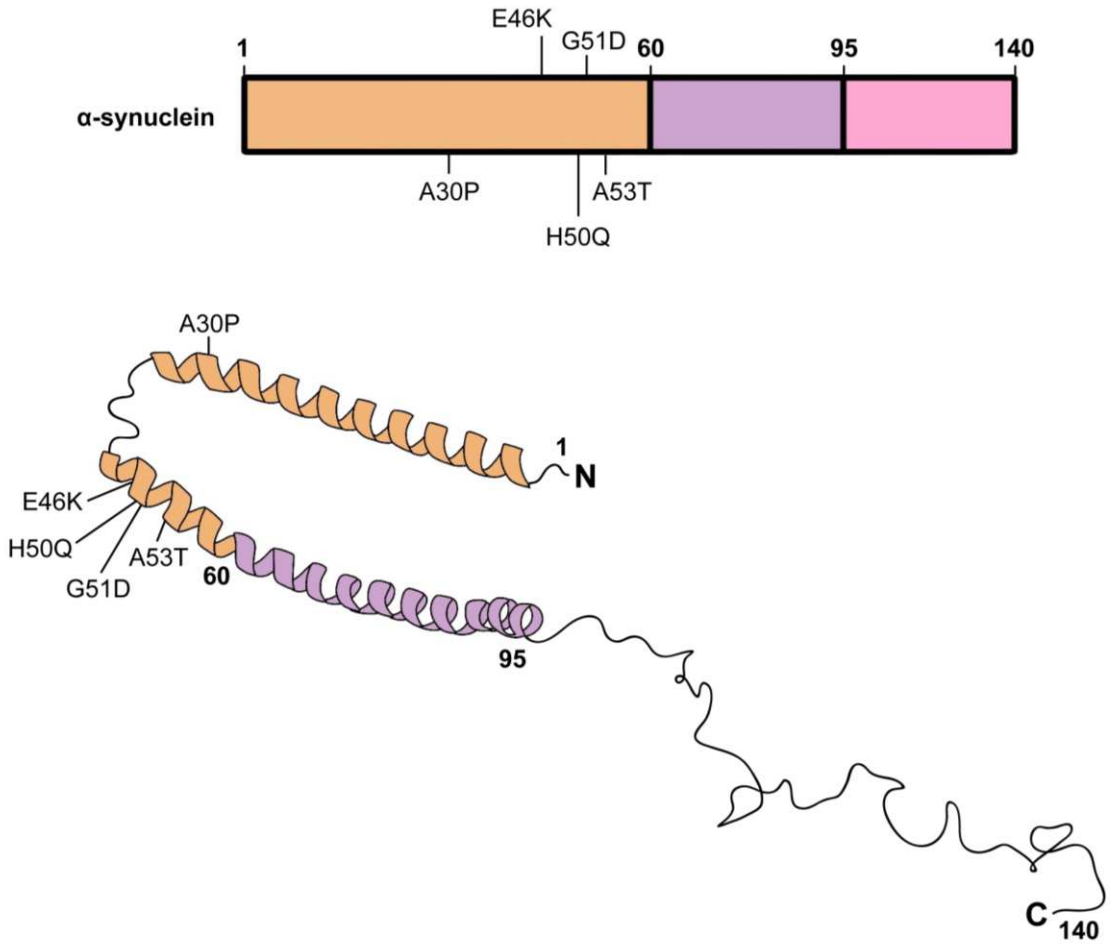

Figure 10: Schematic showing protein domains and structure of α-synuclein

α-synuclein is a 140 amino acid protein made of 3 structural domains: the N-terminus (orange), NAC domain (purple) and the C-terminus (pink/black). Many common point mutations associated with Parkinson's disease occur in the N-terminus, including A30P, E46K, H50Q, G51D and A53T.

1.4.1.2 Synuclein family members

The synuclein family consists of not only 140-AA α-synuclein, but 134-AA β-synuclein and 127-AA γ-synuclein (**Figure 11**) (George, 2001). Though only α-synuclein is associated with PD, there is some structural and functional homology between the proteins. β-synuclein is the most similar to α-synuclein with 78% AA sequence homology, and the 2 proteins are often co-expressed throughout the nervous system (Goedert, 2001). It has an N-terminal segment that closely resembles that of α-synuclein, but lacks a large portion of the aggregatory NAC domain (Williams et al., 2018). The C-terminus is also much less flexible in β-synuclein, giving it a more rigid structure. Accordingly, β-synuclein has a much lower propensity to aggregate (Barba et al., 2022). γ-synuclein has 60% similarity with α-synuclein, and is less well-characterised (Goedert,

2001). It is primarily expressed in the peripheral nervous system and has been implicated in the development of breast cancer (Liu et al., 2005). Its N-terminus also has high homology with that of α-synuclein, but it does not have α-synuclein's high aggregation propensity. While γ-synuclein can aggregate, it has only been shown to do so more slowly and at high concentrations, due to differences in both its NAC domain and C-terminus (Uversky et al., 2002).

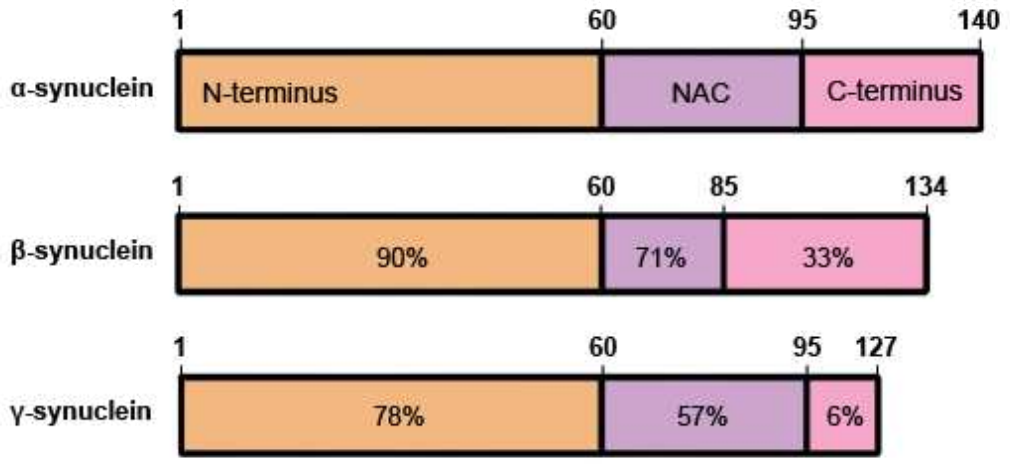

Figure 11: Schematic showing protein domains of α-, β- and γ-synuclein

The synuclein family comprises α-, β- and γ-synuclein which have different levels of homology in their amino acid sequence. The highest homology is seen in the 3 N-terminal domains, with the C-terminus the most variable. α- and β-synuclein have the greatest structural similarity.

1.4.1.3 Aggregation of α-synuclein

Pathology of α-synuclein is dependent on its aggregation. LBs observed in the PD brain primarily contain α-synuclein fibrils, though mechanisms regulating the formation of these species are not fully understood (Cremades & Dobson, 2018). Physiologically, α-synuclein exists as both a soluble, unfolded monomer and a membrane-bound α-helical form. Monomeric α-synuclein is intrinsically disordered, meaning its structure continuously oscillates from an unfolded to a fully folded protein (Robustelli et al., 2018). When aggregation is triggered, native monomeric species can interact to form β-sheets. Multiple β-sheets can connect with each other to form intermediate species classified as oligomers, which are thought to be one of the most toxic structural α-synuclein conformations (Winner et al., 2011). Oligomers can stabilise into insoluble protofibrils, and finally polymerise into amyloid fibrils. Interestingly, several PD-

associated mutations in SNCA confer an increased aggregation propensity that enhances formation of these large α-synuclein species (**Figure 12**). One example of this is A53T, a point mutation which describes an alanine to threonine substitution at position 53 (Polymeropoulos et al., 1997). Since this mutation does not impact the aggregatory NAC domain, it is proposed to enhance aggregation by promoting the formation of β-sheets which oligomerise more easily (S. Kumar et al., 2009; Ohgita et al., 2022).

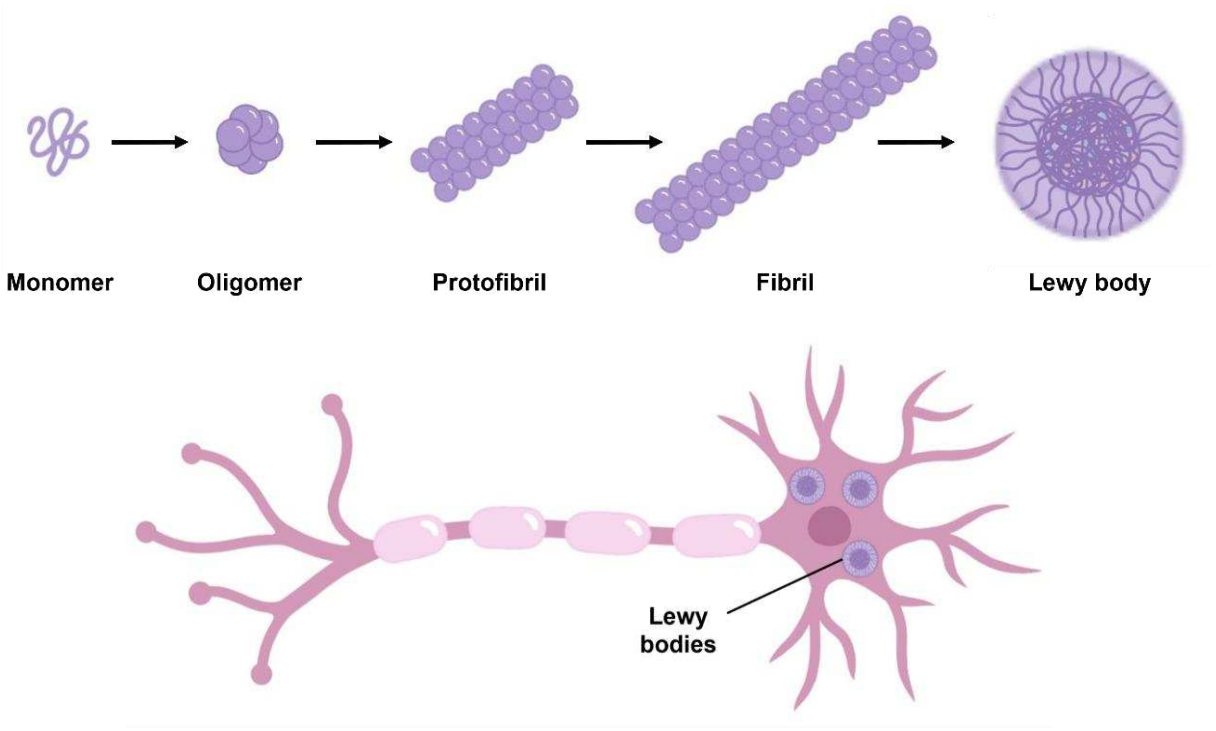

Figure 12: Schematic showing aggregation of α-synuclein

α-synuclein primarily exists as a disordered monomer, which can bind other α-synuclein proteins to form oligomeric structures. These can associate with other oligomers to form protofibrils, which eventually extend into longer fibrils. Fibrillar α-synuclein can form Lewy bodies, which encapsulate other damaged proteins from the cell. Lewy bodies are found intracellularly in dopaminergic neurons from the brains of PD patients.

1.4.2 Physiological function of α-synuclein

As mentioned, α-synuclein exists as an unfolded monomer that shuttles between the cytoplasm and phospholipid membranes, where it binds and adopts a helical structure (Burré, 2015; Emamzadeh, 2016). Investigations into the membrane binding capability of α-synuclein using nuclear magnetic resonance (NMR) revealed that it has high affinity for unsaturated lipids with small anionic head groups and polyunsaturated acyl chains, which have large spaces between phospholipid groups (Pfefferkorn et al., 2012; G. F. Wang et al., 2010). These preferences enable α-synuclein to act as a curvature sensor, and facilitate its range of physiological functions (Drin & Antonny, 2010).

1.4.2.1.1 Synaptic vesicle regulation

First identified in synaptic vesicles from *Torpedo californica*, the primary function of α-synuclein is considered to be regulation of neurotransmission (Maroteaux et al., 1988). Its affinity for binding highly curved membranes enables it to bind synaptic vesicles, where it has a role in mediating their release from the presynaptic terminal (V. Gao et al., 2023; W. J. Hong & Lev, 2014). Specifically, it has been shown to promote the assembly of SNARE complexes through a direct interaction with synaptobrevin-2 (Burré et al., 2010). SNARE complexes facilitate membrane fusion between synaptic vesicles and the plasma membrane, so α-synuclein is important for both vesicle docking and exocytosis. In addition, α-synuclein has been shown to impact the clustering and trafficking of synaptic vesicles, enabling it to regulate the number of vesicles docked at the membrane (Auluck et al., 2010; Diao et al., 2013).

1.4.2.1.2 Molecular chaperone activity

α-synuclein also exhibits sequence homology with members of the versatile chaperone protein family, 14-3-3 (Ostrerova et al., 1999). It has been shown that α-synuclein can bind molecular targets of 14-3-3 proteins, which include protein kinase C (PKC), extracellular-signal-regulated kinase (ERK) and Bcl-2-associated death promoter (BAD) (Ostrerova et al., 1999). Alterations in α-synuclein can influence the cell signalling cascades governed by these proteins, confirming the ability of α-synuclein to act as a molecular chaperone (Jin et al., 2011; Sang et al., 2002).

1.4.2.1.3 Dopamine regulation

Another important function performed by α-synuclein is regulation of dopamine homeostasis. Firstly, α-synuclein has been shown to interact with tyrosine hydroxylase (TH), the rate-limiting enzyme involved in the conversion of tyrosine to the dopamine precursor, L-3, 4-dihydroxyphenylalanine (L-DOPA) (Perez et al., 2002a). Physiologically, it is thought to inhibit TH

and thus downregulate dopamine synthesis (X. M. Peng et al., 2005; Perez et al., 2002a). Through its action at pre-synaptic terminals, α-synuclein can also influence dopaminergic transmission through modulating the release of dopamine-containing synaptic vesicles (Burré, 2015). Further to this, α-synuclein has also been suggested to regulate function of the dopamine transporter (DAT) responsible for reuptake of dopamine from the synaptic cleft (F. J. S. Lee et al., 2001; Wersinger & Sidhu, 2003). Together, this highlights the importance of α-synuclein's physiological function in dopaminergic neurons, which could be a factor contributing to their selective degeneration in PD.

1.4.2.1.4 Neuronal differentiation

In addition to its role in mature neurons, α-synuclein has been implicated in the processes of neuronal development and differentiation, though the mechanisms involved in this are still unknown. Though α-synuclein has mostly been investigated in the adult brain, its expression actually peaks during gestation and slowly reduces with age, indicating that it may have a role during early development (Alejandra Morato Torres et al., 2020; Raghavan et al., 2004). Interestingly, localisation of α-synuclein switches from the cell body to the axon during the process of neuronal maturation (Robertson et al., 2004; Zhong et al., 2010). This also indicates a developmental role, suggesting that α-synuclein may function in the cell body in immature neurons prior to its axonal role in modulating the synaptic vesicle pathway.

One hypothesis is that through its activity as a molecular chaperone, α-synuclein can activate Ras GTPases which act as master regulators in a range of signalling cascades (Emamzadeh, 2016; Fu et al., 2024). This includes the ERK/mitogen-activated protein kinase (MAPK) pathway which has been heavily implicated in directing fate-decisions of neural progenitors, differentiation of neuronal cells, and regulation of myelin formation (Emamzadeh, 2016; Ishii et al., 2014).

1.4.3 Pathological α-synuclein

LBs are the hallmark feature of PD pathology that can be identified post-mortem (Cremades & Dobson, 2018). These primarily contain α-synuclein species, the majority of which are phosphorylated at its S129 residue (pS129) (Anderson et al., 2006). Studies investigating this found that under physiological conditions, only 4% of monomeric α-synuclein was phosphorylated at S129 (Anderson et al., 2006; H. Fujiwara et al., 2002). Comparatively, approximately 90% of α-synuclein species were shown to exhibit the pS129 modification in purified LBs from PD brains (Anderson et al., 2006; H. Fujiwara et al., 2002). Accordingly, pS129 α-synuclein has become a common marker of PD pathology in both patients and animal models (Lashuel et al., 2022). Despite suggestions that this PTM may increase α-synuclein's aggregation

propensity, how it impacts α-synuclein structure and function is not well understood (Lashuel et al., 2022).

Though LBs contain mostly fibrillar α-synuclein, it is the smaller, oligomeric intermediate species that are considered to induce the most damage (H. L. Roberts & Brown, 2015; Winner et al., 2011). Current work is trying to establish the molecular features of these oligomers that confer toxicity, with one suggestion being that unlike α-synuclein fibrils, oligomers can bind and permeabilise phospholipid membranes because of their flexible structure (H. L. Roberts & Brown, 2015). Interestingly, non-toxic oligomeric species have been shown to only bind membranes weakly and not to cause permeabilisation, providing support for this lipid binding-based hypothesis of oligomer toxicity (Campioni et al., 2010). Permeabilisation of membranes by α-synuclein causes hydrophobic surfaces to be exposed, which has been shown to induce lipid peroxidation, production of ROS and apoptosis (Campioni et al., 2010; Zampagni et al., 2011). Membrane binding has also been shown to induce aggregation of α-synuclein, triggering a feedback loop that perpetuates mitochondrial dysfunction (Kamano et al., 2024). Interestingly, this has recently been shown to occur at mitochondria, where binding of α-synuclein A53T to the IMM was shown to trigger its oligomerisation, leading to mitochondrial membrane permeabilisation and cell death (M. L. Choi et al., 2022).

1.5 Mitochondria and α-synuclein in PD

The ability of α-synuclein to bind mitochondria and induce dysfunction highlights the connection between these two key drivers of PD pathology. Several studies have significantly improved our understanding of α-synuclein's relationship with mitochondria, providing insight into how the association between them may be a potential driver of PD pathogenesis (Chinta et al., 2010; Devi et al., 2008; Ludtmann et al., 2016).

1.5.1 Mitochondria-α-synuclein interactions

Firstly, the proposed hypothesis of a pathological interaction between α-synuclein and mitochondria was supported by investigations in the PD brain, where α-synuclein accumulation was coupled to a dramatic increase in α-synuclein localisation to mitochondria in the SNpc (Devi et al., 2008). Further investigation revealed that in human dopaminergic neurons, α-synuclein was imported into mitochondria where it associated with the IMM (Devi et al., 2008). The selective localisation of α-synuclein to mitochondria was supported by the identification of a cryptic 32-AA mitochondrial-targeting sequence in the N-terminus of α-synuclein (Devi et al., 2008). The existence of this signal alluded to a potential physiological relationship between α-synuclein and mitochondria. Supporting this suggestion, α-synuclein has been shown to directly interact with essential proteins in the ETC and modulate ATP synthase (Ludtmann et al., 2016). Mouse models lacking α-synuclein showed a reduction in the activity of both complex I and ATP synthase, confirming α-synuclein as a regulator of mitochondrial ATP production (Ellis et al., 2005; Ludtmann et al., 2016).

1.5.1.1 α-synuclein & the OMM

To facilitate its mitochondrial internalisation, α-synuclein must first interact with and traverse the OMM. Mitochondrial import of α-synuclein has been suggested to occur through the outer membrane translocase, TOM40, since blockage of this channel inhibited α-synuclein internalisation (Devi et al., 2008). Other studies have shown that α-synuclein can also enter mitochondria through VDAC, which it binds with high affinity (Hoogerheide et al., 2017; T. K. Rostovtseva et al., 2015). Interestingly, import of α-synuclein has been shown to be dependent on an intact $\Delta\Psi m$ and was blocked upon inhibition of ATP synthase in a mammalian cell model, suggesting that it occurs in healthy mitochondria (Devi et al., 2008).

Interestingly, one study suggested that mitochondria can act as a scavenger for aggregatory proteins such as α-synuclein, through a hypothesised process called MAGIC (mitochondria as guardian in cytosol) (Ruan et al., 2017). The authors theorise that mitochondrial proteases can degrade aggregated proteins, easing the burden of these in the

cytosol and maintaining cellular integrity (Ruan et al., 2017). This provides another physiological purpose for mitochondrial import of α-synuclein alongside regulation of ATP synthase.

However, interactions between α-synuclein and mitochondrial import machinery not only facilitate its own import, but represent an opportunity for pathological damage. Other aggregation-prone proteins such as amyloid-precursor protein (APP) have been shown to impede protein import by obstructing the TOM40 subunit (Gottschalk et al., 2014). This has also been shown in the context of α-synuclein, with pathological species shown to induce degradation of TOM40 (Bender et al., 2013; Hegde et al., 2024). Pathologically, α-synuclein aggregates have also been shown to impact protein import by binding another translocase, TOM20, preventing the interaction between TOM20 and its co-receptor, TOM22 (Di Maio et al., 2016).

1.5.1.2 α-synuclein & the IMM

As mentioned, several studies have shown an enrichment of α-synuclein at the IMM under pathological conditions, which has been linked to its interaction with CL (Devi et al., 2008; K. Nakamura et al., 2011; Robotta et al., 2014). Several studies have shown that α-synuclein's affinity for unsaturated lipids leads it to preferentially bind mitochondrial membrane domains that contain CL, which in turn can facilitate the assembly of α-synuclein species into helical structures (Grey et al., 2011; Ramakrishnan et al., 2003). Once associated with the IMM, α-synuclein is able to modulate ATP synthase (Ludtmann et al., 2016). Interestingly, the internalisation of α-synuclein appears to be irreversible at high concentrations, since only low levels could be washed out in isolated mitochondria from rat brain tissue (Martínez et al., 2018). This could be related to the formation of oligomeric species, since evidence for α-synuclein's physiological role in mitochondrial ATP production has mostly been characterised in terms of monomeric α-synuclein (Ludtmann et al., 2016; Tripathi & Chattopadhyay, 2019). Since the aggregation potential of α-synuclein increases with protein concentration, high levels of α-synuclein inside mitochondria could result in the formation of oligomers which may cause mitochondrial toxicity (Afitska et al., 2019).

1.6 Mito-QC & α-synuclein

Despite the direct interactions between α-synuclein and mitochondria described in both physiological and pathological circumstances, limited research has investigated whether this relationship extends to mito-QC (Eldeeb et al., 2022; Henderson et al., 2019). Monomeric α-synuclein's affinity for mitochondria alongside its ability to bind and remodel phospholipid membranes makes it a suitable candidate for a role in co-ordination of mito-QC (Ellis et al., 2005; Ludtmann et al., 2018). However, there is a considerable lack of research exploring this. Though mitochondrial dynamics and the generation of MDVs both require dynamic remodelling of the mitochondrial network through alterations in mitochondrial membranes, current research has not assessed whether α-synuclein may have a physiological role in these processes.

Whether dysfunctional mito-QC could represent a key mechanism behind α-synuclein-induced cell death is an important question to be addressed. Given that many genes carrying PD-associated mutations are involved in mito-QC pathways and that SNpc neurons are especially vulnerable to mitochondrial dysfunction, a potential explanation for selective SNpc death could be an α-synuclein-induced impact on the activity of mito-QC. Investigations into this have found that pathological α-synuclein can directly interact with key mito-QC proteins such as Parkin, and can cause disruption to mitochondrial fission, fusion and mitophagy (Krzystek et al., 2021; K. Nakamura et al., 2011; Wilkaniec et al., 2019).

1.6.1 α-synuclein in mitochondrial dynamics

1.6.1.1 Increased fission activity

Pathological α-synuclein has been associated with fragmentation of the mitochondrial network in both animal models and mammalian cells (Butler et al., 2012; Furlong et al., 2020; Kamp et al., 2010; Krzystek et al., 2021; K. Nakamura et al., 2011). In a humanised *Drosophila melanogaster* model, overexpression of full-length α-synuclein led to mitochondrial fragmentation which persisted in the absence of both the C-terminus and NAC domain, demonstrating that the response was independent of α-synuclein's propensity to aggregate (Krzystek et al., 2021). Fragmentation instead required an intact N-terminus, implying that the response was due to alterations in the biophysical properties of mitochondrial membranes resulting from the α-synuclein interaction (Krzystek et al., 2021). Reduction of the essential mitochondrial fission machinery, Drp1, in the context of α-synuclein overexpression resulted in a complete rescue of mitochondrial morphology, suggesting that α-synuclein-induced fragmentation was dependent on Drp1 activity (Krzystek et al., 2021). Overexpression of the fusion protein, Mfn2, did not evoke the same rescue, confirming that fragmentation was the

result of an increase in fission rather than a decrease in fusion. A suggested mechanism behind this is that pathological α-synuclein increases recruitment of Drp1 to the OMM, which has been observed in response to α-synuclein overexpression (Gui et al., 2012; Youle & Van Der Bliek, 2012). These data suggest a functional relationship between α-synuclein and Drp1 that could alter mitochondrial dynamics. Drp1 has also been implicated in the scission of MDVs as well as in autophagy, apoptosis and cytoskeletal remodelling, so α-synuclein-induced alterations in Drp1 function could have broad cellular impacts (Duan et al., 2020; Frank et al., 2001; König et al., 2021).

Interestingly, this contradicts previous work which indicated that α-synuclein-induced mitochondrial fragmentation was completely independent of Drp1 (K. Nakamura et al., 2011). In this context, suppression of Drp1 was not sufficient to rescue the fragmentation induced by transient overexpression of α-synuclein. It was instead suggested that the direct association of α-synuclein to the mitochondrial membrane was driving the fragmentation, since this was abolished with overexpression of the A30P mutant of α-synuclein which has no membrane-binding ability (Jo et al., 2002; K. Nakamura et al., 2011). Intermediate oligomeric α-synuclein species were also shown to directly fragment artificial phospholipid membranes *in vitro*, supporting α-synuclein's potential as a direct modulator of membrane dynamics (K. Nakamura et al., 2011). Fragmentation was not observed with α-synuclein monomers, mature oligomers or fibrils, also suggesting that this effect was exclusively caused by small, intermediate oligomeric species (K. Nakamura et al., 2011). Though the majority of research has focused on pathological α-synuclein, one loss-of-function study showed that α-synuclein-null mice had no change in Drp1 levels, suggesting that differences in Drp1 are due to toxic gain-of-function of α-synuclein rather than loss-of-function (Faustini et al., 2019). Though there is a consensus that α-synuclein overexpression can stimulate mitochondrial fission, there are still discrepancies about the mechanisms that drive this. One consideration is that α-synuclein may preferentially influence fission through an interaction with Drp1 when it is available, but in the absence of Drp1 it may be able to stimulate fragmentation directly depending on its expression level and protein conformation.

1.6.1.2 Decreased fission activity

Conversely, several studies report an enlargement in mitochondria in models of α-synuclein pathology, correlating with a decrease in mitochondrial Drp1 translocation (Ordonez et al., 2018; Portz & Lee, 2021). In a human α-synuclein transgenic *Drosophila melanogaster* model, a decrease in mitochondrial fission was shown to occur through abnormal stabilisation of the actin cytoskeleton via an association with spectrin, preventing trafficking of Drp1 to mitochondria (Korobova et al., 2013; Ordonez et al., 2018). This was rescued by genetic

manipulation of actin, supporting the case for an association between α-synuclein and the cytoskeleton (Ordonez et al., 2018). This mechanism of cytoskeletal modification by aggregate-prone proteins has previously been described in the context of other neurodegenerative diseases such as AD, where microtubule destabilisation by hyperphosphorylated Tau drives toxic effects on both mitochondria and protein trafficking (DuBoff et al., 2012). In the context of α-synuclein, this occurs through interactions with the actin cross-linking protein, spectrin, disrupting cytoskeletal dynamics (Machnicka et al., 2012; Ordonez et al., 2018).

However, modifications of the actin cytoskeleton not only impact mitochondrial dynamics, but also directly impact mitophagy (Sarkar et al., 2021). Specifically, pathogenic α-synuclein-induced actin stabilisation has been shown to disrupt autophagosome trafficking to the lysosome, resulting in impaired autophagosome maturation (Sarkar et al., 2021). By the same reckoning, there is potential for alterations in the actin cytoskeleton to disrupt trafficking of cellular components on a global scale, which would include MDVs and other endolysosomal compartments (Oliveira da Silva & Liz, 2020).

A summary of the proposed associations between α-synuclein and regulators of mitochondrial dynamics is shown in **Figure 13**.

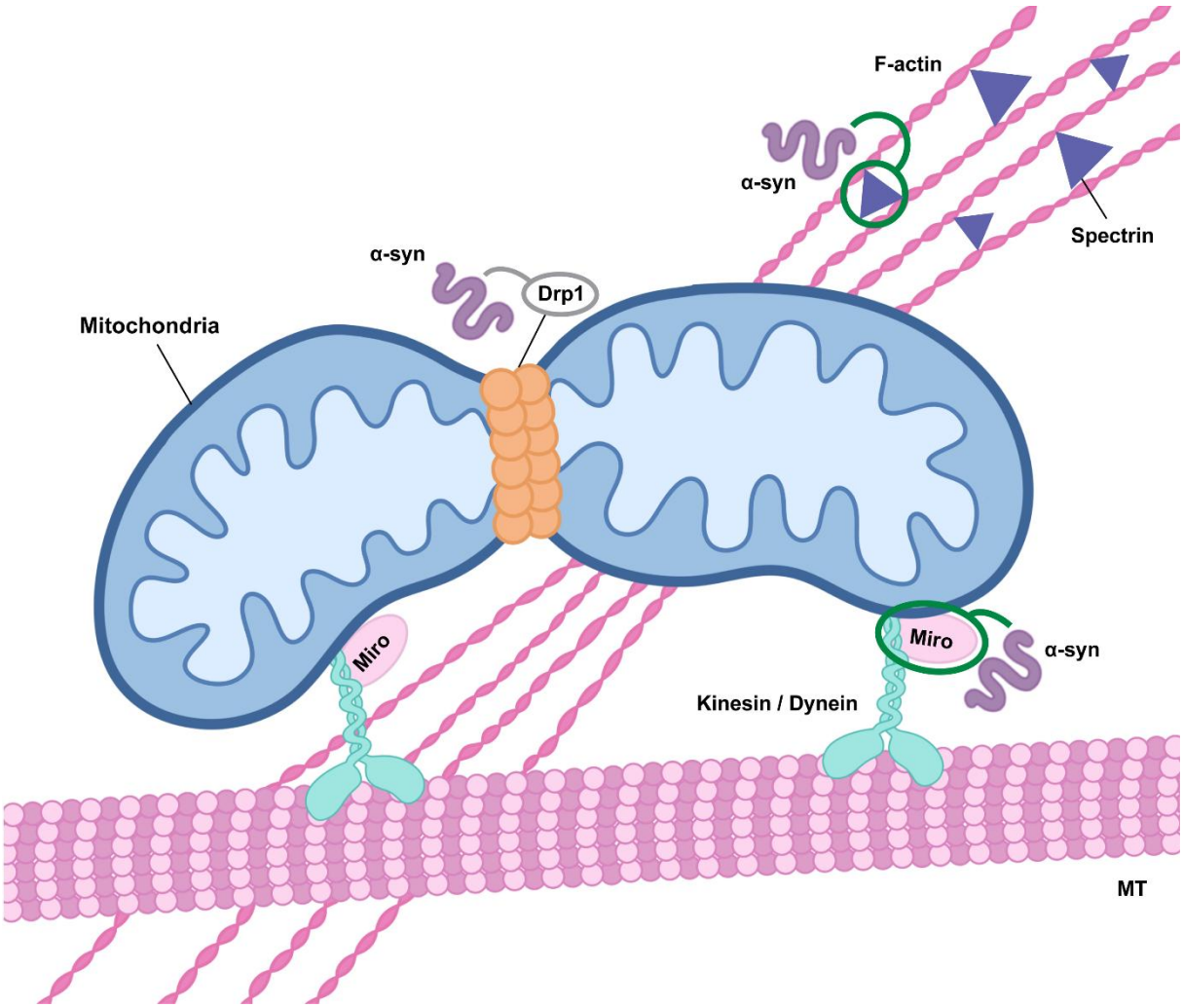

Figure 13: Schematic showing proposed interactions between α-synuclein and fission/fusion machinery

α-synuclein influences mitochondrial transport and fission. Alterations in α-synuclein function may affect mitochondrial fission through direct effects on Drp1 activity and mitochondrial translocation, although the precise impact has not been clearly defined (indicated in grey). Oligomeric α-synuclein may also inhibit Drp1 trafficking to mitochondria as a result of alterations in actin cytoskeletal dynamics mediated by an association with the actin-cross linker spectrin. In addition, α-synuclein oligomers modulate Miro activity, either through promotion of Miro protein stability or retention in the OMM influencing microtubule (MT) transport via dysregulation of kinesin or dynein activity. Repurposed from Thorne & Tumbarello, 2022.

1.6.2 α-synuclein in mito-QC

1.6.2.1 Interactions with PINK1/Parkin

The functions of essential mitophagy regulators, PINK1 and Parkin, have been shown to be directly impacted by α-synuclein pathology (Krzystek et al., 2021; Wilkaniec et al., 2019). Parkin is functionally associated with several aspects of mito-QC distinct from mitophagy, such as the MDV pathway where it has been shown to mediate both formation and trafficking of different MDV subtypes (McLelland et al., 2014; T. A. Ryan et al., 2020; Shimura et al., 2000). In a neuronal model, addition of exogenous α-synuclein oligomers or fibrils led to a reduction in Parkin expression alongside loss of ΔΨm, decreased ATP production and increased mitochondrial ROS (Wilkaniec et al., 2019, 2021). Further assessment revealed alterations in mitophagy, exhibited by a reduction in mitochondrial protein ubiquitylation and subsequently less mitochondria inside autophagosmes (Wilkaniec et al., 2021). These phenotypes could be rescued by Parkin overexpression, suggesting that an α-synuclein-induced downregulation of Parkin was responsible for mitochondrial dysfunction (Wilkaniec et al., 2021). Previous work has indicated that exogenous α-synuclein oligomers induce oxidative and nitrative stress, resulting in PTMs to Parkin. In particular, *S*-nitrosylation of Parkin results in its autoubiquitination and degradation (Kazmierczak et al., 2008; Wilkaniec et al., 2019; Yao et al., 2004). This suggests a mechanism by which pathogenic α-synuclein can evoke Parkin downregulation, resulting in a damaging feedback loop that exacerbates mitochondrial damage due to loss of Parkin's protective role (Jęśko et al., 2019). Several studies report the ability of Parkin to restore mitochondrial morphology and function following α-synuclein-induced alterations, but it is unclear whether this is through a direct association with α-synuclein or due to its general neuroprotective role in regulating mitochondrial protein degradation (Jęśko et al., 2019; Kamp et al., 2010; Krzystek et al., 2021; Lonskaya et al., 2013). In line with this, a functional relationship has been suggested between PINK1/Parkin activity and α-synuclein, since their overexpression was able to rescue α-synuclein-induced mitochondrial fragmentation, depolarisation and dysfunction (Krzystek et al., 2021). This association between PINK1/Parkin and α-synuclein is proposed to occur through membrane interactions, since it was dependent on the C-terminus of α-synuclein which can interact with small molecules like Ca^{2+} to enhance its lipid-binding capacity (Krzystek et al., 2021; Lautenschläger et al., 2018). Alternatively, PINK1 has been shown to form a complex with α-synuclein in the cytoplasm which initiates autophagy, potentially providing a protective mechanism against α-synuclein pathology (Liu et al., 2017).

1.6.2.2 Impacts on mitochondrial motility

α-synuclein may also influence mitophagy independently of PINK1/Parkin, instead through an interaction with mitochondrial rho GTPase (Miro) proteins which are essential components of mitochondrial motility machinery (Shaltouki et al., 2018). Functional mitochondria require Miro on their OMM to facilitate movement along microtubules, but it must be promptly degraded upon mitochondrial damage to halt motility and enable the initiation of mitophagy (Hsieh et al., 2016). Miro expression has been shown to be increased in PD brains relative to healthy controls, human neurons and a *Drosophila melanogaster* model overexpressing α-synuclein (Shaltouki et al., 2018). They displayed no changes in PINK1/Parkin expression or recruitment, but exhibited a delay in mitophagy that could be rescued by Miro downregulation (Shaltouki et al., 2018). α-synuclein did not evoke alterations in expression of Miro messenger RNA (mRNA) but was incorporated into the membrane-bound Miro complex (Shaltouki et al., 2018; Wang et al., 2011). Using skin fibroblasts from PD patients, a recent study found that more than 94% of patient cell lines were unable to extract Miro from the OMM following depolarisation, indicating that α-synuclein-induced defects in Miro removal could be the mechanism behind this delay in mitophagy (Hsieh et al., 2019). Intriguingly, Miro proteins have also been implicated in MDV biogenesis, with super-resolution microscopy revealing that mitochondrial membrane protrusions extend using microtubule filaments dependent on the activity of Miro (König et al., 2021). Miro stabilisation as a result of α-synuclein pathology therefore has the potential to disrupt multiple mito-QC mechanisms. Since many of these studies have looked at pathological α-synuclein, it would be valuable to better define the relationship between Miro and endogenous α-synuclein to investigate whether these interactions may have a physiological function in the OMM-bound Miro complex.

1.6.2.3 Impacts on autophagosome formation

Pathogenic overexpression of α-synuclein also elicits alterations in autophagosome formation, maturation and autophagosome-lysosome fusion (Sarkar et al., 2021; Tang et al., 2021; Winslow et al., 2010). This has been characterised by reductions in autophagosome-associated LC3II and accumulation of known autophagy substrates, such as pathogenic forms of Huntingtin polyglutamine protein (Winslow et al., 2010). Previous research has implicated a protective role for the small GTPase, Rab1, against α-synuclein toxicity in the context of ER-Golgi vesicular trafficking and autophagy (Cooper et al., 2006; Winslow et al., 2010). Supporting this, knockdown of Rab1a mirrored an α-synuclein-induced reduction in autophagosomes, and overexpression of Rab1a rescued this, insinuating that the 2 proteins were acting at similar stages of the autophagy pathway (Winslow et al., 2010). This was suggested to be early during autophagosome formation, since α-synuclein has also been shown to disrupt localisation of

autophagy-related protein 9 (Atg9) to LC3-positive compartments; a step known to facilitate the delivery of membrane required for autophagosome expansion (Feng & Klionsky, 2017). Interestingly, defects in autophagosome formation were specific to wild-type α-synuclein in this model and were not observed with A53T or A30P missense mutants (Winslow et al., 2010). Since these point mutations exist within the N-terminus of α-synuclein, their lack of influence on autophagosome formation may be due to altered membrane binding properties (Jo et al., 2000, 2002).

1.6.2.4 Influence on autophagosome-lysosome fusion

Several studies have also indicated that excess α-synuclein may impair autophagy further downstream, illustrated by a decrease in autophagic turnover as a result of defective autophagosome-lysosome fusion (Sarkar et al., 2021; Tang et al., 2021). This fusion process is mediated by a SNARE complex comprising syntaxin 17, synaptosomal-associated protein 29 (SNAP29) and vesicle-associated membrane protein 8 (VAMP8) or YKT6, tethering together the two compartments to facilitate autophagosome maturation (Guo et al., 2014; Itakura et al., 2012; Matsui et al., 2018). Given α-synuclein's role in the assembly of SNARE complexes at the synapse, its interaction with SNAREs in the context of autophagosome-lysosome fusion was investigated (Tang et al., 2021). SNAP29 was found to be significantly less abundant in models of α-synuclein overexpression, with subsequent co-expression of SNAP29 and α-synuclein able to restore autophagic flux (Tang et al., 2021). Interestingly, a reduction in SNAP29 was also seen in human SNpc neurons from patients with LB pathology, supporting a potential role for pathogenic α-synuclein in evoking dysfunction in the autophagic SNARE complex (Tang et al., 2021). Since autophagy is essential for the removal of aggregatory proteins such as α-synuclein, disruption of these pathways would also generate a destructive feedback loop, potentiating the pathology (Ebrahimi-Fakhari et al., 2011; Gidalevitz et al., 2006; Tang et al., 2021). Though the impact of α-synuclein has been studied in pathological terms, there is unexplored potential for the loss-of-function of α-synuclein to alter SNARE complex formation during autophagy as it does at the synapse.

A summary of the proposed associations between α-synuclein and regulators of mitochondrial dynamics is shown in **Figure 14**.

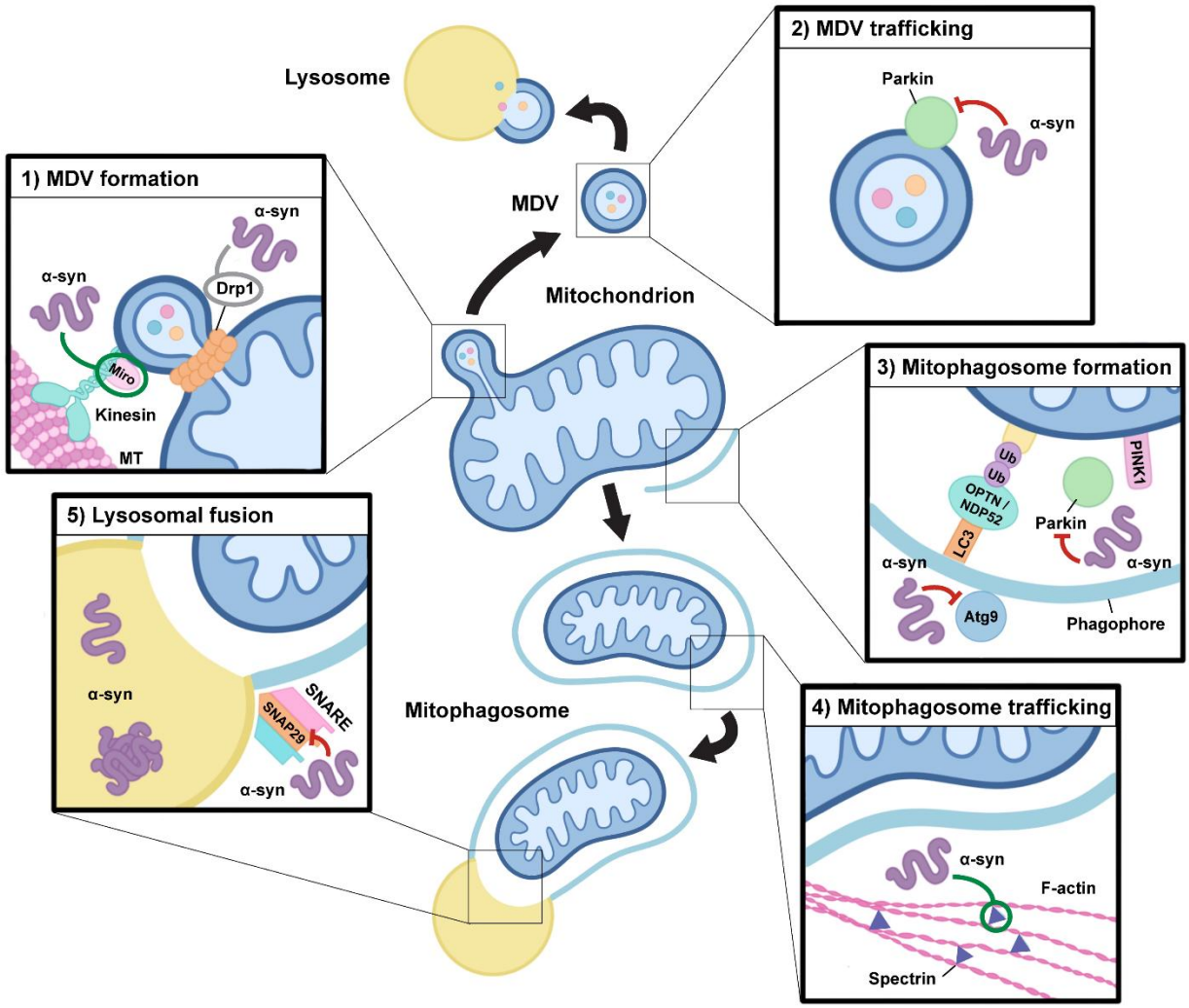

Figure 14: Schematic showing proposed interactions between α-synuclein and mito-QC machinery

Alterations in α-synuclein function may impact mitochondrial quality control pathways. α-synuclein function and its aggregation may have an impact at multiple levels during both mitophagy and the mitochondrial-derived vesicle pathway. (1) MDV formation: Drp1 and Miro proteins are required for mitochondrial-derived vesicle (MDV) fission from the mitochondrion in response to local oxidative damage, which may be directly influenced by alterations in α-synuclein function. α-synuclein oligomers can stabilize Miro on the mitochondrial membrane and modulate Drp1 localisation, although the precise impact of α-synuclein-induced alterations in Drp1 function is still a point of contention (indicated in grey). (2) MDV trafficking: Oligomeric species of α-synuclein may downregulate Parkin expression and alter its localization, which could have negative impacts on MDV formation and trafficking to the lysosome. (3) Mitophagosome formation: Mitophagy requires the action of PINK1 and Parkin to trigger the ubiquitylation of outer membrane proteins which leads to the recruitment of autophagy receptors, including NDP52 and OPTN, which facilitate the capture of damaged mitochondria within a phagophore, which matures into a mitophagosome. α-synuclein may impact this process through alterations in Parkin activity and by inhibiting the recruitment of Atg9-

positive vesicles which are required for autophagosomal membrane expansion. (4) Mitophagosome trafficking: Through interactions with spectrin, overexpression and accumulation of α-synuclein oligomers alters actin cytoskeletal dynamics resulting in its aberrant stabilization, which may negatively impact the maturation and trafficking of mitophagosomes required for endosomal and lysosomal fusion. (5) Lysosomal fusion: To enable cargo degradation, the mitophagosome requires the action of SNARE protein complexes to facilitate lysosomal fusion. Pathogenic overexpression of α-synuclein may alter SNAP29 activity, thus influencing the ability of mitophagosomes to fuse with lysosomes. In addition, accumulation of monomeric and oligomeric species of α-synuclein within lysosomes alters their activity, which may result in negative impacts on cargo degradation in both the mitophagy and MDV pathways. Repurposed from Thorne & Tumbarello, 2022.

1.7 Aims & objectives

Though α-synuclein has been extensively suggested throughout the literature as a driver of PD pathology via interactions with mitochondria, limited research has investigated its relationship with mito-QC. Though recent studies have shown that pathological α-synuclein can cause dysfunctions in mitochondrial health and can associate with molecular players in mito-QC pathways, the direct impact of α-synuclein on mito-QC has not been well-established. Further investigations are required to delineate this relationship between α-synuclein and mito-QC, and establish whether defective mitochondrial phenotypes observed in PD models are the result of a toxic gain-of-function of α-synuclein or loss of its physiological function. This study aims to address this by assessing the impacts of perturbations in α-synuclein on mitochondrial function and mito-QC in a mammalian cell model. Further, I aim to develop a neuronal-like model to enable investigation of mito-QC, and assess the impact of manipulating α-synuclein on neuronal phenotypes.

AIM 1: Investigate the role of endogenous α-synuclein in mitochondrial health and mito-QC

1) Develop a model of α-synuclein loss-of-function in SH-SY5Y cells
2) Utilise the α-synuclein loss-of-function model to assess whether α-synuclein has a physiological role in mitochondrial function and dynamics
3) Utilise the α-synuclein loss-of-function model to assess whether α-synuclein has a physiological role in mito-QC pathways

AIM 2: Investigate the impact of pathological α-synuclein overexpression on mitochondrial health and mito-QC

1) Develop gain-of-function models of α-synuclein wild-type and A53T in SH-SY5Y cells
2) Utilise the gain-of-function models to assess the impact of wild-type and A53T α-synuclein overexpression on mitochondrial function and dynamics
3) Utilise the gain-of-function models to assess the impact of wild-type and A53T α-synuclein overexpression on mito-QC pathways

AIM 3: Develop a neuronal model and investigate the impact of alterations in α-synuclein on neuronal differentiation

1) Optimise and validate a protocol for differentiating SH-SY5Y cells and characterise differentiated neuronal phenotypes in wild-type cells
2) Investigate the impact of α-synuclein loss-of-function on differentiation of SH-SY5Y cells
3) Investigate the impact of α-synuclein overexpression on differentiation of SH-SY5Y cells

Chapter 2 Materials & methods

2.1 Antibodies and reagents

2.1.1 Antibodies

Primary antibodies were used for Western blot and immunocytochemistry at the dilutions indicated in **Table 4**. Secondary antibodies for Western blot visualisation with LiCOR® were a combination of IRDye® 680 and IRDye® 800 (LiCOR®), either anti-rabbit or anti-mouse and all used at a dilution of 1:5,000. Secondary antibodies for immunocytochemistry were AlexaFluor™, raised in goat and used at a dilution of 1:200. Details are indicated in **Table 5**.

Table 4: Primary antibodies used for Western blotting (WB) and immunofluorescence (IF)

Antibody	Species	WB	IF	Company	Code
α-synuclein (211)	Mouse IgG1	1:1,000	1:500	Santa Cruz	sc-12767
α-synuclein (LB509)	Mouse IgG1	1:1,000	N/A	Santa Cruz	sc-58480
α-synuclein	Rabbit polyclonal	N/A	1:50	ProteinTech	10842-1-AP
α-tubulin	Rabbit polyclonal	1:1,000	N/A	ProSci	7597
β-actin	Mouse monoclonal	1:10,000	N/A	ProteinTech	60008-1-Ig
β-III-tubulin	Rabbit monoclonal	1:1,000	1:1,000	Cell Signalling	5568
Calnexin	Mouse monoclonal	1:1,000	N/A	Chemicon	MAB3126
CoxII (MTCO2)	Mouse IgG2A	1:1,000	N/A	Abcam	ab110258
Cytochrome c	Mouse IgG1	N/A	1:1,000	BioLegend	612302
GAP43	Mouse monoclonal	1:1,000	N/A	Merck Millipore	MAB347
GAPDH	Rabbit polyclonal	1:20,000	N/A	ProteinTech	10494-1-AP
GFP	Rabbit polyclonal	1:5,000	1:1,000	Sigma Aldrich	SAB4301138
LAMP1 (CD107α)	Mouse IgG1K	N/A	1:1,000	BD Biosciences	555798
LC3II	Rabbit polyclonal	1:2,000	N/A	Novus	NB100-2220
Mfn2 (D2D10)	Rabbit monoclonal	1:1,000	N/A	Cell Signalling	9842
PS129 α-synuclein	Mouse IgG2A	1:1,000	1:1,000	BioLegend	825702
Parkin	Mouse monoclonal	1:1,000	N/A	Cell Signalling	4211
PDH (A1-α subunit)	Mouse IgG1	N/A	1:1,000	Abcam	Ab110330

Antibody	Species	WB	IF	Company	Code
PINK1 (D8G3)	Rabbit monoclonal	1:1,000	N/A	Cell Signalling	6946
pUb S65	Rabbit polyclonal	1:1,000	1:500	Merck Millipore	ABS1513-I
Tyrosine hydroxylase	Rabbit	1:1,000	N/A	Sigma Aldrich	AB152
TOM20	Rabbit polyclonal	N/A	1:2,000	Abcam	ab78547
Vinculin	Mouse monoclonal	1:1,000	N/A	Merck Millipore	MAB3574-C

Table 5: AlexaFluor™ secondary antibodies used for immunofluorescence

Conjugate	Species	Immunogen	Company	Code
AlexaFluor™ 488	Mouse	Gamma immunoglobulin (H + L)	Invitrogen	A11029
AlexaFluor™ 488	Rabbit	Gamma immunoglobulin (H + L)	Invitrogen	A11034
AlexaFluor™ 568	Mouse	Gamma immunoglobulin (H + L)	Invitrogen	A11031
AlexaFluor™ 568	Rabbit	Gamma immunoglobulin (H + L)	Invitrogen	A11036
AlexaFluor™ 647	Mouse	Gamma immunoglobulin (H + L)	Cell Signalling	4410S
AlexaFluor™ 647	Rabbit	Gamma immunoglobulin (H + L)	Invitrogen	A21245

2.2 Cell culture

2.2.1 Cell maintenance

SH-SY5Y cells were maintained in Dulbecco's modified eagle medium (DMEM)/Nutrient Mixture F12 media with GlutaMAX (Gibco™, 11320-074), supplemented with 10% fetal bovine serum (FBS) (Gibco™, 10270-106), 1% penicillin/streptomycin solution (P/S) (Gibco™, 15140-122) and 1% non-essential amino acids (NEAA) (Gibco™, 11140-050). HEK239/T cells were maintained in DMEM high glucose media (Sigma Aldrich, D6429) supplemented with 10% FBS, 1% P/S and 1% L-glutamine (Sigma Aldrich, G7513).

Cells were thawed from liquid nitrogen stocks by suspending vials in a 37°C water bath and adding cells to fresh media. Cells were centrifuged for 3 minutes at 500G to form a pellet which was resuspended in fresh media prior to seeding in either a 6cm or 10cm plate depending on

pellet size. To passage cells when confluent, serum was removed by gently washing with sterile Dulbecco's phosphate buffered saline (DPBS) (Gibco™, 14190-094) before the addition of 0.05% Trypsin-EDTA (Gibco™, 25300-054) appropriate to plate volume. Trypsinised cells were incubated at 37°C for 3 minutes or until dissociated from the surface of the plate. Fresh media was added, and cells were triturated to create a single cell suspension before being counted with a haemocytometer and seeded as appropriate for experiments as detailed in **Table 6**. Cell populations being expanded for future experiments were diluted approximately 1:3 and seeded into 10cm plates.

All cell lines were kept incubated at 37°C under 5% carbon dioxide (CO_2). For freezing, cells at approximately 70% confluency were trypsinised and incubated at 37°C for 3 minutes or until dissociated from the surface. Cells were collected in fresh media and centrifuged at 1000RPM for 3 minutes at room temperature. The cell pellet was resuspended in freezing media (90% FBS, 10% dimethyl sulfoxide (DMSO) (Sigma Aldrich, 472301) and flash-frozen on dry ice in 1ml aliquots. Vials were kept at -80°C for 2-3 weeks before being transferred to liquid nitrogen at approximately -160°C for long term storage.

Table 6: Plating conditions for SH-SY5Y cells according to experimental use

Experimental use	Vessel	Number of cells plated
Harvesting lysates	6-well plate	500,000/well
Immunocytochemistry	12-well plate on coverslips	80,000/well
Live imaging	3cm glass-bottom plate	150,000/well
ATP assay	96-well plate	40,000/well
Seahorse mito stress test	96-well Seahorse assay plate	50,000/well

2.2.2 Treatment with mitochondrial stressors

To evoke mitochondrial stress in SH-SY5Y cells, oligomycin and Antimycin A were used together (referred to as A/O) at concentrations defined in **Table 7**. These inhibitors were diluted in fresh media and added dropwise to cells plated 24-hours prior. Cells were treated for various time periods to evoke measurable mito-QC mechanisms and either fixed or lysed depending on the experiment. Bafilomycin A1 and Bortezomib were used in combination with A/O treatment to

block autophagosome-lysosome fusion and proteasomal degradation respectively. Concentrations for these inhibitors are also defined in **Table 7**.

Table 7: Reagents used to evoke mitochondrial damage

Reagent	Diluent	Working conc.	Company	Code
Antimycin A	Ethanol	5uM	Sigma Aldrich	A8674
Oligomycin	Ethanol	10uM	Millipore	495455
Bafilomycin A1	DMSO	100nM	ARCOS Organics	A0360555
Bortezomib	DMSO	1μM	UBP Bio	F1200
CCCP	DMSO	10nM	ThermoFisher Scientific™	LO6932

2.2.3 Differentiation

To differentiate SH-SY5Y cells, a 14-day protocol based on Shipley et al. (2016) was used.

2.2.3.1 Days 0-5

To plate cells for differentiation (day 0), a confluent 10cm plate of SH-SY5Y cells was split as described in 2.2.1 and 1/3 of the cells were replated into a new 10cm plate. On days 1, 3 and 5, these cells were refed with reduced-serum media referred to as “Differentiation Media 1”. This media consisted of DMEM/F12 with GlutaMAX, supplemented with 1% P/S, 1% NEAA, 2.5% FBS and 10μM retinoic acid (RA) (Sigma Aldrich, R2625).

2.2.3.2 Days 6-7

On day 6, plates were prepared ready for plating on day 7 for either immunocytochemistry (12-well plates with acid-washed sterile coverslips, see Section X) or Western blot analysis (6-well plates) by coating with 40uM poly-D-lysine (PDL) (Sigma Aldrich, P7886) in PBS. Plates required for seeding cells were coated with approximately 0.5-1ml PDL/well dependent on well volume. Plates were then incubated at 37°C overnight. On day 7, plates were removed from the incubator and PDL was removed. Plates were washed 3 times with sterile DPBS and then left to dry in the cell culture hood for approximately 30 minutes before cells were seeded.

Cells were washed with 5ml DPBS and rinsed with 2ml TrypLE™ (Gibco™, 12605-010) and incubated at 37°C for 3 minutes or until dissociated from the surface of the plate. Cells were collected into 4mls of Differentiation Media 1 and triturated to create a single cell suspension before being counted with a haemocytometer. Those used for immunocytochemistry were seeded on PDL-coated acid-washed coverslips at approximately 60,000 cells/well, and those for Western blot were seeded on PDL-coated plates at approximately 150,000 cells/well.

2.2.3.3 Days 8-14

On day 8, Differentiation Media 1 was removed and replaced with serum-free media referred to as "Differentiation Media 2". This media consisted of DMEM/F12 with 2mM GlutaMAX, supplemented with 1% PS, 1% NEAA, 10µM RA, 50ng/µl BDNF (brain-derived neurotrophic factor) (Bio-Techne, 11166-BD), 1X B27 (Gibco™, 17504-044) and 20mM KCl (potassium chloride). On days 11 and 14, cells were refed with Differentiation Media 2. On day 14, cells were considered differentiated and so were either fixed or lysed for analysis or treated with mitochondrial stressors for mito-QC experiments.

2.2.4 Transfection & transduction

For transfection with DNA constructs, cells were seeded 12-24-hours prior at approximately 500,000 cells/well for SH-SY5Y cells and 1,000,000 cells/well for HEK239/T cells. 5µl of polyethylenimine (PEI) transfection reagent (ratio of 5:1 PEI to DNA) and 100µl OptiMEM (Gibco™, 11058-021) were incubated for 5 minutes at room temperature before the addition of plasmid DNA (1µg for transient transfection; as described in **2.5.1** for lentiviral production) and further incubated for 15-20 minutes at room temperature. Cells were refed with fresh media and the DNA solution was added to them dropwise.

2.3 Plasmids & cloning

Subcloning was used to move GFP-α-syn sequences from EGFP-alphasynuclein-WT (Addgene #40822, a gift from David Rubinsztein http://n2t.net/addgene:40822; RRID: Addgene_40822) and EGFP-alphasynuclein-A53T (Addgene #40823, a gift from David Rubinsztein http://n2t.net/addgene:40823; RRID: Addgene_40823) plasmids into a lentiviral pLJM1-EGFP vector (Addgene #19319, a gift from David Sabatini http://n2t.net/addgene:19319; RRID: Addgene_19319) in order to generate cell lines stably overexpressing GFP-α-syn (**Figure 15**). This chapter provides details for each step of the cloning process, some of which were also used in the creation of the SNCA knockout cell line by CRISPR/Cas9.

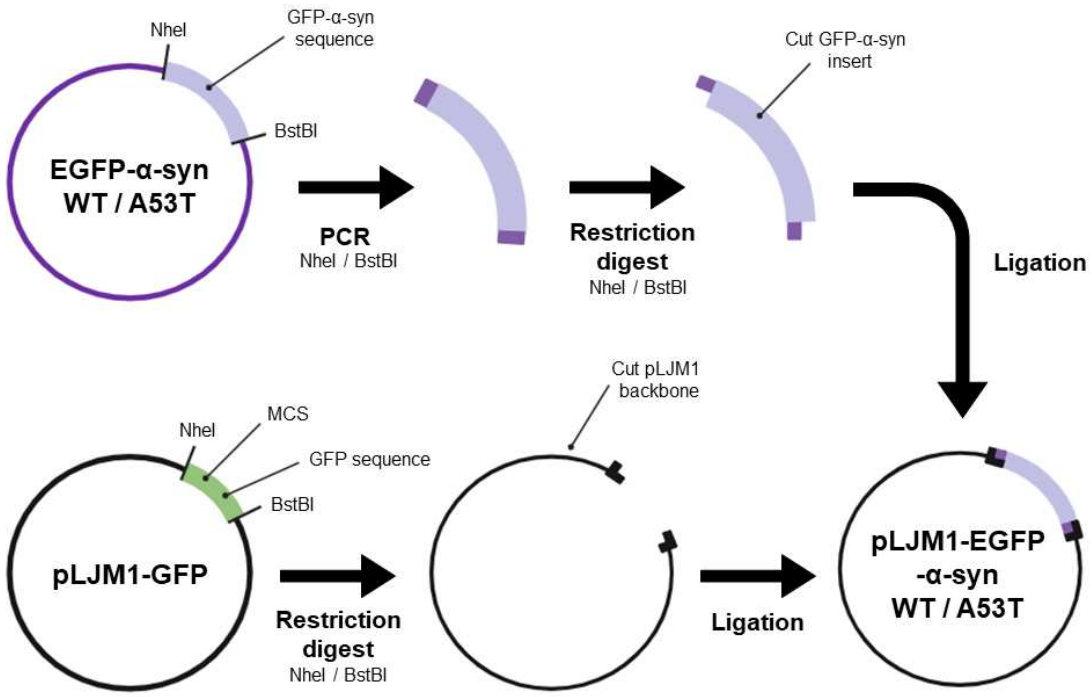

Figure 15: Generation of pLJM1-EGFP-α-syn-WT and pLJM1-EGFP-α-syn-A53T constructs

Schematic diagram showing the process of generating pLJM1-EGFP-α-syn-WT and -A53T constructs. pLJM1-GFP was digested with NheI and BstBI restriction enzymes to excise the GFP sequence, leaving the empty pLJM1 backbone. EGFP-α-syn-WT and -A53T sequences were amplified with PCR and digested with the same restriction enzymes to leave complementary sticky ends. The cut EGFP-α-syn-WT and -A53T sequences and empty pLJM1 backbone were ligated to form the final lentiviral construct.

2.3.1 PCR amplification

PCR was performed on EGFP-alphasynuclein-WT and EGFP-alphasynuclein-A53T plasmids using specific oligonucleotide primers (Sigma Aldrich) (**Table 8**) to amplify the GFP-α-syn sequences (**Figure 16**).

Table 8: Primers used for PCR amplification of EGFP-α-syn-WT and -A53T sequences

Primer	Sequence	Complimentary sequence
NheI FWD	G^CTAG CATGGTGAGCAAGGGC	CGGTG GTACCACTCGTTCCCG
BstBI REV	TT^CGAATTAGGCTTCAGGTTC	CTTAAG AATCCGAAGTCCAAG

a)

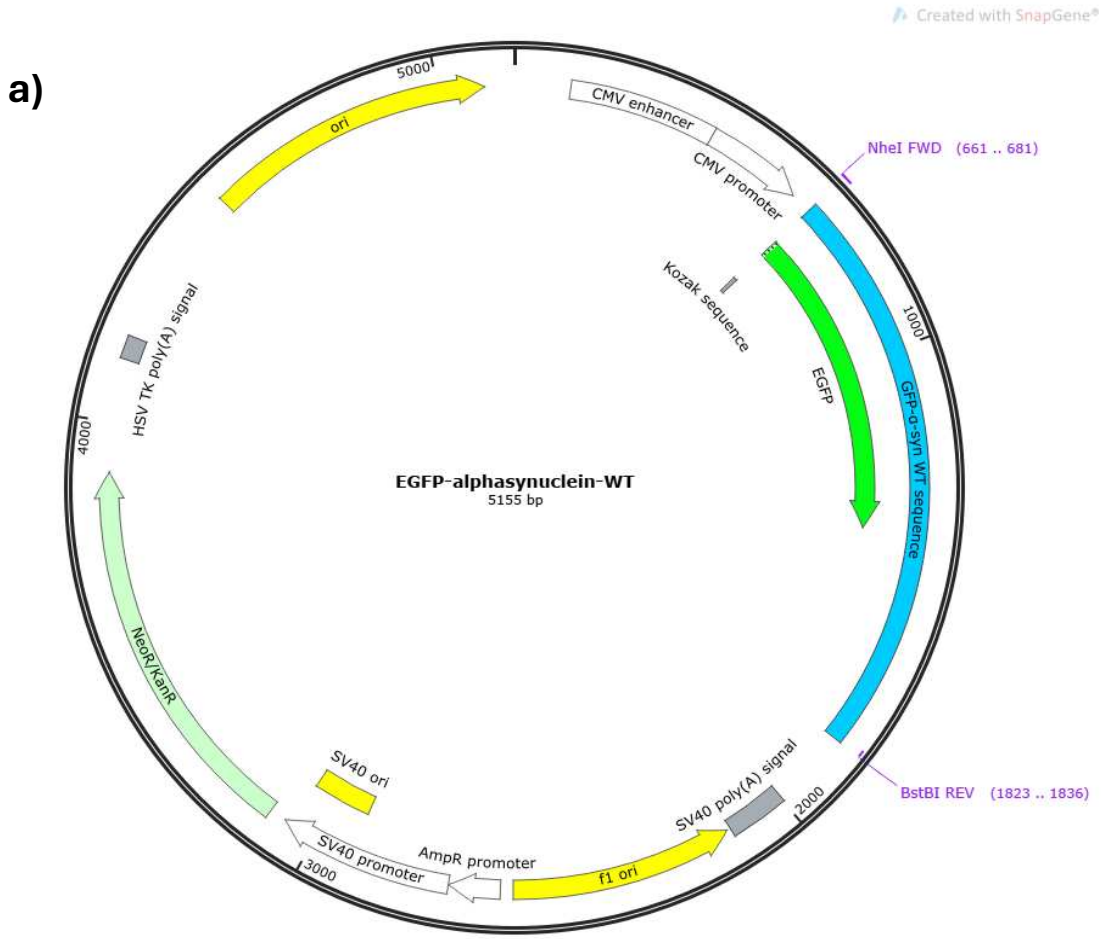
Created with SnapGene®
5000
ori
CMV enhancer
CMV promoter
NheI FWD (661 .. 681)
Kozak sequence
EGFP
1000
GFP-α-syn WT sequence
HSV TK poly(A) signal
4000
EGFP-alphasynuclein-WT
5155 bp
NeoR/KanR
SV40 ori
SV40 poly(A) signal
BstBI REV (1823 .. 1836)
2000
SV40 promoter
AmpR promoter
f1 ori
3000

b)

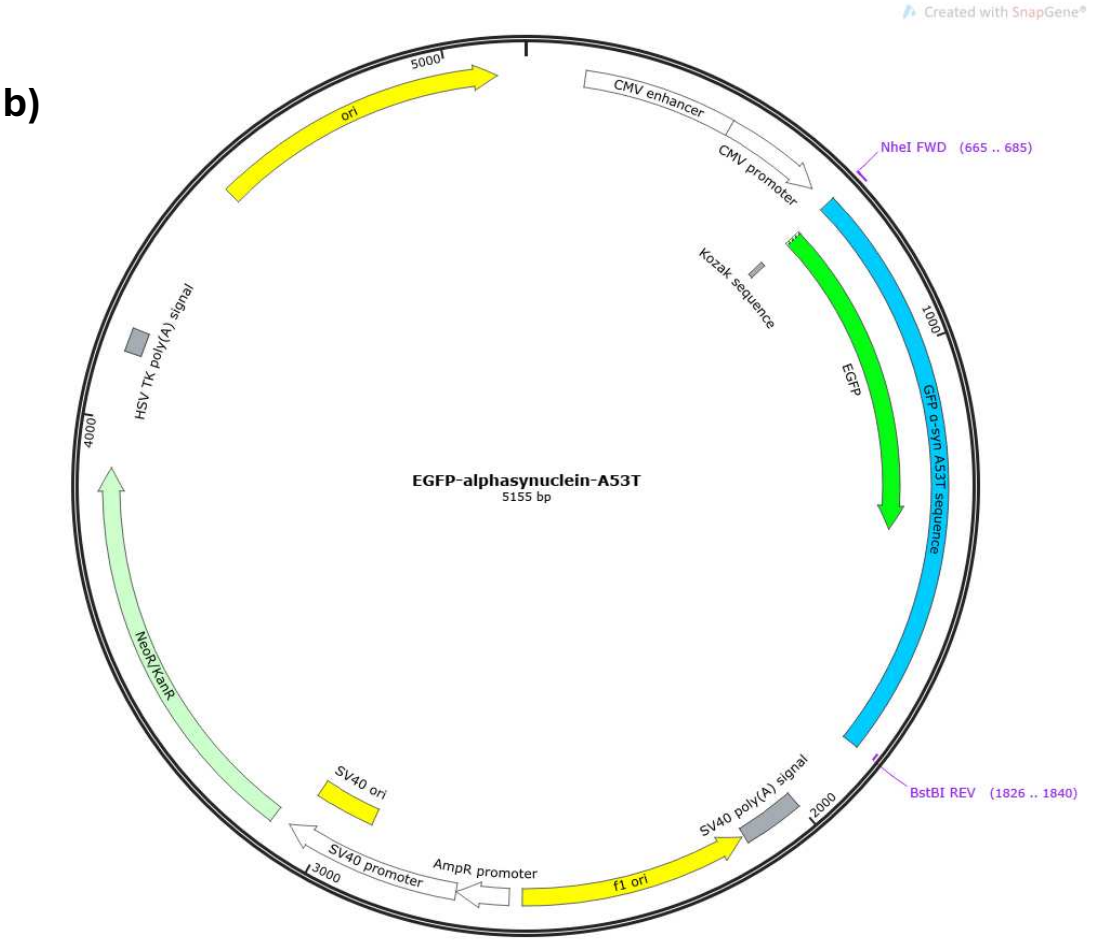
Created with SnapGene®
5000
ori
CMV enhancer
CMV promoter
NheI FWD (665 .. 685)
Kozak sequence
EGFP
1000
GFP α-syn A53T sequence
HSV TK poly(A) signal
4000
EGFP-alphasynuclein-A53T
5155 bp
NeoR/KanR
SV40 ori
SV40 poly(A) signal
BstBI REV (1826 .. 1840)
2000
SV40 promoter
AmpR promoter
f1 ori
3000

Figure 16: Plasmid maps showing primer binding sites used for PCR amplification of EGFP-α-syn-WT and -A53T sequences

Plasmid maps of EGFP-α-syn-WT (a) and EGFP-α-syn-A53T (b) plasmids, with NheI FWD and BstBI REV primer binding sites indicated. These primers were used to amplify EGFP-α-syn-WT and -A53T sequences, shown in blue, using PCR.

For the PCR reaction, 100ng EGFP-alphasynuclein-WT and EGFP-alphasynuclein-A53T DNA were incubated on ice with 10µl 5X Phusion HF buffer (ThermoScientific™, F-518), 10mM dNTPs (NEB, N0447S), 100mM forward primer (NheI FWD), 100mM reverse primer (BstBI REV) and 0.5µl Phusion DNA polymerase (ThermoScientific™, F-530S, made up to 50µl with nuclease-free water (Ambion™, 991467). The mixture was then incubated in a thermocycler (BioRAD, T100) with the parameters detailed in **Table 9**.

Table 9: PCR parameters for amplification of EGFP-α-syn-WT and -A53T sequences

Step	Temperature	Time
1. Denaturation	98ºC	30 seconds
2. Cycling (30 cycles)	98ºC	10 seconds
	60ºC	30 seconds
	72ºC	1 minute
3. Final extension	72ºC	10 minutes
4. Extended incubation	10ºC	Infinite hold

2.3.2 Gel electrophoresis and purification

Gel electrophoresis was used to separate out amplified or cut sequences from the rest of the plasmid DNA. Agarose powder (Fisher Bioreagents™, BP160-500) was dissolved in 1X TBE to make a 10% agarose gel. Once cool, SyBRSafe nucleic acid stain (Invitrogen™, S33102) (1:50,000; ThermoFisher) was added. The gel was poured into a tank and left to set for 30 minutes at room temperature. Once set, the gel was covered in 1X TBE. PCR product was mixed with 1X loading dye and loaded on the gel alongside 5µl 1kb GeneRuler DNA ladder (ThermoFisher Scientific™, SM1331) to allow identification of band size. The tank was attached to a powerpack, and the gel was run at 60V for approximately 45 minutes or until samples were

separated. DNA bands were visualised using a G:BOX blue light transilluminator (Syngene) and bands containing the DNA sequences of interest were cut out using a razor blade (approximate sizes in **Table 10**). DNA within the excised gel band was purified using a GeneJet extraction kit (ThermoFisher Scientific™, K0503) according to the protocol provided in the kit. Recipes for buffers used can be found in **Appendix A** (**Table 20**).

Table 10: Approximate sizes of DNA sequences of interest

Sequence of interest	Size (bp)	Origin plasmid
EGFP-α-syn-WT	1171	EGFP-alphasynuclein-WT
EGFP-α-syn-A53T	1171	EGFP-alphasynuclein-A53T
pLJM1	7366	pLJM1-EGFP

2.3.3 Restriction digest

The pLJM1-EGFP vector was digested using restriction enzymes NheI and BstBI (**Table 11**) to cut out the GFP sequence (**Figure 17**), leaving an empty pLJM1 backbone (vector). The purified EGFP-α-syn-WT and -A53T sequences (inserts) were digested using the same restriction enzymes to create sticky ends complimentary to those of the pLJM1 backbone.

Table 11: Restriction enzymes used to create sticky ends in the empty pLJM1 backbone and EGFP-α-syn-WT and -A53T sequences

Restriction enzyme	Cut site (5'-3')	Company	Code
NheI	1171	Roche	885 851
BstBI	1171	NEB	R0519S

2µg of DNA to be digested was mixed with 1µl of each restriction enzyme (NheI and BstBI) and 3µl 10X Tango buffer (ThermoFisher Scientific™, BY5), made up to 30µl with nuclease-free water. The vector was dephosphorylated by incubating with 1µl FastAP enzyme and 3µl FastAP buffer (ThermoFisher Scientific™, EF0654) at 37ºC for 10 minutes to prevent self-ligation. The mixture was incubated at 37ºC for 1.5 hours. The digested DNA products were then run on an electrophoresis gel, excised, and purified (as in **2.3.2**).

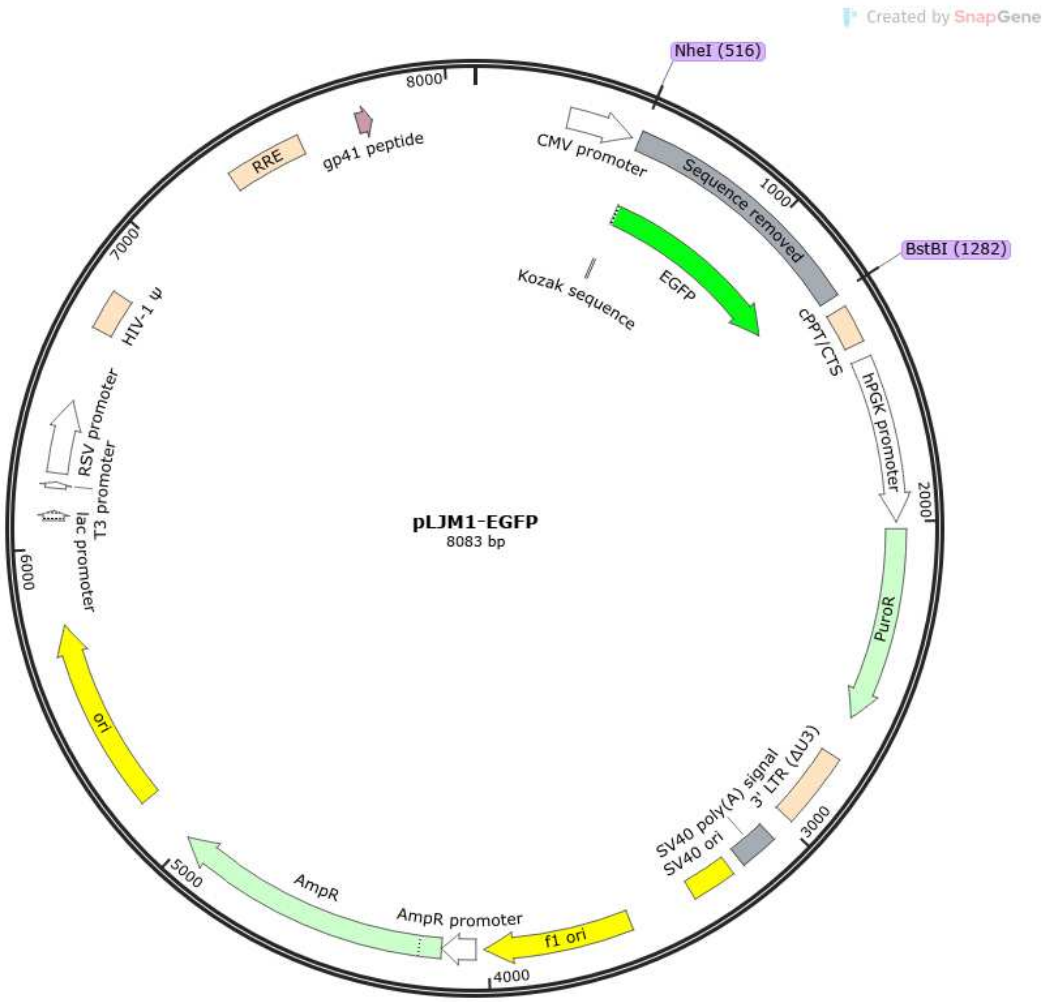

Figure 17: Plasmid map showing restriction sites used to digest pLJM1-EGFP

Plasmid map of pLJM1-EGFP with the NheI and BstBI restriction sites indicated. These restriction enzymes were used to cut out the EGFP sequence (shown by a green arrow), leaving an empty pLJM1 backbone with sticky ends.

2.3.4 Plasmid purification

The construct of interest was transformed into competent Stbl3™ bacteria (OneShot™; Invitrogen™, C737303) by incubating on ice for 30 minutes and heat shocking for 45 seconds at 42ºC. Bacteria were incubated and shaken in 400µl SOC growth media (Invitrogen, 15544-034) for 1 hour at 37ºC. The bacterial suspension was spread onto LB-Agar plates containing either ampicillin (100µg/ml) (ThermoFisher Scientific™, BP1760-5) or kanamycin (25µg/ml) (Fisher BioReagents, BP906-5) depending on the antibiotic resistance gene expressed in the plasmid. Plates were incubated for 16-18 hours at 37ºC to allow formation of bacterial colonies. Individual colonies were selected, incubated, and shaken in LB-Agar for 16-18 hours at 37ºC. The bacterial culture was centrifuged at 3500RPM for 10 minutes at 10 ºC to generate a pellet

and LB-Agar was removed. Plasmid DNA from the resulting bacterial culture was isolated and purified using the NucleoSpin™ Plasmid MiniPrep kit (Macherey-Nagel™, 740588.50) according to the protocol provided.

2.3.5 Ligation and transformation

Inserts and vectors (shown in **Table 12**) were ligated together at a 3:1 ratio of insert: vector, made up to 10µl with nuclease free water. 10µl of Quick Ligation buffer (NEB, B2200S) and 0.5µl of T4 Quick Ligase enzyme (NEB, M2200S) were added and the mixture was incubated at room temperature for 10 minutes. 2µl of ligation product was added to 30µl of competent Stbl3 cells which were transformed and grown out as described in **2.3.4**. Plasmid maps of final constructs can be found in **Appendix A** (**Figure 113**, **Figure 114**, **Figure 116**).

Table 12: Vector-insert pairings used to create final constructs

Vector	Insert	Final construct
pLJM1	EGFP-α-syn-WT	pLJM1-GFP-α-syn-WT
pLJM1	EGFP-α-syn-A53T	pLJM1-GFP-α-syn-A53T
pLentiCRISPRv2	SNCA KO	pLentiCRISPRv2-SNCA KO

2.3.6 Screening

New pLJM1-GFP-α-syn constructs were screened for successful ligation by redigesting to check for the presence of both the vector and insert DNA sequences by size. 1µg of DNA from the constructs was incubated in LB Agar and spread onto Agar plates as described in 2.3.4. Purified plasmid DNA was redigested as described in 2.3.3 and run on an agarose gel as described in 2.3.2 to check for the presence of the GFP-α-syn WT and A53T inserts and the pLJM1 vector (sizes indicated in **Table 10**). If constructs were positive, purified plasmid DNA was taken forward for experiments. Glycerol stocks of positive constructs were made with 500µl of positive bacterial culture and 250µl of 50% glycerol (Fisher Bioreagents™, G/0650/08), before storing at -80 ºC.

2.4 CRISPR/Cas9

CRISPR/Cas9 gene editing was used to selectively inactivate the human gene encoding α-synuclein (SNCA) to create an αn α-synuclein knockout cell line (SNCA KO). The SNCA gene was analysed using Benchling and 2 guide sequences (gRNAs) were chosen that targeted regions in exon 2. Oligonucleotide gRNAs (purchased from Sigma-Aldrich) are shown in **Table 13**, with the gRNA sequence shown in bold.

Table 13: gRNA sequences used to target the SNCA gene (5'-3')

gRNA	Forward	Reverse
1	CACCG **AGGACTTTCAAAGGCCAAGG**	AAAC **CCTTGGCCTTTGAAAGTCCT**C
2	CACC **GCTGCTGAGAAAACCAAACA**	AAAC **GTTTGGTTTTCTCAGCAGC**

The annealed oligonucleotide pair was ligated into a BsmBI-digested pLentiCRISPRv2 backbone plasmid (Addgene #52961, a gift from Feng Zhang; http://n2t.net/addgene:52961; RRID: Addgene_52961, **Appendix A**, **Figure 115**) and transformed into Stbl3 bacteria as described in **2.3.5**. The purified pLentiCRISPRv2-SNCA KO DNA was screened for insertion of the oligonucleotide gRNAs by Sanger sequencing using the primer detailed in **Table 14**.

Table 14: Sequence of primer used for Sanger sequencing

Primer	Forward
U6 FWD	ACTATCATATGCTTACCGTAAC

2.5 Lentiviral DNA delivery

To generate stable cell lines in SH-SY5Y cells, plasmid DNA was integrated into the host cell genome using a lentiviral system, summarised in **Figure 18**. Alongside experimental cell lines with perturbations in α-synuclein, control cell lines were generated with the same system to rule out possible effects of the viral transduction process on cell phenotypes.

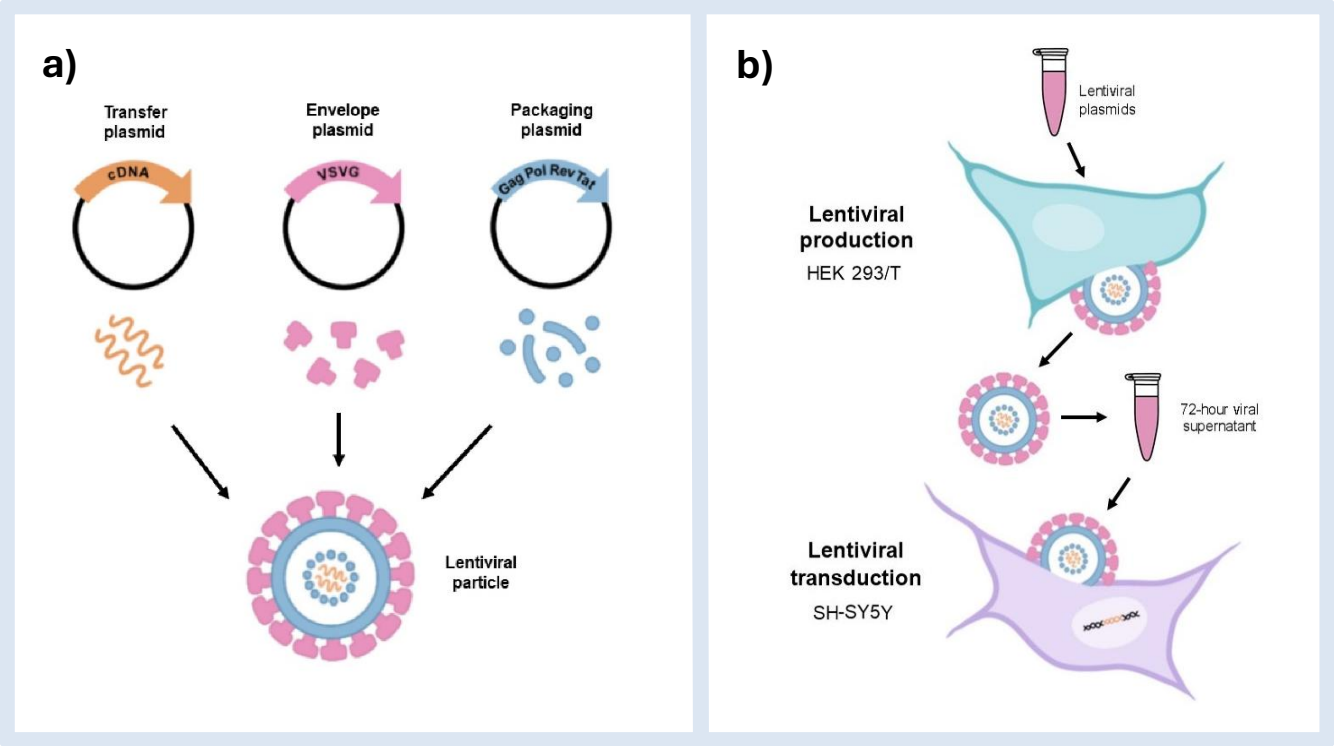

Figure 18: Formation of 2nd generation lentiviral particles, their production from HEK293 cells and their transduction into SH-SY5Y cells

a) 3 plasmids come together to form lentivirus: a transfer plasmid containing a lentiviral backbone with the DNA of choice (orange), an envelope plasmid encoding proteins on the viral surface (pink) and a packaging plasmid containing core viral components (blue)

b) To generate lentivirus, the transfer, envelope and packaging plasmids are transfected into HEK239/T cells, where they are taken up and expressed in the form of lentiviral particles. Supernatant containing the virus is collected used to transduce the host, SH-SY5Y cells. DNA from the lentivirus is integrated into the host cell genome where it can be stably expressed.

2.5.1 Lentiviral production in HEK239/T cells

HEK293/T cells were seeded in 6-well plates and transfected as described in **2.2.4** with a puromycin-resistant transfer plasmid, psPAX2 (Addgene #12260, a gift from Didier Trono; http://n2t.net/addgene:12260; RRID: Addgene_12260) and Pmd2.G (Addgene #12259, a gift from Didier Trono; http://n2t.net/addgene:12259; RRID: Addgene_12259) at the concentrations defined in **Table 15**.

Table 15: Plasmids used to generate lentivirus in HEK239/T cells

Plasmid	Function	Composition	Concentration
Variable	Transfer plasmid	DNA to be expressed	1.140μM
psPAX2	Packaging plasmid	Gag-pol-rev-tat	0.750μM
pMD2.G	Envelope plasmid	VSVG	0.375μM

Transfer plasmids were variable depending on the cell line being created. Details of each transfer plasmid and the cell line it was used to generate are shown in **Table 16**.

Table 16: Transfer plasmids used to generate each cell line

Transfer plasmid	Cell line	Model
pLJM1-EGFP	GFP only control	Overexpression
pLJM1-GFP-α-syn-WT	GFP-α-syn WT	Overexpression
pLJM1-GFP-α-syn A53T	GFP-α-syn A53T	Overexpression
pLentiCRISPRv2	EV control	Knockout
pLentiCRISPRv2-SNCA KO 1	SNCA KO 1	Knockout
pLentiCRISPRv2-SNCA KO 2	SNCA KO 2	Knockout

HEK293/T cells transfected with pLJM1-EGFP were used as a positive control and visualised using a ZOE™ Fluorescent Cell Imager (Bio-Rad, 1450031) to check for GFP fluorescence to confirm transfection. After 24 and 48 hours, media was removed and replaced with 2ml of fresh media. 72-hours post-transfection, viral supernatant was removed and put through a 0.45µM filter to remove cell debris. Virus was then used immediately for transduction.

2.5.2 Lentiviral transduction of SH-SY5Y cells

SH-SY5Y cells were seeded in 6-well plates at 500,000 cells/well approximately 24 hours prior to viral transduction. Filtered viral supernatant was added dropwise to SH-SY5Y cells with 5µg/ml hexadimethrine bromide (polybrene) (Merck Millipore, 107689). After 6 hours, viral supernatant was removed and replaced with 2ml of fresh media. 48 hours after transduction, 1.5µg/ml puromycin (Fisher Bioreagents™, BP2956-100) was added for 2 days to allow for selection of only cells expressing the transfer plasmid. A visual representation of this is shown in **Figure 18b**. Cells were then allowed to expand before being screened for knockout or overexpression by Western blot. Positive cell lines were frozen as described in **2.2.1** and taken forward for experiments.

2.6 Protein extraction

2.6.1 Cell lysis

Cells were washed gently with cold 1X phosphate buffered saline (PBS) before being lysed with radioimmunoprecipitation assay buffer (RIPA) (**Appendix A**, **Table 20**) and scraped from the plate. Lysates were collected, centrifuged at 10,000RPM for 10 minutes at 4°C and the pellet was removed.

2.6.2 BCA assay

A Pierce™ bicinchoninic acid (BCA) Protein Assay Kit (ThermoScientific™, 23250) was used according to instructions to determine the protein concentration of each lysate. In duplicate, 10ul of each experimental lysate was pipetted into a 96-well plate in alongside 10ul of each bovine serum albumin (BSA) standard, made up from the kit. For cells in 96-well plates for normalisation to total protein, 25ul of RIPA buffer was added to each well containing cells and 25ul of each standard was pipetted in duplicate into empty wells of the same plate. The standards were at the following concentrations: 0µg/ml (control), 25µg/ml, 125µg/ml, 250µg/ml, 500µg/ml, 750µg/ml, 1000µg/ml, 1500µg/ml, and 2000µg/ml. 200µl of BCA working reagent was

added to each well and the plate was incubated at 37°C for 30 minutes. The absorbance of each well was read with a POLARstar Omega plate reader (BMG Labtech) at a wavelength of 562nm. Duplicate readings were averaged and the background measurement from the control standard were subtracted from all other readings. The absorbances of the known standards were used to create a standard curve. The equation for the gradient of this curve was used to calculate protein concentrations of experimental lysates.

2.6.3 Mitochondrial isolation

Mitochondria were isolated from cells using a Mitochondria Isolation Kit for Cultured Cells (Abcam, ab110170). Cells were washed gently with cold 1X PBS before 500µl 1X PBS was added to each of 3 plates. Cells were scraped from the plates, collected together, and centrifuged at 1000G for 5 minutes at 4°C. The pellet was flash frozen on dry ice and then thawed to weaken cell membranes. The pellet was resuspended in reagent A at a concentration of 5mg/ml and incubated on ice for 10 minutes. Cells were then homogenised with a dounce homogeniser (30 strokes) and centrifuged at 1000G for 5 minutes at 4°C. The supernatant was kept and the pellet was resuspended in reagent B at a concentration of 5mg/ml. The same rupture process was repeated and the supernatants from both steps were added together. The combined supernatants were centrifuged at 12,000G for 15 minutes at 4°C and the supernatant was kept as the cytosolic fraction. The pellet was resuspended in 500µl reagent C as the mitochondrial fraction. 1X protease inhibitor was added and fractions were frozen at -80°C.

2.7 Western blot

2.7.1 Casting gels

SDS-Page gels were made according to protocols for the SDS-Page Mini setup (Bio-Rad) (**Appendix A**, **Table 22**). Resolving gels were made at either 10% or 15% acrylamide depending on the expected molecular weight of proteins of interest. Gels were covered with 70% ethanol (Sigma Aldrich, 32221-M) and left to set for 30 minutes at room temperature. Ethanol was rinsed out with dH_2O and stacking gels were added on top of resolving gels. Combs were inserted to form the sample wells and the gel was left to set for 45 minutes at room temperature. Once set, gels were stored at 4°C until use.

2.7.2 SDS-Page

Based on the BCA assay, cell lysates were diluted in RIPA buffer to enable equal loading of protein, and each mixed with the same volume of 1X sodium dodecyl sulfate (SDS) loading buffer (diluted from 6X). Lysates were then denatured by boiling at 95°C for 5 minutes and cooled on ice for 2 minutes prior to loading into the gel. Proteins were separated on SDS-Page gels alongside a molecular weight ladder (PageRuler™, ThermoScientific™, 26616; EZ Run™, Fisher Bioreagents™, BP3603-500) in 1X running buffer (10% Laemmli buffer in dH_2O) at 100V for approximately 1 hour 30 minutes (10% gels) or 2 hours (15% gels). A polyvinylidene difluoride (PVDF) membrane (Millipore, IPFL00010) was activated by submerging it in methanol (Fisher Bioreagents™ M/3900/17) for 2 minutes prior to transfer. Proteins in the gel were transferred to the activated PVDF membrane by applying a current of 350mA for 1 hour in 1X transfer buffer. To enable detection of α-synuclein, membranes were subsequently incubated in 4% paraformaldehyde (PFA) (Polysciences, Inc., 04018-1) in PBS for 30 minutes at room temperature to allow cross-linking of monomers to the membrane. Membranes were incubated in blocking solution (either 5% non-fat milk or 3% BSA (Fisher Bioreagents™, BP9701-100) in Tris-buffered saline (TBS) for 30 minutes at room temperature. Primary antibodies were diluted in blocking solution according to recommendation (**Table 4**) and membranes were incubated in this solution overnight at 4°C. Membranes were then washed 3 times in 0.1% TBS-Tween® wash buffer (TBS-T) at room temperature. Secondary antibodies were diluted in TBS-T according to recommendation (**Table 5**) with 2µl SDS (Fisher Bioreagents™, BP1311-200) to reduce background signal. Membranes were incubated in this solution for 1 hour at room temperature before 3 final washes in TBS-T at room temperature. Membranes were washed once in TBS at room temperature, placed into fresh TBS and then visualised using the Li-COR® Odyssey® infrared imaging system. Blots were processed using ImageStudio® software. Recipes for buffers used can be found in Appendix A (**Table 20**).

2.8 ATP assay

SH-SY5Y cells were cultured in glucose or galactose in the presence or absence of oligomycin to allow measurements of ATP under different metabolic conditions. The rationale behind this is detailed in **Appendix A** (**Figure 117**).

Cells were plated identically in two 96-well plates – one for the ATP assay using the Mitochondrial ToxGlo Assay (Promega, G8000) and one for a BCA assay to allow normalisation of ATP readouts against protein concentration. Cells were plated in triplicate for each of 4

experimental conditions. After 24-hours, cells were washed twice with media and refed with 100µl in the following conditions: 1) glucose media; 2) glucose media with 10µM oligomycin; 3) galactose media; 4) galactose media with 10µM oligomycin. Glucose media refers to DMEM/F12 as described in **2.2.1**. Galactose media refers to DMEM no glucose (ThermoScientific™, 11966025) supplemented with 1% PS, 1% NEAAs, 10% FBS and 10mM galactose (Sigma Aldrich, G0750). A well with no cells and galactose media was used as a negative control. Cells were incubated at 37°C for 2 hours before plates were processed.

For the ATP assay plate, media was removed and 100µl ATP detection reagent from the kit was added to each well. Samples were gently mixed without pipetting and transferred to a white 96-well plate. Luminescence was measured in relative light units (RLU) using a GloMax® Multi+ detection system (Promega). The values for each condition were averaged and the negative control was subtracted from the experimental readings. For the BCA assay plate, media was removed and cells were washed with cold PBS. 25µl of RIPA buffer was added to each experimental well and 25µl of each BSA standard from the BCA Assay kit was added to the plate in duplicate. The BCA was then carried out as described in **2.6.2**. Luminescence vales were divided by the protein concentration for each experimental well to give ATP levels normalised to total protein (RLU/µg).

2.9 Oxygen consumption rate

Oxygen consumption rate (OCR) was measured using a Mito Stress Test with the Agilent Seahorse XF Pro analyser. The theory behind how this test manipulates complexes of the respiratory chain to enable measurement of mitochondrial output is explained in **Appendix A** (**Figure 118, Figure 119**). 24-hours prior to the assay, cells were seeded at 50,000 cells/well in a 96-well Seahorse culture plate and left at room temperature for 30 minutes to ensure even spreading before cells adhered. At least three replicate wells were plated per experimental group. Seahorse XF Calibrant (Agilent, 100840-000) was added to each well of the calibration plate and the hydrobooster was inserted. The calibration plate was incubated overnight at 37°C without CO_2. Cells were plated in duplicate in a 96-well plate for normalisation.

On the day of the assay, media was removed from the cells and replaced with Seahorse XF DMEM pH 7.4 (Agilent, 103575-100) supplemented with 1M glucose (Agilent, 103577-100), 100mM pyruvate (Sigma Aldrich, S8636) and 200mM L-glutamine. The calibration plate was removed from the incubator and injection ports on the sensor cartridge were loaded with the Seahorse Mito Stress Test compounds (Agilent, 103015-100) at the following concentrations:

1.5μM oligomycin, 2μM CCCP, 0.5μM antimycin A/rotenone. The plate was then inserted into the Seahorse analyser for machine calibration. The cell plate was incubated for approximately 45 minutes at 37°C without CO_2 to acclimate, then inserted into the Seahorse analyser for the assay to be run. During the run, the duplicate 96-well plate was used to run a BCA assay as described in **2.6.2**. Using Agilent Wave Pro software, OCR vales were divided by the protein concentration for each experimental well to give OCR normalised to total protein (OCR/μg). Graphs and calculations of respiratory parameters were all automatically generated from the data with Agilent Wave Pro software.

2.10 Immunofluorescence

2.10.1 Acid-washing coverslips

Differentiating SH-SY5Y cells were plated on acid-washed coverslips to enhance cellular attachment to the glass. To acid-wash, coverslips were shaken in 1M NaOH for an hour at room temperature, rinsed 5 times in dH_2O and then shaken in 1M HCl overnight at room temperature. Coverslips were rinsed a further 5 times in dH_2O and shaken in 70% ethanol for 15 minutes at room temperature and then left in fresh 70% ethanol until use.

2.10.2 Immunocytochemistry

SH-SY5Y cells were cultured on ethanol-sterilised coverslips in 12-well plates. Prior to staining, cells were washed with 1X PBS and fixed in 4% PFA in PBS for 20 minutes at room temperature. Coverslips were washed again in 1X PBS and membranes were permeabilised with 0.1% Triton-X-100 (Acros Organics, 215682500) in PBS for 2 minutes at room temperature. Coverslips were washed a final time in 1X PBS before being incubated in blocking solution (1% BSA in PBS) for 20 minutes at room temperature. Primary antibodies were diluted as recommended in blocking solution (**Table 4**). Coverslips were incubated in primary antibody solution for 1 hour 30 minutes at room temperature in a humidified incubation chamber. Secondary antibodies were also diluted as recommended (**Table 5**) in blocking solution with the addition of Hoechst nuclear stain (1:10,000). Coverslips were washed in 1X PBS before incubation with secondary antibody solution for 45 minutes at room temperature in a dark humidified incubation chamber. Coverslips were washed in 1X PBS for a final time, rinsed in dH_2O and mounted onto sterile glass slides with FluorSave® mounting medium (Merck Millipore, 345789). Immunofluorescence images were obtained using either a Zeiss Axioplan microscope with a 63X oil immersion objective or an Olympus IX83 inverted fluorescence microscope with a 100X or 60X oil

immersion objective or a 40X air objective. Images were subsequently processed with ImageJ® software.

2.10.3 Saponin treatment

To look at localisation of α-synuclein and pS129 α-synuclein in cells overexpressing GFP-α-syn-WT or -A53T, saponin was used to clear the cytoplasm, highlighting any GFP-α-synuclein left behind. In these cases, cells on coverslips were washed with 1X PBS and then incubated in 0.03% saponin (Sigma Aldrich, S4521) in PBS for 30 seconds at room temperature prior to fixation with 4% PFA. The rest of the staining protocol was carried out as detailed in **2.10.2**.

2.11 Live imaging of ΔΨm

ImageIT™ tetramethylrhodamine (TMRM) reagent (Invitrogen, I34361) was used in live cells to assess mitochondrial membrane potential **(**ΔΨm)**.** Cells were plated as described in **2.2.1**. 24-hours prior to imaging, DMEM/F12 media was removed and replaced with media without phenol red, FluoroBrite™ DMEM (Gibco, A1896701) supplemented with 10% FBS, 1% PS and 1% NEAAs. On the day of imaging, ImageIT™ TMRM reagent was diluted and added to cells in fresh media to a final concentration of 10nM. Cells were incubated at 37°C in 5% CO_2 for 30 minutes and then imaged with a 63X objective on a DeltaVision™ Elite live imaging microscope. Z-stacks were taken to capture whole cells in 3D, with approximately 15 Z-slices per cell. Images of 10 different fields of view were taken for TMRM fluorescence intensity measurements as readouts of steady state ΔΨm**.**

As a positive control, cells were incubated with TMRM as above and one field of view was imaged. 10μM CCCP was added to induce depolarisation of the mitochondrial membrane, and images of the same field of view were taken once per minute over a 10-minute period, showing a decrease in fluorescence intensity. This data is shown in **Appendix A** (**Figure 121**) as proof-of-concept.

2.12 Data analysis

2.12.1 Western blot quantification

ImageJ® software was used to determine protein levels from Western blots. For each blot, mean grey value measurements were taken of proteins of interest, loading control and background. Background measurements were subtracted from protein measurements to reduce noise. Expression levels of the protein of interest were expressed relative to the loading control, or in some cases to a comparative protein. Calculated protein expression was directly plotted on bar graphs and differences between groups were statistically analysed.

2.12.2 Quantification of GFP puncta in GFP-α-syn overexpressing cells

GFP only, GFP-α-syn-WT and GFP-α-syn-A53T overexpressing cell were fixed, underwent cytoplasmic clearance with saponin and immunocytochemically stained for GFP. The number of GFP-positive puncta remaining was quantified as a readout of potential aggregated species.

GFP images were first adjusted using “brightness/contrast” before the number of GFP-positive puncta per cell was then manually counted (**Figure 19**). Care was taken to only quantify this in cells exhibiting a level of background GFP to ensure that only cells overexpressing GFP or GFP-α-syn were included. Criteria for counting a staining feature as a GFP-positive puncta were firstly that it was rounded and punctate in shape, and secondly that it displayed an increased brightness that enabled it to be distinguished from background GFP. The number of GFP-positive puncta was counted in 16 cells per experimental group, per repeat, with the means of each group taken forward for statistical analysis.

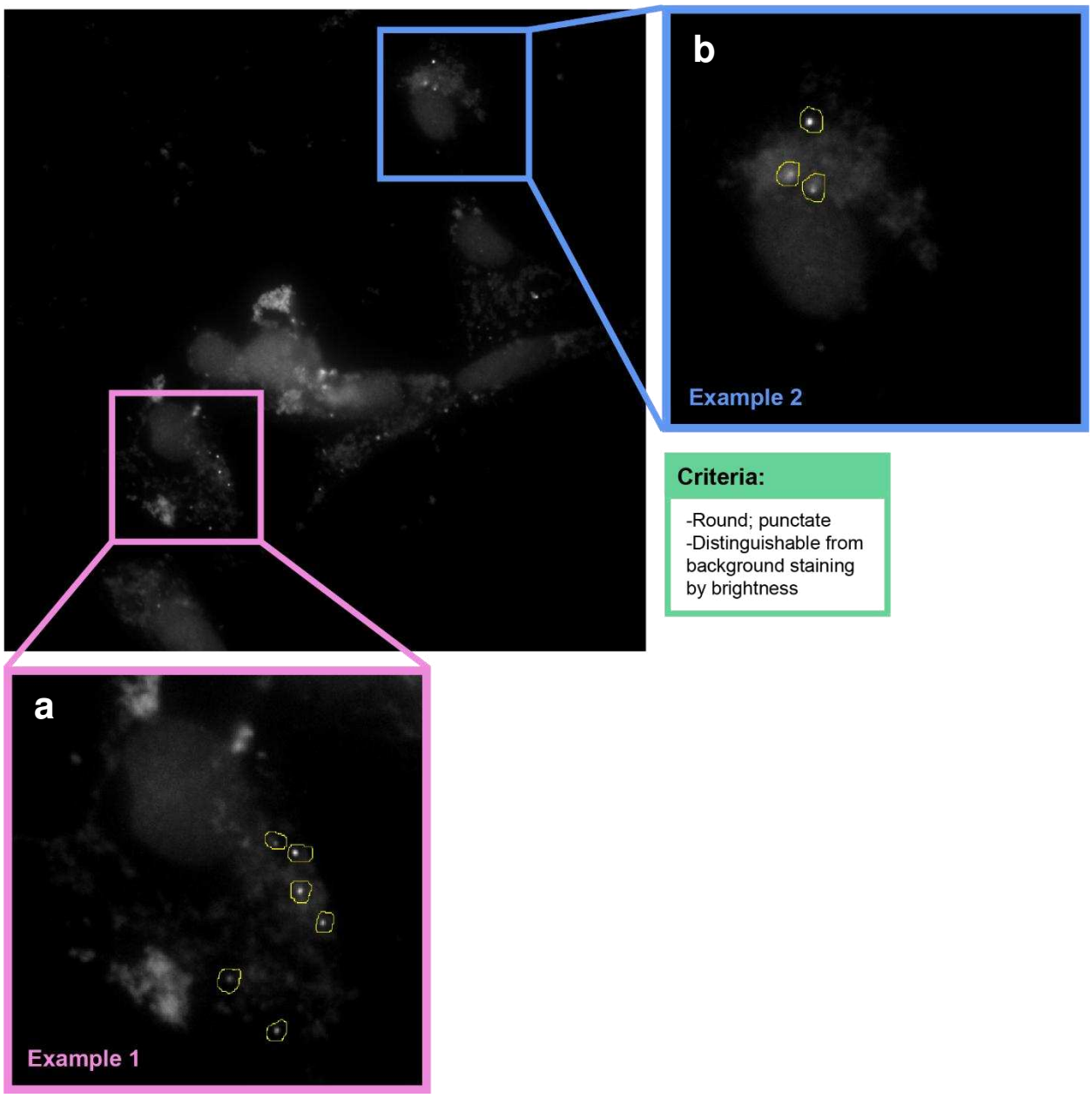

Figure 19: Examples of GFP puncta in GFP-α-syn overexpressing cells

Cells overexpressing GFP or GFP-α-syn were fixed and underwent cytosolic clearance with saponin to leave only punctate staining. GFP images were adjusted manually with the "brightness/contrast" tool before individual cells were assessed for punctate staining which could potentially reflect aggregates. The number of GFP-positive puncta per cell was counted manually. Criteria denoting punctate staining was that staining features were round and so bright that they could be clearly distinguished from background staining. Examples of cells with GFP-positive puncta identified are shown in (a) and (b).

2.12.3 MDV quantification

MDVs were quantified manually with ImageJ® software from immunofluorescence images taken on a 100X objective. Background was subtracted to reduce noise using a rolling ball radius of 30-50 pixels and brightness/contrast was enhanced. Images of TOM20, PDH and nuclei stained with 4', 6-diamidino-2-phenylindole (DAPI) were merged to allow identification of individual cells. IMM-derived MDVs were defined as PDH+/TOM20- puncta, identified by PDH+ puncta that did not colocalise with TOM20 (**Figure 20a**). OMM-derived MDVs were defined as TOM20+/PDH- puncta, identified by TOM20+ puncta that did not colocalise with PDH (**Figure 20b**). The multi-point tool was used to select individual MDVs, and the total number of points was counted for 10 cells per condition. The same cells were used to quantify both OMM- and IMM-derived MDVs. Numbers of MDVs were plotted on a scatter dot plot alongside and differences between groups were statistically analysed.

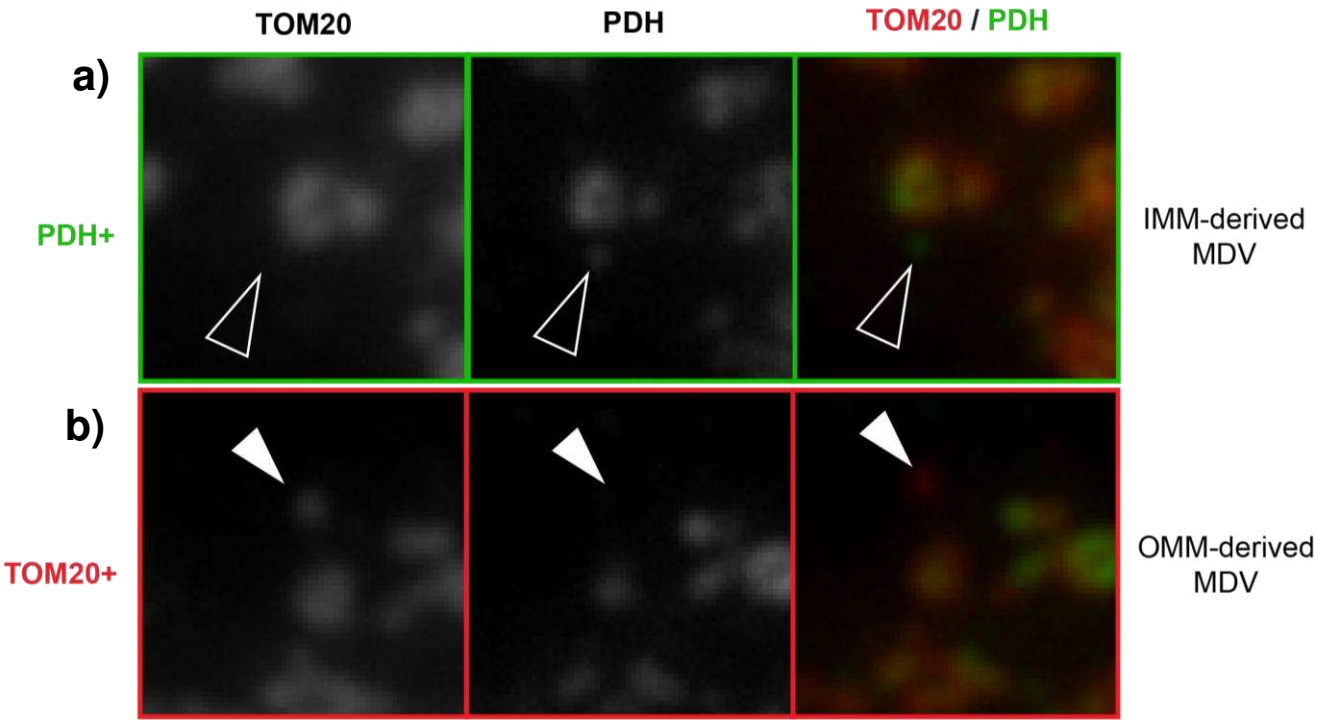

Figure 20: Identification of MDVs with ImageJ® using TOM20 and PDH staining

MDVs were distinguishable from the rest of the mitochondrial network since the network expressed both the IMM marker, PDH, and the OMM marker, TOM20. MDVs only expressed one of these two depending on its origin. IMM-derived MDVs were defined as being PDH+ but TOM20- (a). OMM-derived MVs were defined as being TOM20+ but PDH-.

2.12.4 Mitochondrial network analysis

To analyse the mitochondrial network, immunofluorescence microscopy images of cells stained with a mitochondrial marker (either TOM20 or cytochrome C (henceforth referred to as CytC) were processed using an ImageJ® analysis workflow developed based on Chaudhry et al., 2020.

2.12.4.1 Thresholding

Images were first adjusted and thresholded using a 7-step process to leave a binary image. First, the "subtract background" command was used with a rolling ball to remove uneven background and then the "sigma filter plus" plugin was then used to smooth the image. The "enhance local contrast (CLAHE)" plugin was used alongside the "gamma" correction function to adjust brightness and contrast. Thresholding was achieved with the "adaptive threshold" plugin which accounts for heterogeneous image feature intensities. Noise was reduced using the "despeckle" and "remove outliers" commands. Examples of image outputs at each thresholding stage area shown in **Figure 21**, and the specific parameters for any variable commands or plugins are detailed in **Table 17**.

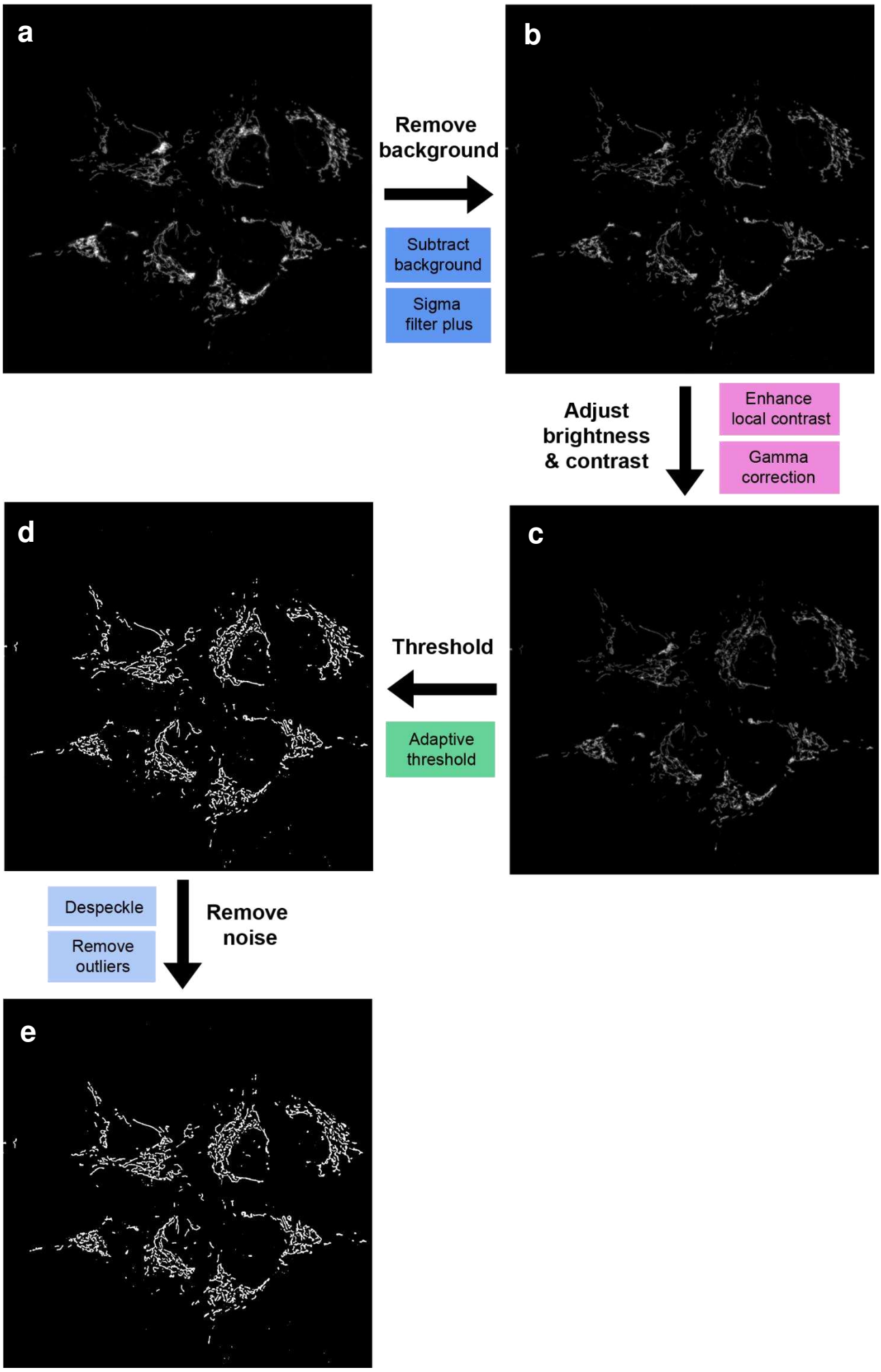
a
b
Remove background
Subtract background
Sigma filter plus
Adjust brightness & contrast
Enhance local contrast
Gamma correction
c
d
Threshold
Adaptive threshold
Despeckle
Remove outliers
Remove noise
e

Figure 21: Steps for image thresholding with ImageJ® prior to analysis

A 7-step thresholding process was used to create a binary image to be used for analysis. Starting with a raw image (a), background was removed to leave a cleaner image (b). Brightness was then adjusted, leaving an image with enhanced contrast (c). Thresholding was then carried out to leave a binary image (d) which then underwent noise removal to leave a clean final processed image (e) ready for analysis. Coloured boxes detail the specific ImageJ® plugins or commands used at each stage.

Table 17: Parameters used for thresholding prior to mitochondrial network analysis

Thresholding function	Parameter 40X	Parameter 100X
Subtract background rolling ball size	6.2713	15.6200
Sigma filter plus radius	0.62713	0.1562
Enhance local contrast block size	64	64
Enhance local contrast slope	0	0
Gamma correction value	0.8	1.1
Adaptive threshold block size	7.84	19.53
Adaptive threshold subtract	-1	-4
Remove outliers radius	0.94	3.34
Remove outliers threshold	50, bright	50, bright

2.12.4.2 Isolation of individual cells

Once images of staining were thresholded, the resulting binary image was merged with either DAPI (for EV and SNCA KO cells) or GFP (for GFP only, GFP-α-syn-WT and GFP-α-syn-A53T cells) to enable identification and selection of individual cells. 20 cells were selected per experimental group, per repeat, with up to 5 cells selected per image. Cells were manually selected using the "freehand selections" tool and saved as individual regions of interest (ROIs) (**Figure 22b**). For a given image, all ROIs were then overlayed onto the image, filled and inverted to create a mask. This mask was used with the "image calculator" tool to subtract the staining within ROIs from the rest of the image, leaving only an image with the cells of interest. Individual

cells were isolated from the rest of this image in the same way: an individual ROI was overlayed onto the image, filled and inverted to create a mask which was then subtracted from the image, leaving an image containing only one cell (**Figure 22c**).

2.12.4.3 Analysis of network

For each cell, a 2-step analysis workflow was carried out. Firstly, the "analyse particles" function was used directly on the processed images to capture morphological information including the total number of discrete staining features (considered to be individual mitochondria) as well as the area, perimeter, aspect ratio and circularity of each one (**Figure 22d**). Then, the "skeletonise 2D/3D" plugin was used to generate a skeletonised image for information on connectivity (**Figure 22e**). The "analyse skeleton" function was used to measure the total number of branches (considered to be individual mitochondria) as well as the length of each branch and the number of junctions between branches (**Figure 22f**). Individual morphology and connectivity measurements were then averaged for each cell. These values were used to calculate the overall mean of the 20 cells for each experimental group. SuperPlots were generated from this data to display each individual data point and statistical analysis was carried out.

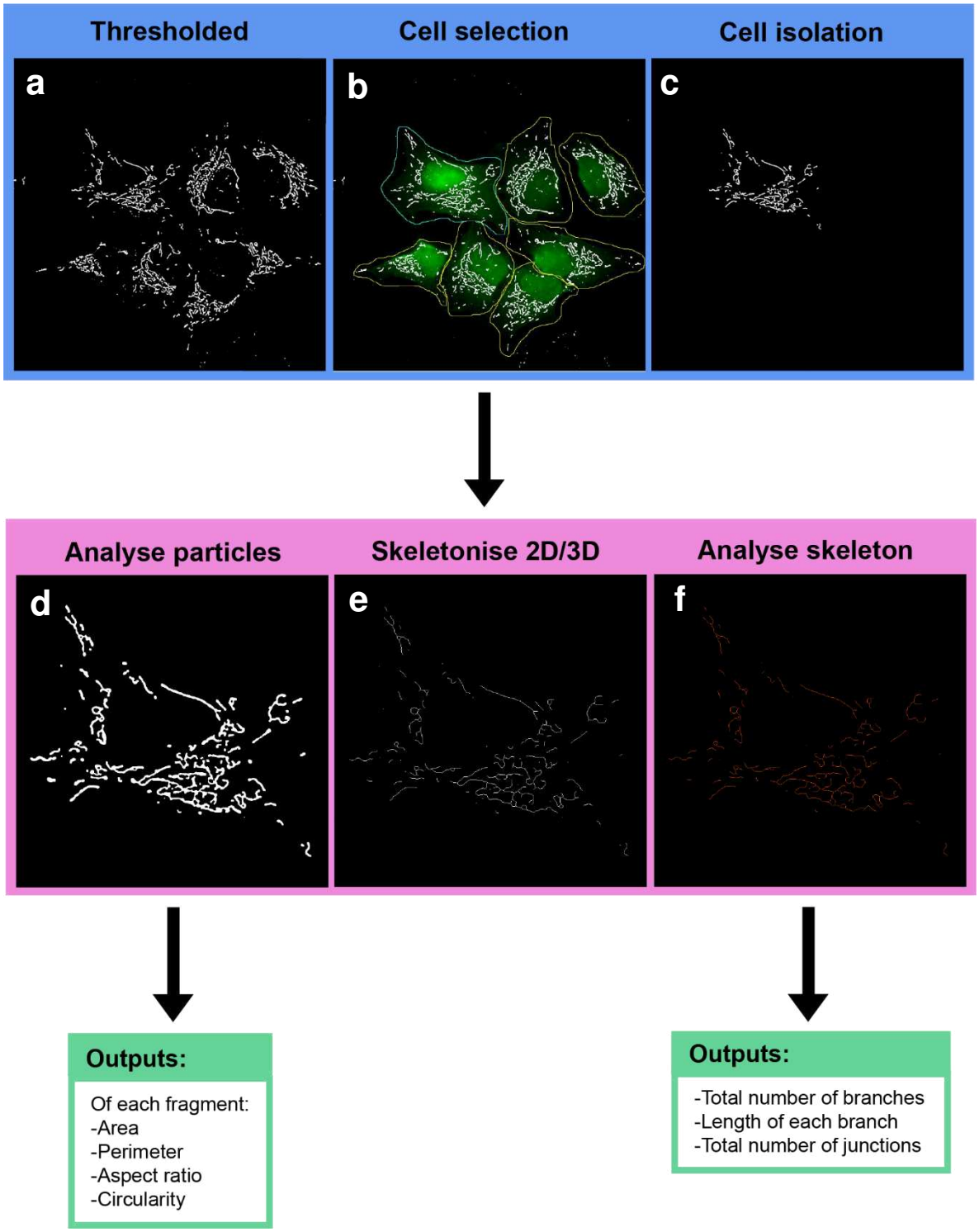

Figure 22: Steps for selecting, isolating and analysing mitochondria in individual cells with ImageJ®

Individual cells were isolated from a thresholded image (a) using the ROI manager. Cells were manually drawn around with the "freeform selections" tool (b). By filling these ROIs, creating masks and subtracting these from the thresholded image, individual cells could be isolated to leave images containing only one cell, ready for analysis (c). This image was directly assessed using "analyse particles" (d) to generate morphology measurements for each individual staining feature. The image was then processed with "skeletonise 2D/3D" (e) and "analyse skeleton" (f) was used to generate a tagged skeleton of the cell (branches in orange, junctions in pink, endpoints in blue). Connectivity measurements were taken from this image.

2.12.5 Lysosome analysis

Lysosomal phenotypes were measured from cells stained with antibodies against the lysosomal marker, LAMP1 and the OMM marker, TOM20. Images taken by immunofluorescence microscopy on a 100X objective were put through an ImageJ® analysis workflow developed to assess the number and total area of lysosomal puncta within a cell, and percentage of lysosomal puncta and area that colocalised with mitochondrial staining. These measures were all taken from the same cells. 20 cells were analysed per experimental group, per repeat.

2.12.5.1 Thresholding

Firstly, raw images were adjusted and thresholded to leave binary images. The TOM20 image was thresholded as previously described in **2.12.4.1** (**Figure 21**). The LAMP1 image was processed using the "subtract background" command with a rolling ball size of 5, and the "auto threshold" function (**Figure 23**).

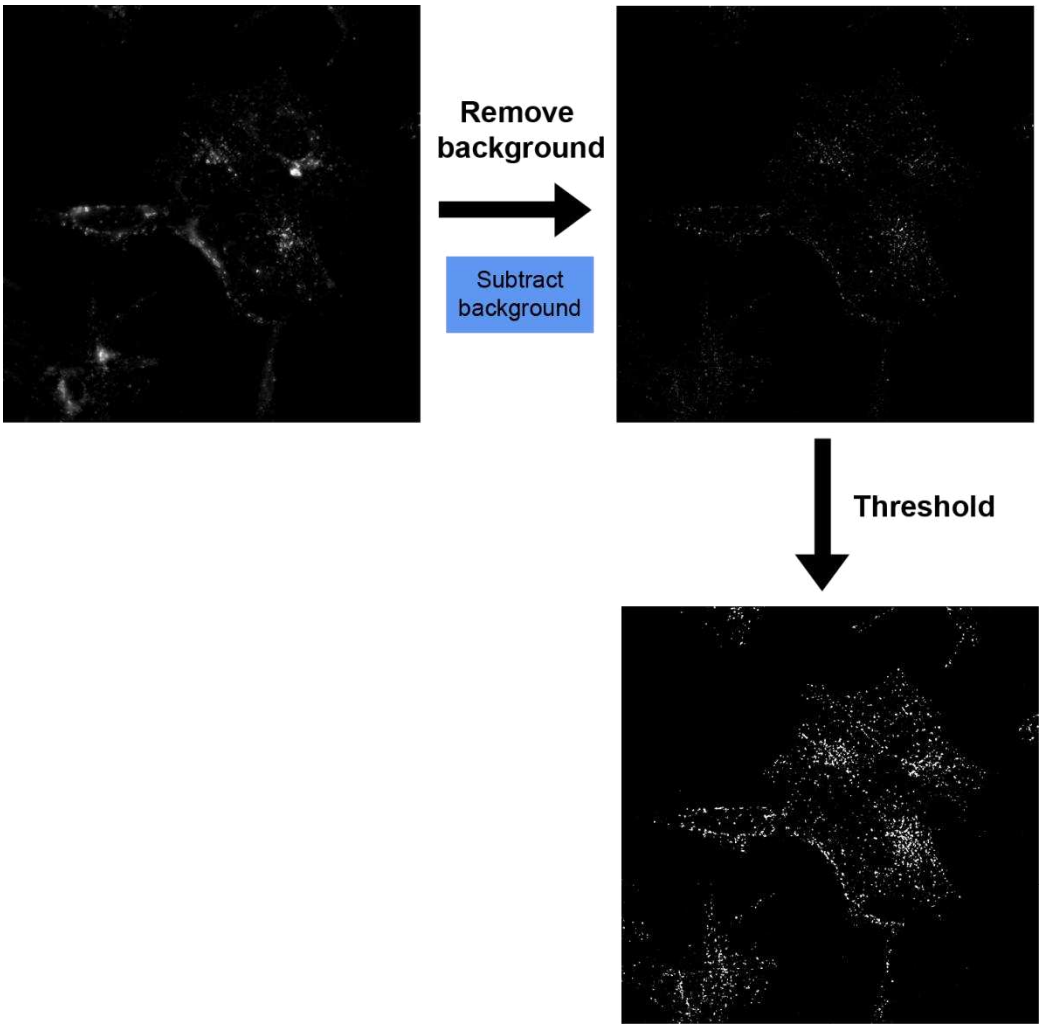

Figure 23: Steps for adjusting and thresholding LAMP1 images

To process LAMP1 images, background was removed from raw images to leave a cleaner image. This was then thresholded to generate a binary image of LAMP1 staining ready for analysis.

2.12.5.2 Isolation of individual cells

Thresholded binary images of TOM20 and LAMP1 staining were then merged with either DAPI (for EV and SNCA KO cells) or GFP (for GFP only, GFP-α-syn-WT and GFP-α-syn-A53T cells) to allow selection of individual cells for analysis. Individual cells were manually drawn around with the "freehand selection" tool, with each saved as an individual ROI.

The thresholded, binarized TOM20 and LAMP1 images were merged in colour alongside DAPI or GFP to enable identification of individual cells (**Figure 24a**). The "freehand selection" tool was used to manually draw around individual cells which were each saved as a separate ROI (**Figure 24b**). For binary LAMP1 and TOM20 images, all ROIs were overlayed, filled and inverted to create a mask. This was used to subtract staining within the ROIs from the rest of the image. Individual cells were isolated in the same way: an individual ROI was overlayed onto the image, filled and inverted to create a mask which was then subtracted from the image, leaving an image containing staining from a single cell (**Figure 24c**). For each cell, this generated one image of isolated LAMP1 and one of isolated TOM20.

2.12.5.3 Analysis of LAMP1 and LAMP1/TOM20 colocalisation

To measure LAMP1+ puncta, the "analyse particles" command was used directly on this isolated LAMP1 image to generate readouts of the total number of LAMP1+ puncta and the total area of LAMP1+ puncta per cell (**Figure 24d**). To assess colocalisation of LAMP1 and TOM20, the "image calculator" function was used to create a composite from the binary LAMP1 and TOM20 images. This composite was comprised only of pixels that were positive for staining in both the LAMP1 "and" the TOM20 images (**Figure 24e**). The "analyse particles" command was then used to generate readouts of the total number of colocalised puncta per cell and the total area of colocalised puncta per cell. The colocalised puncta and area were normalised against total lysosomal puncta and area respectively to provide the percentage of all lysosomes that colocalised with mitochondria.

Total LAMP1+ puncta per cell, total area of LAMP1+ puncta per cell, percentage of LAMP1 puncta colocalised with TOM20 per cell and percentage of LAMP1 area colocalised with TOM20 per cell were presented. The values from each of the 20 cells per group were used to calculate an overall group mean. SuperPlots were generated from this data to display each individual data point and statistical analysis was carried out.

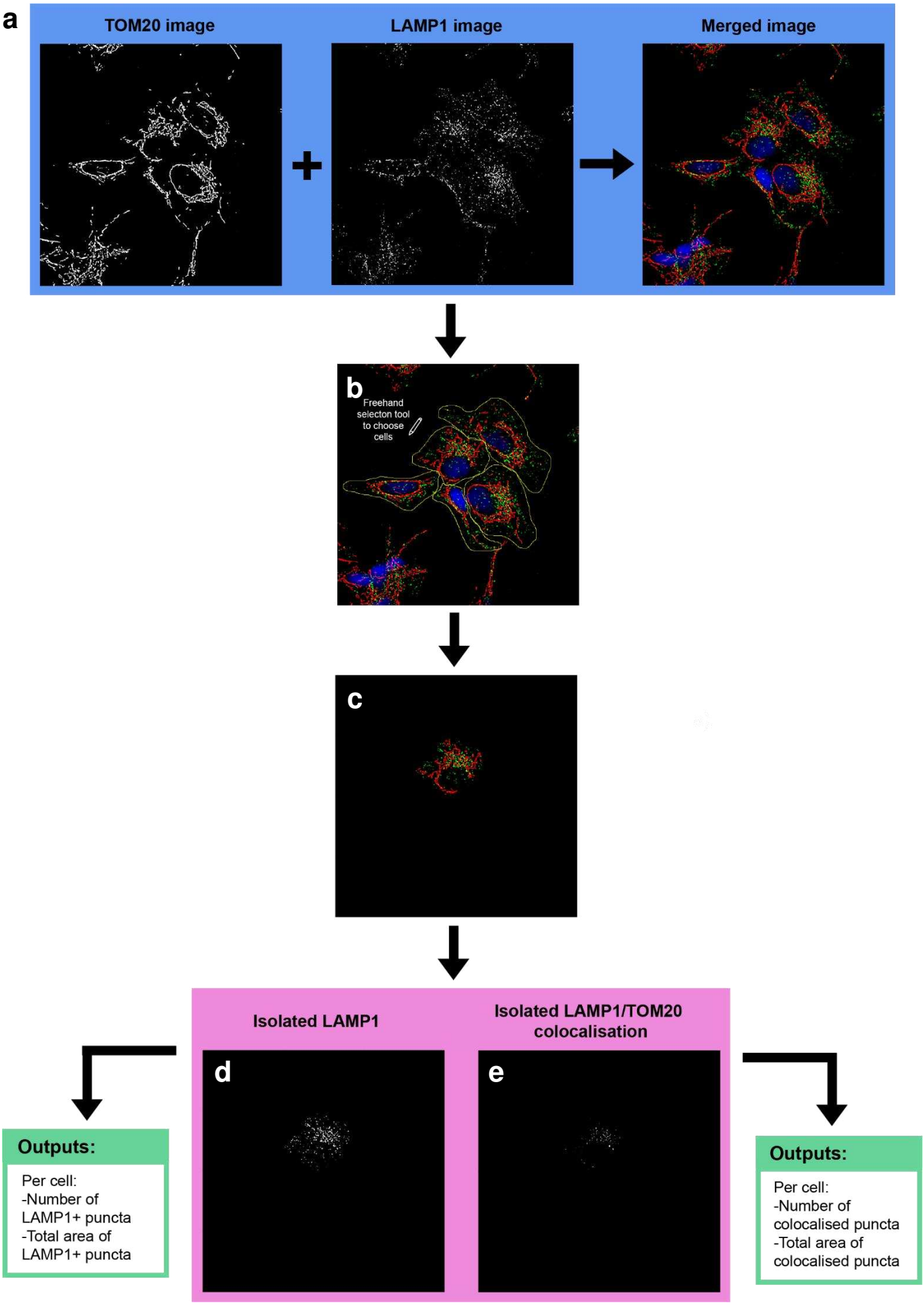
a
TOM20 image
LAMP1 image
Merged image
b
Freehand selecton tool to choose cells
c
Isolated LAMP1
Isolated LAMP1/TOM20 colocalisation
d
e
Outputs:
Per cell:
-Number of LAMP1+ puncta
-Total area of LAMP1+ puncta
Outputs:
Per cell:
-Number of colocalised puncta
-Total area of colocalised puncta

Figure 24: Steps for analysis of LAMP1 morphology and LAMP1/TOM20 colocalisation with ImageJ®

Thresholded, binary TOM20 and LAMP1 images were merged with either DAPI or GFP to enable identification of individual cells (a). These were selected manually using the "freehand selection" tool and each cell was saved as an ROI (b). Staining in individual ROIs was subtracted from the rest of the cell through the creation of masks, leaving behind images only containing one cell (c). Isolated LAMP1 staining was directly measured using "analyse particles", generating readouts of total LAMP1 puncta and area per cell (d). Using "image calculator", composite images were created to show pixels that were positively stained in both LAMP1 and TOM20 images as a readout of colocalisation (e). The number and area of colocalised puncta were measured using "analyse particles".

2.12.6 Quantitation of mitochondrial pUb S65

Levels of mitochondrial pUb S65 were measured from cells stained with the mitochondrial marker, CytC, and pUb S65. Images taken by immunofluorescence microscopy on a 100X objective were put through an ImageJ® analysis workflow developed to the number of mitochondrial pUb S65 puncta and the total area of mitochondrial pUb S65 staining per cell. 20 cells were selected per experimental group, per repeat.

This process measured colocalised puncta and area and was very similar to that used for measuring colocalised LAMP1 and TOM20, so this workflow is referenced throughout.

2.12.6.1 Thresholding

Firstly, raw images were adjusted and thresholded to leave binary images. The CytC image was thresholded as previously described in **2.12.4.1** (**Figure 21**), but parameters were slightly adjusted due to differences in signal between TOM20 and CytC (

Table 18). The pUb S65 image was processed using the "subtract background" command with a rolling ball size of 5, and the "auto threshold" function (**Figure 25**).

Thresholding function	**Parameter**
Subtract background rolling ball size	15.6200
Sigma filter plus radius	0.5
Enhance local contrast block size	64
Enhance local contrast slope	0
Gamma correction value	1.10
Adaptive threshold block size	21
Adaptive threshold subtract	-1
Remove outliers radius	2.34
Remove outliers threshold	50, bright

Table 18: Parameters used for thresholding of CytC images prior to pUb S65 analysis

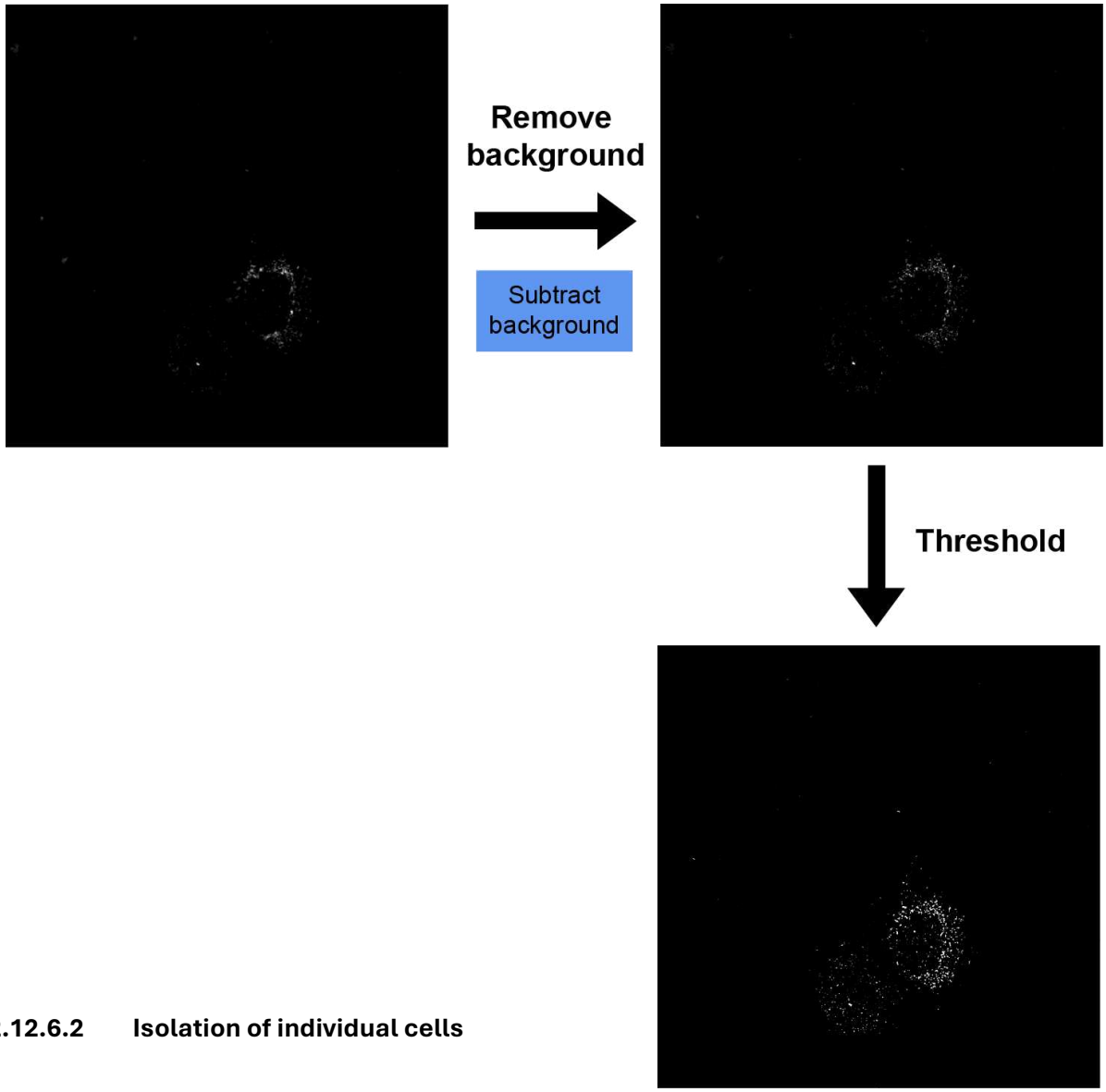

2.12.6.2 Isolation of individual cells

Figure 25: Steps for adjusting and thresholding pUb S65 images

To process pUb S65 images, background was removed from raw images to leave a cleaner image. This was then thresholded to generate a binary image of LAMP1 staining ready for analysis.

Thresholded binary images of pUb S65 and CytC were merged, and cells were selected in the same way as described in **2.12.5.2**. For each cell, this generated one image of isolated CytC and one of isolated pUb S65. This is shown in context in **Figure 26**.

2.12.6.3 Analysis of mitochondrial pUb s65

Mitochondrial pUb S65 was defined as puncta of pUb S65 staining that colocalised with CytC. This was because to avoid skewing of data since some images had a lot of background nuclear pUb S65 staining. To assess colocalisation between pUb S65 and CytC, the “image calculator” function was used to create a composite from the binary pUb S65 and CytC images. This composite was comprised only of pixels that were positive for staining in both the pUb S65

"and" CytC images. The "analyse particles" command was then used to generate readouts of

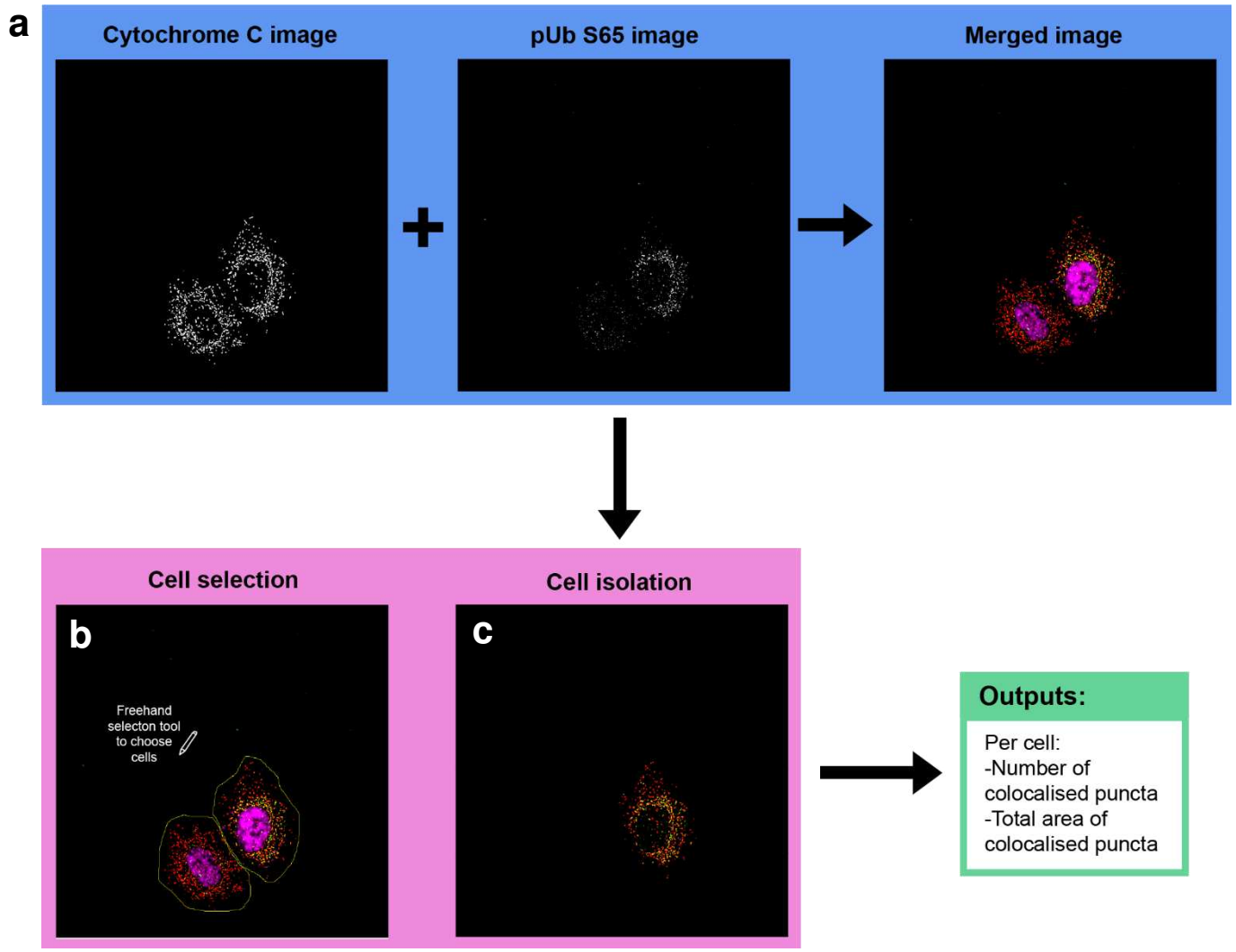

Figure 26: Steps for analysis of pUb S65/CytC colocalisation with ImageJ®

Thresholded, binary TOM20 and LAMP1 images were merged with either DAPI or GFP to enable identification of individual cells (a). These were selected manually using the "freehand selection" tool and each cell was saved as an ROI (b). Staining in individual ROIs was subtracted from the rest of the cell through the creation of masks, leaving behind images only containing one cell (c). Using "image calculator", composite images were created to show pixels that were positively stained in both pUb s65 and cytochrome c images as a readout of colocalisation (shown in yellow on this diagram). The number and area of colocalised puncta were measured using "analyse particles".

2.12.7 TMRM fluorescence intensity analysis

To measure changes **in** ΔΨm, I analysed fluorescence intensity in Z-stack images of TMRM signal in live cells. To exclude areas outside the cell and regions between mitochondrial staining, only pixels positive for TMRM were assessed using a 3-step image processing workflow developed with ImageJ® with help from Jacob Trend. Z-stacks were first opened and duplicated – one used to create the mask (**2.12.7.1**) and one used to generate data (**2.12.7.2**, **2.12.7.3**)**.** This process was repeated until information from 20 cells per group, per experimental repeat had been obtained.

2.12.7.1 Creation of mitochondrial masks

Firstly, a mitochondrial mask was created to enable isolation of positive TMRM signal using one of the duplicate Z-stacks (**Figure 27**). The "multiply" function was applied to enhance the

difference between positive and negative signal followed by “3D sharpen” to enhance border definition and “3D Gaussian blur” to reduce noise (**Figure 27a**). The Z-stack was then compressed into a single 2D image using the “Z-projection” function with “sum slices” to add values from each slice of the Z-stack together for any given pixel. To enable accurate capture of the positive and negative staining within the mitochondrial network, sharp boundaries were then detected using “find edges”. The “threshold” command was then used to create a binary outline image of all stained areas, using a “Huang dark autothreshold”. These outlines were filled and inverted, leaving behind only regions with positively stained pixels that tightly followed the mitochondrial staining. This mask was then used to isolate positive signal (**Figure 27b**).

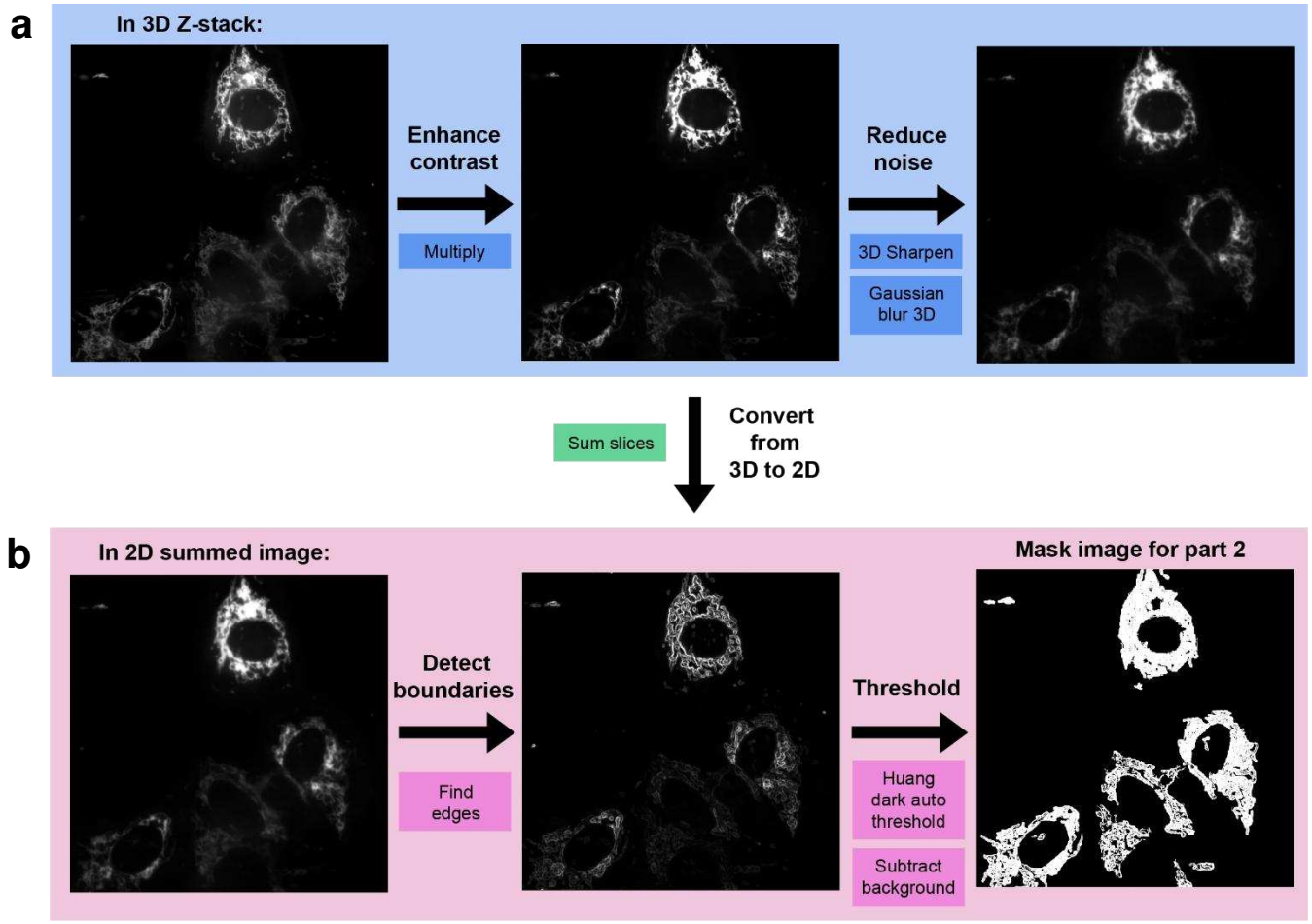

Figure 27: TMRM fluorescence intensity analysis part 1: creating the mitochondrial mask

To measure fluorescence intensity of TMRM staining in individual cells, a mask of mitochondrial staining first had to be generated. To create this, raw Z-stacks underwent contrast enhancement and noise reduction (a) before being compressed from a Z-stack to a 2D image using "sum slices". In the resulting image, sharp boundaries were detected and then images were thresholded to create a binary outline image. Any non-specific staining was then removed, leaving a mask containing only pixels positive for TMRM that tightly followed the contours of mitochondrial membranes (b). This mask was taken forward for part 2 (**Figure 28**) to isolate positive signal.

2.12.7.2 Isolation of positive signal

The second duplicate Z-stack was compressed into a single 2D image using the "Z-projection" function with "sum slices" (**Figure 28a**). The mask image from **2.12.7.1** was then subtracted from this using "image calculator", generating an image showing only positive signal within those masked regions (**Figure 28b**). Cells were manually selected from this positive signal image using the "freehand selection" tool and saved as individual ROIs (**Figure 28c**). 20 cells were selected per experimental group, per repeat, with up to 5 cells selected per image.

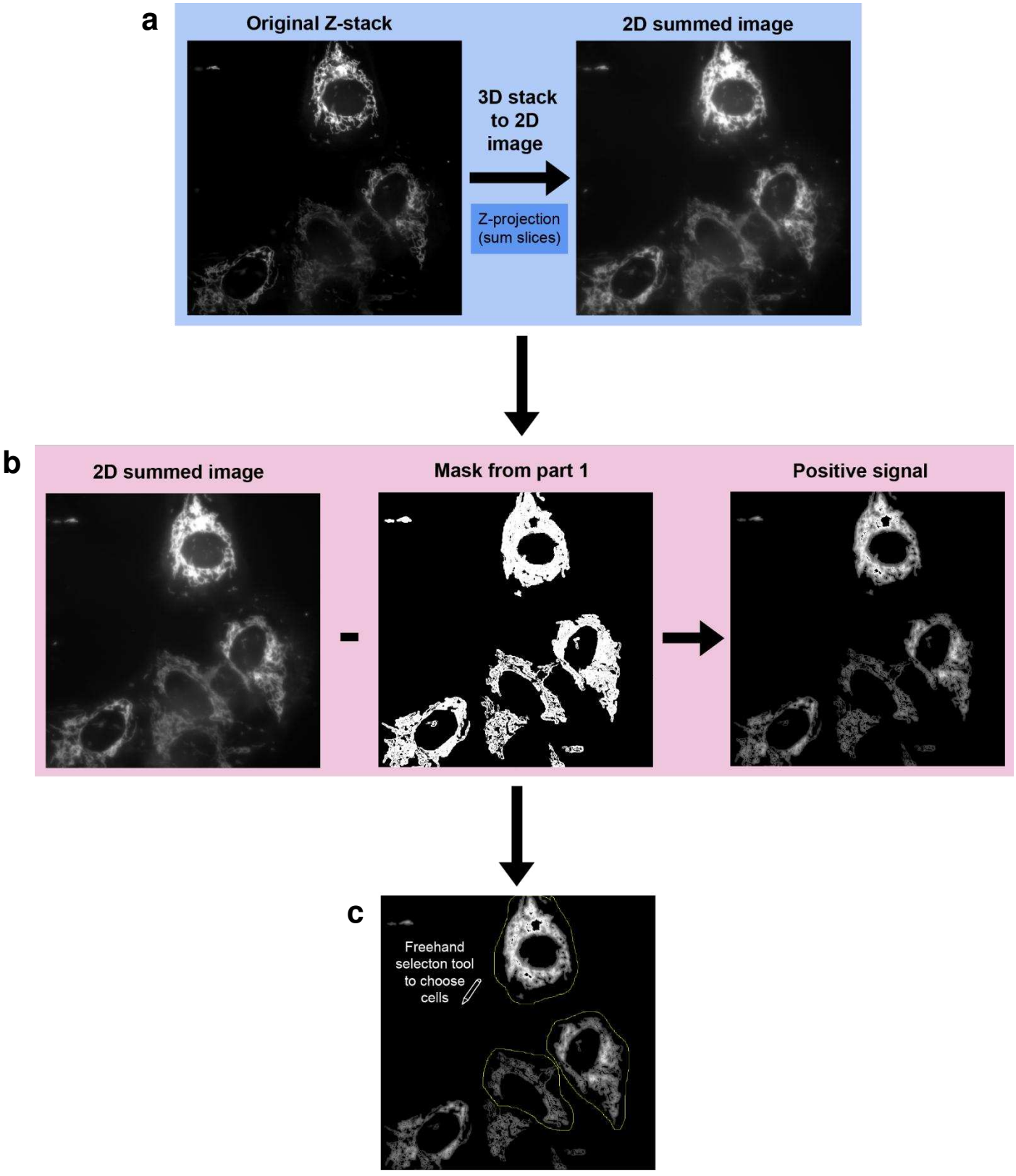
a
Original Z-stack
2D summed image
3D stack to 2D image
Z-projection (sum slices)
b
2D summed image
Mask from part 1
Positive signal
c
Freehand selecton tool to choose cells

Figure 28: TMRM fluorescence intensity analysis part 2: isolating positive signal & selecting cells

To measure fluorescence intensity of TMRM staining in individual cells, the mask created in part 1 (**Figure 27**) was used to isolate only TMRM-positive pixels. Raw Z-stacks were compressed to 2D images using "sum slices" (a), and the mitochondrial mask was then subtracted to leave an image showing positive signal, tightly following the contours of mitochondrial membranes specified by the mask (b). The "freehand selection" tool was then used to manually draw around individual cells, with each cell outline saved as an ROI (c). These selected ROIs were then analysed in part 3 (**Figure 29**).

2.12.7.3 Isolation of cells & histogram analysis

Individual ROIs were overlayed onto the image, filled and inverted to create a mask. This mask was used with the "image calculator" tool to subtract this from the rest of the image, leaving behind an image containing only one cell (**Figure 29**). Pixels were separated into 3 intensity bins: 0, 1-254 and 255. The "fill" tool was used to infill pixels outside the ROI with a maximum intensity of 255 and negatively stained pixels within the bounds of the mitochondrial mask (e.g. gaps between mitochondrial filaments) an intensity of 0. As such, any positive pixels had values of 1-254. The "analyse histogram" function was then used to generate a readout of the distribution of pixel values from 0-255. Intensity information from this histogram was taken forward for analysis.

2.12.7.4 Quantitative intensity analysis

The output of the histogram was the number of pixels attributed to each intensity bin from 0-255. 0 indicated non-positively stained pixels within the mitochondrial network (e.g. gaps between mitochondrial filaments) and 255 indicated background from outside the mitochondrial network (e.g. space between the bounds of the network and the edge of the drawn ROI). Pixels in these 2 bins were discarded from analysis to avoid skewing of data by pixels not positive for TMRM. Pixels between 1-10 were classified as noise, and pixels from 200-254 were discarded as background. This left pixels between 10-200 which were considered to be positive for TMRM and thus were quantified.

The number of pixels in each bin was used to calculate a weighted average, yielding an average image intensity value per cell. Image intensities from each of the 20 cells per group were then used to generate a group mean. SuperPlots were generated from this data to display each individual data point and statistical analysis was carried out.

2.12.7.5 Validation with positive control

To validate that quantitation of TMRM fluorescence intensity could capture a decrease in ΔΨm, intensities were quantified in the same cells before and after the addition of 10μM CCCP. 15 cells were chosen from the pre-treatment image, isolated and quantified as described. The same 15 cells were quantified in images of the same field of view taken 1-10 minutes after the addition of CCCP. The average fluorescence intensity for each cell at each time point was plotted on a graph, enabling visualisation of a decrease in intensity after CCCP. Image intensities from each of the 15 cells were used to generate a mean for each time point. SuperPlots were generated from this data to display each individual data point, shown in **Appendix A** (**Figure 122**).

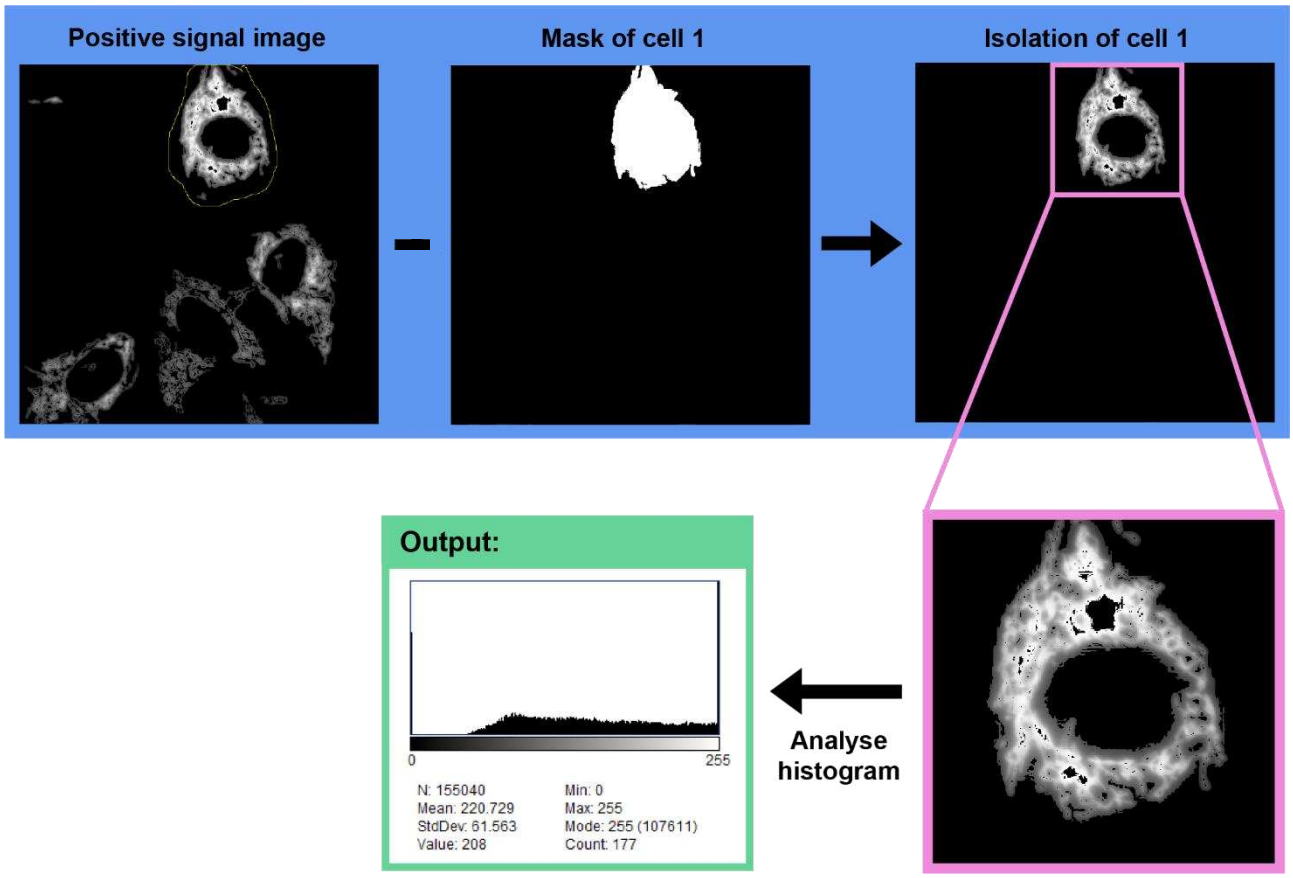

Figure 29: TMRM fluorescence intensity analysis part 3: isolating cells & creating histograms

To measure fluorescence intensity of TMRM staining in individual cells, ROIs from part 2 (**Figure 28**) were used to selectively isolate cells for analysis. By filling these ROIs, creating masks and subtracting these from the thresholded image, individual cells could be isolated to leave images containing only one cell, ready for analysis. The "fill" tool was used to give pixels outside the cell an intensity of 255 and pixels in gaps within the mitochondrial network an intensity of 0, leaving positively stained mitochondrial pixels between 1 and 254. A visual representation of this was generated using "analyse histogram" and the values from this were inputted into excel for further analysis.

2.12.8 Neuronal analysis

To evaluate the morphology of differentiated cells, immunofluorescence microscopy images of cells stained with B-III-tubulin and DAPI were analysed with ImageJ®.

2.12.8.1 Neurite measurements

To measure the number of neurites for each cell, B-III-tubulin and DAPI images were merged to allow identification of individual cells. The "multi-point" tool was then used to label individual neurites, defined as B-III-tubulin-positive projections from the cell body (**Figure 30a**). The number of neurites was counted for 20 cells per experimental group, per repeat, and the mean of each group was taken to give the average number of neurites per cell and statistically analysed.

To measure the length of the primary neurite in each cell, images showing B-III-tubulin were opened with the "NeuronJ" plugin which enables precise tracing of neurite paths. The "add tracings" command was used to select individual neurites to be measured. For the longest neurite in each cell, the first tracing point was placed at the edge of the cell body and the final tracing point was placed at the end of the neurite. The "measure tracings" command was used to generate the lengths of each traced neurite (**Figure 30b**). Primary neurite length was measured for 20 cells per experimental group, per repeat, and the mean of each group was taken to give the average primary neurite length per cell and statistically analysed.

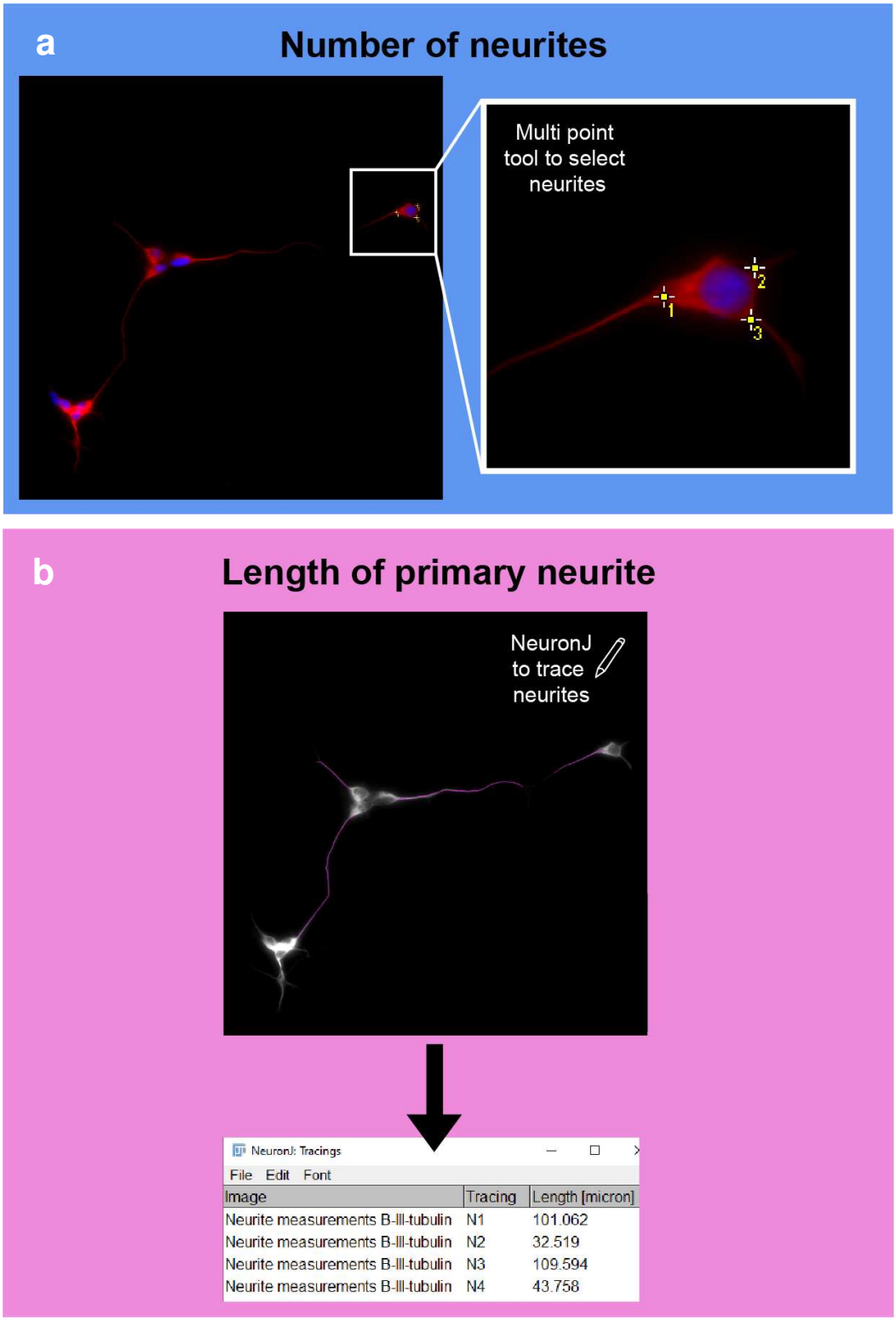

Figure 30: Steps for measuring neurites in differentiated cells with ImageJ®

a) To measure the number of neurites per differentiated cell, B-III-tubulin and DAPI images were merged and the “multi-point” tool was used to select individual B-III-tubulin-positive projections from the cell body.

b) To measure the length of the primary neurite, the “NeuronJ” plugin was used to trace the longest B-III-tubulin-positive neurite in each cell. The “measure tracings” command was used to measure the length of each tracing.

2.12.8.2 Nuclear measurements

To measure nuclear morphology in differentiated cells, DAPI images were first thresholded. The "subtract background" command was used with a rolling ball size of 50 to remove uneven background and then the "auto threshold" command was used since DAPI staining was generally very clean. Merged images showing DAPI staining with B-III-tubulin staining were then opened alongside this thresholded image to visualise differentiated cells, ensuring that in the next steps only nuclei in cells with B-III-tubulin-positive neurites were selected. Nuclei from individual differentiated cells were selected using the "freeform selection" tool, with each being added individually to the ROI manager. 20 cells were selected per experimental group, per repeat, with up to 5 cells selected per image. Care was taken to only select nuclear staining which had a clear boundary and were not touching nuclear staining from other cells.

For a given image, all ROIs were then overlayed onto the image, filled and inverted to create a mask. This mask was used with the "image calculator" tool to subtract the staining within ROIs from the rest of the image, leaving only an image with the cells of interest. Individual cells were isolated from the rest of this image in the same way: an individual ROI was overlayed onto the image, filled and inverted to create a mask which was then subtracted from the image, leaving an image containing only one cell. The "analyse particles" command was used on these images to generate readouts of nuclear morphology. A summary of this process is shown in **Figure 31**. Nuclear area and aspect ratio were measured for 20 cells per experimental group, per repeat and statistically analysed.

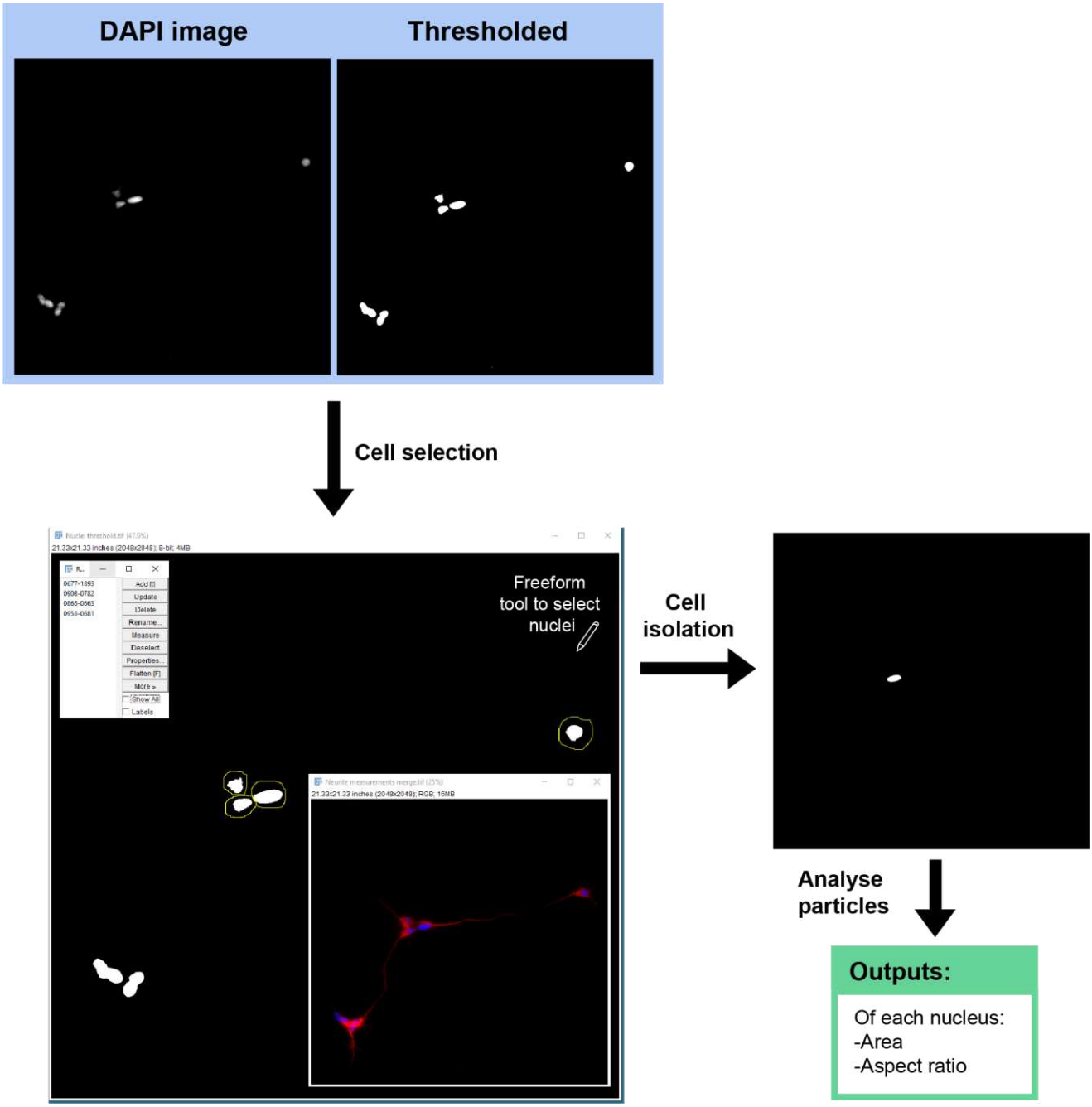

Figure 31: Steps for measuring nuclear morphology in differentiated cells with ImageJ®

To measure nuclear morphology, DAPI staining was first thresholded to create a clean, binary image. The "freeform selection" tool was used manually draw around nuclei and each was saved as an ROI. A merged image of DAPI with B-III-tubulin staining was opened alongside the thresholded DAPI image to ensure that only cells considered differentiated were selected. By filling these ROIs, creating masks and subtracting these from the thresholded image, nuclei from individual cells could be isolated to leave images containing only one cell nucleus, ready for analysis. This image was directly assessed using "analyse particles" to generate morphology measurements of area and

2.12.9 Generation of SuperPlots

For all measurements generated from immunofluorescence microscopy images, data was presented as a SuperPlot. A SuperPlot describes a graph which displays all data colour coded by repeat to enhance communication of the experimental design and results. This enables the reader to visualise technical and biological replicates, though does sometimes reveal inconsistencies between replicates (e.g. as in **Figure 79**). SuperPlots were generated with GraphPad Prism based on Lord et al. (2020) by overlaying 2 graphs: one displaying each data point and one displaying means and SEM, both coded with the same colours (**Figure 32**).

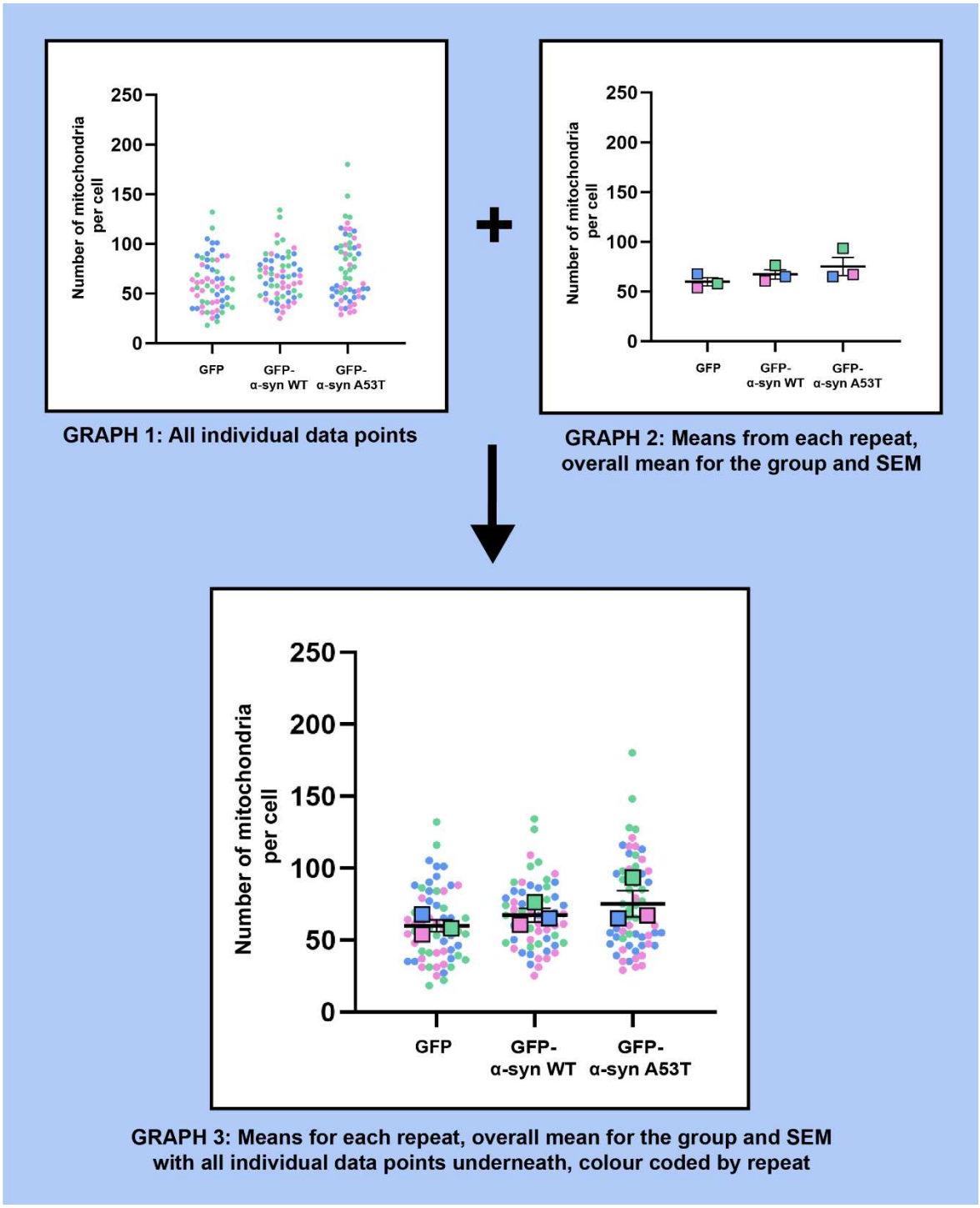

Figure 32: Generation of SuperPlots using GraphPad Prism

To generate SuperPlots, two individual graphs were created and then overlayed. Firstly, a graph displaying all individual data points was made, with data points colour coded by biological repeat. Secondly, a graph displaying the means of each group, the overall mean from the 3 biological repeats and the SEM. Means were colour coded by biological repeat in the same way. These graphs were then overlayed to show all this information on a single set of axes.

2.13 Statistical analysis

Statistical analysis was performed on all quantitative data with at least 3 biological repeats using GraphPad Prism 10 for Windows (Boston, Massachusetts, USA). Parametric tests were carried out on means where data was approximately normally distributed and had equal variance.

Different tests were performed dependent on the number of groups and variables being analysed. T-tests were used when analysing how one factor (e.g. cell line) affects a response variable in 2 groups. One-way ANOVAs were used when analysing how one factor (e.g. cell line) affects a response variable in 3 or more groups. 2-way ANOVAs were used when analysing how two factors (e.g. cell line and A/O treatment) affect a response variable in 3 or more groups. With ANOVAs, post-hoc tests were used for multiple comparisons tests as recommended by the software. Tukey's test was used to compare every mean was with every other mean. Sídák's test was used when selected means were compared with each other.

For most analyses, pairing (t-tests) or repeated measures (ANOVAs) were used to signify those particular values came from the same experimental groups. For example, values from the same cell line would be matched, and values from the same biological repeat would be matched. This enables the software to compare means knowing which values came from which biological repeat, adding power to the analysis.

Differences between groups where $p<0.05$ were considered statistically significant. Significant differences between groups are indicated on graphs throughout using stars: * = $p<0.05$, ** = $p<0.01$, *** = $p<0.001$, **** = $p<0.0001$.

Chapter 3 Investigating the role of endogenous α-synuclein in mitochondrial health and quality control

3.1 Introduction

The majority of literature on α-synuclein in PD has hypothesised that its neurotoxicity is the result of toxic gain-of-function: pathological α-synuclein is aggregating and exhibiting new functions that allow it to disrupt cell health (Betzer et al., 2018; Chen et al., 2015; Di Maio et al., 2016; Hoffmann et al., 2019). The idea that a loss-of-function of endogenous α-synuclein may be responsible for these pathological changes has not been well explored. Some research has addressed this, with a lack of α-synuclein shown to cause neuronal degeneration in non-human primates and disrupt normal immune responses in mouse models (Alam et al., 2022; Collier et al., 2016). However, current investigations have not explored whether α-synuclein loss-of-function could contribute to the mitochondrial dysfunction observed in PD patients and models (Bender et al., 2006; Devi et al., 2008; Martin et al., 2006).

Physiological α-synuclein has known functions in neuronal cells, regulating key signalling processes required for communication. Enriched at pre-synaptic terminals, α-synuclein has defined roles in co-ordinating vesicle recycling, facilitating neurotransmitter release and modulating synaptic plasticity (Burré, 2015; Cheng et al., 2011). Aside from localising and operating at synapses, α-synuclein has been shown to associate with mitochondria (Nakamura et al., 2008). Interestingly, α-synuclein has exhibited a preferential binding affinity for mitochondrial membranes over those of other organelles, and has even been suggested to have a mitochondrial-targeting sequence in its N-terminus; the structural segment involved in lipid binding (Bernal-Conde et al., 2020; Devi et al., 2008; Nakamura et al., 2008 et al., 2020). In addition to binding the OMM, α-synuclein has been shown to enter mitochondria through the TOM complex, facilitating interactions with IMM proteins such as cardiolipin and notably, the key respiratory enzyme ATP synthase (Devi et al., 2008; Ghio et al., 2016; Gilmozzi et al., 2020; Tripathi & Chattopadhyay, 2019). These observations suggest a functional interaction between α-synuclein and mitochondria.

The role of α-synuclein in synaptic vesicle release and recycling relies on its interactions with phospholipid membranes; α-synuclein's ability to remodel these structures enables membrane fusion and subsequent exocytosis of vesicles (Huang et al., 2019; Snead & Eliezer, 2014). Alongside its ability to bind mitochondria, the capacity of α-synuclein to reshape and

restructure membranes raises questions about whether it could function physiologically in mito-QC, since these systems rely on the remodelling of mitochondrial membranes. For example, the key processes co-ordinating mitochondrial morphology, fission and fusion, rely on the selective division and connection of mitochondrial membranes, with membrane-bound machinery to facilitate this (Franchino et al., 2024; Ugarte-Uribe et al., 2014; von der Malsburg et al., 2023). In addition, the biogenesis of MDVs relies on membrane budding and scission; both of which require remodelling of at least one mitochondrial membrane (Neuspiel et al., 2008; Soubannier et al., 2012a). As such, mitochondrial α-synuclein could conceivably function in these pathways through its membrane-remodelling capacity.

In this chapter I aimed to test the hypothesis that α-synuclein loss-of-function alters mitochondrial function and quality control, and that loss of physiological α-synuclein function leads to pathological consequences for mitochondria in PD. Here, I used SH-SY5Y cells to investigate the role of endogenous α-synuclein in mitochondrial health, dynamics and mito-QC. To examine the impact of α-synuclein loss-of-function, I used CRISPR/Cas9 to generate an α-synuclein knockout cell line and assessed cellular responses to mitochondrial damage.

Aims:

1) Develop a model of α-synuclein loss-of-function in SH-SY5Y cells
2) Utilise the α-synuclein loss-of-function model to assess whether α-synuclein has a physiological role in mitochondrial function and dynamics
3) Utilise the α-synuclein loss-of-function model to assess α-synuclein's physiological role in mito-QC

3.2 Results

3.2.1 SH-SY5Y cells express endogenous α-synuclein

SH-SY5Y cells are an immortal cell line created in 1970, originating from a metastatic neuroblastoma (Biedler et al., 1973, 1978). These cells have some similarities to the those degenerated in PD and as such, are widely used in PD research (Xicoy et al., 2017). They can be differentiated to enhance their neuronal phenotype but are often used in their undifferentiated form, where they express immature neuronal markers but still proliferate (Kovalevich & Langford, 2013; Påhlman et al., 1995). Previous research from our lab has used SH-SY5Y cells to investigate mito-QC mechanisms, since they express physiological levels of key proteins such as PINK1 and Parkin (Pawlyk et al., 2003). Importantly, they have been shown to undergo PINK/Parkin-dependent mechanisms such as mitophagy and MDV release without requiring overexpression of these proteins (Ryan et al., 2020; Collier et al., in prep). As such, they are a useful model for studying these pathways physiologically, without the need for artificial intervention.

The Human Protein Atlas reports that SH-SY5Y cells express endogenous α-synuclein, so they were our chosen candidate for creating an α-synuclein loss-of-function model (Thul et al., 2017). These cells have relatively low expression of the protein compared to other neuroblastoma cell lines, so I first aimed to characterise endogenous α-synuclein in wild-type SH-SY5Y cells (Thul et al., 2017).

A Western blot was performed to confirm the expression of α-synuclein in proliferating SH-SY5Y cells. The cells expressed endogenous α-synuclein, as seen by the presence of a band at approximately 18kDa (**Figure 33**). Though the protein is 14kDa in size, it appears slightly higher, as previously reported in the literature (Huang et al., 2005). This detectable expression confirmed that the SH-SY5Y cell line would be suitable to create a loss-of-function model.

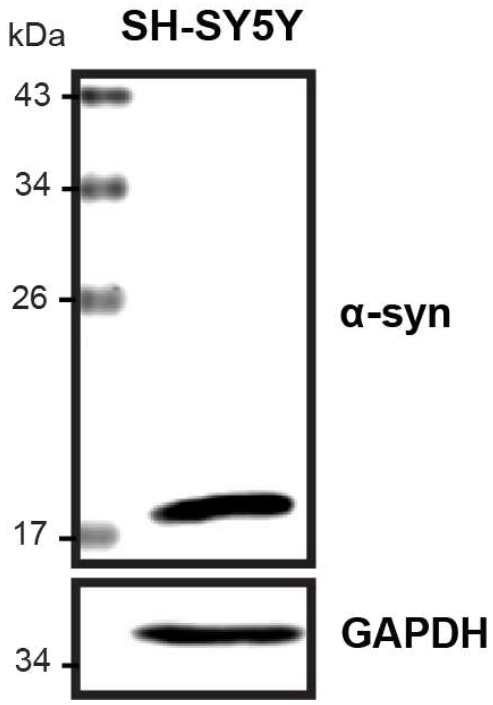

Figure 33: SH-SY5Y cells express endogenous α-synuclein

Wild-type SH-SY5Y cells were lysed and protein expression was assessed by Western blot with antibodies against α-synuclein and GAPDH as a protein loading control. (**n=1**).

3.2.2 Mitochondrial damage triggers degradation of endogenous α-synuclein by proteasomal and autophagic mechanisms

Limited research has explored the relationship between endogenous α-synuclein and mito-QC. Accordingly, the impact of mitochondrial damage on physiological α-synuclein is not clear from the literature, as most work is focused on pathological forms of the protein (Lin et al., 2019; Melo et al., 2018). After establishing that SH-SY5Y cells expressed a detectable level of α-synuclein, I next aimed to investigate whether inflicting mitochondrial damage caused any direct changes to α-synuclein expression.

To examine this, a Western blot was performed to assess any changes in the expression of α-synuclein in response to mitochondrial damage. This was evoked with a combination of antimycin A and oligomycin (A/O): a complex III inhibitor and ATP synthase inhibitor, respectively (Lardy et al., 1958; Ma et al., 2011). Treatment with these compounds is known to induce mitochondrial damage via disruption of the electron transport chain, with previous work from our lab showing that these treatment times enable observation of MDV upregulation (2 hours), PINK1/Parkin induction (6 hours) and whole mitochondrial clearance (24 hours) (McLelland et al., 2014; Ryan et al., 2020, Collier et al., in prep). Therefore, these treatment

times were chosen to capture changes in α-synuclein expression over a course of accrued damage.

Treatment of cells with A/O was shown to decrease expression of endogenous α-synuclein compared to untreated cells (**Figure 34**). Longer treatment times resulted in lower α-synuclein levels, with cells treated for 24 hours expressing significantly less α-synuclein than cells left untreated (p=0.0023) or treated for 2 hours (p=0.0059). This reduction in expression is reflective of α-synuclein degradation in response to mitochondrial damage.

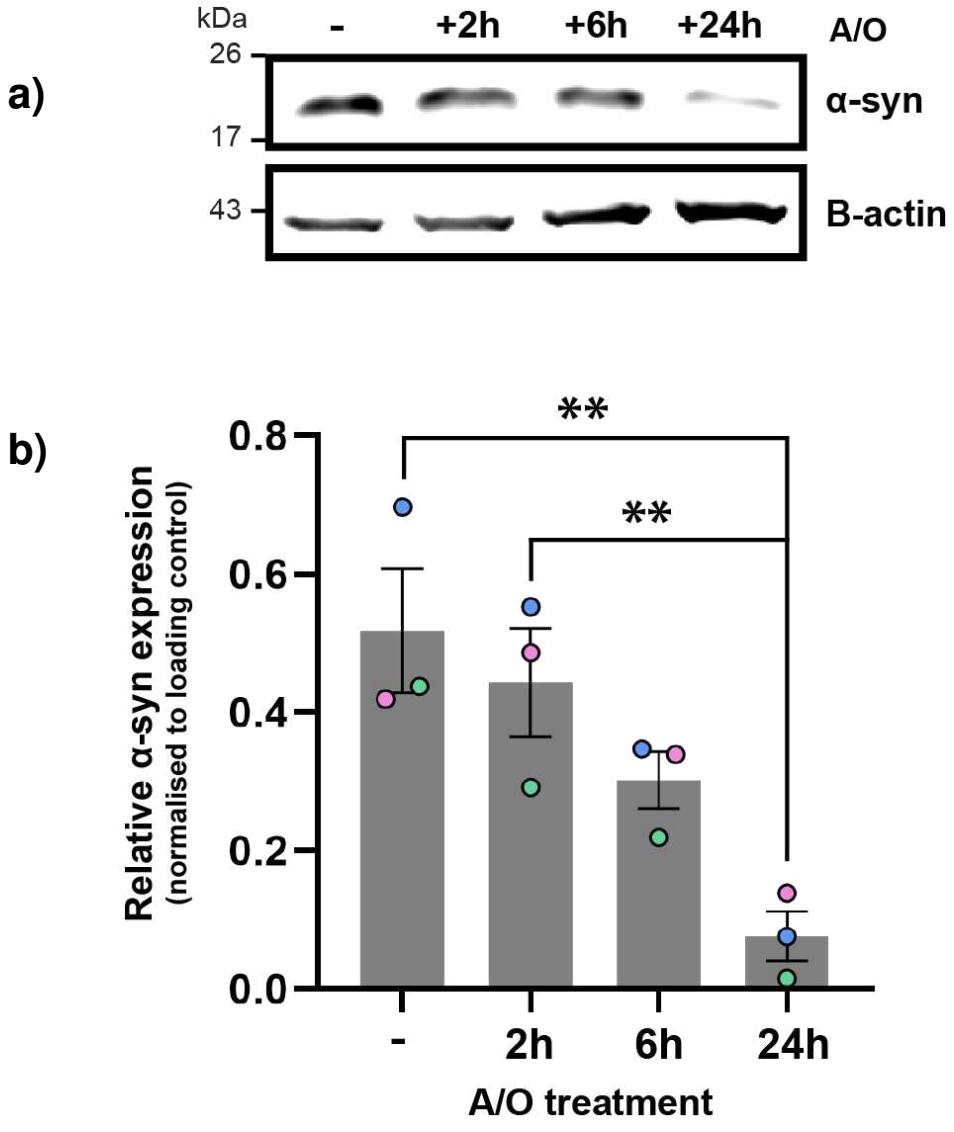

Figure 34: α-synuclein expression is decreased in response to mitochondrial damage

a) Wild-type SH-SY5Y cells were left untreated (-) or treated for 2 hours, 6 hours or 24 hours with A/O to induce mitochondrial damage. Lysates were processed for Western blot with antibodies against α-synuclein and B-actin as a protein loading control.

b) From Western blot data, α-synuclein expression in response to A/O treatment was normalised to B-actin expression to account for differences in protein loading. α-synuclein expression is represented here by the raw values of this calculation. Biological repeats are colour coded, with circles representing the means of each repeat, bars representing the mean of the 3 repeats and black lines representing the SEM. Statistical analysis was performed using a repeated measures one-way ANOVA with Tukey's multiple comparisons test. Significant differences: untreated V 24-hour A/O p=0.0023 (**); 6-hour A/O V 24h A/O p=0.0059 (**). (**n=3**).

Since I observed that mitochondrial damage had a direct effect on the expression level of endogenous α-synuclein, I considered whether it may have any impact on expression of post-translationally modified forms of α-synuclein. Post-translational modifications have been suggested to be of particular importance in α-synuclein regulation, including in turnover of the protein (Brembati et al., 2023). One example of such a modification is pS129 α-synuclein, which has been highly implicated in PD pathology due to its abundance in the Lewy bodies of PD patients (Anderson et al., 2006). Due to this observation, investigations into pS129 α-synuclein have been focused on its impacts on aggregation in the pathological form of the protein (Ghanem et al., 2022). However, there is evidence to support the incidence of physiological pS129 α-synuclein, with a recent paper finding that pS129 α-synuclein even correlated with α-synuclein membrane interactions (Ramalingam et al., 2023). As such, I investigated the occurrence of endogenous p129 α-synuclein and explored whether its expression may correlate with the mitochondrial damage response.

In the same lysates from asynchronously proliferating SH-SY5Y cells, pS129 α-synuclein was not observed by Western blot, implying that α-synuclein with this post-translational modification was not detectable. In cells treated with A/O for 2, 6, or 24 hours to induce mitochondrial damage, pS129 α-synuclein was still not detected (**Figure 35**). These observations imply that pS129 α-synuclein is not present in measurable levels at baseline was not seen to be upregulated in response to mitochondrial damage or associated with α-synuclein degradation in this context.

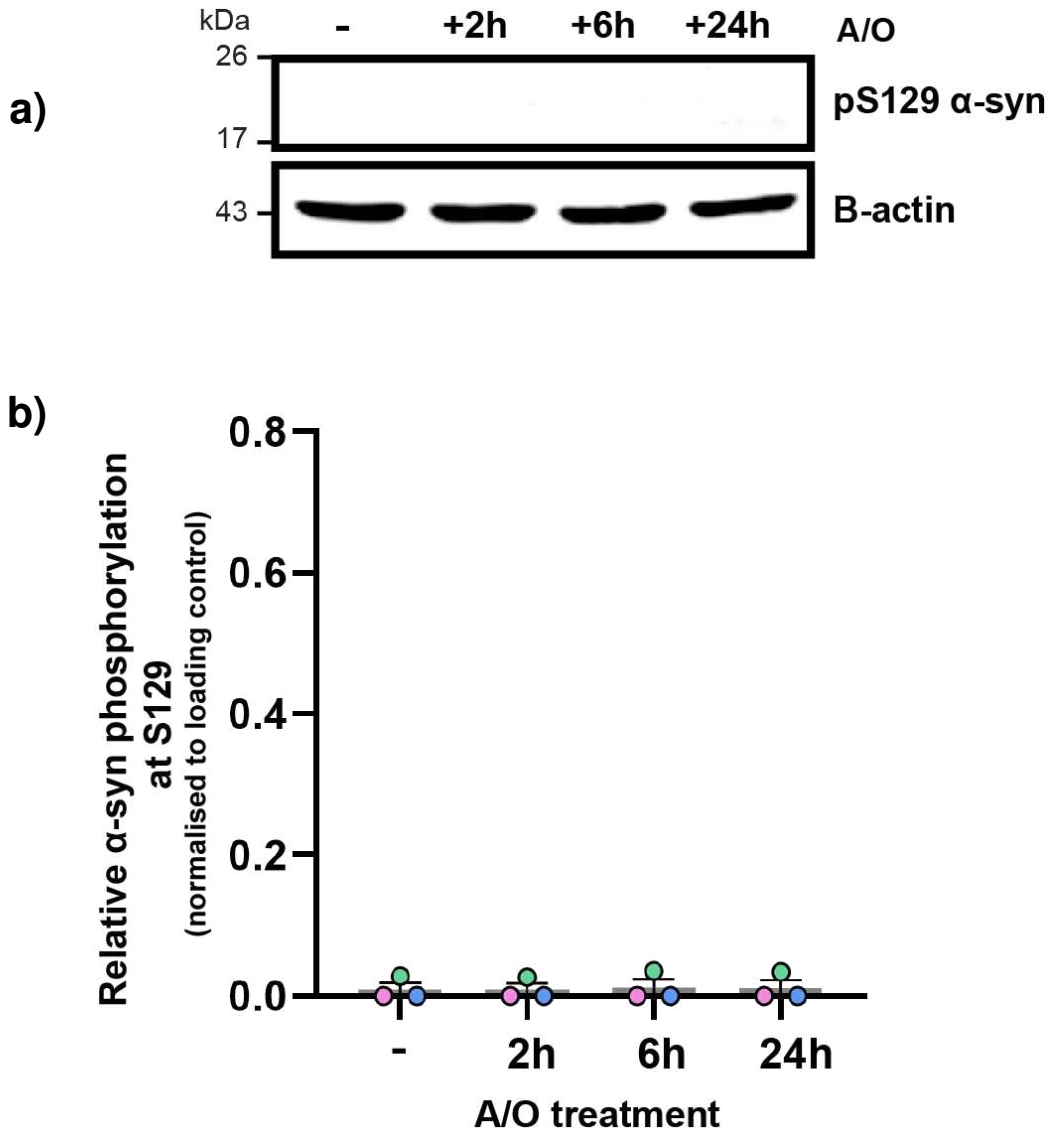

Figure 35: Endogenous phospho-S129 α-synuclein is not detected in wild-type SH-SY5Y cells

a) Wild-type SH-SY5Y cells were left untreated (-) or treated for 2, 6 or 24 hours with A/O to induce mitochondrial damage. Lysates were processed by Western blot with antibodies against phospho-S129 α-synuclein and B-actin as a loading control.

b) Phospho-S129 α-synuclein expression in response to A/O treatment was normalised to B-actin expression to account for differences in protein loading. Expression of phospho-S129 α-synuclein is represented here by the raw values of this calculation. Biological replicates are colour coded, with circles representing the means of each repeat, bars representing the mean of 3 repeats and black lines representing the SEM. (**n=3**).

The observation that endogenous α-synuclein expression was reduced in response to A/O treatment raised questions about which pathways were operating to degrade the protein. Research in rat neuronal cultures has suggested that endogenous α-synuclein is degraded in lysosomes but not through macroautophagic mechanisms, though this was not studied in the context of mitochondrial damage (Cuervo et al., 2004). In the same study, human α-synuclein was shown to be degraded by both macroautophagy and chaperone-mediated autophagy in PC12 cells, but they transfected in wild-type α-synuclein rather than studying the endogenous protein (Cuervo et al., 2004; Stefanis et al., 2001). In order to investigate the mechanisms of endogenous α-synuclein degradation in response to mitochondrial damage, cells were treated with A/O alongside inhibitors of protein degradation systems to assess whether suppression of specific quality control pathways could rescue α-synuclein degradation.

The ubiquitin/proteasome system is a key player in the removal of proteins from the cell, both in degrading dysfunctional and misfolded proteins as well as in the turnover of important regulatory proteins (Hershko & Ciechanover, 1998). Bortezomib (Btz) can be used to block this system, binding the 26S subunit of the proteasome and inhibiting its action (Ling et al., 2002). To examine whether endogenous α-synuclein was degraded by the proteasome in response to mitochondrial stress, cells were treated with A/O and Btz in combination. Proteasomal inhibition rescued the reduction of α-synuclein to some extent; there was still a decrease in α-synuclein with increasing treatment times, but this was less pronounced as compared to A/O alone (**Figure 36**). The lack of a clear stepwise reduction in α-synuclein implies that inhibition of the proteasomal system does rescue some mitochondrial damage-induced α-synuclein degradation.

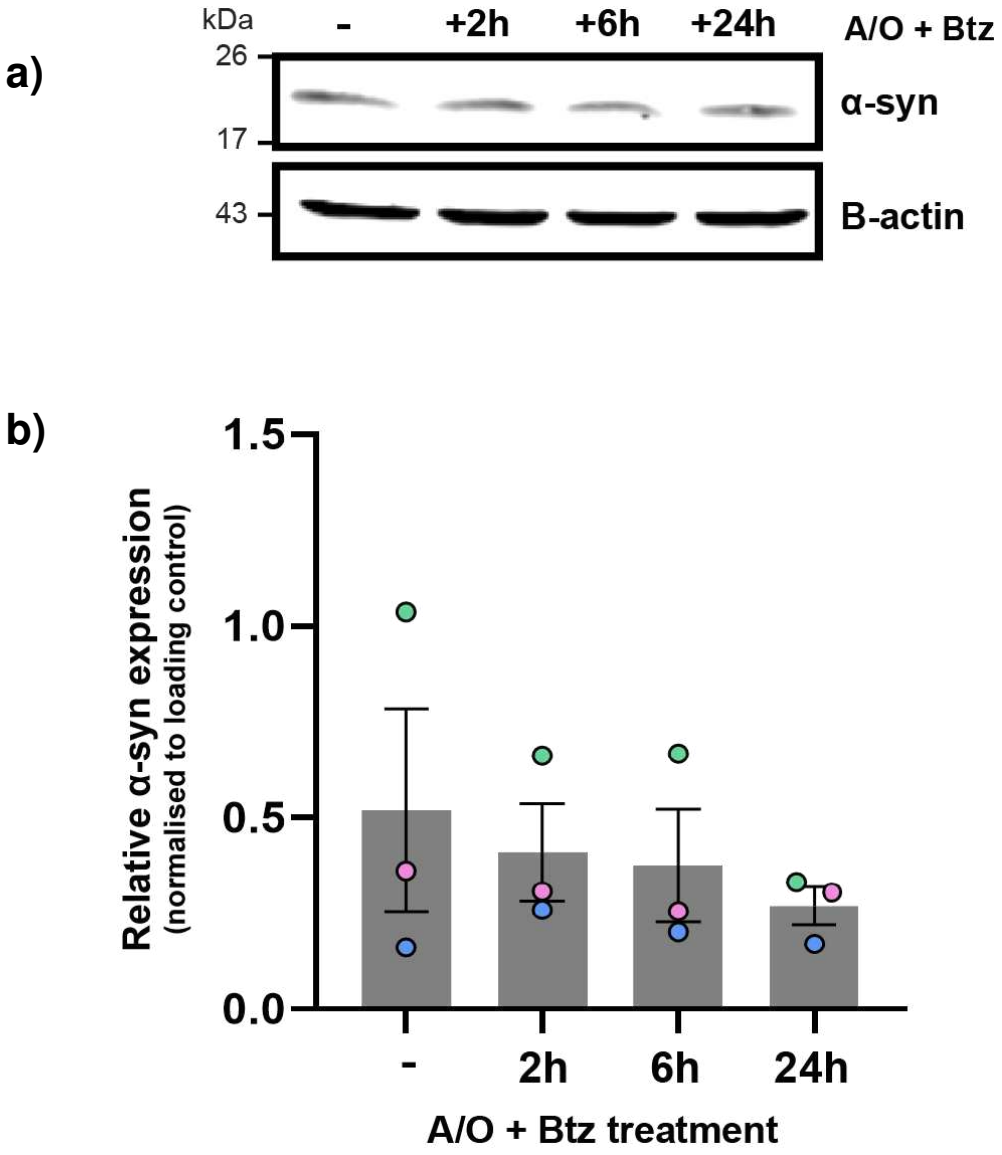

Figure 36: Proteasome inhibition partially rescues a mitochondrial damage-induced reduction in α-synuclein

a) Wild-type SH-SY5Y cells were left untreated (-) or treated for 2, 6 or 24 hours with A/O and Btz to induce mitochondrial damage and inhibit proteasomal activity. Lysates were processed by Western blot with antibodies against α-synuclein and B-actin as a loading control.

b) α-synuclein expression in response to A/O and Btz treatment was normalised to B-actin expression to account for differences in protein loading. α-synuclein expression is represented here by the raw values of this calculation. Biological replicates are colour coded, with circles representing the means of each repeat, bars representing the mean of the 3 repeats and black lines representing the SEM. Statistical analysis was carried out using a repeated measures one-way ANOVA with Tukey's multiple comparisons test. There were no significant differences. (**n=3**).

Another cellular system involved in protein and organelle removal is mitophagy. Like the ubiquitin/proteasome system, this pathway is active basally to maintain organelle health but can also be upregulated in response to stress (Palikaras et al., 2018). This process is mitochondria-specific, so only degrades proteins directly inside, attached to or in very close proximity to these organelles. Like other macroautophagy mechanisms, mitophagy triggers recruitment of autophagosomes to engulf damaged mitochondria and co-ordinate their degradation through lysosomal enzymes (Palikaras et al., 2018). This system can be blocked using BafA1, an inhibitor of the vacuolar H+ ATPase (V-ATPase) that maintains lysosomal pH gradients (Yamamoto et al., 1998). This prevents lysosomal acidification; a necessary step for autophagosomes to bind and facilitate degradation of their contents. As such, BafA1 is considered an inhibitor of autophagosome-lysosome fusion and is used to block autophagic pathways.

To assess whether endogenous α-synuclein was degraded by autophagy pathways in response to mitochondrial stress, cells were treated with a combination of A/O and BafA1. Inhibition of autophagy still resulted in a reduction in α-synuclein expression when cells were treated for 2 or 6 hours, suggesting that some degradation was taking place through non-autophagic systems (**Figure 37**). However, at the longer treatment time of 24 hours, α-synuclein expression was completely rescued back to, or higher than, the level seen in untreated cells. Since the 24-hour time point is where I observed most degradation in cells treated with A/O alone, the rescue in α-synuclein expression identified with BafA1 implies its degradation was likely mediated by lysosomes.

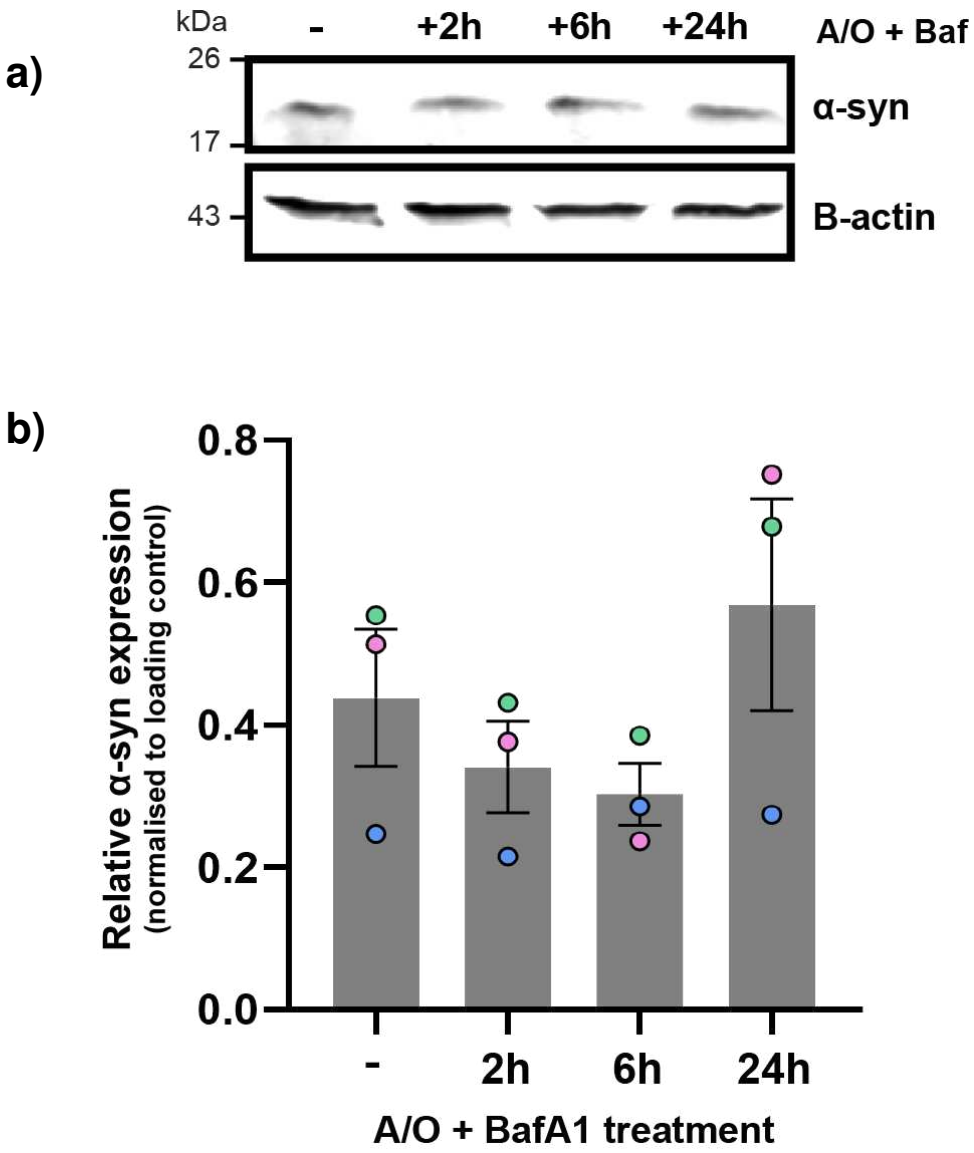

Figure 37: Inhibition of autophagosome-lysosome fusion rescues a mitochondrial damage-induced reduction in α-synuclein

a) Wild-type SH-SY5Y cells were left untreated (-) or treated for 2, 6 or 24 hours with A/O and BafA1 to induce mitochondrial damage and inhibit autophagosome-lysosome fusion. Lysates were processed by Western blot with antibodies against α-synuclein and B-actin as a loading control.

b) α-synuclein expression in response to A/O and BafA1 treatment was normalised to B-actin expression to account for differences in protein loading. α-synuclein expression is represented here by the raw values of this calculation. Biological replicates are colour coded, with circles representing the means of each repeat, bars representing the mean of the 3 repeats and black lines representing the SEM. Statistical analysis was carried out using a repeated measures one-way ANOVA with Tukey's multiple comparisons test. There were no significant differences. (**n=3**).

3.2.3 Endogenous α-synuclein is not detectable in isolated mitochondria

Since I demonstrated that mitochondrial damage-induced α-synuclein degradation was rescued with inhibition of autophagy, I hypothesised that α-synuclein removal may be occurring through the mitophagy pathway. To investigate whether α-synuclein was localised to mitochondria at baseline or as part of the damage response, mitochondrial fractionation was performed, resulting in biochemical separation of mitochondrial and cytosolic cell content. To look at the impact of mitochondrial damage, cells were treated for 6 hours with A/O – enough time for the induction of mitophagy but not so long that most mitochondrial proteins were already degraded. Western blots were then performed on lysates containing isolated mitochondrial fractions.

Successful isolation was confirmed since enrichment of the mitochondrial marker, CoxII, was observed in the mitochondrial fractions and not the cytosolic fractions. Cytosolic markers such as vinculin and α-tubulin were greatly increased in the cytosol and were barely detected in the mitochondrial fractions, further corroborating the selectivity of the isolation protocol (**Figure 38**). In terms of α-synuclein, a low level of protein was visible in the whole-cell lysate from both the untreated and A/O treated cells. Aside from this, the only α-synuclein detected was in the cytosolic fraction of the untreated cells, but at a very low level. No endogenous α-synuclein was visible in either mitochondrial fraction, suggesting that its association with mitochondria was not detected using this method.

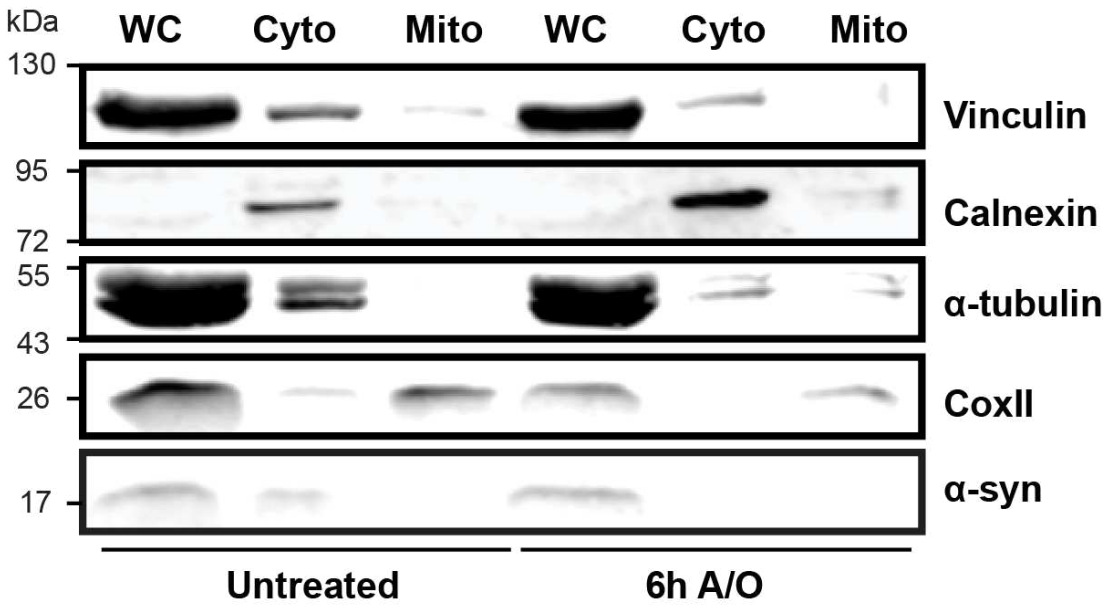

Figure 38: Endogenous α-synuclein was not detected in isolated mitochondria

Wild-type SH-SY5Y cells were left untreated or treated for 6 hours with A/O to induce mitochondrial damage. Mitochondrial and cytosolic fractions were isolated from cells and a whole-cell lysate was generated from the same cell population. Lysates were processed by Western blot with antibodies against α-synuclein as well as control proteins from different organelles to confirm isolation of mitochondria: vinculin (cytoplasm), calnexin (ER), α-tubulin (cytoplasm) and CoxII (mitochondria). (WC = whole cell lysate; cyto = cytosolic fraction; mito = mitochondrial fraction). (**n=1**).

3.2.4 Development and validation of an α-synuclein loss-of-function model in SH-SY5Y cells using CRISPR/Cas9

To investigate physiological roles of α-synuclein more directly, CRISPR/Cas9 technology was used to generate an α-synuclein loss-of-function model in SH-SY5Y cells. In this system, a lentiviral vector containing a Cas9 nuclease enzyme is expressed alongside suitable gRNA sequences to target a gene; in this case, the α-synuclein gene, SNCA. The Cas9 enzyme induces a double-stranded DNA break at the site specified by the gRNA – these were designed to be in exon 2 to ensure disruption early-on in the gene sequence. Due to the error-prone repair mechanisms that cells can employ, repair of DNA often results in the use of incorrect bases to fix the sequence and the induction of a mutation that leaves the protein non-functional and so "knocked out" (Jinek et al., 2012; Ran et al., 2013). The CRISPR/Cas9 system relies on this faulty repair mechanism and as such, creates cells with specific gene knockouts (Ran et al., 2013).

Alongside the α-synuclein loss-of-function model, a control cell line was created by transducing wild-type SH-SY5Y cells with the lentiviral vector containing the Cas9 enzyme, but without any gRNA sequences. This cell line was termed "EV" for "empty vector" and was used as a control to ensure that any differences in phenotypes were the result of the gene knockout rather than any features of the lentiviral process.

The CRISPR/Cas9 system very efficiently knocked out the functionality of the SNCA gene with two separate gRNAs that targeted different regions within exon 2. Western blot analysis showed that α-synuclein was completely undetected in these cells (**Figure 39**). Since they were observed to be 100% knockout, they are referred to as "SNCA KO".

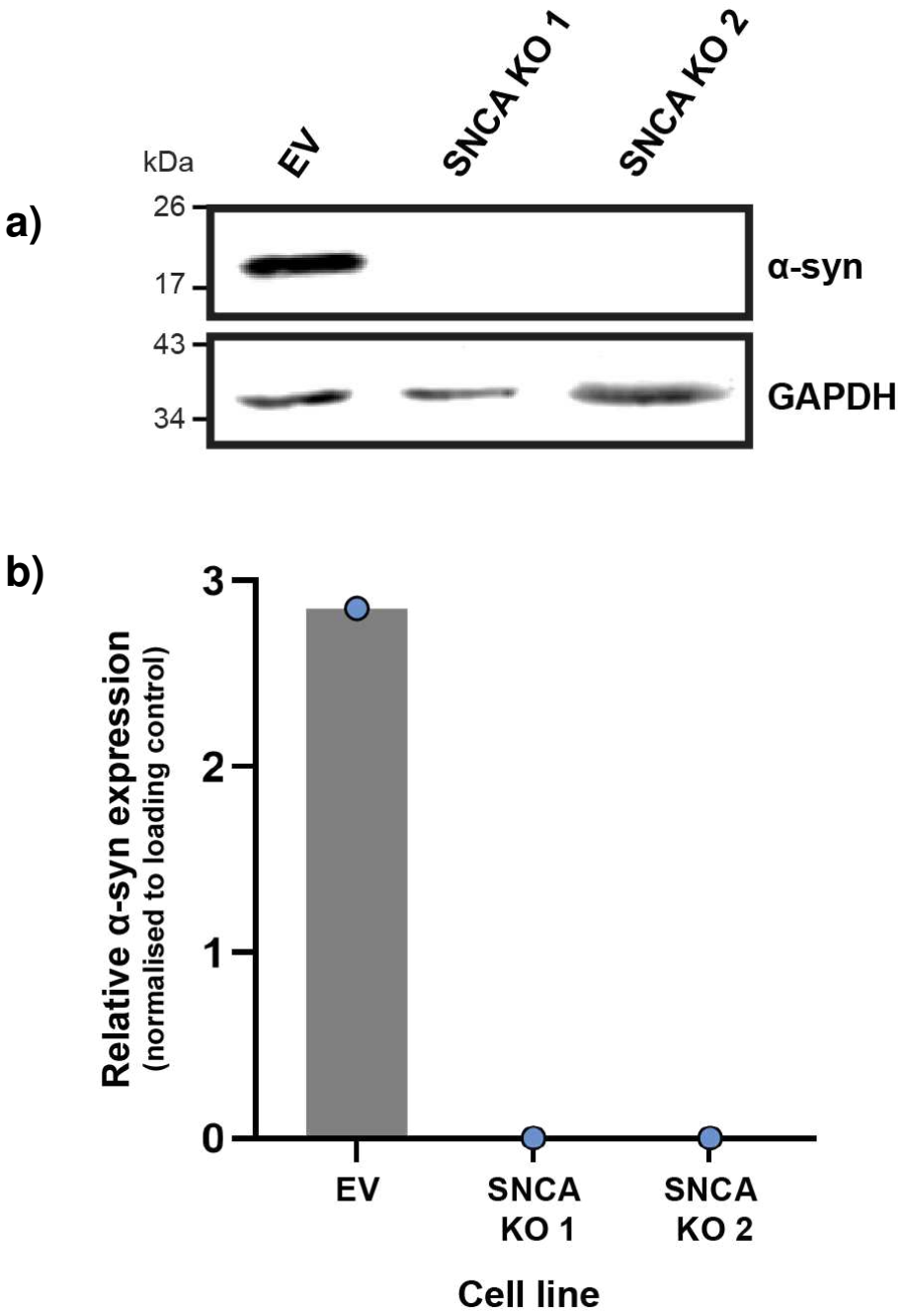

Figure 39: α-synuclein expression is eliminated in SNCA KO cells

a) Wild-type SH-SY5Y cells were transduced with virus from HEK cells transfected with either lentiviral vector alone (EV) or lentiviral vector with gRNAs targeting the SNCA gene (SNCA KO). Lysates were processed by Western blot with antibodies against α-synuclein and GAPDH as a protein loading control.

b) Expression of α-synuclein was normalised to GAPDH to account for differences in protein loading. Raw values of this calculation are plotted as relative α-synuclein expression. (**n=1**).

Generation of SNCA KO cells also enabled the specificity of antibodies against endogenous α-synuclein to be tested, especially those which were not knockout-validated by their respective companies. After confirming α-synuclein knockout with Western blotting, I verified the specificity of three antibodies: LB509 mouse monoclonal (Santa Cruz), 211 mouse monoclonal (Santa Cruz) and 10842-1-AP rabbit monoclonal (Proteintech). Immunofluorescence imaging revealed that although all three antibodies appeared to show endogenous α-synuclein in EV cells, in fact, the staining detected by both LB509 and 211 antibodies was non-specific (**Figure 40**). This was concluded from the fact that immunofluorescence staining of EV and SNCA KO cells was not visibly different, and the two cell lines could not be distinguished from each other based on this staining. The 10842-1-AP antibody is the only one that showed a visible reduction in cytoplasmic fluorescence signal between EV and SNCA KO cells (**Figure 41**Figure 40). This observation knockout-validated this antibody in my hands since it could be used to distinguish between the presence or absence of α-synuclein by immunofluorescence microscopy.

Based on staining by the 10842-1-AP antibody in EV cells, endogenous α-synuclein is present as diffuse staining across the whole cell and does not appear to localise to any distinct structures. Large, bright puncta are seen inside nuclei, but these can be discounted as non-specific staining as they are still present in the SNCA KO cells.

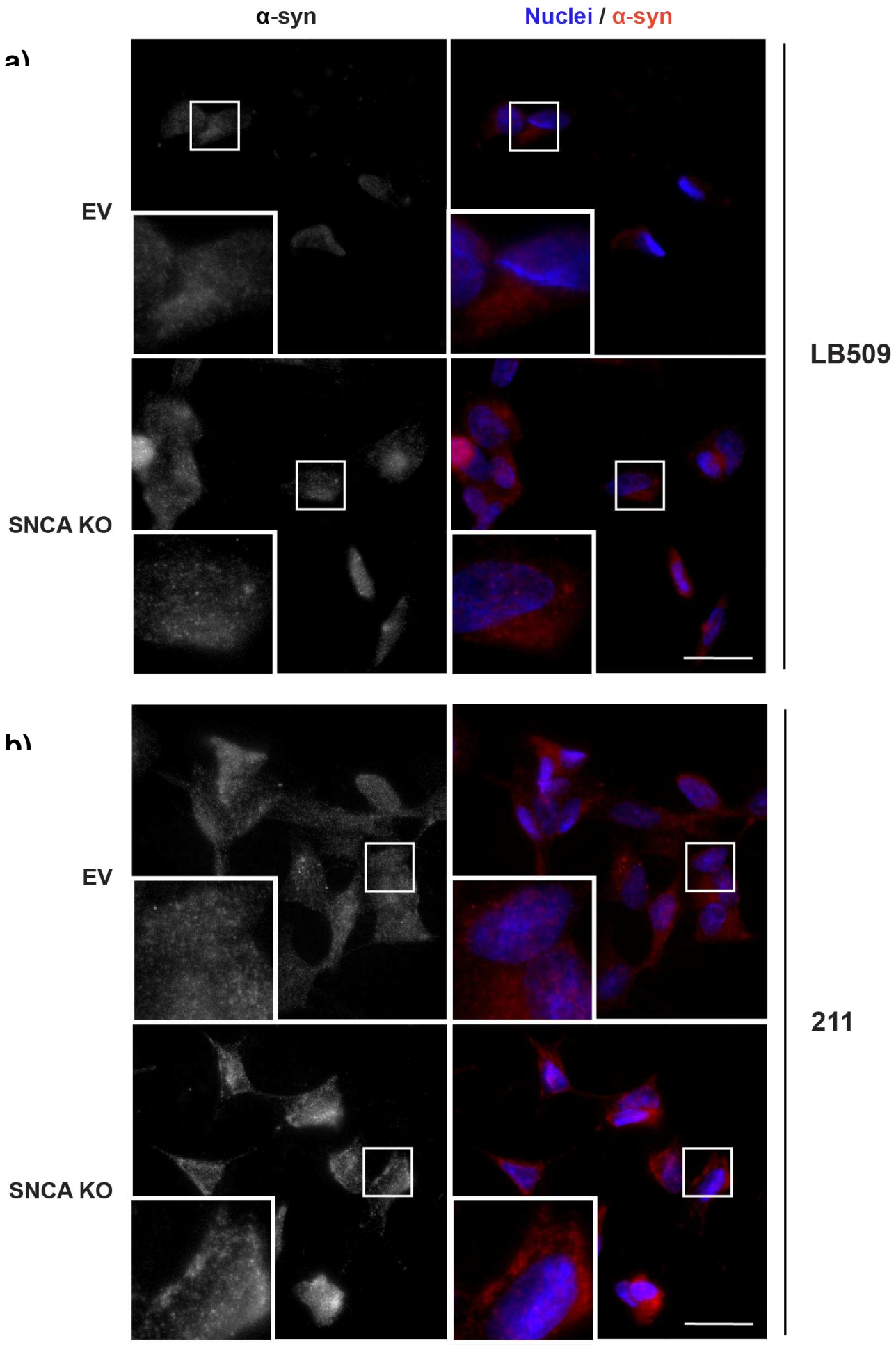
α-syn
Nuclei / α-syn
a)
EV
SNCA KO
LB509
b)
EV
SNCA KO
211

Figure 40: LB509 and 211 mouse monoclonal antibodies are not selective for endogenous α-synuclein by immunofluorescence microscopy

EV and SNCA KO cells were fixed and immunostained with antibodies against α-synuclein (red): a) LB509; b) 211. Nuclei were labelled with Hoechst (blue). Images were taken using widefield immunofluorescence microscopy on a 100X objective. Scale bar = 20µm. Figure shows representative images. (**n=1**).

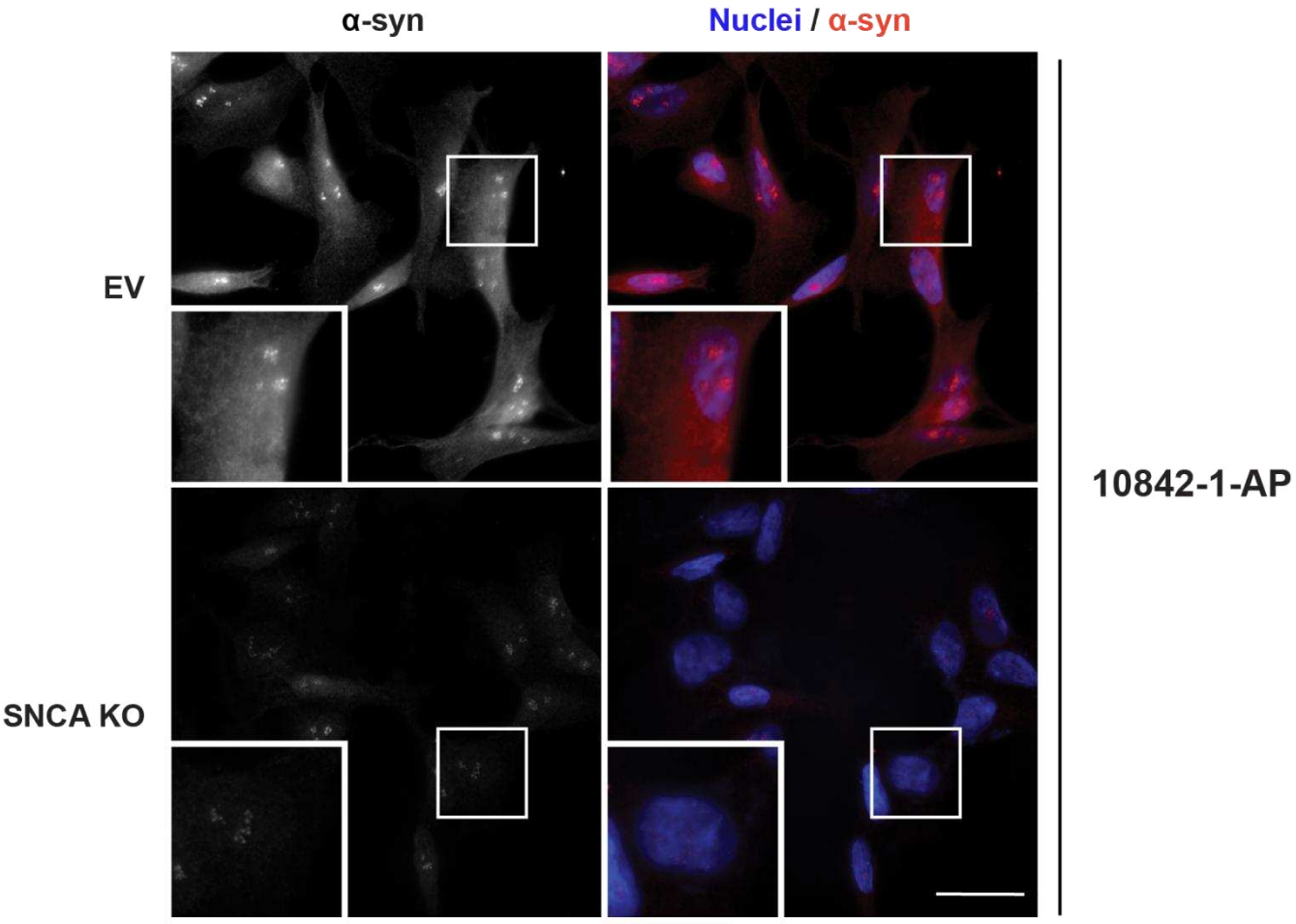

Figure 41: The 10842-1-AP rabbit polyclonal antibody is selective for endogenous α-synuclein by immunofluorescence microscopy

EV and SNCA KO cells were fixed and immunostained with antibodies against α-synuclein (red). Nuclei were labelled with Hoechst (blue). Images were taken using widefield immunofluorescence microscopy on a 100X objective. Scale bar = 20µm. Figure shows representative images (**n=1**).

3.2.5 Lack of α-synuclein increases mitochondrial energy production through glycolytic pathways

The production of ATP is widely considered to be the primary function of mitochondria. The ATP they create is a major source of energy, fuelling metabolic reactions and regulatory processes required for cell survival (Schapira, 2006). It relies on the movement of electrons through a series of transport proteins embedded in the IMM, ending with the generation of energy molecules by the ATP synthase pump (Nunnari & Suomalainen, 2012). This key process can be disrupted when mitochondria are not healthy, with ATP production directly affected. For example, cells from PD patients with mutations in PINK1 and Parkin were shown to experience electron transport chain dysfunction and decreased ATP production (Abramov et al., 2010; Mortiboys et al., 2008; Rakovic et al., 2010). Investigating ATP production is a direct readout of mitochondrial function and health, so measuring this in my SNCA KO model would demonstrate whether α-synuclein loss-of-function has any impact on bioenergetics.

Interestingly, α-synuclein has been shown to interact with ATP synthase; a key determinant of ATP production (Ludtmann et al., 2016, 2018; Tripathi & Chattopadhyay, 2019). As well as evidence that oligomeric α-synuclein binds ATP synthase and induces mitochondrial damage, research has found that monomeric α-synuclein also interacts with the pump to positively modulate its function (Ludtmann et al., 2016, 2018). Further, this study found that lack of α-synuclein reduced ATP levels, proposing a potential physiological function for α-synuclein in regulating mitochondrial energy production (Ludtmann et al., 2016). I wanted to test this hypothesis in my loss-of-function model to see whether I could recapitulate these observations.

Firstly, a luminescence-based assay was performed to capture any overall changes to ATP level. In this method, cells are cultured under specific media conditions to manipulate ATP production pathways, allowing measurement of ATP produced by the glucose-conversion pathway, glycolysis, and mitochondrial OXPHOS (**Appendix A**, **Figure 117**). Under normal growth conditions, cells are able to generate ATP by OXPHOS and by metabolising glucose through glycolysis. Conditions can be manipulated so that cells can only use the glycolytic pathway by inhibiting OXPHOS with the ATP synthase inhibitor, oligomycin (Lardy et al., 1958). Conversely, cells can be grown in galactose media, where they have no glucose available for glycolysis and thus can only generate ATP through OXPHOS (Rossignol et al., 2004). When oligomycin is added to these conditions, this inhibits OXPHOS and thus leaves cells unable to generate ATP through either pathway. This assay therefore provides insight into ATP production through both mitochondrial and non-mitochondrial means.

EV and SNCA KO cells were cultured under these different media conditions, and ATP levels were measured by luminescence. In EV cells, ATP levels were almost equal whether cells used glycolysis (glucose + oligomycin), OXPHOS (galactose) or both (glucose) (**Figure 42a**). In SNCA KO cells, ATP levels produced with OXPHOS (galactose) were significantly lower ($p=0.0214$) than with glycolysis (glucose + oligomycin) (**Figure 42b**). When both pathways were inhibited (galactose + oligomycin), ATP levels significantly dropped as expected in both cell lines ($p<0.0001$) (**Figure 42**). Comparatively, SNCA KO cells were seen to produce significantly more ATP by glycolysis alone (glucose + O) and when both pathways were used together (glucose) than EV cells (**Figure 43**). It is interesting to note that this trend holds true in all three biological repeats and suggests that α-synuclein may play a role in ATP production.

Exposing mitochondria to energy-challenging conditions may initiate compensatory mechanisms such as an increase in mitochondrial load to try and boost ATP production. To ensure that this was not the case and was not the cause of changes in ATP levels recorded, expression of the mitochondrial marker, CoxII, was measured as a readout of mitochondrial load. Expression level was deemed similar between cells in different experimental conditions, reflecting no overall change in mitochondrial load **(Figure 43**).

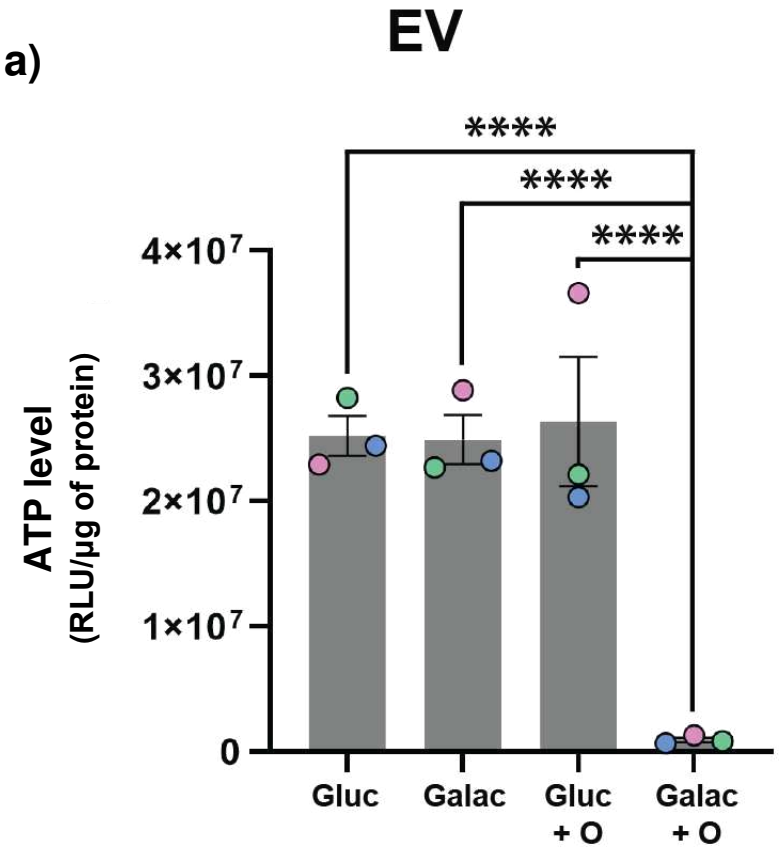
a)
EV
****
****
****
4×10^7
3×10^7
2×10^7
1×10^7
0
ATP level
(RLU/µg of protein)
Gluc
Galac
Gluc + O
Galac + O

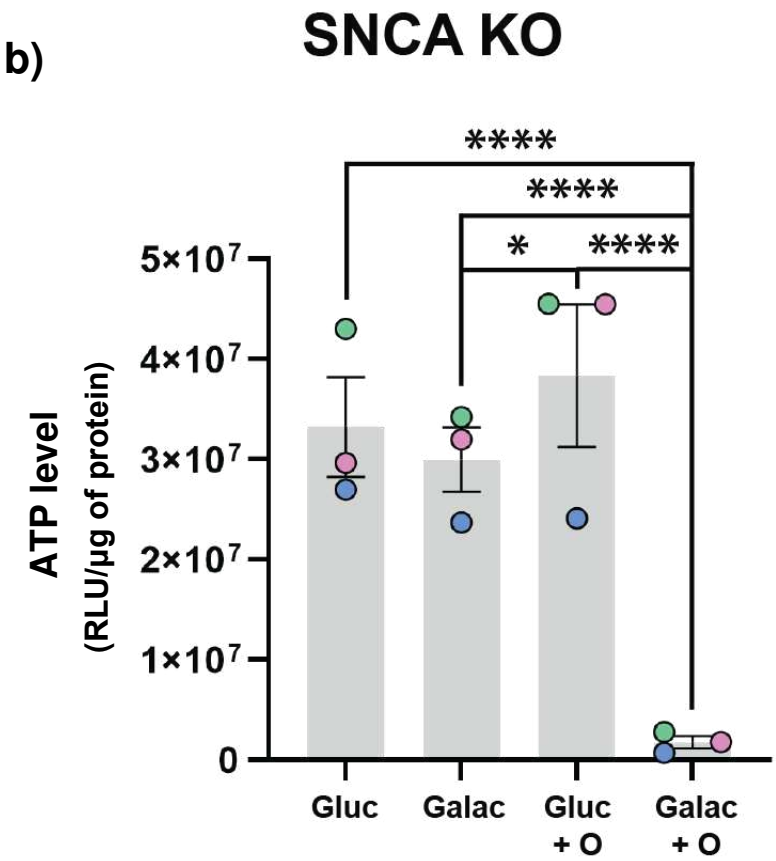
b)
SNCA KO
****
****
*
****
5×10^7
4×10^7
3×10^7
2×10^7
1×10^7
0
ATP level
(RLU/µg of protein)
Gluc
Galac
Gluc + O
Galac + O

Figure 42: Cells lacking α-synuclein produce more ATP through glycolysis than OXPHOS

EV and SNCA KO cells were grown in different media compositions to enable measurement of ATP from glycolysis and/or OXPHOS: glucose (glycolysis and OXPHOS), galactose (OXPHOS only), glucose with oligomycin (glycolysis only) or galactose with oligomycin (negative control). An ATP kit was used to obtain luminescence readings proportional to ATP in the media. Luminescence readings were measured as relative light units (RLU), and this was normalised to total protein concentration. ATP level here is shown by RLU per µg of protein. Graphs show within-cell line comparisons between a) EV and b) SNCA KO cells under different media conditions. Biological replicates are colour coded, with circles representing the means of each repeat, bars representing the mean of the 3 repeats and black lines representing the SEM. Statistical analysis for differences within groups was performed using a repeated measures 2-way ANOVA with Sídák's multiple comparisons test. Significant differences: a) EV: glucose, galactose and glucose + oligomycin V galactose + oligomycin, $p<0.0001$ (****). b) SNCA KO: glucose, galactose and glucose + oligomycin V galactose + oligomycin, $p<0.0001$ (****), galactose V glucose + O, $p=0.0214$ (*). (**n=3**).

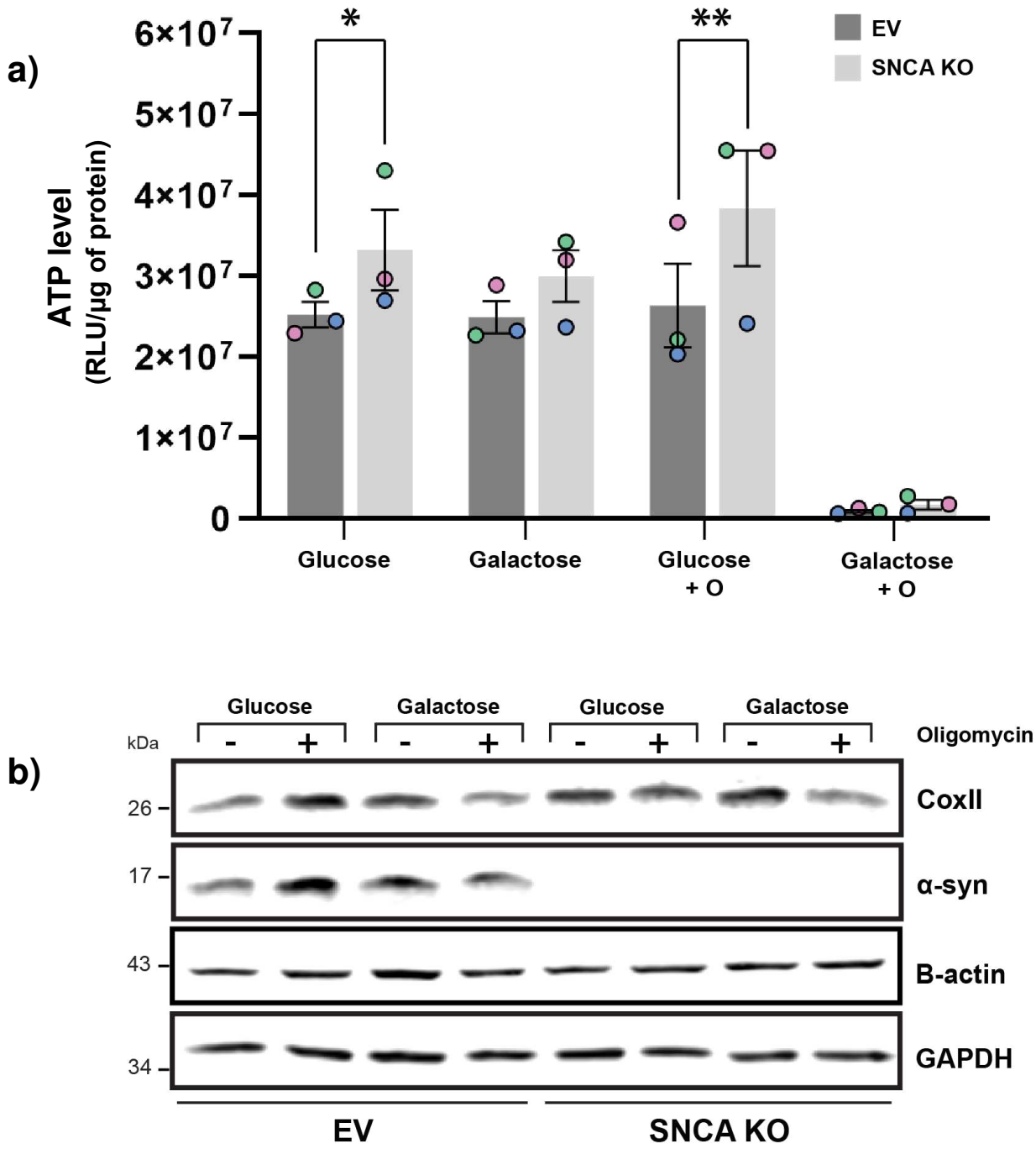
a)
ATP level
(RLU/µg of protein)
6×10^7
5×10^7
4×10^7
3×10^7
2×10^7
1×10^7
0
*
**
EV
SNCA KO
Glucose
Galactose
Glucose + O
Galactose + O
b)
Glucose
Galactose
Glucose
Galactose
Oligomycin
kDa
- + - + - + - +
26
17
43
34
CoxII
α-syn
B-actin
GAPDH
EV
SNCA KO

Figure 43: Cells lacking α-synuclein produce more ATP via glycolytic pathways than EV control cells

a) The same luminescence values from the ATP assay on EV and SNCA KO cells are shown comparatively on the same graph. Luminescence readings were measured as relative light units (RLU) and was normalised to total protein concentration. ATP level here is shown by RLU per μg of protein. The graph shows between-cell line comparisons between EV and SNCA KO cells under different media conditions. Biological replicates are colour coded, with circles representing the means of each repeat, bars representing the mean of the 3 repeats and black lines representing the SEM. Statistical analysis for differences between groups was performed using a repeated measures 2-way ANOVA with Sídák's multiple comparisons test. Significance was found between ATP level in EV and SNCA KO cells cultured in glucose (p=0.0136, *) and in glucose + oligomycin (p=0.0023, **). (**n=3**).

b) EV and SNCA KO cells were kept under the same growth conditions as for the ATP assay but were instead lysed and processed by Western blot. An antibody against CoxII was used to confirm no differences in mitochondrial load and an antibody against α-synuclein was used to confirm that SNCA KO cells used for the assay had no α-synuclein expression. GAPDH and B-actin were used as protein loading controls. (**n=1**).

Though the ATP assay provides useful initial information, it is only able to provide one readout: ATP level. Recently, a system has been developed to generate more specific readouts of mitochondrial health and energy generation. The Seahorse mito-stress test is an assay that directly measures cellular oxygen consumption rate (OCR) in live cells, quantifying the bioenergetics of mitochondria in real time rather than just measuring the end-product (Gu et al., 2021). It works by manipulating components of the electron transport chain with selective inhibitors of mitochondrial respiratory complexes, described in **Appendix A** (**Figure 118**). Exposure to these inhibitors in a specific profile enables measurement of key energetic parameters (**Appendix A**, **Figure 119**).

There was little difference in oxygen consumption over the course of the mito-stress test between the two cell lines, both at baseline and in response to mito-stress compounds, with the trace of the means from 3 repeats showing almost identical profiles (**Figure 44**). This trace normalises both cell lines to their respective baseline OCR from each repeat to allow visualisation of the two cell lines on top of each other, clarifying the profiles. The raw trace can be seen in **Appendix A** (**Figure 120**).

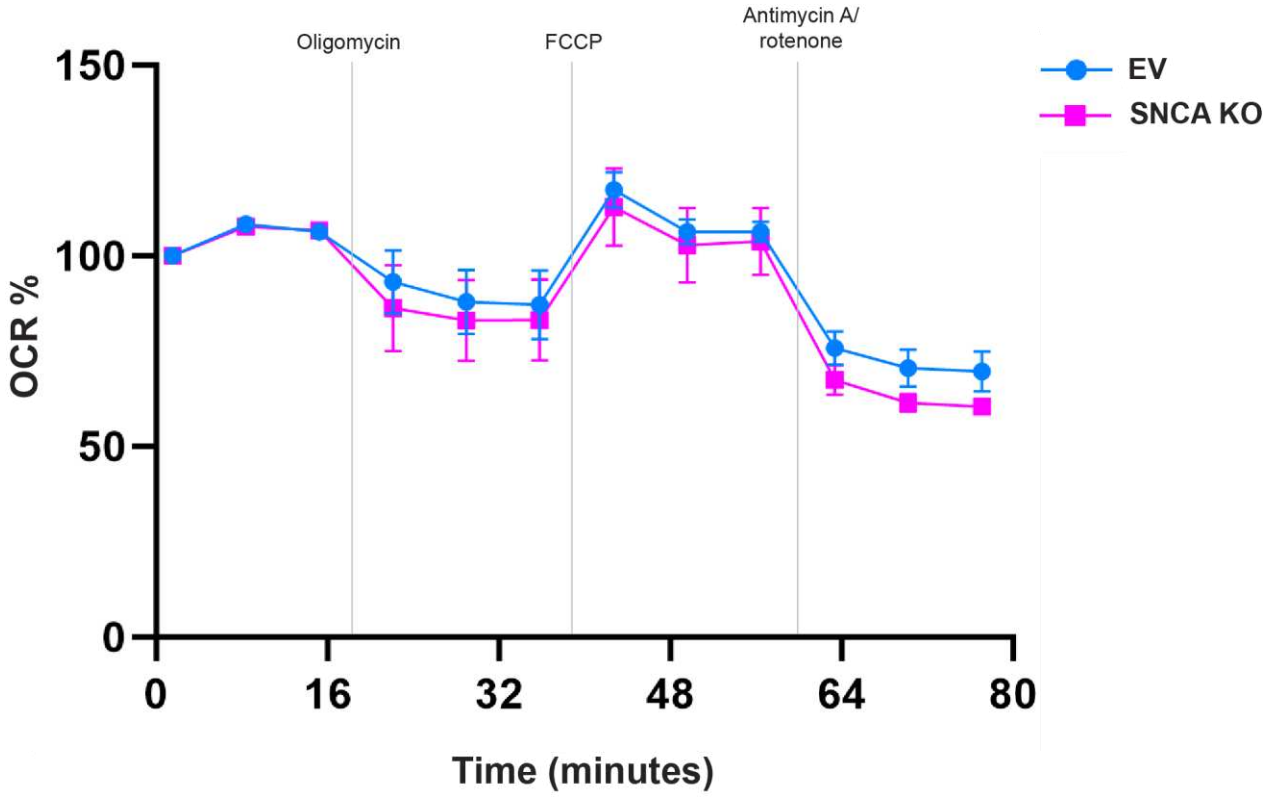

Figure 44: Cells lacking α-synuclein have similar oxygen consumption to EV controls over the course of the Seahorse mito-stress test

EV and SNCA KO cells were plated in a 96-well plate and underwent a Seahorse mito-stress test. Oligomycin, FCCP and a combination of antimycin A and rotenone were applied at different time points. Oxygen consumption rate (OCR) was measured over 80 minutes. This graph is a trace of the means from 3 biological replicates. EV cells are shown in blue and SNCA KO in pink. Data points are shown relative to the first baseline OCR reading, shown as 100%, for each cell line. Data has been normalised to total protein concentration to account for differences in cell density. (**n=3**).

There were small differences between the respiratory parameters measured by the mito-stress test in EV and SNCA KO cells, but none were statistically significant. Basal respiration, the OCR under basal conditions before the addition of oligomycin, were consistently increased in SNCA KO cells, consistent with data from the ATP assay (**Figure 45a**). This can be visualised more clearly in the raw trace shown in **Appendix A** (**Figure 120**). ATP-linked respiration, the proportion of basal oxygen consumption directly linked to ATP production, was also increased in SNCA KO cells, likely due to the overall higher basal respiration (**Figure 45b**). The remaining proportion of basal respiration reflects the proton leak, which was also increased, likely for the same reason (**Figure 45c).** In keeping with these observations, maximal respiration was slightly increased in SNCA KO cells, implying that these cells have a greater capacity to produce ATP (**Figure 45d**). There was no difference in spare respiratory capacity between EV and SNCA KO cells, which is defined as the difference between maximal and basal respiration (**Figure 45e**). This measure is commonly used to measure fitness of the cells as it reflects their ability to respond to changes in energy demand (Divakaruni & Jastroch, 2022; Gu et al., 2021). Finally, there was a subtle difference in non-mitochondrial respiration between the cell lines, indicating that SNCA KO cells consume less oxygen through other cellular pathways, such as enzymatic reactions (**Figure 45f**). Overall, the mito-stress test suggests that mitochondria in SNCA KO cells consume more oxygen at baseline and can push this consumption further than EV cells. Despite this, the fact that they have no difference in spare respiratory capacity shows that this ability does not make them any more able to react to changes in energy demand.

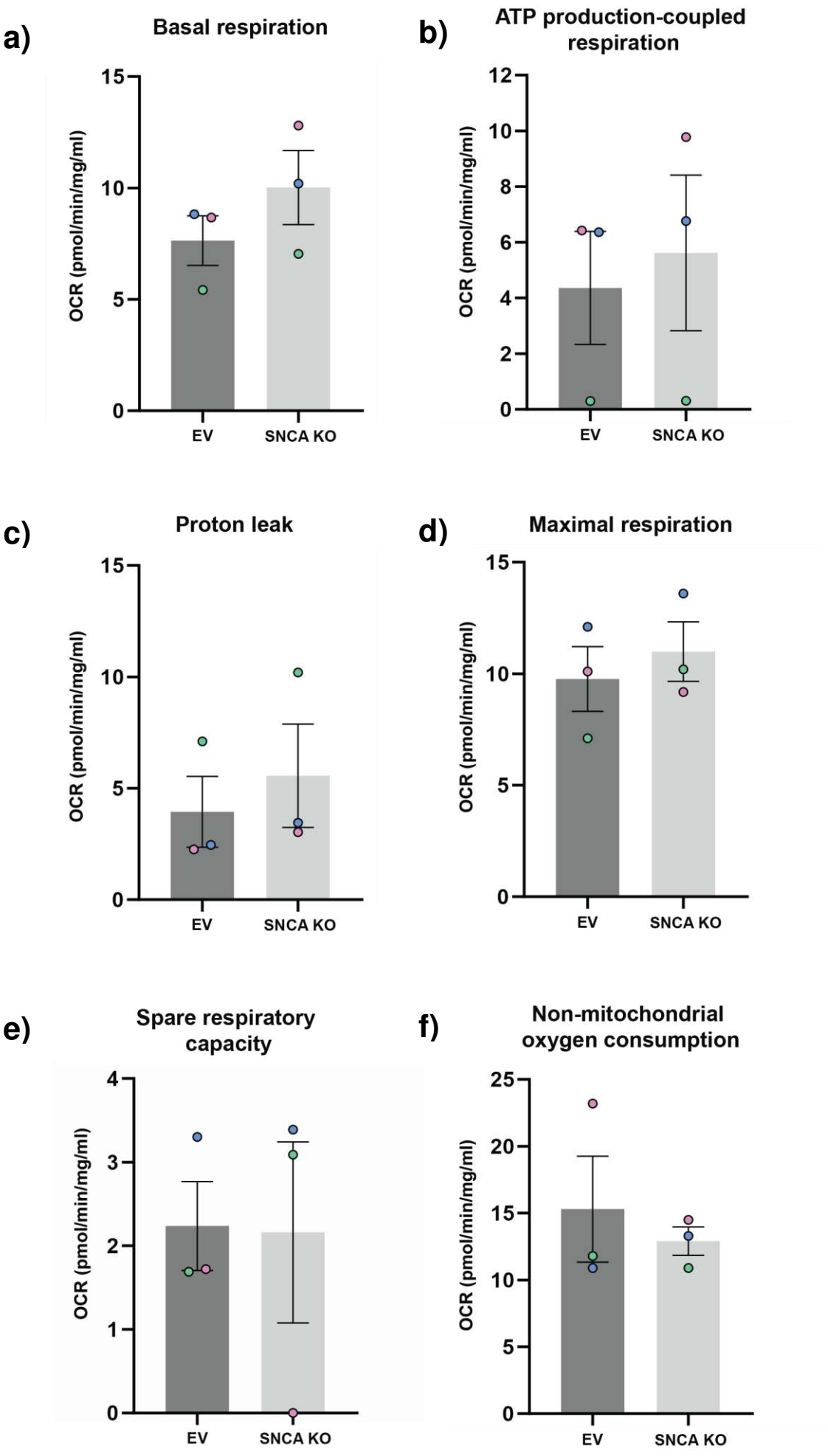
a)
Basal respiration
OCR (pmol/min/mg/ml)
15
10
5
0
EV
SNCA KO
b)
ATP production-coupled respiration
OCR (pmol/min/mg/ml)
12
10
8
6
4
2
0
EV
SNCA KO
c)
Proton leak
OCR (pmol/min/mg/ml)
15
10
5
0
EV
SNCA KO
d)
Maximal respiration
OCR (pmol/min/mg/ml)
15
10
5
0
EV
SNCA KO
e)
Spare respiratory capacity
OCR (pmol/min/mg/ml)
4
3
2
1
0
EV
SNCA KO
f)
Non-mitochondrial oxygen consumption
OCR (pmol/min/mg/ml)
25
20
15
10
5
0
EV
SNCA KO

Figure 45: Lack of α-synuclein does not significantly impact mitochondrial oxygen consumption rate in the Seahorse mito stress test

Respiratory parameters for EV and SNCA KO cells were calculated from oxygen consumption rate (OCR) data from the Seahorse mito-stress test. Seahorse WavePro software was used to collect data from each biological replicate. Graphs display measurements of a) basal respiration, b) ATP-coupled respiration, c) proton leak, d) maximal respiration, e) spare respiratory capacity and f) non-mitochondrial oxygen consumption. OCR is shown normalised to protein concentration in mg/ml. Bars show EV cells in dark grey and SNCA KO cells in light grey. Biological replicates are colour coded, with circles representing the means of each repeat, bars representing the mean of the 3 repeats and black lines representing the SEM. Statistical analysis was carried out using a paired t-test. There were no significant differences found between the groups. (**n=3**).

For completeness, I also investigated whether there were any differences in mitochondrial membrane potential (ΔΨm) in SNCA KO cells. Generated by electron transport chain complexes, ΔΨm is a key indicator of mitochondrial health, and its maintenance is extremely important for ATP synthesis (Zamzami et al., 1995; Zorova et al., 2018). The ΔΨm is kept constant at baseline, so complete loss of ΔΨm (i.e., depolarisation) has grave consequences for the mitochondria, triggering accumulation of PINK1 on the OMM and the start of mitophagy (Kondapalli et al., 2012). I assessed this baseline ΔΨm in EV and SNCA KO cells to determine whether it was impacted by a lack of α-synuclein.

Measured by fluorescence intensity of the ΔΨm probe, TMRM, EV and SNCA KO cells exhibited a similar ΔΨm at baseline in living cells, indicating that α-synuclein loss-of-function does not impact the ability of cells to maintain their ΔΨm under normal conditions (**Figure 46**).

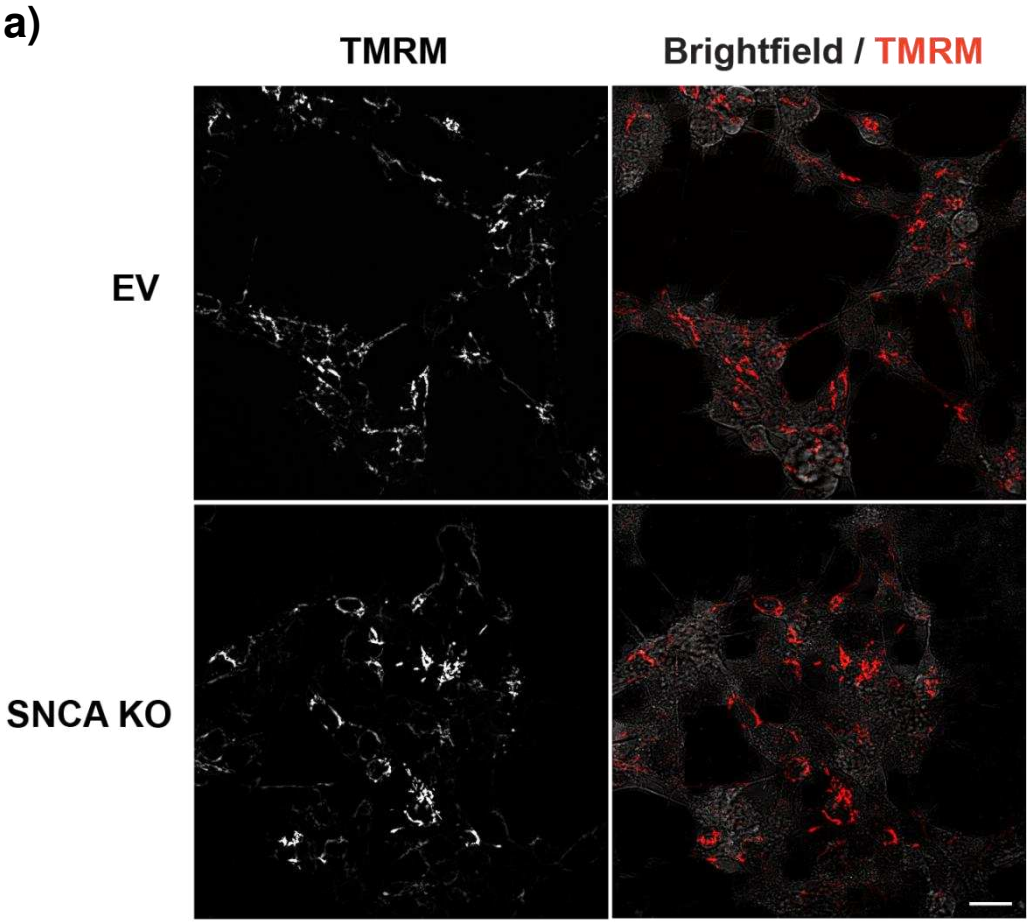
a)
TMRM
Brightfield / TMRM
EV
SNCA KO
b)
Average TMRM fluorescence intensity per cell
150
100
50
0
EV
SNCA KO

Figure 46: Lack of α-synuclein has no impact on baseline ΔΨm

a) ΔΨm was measured at baseline in live EV and SNCA KO cells using TMRM, a voltage-sensitive probe. Images are representative and show TMRM staining (red) with cells shown by brightfield (grey) from 1 repeat. Images were taken on a DeltaVision Elite live imaging system with a 60X objective.

b) Fluorescence intensity of TMRM-positive mitochondria was measured in 20 cells per cell line, per biological repeat. Average fluorescence intensity for each individual cell is represented by a dot, with the mean of each biological repeat shown by a square and the mean of all 3 repeats shown by a black bar. SEM is shown by vertical black lines. Data points are colour coded by biological repeat. Statistical analysis was carried out by a paired t-test and reported no significant differences between the groups. (**n=3**).

3.2.6 Lack of α-synuclein has no overall impact on the organisation of the mitochondrial network

Though no impact on mitochondrial function was observed in my α-synuclein loss-of-function model, I next aimed to investigate whether a lack of α-synuclein caused any alterations to mitochondrial network morphology and organisation.

Mitochondria exist as a dynamic network, with constant fission and fusion events remodelling these organelles to promote their health (Youle & Van Der Bliek, 2012). A physiological role for α-synuclein in this context would be reflected by changes to the mitochondrial network in a loss-of-function environment. As such, mitochondrial morphology and connectivity was assessed at steady state and in response to treatment with A/O for 2, 6 or 24 hours to capture both basal and stress-induced network changes (**Figure 47**).

To measure mitochondrial morphology, an analysis workflow was developed which enabled measurement of the number of mitochondria per cell alongside the average area, perimeter, circularity, and aspect ratio of mitochondrial regions per cell. It is known that cellular stressors cause mitochondria to become fragmented through an upregulation of mitochondrial fission processes, since smaller mitochondria are not only easier to be engulfed by autophagosomes, but easier to transport (Preminger & Schuldiner, 2024). Fission is therefore a prerequisite for mitophagy and has even been suggested to promote it (Fukuda et al., 2023; Kleele et al., 2021; Twig et al., 2008). I first confirmed the sensitivity of these measurements by ensuring they could recapitulate damage-induced changes to the mitochondrial network in EV cells. With increasing A/O treatment, the number of mitochondria per cell increased as the average mitochondrial

area and perimeter decreased, reflecting an increase in mitochondrial fission. Mitochondrial shape also corroborated this, with circularity and aspect ratio of mitochondrial fragments both measuring more rounded mitochondria with increasing A/O treatment (**Figure 48**)**.** In terms of mitochondrial connectivity and intricacy, the workflow measured the average number of mitochondrial branches, number of mitochondrial junctions, average mitochondrial branch length and maximum mitochondrial branch length per cell. All four of these measurements decreased with increasing A/O treatment, capturing the decrease in mitochondrial connections and network cohesion as a result of damage-induced fission and mitophagy. Comparatively, SNCA KO cells had a very similar mitochondrial profile (**Figure 49**). Measurements were similar to those of the EV cells for all parameters, with no significant differences found in network morphology or connectivity either at baseline or in response to damage.

Though not statistically significant, I noticed that untreated SNCA KO cells appeared to be slightly smaller and rounder according to morphological measurements. Since the analysis was based on images taken at 40X magnification, I thought it possible that phenotypes may have been missed due to limited resolution. I endeavoured to exclude this possibility by reimaging untreated EV and SNCA KO cells at 100X and reanalysing to resolve this (**Appendix B**, **Figure 123**, **Figure 124**). This analysis did not result in any significant differences between the cell lines, confirming that there is limited impact of α-synuclein loss on steady state mitochondrial morphology and connectivity.

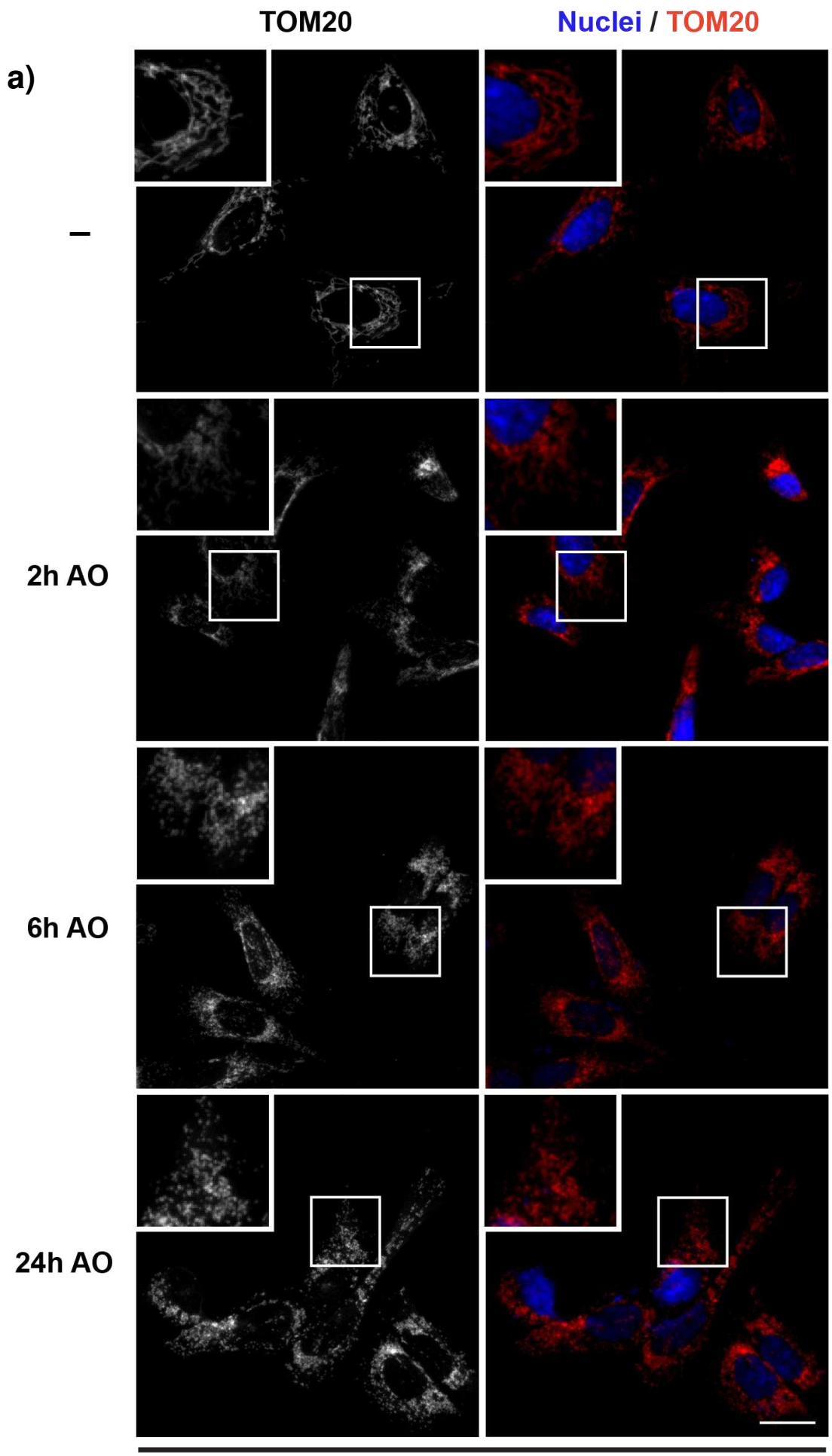
a)
TOM20
Nuclei / TOM20
–
2h AO
6h AO
24h AO
EV

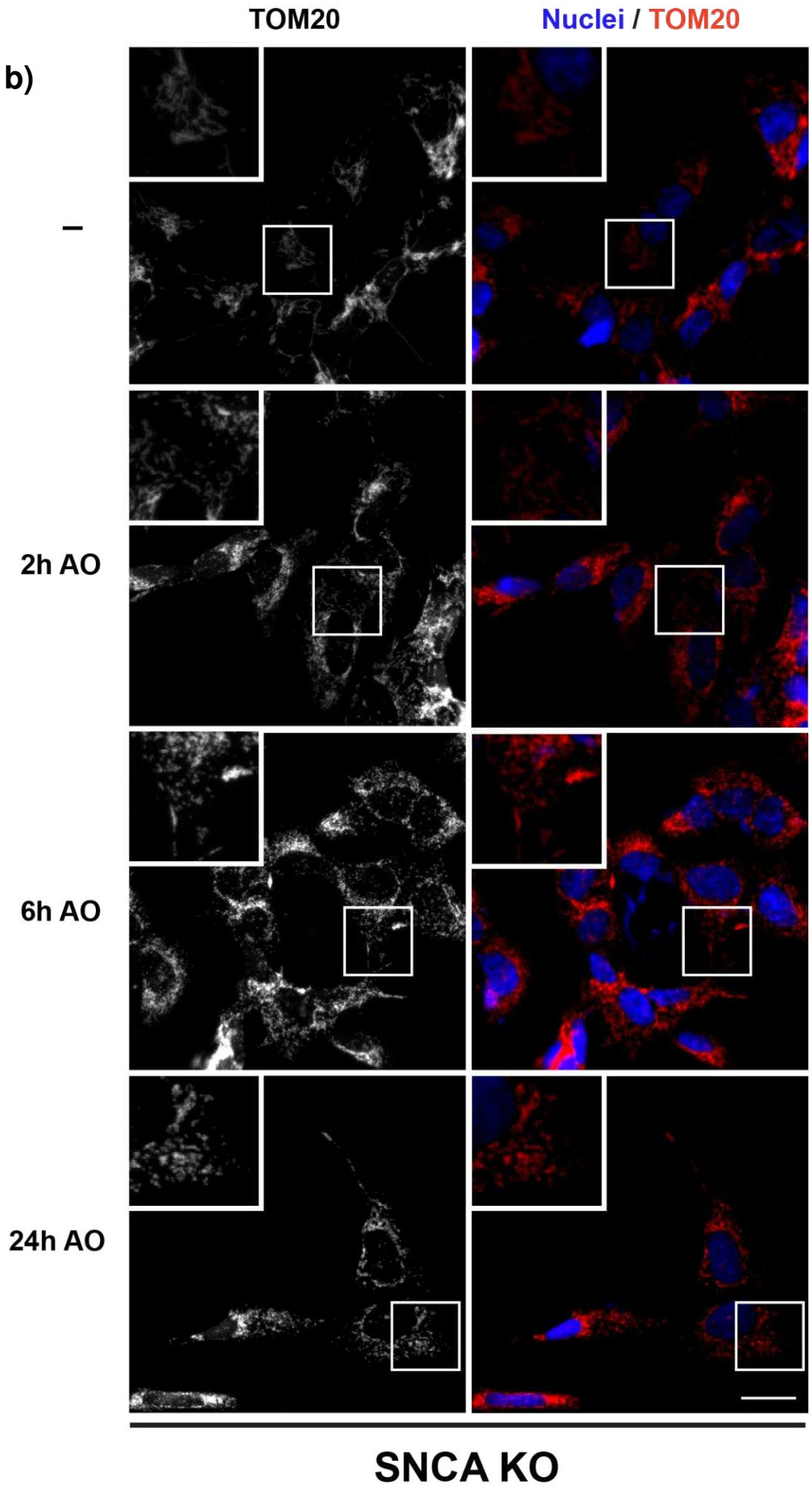
b)
TOM20
Nuclei / TOM20
–
2h AO
6h AO
24h AO
SNCA KO

Figure 47: Loss of α-synuclein has no impact on the organisation of the mitochondrial network

EV (a) and SNCA KO (b) cells were left untreated (-) or treated for 2, 6 or 24 hours with A/O to induce mitochondrial damage. Cells were fixed and stained with an antibody against TOM20 (red) with nuclei labelled by Hoechst (blue). Images shown are representative and originate from 1 biological repeat. Images were taken using widefield immunofluorescence microscopy on a 40X objective. Scale bar = 20µm.

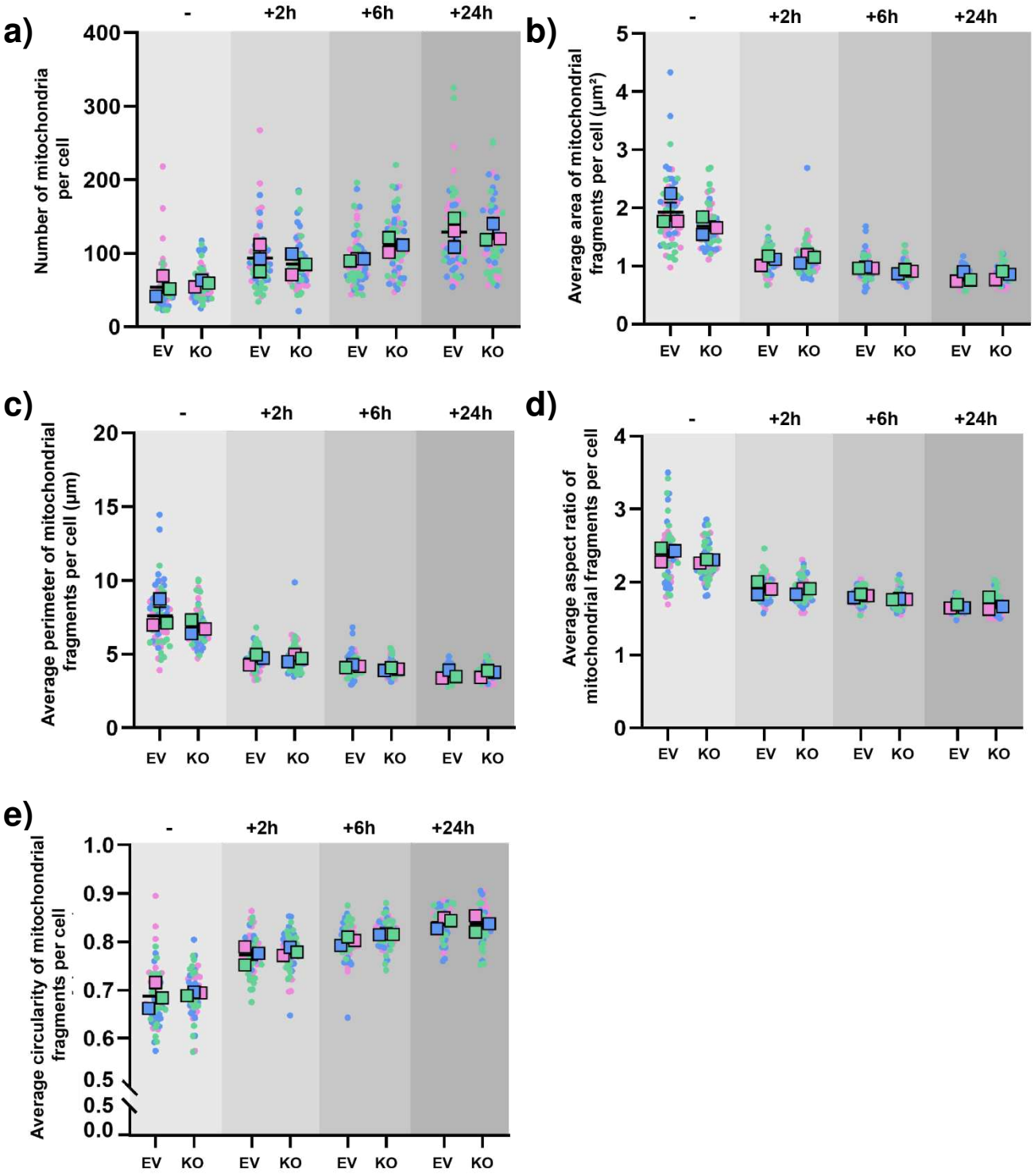

Figure 48: Lack of α-synuclein has no effect on mitochondrial morphology at baseline or in response to mitochondrial damage

Quantitative measurements of mitochondrial morphology were obtained using an image analysis workflow on ImageJ to isolate individual cells and analyse particles within them that were positive for TOM20. Measurements were taken from EV and SNCA KO cells left untreated (-) or treated for 2, 6 or 24 hours with A/O to induce mitochondrial damage. Parameters measured were a) number of mitochondria per cell; b) average area of mitochondrial fragments per cell; c) average perimeter of mitochondrial fragments per cell; d) average aspect ratio of mitochondrial fragments per cell and e) average circularity of mitochondrial fragments per cell. 20 cells were analysed per condition, per biological repeat. Measurements from each individual cell are shown by a dot, with the mean of each biological repeat shown by a square and the mean of all 3 repeats shown by a black line. SEM is shown by vertical black lines. Data points are colour coded by biological repeat. Statistical analysis was performed by repeated measures 2-way ANOVA with Sídák's multiple comparisons test, which did not report any significant differences between EV and SNCA KO cells in any measure. (**n=3**).

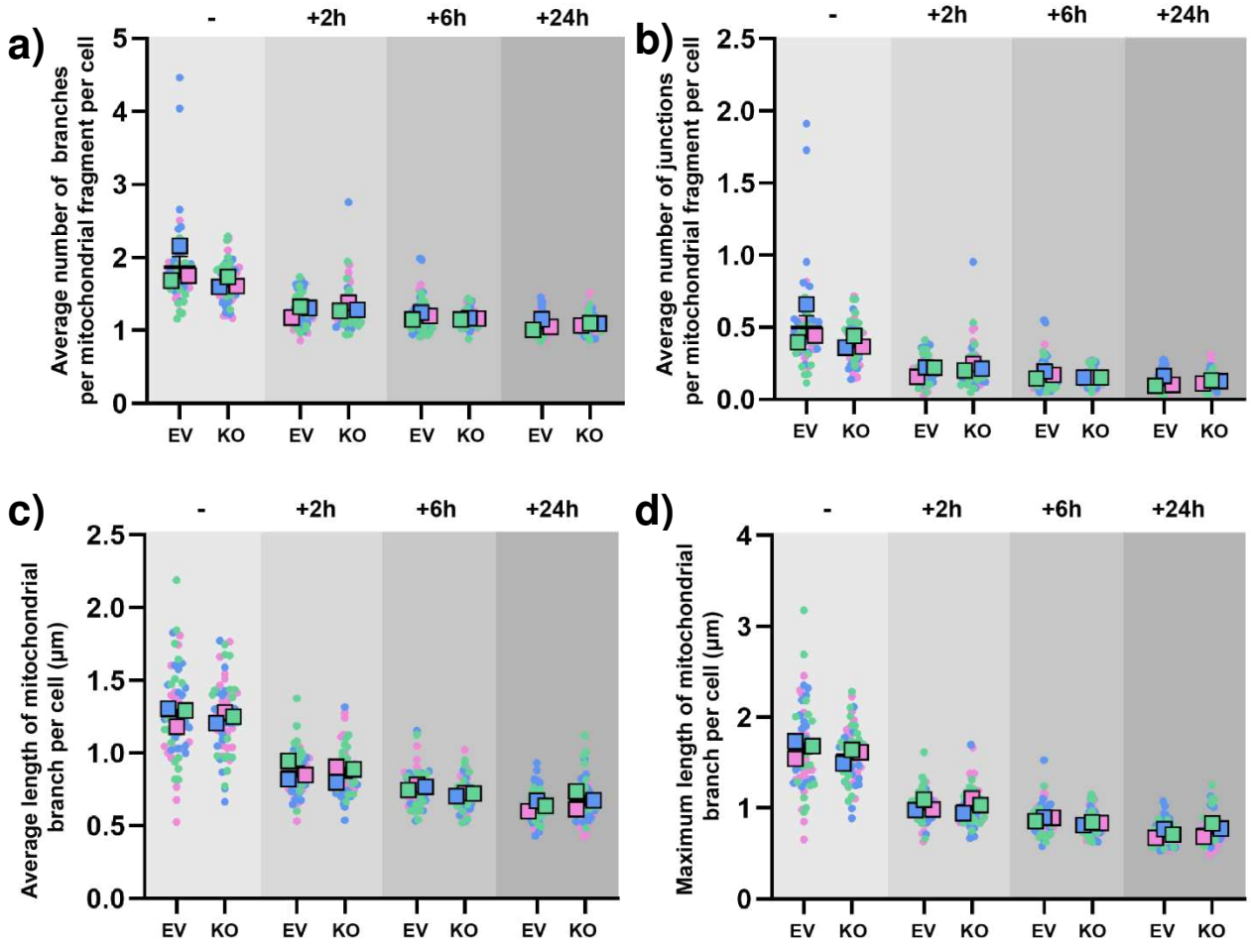

Figure 49: Lack of α-synuclein has no effect on mitochondrial connectivity at baseline or in response to mitochondrial damage

Quantitative measurements of mitochondrial connectivity were obtained using an image analysis workflow on ImageJ to isolate individual cells and analyse skeletons within them. Measurements were taken from EV and SNCA KO cells left untreated (-) or treated for 2, 6, or 24 hours with A/O to induce mitochondrial damage. Parameters measured were a) average number of branches per mitochondrial fragment per cell; b) average number of junctions per mitochondrial fragment per cell; c) average length of mitochondrial branches per cell and d) maximum length of mitochondrial branches per cell. 20 cells were analysed per condition, per biological repeat. Measurements from each individual cell are shown by a dot, with the mean of each biological repeat shown by a square and the mean of all 3 repeats shown by a black line. SEM is shown by vertical black lines. Data points are colour coded by biological repeat. Statistical analysis was performed by repeated measures 2-way ANOVA with Sídák's multiple comparisons test, which did not report any significant differences between EV and SNCA KO cells in any measure. (**n=3**).

3.2.7 α-synuclein loss-of-function increases Parkin expression at baseline, but has limited overall impact on PINK1/Parkin mitophagy

Since a lack of α-synuclein had limited impact on mitochondrial energy production or network organisation, I next aimed to evaluate whether α-synuclein loss-of-function had any effect on cellular responses to mitochondrial damage through mito-QC systems.

α-synuclein has a physiological role in synaptic transmission, where it modulates vesicle release and recycling through binding phospholipid membranes (Cheng et al., 2011). This lipid-binding activity is mediated by the N-terminus of α-synuclein, suggesting an intrinsic functionality to the relationship between α-synuclein and membranes (Emamzadeh, 2016). This interaction and thus a potential physiological function for α-synuclein has not been well-studied in the context of mitochondrial membranes, despite evidence that α-synuclein preferentially binds these organelles (Devi et al., 2008; Guardia-Laguarta et al., 2014; Zigoneanu et al., 2012). The ability of α-synuclein to reshape phospholipid membranes lends it to a role in mito-QC mechanisms, where the dynamic remodelling of mitochondrial membranes facilitates mitochondrial and cellular health. I consider the possibility that α-synuclein is a physiological player in these pathways, such as PINK1/Parkin-mediated mitophagy.

In response to high levels of damage, mitochondria undergo fission activity to sequester damaged components into individual organelles, in preparation for degradation (Burman et al.,

2017). PINK1/Parkin mitophagy is initiated, and mitochondria that are deemed beyond repair are engulfed by an autophagosome and subsequently degraded by the lysosome (Montava-Garriga & Ganley, 2020). These processes all necessitate membrane remodelling by the mitochondria as well as the autophagosome and lysosome, offering potential for physiological involvement of α-synuclein. Additionally, evidence has shown that pathological forms of α-synuclein can cause downregulation of Parkin (Wilkaniec et al., 2021). These impacts are considered to be the result of toxic gain-of-function, but it is possible some of these phenotypes could result from the loss of a physiological function of α-synuclein in a pathological context.

To address the question of whether α-synuclein has a physiological role in PINK1/Parkin mitophagy, EV and SNCA KO cells were subject to mitochondrial damage and mitophagy was evaluated (**Figure 50a**). CoxII, an electron transport chain protein embedded in the IMM, was used as a readout of mitochondrial load to assess whole mitochondrial turnover. CoxII was found to be significantly decreased in response to 24 hours of A/O treatment in both EV ($p=0.0295$) and SNCA KO ($p=0.0294$) cells, reflecting mitochondrial degradation by mitophagy (**Figure 50b**). Both cell lines exhibited a CoxII reduction of approximately 50% upon A/O treatment, showing that α-synuclein loss-of-function had no impact on the ability of cells to clear damaged mitochondria.

To confirm this phenotype and assess PINK1/Parkin more directly, I assessed expression of PINK1 itself. Degraded in the cytosol of healthy cells, PINK1 only stabilises on the OMM of damaged mitochondria in response to changes in mitochondrial membrane potential (Matsuda et al., 2013). In both EV and SNCA KO cells, this accumulation of PINK1 on the mitochondria is seen by the significant increase in PINK1 expression ($p=0.0006$) upon mitochondrial damage with A/O (**Figure 50c**). Expression was increased to a similar level in both cell lines, reflecting that PINK1 stabilisation is unaffected by loss of α-synuclein. On the OMM, PINK1 is able to recruit Parkin to ubiquitinate membrane proteins as a degradation signal, triggering engagement of the autophagosome. Mfn2, a fusion co-ordinating protein, is a substrate of Parkin and has been shown to be ubiquitinated as part of the mitochondrial degradation process (Chen & Dorn, 2013). This was measured as an additional readout of PINK1/Parkin mitophagy, with the appearance of a higher molecular weight band (highMW Mfn2) by Western blot considered to be a ubiquitinated form of Mfn2, as described in previous literature (Gegg et al., 2010; Ziviani et al., 2010). Ubiquitinated Mfn2 was observed to significantly increase in response to A/O in both cell lines ($p<0.0001$) with significantly higher expression in SNCA KO cells compared to EV controls ($p=0.0029$) (**Figure 50d**). This suggests that damage-induced ubiquitination of mitochondrial proteins may be increased by α-synuclein loss-of-function.

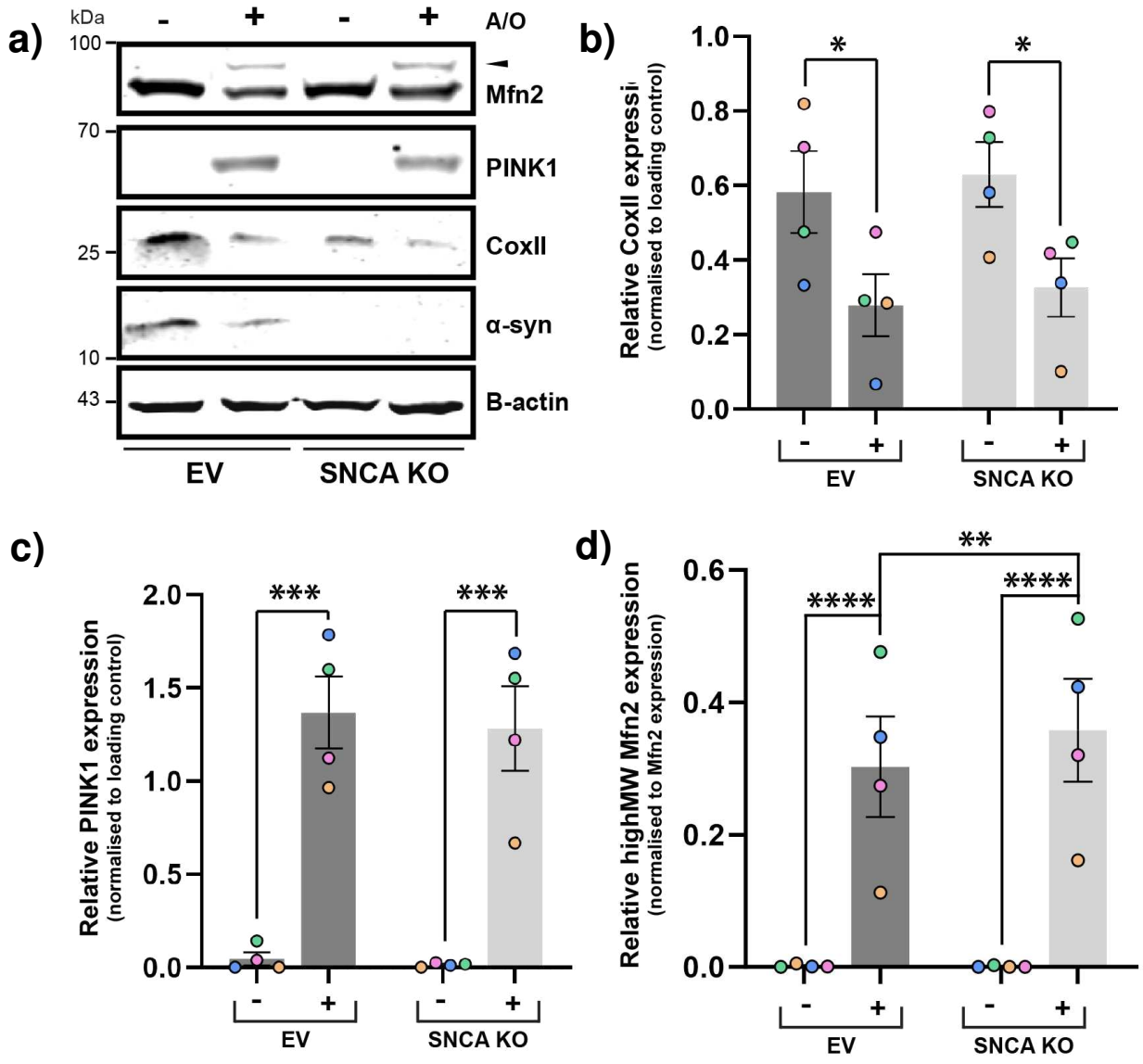
a)
kDa
A/O
100
70
25
10
43
Mfn2
PINK1
CoxII
α-syn
B-actin
EV
SNCA KO
b)
Relative CoxII expressi
(normalised to loading control)
c)
Relative PINK1 expression
(normalised to loading control)
d)
Relative highMW Mfn2 expression
(normalised to Mfn2 expression)

Figure 50: Loss of α-synuclein has no impact on mitochondrial degradation but increases highMW Mfn2 in response to mitochondrial damage

EV and SNCA KO cells were left untreated (-) or treated for 24 hours with A/O to induce mitochondrial damage. Lysates were processed by Western blot (a) with antibodies against CoxII, PINK1 and Mfn2 alongside B-actin as a loading control and α-synuclein to confirm knockout in SNCA KO cells. Graphs show expression of b) CoxII, c) PINK1 and d) Mfn2. Expression of CoxII and PINK1 were normalised to B-actin to account for differences in protein loading, with the raw value of these calculations shown on the graphs. For higher molecular weight (highMW, denoted on (a) by the arrowhead) Mfn2, expression was normalised to total Mfn2 expression (both upper and lower bands), thus is presented as a proportion of total Mfn2. Biological replicates are colour coded, with circles representing the means of each repeat, bars representing the mean of the 4 repeats and black lines showing SEM. Dark grey bars represent EV while light grey represents SNCA KO. Statistical analysis was carried out using a repeated measures 2-way ANOVA with Sídák's multiple comparisons test. CoxII was significantly decreased with A/O treatment in EV ($p=0.0295$, *) and SNCA KO cells ($p=0.0294$, *). PINK1 was significantly increased with A/O treatment in EV and SNCA KO cells (both $p=0.0006$, ***) and so was highMW Mfn2 (both $p<0.0001$, ****). In SNCA KO cells treated with A/O, highMW Mfn2 was significantly higher than in EV cells ($p=0.0029$, **). (**n=4**).

Although cells lacking α-synuclein had no difference in damage-induced mitochondrial clearance, the observation that loss of α-synuclein resulted in higher levels of ubiquitinated Mfn2 in response to mitochondrial damage raised questions about the relationship between α-synuclein and Parkin. There is limited research on this in the context of endogenous α-synuclein, but evidence from studies on the pathological form of the protein do suggest a functional interaction between α-synuclein and Parkin (Jęśko et al., 2019; Madsen et al., 2021; Wilkaniec et al., 2021). It has been shown that exogenous α-synuclein oligomers result in post-translational modifications to Parkin that result in its autoubiquitination and degradation (K Chung et al., 2001; Wilkaniec et al., 2019; Yao et al., 2004). This suggestion that pathological α-synuclein can alter Parkin expression led me to investigate whether perturbation of endogenous α-synuclein may also influence Parkin levels.

To assess this, EV and SNCA KO cells were treated with A/O for 24 hours to evoke mitophagy, but also for shorter time periods to capture any impacts on early damage responses as well as when damage is accrued. Degradation of Parkin was seen in both cell lines in response to mitochondrial damage, with the lowest Parkin expression remaining at the latest time point where the most damage had accrued (**Figure 51**Error! Reference source not found.). There was n o impact of α-synuclein loss on damage-induced Parkin degradation. Interestingly, a difference

in Parkin expression between EV and SNCA KO cells was observed at baseline. SNCA KO cells were observed to express significantly higher levels of Parkin (p=0.0072) than EV controls in untreated conditions.

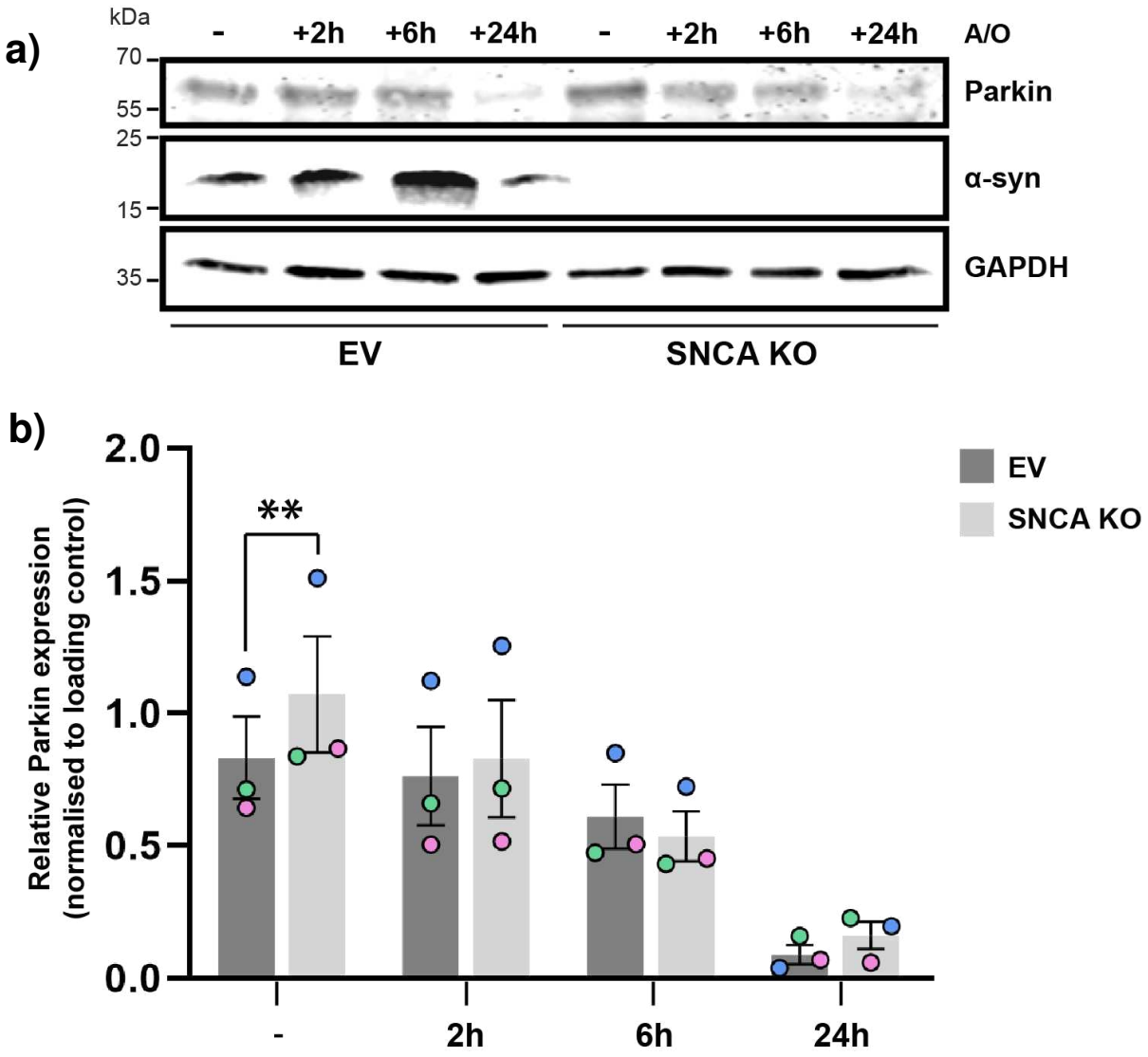

Figure 51: Loss of α-synuclein increases baseline Parkin expression

a) EV and SNCA KO cells were left untreated (-) or treated for 2, 6 or 24 hours with A/O to induce mitochondrial damage. Lysates were processed for Western blot with antibodies against Parkin, GAPDH as a protein loading control and α-synuclein to confirm knockout in SNCA KO cells.

b) From Western blot data, Parkin expression in EV and SNCA KO cells in response to A/O was normalised to GAPDH expression to account for differences in protein loading. Parkin expression is represented by the raw values of this calculation. Biological repeats are colour coded, with circles representing the means of each repeat, bars representing the mean of the 3 repeats and black lines representing SEM. Dark grey bars represent EV and light grey bars represent SNCA KO. Statistical analysis was performed with a repeated measures 2-way ANOVA with Sídák's multiple comparisons test. In untreated cells, the difference in Parkin expression levels between EV and SNCA KO cells was significant (p=0.0072, **). (**n=3**).

After observing that α-synuclein had no impact on PINK1 expression and caused an increase in Parkin expression at baseline, I explored whether α-synuclein loss-of-function directly influenced PINK1/Parkin functionality through measuring phospho-ubiquitin at serine 65 (pUb S65). Upon the induction of mitophagy, PINK1 phosphorylates ubiquitin serine 65. This recruits Parkin to bind phosphorylated ubiquitin, allowing PINK1 to also phosphorylate Parkin at its serine 65 residue to activate Parkin's E3 ubiquitin ligase activity and therefore enable mitophagy (Kane et al., 2014; Koyano et al., 2014; McWilliams et al., 2018). Since PINK1 is the only kinase known to phosphorylate ubiquitin, pUb S65 can be used as a direct and specific readout of PINK1/Parkin activity. In this experiment, the area and number of pUb S65 puncta per cell were evaluated in response to mitochondrial damage (**Figure 52**). Only puncta colocalising with mitochondrial staining were measured to reduce capture of non-specific background staining elsewhere in the cell.

Both EV and SNCA KO cells displayed an increase in mitochondrial pUb S65 staining with increasing A/O treatment. The greatest level of pUb S65 staining was induced with 24 hours of A/O in measures of both average number of pUb S65 puncta and average pUb S65 area per cell (**Figure 53**). When the two cell lines were statistically compared, there were no significant differences between pUb S65 staining at any of the time-points, showing that loss of α-synuclein had no impact on pUb S65 at early time points following damage. However, both total mitochondrial pUb S65 area and number of mitochondrial pUb S65 puncta were both slightly lower in SNCA KO cells than EV controls after 24 hours of A/O, suggesting that lack of α-synuclein slightly lessens the response in situations where damage is accrued over a long time period.

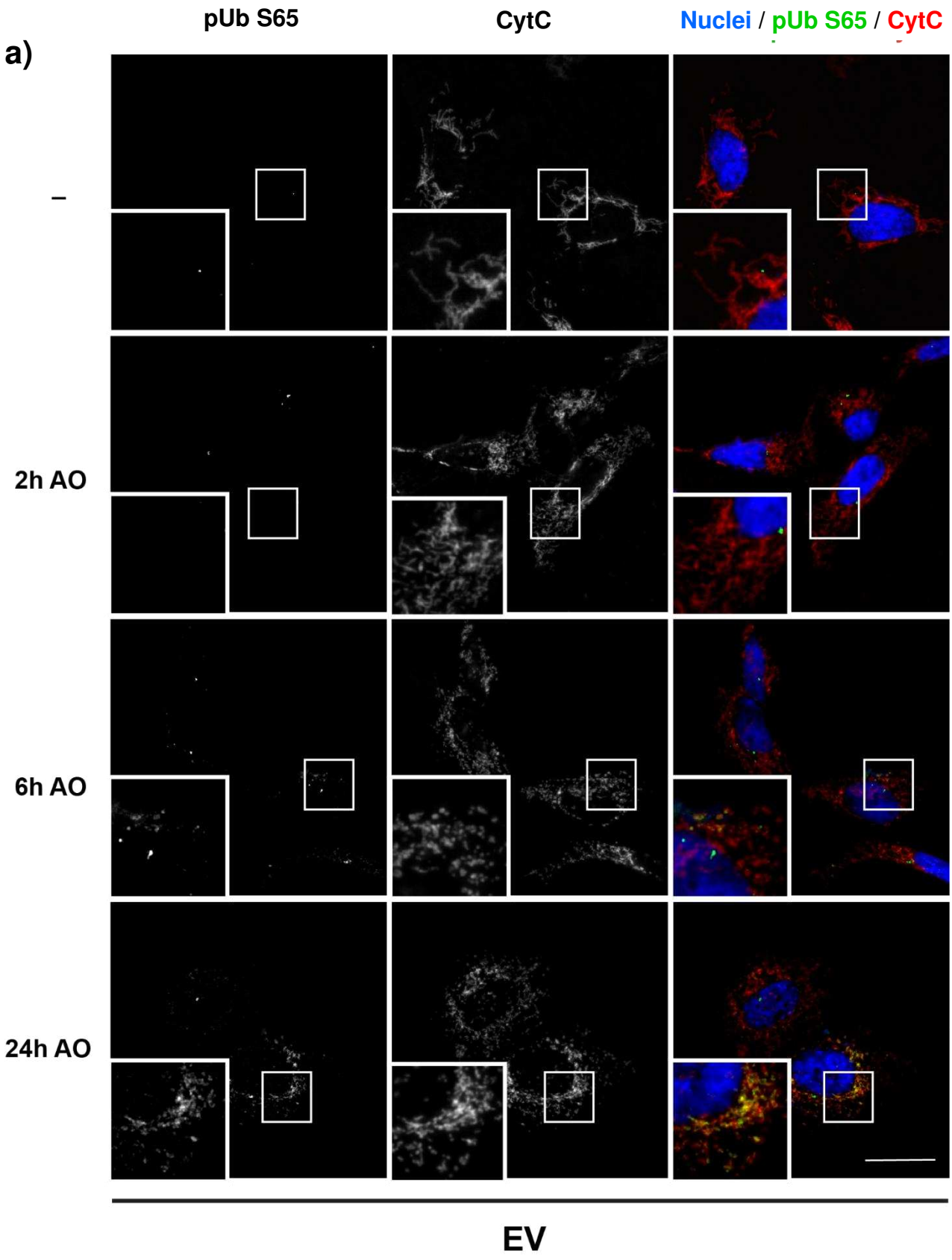
a)
pUb S65
CytC
Nuclei / pUb S65 / CytC
–
2h AO
6h AO
24h AO
EV

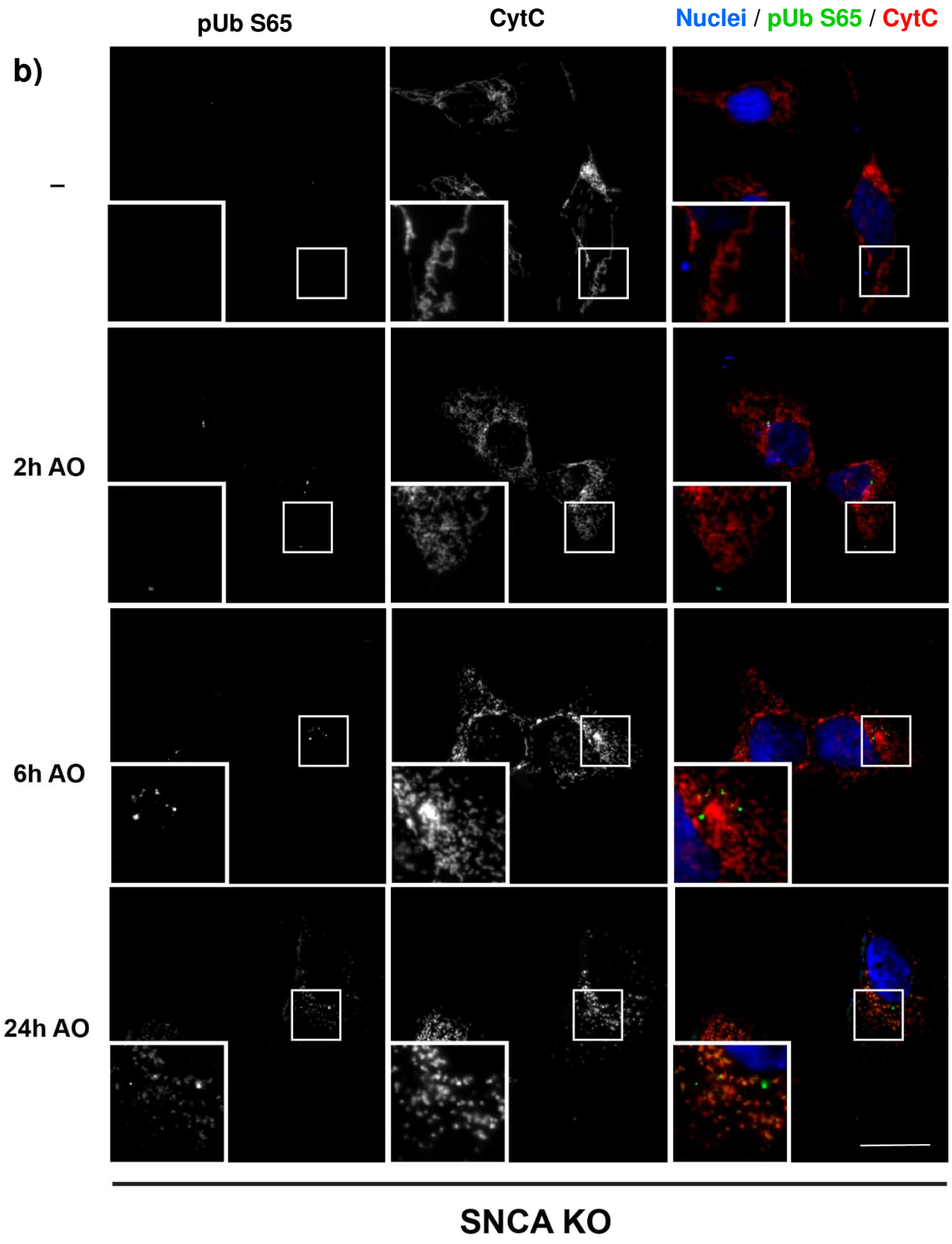
b)
pUb S65
CytC
Nuclei / pUb S65 / CytC
–
2h AO
6h AO
24h AO
SNCA KO

Figure 52: Loss of α-synuclein has limited impact on pUb S65 in response to mitochondrial damage

EV (a) and SNCA KO (b) cells were left untreated (-) or treated for 2, 6 or 24 hours with A/O to induce mitochondrial damage. Cells were fixed and immunostained with antibodies against pUb S65 (green) and cytochrome c (red), with nuclei labelled by Hoechst (blue). Colocalisation between pUb S65 and cytochrome c is reflected by yellow staining. Images shown are representative and originate from 1 biological repeat. Images were taken with widefield immunofluorescence microscopy on a 100X objective. Scale bars = 20µm.

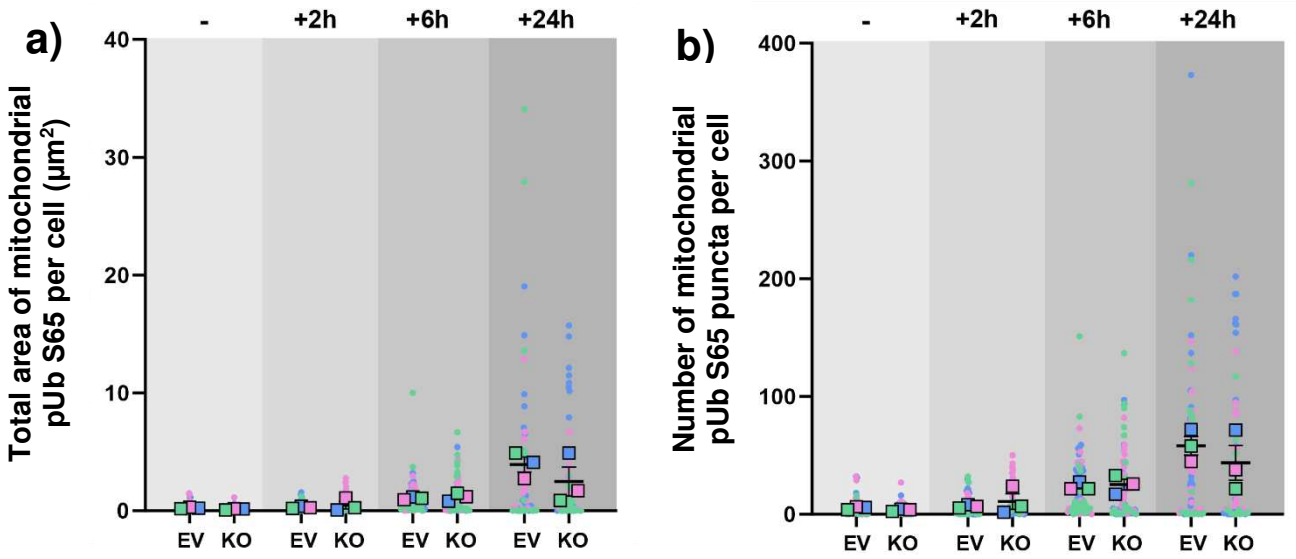

Figure 53: Loss of α-synuclein has no significant impact on pUb S65 upregulation in response to 24 hours of mitochondrial damage with A/O

EV and SNCA KO cells were left untreated (-) or treated for 2, 6 or 24 hours with A/O to induce mitochondrial damage. Cells were fixed and immunostained for pUb S65 and cytochrome c. Colocalisation between the 2 was ensured by only quantifying image pixels positive for both stains. The total area and number of puncta of colocalised staining were measured per cell in 20 cells per condition, per biological repeat. Graph a) presents the total area of mitochondrial pUb S65 staining per cell, and graph b) presents the total number of mitochondrial pUb S65 puncta. Measurements from each individual cell are shown by a dot, with the mean of each biological repeat shown by a square and the mean of all 3 repeats shown by a black bar. SEM is shown by vertical black lines. Data points are colour coded by biological repeat. (n=3). Statistical analysis carried out by repeated measures 2-way ANOVA with Sídák's multiple comparisons test for differences between cell lines reported no significance. (**n=3**).

3.2.8 Lack of α-synuclein results in a delay in the autophagosome response

We have shown that α-synuclein loss-of-function has limited impact on PINK1/Parkin activity and whole mitochondrial clearance in response to damage with A/O. To be thorough, I next investigated whether α-synuclein had any impact on the endpoints of the pathway: autophagosomes and lysosomes. As another aspect of mitochondrial quality control that requires membrane remodelling, there is potential for α-synuclein to act in a physiological capacity in autophagosome-lysosome interactions. This has not been explored in the literature, rather the focus has been on the impact of pathological α-synuclein, which has been shown to cause defects in several aspects of autophagosome function (Sarkar et al., 2021; Tang et al., 2021; Winslow et al., 2010).

When autophagosomes are formed, LC3I is modified in the isolation membrane to become LC3II (Kabeya et al., 2000). As such, levels of LC3II can be monitored and used as a readout of autophagosome number. LC3II expression was measured in EV and SNCA KO cells by Western blot in response to mitochondrial damage with A/O. Both cell lines showed an upregulation of LC3II expression with increasing A/O treatment times, but SNCA KO cells showed lower LC3II levels, particularly following 2 and 6 hours of A/O treatment (**Figure 54**Error! Reference source n ot found.). This difference between the cell lines was significant at the 6-hour time point ($p=0.0396$). This difference was negligible in the 24-hour A/O treated cells, suggesting that any impact of α-synuclein was resolved at later time points.

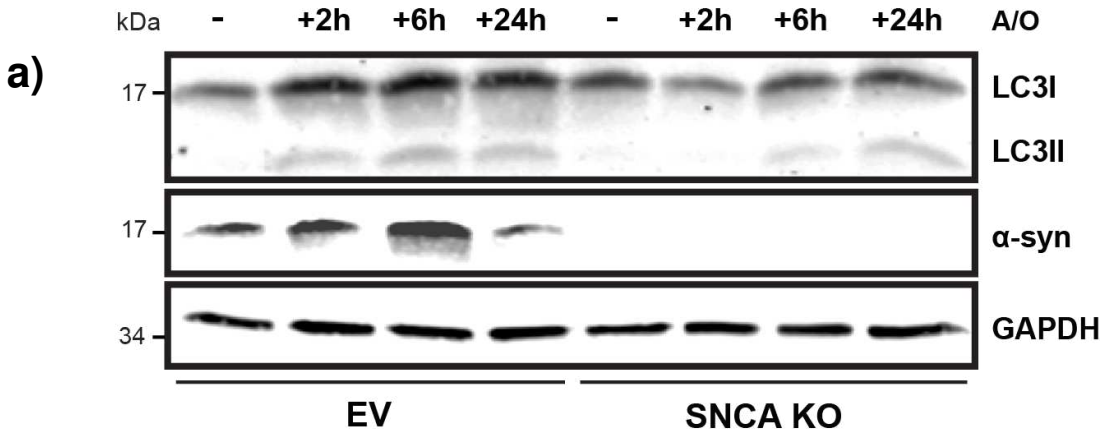
a)
kDa
-
+2h
+6h
+24h
-
+2h
+6h
+24h
A/O
17
LC3I
LC3II
17
α-syn
34
GAPDH
EV
SNCA KO

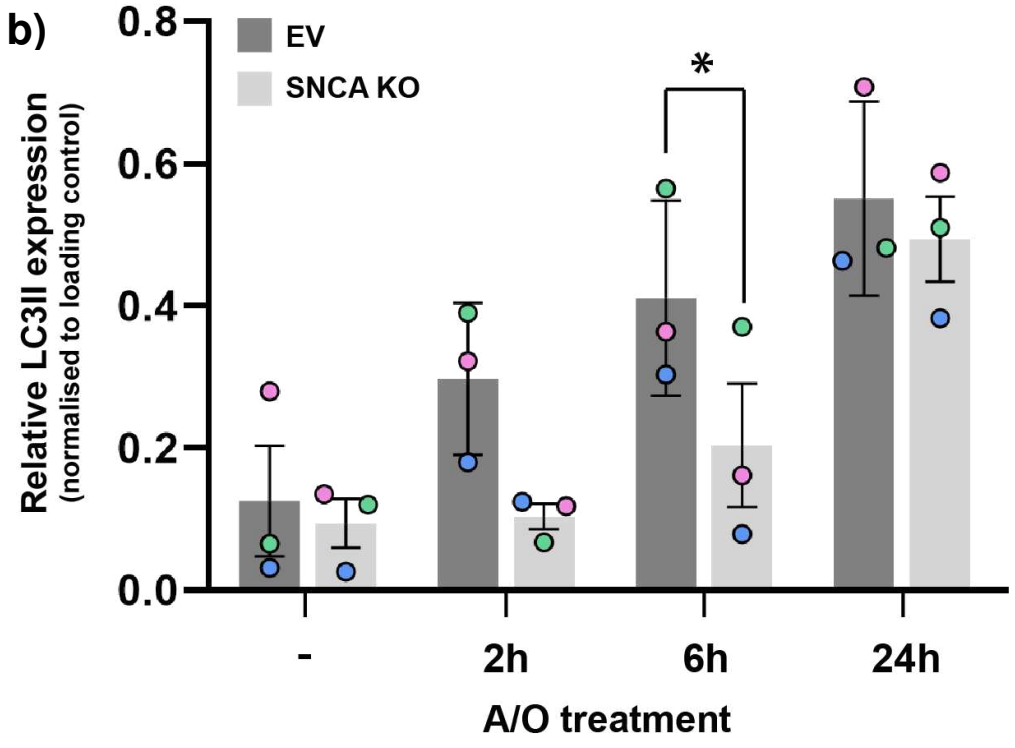
b)
EV
SNCA KO
*
Relative LC3II expression
(normalised to loading control)
0.8
0.6
0.4
0.2
0.0
-
2h
6h
24h
A/O treatment

Figure 54: Loss of α-synuclein causes a lower level of LC3II at early time points following induction of mitochondrial damage

a) EV and SNCA KO cells were left untreated (-) or treated for 2, 6 or 24 hours with A/O to induce mitochondrial damage. Lysates were processed by Western blot with antibodies against LC3, GAPDH as a protein loading control and α-synuclein to confirm knockout in SNCA KO cells (same membrane as shown in **Figure 51**)Error! Reference source not found..

b) From Western blot data, LC3II expression in EV and SNCA KO cells in response to A/O was normalised to GAPDH expression to account for differences in protein loading. LC3II expression is represented by the raw values of this calculation. Biological repeats are colour coded, with circles representing the means of each repeat, bars representing the mean of all 3 repeats and black lines showing SEM. Dark grey bars represent EV and light grey bars represent SNCA KO. Statistical analysis was performed with a repeated measures 2-way ANOVA with Sídák's multiple comparisons test. In cells treated with A/O for 6 hours, the difference in LC3II expression levels between EV and SNCA KO cells was significant (p=0.0396, *). (**n=3**).

To investigate whether the impact of α-synuclein on LC3II levels in response to mitochondrial damage was due to defects in autophagosome formation, the experiment was repeated in the presence of BafA1. Since BafA1 blocks all autophagosome-lysosome fusion, it prevents the degradation of autophagosomal cargo and thus causes accumulation of autophagosomes. Interestingly, the reduction of autophagosomes seen at early time points in SNCA KO cells is recovered in the presence of BafA1 (**Figure 55**). This suggests that this phenotype was not the result of a defect in autophagosome formation, instead suggesting that there is increased autophagic flux in SNCA KO cells at earlier time points following mitochondrial damage.

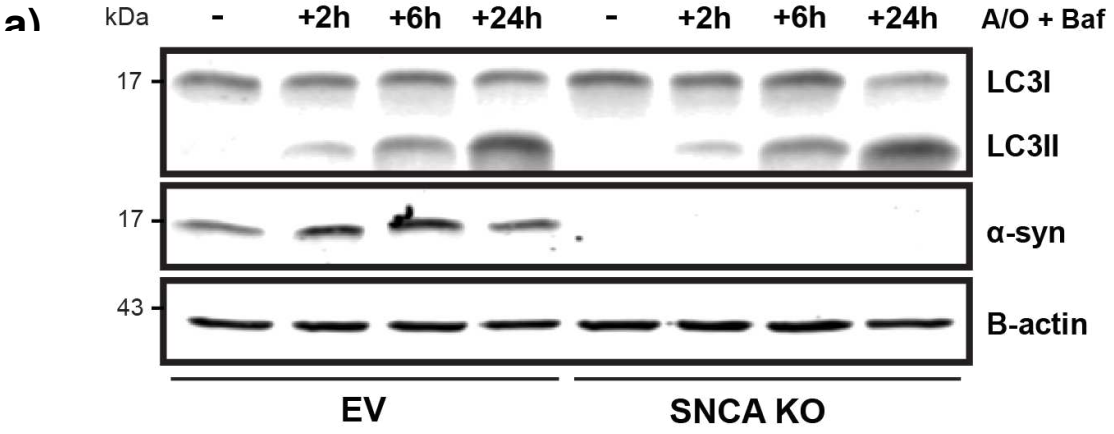
a)
kDa
-
+2h
+6h
+24h
-
+2h
+6h
+24h
A/O + Baf
17
LC3I
LC3II
17
α-syn
43
B-actin
EV
SNCA KO

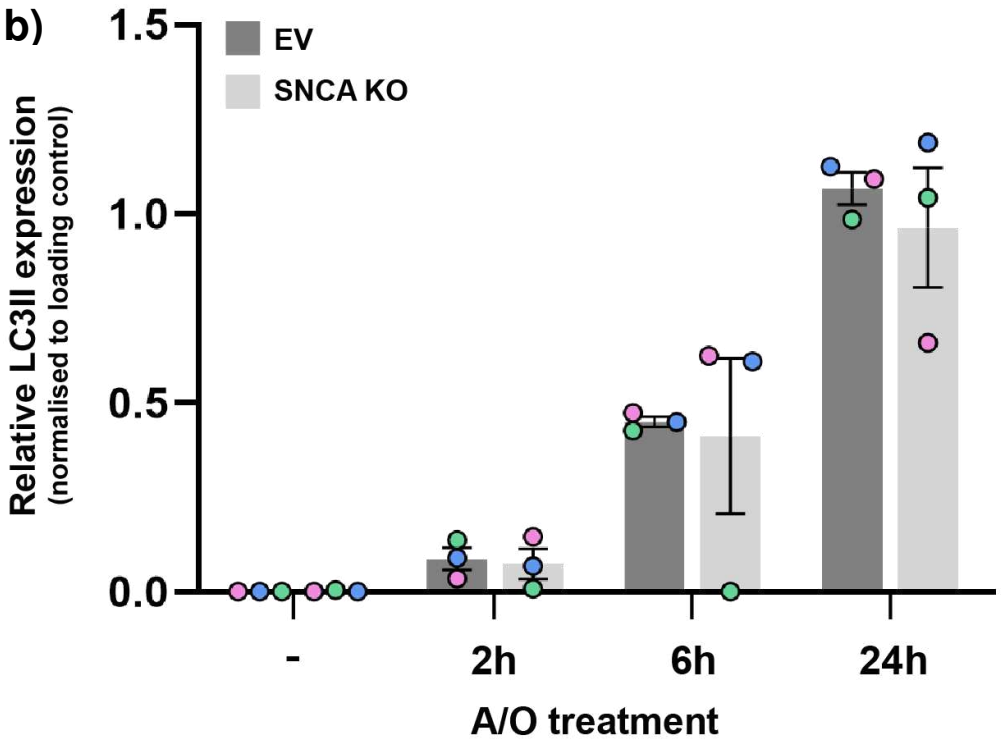
b)
1.5
1.0
0.5
0.0
EV
SNCA KO
Relative LC3II expression
(normalised to loading control)
-
2h
6h
24h
A/O treatment

Figure 55: The lower level of LC3II at early time points following mitochondrial damage in SNCA KO cells is rescued upon inhibition of autophagosome-lysosome fusion

a) EV and SNCA KO cells were left untreated (-) or treated for 2, 6, or 24 hours with A/O and BafA1 to induce mitochondrial damage. Lysates were processed by Western blot with an antibody against LC3, GAPDH as a loading control and α-synuclein to confirm knockout in SNCA KO cells.

b) From Western blot data, LC3II expression in EV and SNCA KO cells in response to A/O was normalised to GAPDH expression to account for differences in protein loading. LC3II expression is represented by the raw values of this calculation. Biological repeats are colour coded, with circles representing the means of each repeat, bars representing the mean of all 3 repeats and black lines showing SEM. Dark grey bars represent EV and light grey bars represent SNCA KO. Statistical analysis was performed with a repeated measures 2-way ANOVA with Sídák's multiple comparisons test and reported no significant differences between groups (**n=3**).

Following the observation that autophagosome flux appears to be increased in SNCA KO cells at early time points, I next evaluated whether a lack of α-synuclein had any measurable effect on lysosomes. Firstly, I assessed whether there were any differences in the morphological characteristics of lysosomes. Lysosomes are able to constantly modify their number and size, with these features shown to influence their ability to function (de Araujo et al., 2020). One example of machinery shown to regulate both lysosomal size and fusion of autophagic membranes is SNARE complexes (de Araujo et al., 2020; W. J. Hong & Lev, 2014; Y. Wang et al., 2016). Interestingly, α-synuclein is known to assemble and interact with SNARE complexes at the synapse to execute its physiological function in the synaptic vesicle cycle (V. Gao et al., 2023). As such, it is possible there may be a role for α-synuclein in regulating lysosomal structure through an interaction with SNAREs, which could impact autophagosome-lysosome fusion events.

Morphological differences in lysosomes were measured in cells at baseline or subject to 24 hours of accrued mitochondrial damage with A/O, when our previous data suggests that the mitophagy response is greatest (**Figure 56**). There were no significant differences in the number of lysosomal puncta per cell (**Figure 57a**) or the total area of lysosomal staining per cell (**Figure 57b**) between EV and SNCA KO cells regardless of mitochondrial damage, though the measurements in SNCA KO cells were trending slightly higher. In calculations of the average area of LAMP1+ puncta per cell, EV cells exhibited a slight increases upon A/O treatment, but this was not seen in SNCA KO cells, suggesting that suggesting that lack of α-synuclein may impact the ability of cells to increase lysosomal size in response to mitochondrial damage (**Figure 57c**).

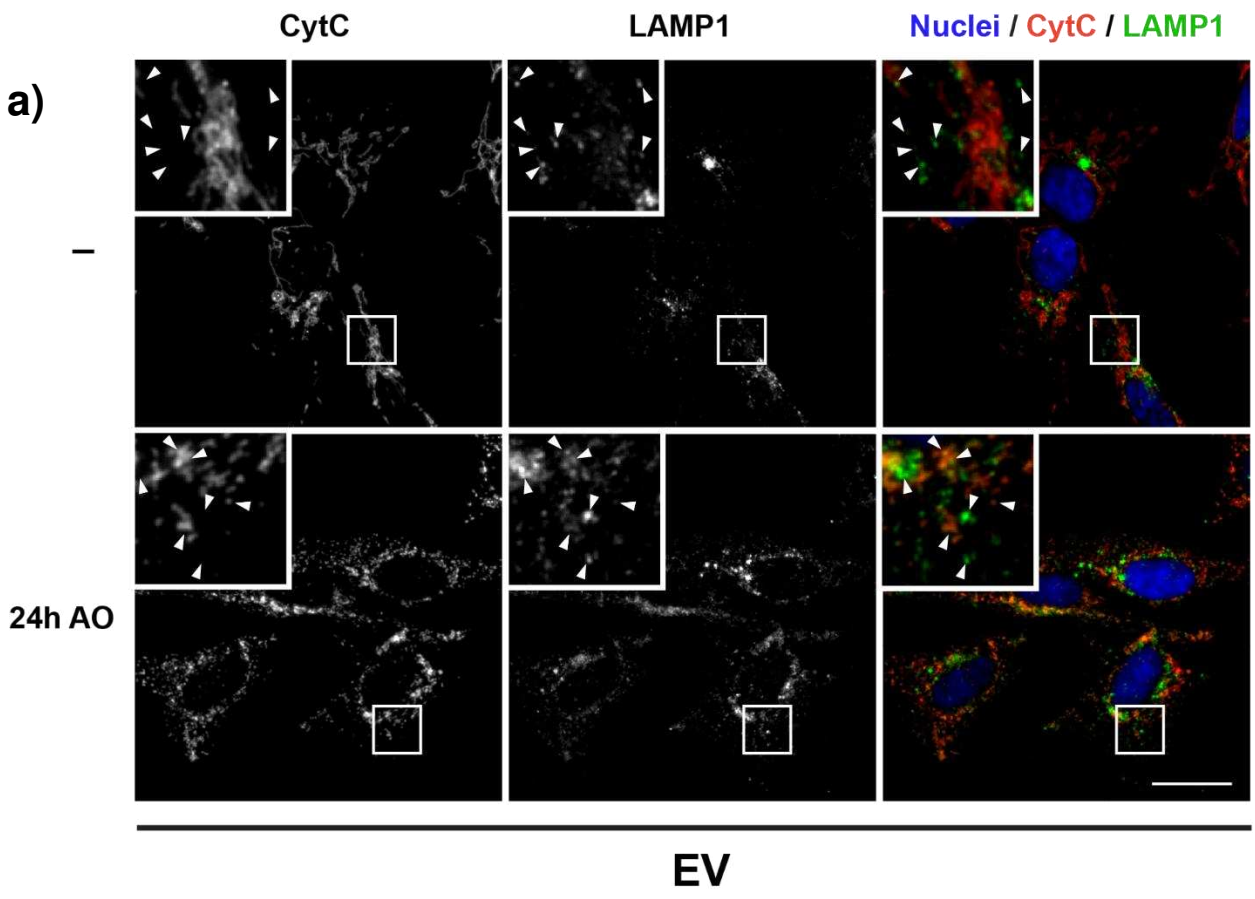
a)
CytC
LAMP1
Nuclei / CytC / LAMP1
–
24h AO
EV

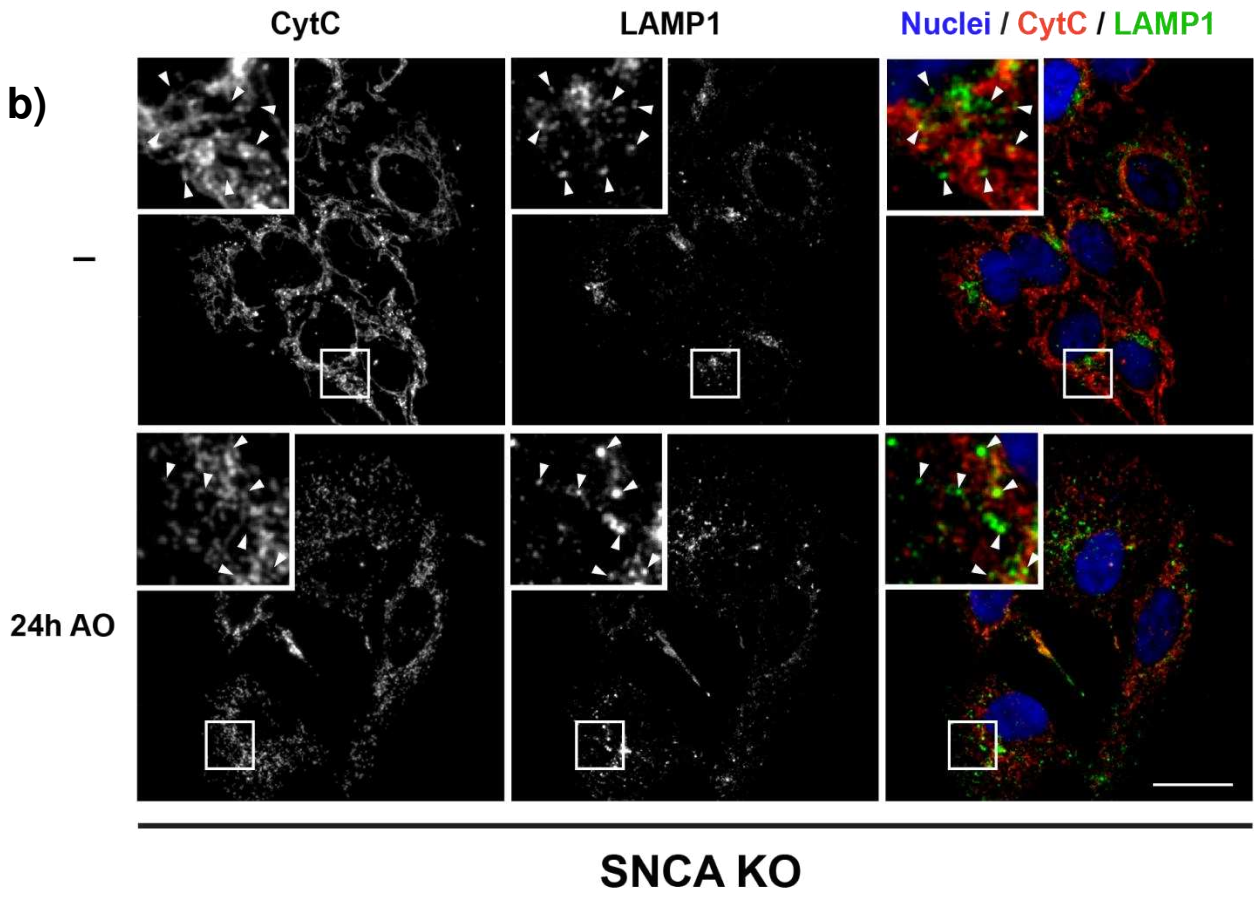
b)
CytC
LAMP1
Nuclei / CytC / LAMP1
–
24h AO
SNCA KO

Figure 56: Lack of α-synuclein causes bigger lysosomes at steady state, resulting in a less pronounced enlargement of lysosomes in response to mitochondrial damage

EV (a) and SNCA KO (b) cells were left untreated (-) or treated for 24 hours with A/O to evoke mitochondrial damage. Cells were fixed and immunostained with antibodies against cytochrome c (red) and LAMP1 (green), with nuclei labelled by Hoechst (blue). Colocalisation between cytochrome c and LAMP1 is shown in yellow. White arrows point to examples of lysosomes in each cell line across the channels, enabling visualisation of lysosome size as well as colocalisation with mitochondria. Images are representative and originate from 1 biological repeat. Images were taken using widefield immunofluorescence microscopy with a 100X objective. Scale bars = 20µm.

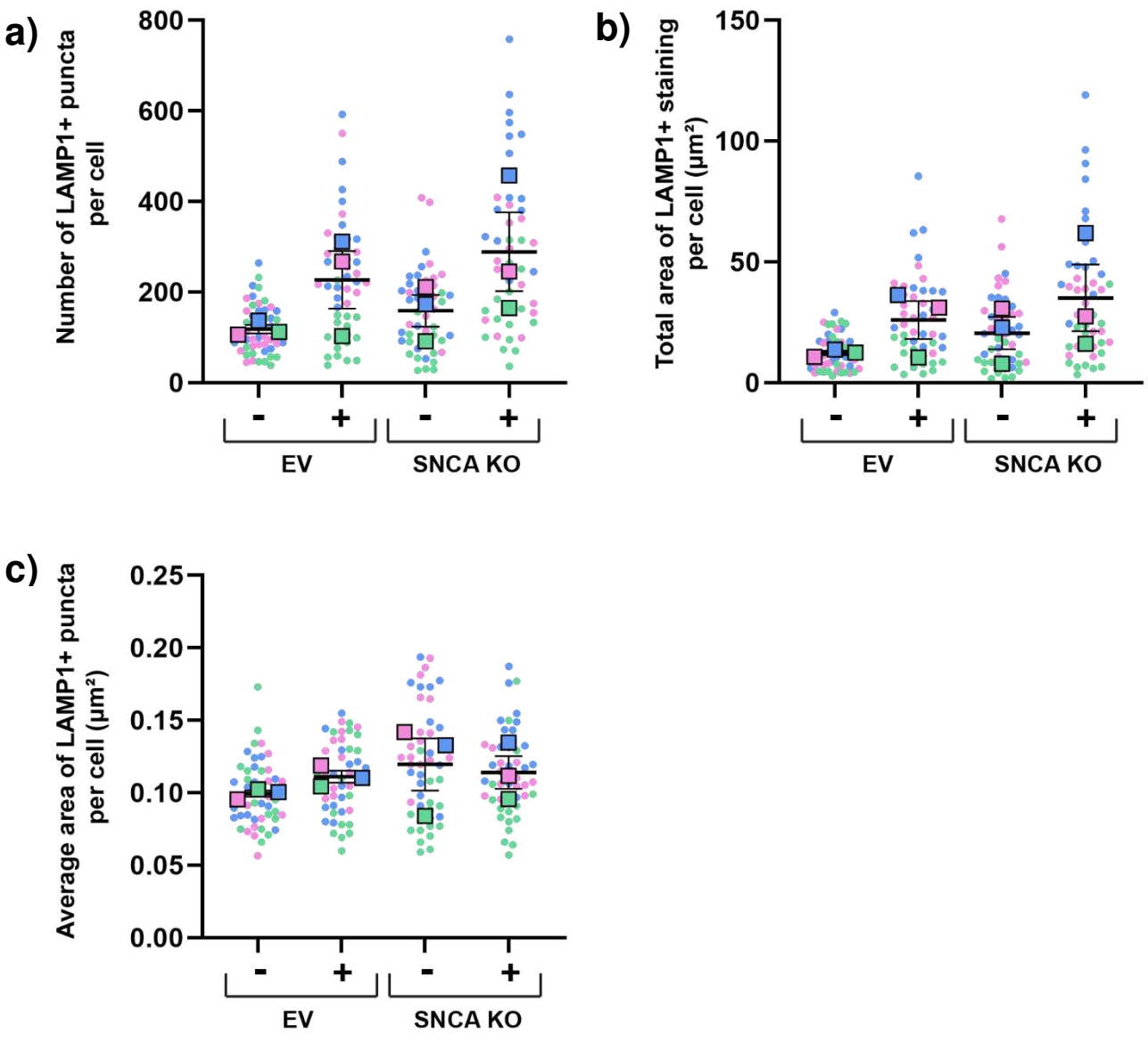

Figure 57: Lack of α-synuclein does not significantly impact lysosomes at steady state

In EV and SNCA KO cells either left untreated (-) or treated with A/O for 24 hours, lysosomal morphology was analysed by isolating cells and within each cell, isolating pixels positive for LAMP1. a) Indicates the number of LAMP1+ puncta per cell, measured by counting the number of individual puncta positive for LAMP1 staining in each individual cell. b) Indicates the total area of LAMP1+ staining per cell, measured by calculating the combined area of all individual LAMP1+ puncta in a given cell. c) Indicates the average area of individual LAMP1+ puncta per cell, calculated by dividing the total area of LAMP1+ staining by the number of LAMP1+ puncta in the same cell. For each measure, 20 cells were analysed per condition, per biological repeat. Measurements from each individual cell are shown by a dot, with the mean of each biological repeat shown by a square and the mean of all 3 repeats shown by a black bar. SEM is shown by vertical black lines. Data points are colour coded by biological repeat. Statistical analysis carried out by repeated measures 2-way ANOVA with Sídák's multiple comparisons test reported no significant differences. (**n=3**).

Given that lysosomes were not observed to increase their average area upon mitochondrial damage in SNCA KO cells, I wanted to investigate whether there were any alterations in the association between mitochondria and lysosomes. Damaged mitochondria are captured by autophagosomes and trafficked to lysosomes for degradation, so I would expect to see mitochondria and lysosomes in association in response to damage. To assess this, I measured colocalisation between the two organelles. This was measured as a percentage of all lysosomes, to provide an idea of how the lysosomal pool shifts in response to 24 hours of A/O, causing accrued damage and triggering mitophagy.

In terms of both lysosomal puncta and area, EV cells were able to upregulate the percentage of lysosomes that colocalised with mitochondria in response to A/O treatment, reflecting trafficking of damaged mitochondria to the lysosome for degradation (**Figure 58a**). However, this increase in the proportion of lysosomal staining associated with mitochondria was not observed in SNCA KO cells. Interestingly, the percentage of lysosomes colocalising with mitochondria was higher at baseline in SNCA KO cells than in EV cells, but was not upregulated in response to mitochondrial stress (**Figure 58b**). This implies that α-synuclein loss-of-function impacts the association between these organelles upon accrued damage, which may relate to a defect in the trafficking of mitochondria to lysosomes.

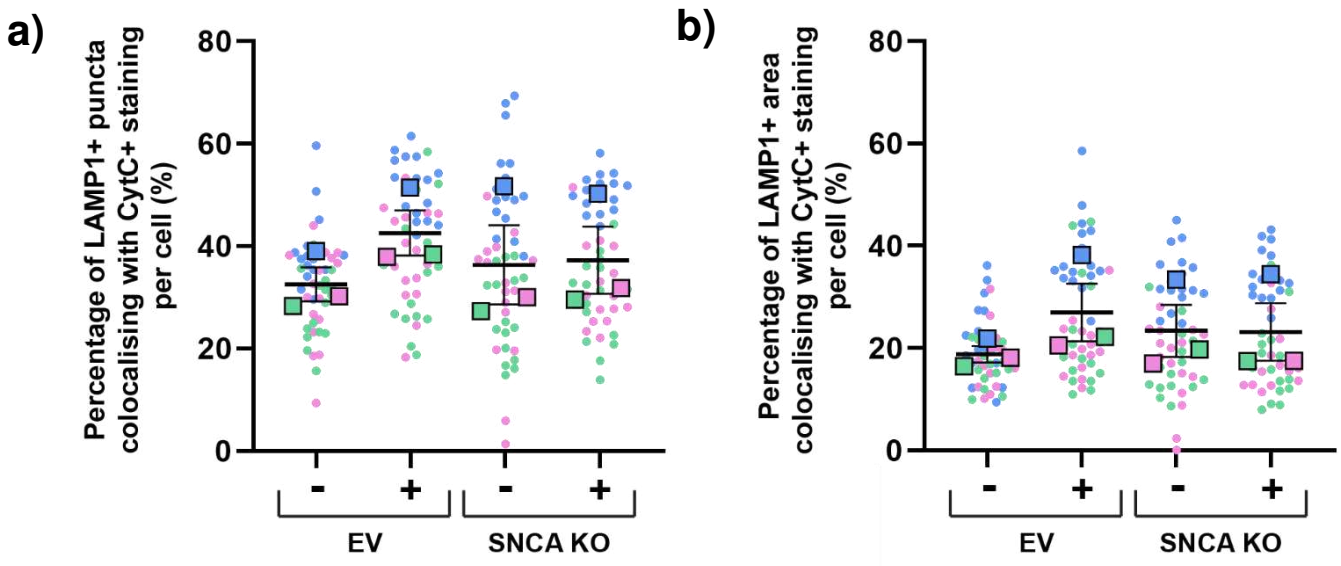

Figure 58: Loss of α-synuclein prevents the upregulation of lysosome-mitochondria colocalisation in response to mitochondrial damage

In EV and SNCA KO cells left untreated (-) or treated with A/O for 24 hours, the colocalisation between lysosomal and mitochondrial staining was measured as a proportion of total lysosomal staining. Image pixels positive for both LAMP1 and cytochrome c were measured, per cell, and presented as a percentage of total LAMP1 (shown in Figure 25a, b). a) Indicates the percentage of all LAMP1+ puncta colocalising with cytochrome c per cell, calculated by dividing the number of colocalised puncta by the total number of LAMP1+ puncta per cell. b) Indicates the percentage of all LAMP1+ area colocalising with cytochrome c staining per cell, calculated by dividing the colocalised area by the total LAMP1+ area per cell. For each measure, 20 cells were analysed per condition, per biological repeat. Measurements from each individual cell are shown by a dot, with the mean of each biological repeat shown by a square and the mean of all 3 repeats shown by a black bar. SEM is shown by vertical black lines. Data points are colour coded by biological repeat. Statistical analysis performed by repeated measures 2-way ANOVA with Sídák's multiple comparisons test reported no significant differences. (**n=3**).

3.2.9 Lack of α-synuclein has no impact on steady state or damage-induced MDVs

Since I have thoroughly investigated the impact of α-synuclein loss-of-function on whole mitochondrial clearance in response to damage, I next investigated whether SNCA KO cells had any defects in mitochondrial repair pathways. One such mechanism that can be upregulated by mitochondrial damage is the MDV pathway (Soubannier et al., 2012a; Soubannier et al., 2012b). Upon mitochondrial stress, locally damaged mitochondrial components can be sequestered inside vesicles derived from mitochondrial membrane and trafficked away from the organelle (Soubannier et al., 2012a; Soubannier et al., 2012b). This strategic removal of damaged contents maintains the health of the organelle left behind, preventing the induction of high-energy processes like mitophagy (Cadete et al., 2016; T. Peng et al., 2022).

Since α-synuclein has been shown to bind and interact with mitochondrial membranes, it could feasibly impact the formation of MDVs. With a role for α-synuclein in co-ordinating vesicle release and recycling at the synapse, it is possible that this could extend to a relationship with MDVs. Shown to act as a sensor of membrane curvature, α-synuclein preferentially binds to highly curved structures like synaptic vesicles (Drin & Antonny, 2010; Emamzadeh, 2016). As such, this property could be a transferable skill for α-synuclein which could allow it to function in the MDV pathway.

Two main structural subtypes of MDVs have been described: those that are TOM20+/PDH- which derived from the OMM, and those that are PDH+/TOM20- that derive from the IMM (Neuspiel et al., 2008; Soubannier et al., 2012a; Sugiura et al., 2014). Although they still form at steady state, MDVs have been shown to selectively incorporate oxidised cargo in response to mitochondrial stress (Soubannier et al., 2012b). Previous research from our lab has shown that MDVs are upregulated in SH-SY5Y cells in response to 2 hours of A/O treatment, so this stimulus was used to assess whether α-synuclein loss-of-function alters the levels of MDVs (T. A. Ryan et al., 2020). Both OMM- and IMM-derived MDVs were quantified (**Figure 59**), since evidence has shown the ability of α-synuclein to bind both mitochondrial membranes (Devi et al., 2008; Di Maio et al., 2016; K. Nakamura et al., 2008).

In terms of OMM-derived MDVs (TOM20+/PDH-), both EV and SNCA KO cells were able to produce MDVs as a steady state quality control mechanism and to significantly increase the number of MDVs (EV p=0.0251, SNCA KO p=0.0281) in response to AO-induced mitochondrial damage (**Figure 60a**). The same trend was true for IMM-derived MDVs (PDH+/TOM20-), with both cell lines equally able to generate MDVs both at steady state and in response to A/O (**Figure 60b**). This suggests that loss of α-synuclein does not impact the level of MDVs at steady state or in response to mitochondrial damage.

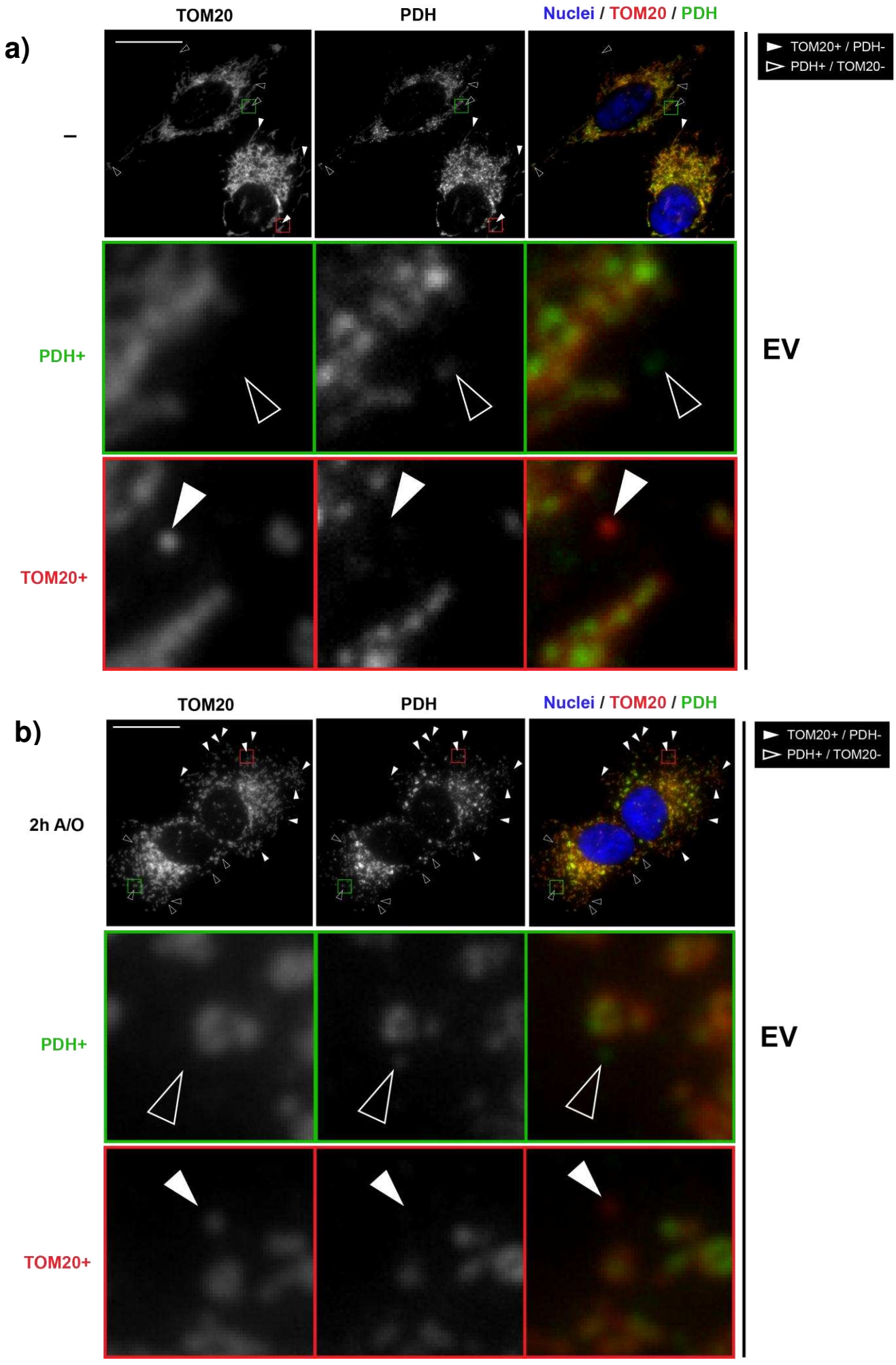
a)
TOM20
PDH
Nuclei / TOM20 / PDH
TOM20+ / PDH-
PDH+ / TOM20-
–
PDH+
TOM20+
EV
b)
TOM20
PDH
Nuclei / TOM20 / PDH
TOM20+ / PDH-
PDH+ / TOM20-
2h A/O
PDH+
TOM20+
EV

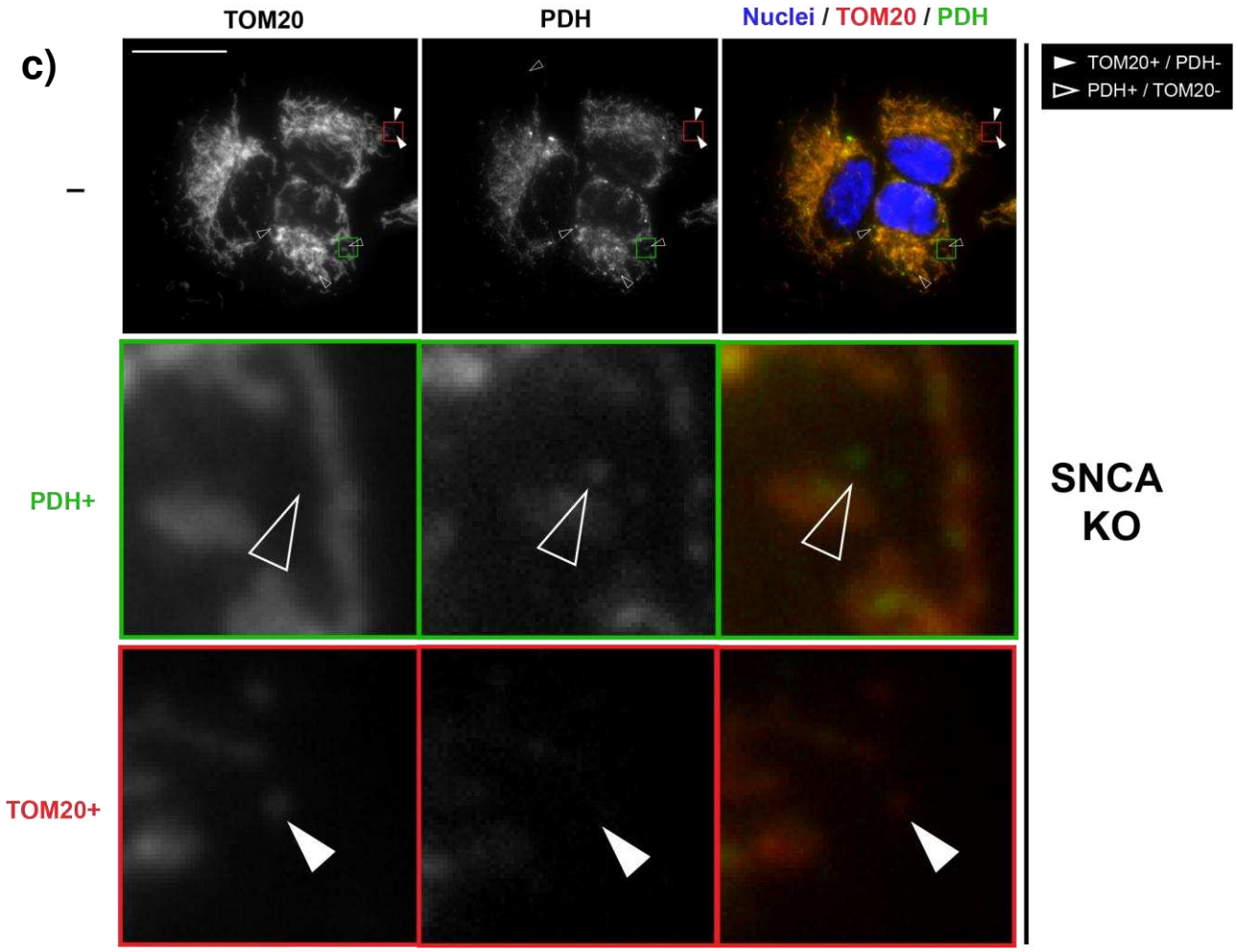
c)
TOM20
PDH
Nuclei / TOM20 / PDH
TOM20+ / PDH-
PDH+ / TOM20-
–
PDH+
TOM20+
SNCA KO

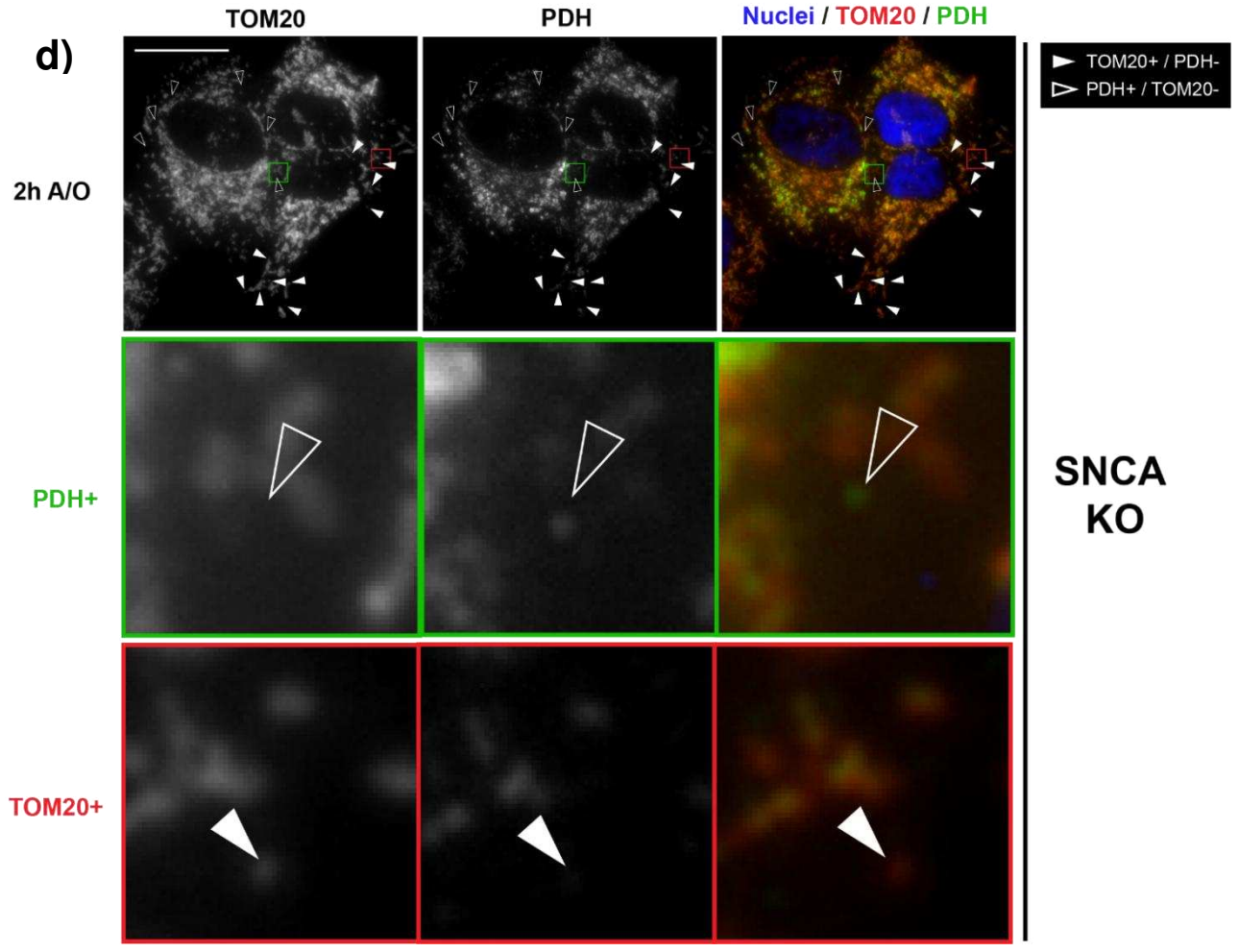
d)
TOM20
PDH
Nuclei / TOM20 / PDH
TOM20+ / PDH-
PDH+ / TOM20-
2h A/O
PDH+
TOM20+
SNCA KO

Figure 59: Cells lacking α-synuclein have more MDVs after 2 hours of mitochondrial damage than at steady state

EV (a, b) and SNCA KO (c, d)cells were left untreated (-) or treated for 2 hours with A/O to evoke mitochondrial damage (b). Cells were fixed and immunostained with antibodies against TOM20 (red) and PDH (green) with nuclei labelled by Hoechst (blue). PDH+/TOM20- MDVs were defined as PDH+ puncta that did not colocalise with TOM20 – these are shown with outlines of white arrowheads, with images in green showing an example of the inclusion of PDH and exclusion of TOM20 in more detail. TOM20+/PDH- MDVs were defined as TOM20+ puncta that did not colocalise with PDH – these are shown with solid white arrowheads, with images in red showing an example of the inclusion of TOM20 and exclusion of PDH in more detail. Images shown are representative and were taken using widefield immunofluorescence microscopy on a 100X objective. Scale bars = 20µm.

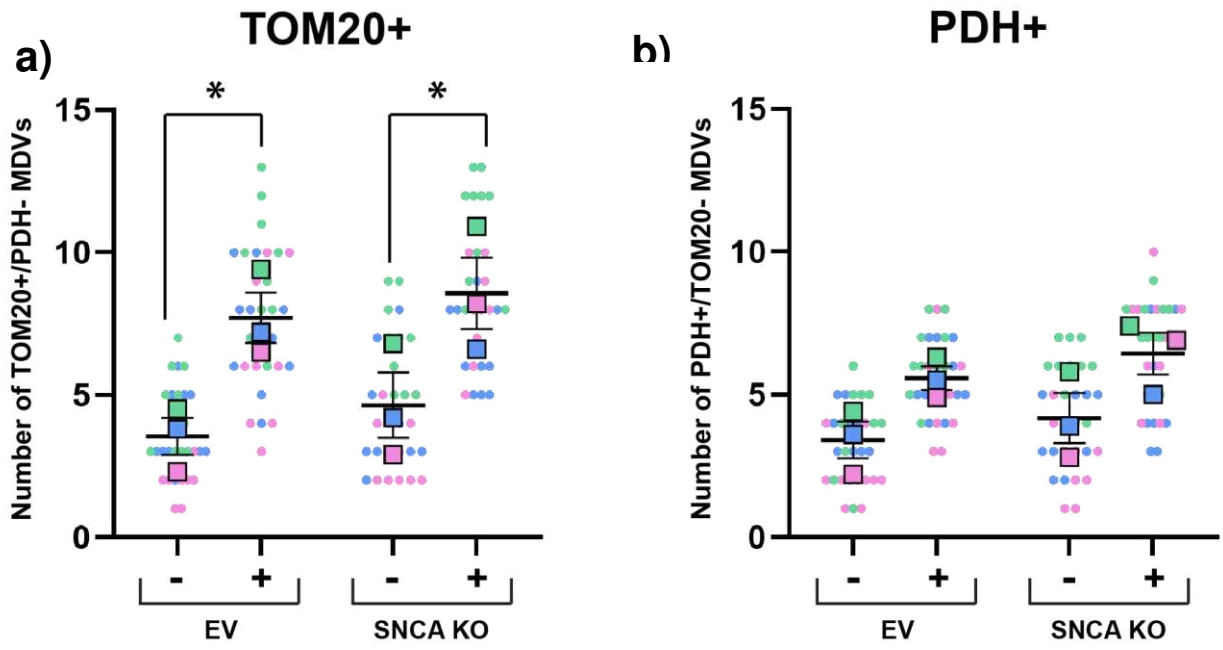

Figure 60: Lack of α-synuclein has no impact on the ability of cells to generate both OMM- and IMM-derived MDVs at steady state or in response to mitochondrial damage

EV and SNCA KO cells were left untreated (-) or treated for 2 hours with A/O to evoke mitochondrial damage. MDVs were counted based on lack of colocalisation of mitochondrial markers TOM20 and PDH. a) Indicates the number of TOM20+/PDH- MDVs, while b) indicates the number of PDH+/TOM20- MDVs. 10 cells were analysed per condition, per biological repeat. Measurements from each individual cell are shown by a dot, with the mean of each biological repeat shown by a square and the mean of all 3 repeats shown by a black bar. SEM is shown by vertical black lines. Data points are colour coded by biological repeat. Statistical analysis performed by repeated measures 2-way ANOVA with Sídák's multiple comparisons test. There was a significant increase in TOM20+ MDVs between untreated cells and those treated with A/O for 2 hours in both EV control cells (p=0.0251, *) and SNCA KO cells (p=0.0281, *), but no differences between cell lines. (**n=3**).

3.3 Discussion

In this chapter, I aimed to investigate the role of α-synuclein in mitochondrial health, function and quality control using an SNCA KO model developed in SH-SY5Y cells. The hypothesis that α-synuclein loss-of-function, rather than toxic gain-of-function, may potentiate some aspects of PD pathology is often overlooked in the literature (Sulzer & Edwards, 2019). Therefore, defining potential physiological roles for α-synuclein in maintaining mitochondrial health and mito-QC mechanisms offers important insight into its wider cellular function, and how the potential loss of these functions may contribute to PD. The results from this chapter indicate that loss of α-synuclein does not cause significant defects in mitochondrial energy production or damage-induced mitochondrial turnover but has minor impacts on early autophagic flux.

Prior to creation of my loss-of-function model, initial investigations in wild-type SH-SY5Y cells characterised the impact of mitochondrial damage on α-synuclein expression. Accrued mitochondrial damage was shown to trigger a decrease in α-synuclein expression that was partially rescued by inhibition of proteasomal and lysosomal pathways, suggesting that damage-induced α-synuclein degradation occurs through both of these mechanisms. This is in support of previous work showing degradation of endogenous α-synuclein by both the proteasome and chaperone-mediated autophagy (Bennett et al., 1999; Cuervo et al., 2004; Tofaris et al., 2001). Given that this degradation was triggered by mitochondrial damage, I considered whether α-synuclein may be associated with, or recruited to, mitochondria under these conditions. Localisation of α-synuclein to mitochondria has mostly been described in a pathological context, where oxidative stress is high and α-synuclein is aggregated (M. L. Choi et al., 2022; Devi et al., 2008), so I sought to assess whether this may occur when α-synuclein is at a physiological level. Assessment of isolated mitochondrial fractions from A/O treated cells did not show any evidence of association between α-synuclein and mitochondria. Unfortunately, mitochondrial localisation of α-synuclein via immunofluorescence microscopy could not be determined due to a lack of antibody specificity. From my data, I consider that α-synuclein was likely not recruited to mitochondria as part of the damage response, but instead may have been degraded as a result of antimycin A-induced production of mitochondrial ROS (Boveris & Cadenas, 1975). Though research has described that ROS can promote aggregation of α-synuclein, this has mostly been observed in terms of chronic, long-term exposure to oxidative stress conditions (Hashimoto et al., 1999; Paxinou et al., 2001; Won et al., 2022). Therefore, it is unlikely that endogenous α-synuclein was aggregated to the point of cellular removal upon 2-24 hours of A/O treatment. Instead, I consider a hypothesis described by Schildknecht et al (2013)

that suggests α-synuclein may act as a scavenger of ROS under physiological conditions, protecting the cellular environment. Oxidation of α-synuclein methionine residues has been suggested as a mechanism to facilitate this, removing damaged ROS from the cell but perhaps making α-synuclein a target for degradation (Glaser et al., 2005; Schildknecht et al., 2013).

After generating and validating an SNCA KO model in SH-SY5Y cells, I began to evaluate the impact of α-synuclein loss-of-function on various mitochondrial phenotypes. Starting with mitochondrial function, I investigated ATP levels, oxygen consumption rates and baseline ΔΨm as readouts of mitochondrial energy production and organelle health. These were all found to be unaffected by the loss of endogenous α-synuclein, suggesting that it does not have an essential role in maintenance of ΔΨm or in regulating mitochondrial energy production. These findings were unexpected, since they contradict a previous study that defined a role for physiological α-synuclein in modulation of the ATP synthase pump (Ludtmann et al., 2016). This study found that mitochondria in cells from α-synuclein knockout mice produced less ATP, which was rescued by the addition of exogenous α-synuclein monomers (Ludtmann et al., 2016). However, they also reported that loss of other synuclein isoforms, β- and γ-synuclein, had similar consequences in their model (Ludtmann et al., 2016). The structure of β-synuclein in particular is highly homologous to α-synuclein, with the N-terminus in both proteins containing KTKEGV sequences that facilitate membrane binding (Hayashi & Carver, 2022; Westphal & Chandra, 2013). Along with the fact that α- and β-synuclein are often co-expressed in the human body, structural similarities between the proteins have led to suggestions that they may have similar or co-operative functions (Hayashi & Carver, 2022). In support of this, β-synuclein has been shown to interact with and modulate synaptic vesicles in a similar way to physiological α-synuclein (Ninkina et al., 2021). In the context of my results, I suggest that the genetic SNCA KO model developed in this study may have adapted to a lack of α-synuclein, with other members of the synuclein family compensating for its cellular role.

Once I established that loss of α-synuclein did not impact mitochondrial energy production in my model, I next investigated whether it caused any alterations in organisation of the mitochondrial network. Given α-synuclein's other cellular functions related to membrane remodelling, whether this extends to mitochondrial membranes is an important question that has not been previously addressed in the literature. I observed that both at steady state and under damage conditions, there were no differences in the morphology and connectivity of mitochondria in SNCA KO cells compared to EV control cells. These data led me to conclude that in my model, α-synuclein is not required to maintain the organisation of the mitochondrial

network. Since mitochondrial morphology is regulated by a fine balance of fission and fusion, I therefore suggest that α-synuclein is not required for these events either at steady state or in response to damage (Bereiter-Hahn & Voth, 1994; H. Chen & Chan, 2004). Though α-synuclein is involved in membrane remodelling at the synapse, I do not see evidence that this extends to a role in regulating mitochondrial morphology (Cheng et al., 2011). This contradicts evidence from murine models which showed that α-synuclein null mice exhibited fragmented mitochondria, but as yet this is the only other study that has investigated the impact of α-synuclein loss-of-function on mitochondrial organisation (Faustini et al., 2019). Consequently, I suggest that the alterations in mitochondrial organisation, morphology and fission-fusion mechanics seen in PD patients are likely due to toxic gain-of-function from pathological α-synuclein and not the result of loss-of-function of pathological α-synuclein (Chen et al., 2023).

In assessing mito-QC, I discovered that α-synuclein loss-of-function did not affect the degradation of mitochondria by mitophagy. The fact that SNCA KO cells were still able to efficiently conduct whole mitochondrial clearance and exhibit increased PINK1/Parkin activity in response to damage indicates that in my model, α-synuclein does not have an essential role in the co-ordination of PINK1/Parkin-dependent mitophagy. However, the observation that Parkin expression was significantly elevated in SNCA KO cells at steady state suggests that a potential regulatory relationship may exist between α-synuclein and Parkin. This fits with previous literature, with earlier work showing that exogenous α-synuclein oligomers can decrease Parkin expression through S-nitrosylation and subsequent degradation of the protein (Wilkaniec et al., 2019, 2021). Such an association has only been described in the context of both pathological α-synuclein and Parkin overexpression, but I provide evidence that this relationship may also exist physiologically at steady state. Interestingly, SNCA KO cells showed slightly lower levels of mitochondrial pUb S65 compared to EV control cells, which could represent an increase in the turnover of damaged mitochondria as a result of increased Parkin availability. I suggest that though the relationship between Parkin and α-synuclein is not required for Parkin function, modulation of Parkin expression by α-synuclein may impact its activity.

Further investigation into the later stages of these mitochondrial degradation pathways revealed that α-synuclein loss-of-function impacted both autophagosomal and lysosomal phenotypes. Measurement of LC3 lipidation demonstrated that cells lacking α-synuclein exhibited less autophagosomes than EV control cells in response to 2 or 6 hours of mitochondrial damage. This early reduction in autophagosomes was recovered to EV control

levels when autophagosome-lysosome fusion was blocked, suggesting that the loss-of-function phenotype may be the result of increased autophagic flux, rather than decreased autophagosome formation. Interestingly, SNCA KO cells did not show the damage-induced increase in colocalisation between the mitochondrial marker, TOM20, and the lysosomal marker, LAMP1, seen in EV control cells. This could be due to increased autophagic flux at early time points, as suggested by the LC3II data. Since colocalisation was visualised after 24 hours of A/O treatment, I only see a snapshot of the response to damage, so it is possible that the highest level of colocalisation between mitochondria and lysosomes may have occurred at an earlier time point in SNCA KO cells which was not captured by these data. One explanation for this could be that SNCA KO cells have an increased availability of lysosomes ready to degrade autophagic contents at these early time points, since immunofluorescence microscopy showed that lack of α-synuclein increased total puncta and area of LAMP1 staining per cell at steady state.

A potential mechanism behind this effect could be that α-synuclein loss-of-function may contribute to disinhibition of transcription factor EB (TFEB), a protein known to promote lysosome biogenesis and autophagy (Cortes & La Spada, 2019; Martina et al., 2014). Under normal circumstances, TFEB interacts with the chaperone protein 14-3-3, leading to its sequestration in the cytoplasm and prevention of its translocation to the nucleus to trigger transcription of autophagy-promoting genes (Martina et al., 2014; Raben & Puertollano, 2016). Interestingly, α-synuclein exhibits both structural and functional homology with 14-3-3, with studies showing its ability to bind 14-3-3 interacting partners which could feasibly include TFEB (Ostrerova et al., 1999; Perez et al., 2002b). Under pathological conditions, α-synuclein and TFEB have been shown to have a direct relationship, with α-synuclein overexpression leading to an increase in cytoplasmic retention of TFEB and a subsequent reduction in autophagy (Decressac et al., 2013). As such, it is possible that α-synuclein may have a physiological role, akin to that of 14-3-3, in the retention of TFEB in the cytoplasm which is lost in my SNCA KO model. Loss of this interaction may therefore increase translocation of TFEB to the nucleus and account for the increase in autophagic flux and LAMP1 staining seen in these cells (**Figure 61**).

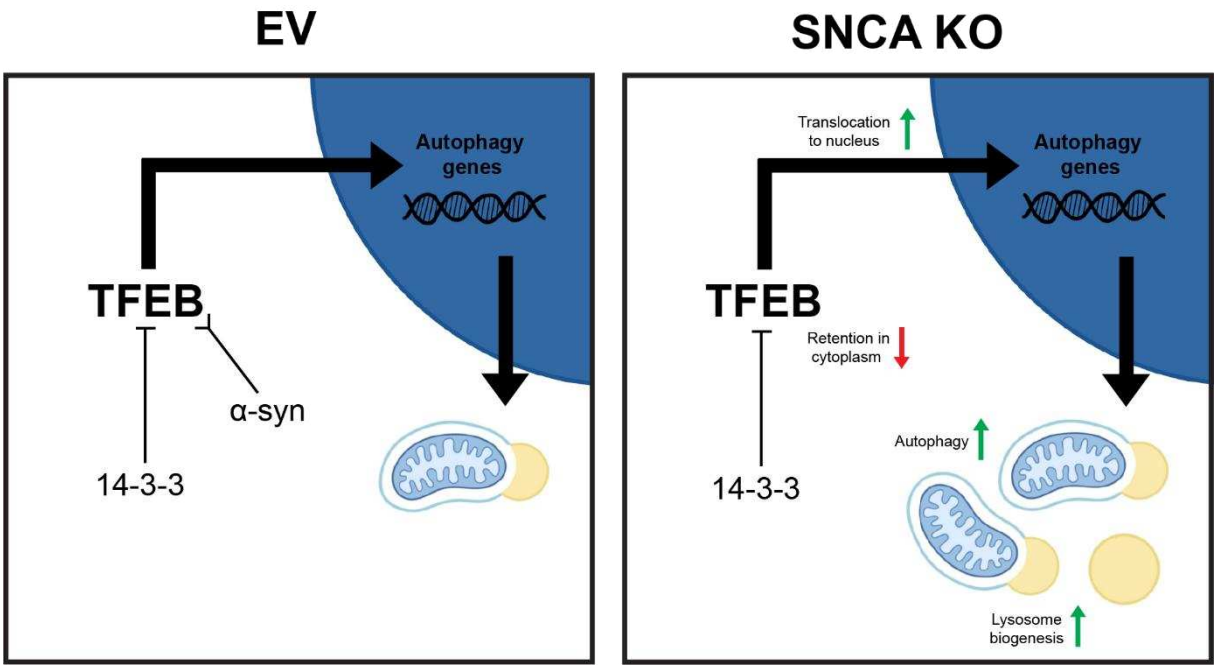

Figure 61: Potential mechanism for increased early autophagy flux and increased steady state lysosome number in SNCA KO cells

We propose that a potential mechanism behind the increase in autophagy flux and lysosomal number could be that SNCA KO cells have a loss of disinhibition of TFEB. Normally, 13-4-4 sequesters TFEB in the cytoplasm to prevent its translocation to the nucleus and promotion of autophagy. Since α-synuclein shares structural and functional homology with 13-4-4, I suggest that it may have a similar role in modulating TFEB. When α-synuclein is lost, less TFEB may be retained in the cytoplasm, leading to an increase in its translocation to the nucleus and subsequent increases in transcription of genes promoting autophagy and lysosome biogenesis.

Given the loss-of-function phenotypes observed at early time points, I felt it important to investigate alternative mitochondrial repair routes known to be active in response to localised oxidative stress. Shown to selectively incorporate oxidised cargo, MDVs are upregulated in response to short-term mitochondrial stress to sequester damaged components away from the organelle, maintaining mitochondrial health (Soubannier et al., 2012a; Soubannier et al., 2012b; Sugiura et al., 2014). Physiological functions of α-synuclein are most well-defined in the synaptic vesicle pathway, where it can remodel phospholipid membranes and facilitate membrane trafficking to modulate vesicle release (Burré, 2015; Drin & Antonny, 2010; H. J. Lee et al., 2011; Murphy et al., 2000). These same mechanisms are required in the MDV pathway, and since α-synuclein has been shown to bind mitochondrial membranes, I considered that its function in vesicle modulation may extend to MDVs. I found that α-synuclein loss-of-function did not impact the number of MDVs at steady state or in response to mitochondrial damage, suggesting that it may not have a physiological role in this pathway despite its affinity for

vesicles. Since α-synuclein's role in vesicle release is facilitated by its preferential binding of highly curved membranes, the fact that MDVs are ~70-150nm in diameter may mean that compared to ~40nm synaptic vesicles, their membranes do not have sufficient curvature to prompt α-synuclein binding (Drin & Antonny, 2010; Middleton & Rhoades, 2010; Neuspiel et al., 2008; Sudhof, 1999). Though α-synuclein has previously been highlighted as one of a wealth of proteins associated with MDVs in a proteomics study, based on my data I suggest that this is likely as cargo rather than as a regulator of the pathway (R. F. Roberts et al., 2021).

Summary

To summarise, this chapter uses a loss-of-function model to provide novel insight into the potential physiological roles of α-synuclein on mitochondrial health and quality control. First, I established that a lack of α-synuclein did not impact ATP level, oxygen consumption rates or maintenance of baseline ΔΨm, suggesting that the physiological function of α-synuclein is not required to facilitate energy production. In terms of mito-QC, I found that loss of α-synuclein did not impact organisation of the mitochondrial network, and thus co-ordination of fission-fusion events. Assessment of responses to localised mitochondrial damage revealed that α-synuclein likely does not have a physiological role in the MDV pathway, since numbers of MDVs at baseline and in response to stress were not impacted by α-synuclein loss-of-function. Though overall damage-induced whole mitochondrial clearance was unaffected by a loss of α-synuclein, levels of pUb s65 indicated a potential increase in mitophagic turnover. In line with this, investigations into autophagosomes and lysosomes suggested increased turnover of both autophagosomes and lysosomes at early time points, indicative of a potential physiological role for α-synuclein in regulating early autophagic flux and lysosomal turnover. I suggest that potential mechanisms behind this could be increased availability of both Parkin and lysosomes at steady state, priming the system for a damage response. Further research is needed to validate these phenotypes in more detail and establish whether α-synuclein loss-of-function could contribute to the dysfunctional autophagy phenotypes reported in PD (Anglade et al., 1997).

Chapter 4 Investigating the impact of pathological α-synuclein overexpression on mitochondrial health and quality control

4.1 Introduction

Mitochondrial dysfunction is widely considered to be a key driver of PD, with clinical research reporting mitochondrial pathology in the brains of PD patients (Bender et al., 2006; Schapira et al., 1989). The relationship between mitochondrial dysfunction and PD pathogenesis has been validated by the discovery that mutations in several key mitochondrial genes are causative for familial forms of the disease (Billingsley et al., 2019). Importantly, many of these genes have defined functions in mito-QC pathways, such as mitophagy co-ordinators PINK1 and Parkin (Kitada et al., 1998; Valente et al., 2004). As such, recent research has considered that mitochondrial dysfunction in PD may be the result of defective mito-QC mechanisms (Chen et al., 2023; Ge et al., 2020).

The most well-characterised aspect of PD pathology is the aggregation of α-synuclein, the protein which forms intracellular Lewy-body inclusions in the PD brain (Spillantini et al., 1997). Though the precise mechanisms of α-synuclein toxicity are not understood, pathological forms have been shown to trigger progressive cell death in animal models (A. Cooper et al., 2006; Sousa et al., 2009). As two established drivers of PD pathology, a potential association between α-synuclein and mitochondrial dysfunction has been explored in the literature. Aggregated α-synuclein has been shown to bind mitochondrial membranes, with accumulation coupled to mitochondrial localisation in PD brains (Devi et al., 2008; X. Wang et al., 2019). These mitochondrial interactions have a direct impact on organelle function, with pathological α-synuclein shown to reduce ATP production through impairment of complex I of the ETC (Chinta et al., 2010; X. Wang et al., 2019). However, limited research has extended these investigations to assess the relationship between α-synuclein and dysfunctions in mito-QC.

Links have been made between pathological α-synuclein and mitophagy, with accumulation of α-synuclein species shown to cause delays in mitochondrial clearance and impairments in both autophagosomal maturation and autophagosome-lysosome fusion (Kinnart et al., 2024; Sarkar et al., 2021; Shaltouki et al., 2018; Tang et al., 2021). A range of mechanisms have been suggested for these phenotypes, including interactions between α-synuclein and proteins known to regulate cargo identification and trafficking in mito-QC, such as Parkin and SNARE complexes (Tang et al., 2021; Wilkaniec et al., 2021). Despite these

suggestions, there is no consensus on the mechanisms behind α-synuclein's ability to disrupt mitophagy. Even less is known about the impact of pathogenic α-synuclein on mechanisms beyond PINK1/Parkin-dependent mitophagy, such as MDVs and mitochondrial dynamics.

Mutant forms of α-synuclein associated with familial PD have been demonstrated to behave slightly differently to the wild-type (WT) protein (Ohgita et al., 2022). With a point mutation in the N-terminus of α-synuclein, the mutant A53T form of the protein has been suggested to have increased aggregation propensity and altered binding to phospholipid membranes (Jo et al., 2000; Ohgita et al., 2022; Polymeropoulos et al., 1997). Interestingly, α-synuclein A53T has been shown to have increased accumulation at mitochondrial membranes compared to the WT protein in human dopaminergic neurons, accompanied by an increase in its mitochondrial import (Devi et al., 2008). Further, recent research has shown that α-synuclein A53T exhibits oligomerisation at mitochondrial membranes that induces toxicity (M. L. Choi et al., 2022). Alongside this, functional studies have shown that overexpression of A53T α-synuclein can cause an increase in mitophagy, contrary to the delay in mitophagy reported for the WT protein (Chen et al., 2015; Choubey et al., 2011; Stefanis et al., 2001). As such, I investigated and compared the impact of both WT and A53T α-synuclein overexpression on mechanisms of mito-QC.

In this chapter, I aimed to test the hypothesis that overexpression of α-synuclein negatively impacts mitochondrial function and quality control through toxic gain-of-function. I investigated this by generating SH-SY5Y cell lines stably overexpressing either GFP-α-syn-WT or GFP-α-syn-A53T. Responses to mitochondrial damage were assessed in these cells to evaluate the impact of α-synuclein overexpression on mitochondrial health, dynamics and mito-QC mechanisms.

Aims:

1) Develop gain-of-function models of α-synuclein in SH-SY5Y cells
2) Utilise the gain-of-function models to assess the impact of WT and A53T α-synuclein overexpression on mitochondrial function and dynamics
3) Utilise the gain-of-function models to assess the impact of WT and A53T α-synuclein overexpression on mito-QC

4.2 Results

4.2.1 Development and validation of α-synuclein gain-of-function models in SH-SY5Y cells

Many studies in this field utilise exogenous α-synuclein in the form of pre-formed fibrils (PFFs) to study toxic gain-of-function. However, evidence suggests that although both oligomeric and fibrillar α-synuclein are harmful, fibrillar α-synuclein is more stable and less damaging (Emin et al., 2022; Winner et al., 2011). Since the oligomerisation process itself is considered to be damaging, models employing PFFs do not capture this key aspect of α-synuclein toxicity. To overcome this, I generated gain-of-function models in SH-SY5Y cells overexpressing WT and A53T forms of GFP-α-synuclein. Since a higher concentration of the protein equates to a higher aggregation propensity, I utilised an overexpression system to provide an environment whereby assembly of de-novo higher order α-synuclein species could occur (Narhi et al., 1999).

Since GFP-tagged α-synuclein has been demonstrated to aggregate and induce toxicity, plasmids containing GFP fused to the N-terminus of α-synuclein were used so that successful overexpression of the protein could be visualised easily (Hansen et al., 2013). These sequences are referred to as GFP-α-syn from this point onwards. Initially, SH-SY5Y cells were transiently transfected with GFP-α-syn-WT and GFP-α-syn-A53T plasmids to confirm detectable overexpression prior to generation of stable cell lines. A plasmid containing only GFP was used as a control to rule out any impacts of the transfection process and confirm that overexpression of GFP did not induce any cellular toxicity. This overexpression was confirmed by both Western blot (**Figure 62**) and immunofluorescence microscopy (**Figure 63**). Since overexpression of GFP-α-syn was confirmed in a transient setting, these sequences were used to generate stable cell lines.

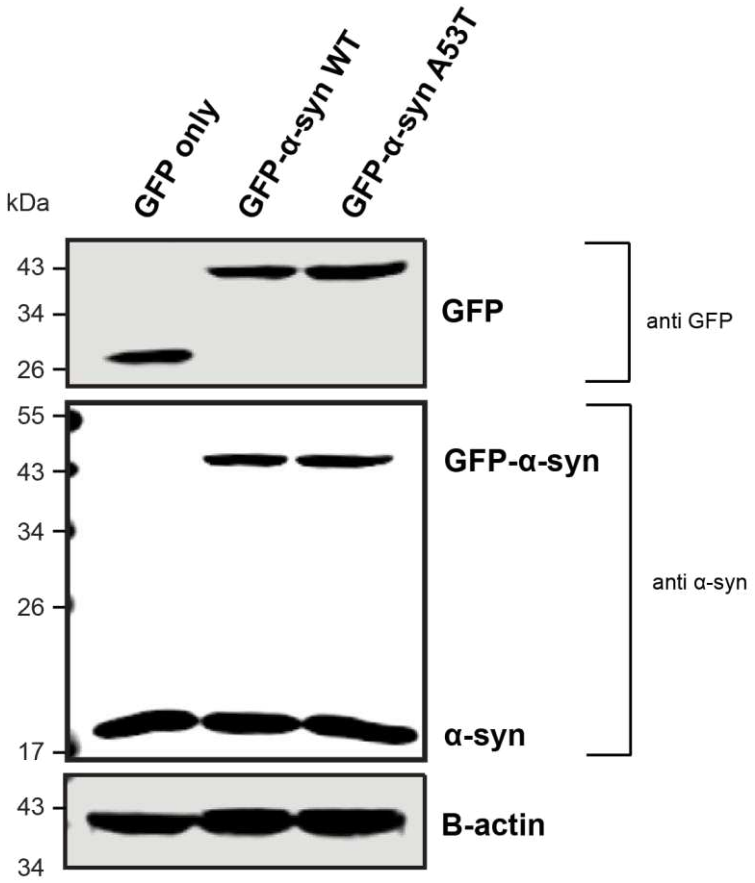

Figure 62: GFP-α-syn is detected by Western blot in SH-SY5Y cells transiently overexpressing GFP-α-syn-WT and GFP-α-syn-A53T plasmids

Wild-type SH-SY5Y cells were transfected with plasmids containing either GFP only, GFP-α-syn-WT or GFP-α-syn-A53T sequences. After 24 hours, lysates were processed by Western blot with antibodies against GFP, α-synuclein and B-actin as a protein loading control. GFP-α-syn is shown detected by both GFP and α-synuclein antibodies.

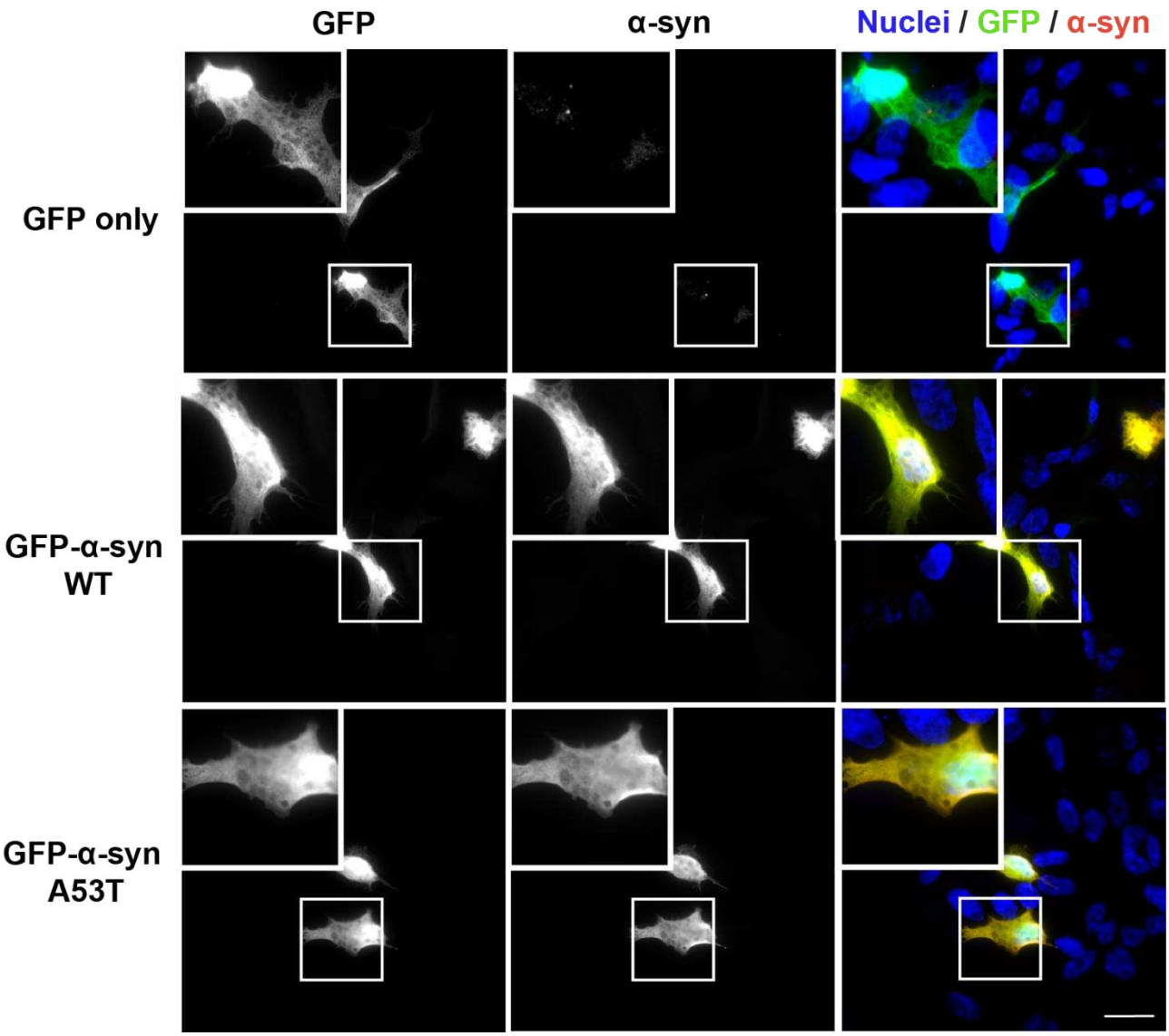

Figure 63: GFP-α-syn is detected by immunofluorescence microscopy in SH-SY5Y cells transiently overexpressing GFP-α-syn-WT and GFP-α-syn-A53T plasmids

Wild-type SH-SY5Y cells were transfected with plasmids containing either GFP only, GFP-α-syn-WT or GFP-α-syn-A53T. After 24 hours, cells were fixed and stained with antibodies against α-synuclein (red) and GFP (green), with nuclei labelled by Hoechst (blue). Colocalisation of α-synuclein and GFP is reflected by yellow staining. Cells were imaged using widefield immunofluorescence microscopy on a 60X objective. Scale bar = 20µm.

After confirming that transfection with these plasmids enabled SH-SY5Y cells to transiently overexpress α-synuclein, I aimed to generate a model that overexpressed this stably using lentiviral vectors.

Lentiviruses are a commonly used genetic tool that facilitate stable expression of chosen genes through their ability to exploit a host cell's replication machinery (Serrao & Engelman, 2016). A

type of retrovirus, they can integrate their own DNA into the genome of a host cell, enabling their consistent expression within that cell and in any daughter cells (Serrao & Engelman, 2016). As such, it is an efficient method for creating stably overexpressing cell lines. Since the GFP-α-syn sequences were not already in retroviral backbones and thus could only be expressed transiently, they were transferred into lentiviral vectors by subcloning.

Lentivirus generated with these new constructs was used to transduce SH-SY5Y cells (**Appendix A**, **Figure 113**, **Figure 114**) and create populations of cells stably overexpressing either GFP only, GFP-α-syn-WT or GFP-α-syn-A53T. Cell lines are referred to by these names from this point on. GFP only cells were used as a control since they had been subject to the same lentiviral process, represented a non-aggregation-prone comparison and to negate any effects of potential GFP toxicity. Stable overexpression of these constructs was confirmed by both Western blot (**Figure 64**) and immunofluorescence microscopy (**Figure 65**).

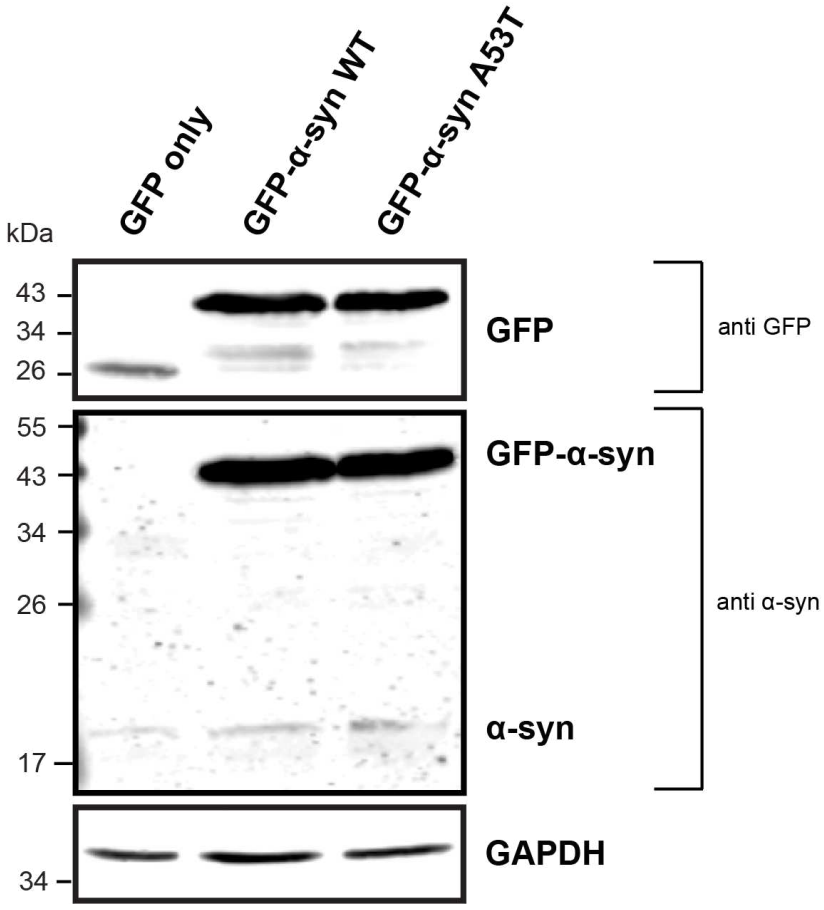

Figure 64: GFP-α-syn is detected by Western blot in SH-SY5Y cells stably overexpressing GFP-α-syn-WT and GFP-α-syn-A53T

Wild-type SH-SY5Y cells were transduced with lentiviral particles to facilitate stable overexpression of GFP only, GFP-α-syn-WT or GFP-α-syn-A53T. Lysates were processed by Western blot with antibodies against GFP, α-synuclein and B-actin as a protein loading control. GFP-α-syn is shown detected by both GFP and α-synuclein antibodies.

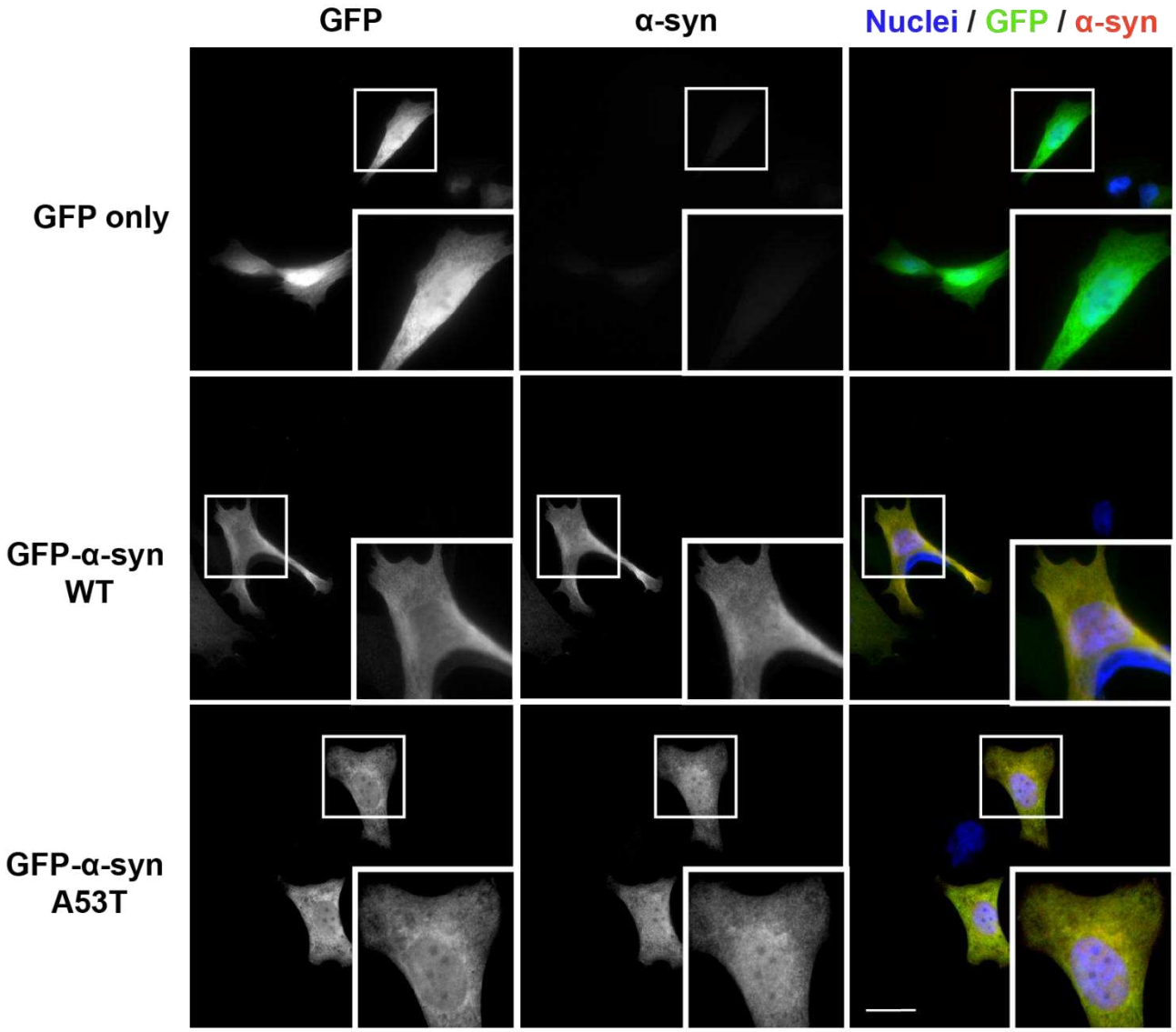

Figure 65: GFP-α-syn is detected by immunofluorescence microscopy in SH-SY5Y cells stably overexpressing GFP-α-syn-WT and GFP-α-syn-A53T

Wild-type SH-SY5Y cells were transduced with lentiviral particles to facilitate stable overexpression of GFP only, GFP-α-syn-WT or GFP-α-syn-A53T. Cells were fixed and stained with antibodies against α-synuclein (red) and GFP (green), with nuclei labelled by Hoechst (blue). Colocalisation of α-synuclein and GFP is reflected by yellow staining. Cells were imaged using widefield immunofluorescence microscopy on a 60X objective. Scale bar = 20µm.

4.2.2 Overexpression of GFP-α-syn-WT and GFP-α-syn-A53T in SH-SY5Y cells results in markers of pathological α-synuclein

After successfully generating SH-SY5Y cell lines stably overexpressing GFP-α-syn, I investigated whether they exhibited any markers associated with pathological α-synuclein. One of the key toxic attributes of α-synuclein is its ability to oligomerise to form aggregates (Winner et al., 2011). Such aggregates have been identified by immunofluorescence microscopy in SH-SY5Y cells overexpressing α-synuclein in several other studies, so I sought to determine whether such aggregates were visible in my own model (Melnikova et al., 2020; Melo et al., 2017).

Since GFP-α-synuclein was highly expressed and showed subcellular localisation to the nucleus and cytoplasm in GFP-α-syn-WT and GFP-α-syn-A53T expressing cells (**Figure 65**), I was unable to visualise any individual α-synuclein by this method. To circumvent this, I cleared out the cytoplasm to investigate the presence of aggregates. Permeabilisation of the cell membrane with saponin prior to fixation allowed cytoplasmic proteins to exit through plasma membrane pores (X. Zheng & Gallot, 2020). This resulted in the detection of small, round GFP-positive puncta in both GFP-α-syn-WT and GFP-α-syn-A53T cells, which were not seen frequently in GFP only control cells (**Figure 66**). These GFP-positive puncta colocalised with α-synuclein staining, suggesting that they consisted of GFP-α-syn species. These were quantified by the percentage of cells exhibiting more than 5 of these GFP-positive puncta, but the individual numbers of these puncta are shown in **Appendix B** (**Figure 125**). GFP-α-syn-WT cells had a significantly higher percentage of these cells than GFP only cells ($p<0.0001$), and though not significant, GFP-α-syn-A53T also showed a higher percentage than GFP only cells (**Figure 67**). I consider that these puncta could possibly be GFP-α-syn aggregates.

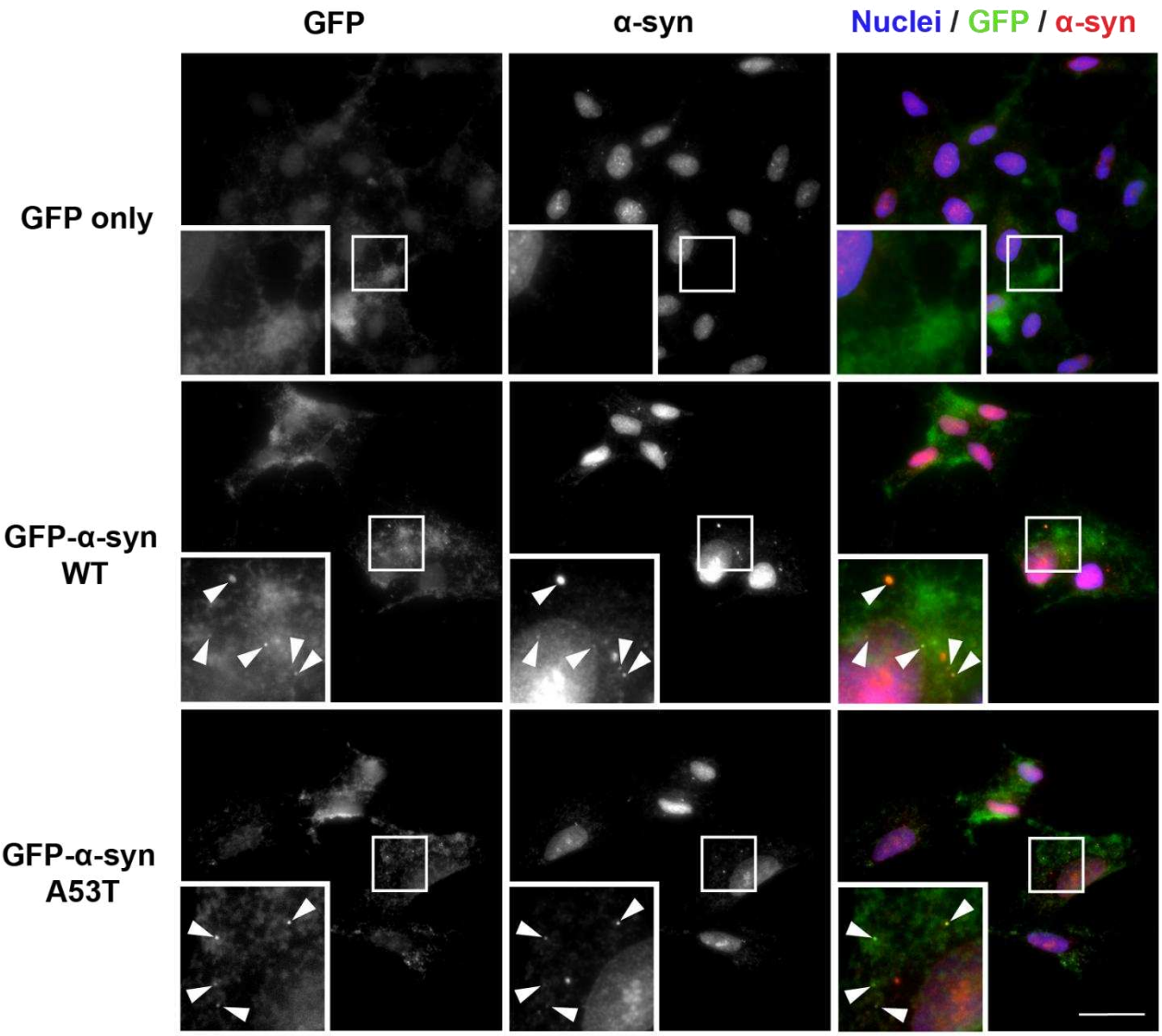

Figure 66: GFP puncta that colocalise with α-synuclein are observed at steady state in cells overexpressing GFP-α-syn-WT and GFP-α-syn-A53T

GFP only, GFP-α-syn-WT and GFP-α-syn-A53T expressing cells were permeabilised with saponin to clear out cytoplasmic proteins. Permeabilised cells were stained with antibodies against GFP (green) and α-synuclein (red), with nuclei labelled by Hoechst (blue) and assessed qualitatively. Cells were visualised using widefield immunofluorescence microscopy on a 100X objective. Scale bar = 20µm.

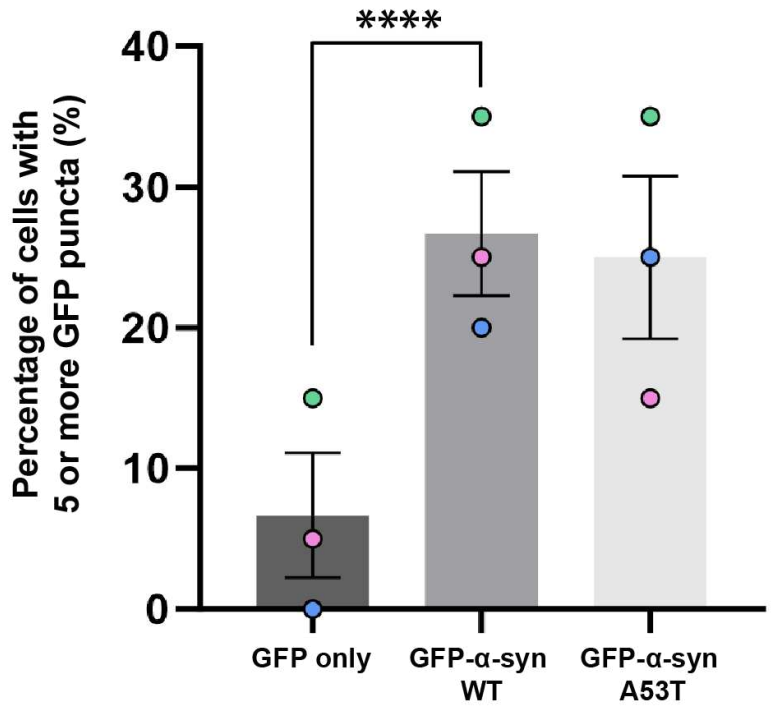

Figure 67: GFP-α-syn-WT and GFP-α-syn-A53T cells have a higher percentage of cells with more than 5 clearly identifiable GFP puncta than GFP only cells

Quantitative measurements of GFP-positive puncta were obtained from GFP only, GFP-α-syn-WT and GFP-α-syn-A53T expressing cells that were fixed and permeabilised with saponin to clear out cytoplasm. The number of bright GFP-positive puncta clearly distinguishable from background GFP staining was counted in 16 cells per cell line, per biological repeat. For each group, the percentage of these 16 cells that had 5 or more of these bright puncta was calculated and is displayed on the graph as a coloured dot. The mean of all 3 repeats is shown by the bar, with SEM shown by vertical black lines. Data points are colour coded by biological repeat. Statistical analysis was performed by a repeated measures one-way ANOVA with Tukey's multiple comparisons test. This reported that a significantly higher percentage of GFP-α-syn-WT cells had 5 or more GFP-positive puncta than GFP only cells ($p<0.0001$, ****). (**n=3**).

The most commonly used indicator of α-synuclein pathology is phosphorylation of the protein at serine 129 (pS129) (Lashuel et al., 2022). This is because pS129 α-synuclein has been well-characterised in Lewy bodies of PD patients, where the majority of α-synuclein exhibits this modification (Anderson et al., 2006). The association between pS129 α-synuclein and aggregated α-synuclein has been shown in both cellular and animal models of PD, with pS129 α-synuclein now widely used as a marker for pathologically aggregated α-synuclein (Anderson et al., 2006; Fujiwara et al., 2002; Okochi et al., 2000).

Accordingly, I evaluated expression of pS129 α-synuclein as a readout of pathological α-synuclein in my GFP-α-syn overexpression models. In untreated cells, pS129 α-synuclein was detected in both GFP-α-syn-WT and GFP-α-syn-A53T cells by Western blotting (**Figure 68**). This species was only seen at the same molecular weight as GFP-α-syn (approximately 43kDa), but not seen at the molecular weight of endogenous α-synuclein (approximately 18kDa), suggesting that the pS129 α-synuclein detected was post-translationally modified GFP-α-syn. In addition, the lack of pS129 α-synuclein observed in GFP only cells verified that its occurrence was the direct result of α-synuclein overexpression.

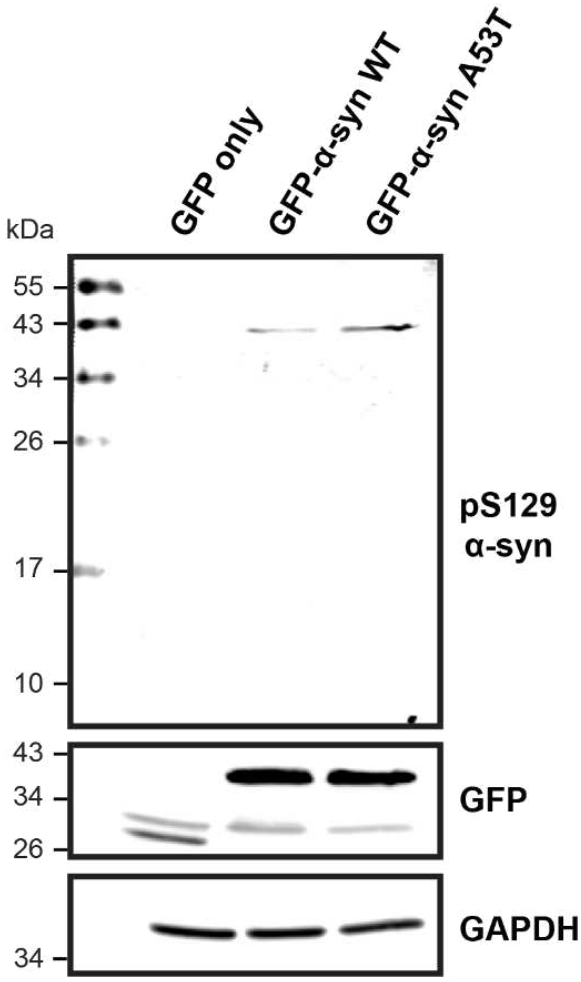

Figure 68: Phospho-S129 α-synuclein is detected at steady state in cells overexpressing GFP-α-syn-WT and GFP-α-syn-A53T by Western blot

Lysates were collected from GFP only, GFP-α-syn-WT and GFP-α-syn-A53T expressing cells at steady state and processed for Western blot. Antibodies against phospho-S129 α-syn and GFP were used, with GAPDH as a protein loading control.

To verify this phenotype, I also visualised pS129 α-synuclein at steady state by immunofluorescence microscopy. Qualitatively, pS129 α-synuclein was more clearly detected in GFP-α-syn-WT and GFP-α-syn-A53T cells compared to the GFP only control, indicating specificity of the antibody. pS129 α-synuclein staining appeared punctate – potentially vesicular – in cells overexpressing GFP-α-syn. GFP-α-syn-A53T cells appeared to have denser pS129 α-synuclein puncta, resulting in brighter staining. Interestingly, this was not consistent between cells. In GFP-α-syn-A53T cells, some exhibited extremely bright pS129 α-synuclein staining, as indicated in **Figure 69**, while others did not. This suggests that the presence of pS129 α-synuclein is variable, and thus may depend on cellular activity and health.

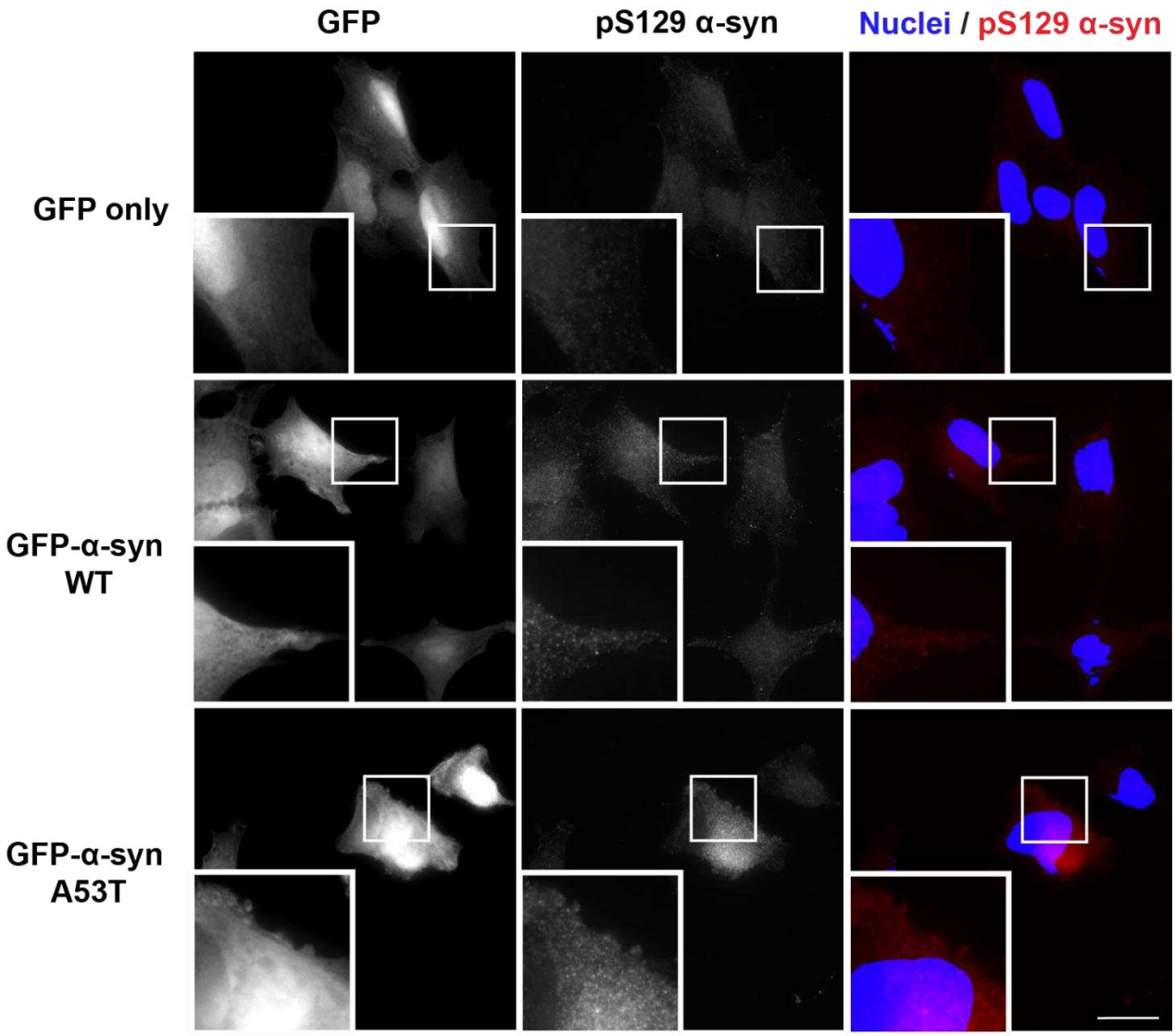

Figure 69: Phospho-S129 α-synuclein is detected at steady state in cells overexpressing GFP-α-syn-WT and GFP-α-syn-A53T by immunofluorescence microscopy

GFP only, GFP-α-syn-WT and GFP-α-syn-A53T cells were fixed and stained with an antibody against phospho-S129 α-synuclein (red) with nuclei labelled by Hoechst (blue). GFP was imaged alongside to ensure only cells with overexpression of the constructs were qualitatively assessed. Phospho-S129 images were taken under the same exposure conditions and left unprocessed to allow for comparison between cell lines. Cells were visualised using widefield immunofluorescence microscopy on a 100X objective. Scale bar = 20µm.

4.2.3 Mitochondrial damage exacerbates markers of pathological α-synuclein in cells overexpressing GFP-α-syn-WT and GFP-α-syn-A53T

Oxidative stress is known to be a key feature of PD pathogenesis (Dias et al., 2013). Having to maintain dopaminergic activity and transport cellular components over long distances means that dopaminergic neurons have higher metabolic demand than many other cell types (Bolam & Pissadaki, 2012; Pacelli et al., 2015). As a result, these cells experience high baseline levels of oxidative stress, with accumulating ROS creating a feedback loop that exacerbates mitochondrial damage (Dias et al., 2013). For example, a recent paper showed that A53T α-synuclein triggers the production of ROS, and this in turn accelerates the oligomerisation of α-synuclein (M. L. Choi et al., 2022). Since mitochondrial damage is a major cause of ROS, I aimed to investigate the impact of A/O exposure on the pathological phenotypes associated with α-synuclein overexpression in my gain-of-function models.

One of the compounds I use to evoke mitochondrial damage, antimycin A, is known to induce the production of ROS through inhibition of the electron transport chain (Balaban et al., 2005; Panduri et al., 2004). As such, I assessed whether treatment of GFP-α-syn-WT and GFP-α-syn-A53T cells with A/O had any impact on the aggregate-like staining observed at steady state. With the cytoplasm cleared out by saponin, GFP-positive puncta were left behind. These tended to puncta colocalise with α-synuclein staining in the overexpressed cells, suggesting that they consisted of GFP-α-syn species. When assessed qualitatively, both GFP-α-syn-WT and GFP-α-syn-A53T expressing cells appeared to have an increase in these GFP-positive puncta in response to accrued mitochondrial damage compared to when untreated (**Figure 70**). This damage-induced increase in GFP-positive puncta, that are potentially aggregates, provided an initial suggestion that mitochondrial damage may impact α-synuclein species.

Interestingly, the only GFP-positive puncta that colocalised with α-synuclein in the GFP only control cells were seen in a doublet formation very close to the nucleus, which I suggest could be the centriole rather than any α-synuclein aggregate.

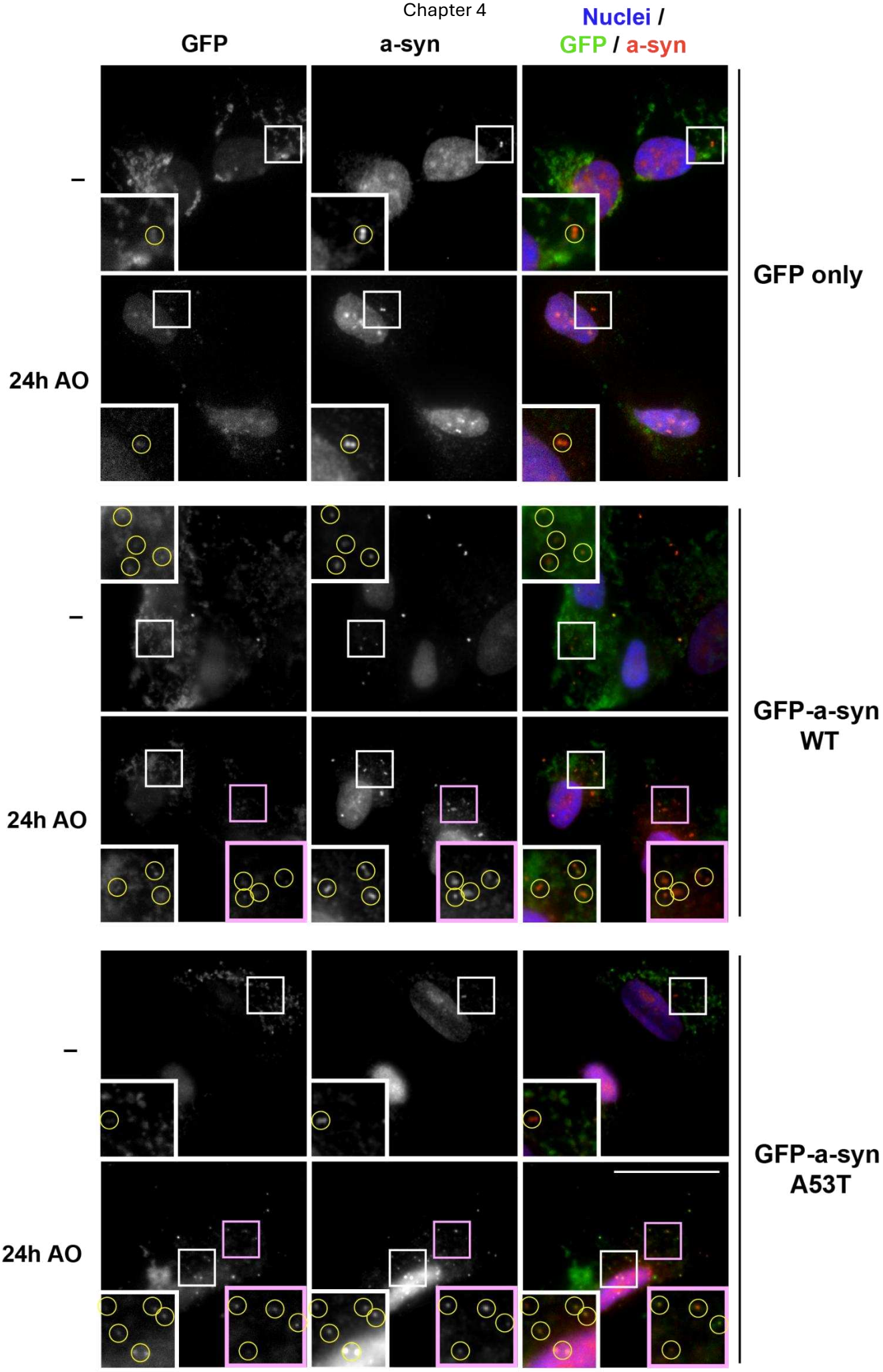
GFP
a-syn
Nuclei /
GFP / a-syn
–
24h AO
GFP only
–
24h AO
GFP-a-syn
WT
–
24h AO
GFP-a-syn
A53T

Figure 70: GFP puncta that colocalise with α-synuclein appear to increase in response to mitochondrial damage in cells overexpressing GFP-α-syn-WT and GFP-α-syn-A53T

GFP only, GFP-α-syn-WT and GFP-α-syn-A53T cells were left untreated (-) or treated with A/O for 24 hours to induce mitochondrial damage. Cells were permeabilised with saponin to clear out cytoplasmic proteins, stained with antibodies against GFP (green) and α-synuclein (red), with nuclei labelled by Hoechst (blue) and assessed qualitatively. Cells were visualised using widefield immunofluorescence microscopy on a 100X objective. Scale bar = 20μm.

To assess this potential damage-induced effect quantitatively, I next explored whether mitochondrial damage induced the expression of pS129 α-synuclein, a marker of pathology. In both GFP-α-syn-WT and GFP-α-syn-A53T overexpressing cells, pS129 α-synuclein expression was similar between cells left untreated and cells treated with A/O for 2 or 6 hours. However, GFP-α-syn-WT and GFP-α-syn-A53T overexpressing cells treated with A/O for 24 hours displayed significantly higher pS129 α-synuclein than in all other treatment conditions (**Figure 71**). These data suggest that accrued mitochondrial damage increases this pathological post-translational modification to α-synuclein. Looking at the increase in pS129 α-synuclein expression from untreated to 24-hour A/O treated cells, GFP-α-syn-WT overexpressing cells had a fold change of 6.14 whereas GFP-α-syn-A53T overexpressing cells only had a fold change of 2.32 (graph in **Appendix B**, **Figure 126**). This difference in phosphorylation between the cell lines was likely because the steady state level of pS129 α-synuclein was greater in GFP-α-syn-A53T cells than in the GFP-α-syn-WT (**Figure 71**).

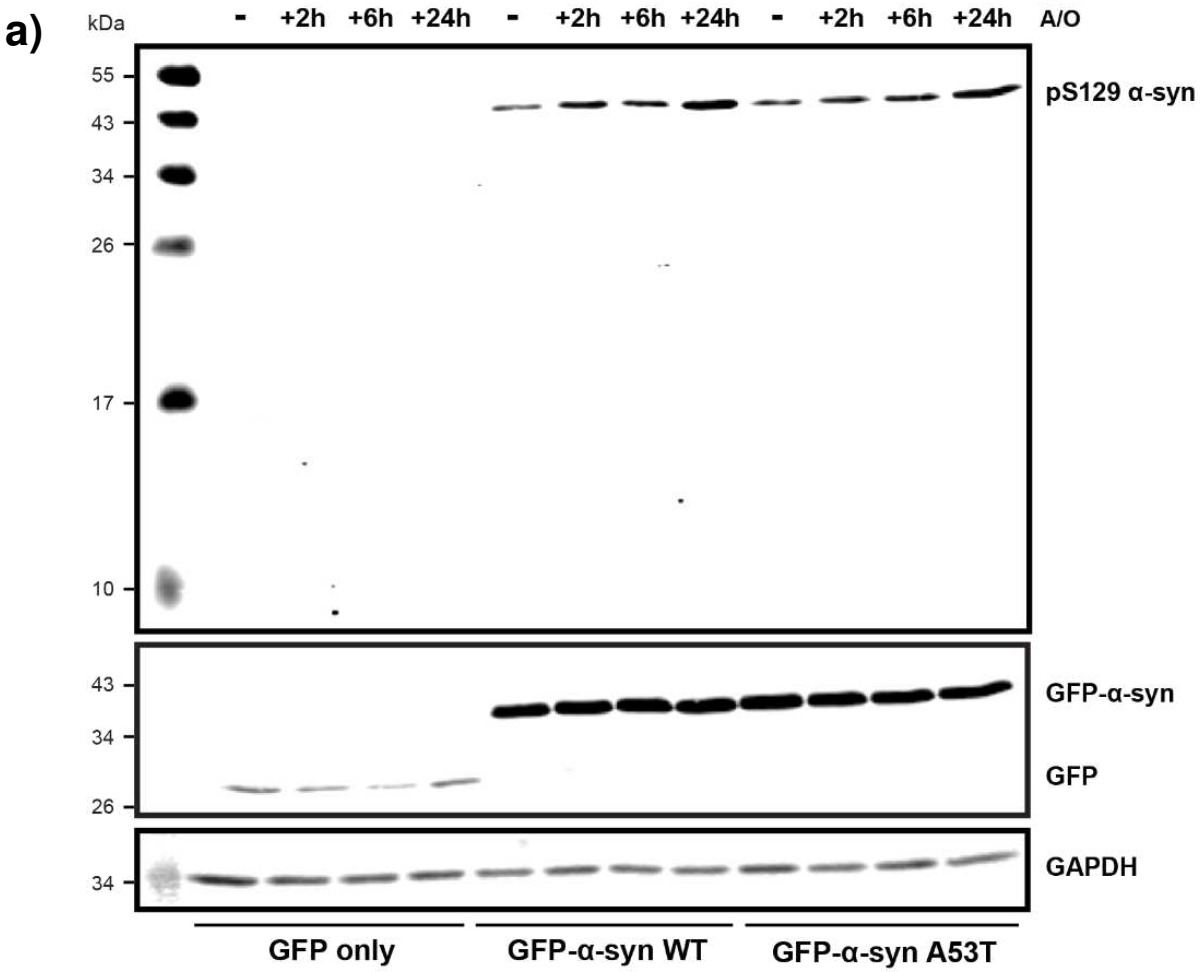
a)
kDa
- +2h +6h +24h - +2h +6h +24h - +2h +6h +24h A/O
55
43
34
26
17
10
pS129 α-syn
43
34
26
GFP-α-syn
GFP
34
GAPDH
GFP only
GFP-α-syn WT
GFP-α-syn A53T

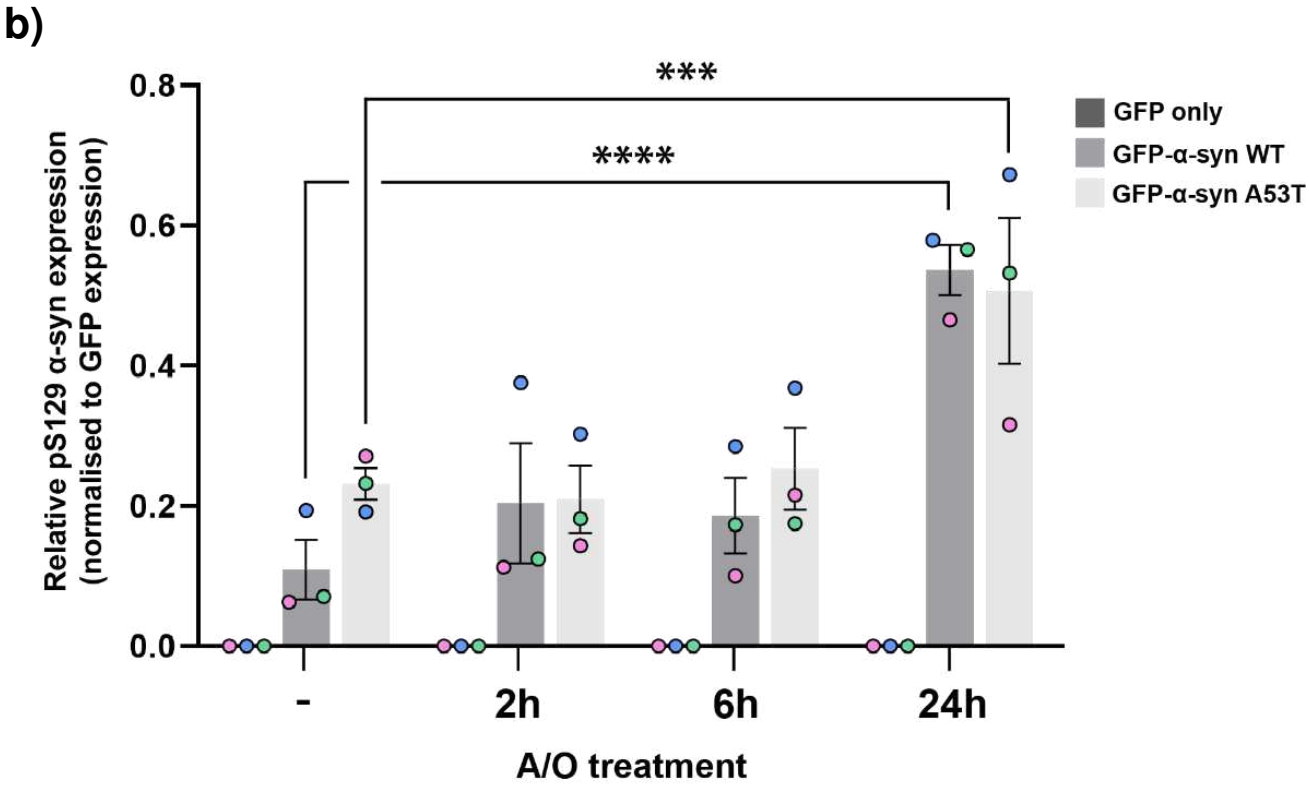
b)
***
****
0.8
0.6
0.4
0.2
0.0
Relative pS129 α-syn expression
(normalised to GFP expression)
GFP only
GFP-α-syn WT
GFP-α-syn A53T
-
2h
6h
24h
A/O treatment

Figure 71: Phospho-S129 α-synuclein is increased following 24 hours of mitochondrial damage in cells overexpressing GFP-α-syn-WT and GFP-α-syn-A53T

a) GFP only, GFP-α-syn-WT and GFP-α-syn-A53T cells were left untreated (-) or treated for 2, 6 or 24 hours with A/O to induce mitochondrial damage. Lysates were processed by Western blot with antibodies against phospho-S129 α-synuclein, GAPDH as a protein loading control and GFP to confirm overexpression of GFP constructs in all cell lines.

b) Phospho-S129 α-synuclein expression in response to A/O treatment was normalised to GFP to account for differences in the level of overexpression. Expression of phospho-S129 α-synuclein is represented by the raw value of this calculation. The results from GFP only cells are shown in dark grey, GFP-α-syn-WT cells in medium grey and GFP-α-syn-A53T in pale grey. Biological replicates are colour coded, with circles representing the means of each repeat, bars representing the mean of 3 repeats and black lines representing SEM. Statistical analysis was performed by a 2-way repeated measures ANOVA with Tukey's multiple comparisons test. No significant differences were found between cell lines, but differences were found within cell lines. In GFP-α-syn-WT cells, treatment with A/O for 24 hours led to significantly higher phospho-S129 expression than cells left untreated ($p<0.0001$, ****), treated for 2 hours ($p=0.0001$, ***) or for 6 hours ($p<0.0001$, ****). In GFP-α-syn-A53T cells, treatment with A/O for 24 hours led to significantly higher phospho-S129 expression than cells left untreated ($p=0.0008$, ***), treated for 2 hours ($p=0.0004$, ***) or for 6 hours ($p=0.0016$, **). Only significance between the untreated and 24-hour treated groups is shown on the graph for clarity. (**n=3**).

4.2.4 GFP-α-syn-WT and GFP-α-syn-A53T overexpressing cells do not show preferential recruitment to mitochondria in response to mitochondrial damage

Since previous data indicates a mitochondrial damage-induced increase in pS129 modified α-synuclein in GFP-α-syn-WT and GFP-α-syn-A53T cells by Western blot, I sought to explore whether pS129 modified α-synuclein demonstrated any localisation to mitochondria. Expression of pS129 α-synuclein was qualitatively observed by microscopy and appeared to be increased in GFP-α-syn-WT and GFP-α-syn-A53T expressing cells upon 24 hours of mitochondrial damage, corroborating my Western blot data (**Figure 71**). As previously seen at steady state (**Figure 69**), pS129 α-synuclein staining was not consistent between GFP-α-syn overexpressing cells, again suggesting that phosphorylation of α-synuclein at the S129 residue is dependent on cell-specific variables such as cell cycle phase and overall health. Expression of pS129 α-synuclein was not observed in GFP only control cells.

In terms of localisation of these pS129 α-synuclein puncta, I did not observe any clear association with mitochondria. Though some damage-induced punctate pS129 α-synuclein expression was colocalised with the mitochondrial marker TOM20 in GFP-α-syn-WT and GFP-α-syn-A53T overexpressing cells, this did not appear to be preferential or specific since there were also puncta across the nucleus and cytoplasm in these cells (**Figure 72**). Since pS129 α-synuclein staining was diffuse, it is possible that colocalisation with mitochondria was observed because of the ubiquitous nature of the diffuse staining, rather than any real mitochondrial recruitment.

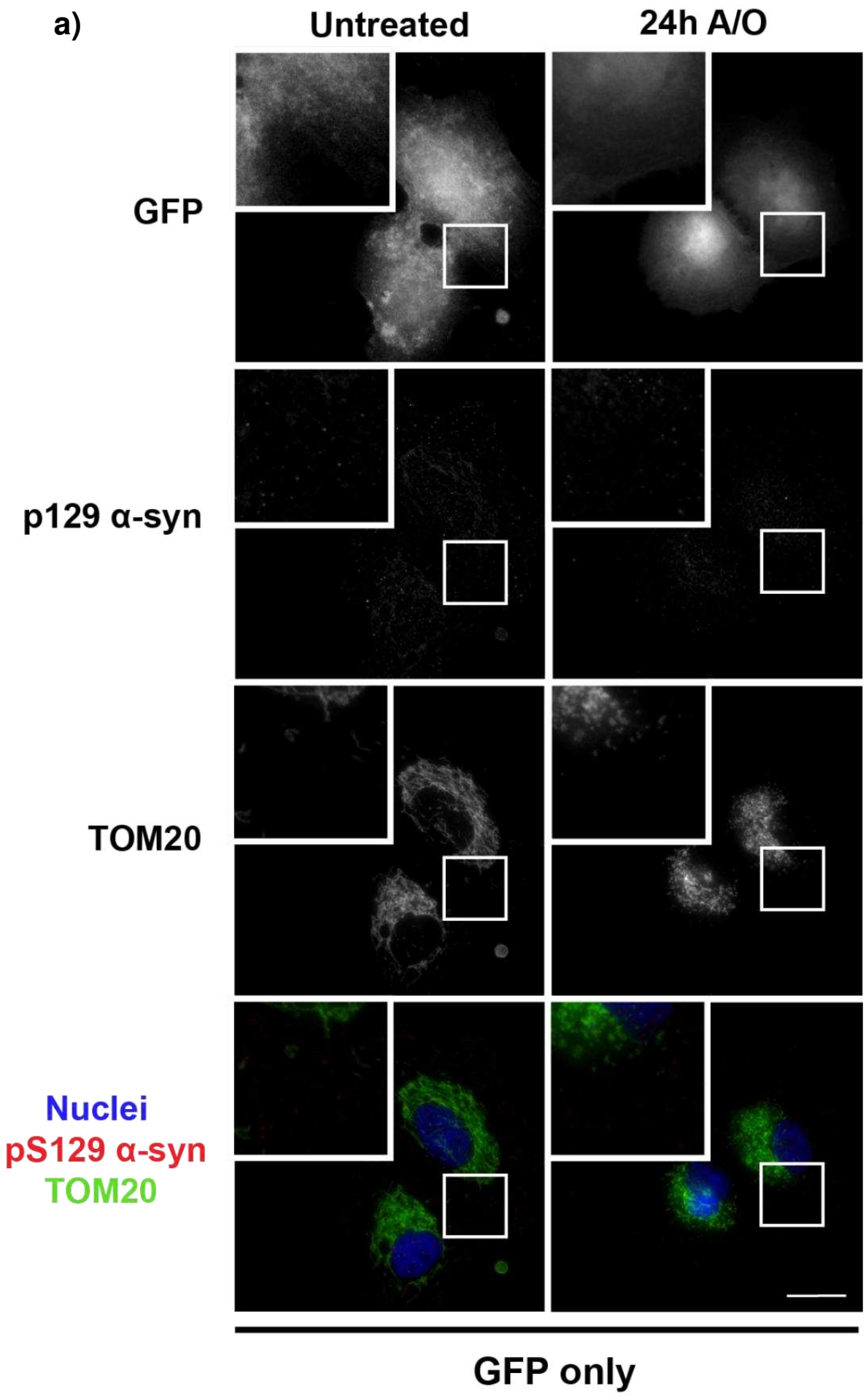
a)
Untreated
24h A/O
GFP
p129 α-syn
TOM20
Nuclei
pS129 α-syn
TOM20
GFP only

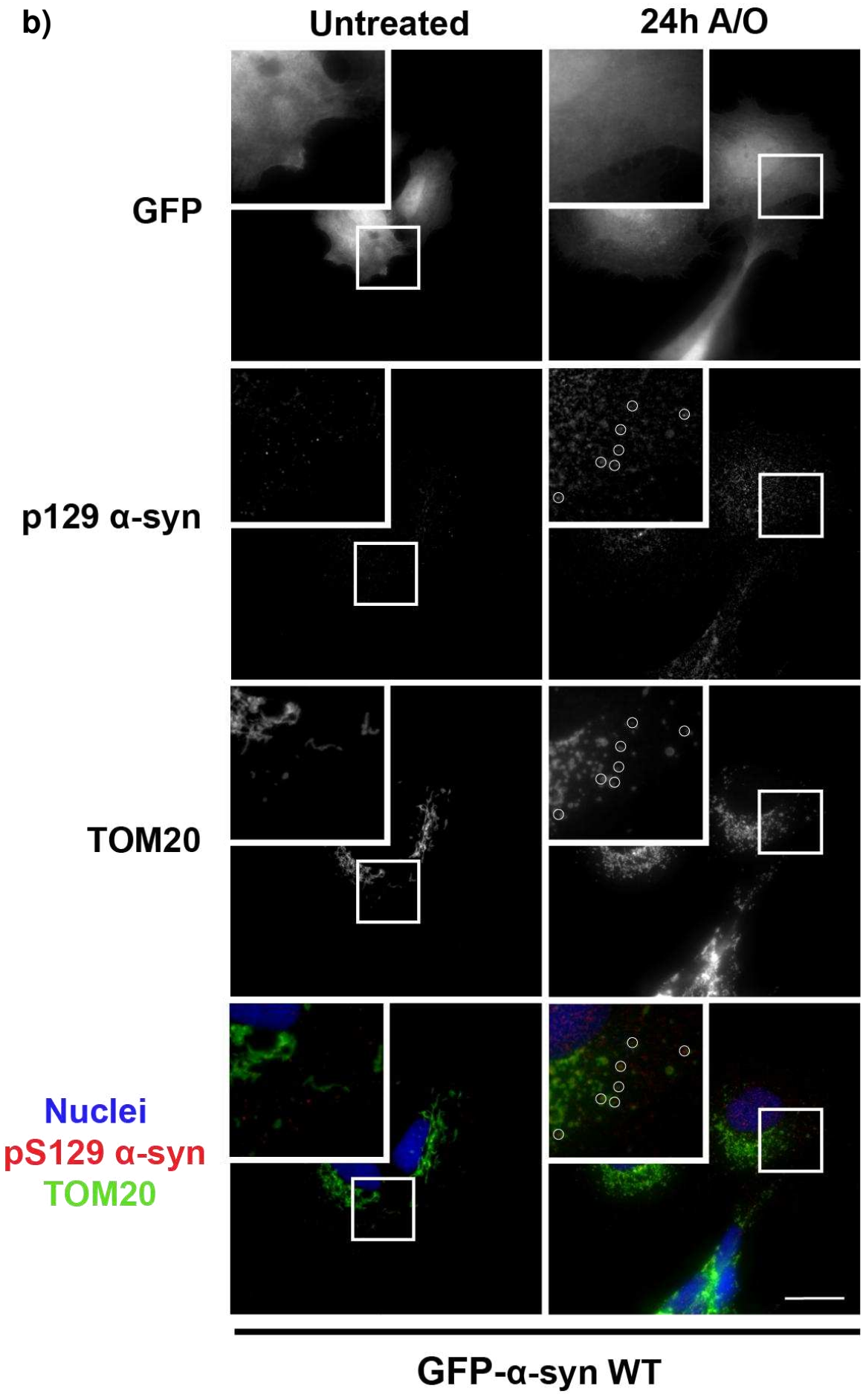
b)
Untreated
24h A/O
GFP
p129 α-syn
TOM20
Nuclei
pS129 α-syn
TOM20
GFP-α-syn WT

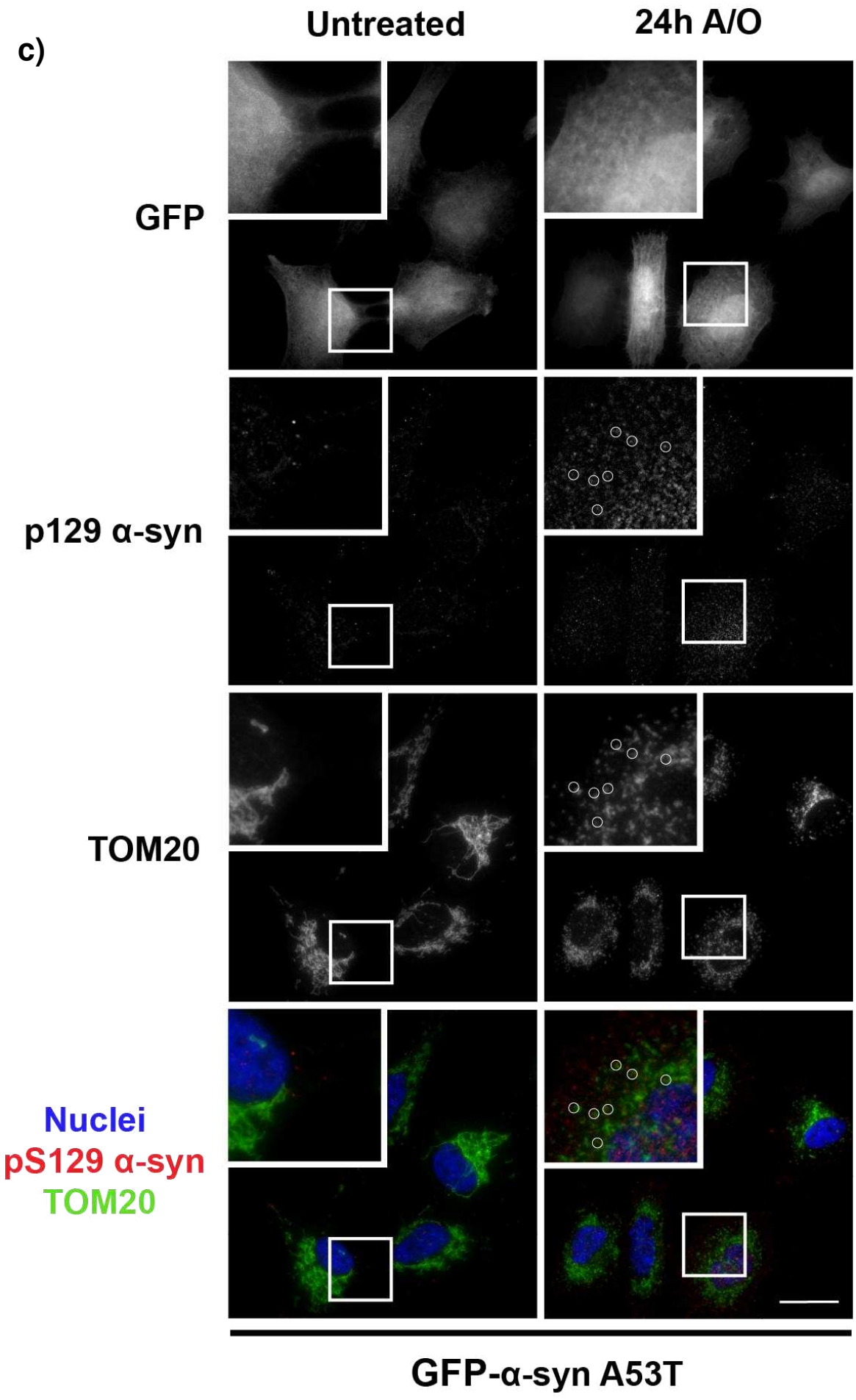
c)
Untreated
24h A/O
GFP
p129 α-syn
TOM20
Nuclei
pS129 α-syn
TOM20
GFP-α-syn A53T

Figure 72: Phospho-S129 α-synuclein is increased following 24 hours of mitochondrial damage in cells overexpressing GFP-α-syn-WT and GFP-α-syn-A53T, but does not show specific mitochondrial recruitment

GFP only, GFP-α-syn-WT and GFP-α-syn-A53T cells were left untreated (-) or treated for 24 hours with A/O to induce mitochondrial damage. Cells were fixed and stained with antibodies against phospho-S129 α-synuclein (red) and TOM20 (imaged in far red, false coloured green for clarity) with nuclei labelled by Hoechst (blue). Cells were stained with GFP to indicate overexpressed cells. In GFP-α-syn- overexpressing cells (b, c), circles indicate examples of colocalisation between TOM20 and pS129 α-synuclein Images were taken using widefield immunofluorescence microscopy on a 100X objective. Scale bar = 20μm.

To more clearly determine whether pS129 α-synuclein was localising to mitochondria, I again applied saponin to clear out cytoplasmic staining and leave only punctate species behind, thus increasing my confidence that any potential mitochondria-pS129 α-synuclein associations were not due to diffuse staining. At steady state, pS129 α-synuclein puncta were visible in both GFP-α-syn-WT and GFP-α-syn-A53T cells. Though a small number of puncta were visualised in proximity to mitochondria, the majority of pS129 α-synuclein was localised to the nucleus. Very few puncta were observed in GFP only control cells, consistent with previous data indicating that pS129 α-synuclein species in these cells were a direct result of α-synuclein overexpression (**Figure 68, Figure 69**).

Upon mitochondrial damage, both GFP-α-syn-WT and GFP-α-syn-A53T cells appeared to exhibit increased pS129 α-synuclein staining, concurrent with previous data (**Figure 71**). In GFP-α-syn-WT cells, the majority of puncta were still observed to be colocalised with nuclear staining, whereas in GFP-α-syn-A53T cells, puncta were often outside of the nuclear stain. Though some pS129 α-synuclein species were seen in proximity to mitochondria, this did not seem to be preferential or suggest specific mitochondrial recruitment, since the majority of pS129 α-synuclein puncta did not localise to mitochondria (**Figure 73**).

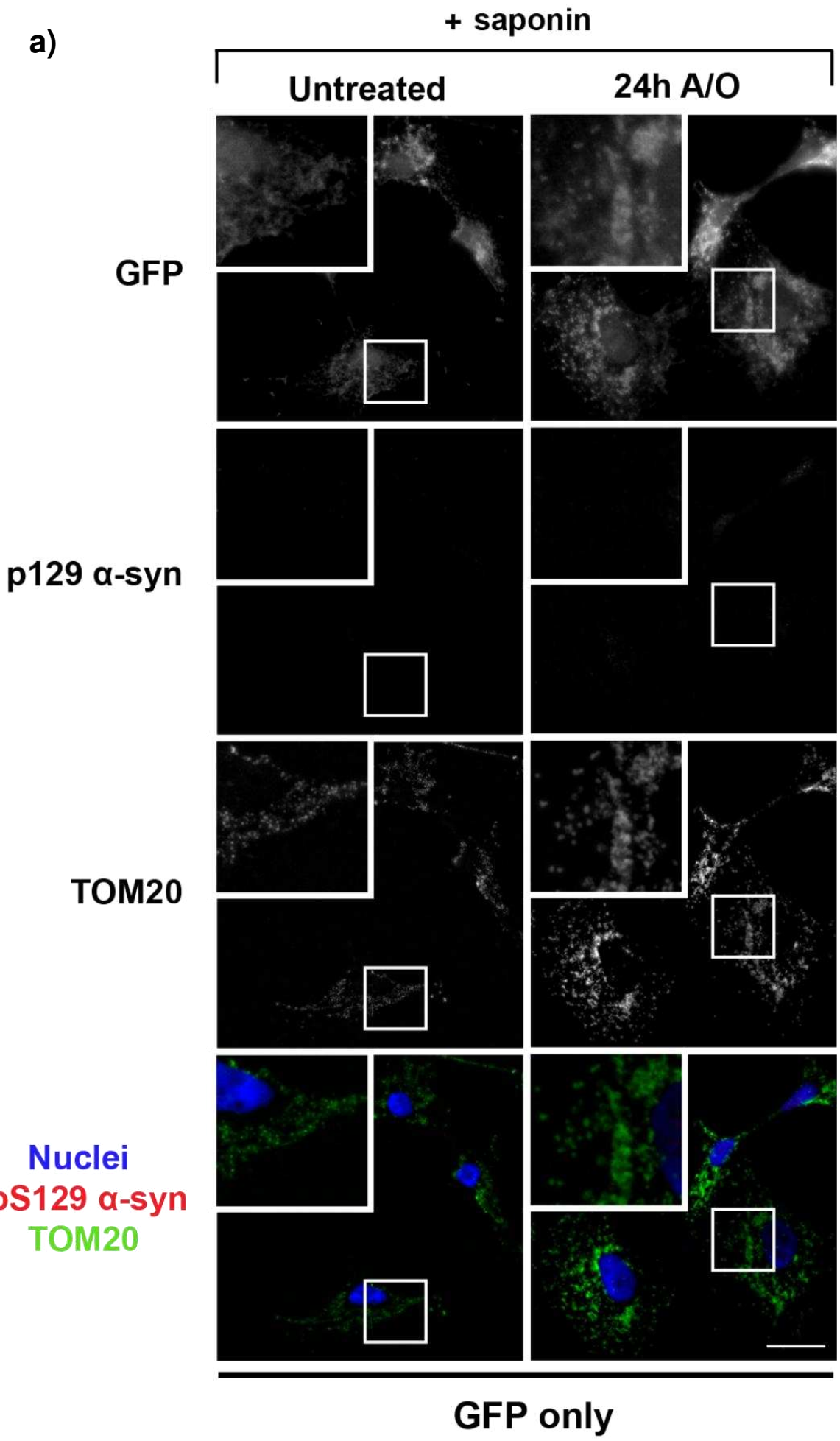
a)
+ saponin
Untreated
24h A/O
GFP
p129 α-syn
TOM20
Nuclei
pS129 α-syn
TOM20
GFP only

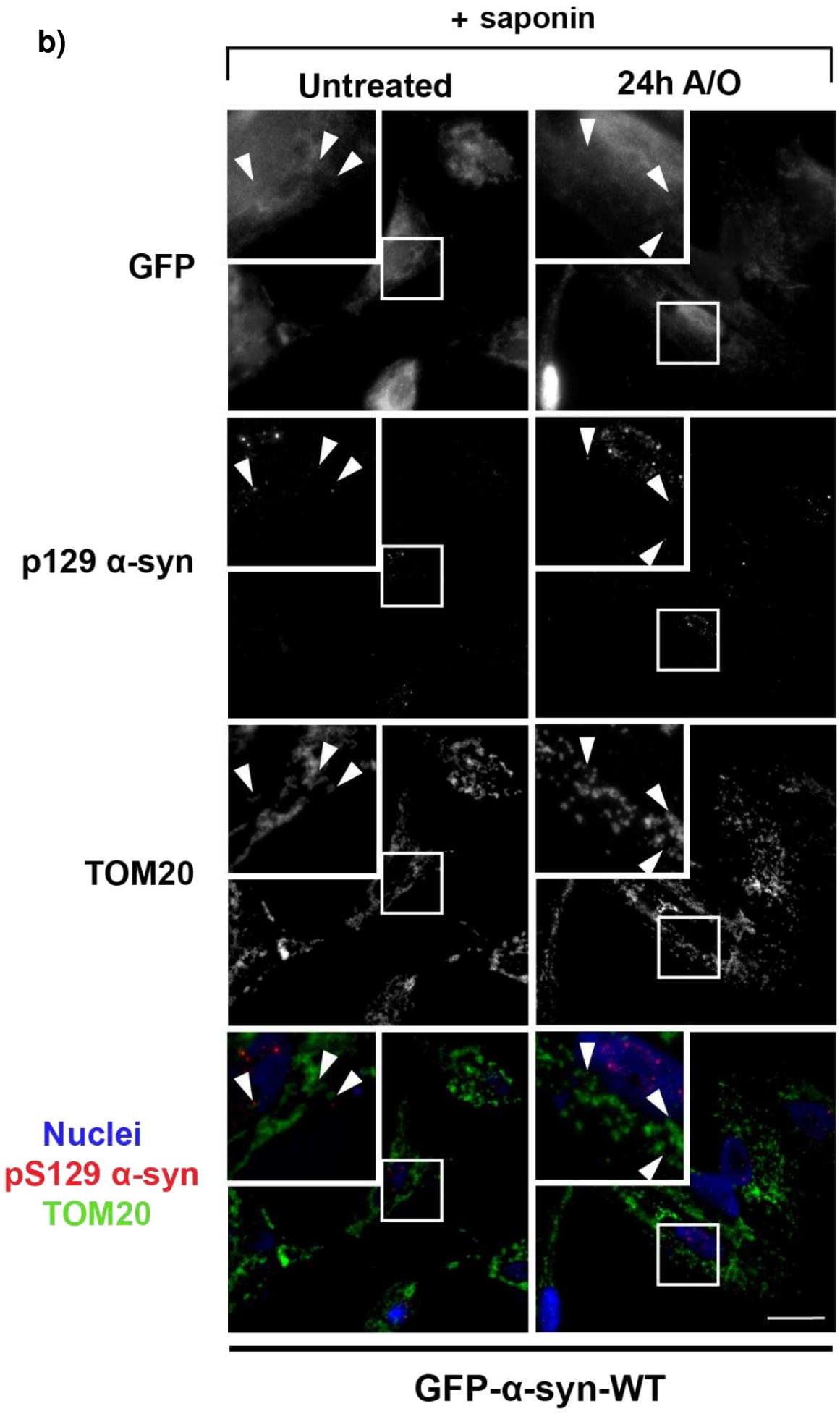
b)
+ saponin
Untreated
24h A/O
GFP
p129 α-syn
TOM20
Nuclei
pS129 α-syn
TOM20
GFP-α-syn-WT

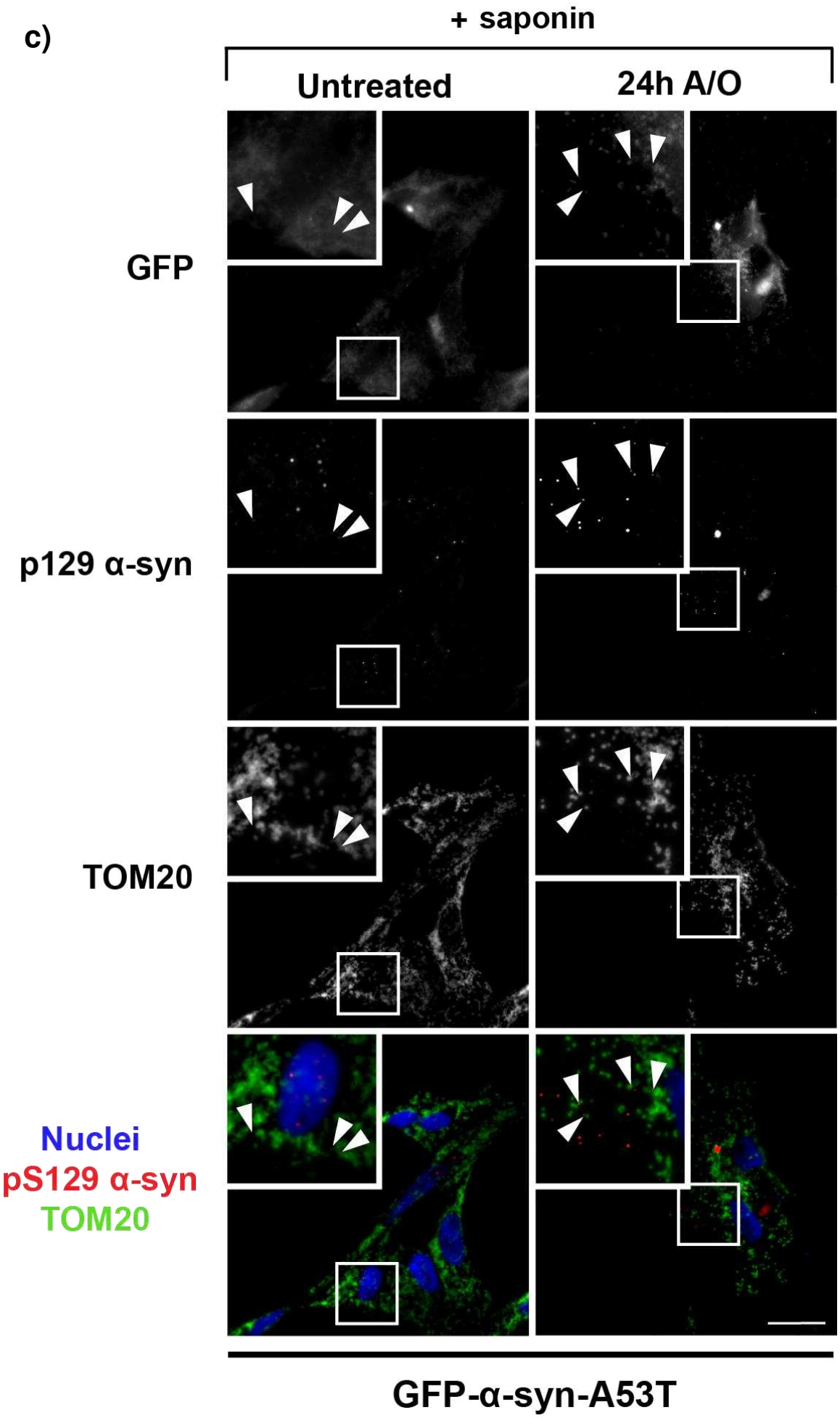
c)
+ saponin
Untreated
24h A/O
GFP
p129 α-syn
TOM20
Nuclei
pS129 α-syn
TOM20
GFP-α-syn-A53T

Figure 73: Phospho-S129 α-synuclein is not observed to be selectively recruited to mitochondria following 24 hours of mitochondrial damage in cells overexpressing GFP-α-syn-WT or GFP-α-syn-A53T

GFP only, GFP-α-syn-WT and GFP-α-syn-A53T cells were left untreated (-) or treated for 24 hours with A/O to induce mitochondrial damage. Cells were fixed and permeabilised with saponin to clear out cytoplasmic proteins. Permeabilised cells were stained with antibodies against phospho-S129 α-synuclein (red) and TOM20 (imaged in far red, false coloured green for clarity), with nuclei labelled by Hoechst (blue). Cells were stained with GFP to ensure that only cells expressing GFP constructs were qualitatively assessed. White arrows indicate examples of pS129 α-synuclein puncta that are in proximity to TOM20 staining. Images were taken using widefield immunofluorescence microscopy on a 100X objective. Scale bar = 20µm.

To further explore a potential mitochondrial localisation of GFP-α-syn in response to mitochondrial damage, I investigated this association biochemically from isolated mitochondria. This was assessed in cells treated for 6 hours with A/O, since this was enough for the induction of mitophagy but not so long that most mitochondria had been degraded.

Isolation of mitochondria was considered to be successful, since the IMM protein CoxII was selectively enriched in the mitochondrial, but not cytosolic, fractions of all three cell lines. This was confirmed by the enrichment of selective markers in the cytosolic, but not mitochondrial, fractions (x). GFP expression was used to assess whether GFP-α-syn was enriched in mitochondrial fractions. In GFP only control cells (**Figure 74a**), the majority of GFP was seen in the cytosol both at steady state and in response to mitochondrial damage, though a comparatively small amount of GFP was present in the mitochondrial fraction upon A/O treatment. In GFP-α-syn-WT cells (**Figure 74b**), GFP was again seen to be greatly enriched in the cytosol both when untreated and in response to mitochondrial damage. GFP-α-syn was not seen to be enriched in the mitochondrial fraction by an antibody against GFP, with barely any GFP detected in these fractions. However, an α-synuclein antibody showed the presence of GFP-α-syn (approx. 43kDa) in mitochondria when untreated and in response to A/O. In GFP-α-syn-A53T cells (**Figure 74c**), a GFP antibody detected GFP-α-syn in both cytosolic and mitochondrial fractions, regardless of treatment with A/O. Confirming this, GFP-α-syn was also detected in all fractions with an α-synuclein antibody.

These data indicate an enrichment of GFP-α-syn in the mitochondrial fraction for cells overexpressing GFP-α-syn-A53T compared to GFP only and GFP-α-syn-WT cells, but this does not appear to be influenced by mitochondrial damage.

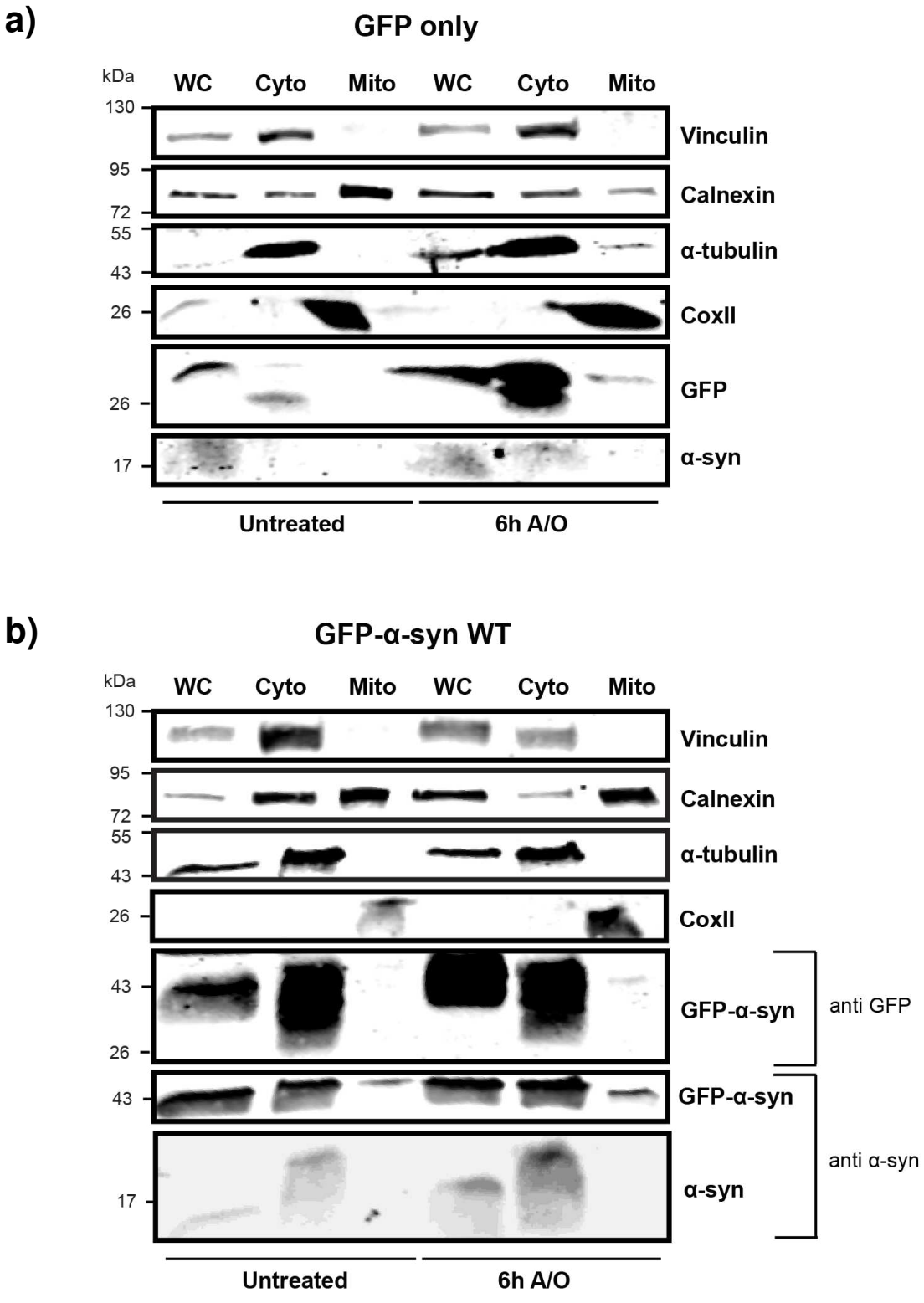
a)
GFP only
kDa
WC
Cyto
Mito
WC
Cyto
Mito
130
95
72
55
43
26
26
17
Vinculin
Calnexin
α-tubulin
CoxII
GFP
α-syn
Untreated
6h A/O
b)
GFP-α-syn WT
kDa
WC
Cyto
Mito
WC
Cyto
Mito
130
95
72
55
43
26
43
26
43
17
Vinculin
Calnexin
α-tubulin
CoxII
GFP-α-syn
GFP-α-syn
α-syn
anti GFP
anti α-syn
Untreated
6h A/O

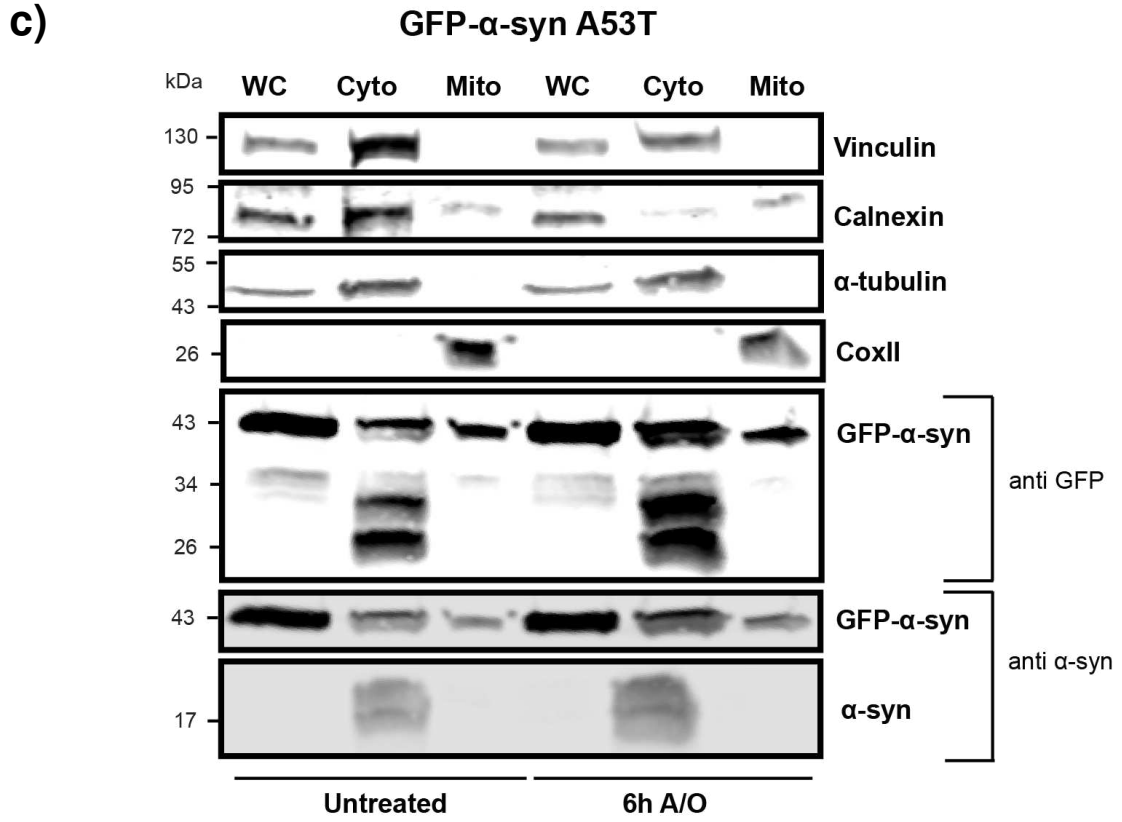

Figure 74: GFP-α-syn is enriched in the mitochondrial fraction in cells overexpressing GFP-α-syn-A53T, but not GFP-α-syn-WT

GFP only (a), GFP-α-syn-WT (b) and GFP-α-syn-A53T (c) cells were left untreated or treated for 6 hours with A/O to induce mitochondrial damage. Mitochondrial and cytosolic fractions were isolated from cells and a whole-cell lysate was generated from the same cell population. Lysates were processed by Western blot with antibodies against α-synuclein and GFP as well as control proteins from different organelles to confirm isolation of mitochondria: vinculin (cytoplasm/cytoskeletal-associated), calnexin (ER), α-tubulin (cytoplasm) and CoxII (mitochondria). (WC = whole cell lysate; cyto = cytosolic fraction; mito = mitochondrial fraction). GFP-α-syn is shown detected by both GFP and α-synuclein antibodies.

4.2.5 Overexpression of GFP-α-syn-WT or GFP-α-syn-A53T has limited impact on mitochondrial energy production

After confirming overexpression and pathogenicity of GFP-α-syn-WT and GFP-α-syn-A53T, I next sought to investigate whether overexpression of GFP-α-syn had any impact on the primary function of mitochondria: energy production.

PD pathology was first linked to dysfunction in ATP production when the mitochondrial complex I inhibitor, MPTP, was shown to induce Parkinsonian-like symptoms in both humans and animal models (Betarbet et al., 2000; Dauer & Przedborski, 2003; William Langston et al., 1983). In accordance with this, a specific deficiency in complex I and a subsequent reduction in ATP has also been observed in PD patients, further suggesting a direct relationship between PD pathology and ATP production (Mortiboys et al., 2008; Rakovic et al., 2010; Schapira, 2006). Mechanistically, it has been suggested that aggregated α-synuclein is able to directly bind complex I to evoke this dysfunction in PD (Reeve et al., 2015). Additionally, α-synuclein aggregates have been shown to induce oxidation of a subunit of ATP synthase, triggering opening of the MPTP and thus reducing mitochondrial function (Ludtmann et al., 2018). Considering that mitochondrial dysfunction has been extensively characterised in PD (Bender et al., 2013; W. Liu et al., 2009; Pickrell et al., 2013), I aimed to explore whether this could be evoked in my gain-of-function models, first by measuring the ATP produced by these cells. This was measured using a luminescence-based assay to capture changes to the ATP level when cells are using glycolysis, OXPHOS or both (**Appendix A**, **Figure 117**).

In GFP only control cells, ATP levels were very similar whether cells used glycolysis (glucose + oligomycin), OXPHOS (galactose) or both (glucose) (**Figure 75a**). This pattern was matched in both GFP-α-syn-WT and GFP-α-syn-A53T cells, where levels of ATP were almost equal across the different conditions (**Figure 75b, c**). When cell lines were compared to each other, there were no significant differences between groups regardless of whether cells were using glycolysis or OXPHOS (**Figure 76a**). However, mitochondrial load appeared to be increased in GFP-α-syn-WT and GFP-α-syn-A53T cells compared to GFP only controls, which could reflect potential compensatory mechanisms to boost mitochondrial ATP production (**Figure 76b**). Overall, overexpression of GFP-α-syn-WT and GFP-α-syn-A53T did not result in any measurable differences in ATP levels.

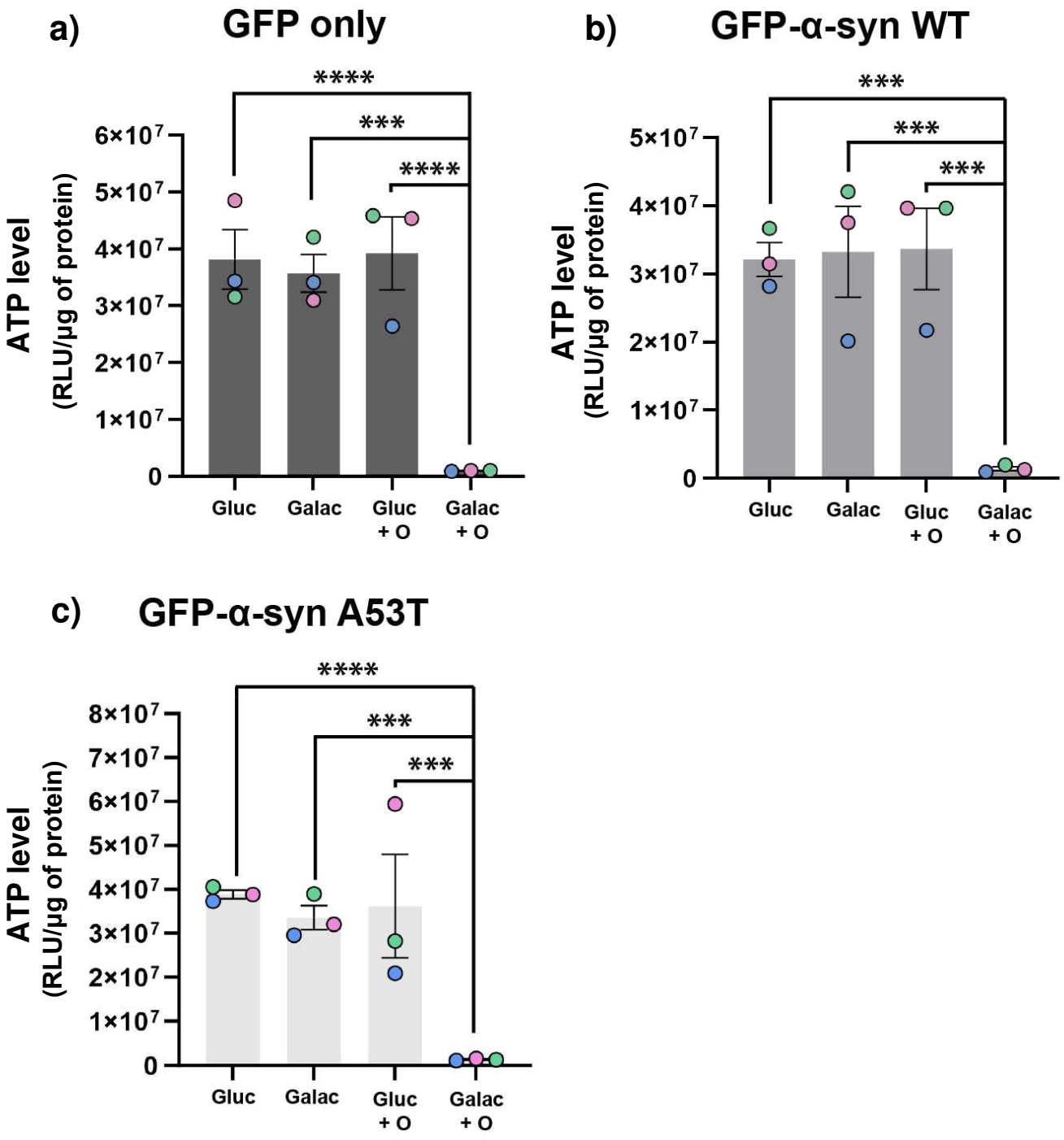
a)
GFP only
ATP level
(RLU/µg of protein)
6×10^7
5×10^7
4×10^7
3×10^7
2×10^7
1×10^7
0
****
***
****
Gluc
Galac
Gluc + O
Galac + O
b)
GFP-α-syn WT
ATP level
(RLU/µg of protein)
5×10^7
4×10^7
3×10^7
2×10^7
1×10^7
0
***
***
***
Gluc
Galac
Gluc + O
Galac + O
c)
GFP-α-syn A53T
ATP level
(RLU/µg of protein)
8×10^7
7×10^7
6×10^7
5×10^7
4×10^7
3×10^7
2×10^7
1×10^7
0
****
***
***
Gluc
Galac
Gluc + O
Galac + O

Figure 75: Overexpression of GFP-α-syn-WT or GFP-α-syn-A53T has no impact on ATP production by glycolysis or OXPHOS

GFP only, GFP-α-syn-WT and GFP-α-syn-A53T cells were grown in different media compositions to facilitate ATP measurements from glycolysis and/or OXPHOS: glucose (glycolysis and OXPHOS), galactose (OXPHOS only), glucose with oligomycin (glycolysis only) or galactose with oligomycin (negative control). An ATP kit was used to read luminescence proportional to ATP in the media. Luminescence readings were measured as relative light units (RLU), normalised to total protein concentrations. ATP level is represented by RLU per µg of protein. Graphs show within-cell line comparisons between a) GFP only, b) GFP-α-syn-WT and c) GFP-α-syn-A53T cells under different media conditions. Biological repeats are colour coded, with circles showing the means of each replicate, bars representing the means of all 3 repeats and black lines representing SEM. Statistical analysis for differences between groups was performed with a repeated measures 2-way ANOVA with Tukey's multiple comparisons test. Significance differences between groups are denoted on the graphs by stars: *** signifies p=0.001, **** signifies p<0.0001. (**n=3**).

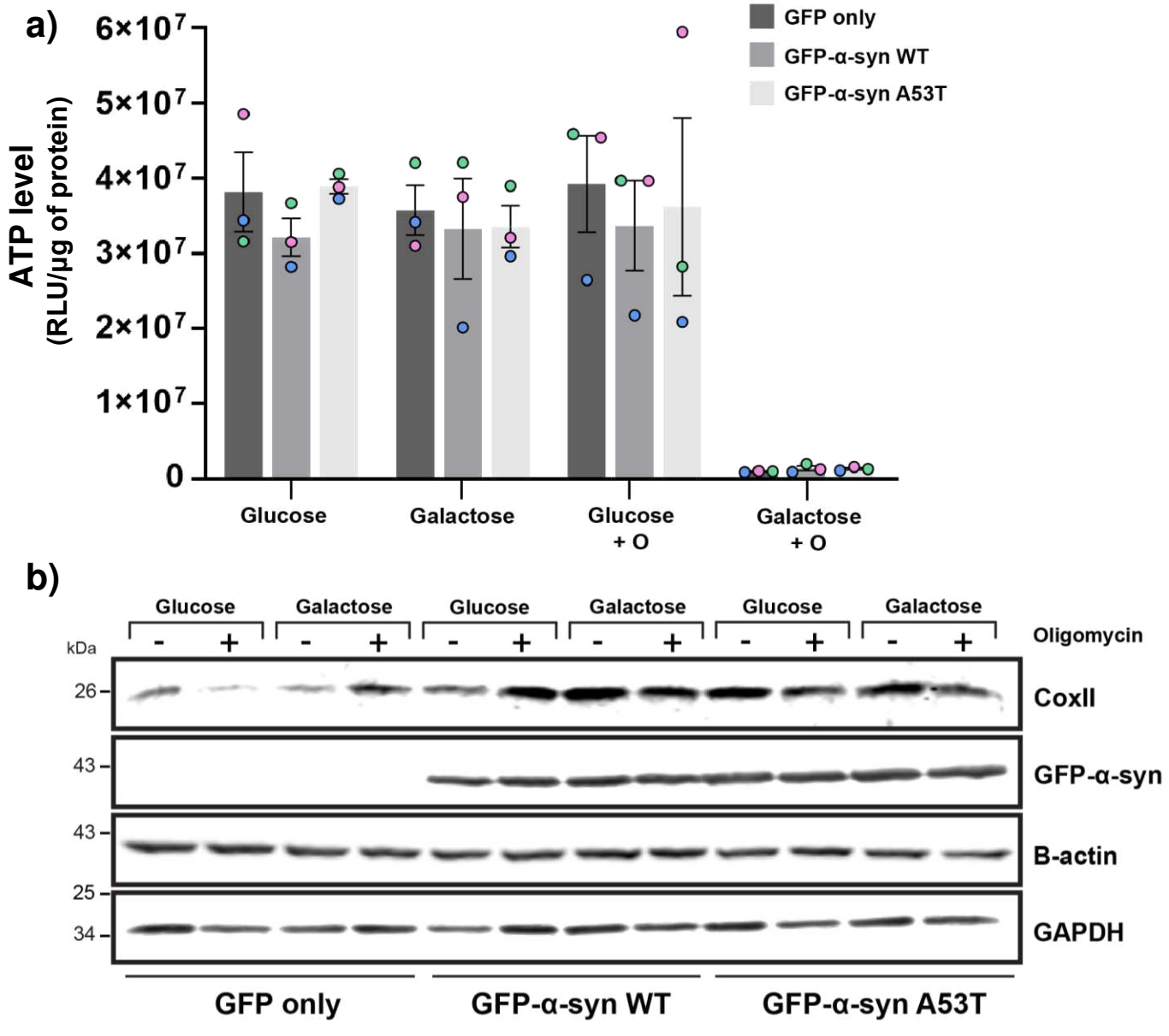
a)
ATP level
(RLU/µg of protein)
6×10^7
5×10^7
4×10^7
3×10^7
2×10^7
1×10^7
0
GFP only
GFP-α-syn WT
GFP-α-syn A53T
Glucose
Galactose
Glucose + O
Galactose + O
b)
Glucose
Galactose
Glucose
Galactose
Glucose
Galactose
Oligomycin
kDa
26
43
43
25
34
CoxII
GFP-α-syn
B-actin
GAPDH
GFP only
GFP-α-syn WT
GFP-α-syn A53T

Figure 76: There are no differences in ATP production between cells expressing GFP only, GFP-α-syn-WT or GFP-α-syn-A53T

a) The luminescence values from the ATP assay on GFP only, GFP-α-syn-WT and GFP-α-syn-A53T cells are shown comparatively on the same graph. Luminescence readings were measured as relative light units (RLU) and normalised to total protein concentration. ATP level is shown by RLU per μg of protein. The graph shows between-cell line comparisons of GFP only, GFP-α-syn-WT and GFP-α-syn-A53T cells under different media conditions. Biological replicates are colour coded, with circles showing the means of each repeat, bars representing the mean of the 3 repeats and black lines representing the SEM. Statistical analysis for differences between groups was performed using a repeated measures 2-way ANOVA with Tukey's multiple comparisons test. No significance was reported. (**n=3**).

b) GFP only, GFP-α-syn-WT and GFP-α-syn-A53T cells were lysed after being grown in the same growth conditions as for the ATP assay and processed by Western blot. An antibody against CoxII was used to check mitochondrial load and an antibody against GFP was used to confirm overexpression of GFP-α-syn. GAPDH and B-actin were used as loading controls.

To investigate energy production more precisely in cells overexpressing GFP-α-syn, I next utilised the Seahorse mito-stress test to measure OCR in living cells. By manipulating the electron transport chain with mitochondrial inhibitors, this test allows me to measure specific metabolic parameters (Gu et al., 2021). The biochemical basis of this method is further explained in **Appendix A** (**Figure 118**).

The raw traces from the mito-stress test each have a different baseline OCR, making the comparison of profiles between cell lines difficult (**Appendix A**, **Figure 120**). As such, representative traces are shown normalised to the respective baseline OCR of each cell line in order to clarify the profiles (**Figure 77**). Looking at these traces showing the means from 3 repeats, each cell line had the same profile, confirming that they all effectively responded to each of the different inhibitors used throughout the test. Though these profiles were very similar, GFP-α-syn-WT cells had the highest OCR percentage when cells were pushed to maximum respiration with FCCP, and GFP-α-syn-A53T cells had the highest OCR percentage after inhibition with antimycin A and rotenone.

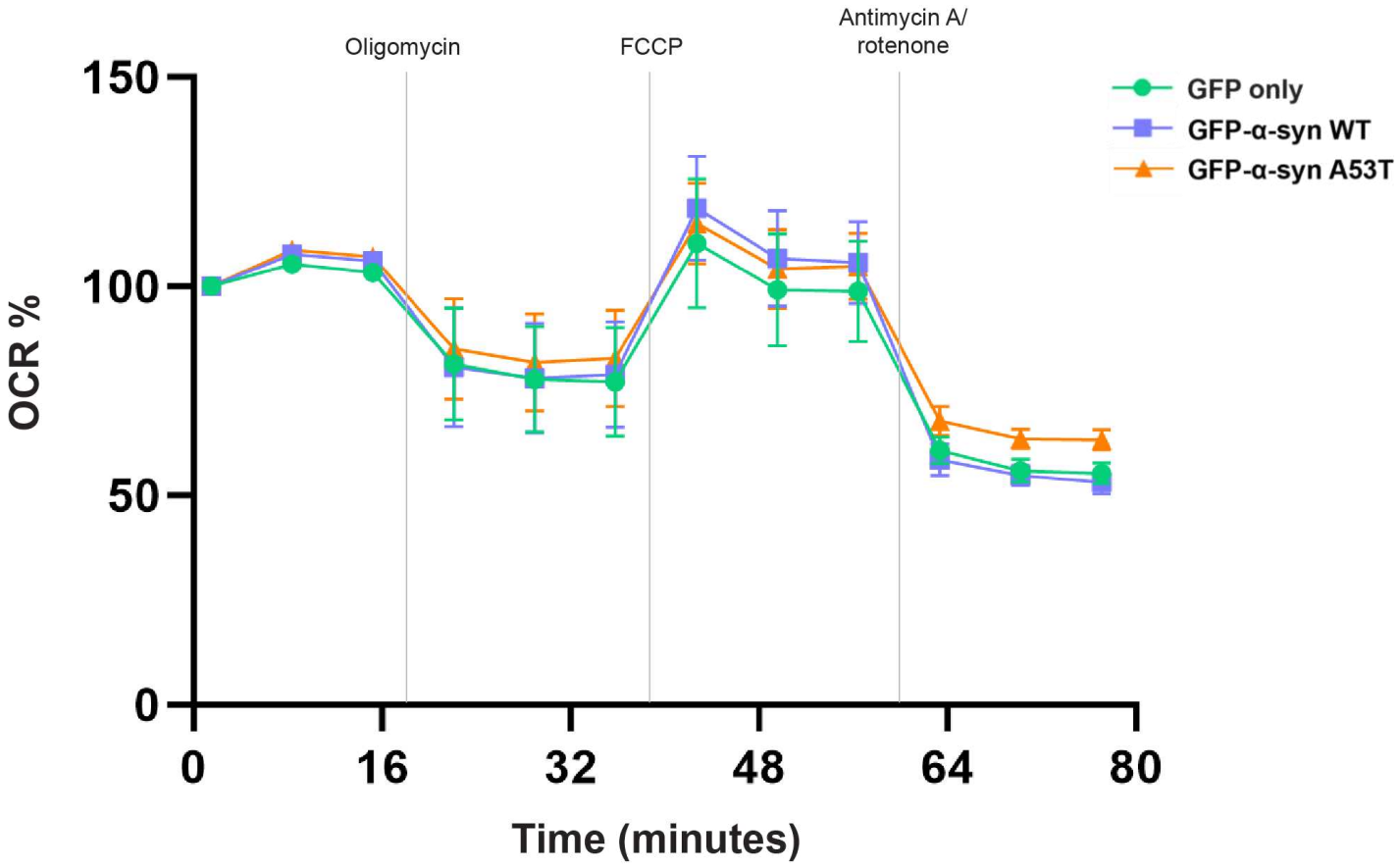

Figure 77: Cells overexpressing GFP-α-syn-WT and GFP-α-syn-A53T have similar oxygen consumption to GFP only controls over the course of the Seahorse mito-stress test

GFP only, GFP-α-syn-WT and GFP-α-syn-A53T cells were plated in a 96-well plate and subjected to a Seahorse mito-stress test. Oligomycin, FCCP and a combination of antimycin A and rotenone were applied at indicated time points. Oxygen consumption rate (OCR) was measured over 80 minutes. This graph is a trace of the means from 3 biological replicates. GFP expressing cells are shown in green, GFP-α-syn-WT expressing cells are shown in purple and GFP-α-syn-A53T expressing cells are shown in orange. Data points are shown relative to the first baseline OCR reading, shown as 100%, for each cell line. Data has been normalised to total protein concentration to account for differences in cell density. (**n=3**).

Measurements from different sections of the mito-stress test trace represent different respiratory parameters (**Appendix A**, **Figure 119**). Though there were no statistically significant differences between the cell lines across any of these indicators, there were some consistent trends. For example, GFP-α-syn-WT cells had higher OCR than GFP only cells in all 6 parameters, with cells overexpressing GFP-α-syn-WT having higher basal and maximal respiration (**Figure 78a, d**). This suggests that overexpression of GFP-α-syn-WT has no negative impact on energy production in my model. In GFP-α-syn-A53T cells, OCR measurements were similar to those from GFP only control cells. There were no clear reductions in OCR, suggesting that overexpression of GFP-α-syn-A53T also does not cause any gross defects in mitochondrial function in my model.

The only measurement which exhibited a clear difference between GFP-α-syn-A53T cells and the GFP only control cells was non-mitochondrial oxygen consumption, where GFP only cells had the lowest measurement (**Figure 78f**). GFP-α-syn-A53T cells had a non-mitochondrial OCR higher than both GFP only and GFP-α-syn-WT cells, which could potentially reflect a compensatory mechanism to increase overall oxygen consumption.

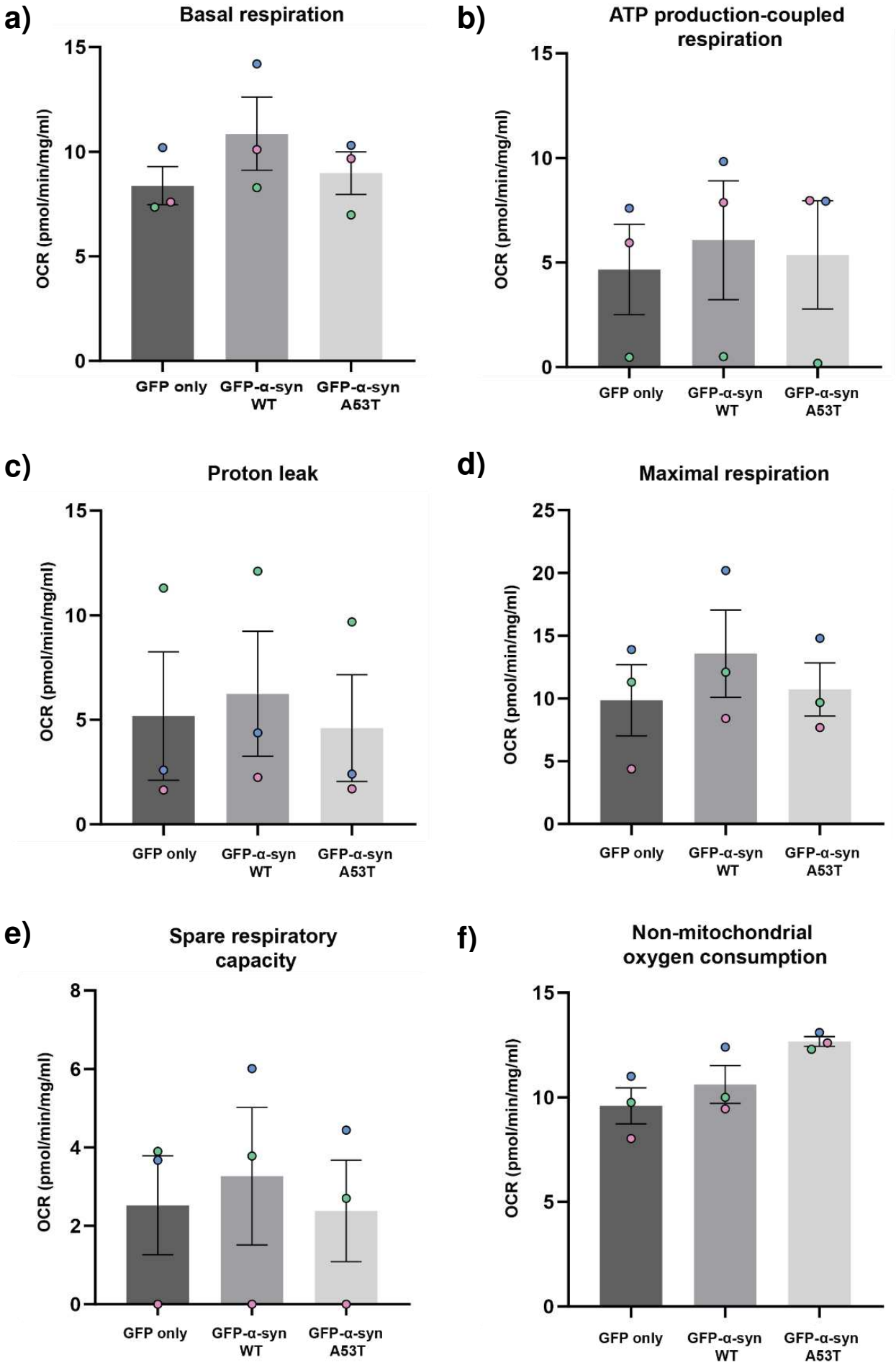
a)
Basal respiration
OCR (pmol/min/mg/ml)
15
10
5
0
GFP only
GFP-α-syn WT
GFP-α-syn A53T
b)
ATP production-coupled respiration
OCR (pmol/min/mg/ml)
15
10
5
0
GFP only
GFP-α-syn WT
GFP-α-syn A53T
c)
Proton leak
OCR (pmol/min/mg/ml)
15
10
5
0
GFP only
GFP-α-syn WT
GFP-α-syn A53T
d)
Maximal respiration
OCR (pmol/min/mg/ml)
25
20
15
10
5
0
GFP only
GFP-α-syn WT
GFP-α-syn A53T
e)
Spare respiratory capacity
OCR (pmol/min/mg/ml)
8
6
4
2
0
GFP only
GFP-α-syn WT
GFP-α-syn A53T
f)
Non-mitochondrial oxygen consumption
OCR (pmol/min/mg/ml)
15
10
5
0
GFP only
GFP-α-syn WT
GFP-α-syn A53T

Figure 78: Overexpression of GFP-α-syn-WT or GFP-α-syn-A53T do not impact mitochondrial oxygen consumption rates

Respiratory parameters were calculated from oxygen consumption rate (OCR) data from the Seahorse mito-stress test. Seahorse WavePro software was used to collect and visualise data. Graphs display measurements of a) basal respiration, b) ATP-coupled respiration, c) proton leak, d) maximal respiration, e) spare respiratory capacity and f) non-mitochondrial oxygen consumption. OCR is shown normalised to protein concentration in mg/ml. Bars show GFP only cells in dark grey, GFP-α-syn-WT cells in medium grey and GFP-α-syn-A53T cells in light grey. Biological replicates are colour coded, with circles representing the means of each repeat, bars showing the mean of all 3 biological repeats and black lines representing the SEM. Statistical analysis was carried out using a repeated measures one-way ANOVA with Tukey's multiple comparisons test. No significant differences were reported. (**n=3**).

To thoroughly explore any impacts on mitochondrial function, I assessed whether cells expressing GFP-α-syn-WT or GFP-α-syn-A53T had any differences in ΔΨm as an indicator of mitochondrial health (Zorova et al., 2018). Maintenance of constant ΔΨm is essential for mitochondrial energy production and organelle health (Zamzami et al., 1995; Zorova et al., 2018). Investigations into the impact of pathological α-synuclein on ΔΨm are conflicting. One study has demonstrated that ex-vivo incubation of isolated rat mitochondria with α-synuclein aggregates resulted in a dose-dependent loss of ΔΨm (Banerjee et al., 2010). However, other research has shown that in an overexpression model, α-synuclein directly bound the OMM without impacting ΔΨm (Kamp et al., 2010). To investigate this in my model, I assessed whether baseline ΔΨm was impacted using the voltage-sensitive probe, TMRM, in live cells.

There was no difference in TMRM fluorescence intensity between GFP only, GFP-α-syn-WT and GFP-α-syn-A53T cells, suggesting that baseline ΔΨm was similar across the cell lines. Though GFP only cells had a higher average fluorescence intensity, this appears to be skewed by one individual biological repeat. These data imply that overexpression of GFP-α-syn-WT and GFP-α-syn-A53T does not impact maintenance of baseline ΔΨm (**Figure 79**).

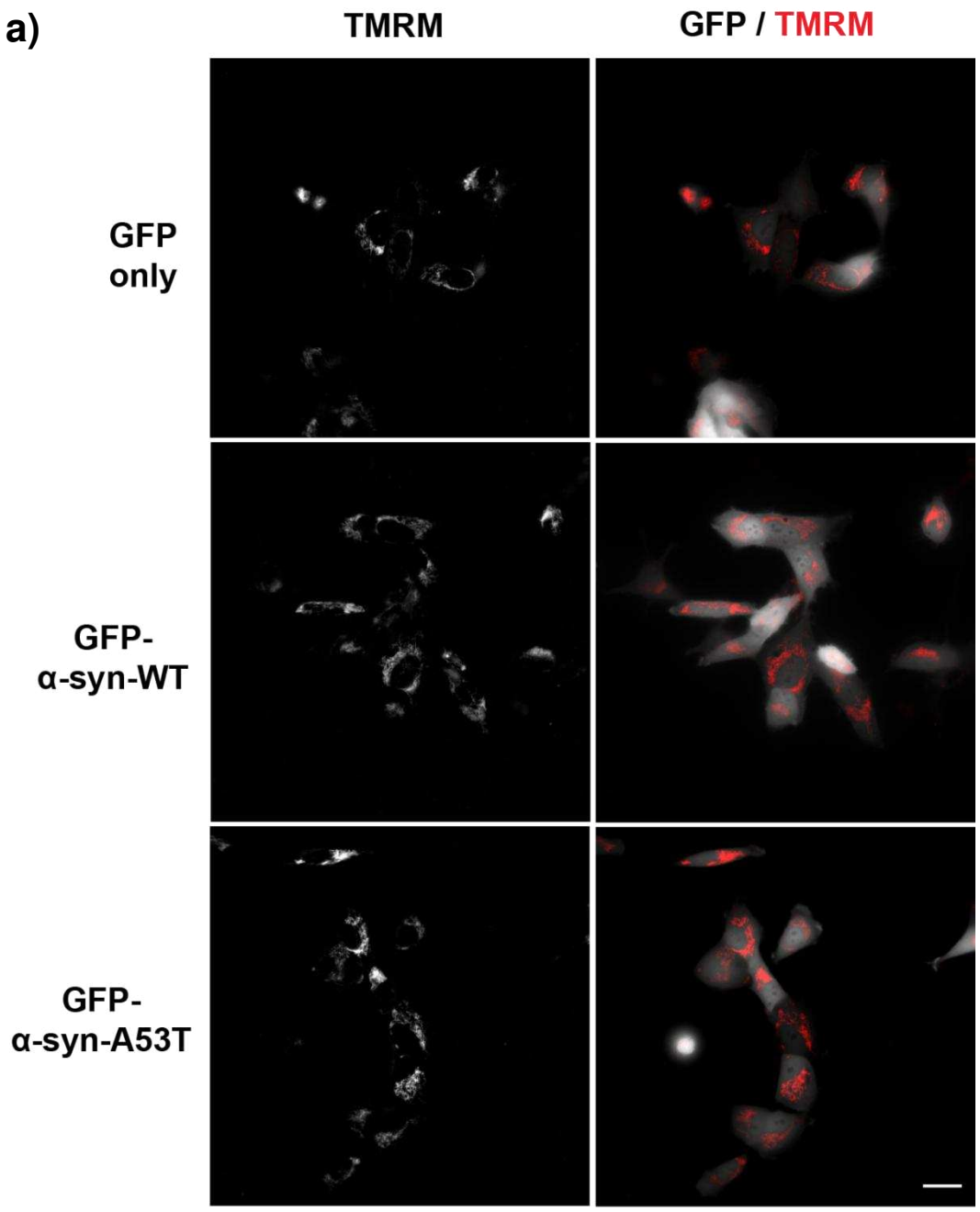
a)
TMRM
GFP / TMRM
GFP only
GFP-α-syn-WT
GFP-α-syn-A53T

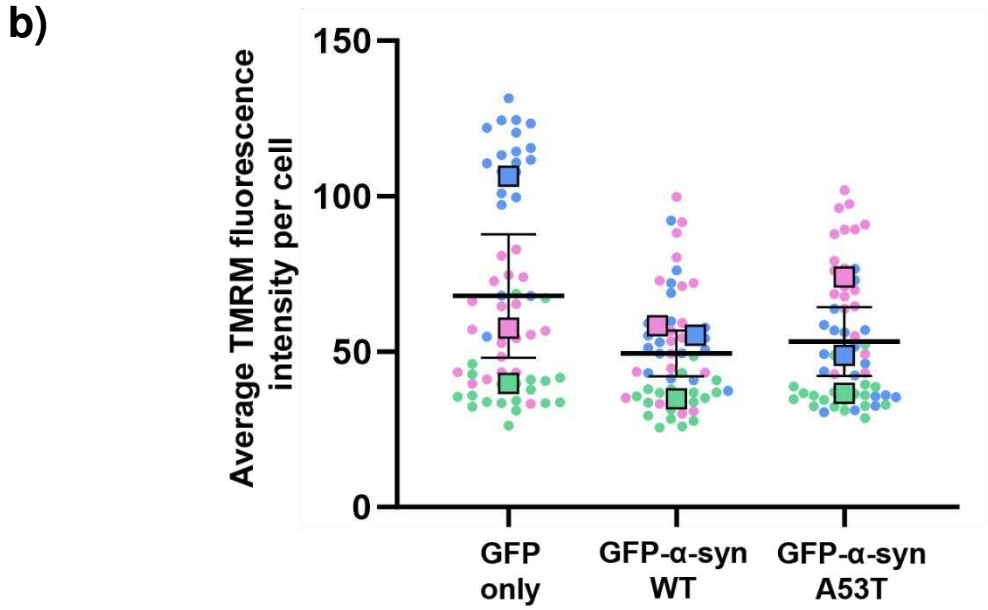
b)
Average TMRM fluorescence intensity per cell
150
100
50
0
GFP only
GFP-α-syn WT
GFP-α-syn A53T

Figure 79: Overexpression of GFP-α-syn-WT and GFP-α-syn-A53T has no impact on baseline ΔΨm

a) ΔΨm was measured at baseline in live cells overexpressing GFP only, GFP-α-syn-WT and GFP-α-syn-A53T using the voltage-sensitive probe, TMRM. Images of TMRM staining (red) are representative and were taken from 1 repeat. GFP staining (shown in grey for clarity) was also imaged to enable selection of only cells expressing GFP or GFP-α-syn. Images were captured on a DeltaVision Elite live imaging system with a 60X objective.

b) Fluorescence intensity of TMRM-positive mitochondria was measured in 20 GFP-positive cells per cell line, per biological repeat. Average fluorescent intensity for each cell is shown by a dot, with the mean of each biological repeat shown by a square and the mean of all 3 biological repeats shown by a black bar. SEM is shown by vertical black lines. Data points are colour coded by biological repeat. Statistical analysis was performed by a repeated measures one-way ANOVA with Tukey's multiple comparisons test but reported no significant differences between the cell lines. (**n=3**).

4.2.6 Overexpression of GFP-α-syn-WT and GFP-α-syn-A53T results in fragmentation of the mitochondrial network at steady state

Maintenance of a healthy mitochondrial network relies on an efficient balance of fission and fusion events (Youle & Van Der Bliek, 2012). Healthy networks are filamentous, with well-connected organelles likely optimising metabolite exchange (McCarron et al., 2013). It is known that in response to damage, mitochondrial fission segregates dysfunctional organelles for mitophagy, resulting in a less tubular, more fragmented network (Twig et al., 2008). Interestingly, an increase in this fragmentation response has been observed in both animal and cellular models of PD (Shah et al., 2019). Of particular relevance, this phenotype has been reported in models of α-synuclein overexpression, suggesting that pathological α-synuclein can influence mitochondrial dynamics (Krzystek et al., 2021; K. Nakamura et al., 2011). It has been proposed that this occurs through a relationship with proteins modulating fission and fusion events (Hsieh et al., 2016; Ordonez et al., 2018; Shaltouki et al., 2018). A major co-ordinator of mitochondrial fission, Drp1 is a GTPase that is recruited to constricted mitochondria to facilitate membrane scission by forming a ring-like structure (Basu et al., 2017). Research has suggested that overexpression of α-synuclein can prevent Drp1 from localising to mitochondria efficiently through stabilisation of the cytoskeleton, reducing fission and thus impacting mitochondrial morphology (Ordonez et al., 2018). Further, α-synuclein has been shown to increase levels of Miro, a key adaptor protein that sits on the OMM and mediates mitochondrial motility in response to damage (Shaltouki et al., 2018). This α-synuclein-induced upregulation of Miro

prevented mitochondrial movement and though the mitochondrial network was not assessed in this study, a delay in mitophagy was observed since Miro prevented normal motility (Shaltouki et al., 2018). These associations between α-synuclein and proteins regulating fission-fusion activity suggest that overexpression of α-synuclein can directly impact mitochondrial morphology.

Given the observations of α-synuclein-induced mitochondrial fragmentation documented in the literature, I next aimed to evaluate whether overexpression of GFP-α-syn-WT or GFP-α-syn-A53T had any consequence on mitochondrial network organisation. Firstly, I assessed the nature of the mitochondrial network at steady state and in response to damage with A/O in SH-SY5Y α-synuclein cell models. I noted that as expected, mitochondria in untreated cells were tubular and filamentous in shape, with many connections forming a clear network. As cells were exposed to accumulating levels of damage with A/O, mitochondria became more fragmented, giving the visual impression of indvidiual mitochondrial puncta throughout rather than one connected network (**Figure 80**). This was true of all cell lines, indicating that GFP-α-syn-WT and GFP-α-syn-A53T overexpressing cells were able to induce fragmentation of the mitochondrial network in response to damage.

Using an analysis workflow, I quantified these changes in mitochondrial morphology and connectivity at steady state and in response to mitochondrial damage from immunofluorescence microscopy images. As well as decreasing in number (**Figure 81a**), mitochondrial fragments in all 3 cell lines exhibited a decrease in the area (**Figure 81b**) and perimeter (**Figure 81c**) in response to increasing mitochondrial damage. In measurements of shape, all cell lines also exhibited an increase in the circularity (**Figure 81d**) and a decrease in the aspect ratio (**Figure 81e**) of mitochondrial fragments, indicating that they became more rounded in response to damage. Measurements of network connectivity showed that with increasing mitochondrial damage, there were fewer mitochondrial branches (**Figure 82a**) and junctions (**Figure 82b**) as well as a reduction in mitochondrial branch length (**Figure 82c, d**) in all 3 cell lines. Together, these readouts indicate numerically the expected fragmentation of the mitochondrial network in response to mitochondrial damage. Since the same pattern of mitochondrial fragmentation was observed in GFP only, GFP-α-syn-WT and GFP-α-syn-A53T cells, I propose that overexpression of GFP-α-syn did not hinder the modulation of fission and fusion in response to damage.

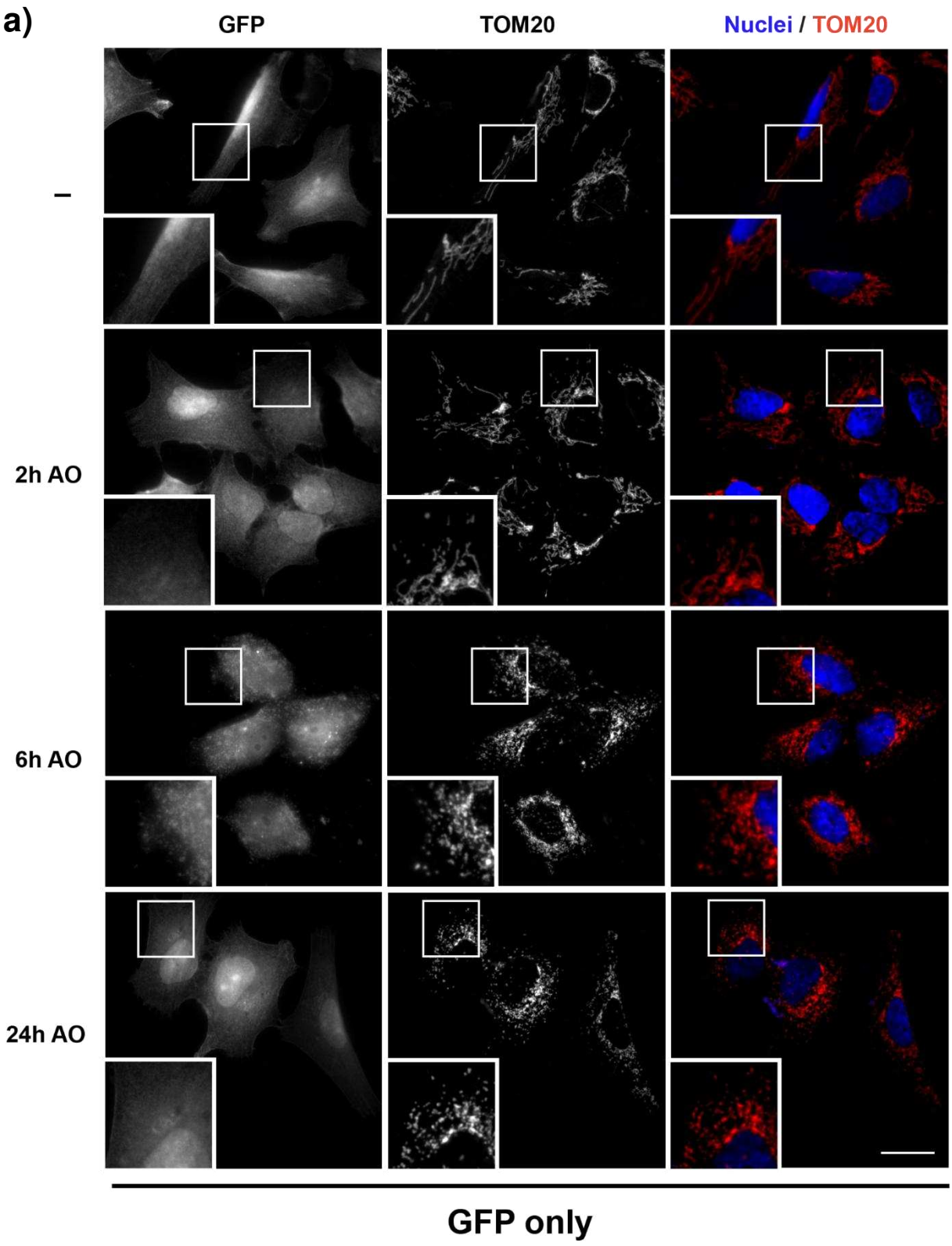
a)
GFP
TOM20
Nuclei / TOM20
–
2h AO
6h AO
24h AO
GFP only

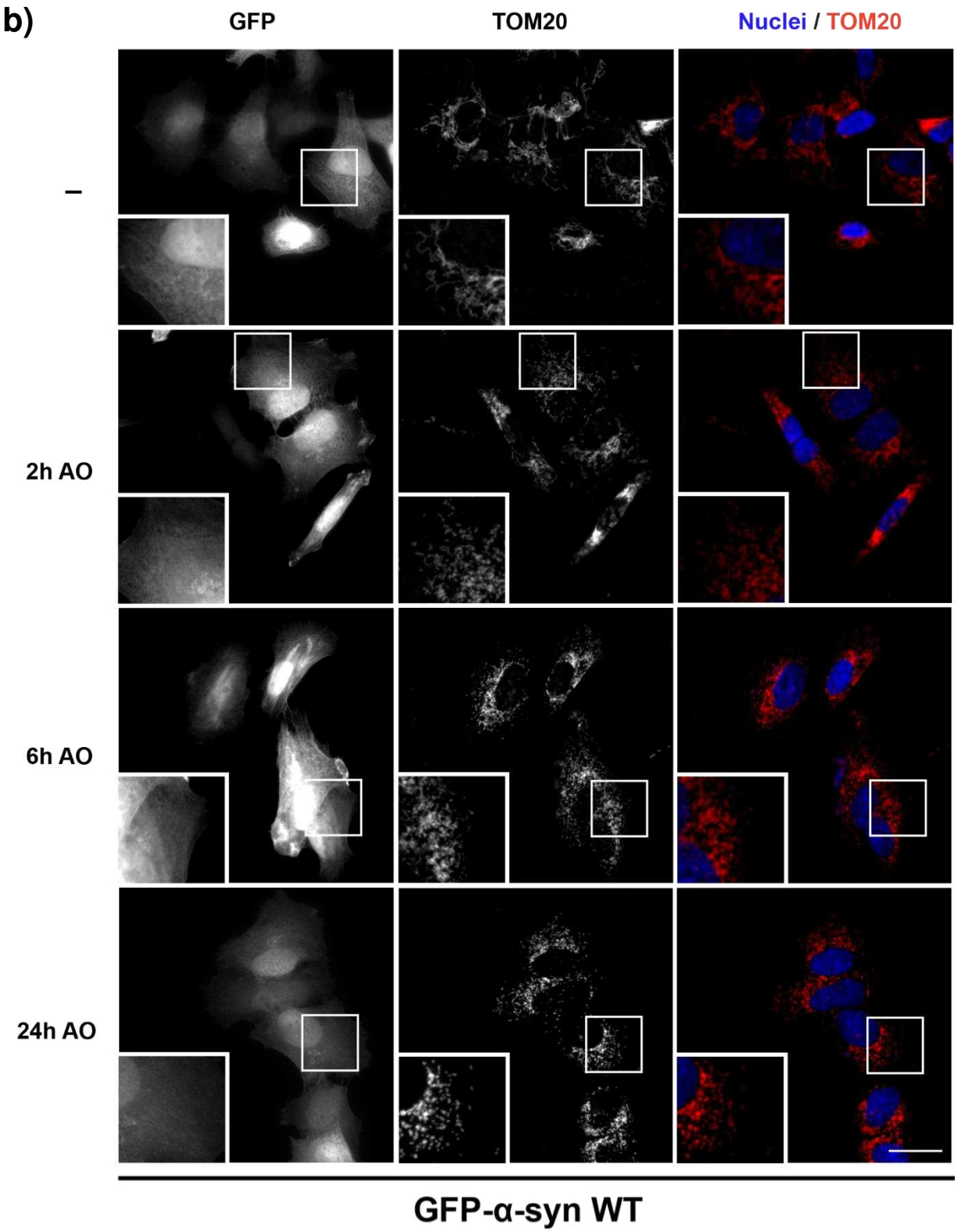
b)
GFP
TOM20
Nuclei / TOM20
–
2h AO
6h AO
24h AO
GFP-α-syn WT

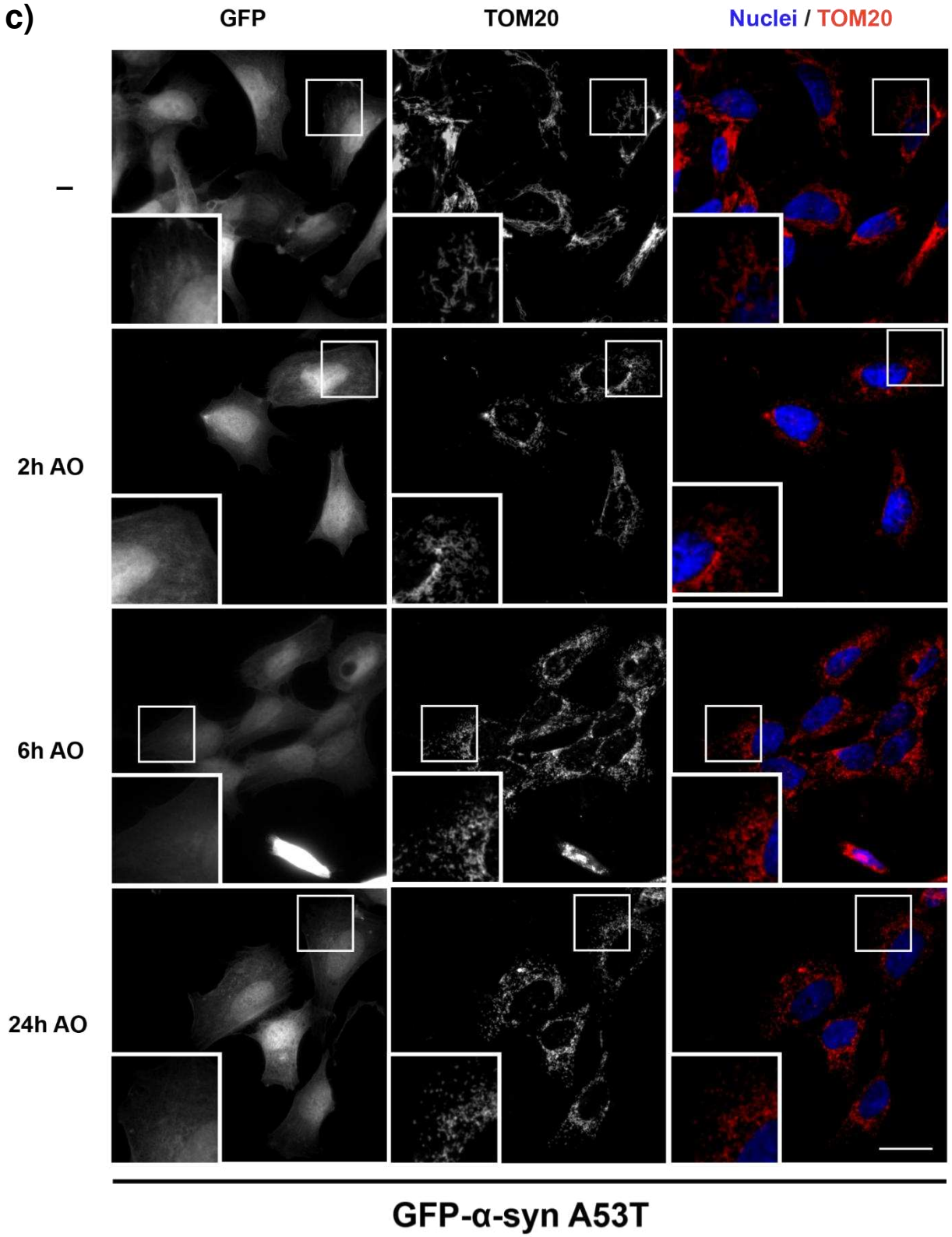
c)
GFP
TOM20
Nuclei / TOM20
–
2h AO
6h AO
24h AO
GFP-α-syn A53T

Figure 80: Overexpression of GFP-α-syn-WT and GFP-α-syn-A53T has no impact on the ability of cells to induce mitochondrial fragmentation in response to accumulating mitochondrial damage

GFP only (a), GFP-α-syn-WT (b) and GFP-α-syn-A53T (c) cells were left untreated (-) or treated for 2, 6 or 24 hours with A/O to induce mitochondrial damage. Cells were fixed and stained with an antibody against TOM20 (red) with nuclei labelled by Hoechst (blue). GFP was imaged to allow selection of only GFP-positive cells for subsequent analysis. Images shown are representative and originate from 1 biological repeat. Images were taken using widefield immunofluorescence microscopy on a 100X objective. Scale bar = 20μm.

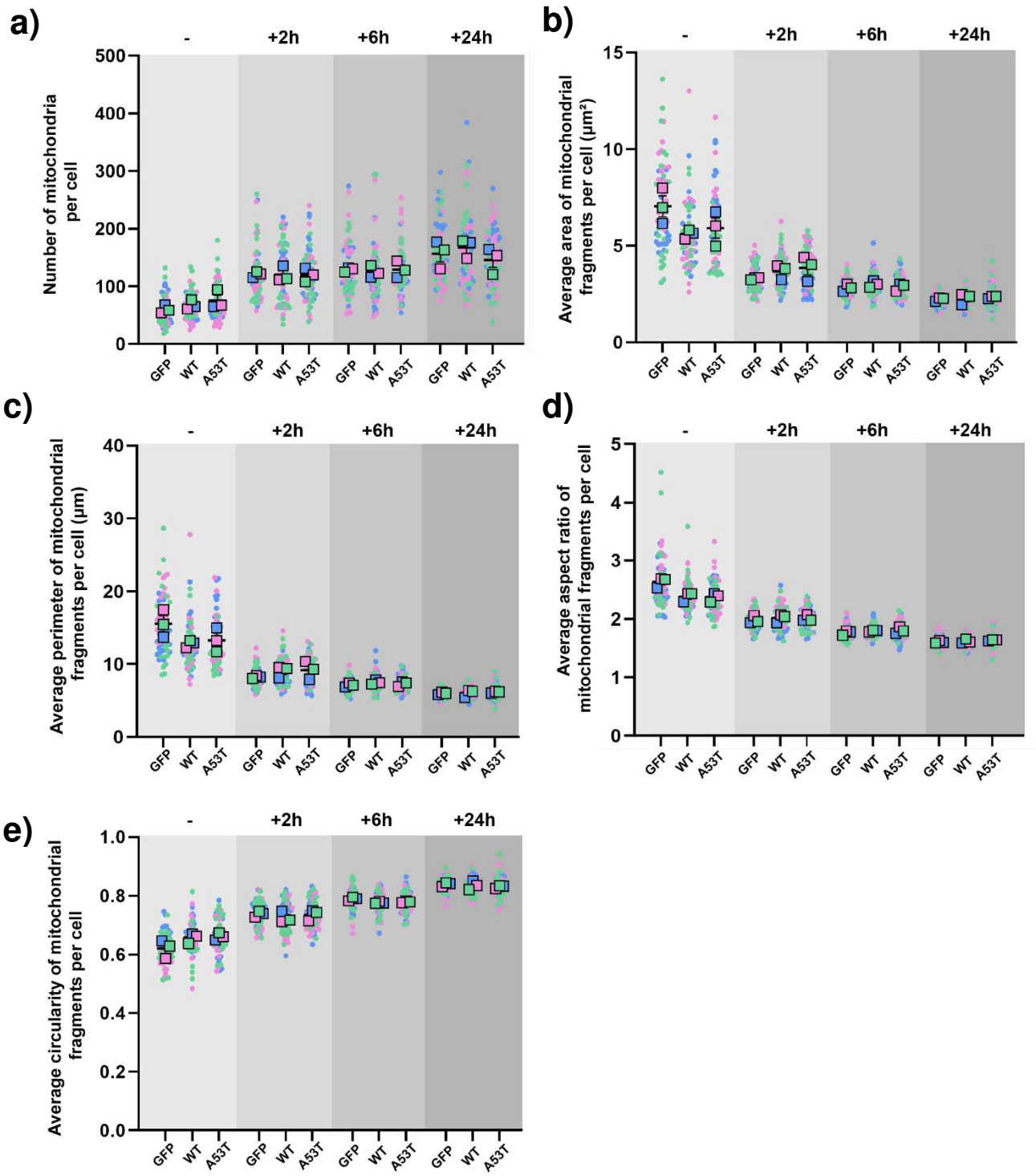
a)
Number of mitochondria per cell
b)
Average area of mitochondrial fragments per cell (µm²)
c)
Average perimeter of mitochondrial fragments per cell (µm)
d)
Average aspect ratio of mitochondrial fragments per cell
e)
Average circularity of mitochondrial fragments per cell
-
+2h
+6h
+24h
GFP
WT
A53T

Figure 81: Overexpression of GFP-α-syn-WT and GFP-α-syn-A53T does not impact the ability of cells to alter mitochondrial morphology in response to damage

Quantitative measurements of mitochondrial morphology were taken with an ImageJ image analysis workflow to isolate individual, GFP-positive cells and analyse particles within these that were positive for TOM20. Measurements were taken from GFP only (GFP), GFP-α-syn-WT (WT) and GFP-α-syn-A53T (A53T) cells left untreated (-) or treated for 2, 6 or 24 hours with A/O to induce mitochondrial damage. Parameters measured were a) number of mitochondria per cell; b) average area of mitochondrial fragments per cell; c) average perimeter of mitochondrial fragments per cell; d) average aspect ratio of mitochondrial fragments per cell and e) average circularity of mitochondrial fragments per cell. 20 cells were analysed per condition, per biological repeat. Measurements from each individual cell are shown by a dot, with the mean of each repeat shown as a square and the mean of all 3 repeats shown by a black line. SEM is shown by vertical black lines. Data points are all colour coded by biological repeat. Statistical analysis was carried out by a repeated measures 2-way ANOVA with Tukey's multiple comparisons test. Significant differences were only found between the cell lines when untreated, shown in **Figure 83**. (**n=3**).

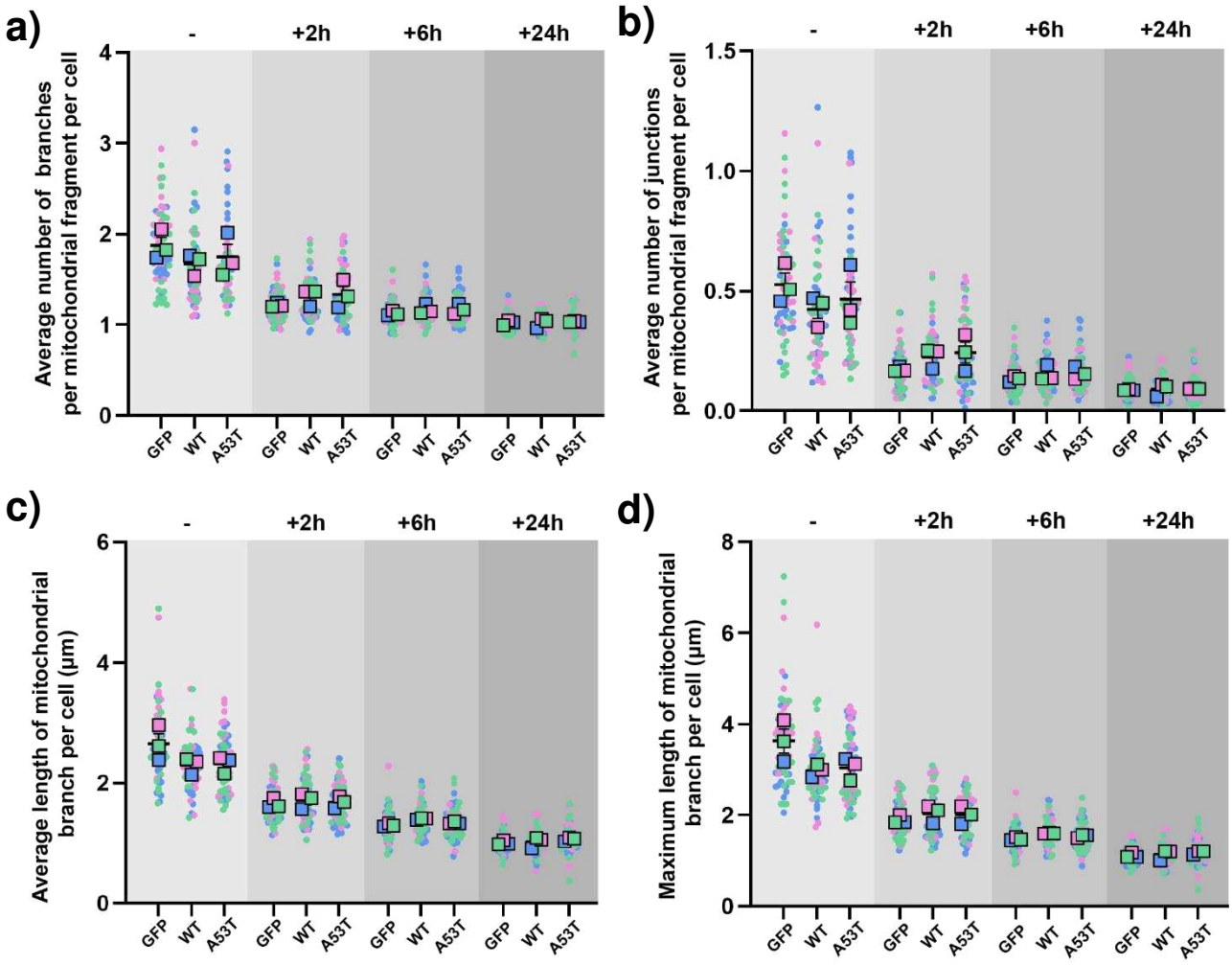

Figure 82: Overexpression of GFP-α-syn-WT and GFP-α-syn-A53T does not impact the ability of cells to alter mitochondrial connectivity in response to damage

Quantitative measurements of mitochondrial connectivity were obtained using an ImageJ image analysis workflow to isolate individual GFP-positive cells and analyse skeletons within them. Measurements were taken from GFP only (GFP), GFP-α-syn-WT (WT) and GFP-α-syn-A53T (A53T) cells left untreated (-) or treated for 2, 6 or 24 hours with A/O to induce mitochondrial damage. Parameters measured were a) average number of branches per mitochondrial fragment per cell; b) average number of junctions per mitochondrial fragment per cell; c) average length of mitochondrial branches per cell and d) maximum length of mitochondrial branches per cell. 20 cells were analysed per condition, per biological repeat. Measurements from each individual cell are shown by a dot, with the mean of each repeat shown by a square and the mean of all 3 repeats represented by a black line. SEM is shown by vertical black lines. Data points are colour coded by biological repeat. Statistical analysis was performed by a repeated-measures 2-way ANOVA with Tukey's multiple comparisons test. Significant differences were only found between the cell lines when untreated, shown in **Figure 84**. (**n=3**).

Of note, statistical analysis revealed that there were significant differences between GFP only, GFP-α-syn-WT and GFP-α-syn-A53T cells when untreated at steady state. In terms of morphology, steady state GFP-α-syn-WT and GFP-α-syn-A53T cells both exhibited significantly lower mitochondrial area (**Figure 83b**), perimeter (**Figure 83c**) and aspect ratio (**Figure 83e**) alongside significantly increased mitochondrial circularity (**Figure 83d**) compared to steady state GFP only cells. Corroborating this, GFP-α-syn-WT and GFP-α-syn-A53T cells also displayed significantly shorter mitochondrial branches than GFP only controls at steady state (**Figure 84c, d**)**.** Interestingly, these differences were all observed in both GFP-α-syn overexpression cell lines, with no significant differences between GFP-α-syn-WT and GFP-α-syn-A53T cells, implying that this phenotype is a general response to excess GFP-α-syn rather than a specific form of the protein. These data suggest that overexpression of GFP-α-syn results in a more fragmented mitochondrial network at steady state, though it does not impact mitochondrial damage-induced changes in network organisation.

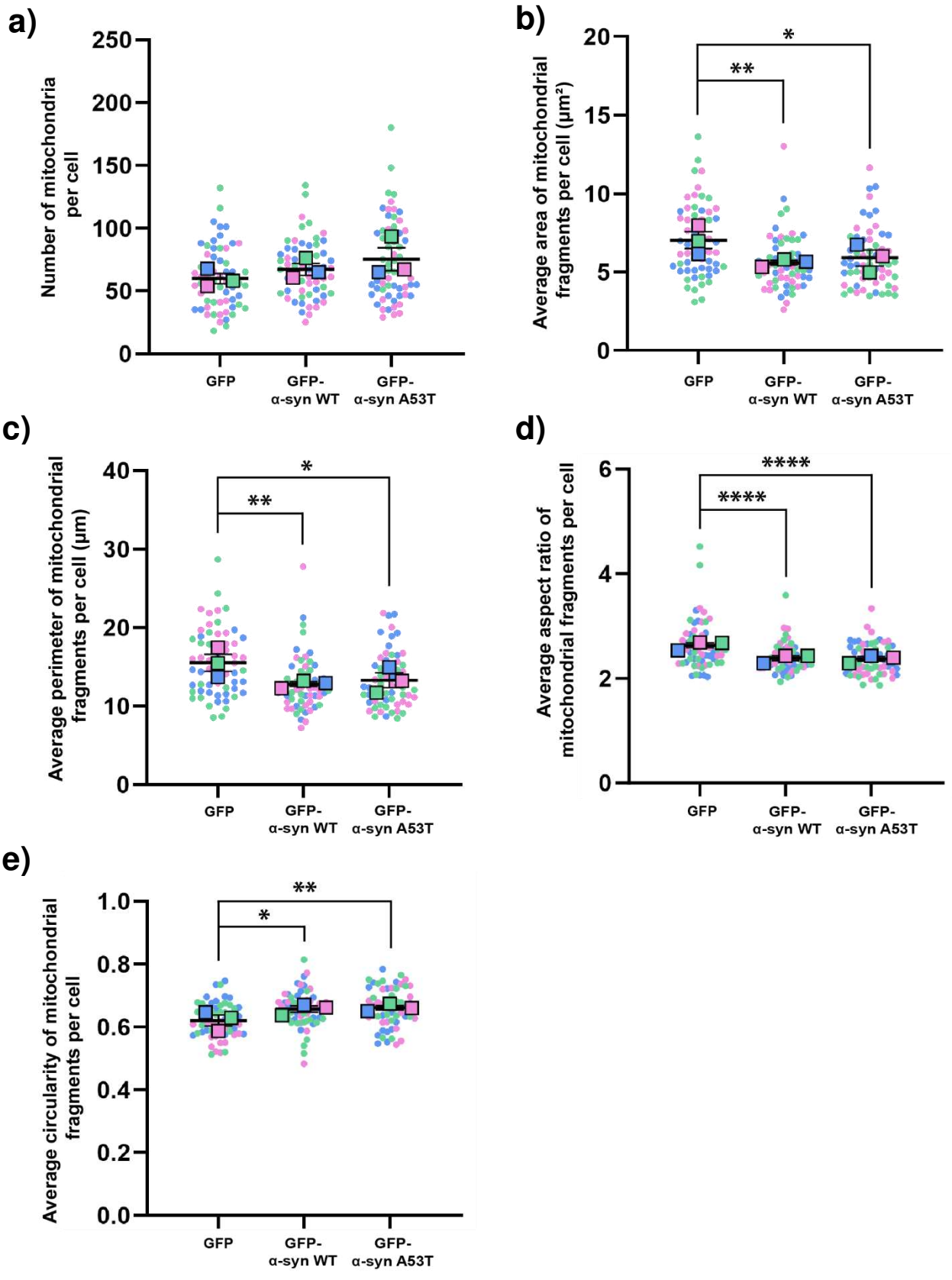
a)
Number of mitochondria per cell
250
200
150
100
50
0
GFP
GFP-α-syn WT
GFP-α-syn A53T
b)
Average area of mitochondrial fragments per cell (µm²)
20
15
10
5
0
*
**
GFP
GFP-α-syn WT
GFP-α-syn A53T
c)
Average perimeter of mitochondrial fragments per cell (µm)
40
30
20
10
0
*
**
GFP
GFP-α-syn WT
GFP-α-syn A53T
d)
Average aspect ratio of mitochondrial fragments per cell
6
4
2
0
****
****
GFP
GFP-α-syn WT
GFP-α-syn A53T
e)
Average circularity of mitochondrial fragments per cell
1.0
0.8
0.6
0.4
0.2
0.0
**
*
GFP
GFP-α-syn WT
GFP-α-syn A53T

Figure 83: Overexpression of GFP-α-syn-WT and GFP-α-syn-A53T results in a more fragmented mitochondrial phenotype at steady state

Graphs show that morphological measurements of mitochondria from untreated GFP only, GFP-α-syn-WT and GFP-α-syn-A53T cells from **Figure 81** in more detail. Parameters measured were a) number of mitochondria per cell; b) average area of mitochondrial fragments per cell; c) average perimeter of mitochondrial fragments per cell; d) average aspect ratio of mitochondrial fragments per cell and e) average circularity of mitochondrial fragments per cell. Measurements from each individual cell are shown by a dot, with the mean of each biological repeat shown by a square and the mean of all 3 repeats shown by a black line. SEM is shown by vertical black lines. Data points are colour coded by biological repeat. Statistical analysis was performed by repeated measures 2-way ANOVA with Sídák's multiple comparisons test. The average area of mitochondrial fragments was significantly lower in GFP-α-syn-WT ($p=0.0021$, **) and GFP-α-syn-A53T ($p=0.0164$, *) cells compared to GFP only. The average perimeter of mitochondrial fragments was significantly lower in GFP-α-syn-WT ($p=0.0025$, **) and GFP-α-syn-A53T ($p=0.0134$, *) compared to GFP only. The average aspect ratio of mitochondrial fragments was also significantly lower in both GFP-α-syn-WT and GFP-α-syn-A53T cells than GFP only (both $p<0.0001$, ****). The average circularity was significantly higher in GFP-α-syn-WT ($p=0.0162$, *) and GFP-α-syn-A53T ($p=0.0065$, **) cells compared to GFP only. (**n=3**).

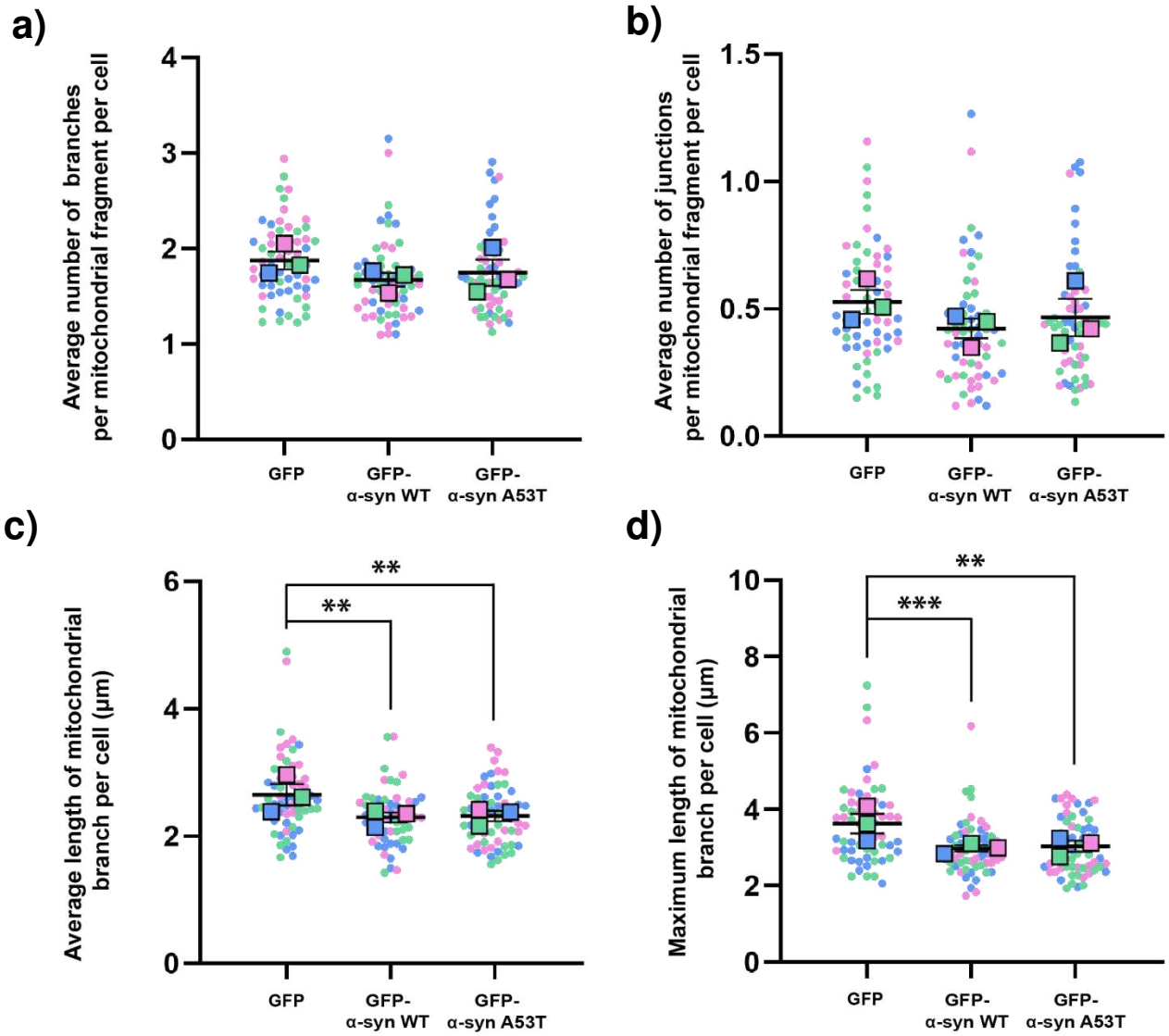

Figure 84: Overexpression of GFP-α-syn-WT and GFP-α-syn-A53T results in a less connected mitochondrial network at steady state

Graphs show the connectivity measurements from untreated GFP only, GFP-α-syn-WT and GFP-α-syn-A53T cells from **Figure 82** in more detail. Parameters measured were a) average number of branches per mitochondrial fragment per cell; b) average number of junctions per mitochondrial fragment per cell; c) average length of mitochondrial branches per cell and d) maximum length of mitochondrial branches per cell. Measurements from each individual cell are shown by a dot, with the mean of each biological repeat shown by a square and the mean of all 3 repeats shown by a black line. SEM is shown by vertical black lines. Data points are colour coded by biological repeat. Statistical analysis was performed by repeated measures 2-way ANOVA with Sídák's multiple comparisons test. The average length of a given mitochondrial branch was significantly lower in GFP-α-syn-WT (p=0.0045, **) and GFP-α-syn-A53T (p=0.0077, **) compared to GFP only. The maximum length of a mitochondrial branch per cell was also significantly lower in GFP-α-syn-WT (p=0.0006, ***) and GFP-α-syn-A53T (p=0.0016, **) cells compared to GFP only. (**n=3**).

4.2.7 Overexpression of GFP-α-syn-WT and GFP-α-syn-A53T have no impact on whole mitochondrial clearance

After exploring the impact of GFP-α-syn-WT and GFP-α-syn-A53T overexpression on mitochondrial function and network organisation, I next investigated whether this had any measurable effect on mito-QC mechanisms in response to damage, starting with mitophagy.

Mitochondrial damage induces depolarisation of the OMM triggering activation of mitochondrial clearance pathways, one of which is PINK1/Parkin mitophagy (D. P. Narendra et al., 2010; Vives-Bauza et al., 2010). Damaged mitochondria are subsequently cleared from the cell by the autophagosome-lysosome pathway, protecting remaining cellular components. Defects in mitophagy have long been associated with PD, since mutations in both PINK1 and Parkin are causative for some familial forms of the disease (Kitada et al., 1998; Pickrell & Youle, 2015; Valente et al., 2004). However, the relationship between pathological α-synuclein and autophagic mechanisms is not well understood. Previous research has shown that exogenous α-synuclein oligomers can reduce mitophagy through a direct interaction with Parkin, leading to reduced ubiquitylation of mitochondrial proteins (Wilkaniec et al., 2021). However, other studies have suggested that α-synuclein aggregation instead induces mitophagy (Lurette et al., 2023). Since there is no consensus on the impact of pathological α-synuclein on mitophagy, I was interested to evaluate this in my model following exposure of cells to 24 hours of A/O treatment.

After exposing cells to A/O for 24 hours, damage-induced degradation of CoxII was assessed as a readout of mitochondrial clearance (**Figure 85a**). In line with the GFP only control cells, GFP-α-syn-WT and GFP-α-syn-A53T cells exhibited a significant reduction of approximately 40% in CoxII expression, signifying that all 3 cell lines were equally able to segregate and remove damaged mitochondria in response to stress (**Figure 85b**). To more directly assess PINK1/Parkin mitophagy, I measured whether PINK1 expression was upregulated in response to damage (**Figure 86a**). A significant increase in PINK1 level was observed in GFP only, GFP-α-syn-WT and GFP-α-syn-A53T cells, suggesting that overexpression of GFP-α-syn did not impact stabilisation of PINK1 on the OMM (**Figure 86b**). Finally, I measured the expression of high molecular weight Mfn2 (highMW Mfn2) as a readout of ubiquitinated Mfn2, since Mfn2 is known to be a substrate of Parkin (Chen & Dorn, 2013). Ubiquitinated Mfn2 was shown to be significantly increased in response to A/O in GFP only, GFP-α-syn-WT and GFP-α-syn-A53T cells (**Figure 86c**)**.** Together, these data suggest that overexpression of GFP-α-syn-WT or GFP-α-syn-A53T does not impact whole mitochondrial clearance in response to mitochondrial damage.

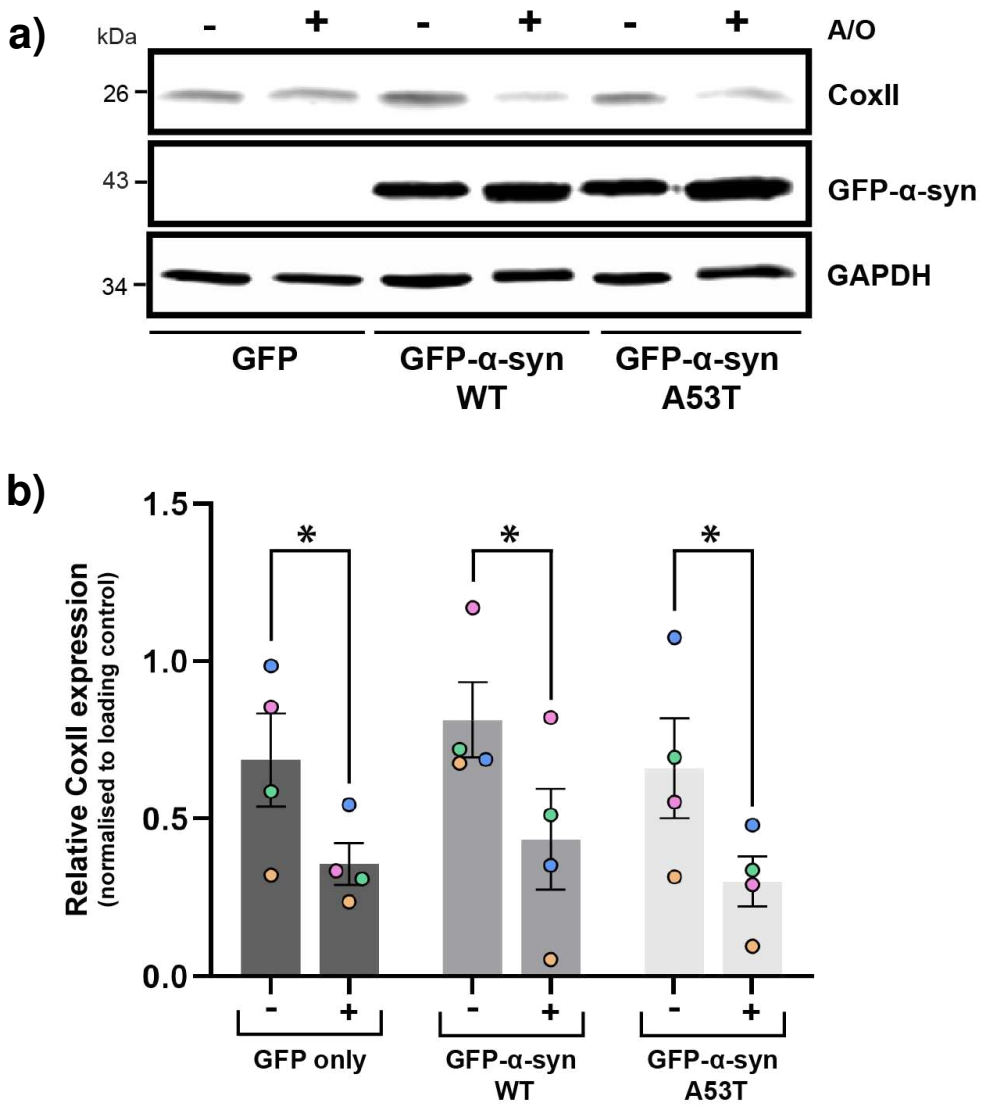

Figure 85: Overexpression of GFP-α-syn-WT and GFP-α-syn-A53T has no impact on damage-induced whole mitochondrial clearance

a) GFP only, GFP-α-syn-WT and GFP-α-syn-A53T cells were left untreated (-) or treated for 24 hours with A/O to induce mitochondrial damage. Lysates were processed for Western blot with an antibody against CoxII alongside α-synuclein to confirm overexpression of GFP-α-syn constructs and GAPDH as a protein loading control.

b) CoxII expression in response to A/O treatment was normalised to GAPDH to account for differences in protein loading. CoxII level is here represented by the raw value of this calculation. Biological replicates are colour coded, with circles representing the means of each repeat, bars representing the mean of the 4 repeats and black lines showing SEM. Bars show GFP only cells in dark grey, GFP-α-syn-WT wells in medium grey and GFP-α-syn-A53T cells in light grey. Statistical analysis was performed by a repeated measures 2-way ANOVA with Sídák's test for multiple comparisons. CoxII was significantly decreased with A/O treatment in GFP only ($p=0.0443$, *), GFP-α-syn-WT ($p=0.0250$, *) and GFP-α-syn-A53T cells ($p=0.0315$, *). (**n=4**).

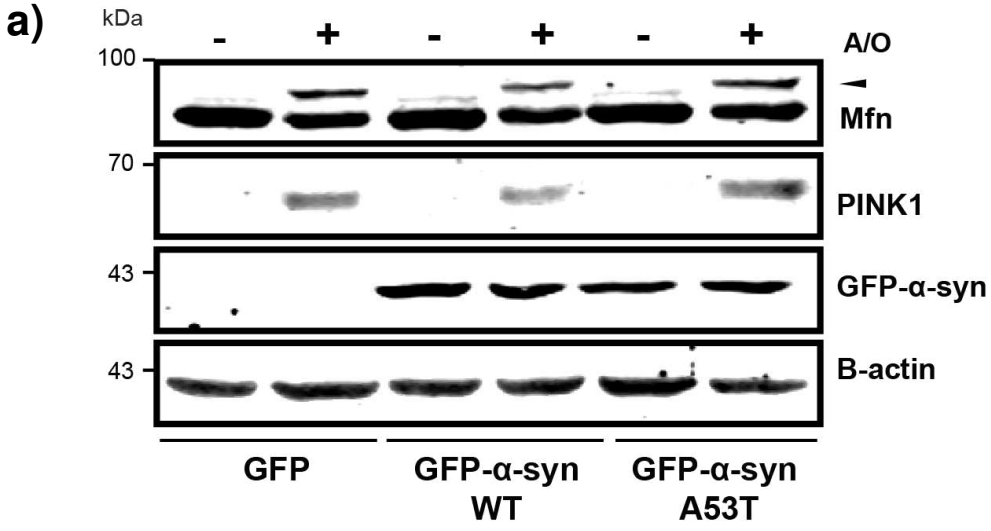
a)
kDa
100
70
43
43
- + - + - +
A/O
Mfn
PINK1
GFP-α-syn
B-actin
GFP
GFP-α-syn WT
GFP-α-syn A53T

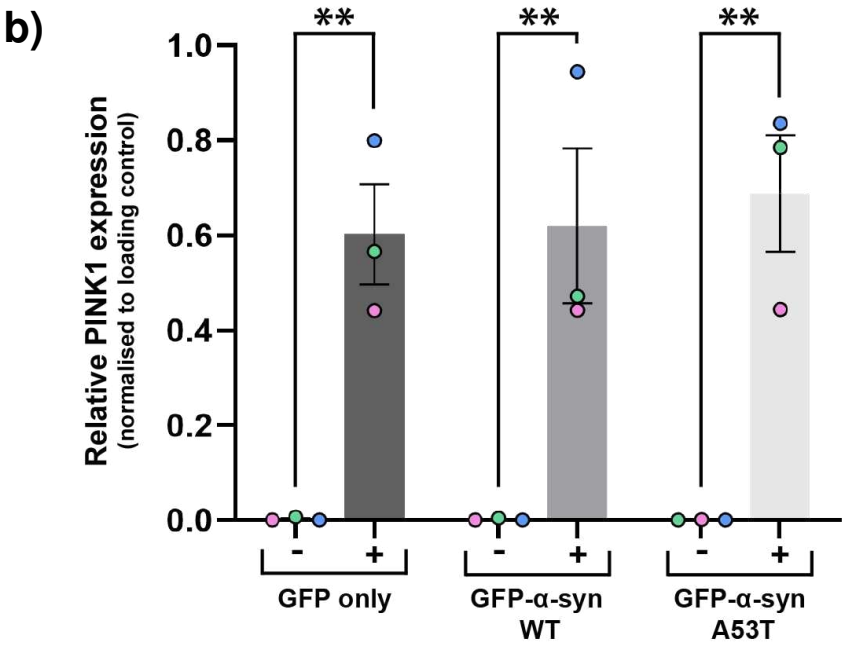
b)
Relative PINK1 expression
(normalised to loading control)
1.0
0.8
0.6
0.4
0.2
0.0
**
**
**
- + - + - +
GFP only
GFP-α-syn WT
GFP-α-syn A53T

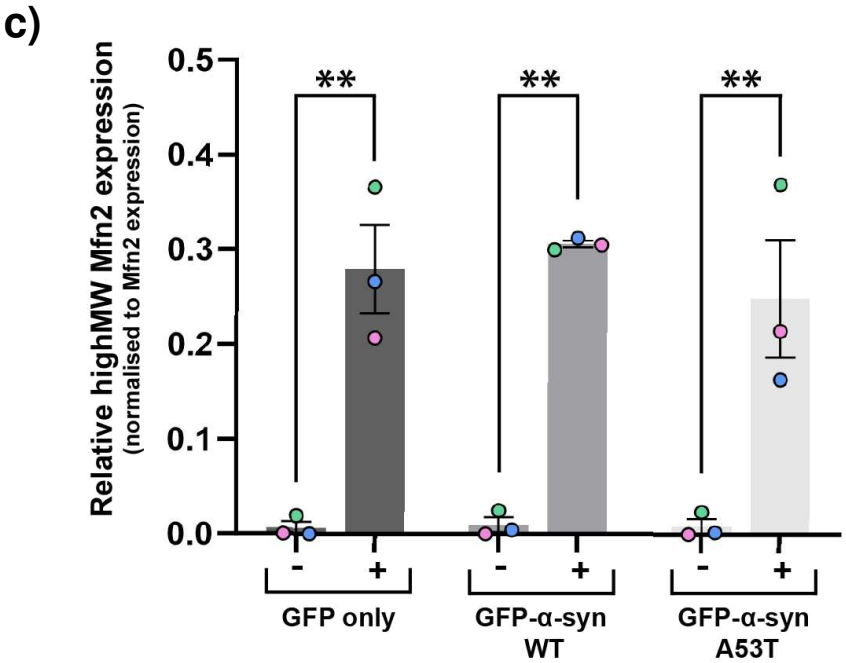
c)
Relative highMW Mfn2 expression
(normalised to Mfn2 expression)
0.5
0.4
0.3
0.2
0.1
0.0
**
**
**
- + - + - +
GFP only
GFP-α-syn WT
GFP-α-syn A53T

Figure 86: Overexpression of GFP-α-syn-WT and GFP-α-syn-A53T has no impact on expression of PINK1/Parkin-dependent mitophagy markers in response to mitochondrial damage

GFP only, GFP-α-syn-WT and GFP-α-syn-A53T cells were left untreated (-) or treated for 24 hours with A/O to evoke mitochondrial damage. Lysates were processed for Western blot (a) with antibodies against PINK1 and Mfn2 alongside α-synuclein to confirm overexpression of GFP-α-syn constructs and GAPDH as a loading control. Graphs b) and c) show quantitation of PINK1 expression high molecular weight (highMW, denoted on (a) by the arrowhead) Mfn2 species, respectively. Expression of PINK1 was normalised to B-actin to account for differences in protein loading. PINK1 level is represented by the raw values of this calculation. HighMW Mfn2 expression was normalised to total Mfn2 expression (both upper and lower bands) and is presented as a proportion of total Mfn2. Biological repeats are colour coded, with circles representing the means of each repeat, bars showing the mean of all 3 repeats and black lines showing SEM. Bars show GFP only cells in dark grey, GFP-α-syn-WT cells in medium grey and GFP-α-syn-A53T cells in light grey. Statistical analysis was carried out by repeated measures 2-way ANOVA with Sídák's multiple comparisons test. PINK1 was significantly increased in response to A/O treatment in GFP only (p=0.0024, **), GFP-α-syn-WT (p=0.0021, **) and GFP-α-syn-A53T cells (p=0.0014, **). HighMW Mfn2 was also significantly increased upon mitochondrial damage in GFP only (p=0.0052, **), GFP-α-syn-WT (p=0.0038, **) and GFP-α-syn-A53T cells (p=0.0083, **). (**n=3**).

Data from the previous chapter showed that a lack of α-synuclein increased Parkin levels at steady state, supporting the theory that α-synuclein may be involved in regulating expression of Parkin. As such, though overexpression of GFP-α-syn did not impact readouts of PINK1/Parkin-dependent mitophagy, I next aimed to investigate whether these α-synuclein models may exhibit alterations in the expression or function of Parkin.

Recent research has suggested that pathological α-synuclein does functionally associate with Parkin. Exogenous α-synuclein oligomers applied to cells were reported to directly result in post-translational modifications to Parkin that cause its degradation, inciting an overall Parkin decrease (Wilkaniec et al., 2019, 2021). However, this study was carried out in a Parkin overexpression background, and an α-synuclein-induced reduction in Parkin has not been observed in other studies. In fact, other research has shown Parkin to be protective against α-synuclein overexpression by altering the balance of phospho-S129 α-synuclein species (Khandelwal et al., 2010). Since SH-SY5Y cells express endogenous Parkin, my models provide a suitable environment in which to investigate the impact of GFP-α-syn-WT and GFP-α-syn-A53T overexpression on Parkin.

In response to mitochondrial damage, Parkin is responsible for ubiquitinating proteins on the surface of mitochondria as a degradation signal (Youle & Van Der Bliek, 2012). However, the removal of ubiquitin chains from Parkin and its degradation is an important step that is required for efficient mitophagy (Durcan et al., 2014). As such, Parkin levels were assessed at steady state and in response to mitochondrial damage with A/O (**Figure 87a**). A gradual decrease in Parkin expression was reported in all 3 cell lines in response to increasing mitochondrial damage, with cells experiencing the most accrued damage (24 hour of A/O), exhibiting the lowest Parkin expression (**Figure 87b**). No significant differences between the cell lines were reported at any of the treatment times, suggesting that overexpression of GFP-α-syn-WT and GFP-α-syn-A53T did not impact Parkin expression at steady state or in response to damage.

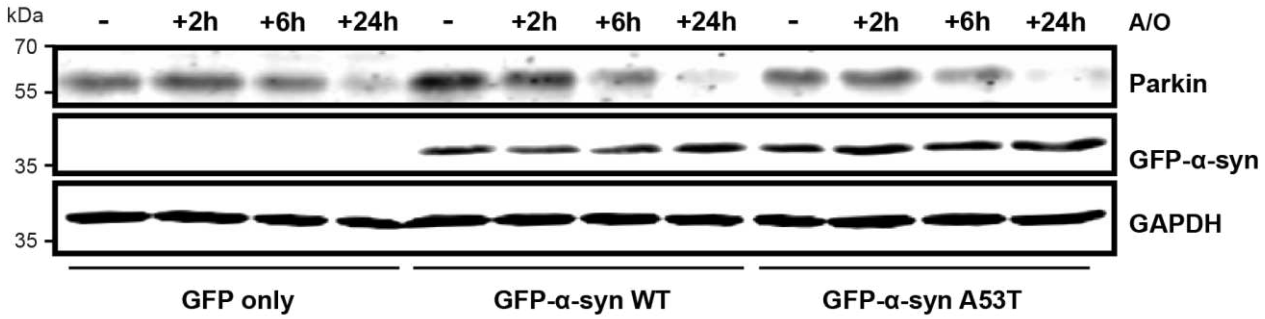

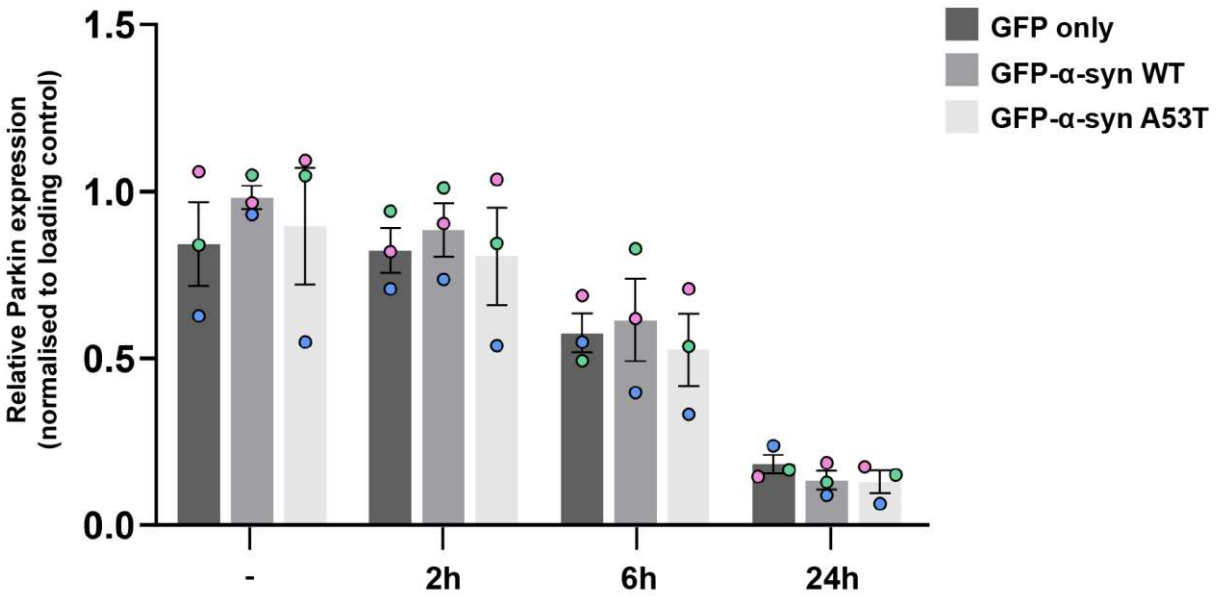

Figure 87: Overexpression of GFP-α-syn-WT and GFP-α-syn-A53T has no impact on Parkin expression or degradation in response to mitochondrial damage

a) GFP only, GFP-α-syn-WT and GFP-α-syn-A53T cells were left untreated (-) or treated for 2, 6 or 24 hours with A/O to induce mitochondrial damage. Lysates were processed for Western blot with an antibody against Parkin alongside α-synuclein to confirm overexpression of GFP-α-syn constructs and GAPDH as a loading control.

b) From Western blot data, Parkin expression was quantified in GFP only, GFP-α-syn-WT and GFP-α-syn-A53T in response to A/O. Parkin was normalised to GAPDH to account for differences in protein loading, and Parkin expression is represented by the raw values of this calculation. Biological repeats are colour coded, with circles showing the mean of each repeat, bars showing the mean of the 3 repeats and black bars representing the SEM. Bars show GFP only cells in dark grey, GFP-α-syn-WT cells in medium grey and GFP-α-syn-A53T cells in light grey. Statistical analysis was performed by repeated measures 2-way ANOVA with Tukey's test for multiple comparisons. No significant differences between cell lines were reported. (**n=3**).

`

Though overexpression of GFP-α-syn did not affect PINK1 or Parkin levels, I lastly measured whether it impacted PINK1/Parkin activity by measuring pUb S65 levels. When mitophagy is triggered, PINK1 phosphorylates ubiquitin at serine 65 which in turn recruits Parkin to damaged mitochondria (Kane et al., 2014; Koyano et al., 2014). As such, pUb S65 levels can be used as a direct readout of PINK1/Parkin-dependent mitophagy. Research has shown that pUb S65 is increased in an age- and disease-dependent manner in post-mortem brain tissue from PD and Lewy-body dementia patients (Hou et al., 2018). Moreover, this study found that pUb S65 correlated with α-synuclein pathology in these specimens, suggesting a direct relationship (Hou et al., 2018). To investigate pUb S65 species, the number of puncta and total area of pUb S65 staining was measured per cell in response to increasing mitochondrial damage. To reduce the capture of background staining, only pUb S65 colocalising with the mitochondrial marker cytochrome c were measured (**Figure 88**).

GFP only, GFP-α-syn-WT and GFP-α-syn-A53T overexpressing cells all displayed an increase in mitochondrial pUb S65 levels with increasing A/O induced damage. Highest levels of pUb S65 were observed when cells were exposed to A/O for 24 hours, both in terms of average number of pUb S65 puncta and average pUb S65 area per cell (**Figure 89**). When cell lines were statistically compared, GFP-α-syn-WT expressing cells showed a significantly higher total area of mitochondrial pUb S65 staining than GFP only cells after 24-hour A/O treatment (p=0.0456) (**Figure 89**). This was also reflected by the number of mitochondrial pUb S65 puncta per cell,

which was significantly higher in GFP-α-syn-WT expressing cells than both GFP only and GFP-α-syn-A53T expressing cells in response to both 6 hours and 24 hours of A/O. Interestingly, this seems to be unique to wild-type α-synuclein since this phenotype was not apparent in GFP-α-syn-A53T cells.

Together, these data show that overexpression of GFP-α-syn-WT and GFP-α-syn-A53T did not impact overall mitochondrial clearance in response to mitochondrial damage and did not impact expression of PINK1 or Parkin. However, overexpression of GFP-α-syn-WT was shown to increase levels of mitochondrial pUb S65 as a readout of PINK1 activity in response to accrued mitochondrial damage compared to GFP only control cells.

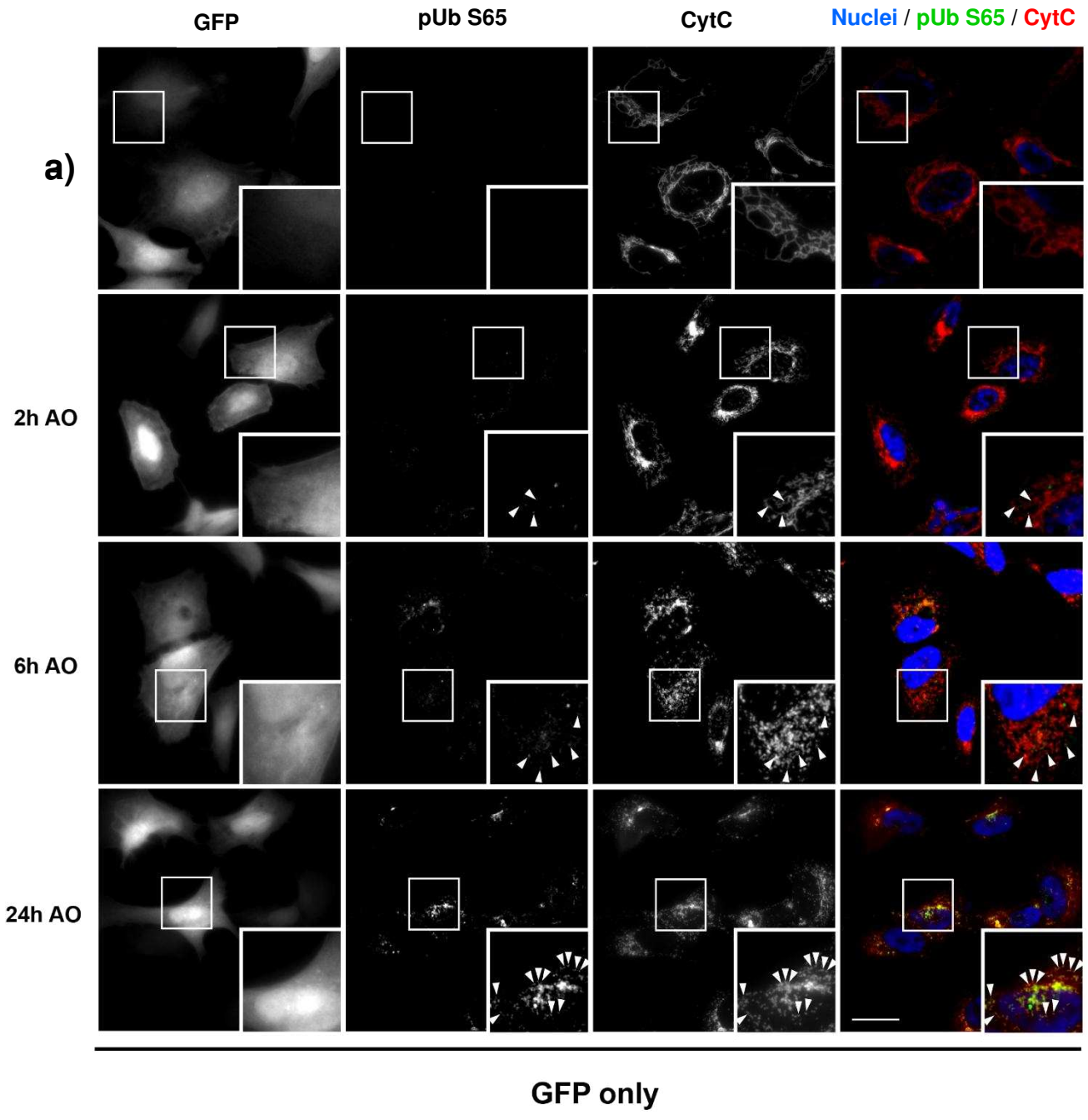

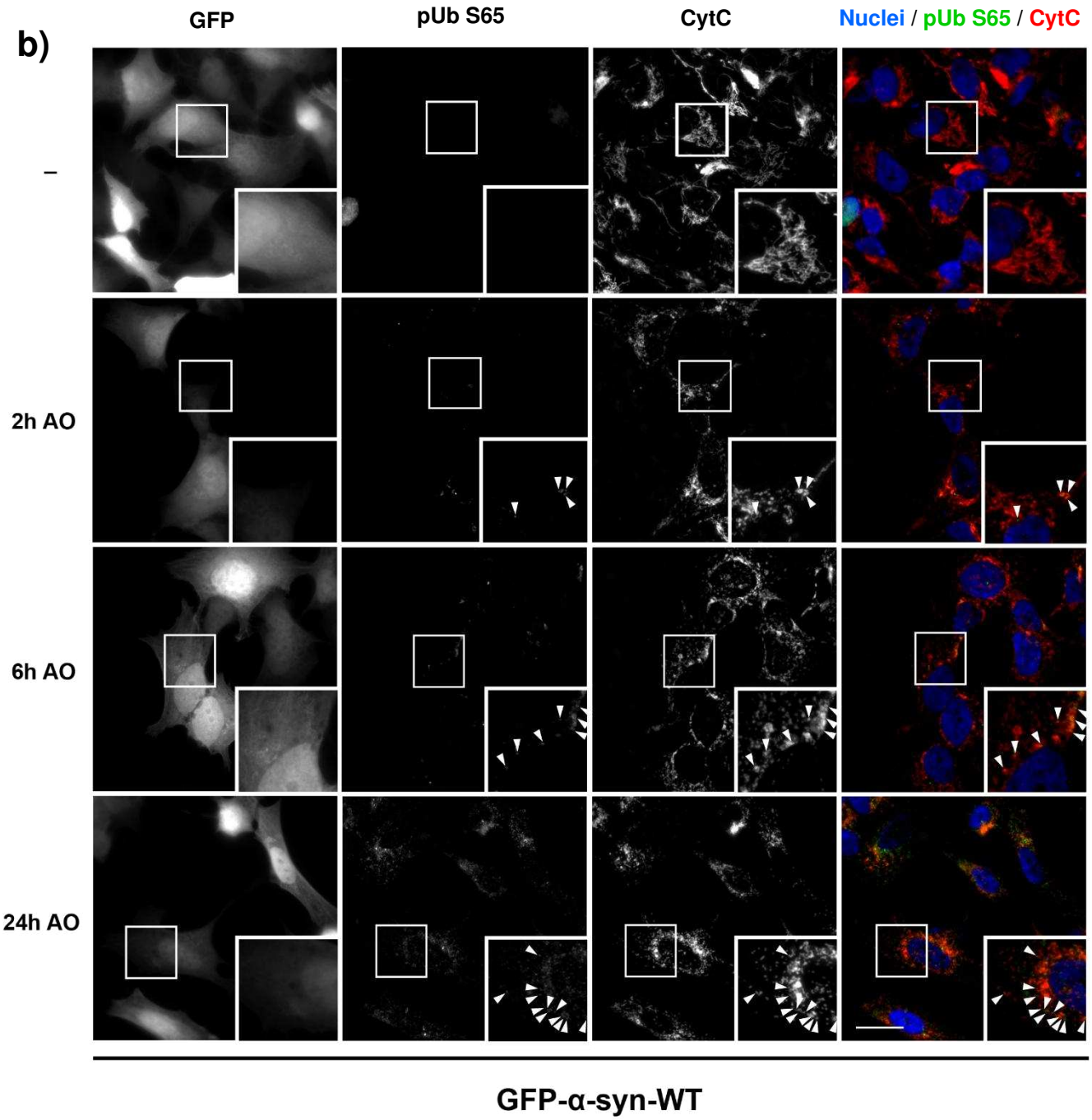
b)
GFP
pUb S65
CytC
Nuclei / pUb S65 / CytC
–
2h AO
6h AO
24h AO
GFP-α-syn-WT

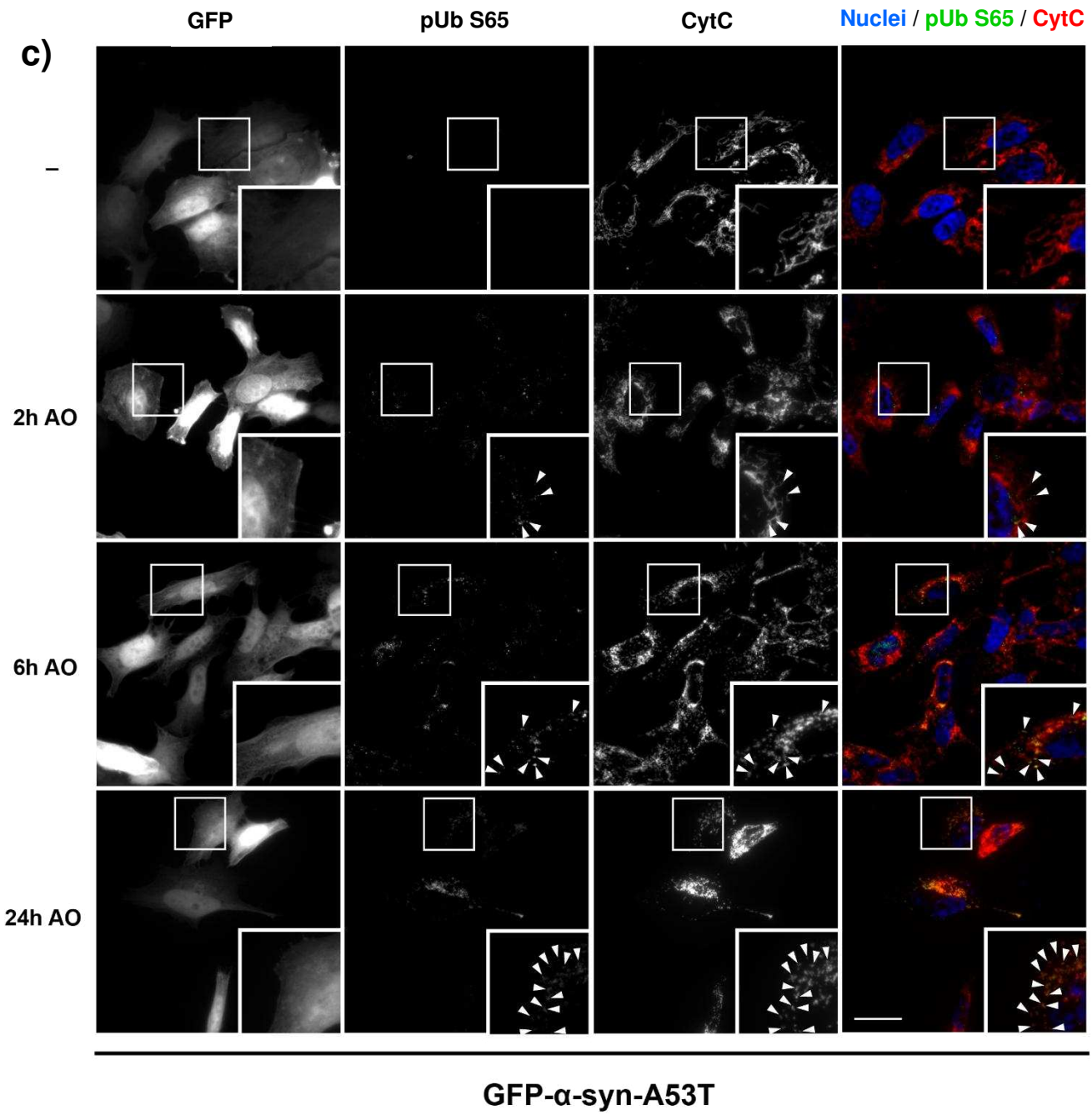

Figure 88: Cells overexpressing GFP-α-syn-WT and GFP-α-syn-A53T show increased pUb S65 levels in response to mitochondrial damage

GFP only (a), GFP-α-syn-WT (b) and GFP-α-syn-A53T (c) cells were left untreated (-) or treated for 2, 6 or 24 hours with A/O to induce mitochondrial damage. Cells were fixed and immunostained with antibodies against pUb S65 (green) and cytochrome c (red), with nuclei labelled by Hoechst (blue). GFP was imaged to allow selection of only GFP-positive cells for subsequent analysis. Colocalisation between pUb S65 and cytochrome c is reflected by yellow staining, with examples of mitochondrial pUb S65 denoted by white arrowheads. Images shown are representative and originate from 1 biological repeat. Images were taken with widefield immunofluorescence microscopy on a 100X objective. Scale bars = 20µm.

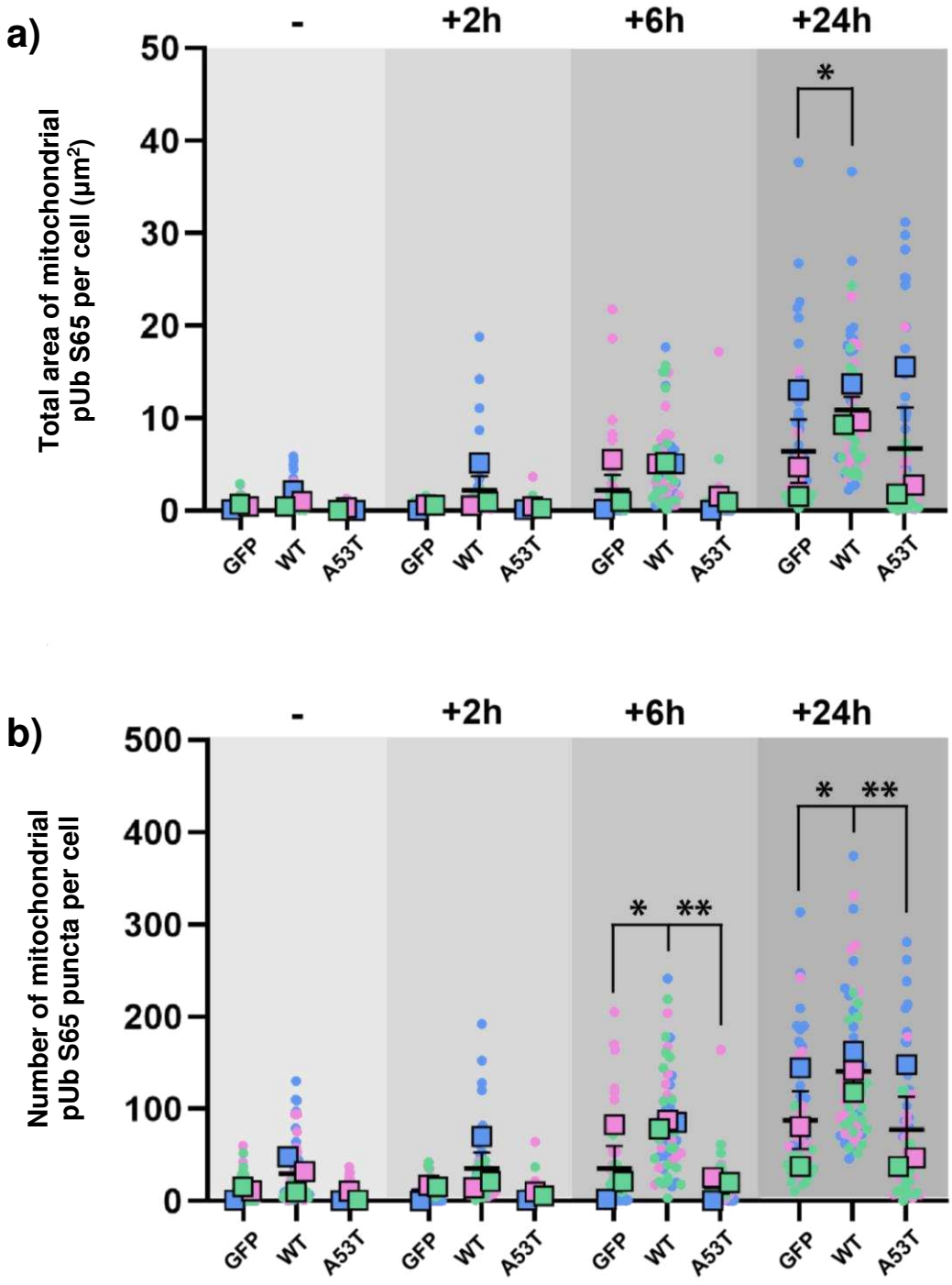
a)
-
+2h
+6h
+24h
Total area of mitochondrial pUb S65 per cell (µm²)
50
40
30
20
10
0
*
GFP
WT
A53T
b)
Number of mitochondrial pUb S65 puncta per cell
500
400
300
200
100
0
* **
* **

Figure 89: Overexpression of GFP-α-syn-WT, but not GFP-α-syn-A53T, results in increased pUb S65 levels in response to accrued mitochondrial damage compared to GFP only controls

GFP only, GFP-α-syn-WT and GFP-α-syn-A53T cells were left untreated (-) or treated for 2, 6 or 24 hours with A/O to induce mitochondrial damage. Cells were fixed and immunostained for pUb S65, cytochrome c and GFP to allow selection of only cells overexpressing GFP constructs. Colocalisation between pUb S65 and cytochrome c was ensured by only quantifying image pixels positive for both stains. The total area and number of puncta of colocalised staining were measured per cell in 20 GFP-positive cells per condition, per biological repeat. Graph a) shows the total area of mitochondrial pUb S65 per cell, and graph b) shows the number of puncta of mitochondrial pUb S65 per cell. In both graphs, biological repeats are colour coded, with measurements from each individual cell shown by a dot, with the mean of each biological repeat shown by a square and the mean of all 3 repeats shown by a black bar. SEM is shown by vertical black lines. Statistical analysis was performed by repeated measures 2-way ANOVA with Tukey's multiple comparisons test for differences *between* cell lines. GFP-α-syn-WT cells had significantly higher mitochondrial pUb S65 area than GFP only cells in response to 24 hours of A/O (p=0.0456, *). In response to 6 hours of A/O treatment, GFP-α-syn-WT cells had a significantly higher number of mitochondrial pUb S65 puncta than both GFP only (p=0.0400, *) and GFP-α-syn-A53T cells (p=0.0051, **). In response to 24 hours of A/O treatment, GFP-α-syn-WT cells had a significantly higher number of mitochondrial pUb S65 puncta than both GFP only (p=0.0243, *) and GFP-α-syn-A53T cells (p=0.0083, **). (**n=3**).

4.2.8 Overexpression of GFP-α-syn-A53T results in a reduction in LC3 lipidation

After thoroughly investigating early markers of mitophagy, I next aimed to determine whether overexpression of GFP-α-syn-WT or GFP-α-syn-A53T impacted later aspects of the pathway, starting with autophagosome formation. Several studies have suggested mechanisms by which pathogenic α-synuclein can impact autophagy, but the directionality of this impact is still contested (Sarkar et al., 2021; Tang et al., 2021; Winslow et al., 2010). The standard practice for assessing autophagy is by measuring levels of LC3II: the lipidated form of LC3 which is conjugated to PE on autophagosomal membranes (Kabeya et al., 2000). By assessing LC3II levels, research has suggested that α-synuclein overexpression can cause a reduction in autophagy (Winslow et al., 2010). However, other studies have found the opposite phenotype, with α-synuclein overexpression shown to increase levels of LC3II in cell models and the lipidation of its fly homolog, Atg8, in *Drosophila melanogaster* (Sarkar et al., 2021; Tang et al., 2021). To establish the impact of GFP-α-syn overexpression on autophagosome formation in my model, I first assessed levels of LC3II in response to mitochondrial damage (**Figure 90a**).

In GFP only cells, LC3II expression was upregulated with increasing mitochondrial damage, reflecting a higher number of autophagosomes as mitochondria are degraded by mitophagy. This increase was also seen in GFP-α-syn-WT and GFP-α-syn-A53T cells, showing that overexpression did not prevent autophagosomes from being upregulated in response to A/O. Though GFP only and GFP-α-syn-WT cells had a similar profile of LC3II expression, GFP-α-syn-A53T cells consistently expressed lower LC3II at each time point. This was most clear after 24 hours of A/O treatment, where LC3II levels were significantly lower in GFP-α-syn-A53T cells than both GFP only (p=0.0365) and GFP-α-syn-WT cells (p=0.0432) (**Figure 90b**). These data suggest that overexpression of GFP-α-syn-A53T results in lower LC3II levels and thus highlights a potential autophagosomal defect.

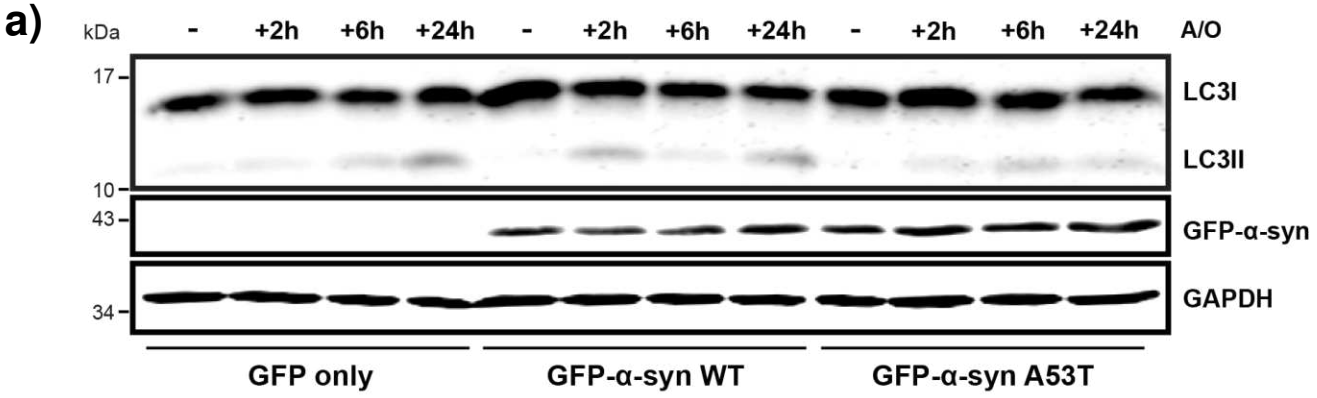

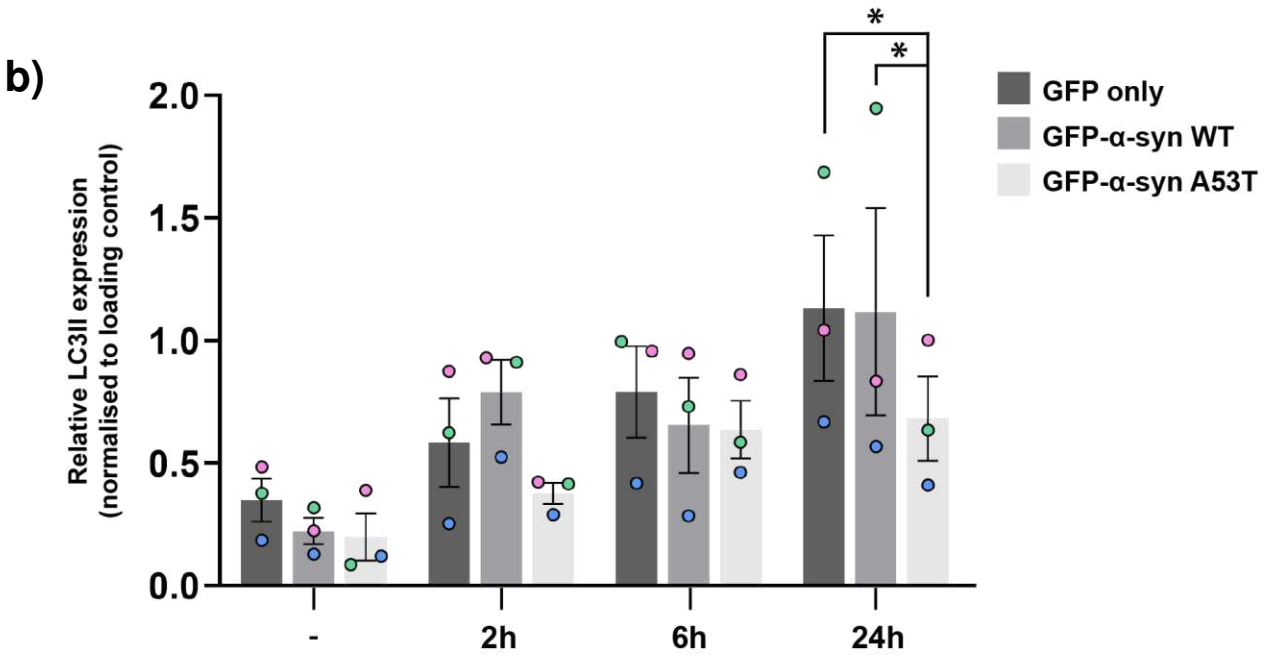

Figure 90: Overexpression of GFP-α-syn-A53T, but not GFP-α-syn-WT, results in decreased LC3II in response to accrued mitochondrial damage

a) GFP only, GFP-α-syn-WT and GFP-α-syn-A53T cells were left untreated (-) or treated for 2, 6 or 24 hours with A/O to induce mitochondrial damage. Lysates were processed by Western blot with antibodies against LC3, α-synuclein to verify overexpression of GFP-α-syn constructs and GAPDH as a protein loading control (same membrane as shown in **Figure 87**).

b) From Western blot data, LC3II expression in GFP only, GFP-α-syn-WT and GFP-α-syn-A53T cells in response to A/O was normalised to GAPDH expression to account for differences in protein loading. LC3II expression is represented by the raw values of this calculation. Biological repeats are colour coded, with circles showing the means of each repeat, bars showing the means of all 3 repeats, and black lines representing the SEM. Bars show GFP only cells in dark grey, GFP-α-syn-WT cells in medium grey and GFP-α-syn-A53T cells in light grey. Statistical analysis was performed by repeated measures 2-way ANOVA with Tukey's test for multiple comparisons. Upon 24 hours of A/O, LC3II expression was significantly lower in GFP-α-syn-A53T cells compared to both GFP only (p=0.0365, *) and GFP-α-syn-WT cells (p=0.0432, *). (**n=3**).

Given that I observed a decrease in LC3II levels in GFP-α-syn-A53T overexpressing cells with accrued mitochondrial damage that may suggest a decrease in autophagosome number, I next aimed to assess whether overexpression of GFP-α-syn resulted in any measurable changes to lysosomal features (**Figure 91**). Previous research has suggested that as well as hindering autophagosome-lysosome fusion, α-synuclein aggregates are able to directly impair lysosomal function (Mazzulli et al., 2011; Sarkar et al., 2021).

Since lysosomal function is thought to be related to morphology, I assessed physical measurements of lysosomes using LAMP1 staining to explore whether overexpression of GFP-α-syn impacted lysosomal reshaping and remodelling in response to mitochondrial damage (de Araujo et al., 2020). Firstly, the number of lysosomal puncta per cell was increased in response to A/O treatment in all cell lines compared to steady state, suggesting an upregulation in the number of lysosomes available to digest damaged cellular components (**Figure 92a**). Those overexpressing GFP-α-syn-WT, and to a lesser extent, GFP-α-syn-A53T, appeared to have a higher steady state total area of LAMP1 per cell compared to GFP only cells, though this was not significant. In response to mitochondrial damage, the total LAMP1 area was increased from untreated in both GFP only and GFP-α-syn-A53T expressing cells, but not in GFP-α-syn-WT expressing cells where the area stayed the same (**Figure 92b**).

Measurements from individual LAMP1 puncta revealed that GFP-α-syn-WT expressing cells had puncta with higher area at steady state than GFP only cells (p=0.0147), suggesting lysosomal swelling (**Figure 92c**). Interestingly, though the average area of individual LAMP1 puncta increased upon mitochondrial damage in GFP only cells, this decreased in GFP-α-syn-WT cells and remained almost the same in GFP-α-syn-A53T cells. This implies that overexpression of GFP-α-syn, especially GFP-α-syn-WT, may impact lysosomes.

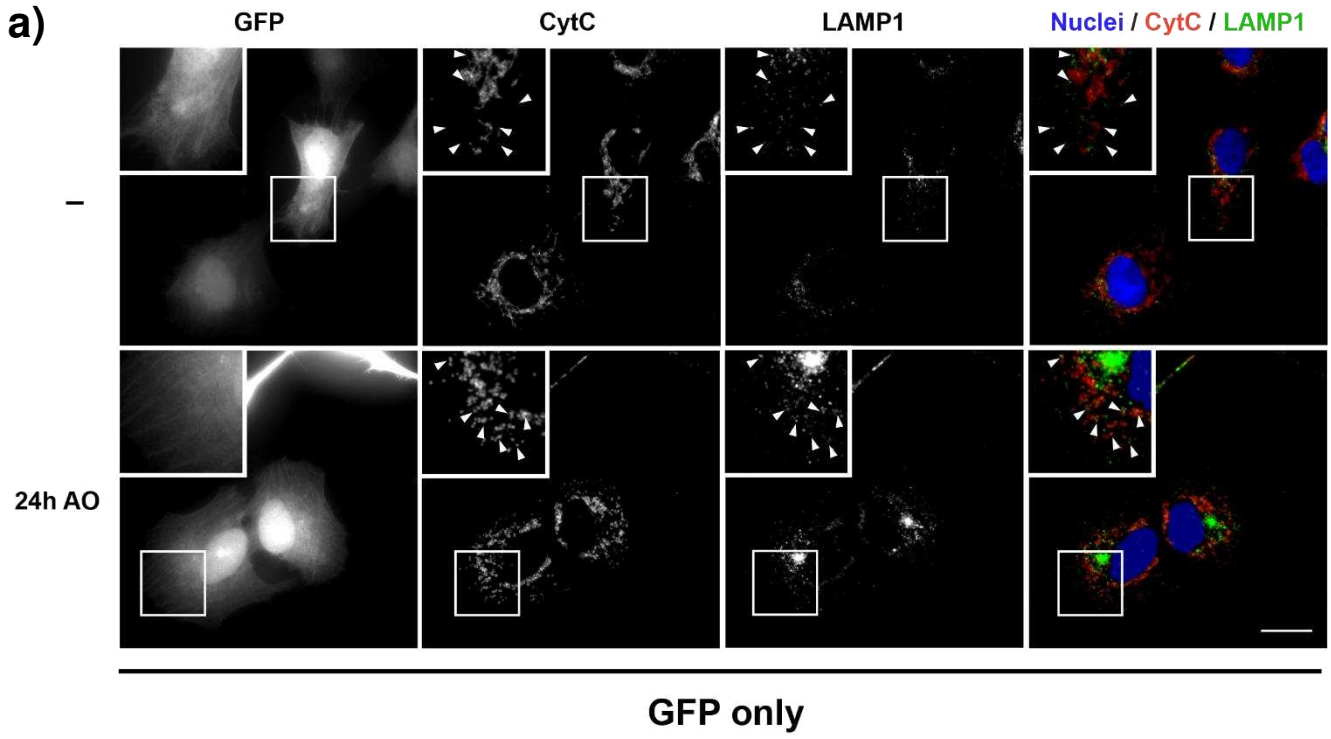

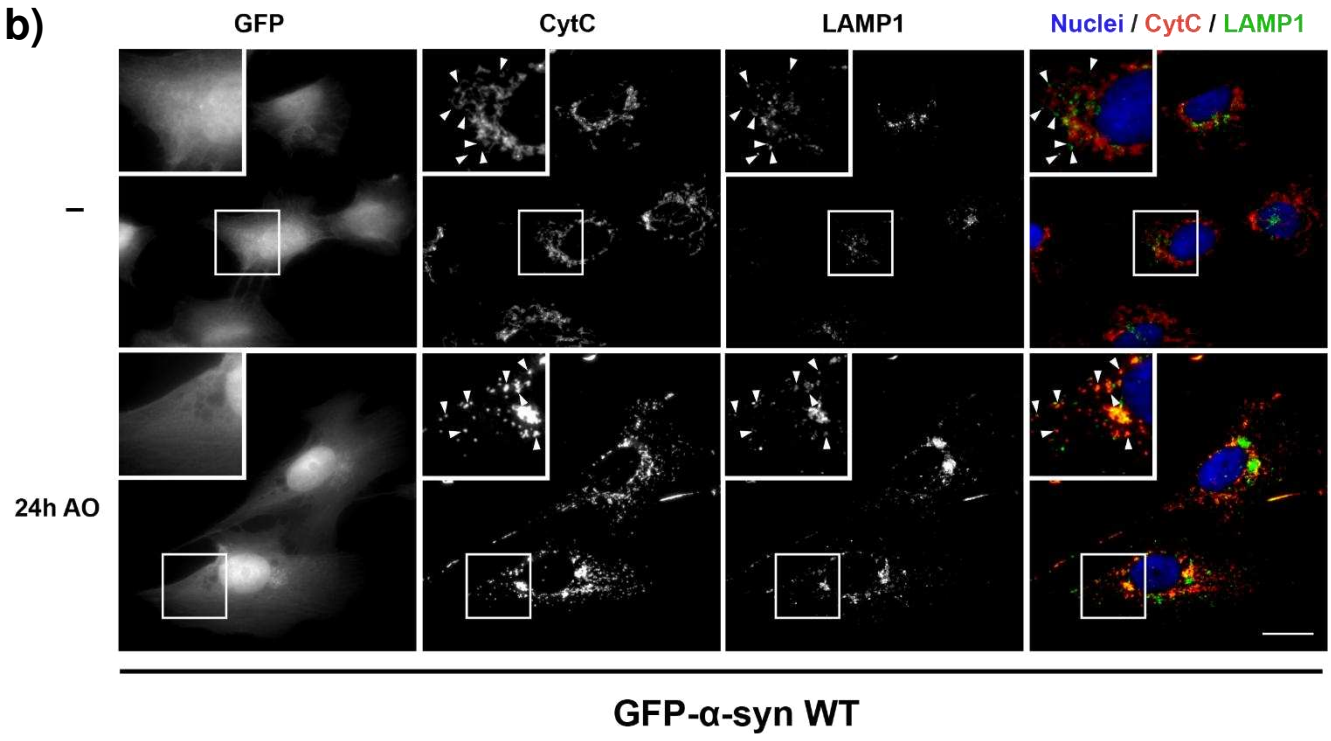

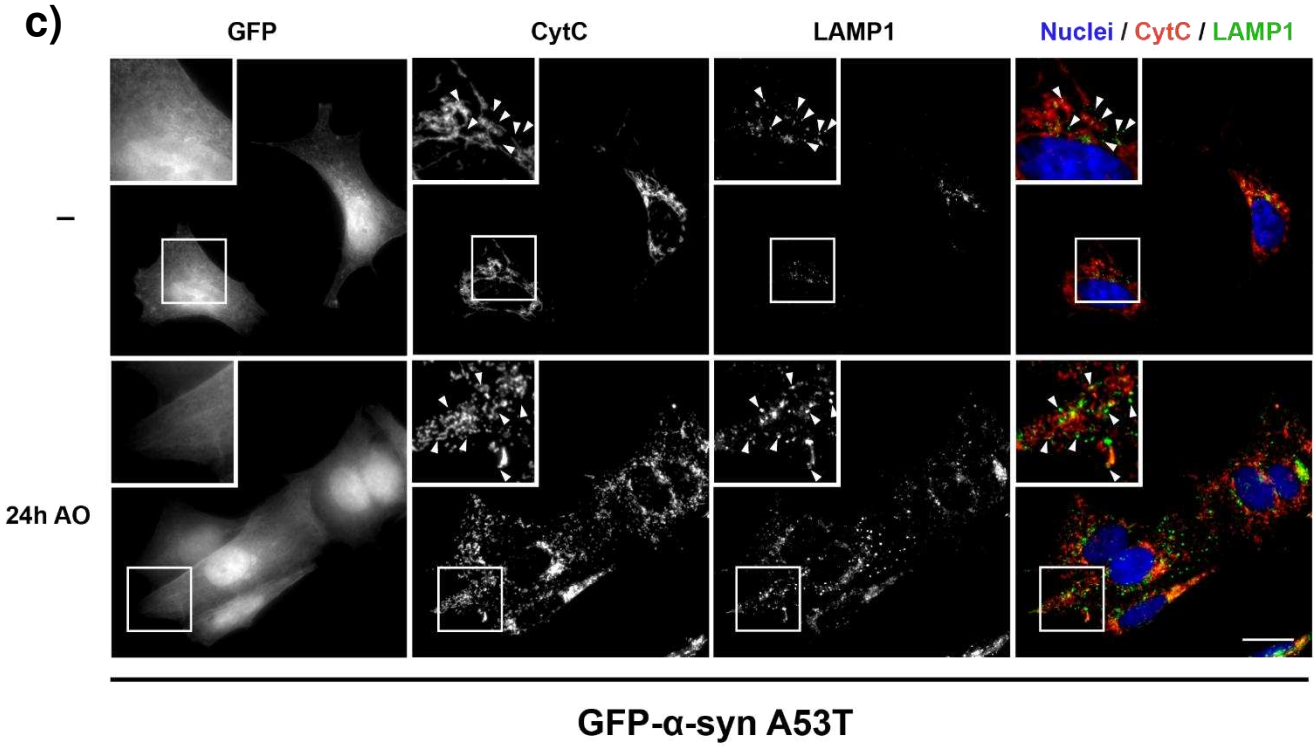

Figure 91: Overexpression of GFP-α-syn impacts readouts of lysosomal staining at steady state and in response to mitochondrial damage

GFP only (a), GFP-α-syn-WT (b) and GFP-α-syn-A53T (c) cells were left untreated (-) or treated for 2, 6 or 24 hours with A/O to induce mitochondrial damage. Cells were fixed and immunostained with antibodies against cytochrome c (red), LAMP1 (green), with nuclei labelled by Hoechst (blue). GFP was imaged to allow selection of only GFP-positive cells for subsequent analysis. Colocalisation between cytochrome c and LAMP1 is shown in yellow. White arrows point to examples of lysosomes in each cell line across the channels, enabling visualisation of lysosome size as well as colocalisation with mitochondria. Images are representative and originate from 1 biological repeat. Images were taken using widefield immunofluorescence microscopy with a 100X objective. Scale bars = 20µm.

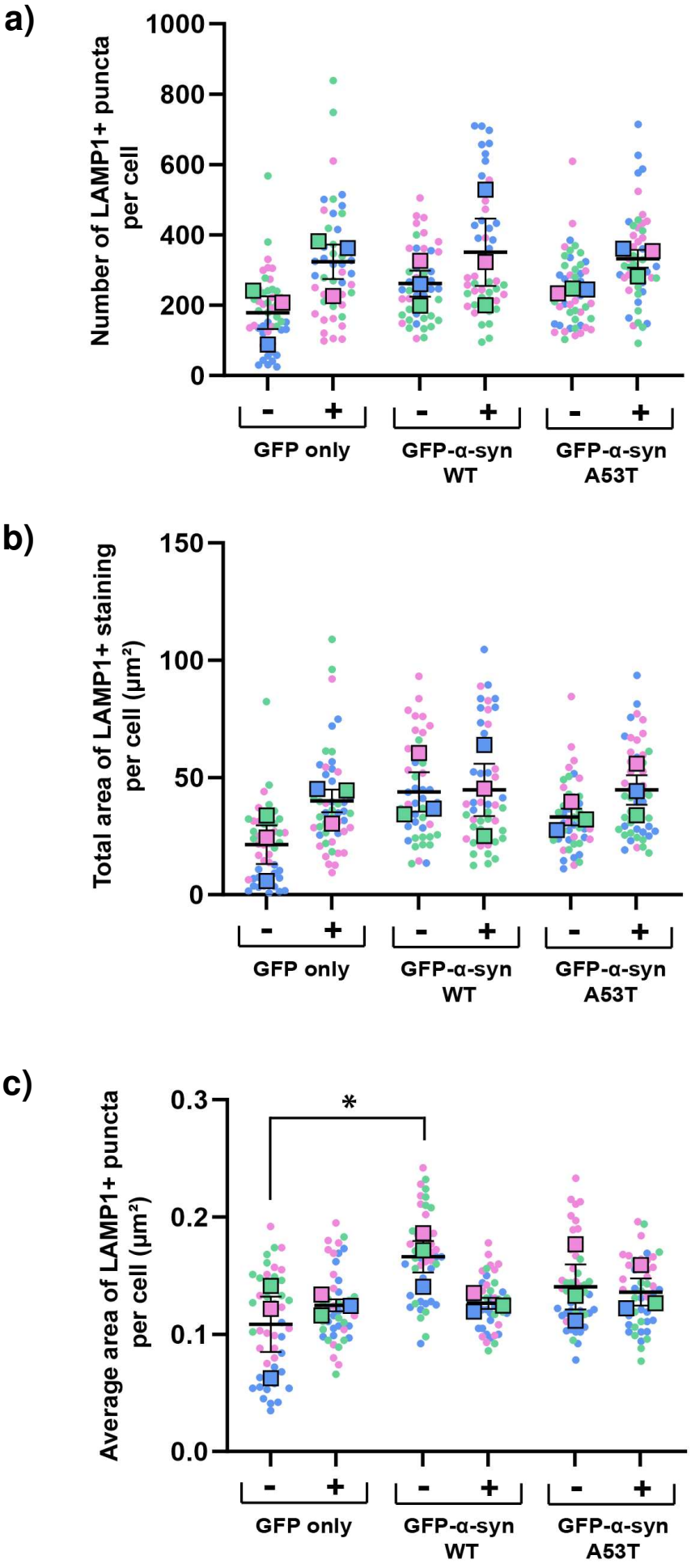
a)
Number of LAMP1+ puncta per cell
1000
800
600
400
200
0
- + - + - +
GFP only
GFP-α-syn WT
GFP-α-syn A53T
b)
Total area of LAMP1+ staining per cell (µm²)
150
100
50
0
- + - + - +
GFP only
GFP-α-syn WT
GFP-α-syn A53T
c)
Average area of LAMP1+ puncta per cell (µm²)
0.3
0.2
0.1
0.0
*
- + - + - +
GFP only
GFP-α-syn WT
GFP-α-syn A53T

Figure 92: Overexpression of GFP-α-syn alters lysosome organisation

In GFP only, GFP-α-syn-WT and GFP-α-syn-A53T cells left untreated (-) or treated with A/O for 24 hours, lysosomal morphology was analysed by isolating pixels positive for LAMP1 within individual cells. a) Indicates the number of LAMP1+ puncta per cell, measured by quantifying the number of puncta positive for LAMP1 staining in individual cells. b) Shows the total area of LAMP1+ staining per cell, measured by calculating the combined area of all LAMP1 puncta in a given cell. c) Indicates the average area of individual LAMP1+ puncta per cell, calculated by dividing the total area of LAMP1+ staining by the number of LAMP1+ puncta in the same cell. For each measure, 20 GFP-positive cells were analysed per condition, per biological repeat. Data points are colour coded by biological repeat, with measurements from each individual cell shown by a dot, the mean of each biological repeat shown by a square and the mean of all 3 repeats shown by a black bar. SEM is shown by vertical black lines. Statistical analysis was performed by repeated measures 2-way ANOVA with Tukey's test for multiple comparisons. The average area of individual LAMP1+ puncta was significantly larger in GFP-α-syn-WT cells than GFP only control cells at steady state (p=0.0147, *). (**n=3**).

To investigate the relationship between lysosomes and mitochondria, I next assessed colocalisation of the two organelles in response to mitochondrial damage. Since dysfunctional mitochondria inside autophagosomes are trafficked to the lysosome for degradation, I aimed to visualise whether this process was occurring as expected in cells overexpressing GFP-α-syn, especially due to lysosomal swelling evident at steady state in GFP-α-syn-WT expressing cells.

The percentage of all LAMP1+ puncta that colocalised with mitochondrial staining was increased in response to mitochondrial damage in all 3 cell lines, reflecting the ability of cells to traffic dysfunctional mitochondria to the lysosome as part of the damage response (**Figure 93a**). Looking at this in terms of LAMP1+ area, the same pattern was evident, with no difference in the colocalisation of mitochondria and lysosomes between the cells overexpressing GFP-α-syn and GFP only controls (**Figure 93b**).

Together these data show that despite the fact that overexpression of GFP-α-syn-WT, and to a lesser extent GFP-α-syn-A53T, appeared to alter lysosomal morphology measurements, this did not results in any alterations to damage-induced colocalisation of mitochondria with lysosomes.

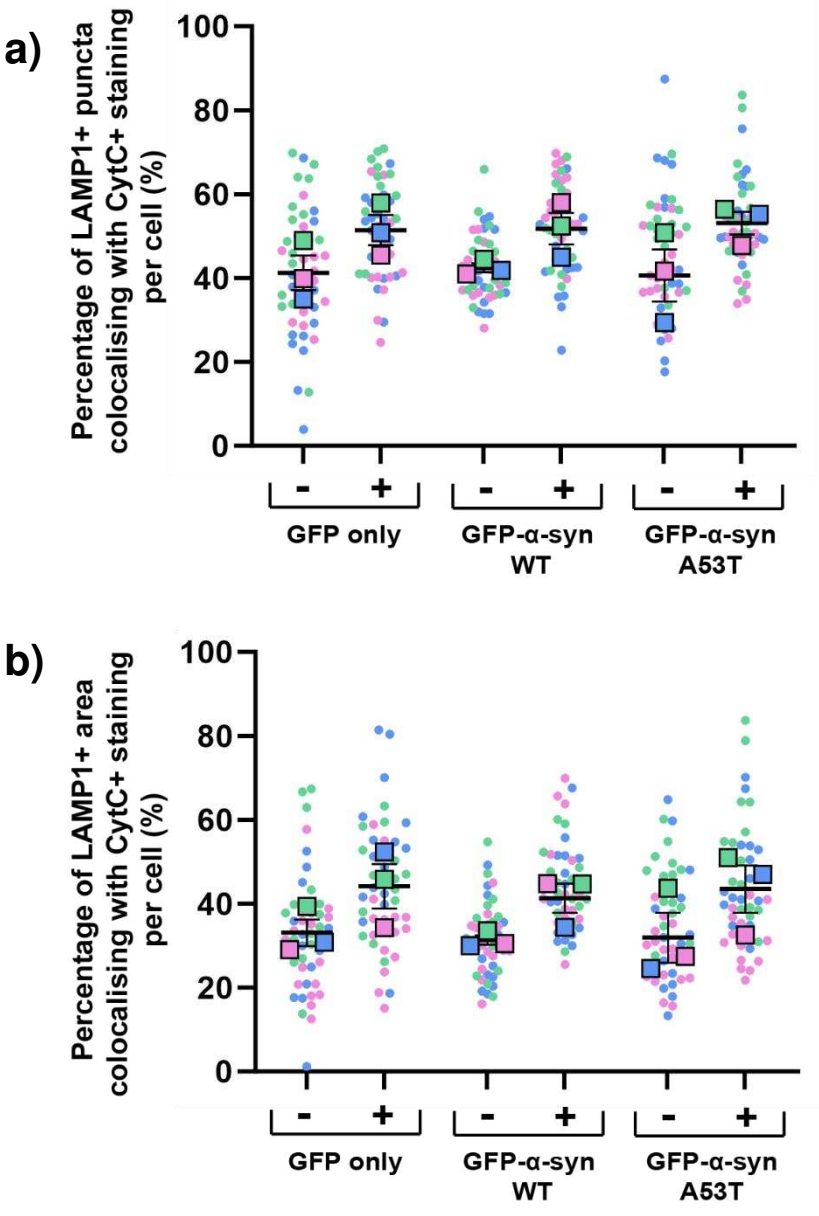
a)
Percentage of LAMP1+ puncta colocalising with CytC+ staining per cell (%)
100
80
60
40
20
0
-
+
-
+
-
+
GFP only
GFP-α-syn WT
GFP-α-syn A53T
b)
Percentage of LAMP1+ area colocalising with CytC+ staining per cell (%)
100
80
60
40
20
0
-
+
-
+
-
+
GFP only
GFP-α-syn WT
GFP-α-syn A53T

Figure 93: Overexpression of GFP-α-syn-WT and GFP-α-syn-A53T has no impact on colocalisation of lysosomes with mitochondria

GFP only, GFP-α-syn-WT and GFP-α-syn-A53T cells left untreated (-) and treated with A/O for 24 hours, the colocalisation between lysosomal and mitochondrial staining was measured. Per cell, pixels positive for both LAMP1 and cytochrome c were measured and presented as a percentage of total LAMP1+ staining (shown in Figure 31a, b). a) Shows the percentage of all LAMP1+ puncta colocalised with cytochrome c per cell, calculated by dividing the number of colocalised puncta by the total number of LAMP1+ puncta per cell. b) Shows the percentage of all LAMP1+ area colocalised with cytochrome c per cell, calculated by dividing the colocalised area by the total area of LAMP1+ per cell. For each measure, 20 GFP-positive cells were analysed per condition, per biological repeat. Data points are colour coded by biological repeat, with measurements from each individual cell shown by a dot, the mean of each biological repeat shown by a square and the mean of all 3 repeats shown by a black bar. SEM is shown by vertical black lines. Statistical analysis was performed by repeated measures 2-way ANOVA with Tukey's test for multiple comparisons but reported no significant differences. (**n=3**).

4.2.9 Overexpression of GFP-α-syn-WT and GFP-α-syn-A53T impacts both steady state and damage-induced MDVs

Finally, I aimed to investigate the impact of GFP-α-syn overexpression on a local repair pathway: MDVs. At steady state, mitochondrial contents can become damaged through exposure to reactive oxygen species produced by physiological processes such as oxidative phosphorylation (Nolfi-Donegan et al., 2020). To combat this damage and protect the rest of the organelle, dysfunctional components can be selectively isolated in MDVs and trafficked away from the mitochondrial network for degradation (Soubannier et al., 2012a; Soubannier et al., 2012b). This mechanism has been shown to be upregulated in response to oxidative stress and can turn over fully assembled mitochondrial complexes, confirming its importance in the acute mitochondrial damage response (König et al., 2021; Soubannier et al., 2012b; Sugiura et al., 2014). Current research in the field of MDV biology has not investigated a link between α-synuclein and MDVs, nor evaluated whether pathological α-synuclein can impact mito-QC through this pathway.

Interestingly, evidence describing the relationship between pathological α-synuclein and mitochondrial proteins hints at the potential for α-synuclein to impact both characterised structural subtypes of MDVs. MDVs derived from the OMM have a double membrane and are

positive for TOM20 but not PDH (Soubannier et al., 2012a; Sugiura et al., 2014). Those derived from the IMM have a single membrane and are positive for PDH but not TOM20 (Neuspiel et al., 2008; Sugiura et al., 2014). Firstly, pathological α-synuclein has been shown to preferentially bind mitochondrial membranes, suggesting that it can localise to the same membranes that MDVs are generated from (Ludtmann et al., 2018; X. Wang et al., 2019). This, alongside the finding that pS129 α-synuclein can interact with the OMM protein TOM20, suggests that α-synuclein could potentially impact these OMM-derived (TOM20+/PDH-) MDVs (Di Maio et al., 2016). Further to this, pathological α-synuclein has been shown to be mitochondrially imported and associated with the IMM in cells from PD brains, meaning that it can access the appropriate mitochondrial compartment involved in the generation of IMM-derived (PDH+/TOM20-) MDVs (Devi et al., 2008). Since α-synuclein could conceivably have a relationship with both OMM- and IMM-derived MDVs, I investigated the numbers of both structural subtypes in GFP-α-syn-WT and GFP-α-syn-A53T cells (**Figure 94**).

In terms of OMM-derived MDVs (TOM20+/PDH-), I identified that at steady state, cells overexpressing GFP-α-syn-WT had significantly more MDVs than in GFP only control cells ($p=0.0061$) (**Figure 95a**). Upon 2 hours of A/O treatment, both GFP-α-syn-WT and GFP-α-syn-A53T cells were still able to increase OMM-derived MDVs in response to damage but to a lesser extent than GFP only cells. These data suggest that overexpression of GFP-α-syn reduces the damage-induced upregulation of OMM-derived MDVs. Interestingly, GFP-α-syn-A53T cells had significantly lower MDVs than GFP-α-syn-WT cells in response to A/O ($p=0.0097$).

There were no differences between the numbers of IMM-derived MDVs (PDH+/TOM20-) at steady state between the cell lines, but differences were observed in response to mitochondrial damage (**Figure 95b**). In GFP only cells, 2 hours of A/O treatment evoked a significant increase in IMM-derived MDVs ($p=0.0481$), but the same level of response was not observed in GFP-α-syn-WT or GFP-α-syn-A53T cells. MDVs were only subtly, not significantly, increased upon damage in these cells, suggesting a potential defect in damage-induced IMM-derived MDV formation. Further to this, GFP-α-syn-A53T cells exhibited significantly less MDVs than GFP only cells in response to damage ($p=0.0450$).

Together, these data indicate that overexpression of GFP-α-syn can impact both structural subtypes of MDVs. GFP-α-syn increased OMM-derived MDVs (TOM20+/PDH-) at steady state and decreased IMM-derived MDVs (PDH+/TOM20-) in response to damage. This suggests that pathological α-synuclein can cause dysfunction in these MDV pathways.

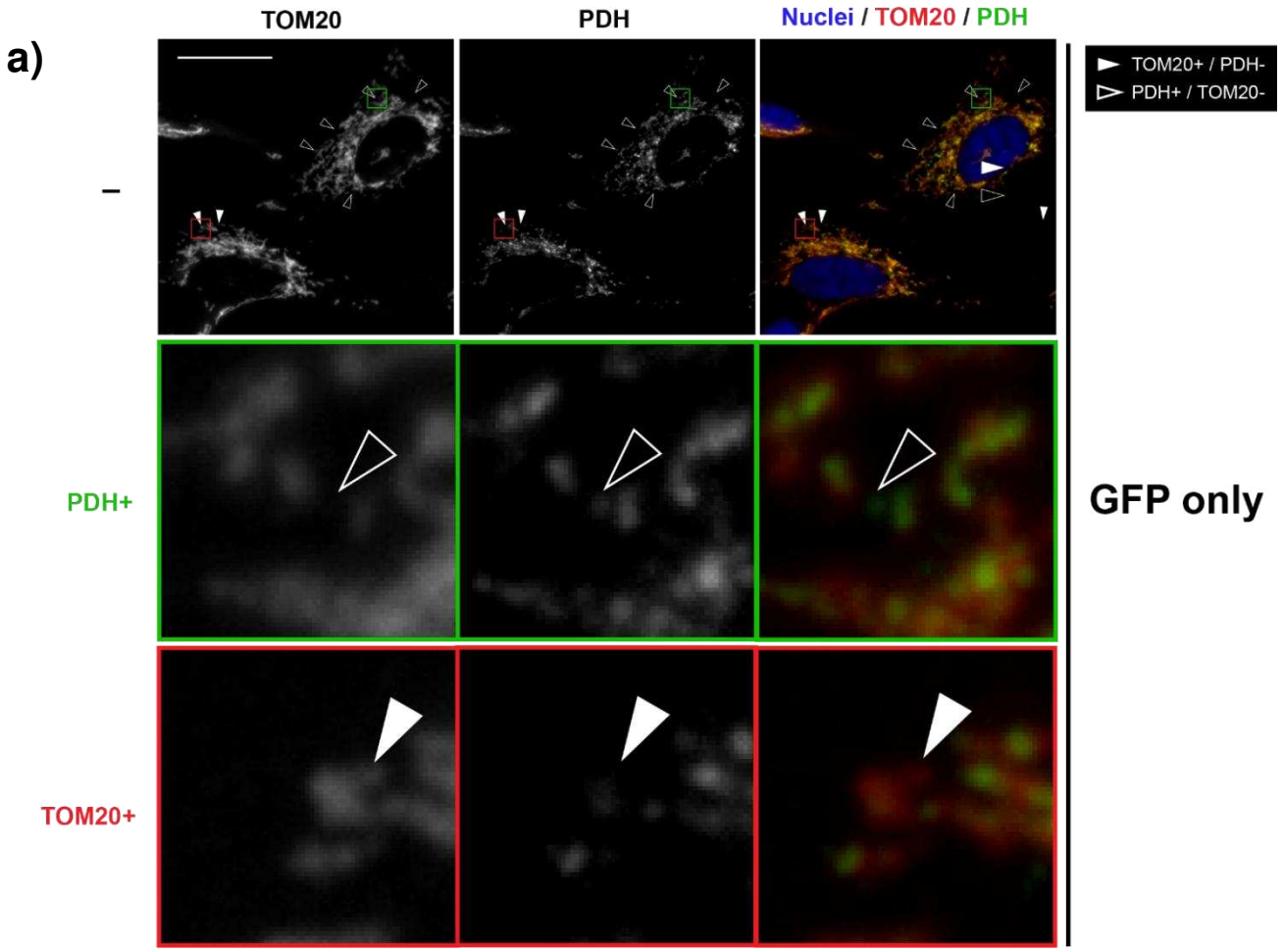
a)
TOM20
PDH
Nuclei / TOM20 / PDH
TOM20+ / PDH-
PDH+ / TOM20-
–
PDH+
GFP only
TOM20+

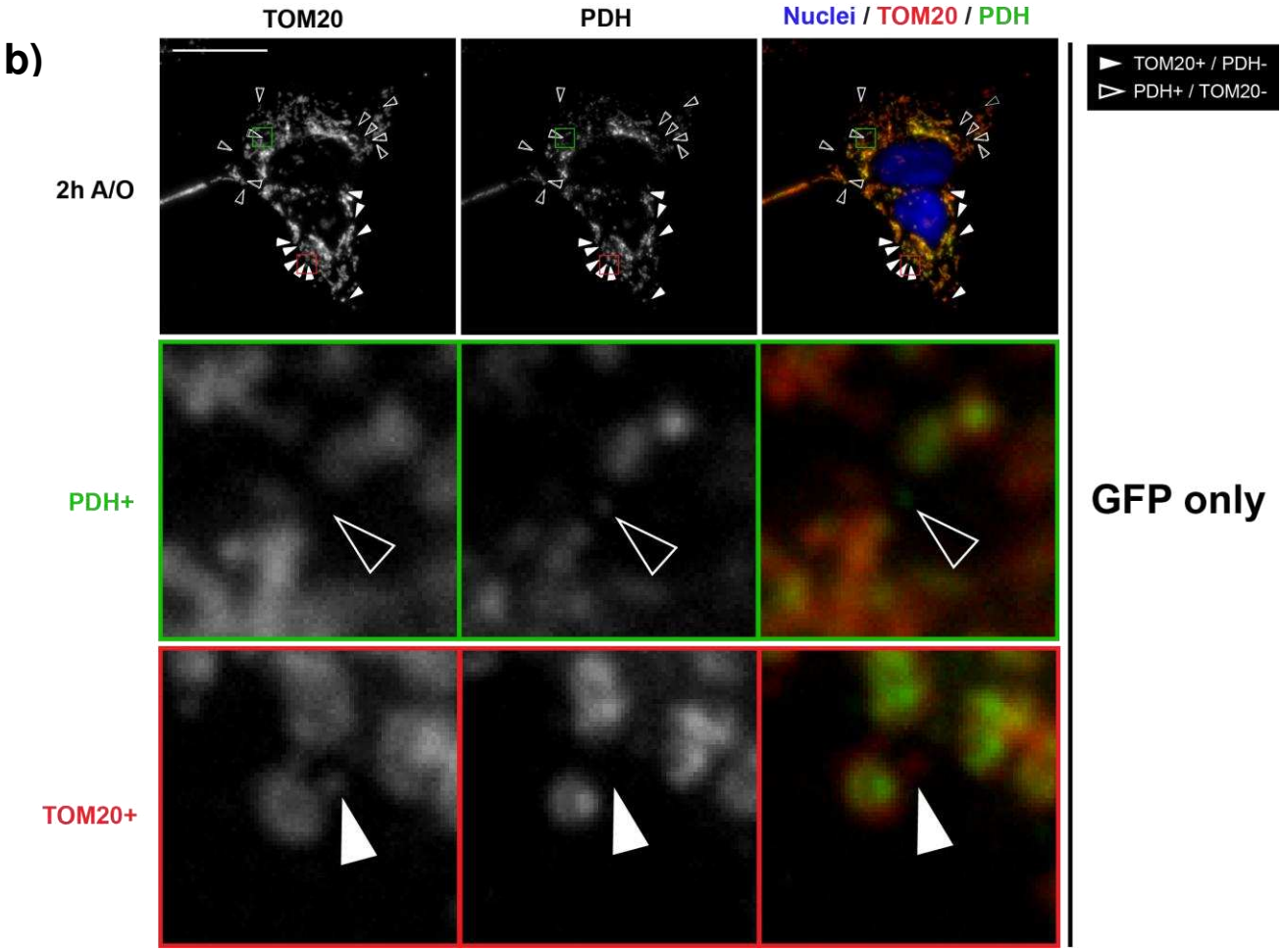
b)
TOM20
PDH
Nuclei / TOM20 / PDH
TOM20+ / PDH-
PDH+ / TOM20-
2h A/O
PDH+
GFP only
TOM20+

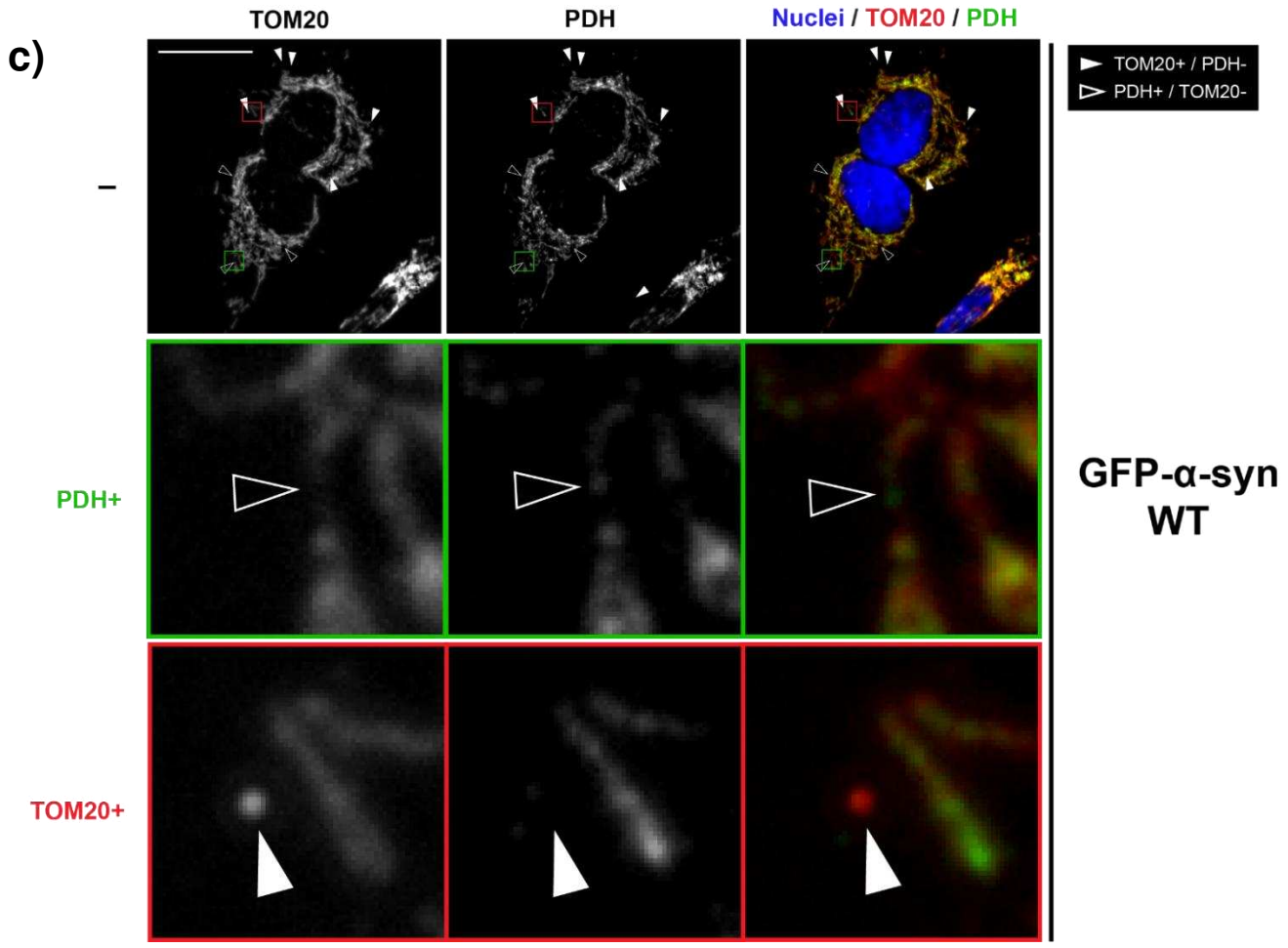
c)
TOM20
PDH
Nuclei / TOM20 / PDH
TOM20+ / PDH-
PDH+ / TOM20-
–
PDH+
TOM20+
GFP-α-syn
WT

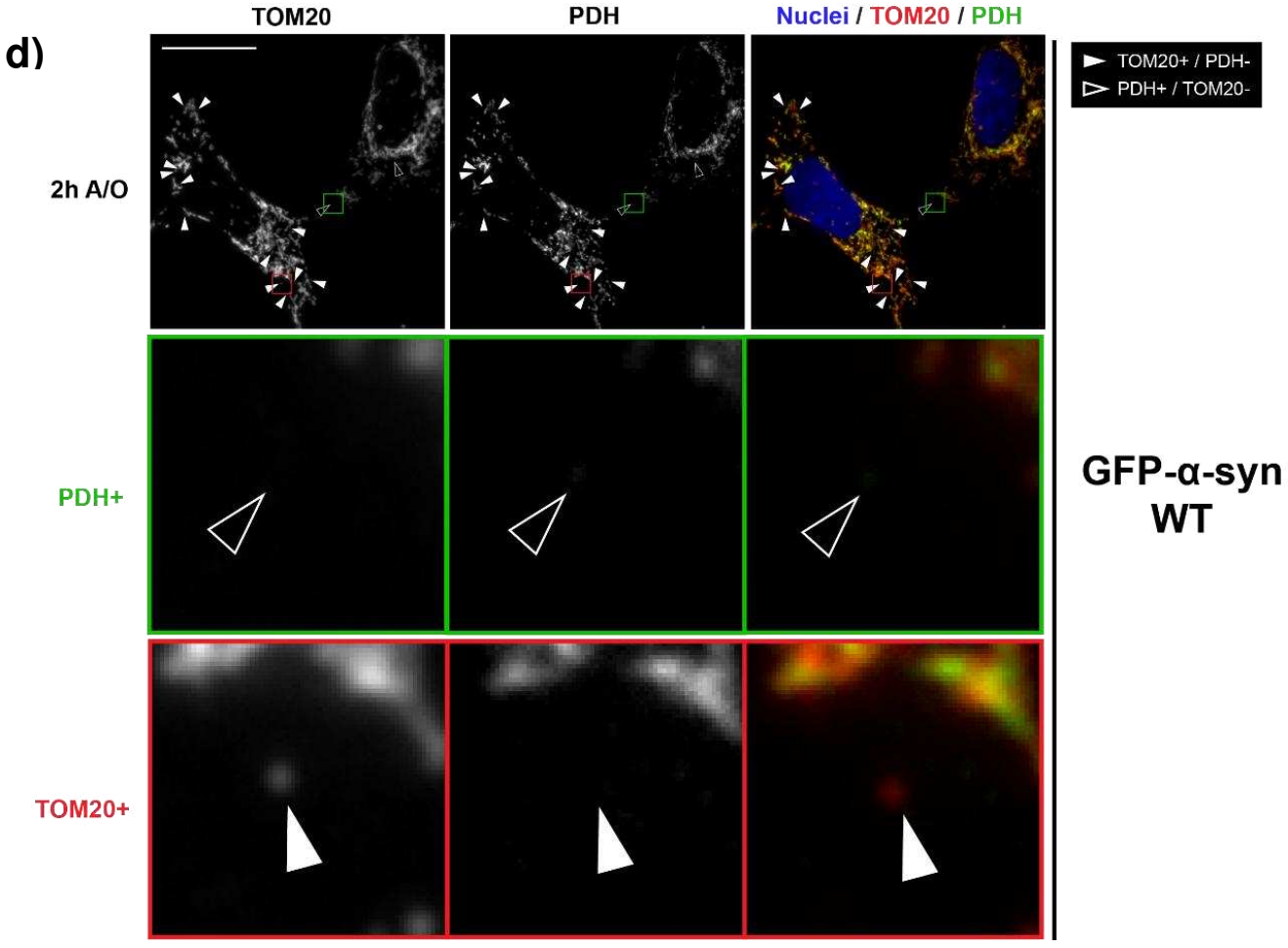
d)
TOM20
PDH
Nuclei / TOM20 / PDH
TOM20+ / PDH-
PDH+ / TOM20-
2h A/O
PDH+
TOM20+
GFP-α-syn
WT

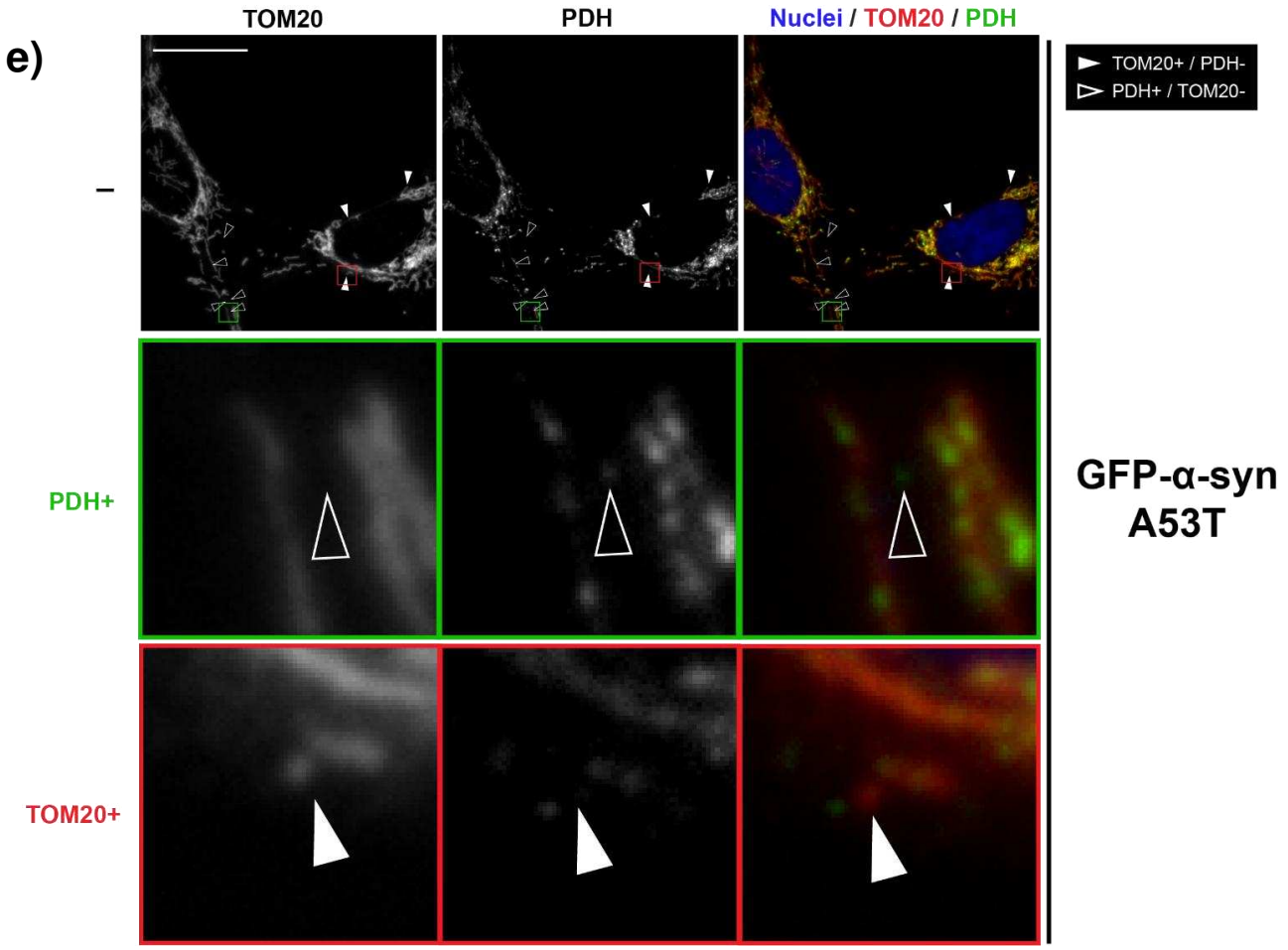
e)
TOM20
PDH
Nuclei / TOM20 / PDH
TOM20+ / PDH-
PDH+ / TOM20-
–
PDH+
TOM20+
GFP-α-syn
A53T

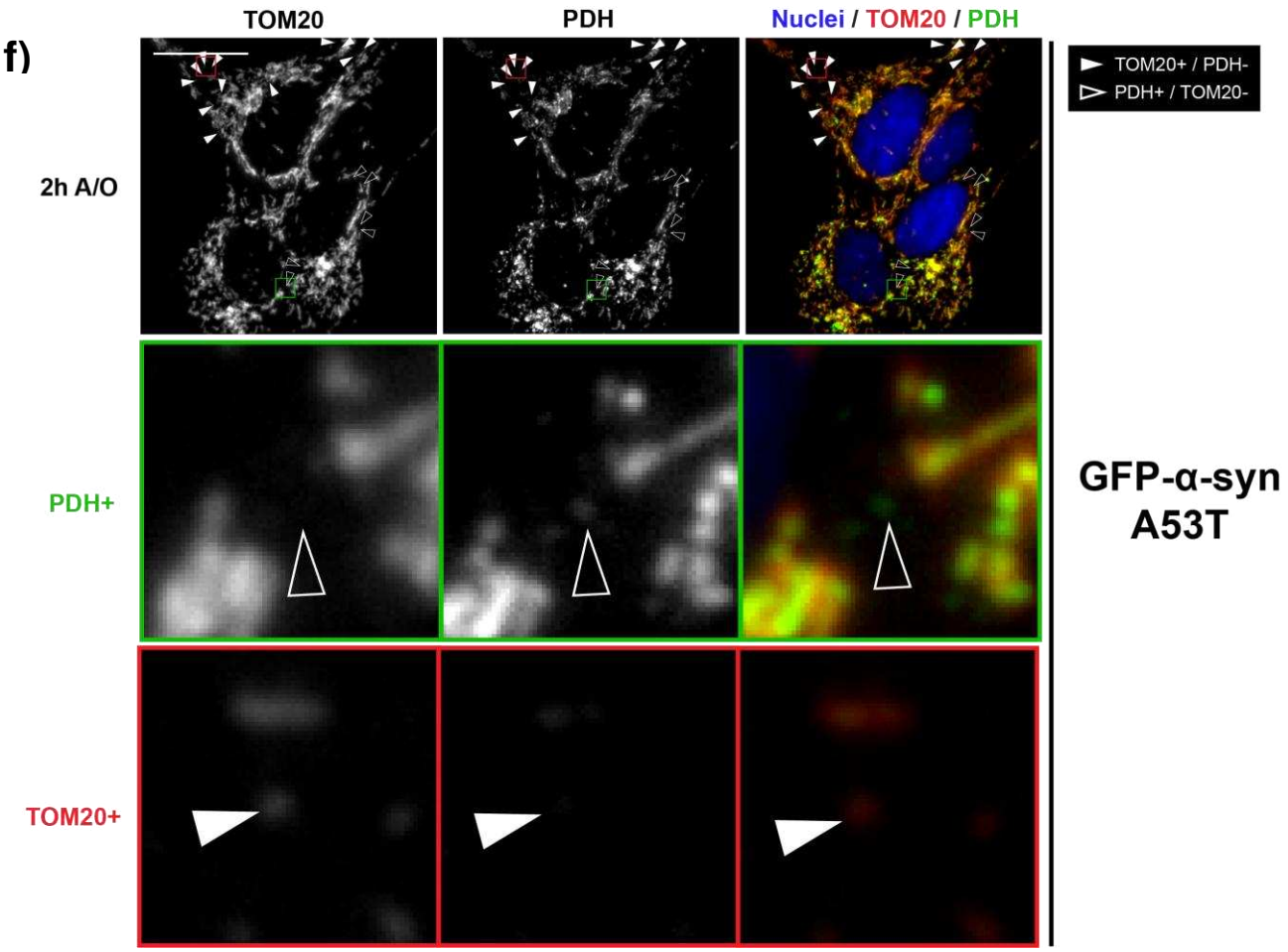
f)
TOM20
PDH
Nuclei / TOM20 / PDH
TOM20+ / PDH-
PDH+ / TOM20-
2h A/O
PDH+
TOM20+
GFP-α-syn
A53T

Figure 94: Cells overexpressing GFP-α-syn-WT and GFP-α-syn-A53T can upregulate OMM-derived, but not IMM-derived, MDVs in response to mitochondrial damage

GFP only (a, b), GFP-α-syn-WT (c, d) and GFP-α-syn-A53T (e, f) cells were left untreated (-) or treated for 2 hours with A/O to induce mitochondrial damage. Cells were fixed and immunostained with antibodies against TOM20 (red) and PDH (green) with nuclei labelled by Hoechst (blue). GFP was imaged to allow selection of only GFP-positive cells for subsequent analysis, shown in **Appendix B** (**Figure 127**). PDH+/TOM20- MDVs were defined as PDH+ puncta that did not colocalise with TOM20 – these are shown with outlines of white arrowheads, with images in green showing an example of the inclusion of PDH and exclusion of TOM20 in more detail. TOM20+/PDH- MDVs were defined as TOM20+ puncta that did not colocalise with PDH – these are shown with solid white arrowheads, with images in red showing an example of the inclusion of TOM20 and exclusion of PDH in more detail. Images shown are representative and were taken using widefield immunofluorescence microscopy on a 100X objective. Scale bars = 20µm.

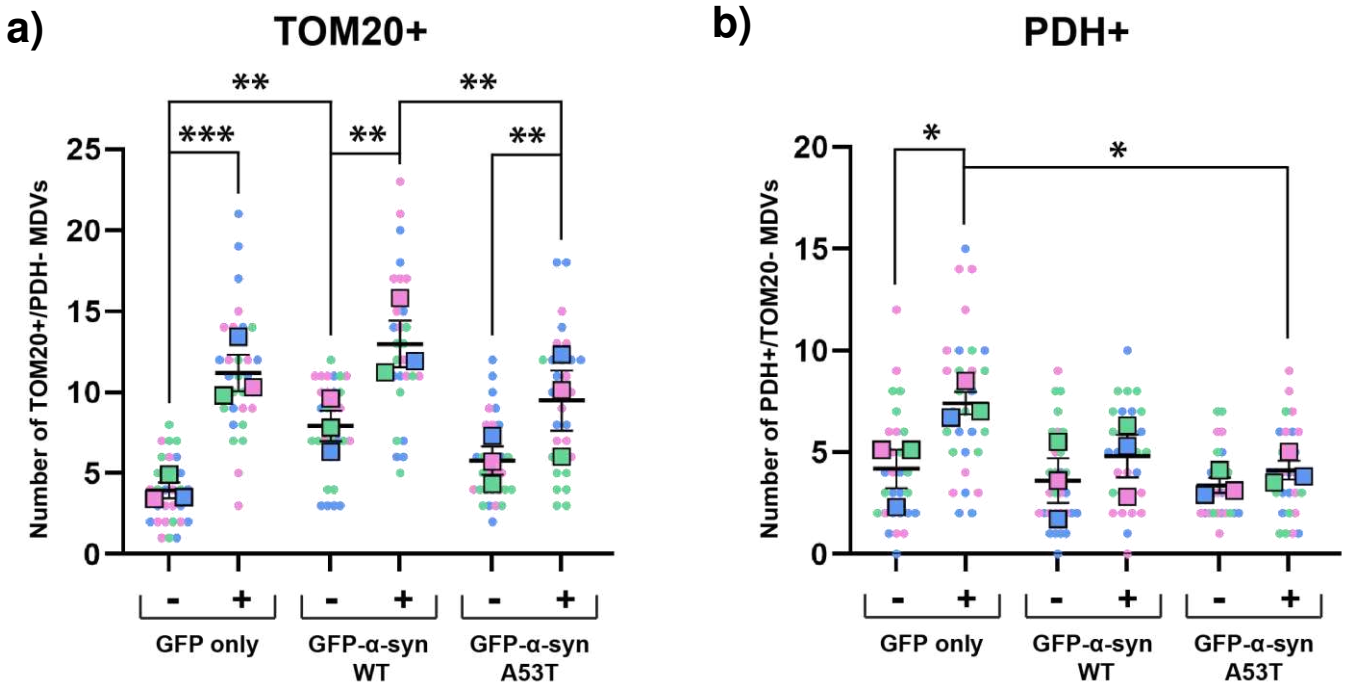

Figure 95: Overexpression of GFP-α-syn-WT and GFP-α-syn-A53T impacts OMM- and IMM-derived MDVs in response to mitochondrial damage

GFP only, GFP-α-syn-WT and GFP-α-syn-A53T cells were left untreated (-) or treated for 2 hours with A/O to evoke mitochondrial damage. MDVs were counted based on lack of colocalisation of mitochondrial markers TOM20 and PDH. a) Indicates the number of TOM20+/PDH- MDVs, while b) shows the number of PDH+/TOM20- MDVs. 10 cells were analysed per condition, per biological repeat. Measurements from each individual are shown by a dot, with the mean of each biological repeat shown by a square and the mean of all 3 repeats shown by a black bar. SEM is shown by vertical black lines. Data points are colour coded by biological repeat. Statistical analysis performed by repeated measures 2-way ANOVA with Sídák's multiple comparisons test. In terms of OMM-derived MDVs, all 3 cell lines were able to significantly upregulate the number of TOM20+/PDH- MDVs in response to mitochondrial damage (GFP only p=0.0006, ***; GFP-α-syn-WT p=0.0024, **; GFP-α-syn-A53T p=0.0079, **). In untreated cells, those overexpressing GFP-α-syn-WT cells had significantly higher TOM20+/PDH- MDVs (p=0.0061, **) than GFP only cells. In 2-hour A/O treated cells, those overexpressing GFP-α-syn-A53T had significantly lower TOM20+/PDH- MDVs (p=0.0097, **) than GFP-α-syn-WT cells. In terms of IMM-derived MDVs, GFP only cells were the only cell line able to significantly upregulate PDH+/TOM20- MDVs (p=0.0481, *) in response to mitochondrial damage. In 2-hour A/O treated cells, those overexpressing GFP-α-syn-A53T had significantly lower PDH+/TOM20- MDVs (p=0.0450, *) than GFP only cells. (**n=3**).

4.3 Discussion

In this chapter, I aimed to investigate the impact of α-synuclein gain-of-function resulting from pathogenic overexpression on mitochondrial health. Though both α-synuclein aggregation and mitochondrial dysfunction are both well-characterised as key drivers of PD pathology, limited research has investigated the relationship between the two (Eldeeb et al., 2022; Henderson et al., 2019). In particular, there is a gap in the literature in understanding how α-synuclein pathology may impact mitochondrial function through perturbation of mitochondrial dynamics and quality control (Thorne & Tumbarello, 2022). I utilised GFP-α-syn-WT and GFP-α-syn-A53T overexpression models in SH-SY5Y cells to investigate the impact of pathological α-synuclein on mito-QC. The results from this chapter indicate that though overexpression of α-synuclein does not alter mitochondrial function or damage-induced whole mitochondrial clearance, it has impacts on numbers of autophagosomes in response to accumulated damage and increases steady state lysosomal size. In addition, I show that α-synuclein overexpression affects the levels of both OMM- and IMM-derived MDVs.

In the field of PD research, a range of tools are used to incite α-synuclein pathology. One method is to induce stable overexpression of α-synuclein, which has been shown to cause nigrostriatal neurodegeneration, dopaminergic dysfunction and motor impairments in animal models (Giasson et al., 2002; Kirik et al., 2002; Lo Bianco et al., 2002; Masliah et al., 2000). Providing an environment where α-synuclein concentration and aggregation propensity is high, overexpression encourages de-novo formation of α-synuclein oligomers (Narhi et al., 1999). In SH-SY5Y cells in particular, α-synuclein overexpression induces aggregated species, visible as α-synuclein-rich cytoplasmic inclusions by immunofluorescence microscopy and positive for the amyloid fibril reporter, thioflavin T (ThT) (Melnikova et al., 2020; Melo et al., 2018; Wördehoff & Hoyer, 2018). In the GFP-α-syn-WT and GFP-α-syn-A53T overexpressing cells developed in my study, I observed a predominant cytoplasmic pool of protein with a subpopulation of α-synuclein-positive puncta, suggesting the presence of potential α-synuclein aggregates. Though I could not verify these as aggregated species using a ThT assay because of overlaps in the emission spectra of GFP and ThT, the puncta I observed bore resemblance to those described by previous studies where aggregates were ThT-positive, cultivating trust in the pathogenic potential of my model (Melnikova et al., 2020; Melo et al., 2018). To further validate pathogenic phenotypes as a result of α-synuclein overexpression, I assessed expression of pS129-modified α-synuclein. Found at high levels in LBs in PD brains, pS129 α-synuclein is considered a biomarker for pathological, aggregated α-synuclein species (Anderson et al., 2006; Fujiwara et al., 2002). In cells overexpressing GFP-α-syn-WT or GFP-α-syn-A53T, I observed expression of

pS129 α-synuclein both biochemically and by immunofluorescence microscopy, which was not present in GFP only control cells, indicative of pathological α-synuclein species. Together, the presence of cytoplasmic α-synuclein-positive inclusions and the expression of pS129 α-synuclein exclusively in GFP-α-syn overexpressing cells led me to conclude that overexpression of α-synuclein did induce pathogenic phenotypes associated with a toxic gain-of-function. Though it can be debated that use of other tools to generate α-synuclein pathology such as the addition of exogenous PFFs or oligomers creates a more exaggerated pathogenic phenotype, I argue that overexpression offers a more physiologically relevant model that enables the impact of organic α-synuclein aggregation to be investigated (Chmielarz & Domanskyi, 2021).

Research has demonstrated that oxidative stress can exacerbate α-synuclein toxicity by promoting its aggregation and inducing PTMs, so I next sought to uncover whether this was apparent in the context of α-synuclein overexpression (Won et al., 2022; Xiang et al., 2013). In line with previous data, I observed that increasing exposure to A/O amplified the appearance of α-synuclein-positive puncta and levels of pS129 α-synuclein, indicating that α-synuclein pathology was augmented by mitochondrial damage. Since aggregated α-synuclein has been shown by others to preferentially bind mitochondrial membranes, I considered that this phenotype may be the result of a direct association between α-synuclein and mitochondria (Choubey et al., 2011; Devi et al., 2008; W. Liu et al., 2009; X. Wang et al., 2019). However, I was unable to visualise selective localisation of α-synuclein to mitochondria by immunofluorescence microscopy. This could be as a result of antibody limitations, since assessing pS129 α-synuclein only enabled me to observe localisation of a specific pool of modified α-synuclein. In addition, since staining predominantly diffuse, saponin was used to clear out the cytoplasm which further reduced the pool of α-synuclein able to be visualised. When localisation was further investigated biochemically, isolated mitochondria from GFP-α-syn-A53T, but not GFP-α-syn-WT, cells exhibited an enrichment of GFP-α-syn that was not altered by mitochondrial damage. This allowed me to make several inferences about the relationship between α-synuclein and mitochondria.

Firstly, though both GFP-α-syn-WT and GFP-α-syn-A53T overexpressing cells had similar pathogenic phenotypes in terms of number of GFP inclusions and levels of pS129 α-synuclein, only GFP-α-syn-A53T cells showed mitochondrial enrichment of GFP-α-syn. This indicates that the A53T form of α-synuclein may have a different relationship with mitochondria than the wild-type protein. Recent work has suggested that the conversion of α-synuclein into aggregated species occurs at mitochondrial membranes specifically for α-synuclein A53T, which could

explain why only the mutant α-synuclein exhibits mitochondrial enrichment in my study (M. L. Choi et al., 2022). In further agreement with this finding, several studies describing an association between α-synuclein and mitochondria have only done so in the context of α-synuclein A53T (Chen et al., 2015; Choubey et al., 2011; Melo et al., 2017; Wang et al., 2019). Secondly, the exacerbation of α-synuclein pathology in response to mitochondrial damage did not appear to be the result of a direct association with mitochondria since mitochondrial enrichment of GFP-α-syn-A53T was not increased in response to A/O. I suggest that the increase in cellular pS129 α-synuclein and α-synuclein-positive cytoplasmic puncta in both GFP-α-syn-WT and GFP-α-syn-A53T overexpressing cells may have been due to the same mechanism: direct modification of α-synuclein by A/O-induced mitochondrial ROS that entered the cytoplasm (Tafani et al., 2016; Won et al., 2022).

After generating and validating α-synuclein gain-of-function models in SH-SY5Y cells, I investigated the impact that α-synuclein overexpression had on mitochondrial function through assessing ATP levels, oxygen consumption and baseline ΔΨm. I found that overexpression of GFP-α-syn-WT or GFP-α-syn-A53T did not significantly alter any of these measurable readouts of mitochondrial function. This was surprising, since other studies have reported that pathological α-synuclein models display reductions in mitochondrial respiration (Ludtmann et al., 2018; Wang et al., 2019). However, both described direct interactions between α-synuclein and mitochondria, including the binding of α-synuclein oligomers to ATP synthase (Ludtmann et al., 2018; Wang et al., 2019). As such, it could be that direct mitochondrial localisation of α-synuclein is required to impact ATP production, which I was unable to observe in my models. It is important to note that these studies both utilised exogenous addition of aggregated α-synuclein species rather than an overexpression model, suggesting that α-synuclein's impact on mitochondrial respiration may be dependent on the presence of high levels of aggregates. An alternative explanation could be that α-synuclein overexpression did influence ATP levels, but this was compensated by the presence of more mitochondria. Measurement of CoxII expression alongside the ATP assay revealed that GFP-α-syn-WT and GFP-α-syn-A53T overexpressing cells exhibited increased mitochondrial load compared to GFP only controls. This led me to consider that these cells may have upregulated their mitochondrial content as an adaptation to account for mitochondrial dysfunction induced by α-synuclein overexpression.

Next, I explored whether α-synuclein overexpression influences mitochondrial dynamics through assessment of mitochondrial morphology and network connectivity. In agreement with previous literature, I report that overexpression of α-synuclein results in significantly increased

fragmentation of the mitochondrial network at steady state (Furlong et al., 2020; Kamp et al., 2010; Krzystek et al., 2021; K. Nakamura et al., 2011). The mechanism behind this mitochondrial phenotype is debated, with suggestions that α-synuclein induces either an increase in mitochondrial fission or a decrease in mitochondrial fusion (Furlong et al., 2020; Krzystek et al., 2021; K. Nakamura et al., 2011). For example, Krzystek et al (2021) proposed that α-synuclein induces mitochondrial fragmentation through alteration in activity of the fission regulator Drp1, since downregulation of this protein rescued the phenotype. Conversely, other studies have reported that α-synuclein does not interact with fission/fusion machinery but instead impacts mitochondrial dynamics through a direct association with mitochondrial membranes (Kamp et al., 2010). Based on my data, I consider the possibility that overexpression induces fragmentation by triggering an increase in fission activity. Since mitochondrial morphology and connectivity is only altered at steady state, I suggest that cells overexpressing α-synuclein have an increased baseline level of oxidative stress that triggers upregulation of mitochondrial fission as a quality control mechanism to preserve mitochondrial health. Though previous work has shown that α-synuclein directly increases oxidative species, assessment of baseline cellular ROS in my GFP-α-syn-WT and GFP-α-syn-A53T overexpressing models would enable this theory to be tested (Hsu et al., 2000; Wilkaniec et al., 2021).

In exploring mito-QC further, I found that overexpression of α-synuclein did not impact expression of PINK1/Parkin-dependent mitophagy markers, or degradation of whole mitochondria in response to mitochondrial damage. Though dysfunctions in mitophagy have been reported in PD, I was unable to recapitulate these in my model (Choubey et al., 2011; W. Liu et al., 2009; Shaltouki et al., 2018; Wilkaniec et al., 2021). Interestingly, many studies which have shown an α-synuclein-induced reduction in mitophagy have utilised tools that create cellular environments with extremely high levels of aggregation, such as the addition of exogenous PFFs or inducible α-synuclein aggregation (Lurette et al., 2023; Wilkaniec et al., 2021). In particular, the study using a newly developed optogenetic system to selectively induce aggregation of α-synuclein is one of the first to discriminate between the impact of α-synuclein expression and α-synuclein aggregation, enabling the authors to conclude that overexpression alone was not sufficient to impact mitophagy in their system (Lurette et al., 2023). This led me to consider that α-synuclein's ability to impact PINK1/Parkin-dependent mitophagy may be conformation-dependent. Though the overexpression models of α-synuclein developed in my study provide an environment for organic aggregation of the protein, the number and size of aggregated species may not reach the same level as in these models where the stepwise fibrillisation process of α-synuclein is either circumvented or artificially accelerated (Iljina et al., 2016).

Despite this, cells overexpressing GFP-α-syn-WT showed increased levels of pUb S65 as a readout of PINK1/Parkin activity upon accumulated mitochondrial damage. Since this was not accompanied by a reduction in overall mitochondrial clearance, I suggest that this phenotype is the result of enhanced mitochondrial damage. However, it is not clear why this is exclusive to GFP-α-syn-WT overexpression. One explanation could be that cells overexpressing GFP-α-syn may require a greater response to mitochondrial damage, since the oxidative stress induced by A/O is exaggerated by overexpression of α-synuclein. As such, GFP-α-syn-WT cells may be able to indirectly increase PINK1/Parkin activity to cope with this, but GFP-α-syn-A53T cells may not.

Upon assessment of autophagosomes by LC3 lipidation, I observed that cells overexpressing GFP-α-syn-A53T had a lower number of autophagosomes compared to GFP only control and GFP-α-syn-WT overexpressing cells. One explanation for this could be a potential interaction between α-synuclein and cardiolipin (CL), a mitochondrial phospholipid that makes up approximately 15-20% of all phospholipids in the IMM (Paradies et al., 2019). Oxidative stress is known to trigger externalisation of CL onto the OMM, where it can bind LC3II on autophagosomes (Chu et al., 2014). However, more recent research has shown that CL is associated with MAMs, which provide a molecular platform for the formation of autophagosomes (Kulkarni et al., 2024; Manganelli et al., 2021). Further to this, CL has been shown to bind machinery known to co-ordinate autophagosome formation such as AMBRA1, BECN1 and WIPI1 (Manganelli et al., 2021). Interestingly, many studies have characterised the ability of α-synuclein to interact with CL and compete with its binding partners (Lurette et al., 2023; Martín-Jiménez et al., 2024; Robotta et al., 2014; Ryan et al., 2018; Stefanovic et al., 2014). Accordingly, I propose that α-synuclein may compete with these molecules to bind CL, resulting in a reduction or delay in autophagosome formation (Martín-Jiménez et al., 2024). The exclusivity of this phenotype to GFP-α-syn-A53T may be explained by its proximity to mitochondria to facilitate this interaction, since I previously showed that GFP-α-syn-A53T, but not GFP-α-syn-WT was enriched in the mitochondrial fraction. Alternatively, the reduction in autophagosomes could indicate an increase in autophagosomal turnover. This could reflect an attempt by the cell to boost autophagic flux in order to degrade damaging α-synuclein A53T when its pathological impacts have been exacerbated by accumulated mitochondrial stress.

Removal of α-synuclein from the cell is known to be co-ordinated by lysosomes, as it is for many aggregate-prone proteins (Mak et al., 2010). Since sequestration of α-synuclein inside lysosomes creates an opportunity for it to impact their function, I explored whether overexpression of α-synuclein in SH-SY5Y cells had any impact on lysosomal phenotypes

(Cuervo et al., 2004; Hoffmann et al., 2019). Interestingly, LAMP1 puncta at steady state were significantly larger in cells overexpressing GFP-α-syn-WT compared to GFP only controls. This is in line with a previous study by Nascimento et al (2020) which also described an increase in lysosomal size in SH-SY5Y cells overexpressing GFP-α-syn-WT. My data demonstrated that an excess of α-synuclein induced a swollen lysosomal phenotype, indicative of undigested materials within the organelle (Hu et al., 2022). This could be explained by α-synuclein's ability to impact the activity of digestive enzymes, since previous research has suggested that pathological α-synuclein can deplete levels of glucocerebrosidase (GCase) and cathepsin D (Hoffmann et al., 2019; Mazzulli et al., 2011). However, this suggestion does not resolve why a more exaggerated phenotype was observed in cells overexpressing GFP-α-syn-WT compared to GFP-α-syn-A53T. As such, I consider an alternative interpretation that lysosomal swelling could be the result of a direct accumulation of wild-type α-synuclein in lysosomes at steady-state as cells try to clear the protein. Previous research has shown that though wild-type α-synuclein is selected for translocation into lysosomes by chaperone-mediated autophagy, α-synuclein A53T is not (Cuervo et al., 2004). In fact, this study found that α-synuclein A53T acts as an uptake blocker on lysosomal membranes, not only inhibiting their own degradation but also that of other proteins (Cuervo et al., 2004). Therefore, transport of wild-type α-synuclein, but not α-synuclein A53T, into lysosomes through the CMA pathway could explain the difference in lysosomal morphology observed between the two cell lines.

Finally, I investigated how overexpression of α-synuclein impacted mito-QC in the context of localised mitochondrial damage by assessing IMM- and OMM-derived MDVs. Given that pathological α-synuclein has been shown to bind both these membranes and enhance oxidative stress, I hypothesised that overexpression of α-synuclein may impact generation of these vesicles (Bender et al., 2013; Devi et al., 2008; K. Nakamura et al., 2008; Robotta et al., 2014). In terms of OMM-derived (TOM20+/PDH-) MDVs, my data demonstrated that cells overexpressing α-synuclein had slightly more at steady state compared to GFP only controls. Since generation of this subtype of MDVs has been shown to be upregulated as an early, protective response to mitochondrial damage, a higher number of MDVs at steady state may reflect an increase in MDV generation due to α-synuclein-induced oxidative stress as previously suggested to explain the increase in steady state fragmentation in these cells (Hsu et al., 2000; Ryan et al., 2020; Soubannier et al., 2012a; Wilkaniec et al., 2021). Alternatively, a higher number of MDVs at steady state could indicate a defect in MDV trafficking, causing them to accumulate. OMM-derived MDVs are shown to shuttle to the lysosome for degradation, but the machinery that facilitates this is still not clear. One protein shown to be involved in trafficking of OMM-derived MDVs is Parkin, which has been suggested to interact with pathological α-

synuclein by several studies (Jęśko et al., 2019; Madsen et al., 2021; McLelland et al., 2014; Ryan et al., 2020; Wilkaniec et al., 2019). Though I did not observe any differences in Parkin expression or function in cells overexpressing α-synuclein in the context of mitophagy, it could be that α-synuclein has a more subtle impact on Parkin that could influence OMM-derived MDV trafficking. Further investigation is needed to establish whether this phenotype is the result of an increase in MDV biogenesis or a defect in MDV trafficking. Despite this, cells were still able to upregulate OMM-derived MDVs upon exposure to A/O, suggesting that the efficiency of the pathway in responding to mitochondrial stressors was not impacted by α-synuclein overexpression.

In assessing IMM-derived (PDH+/TOM20-) MDVs, I observed a more striking phenotype. In response to mitochondrial damage, GFP-α-syn-WT and GFP-α-syn-A53T overexpressing cells were not capable of increasing the number of IMM-derived MDVs compared to GFP only controls. Since the numbers of these MDVs were equal across all cell lines at steady state, I suggest this phenotype is not the result of a general defect in biogenesis of MDVs, but is specific to the generation of MDVs as a direct response to localised oxidative stress. Mechanisms of MDV biogenesis are still poorly understood, with the role of molecular players still being debated and developed. For example, though MDVs were initially described to be independent of the scission protein Drp1, more recent research has suggested otherwise (König et al., 2021; Soubannier et al., 2012a). Given that the co-ordination of MDV biogenesis is not well-understood, we do not know whether the machinery involved may change depending on MDV cargo, such as between oxidised and non-oxidised mitochondrial components. It could be that α-synuclein impacts only machinery that generates MDVs containing oxidised cargo, but more research is needed on regulation of the pathway to establish this.

Summary

To summarise, the work in this chapter develops and uses α-synuclein overexpression models to provide insight into the potential effects of toxic gain of α-synuclein function on mitochondrial health and quality control. Firstly, overexpression of both GFP-α-syn-WT and GFP-α-syn-A53T was shown to induce markers of α-synuclein pathology at steady state which were exacerbated in response to mitochondrial damage. Though immunofluorescence microscopy did not enable me to visualise mitochondrial localisation of α-synuclein, GFP-α-syn-A53T was shown to be enriched in biochemically isolated mitochondria. On assessment of mitochondrial function, I demonstrated that overexpression of α-synuclein did not impact ATP

levels, OCR or maintenance of baseline ΔΨm, which I suggest may be due to lack of a substantial pool of aggregated protein in my model. I observed an elevation in the mito-QC response, illustrated by mitochondrial fragmentation and higher levels of OMM-derived MDVs, which I suggest may be the result of an α-synuclein-induced increase in baseline oxidative stress. I propose that this could be due to increased steady state oxidative stress in the system caused by α-synuclein pathology. Interestingly, α-synuclein overexpression appeared to reduce damage-induced generation of IMM-derived MDVs, though a better understanding of MDV machinery is required to discern the mechanism behind this. Finally, though whole mitochondrial clearance was unaffected by α-synuclein overexpression, lysosomal morphology was altered in GFP-α-syn-WT cells which may reflect an attempt by the cell to remove wild-type α-synuclein by CMA.

Chapter 5 Investigating the impact of alterations in α-synuclein on neuronal differentiation of SH-SY5Y cells

5.1 Introduction

SH-SY5Y cells are commonly used in neurodegenerative research as a neuronal-like model. Originally generated from neuroblastoma cells, they have a morphology similar to immature neurons and express some neuronal markers but, unlike primary neurons, are easy to maintain and highly proliferative (Biedler et al., 1973, 1978; Kovalevich & Langford, 2013). A key advantage of using this cell line in PD research is that they can be differentiated into cells that more closely resemble a mature neuronal phenotype and therefore better recapitulate dopaminergic neurons (Luchtman & Song, 2010). During the differentiation process, SH-SY5Y cells go through several stages that facilitate their development into neuronal-like cells. An important early step is the change in expression of cell cycle genes, causing cells to irreversibly enter the G_0 phase and stop proliferating (Feles et al., 2022; Hardwick et al., 2015). This enables cells to redirect their energy into differentiating, starting with reorganisation of the cytoskeleton to facilitate the growth of neurites (Avila et al., 2020). Actin filaments polymerise to form membrane sprouts at sites where neuritogenesis will occur, and microtubules rearrange to provide these neurites with structural support (Avila et al., 2020; Ponti et al., 2004). Alongside these changes, cells begin to express neuron-specific cytoskeletal components such as β-3-tubulin (Guo et al., 2010). Dynamic, actin-rich growth cones form at the tip of extending neurites, engaging the cytoskeleton to drive neurite outgrowth (Lowery & Vactor, 2009). As neurites increase in length, growth cones also enable them to navigate and turn by responding to guidance cues (Lowery & Vactor, 2009). Cells have recognisably neuronal-like morphology, with a small soma and long neurites, alongside the upregulation of other specific genes involved in neuronal function and synaptogenesis, such as GAP43 (Shipley et al., 2016; Zhao et al., 2012). This also includes the expression of catecholaminergic genes, including machinery required to synthesise neurotransmitters such as noradrenaline and dopamine (Filograna et al., 2015). During this process and in terminally differentiated SH-SY5Y cells, the activity of mitochondria is likely altered to reflect the switch in energy usage (Rangaraju et al., 2019; Sheng & Cai, 2012).

Interestingly, differentiated SH-SY5Y cells also provide an environment where α-synuclein may have a more physiologically relevant role. Primarily expressed in the CNS and

localised at pre-synaptic terminals, α-synuclein has a well-established function in the release and recycling of synaptic vesicles (Burré, 2015; Gao et al., 2023; Kahle et al., 2000). The ability of α-synuclein to sense and enhance membrane curvature enables it to bind these vesicles and facilitate their fusion with the cell membrane, resulting in exocytosis (Sulzer & Edwards, 2019). Interestingly, α-synuclein has been shown to have further functions that impact the homeostasis of dopamine (Venda et al., 2010). As well as modulating vesicle release, α-synuclein has been shown impact dopamine synthesis by an interaction with tyrosine hydroxylase (TH), a key enzyme involved in the conversion of tyrosine into the dopamine precursor, L-3,4-dihydroxyphenylalanine (L-DOPA) (Gao et al., 2007; Peng et al., 2005; Perez et al., 2002). In particular, overexpression of α-synuclein has been suggested to reduce the activity of TH, and therefore levels of dopamine (Gao et al., 2007; Peng et al., 2005; Perez et al., 2002). Additionally, several studies have described a relationship between α-synuclein and the dopamine transporter (DAT), the membrane protein responsible for reuptake of dopamine into the presynaptic bouton (Fountaine & Wade-Martins, 2007; Gosavi et al., 2002). These associations hint that α-synuclein is involved in a range of regulatory functions in neurons, thus α-synuclein may have a precise function in differentiated SH-SY5Y cells that is distinct from its role in undifferentiated cells (Cheng et al., 2011).

As well as being important for activity in mature neurons, it has been suggested that α-synuclein may have a role in neuronal development. This is based on the observation that α-synuclein expression peaks during gestation and slowly reduces into adulthood (Alejandra Morato Torres et al., 2020; Raghavan et al., 2004). Interestingly, research has shown that plasma α-synuclein expression is reduced in children with neurodevelopmental disorders such as ASD, raising further questions about α-synuclein's function in early human development (Sriwimol & Limprasert, 2018). Supporting the theory that α-synuclein has a role in neuronal development, it has been shown to redistribute from the cell body to the axon as neurons undergo maturation (Robertson et al., 2004; Zhong et al., 2010). This alteration in localisation may accompany a functional switch and insinuate that α-synuclein has disparate roles in immature and mature neurons.

Though the potential role of α-synuclein in development is not well established, several studies have investigated this by assessing the impact of alterations in α-synuclein on differentiation and maturation of cultured cells. For example, iPSCs from PD patients with triplication of the SNCA gene exhibited impaired differentiation as well as increased oxidative stress (Byers et al., 2011; Oliveira et al., 2015). However, whether α-synuclein's ability to impact the health and development of immature human neurons was the result of a loss-of-function of physiological α-synuclein or a toxic gain-of-function associated with pathological α-synuclein is

still not understood. I aim to address this by investigating differentiation of SH-SY5Y cells exhibiting either overexpression or knockout of α-synuclein.

Aims:

1) Validate a published protocol for differentiating SH-SY5Y cells and characterise differentiated neuronal phenotypes in wild-type cells
2) Investigate the impact of α-synuclein loss-of-function on differentiation of SH-SY5Y cells
3) Investigate the impact of α-synuclein overexpression on differentiation of SH-SY5Y cells

5.2 Results

5.2.1 Differentiation of wild-type SH-SY5Y cells results in cells with neuronal morphology

Various methods to enable the differentiation of SH-SY5Y cells have been described throughout the literature, but most rely on the addition of retinoic acid (RA) to promote the switch from proliferation to neuronal differentiation (Janesick et al., 2015; Kovalevich & Langford, 2013). RA binds to nuclear retinoic acid receptors (RARs) and retinoid X receptors (RXRs) which interact with retinoic acid response elements (RAREs) in the promotor regions of neuronal target genes, regulating their transcription (Cañon et al., 2004; Johnson et al., 2019). RA also promotes development through modulating the activity of Rho GTPases, key factors important in co-ordinating the rearrangement of cytoskeletal proteins that is required for generation of the growth cone and neurite outgrowth (Johnson et al., 2019; Nayak et al., 2013). In addition, RA has been shown to directly stimulate intracellular signalling molecules that promote neuronal differentiation such as cyclic AMP/protein kinase A (cAMP/PKA)-dependent cAMP response element binding protein (CREB) and phosphatidylinositol-3-kinase (PI3K) (Bastien et al., 2006; Cañon et al., 2004).

Though some papers suggest that as little as 3-7 days with RA is enough to induce a neuronal phenotype, cells often do not exhibit any more neurite outgrowth than observed in undifferentiated cells (Ferreira et al., 2013; Presgraves et al., 2004; Simões et al., 2021). As such, many studies use further supplements in combination with RA to encourage neuronal phenotypes over a longer time period, including growth factors like brain-derived neurotrophic factor (BDNF) (J. Chen et al., 1990; Encinas et al., 2000). Known to promote neuronal differentiation, maturation and survival in human neurons through TrkB receptor signalling, BDNF facilitates the differentiation of SH-SY5Y cells and has been suggested to enhance the effects of RA (Acheson et al., 1995; Arcangeli et al., 1999; Binder & Scharfman, 2004). Alongside a reduction in serum to prevent cellular proliferation, a combination of RA and BDNF has been shown to successfully differentiate SH-SY5Ys into cells with a neuronal phenotype (de Medeiros et al., 2019; Encinas et al., 2000; Jauhari et al., 2017; Shipley et al., 2016).

As such, I aimed to adapt and validate a published protocol for RA/BDNF-induced neuronal differentiation (Shipley et al., 2016). A summary of this 14-day protocol is shown in **Figure 96**.

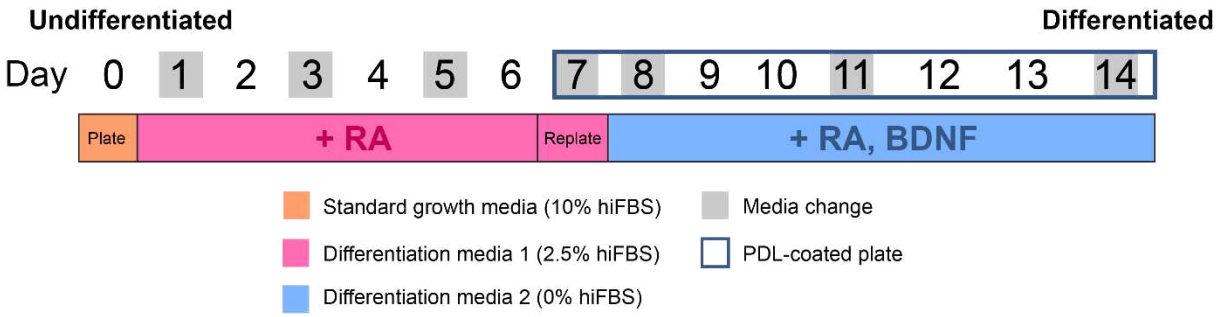

Figure 96: Summary of the protocol used to differentiate SH-SY5Y cells

SH-SY5Y cells were subject to a differentiation protocol adapted from Shipley et al., 2016. Cells were plated in standard growth media, then maintained in low-serum media with RA until day 7 when they were replated on PDL. Cells were then maintained in no-serum media with RA and BDNF until day 14.

To validate this method, wild-type cells were subject to this differentiation protocol and preliminary brightfield images were taken to record changes in cellular morphology throughout the process (**Figure 97**). These images demonstrate the impact of RA over the first 7 days, since with increased exposure to RA, more cells started to extend projections. Though cells had reduced serum in their media, they were still proliferating and thus increased their cell number to confluency on day 7. After cells were replated, they were cultured in a combination of RA, BDNF and other differentiation-inducing factors such as KCl and B27. From this point on, cells were no longer proliferating due to lack of serum and terminal differentiation. With increasing time exposed to RA and BDNF, cells showed projections with appeared to be greater in number and length. Qualitatively, cells showed considerably more neuronal-like morphology on day 14 than on day 1 (with no RA or BDNF) and on day 7 (with RA only).

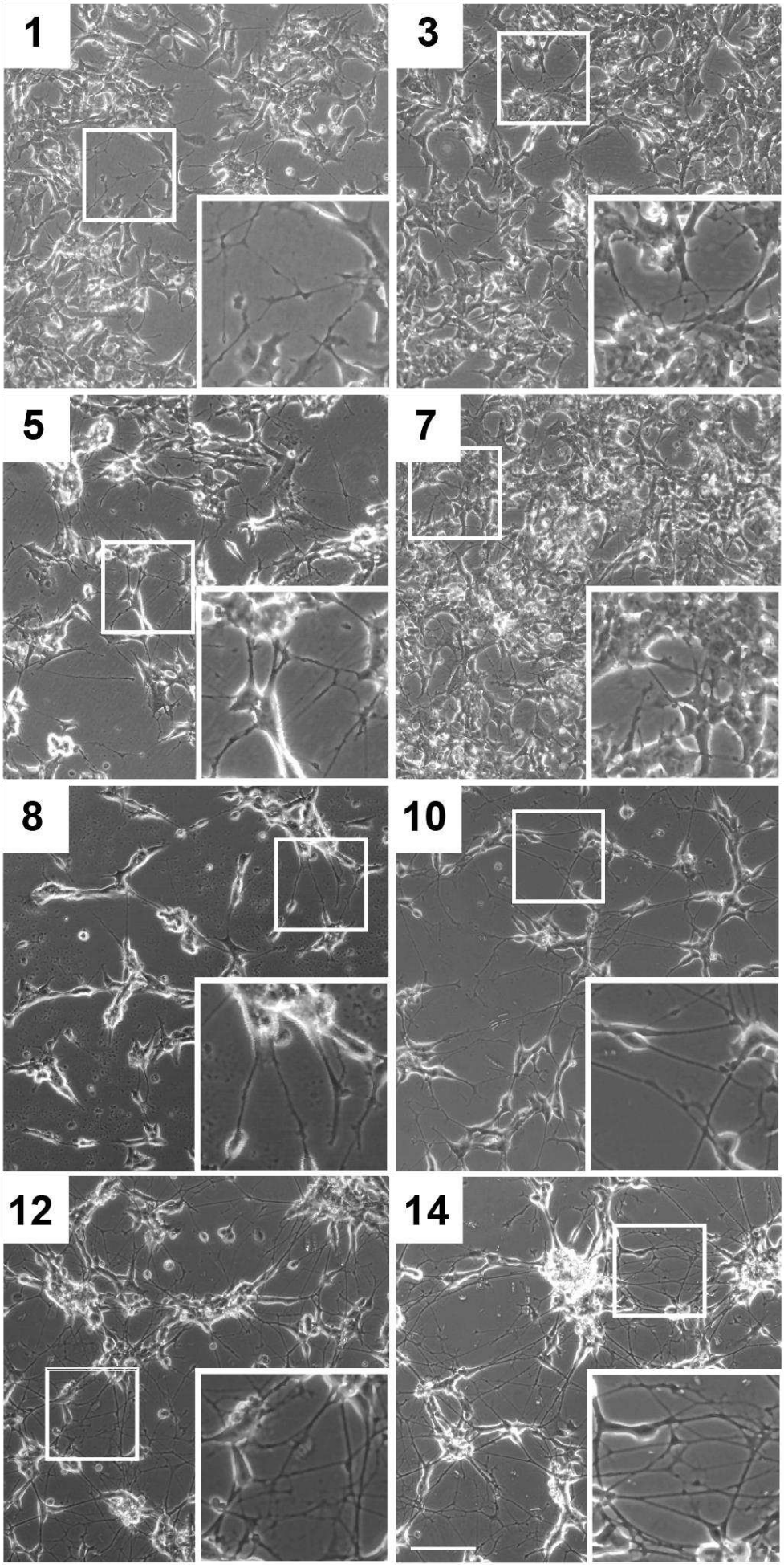
1
3
5
7
8
10
12
14

Figure 97: SH-SY5Y cells exhibit visible neuronal morphology after a 14-day differentiation protocol

Wild-type SH-SY5Y cells were subject to a 14-day differentiation protocol. After plating cells on day 0, cells were imaged on days 1, 3, 5 and 7, prior to replating on PDL. After replating, cells were imaged on days 8, 10, 12 and 14 (as indicated). Images are representative from one biological repeat of the differentiation protocol. Images were captured with a light microscope on a 10X objective. Scale bar = 20μm.

To further investigate the extent of neuronal differentiation, I assessed expression of B-III-tubulin and filamentous actin (F-actin); two cytoskeletal proteins involved in neuronal maturation (Avwenagha et al., 2003; Caccamo et al., 1989). In developing human neurons, B-III-tubulin is enriched in axons while F-actin is distributed in neuronal dendrites and growth cones (Avwenagha et al., 2003). By immunofluorescence microscopy, I was able to use these markers to define cells as "differentiated" or "undifferentiated", since not every cell exhibited neuronal morphology. Cells with no detectable B-III-tubulin expression, no projections and a rounded architecture highlighted by F-actin were considered "undifferentiated" (**Figure 98a**). I noted that these cells tended to have no contact with other cells. Accordingly, cells with a B-III-tubulin-expressing projection with F-actin distributed throughout and enriched at the end (defined as a growth cone) were considered "differentiated" (**Figure 98b**). The longest B-III-tubulin-positive neurite per cell was considered the "primary neurite". Differentiated cells also appeared to have a reduction in nuclear size, with the small nucleus in the cell body defined as the soma. Interestingly, these cells often had direct contact with at least one other cell. From this point on, the presence of at least one B-III-tubulin-rich primary neurite was used to define and distinguish "differentiated" from "undifferentiated" cells by immunofluorescence microscopy.

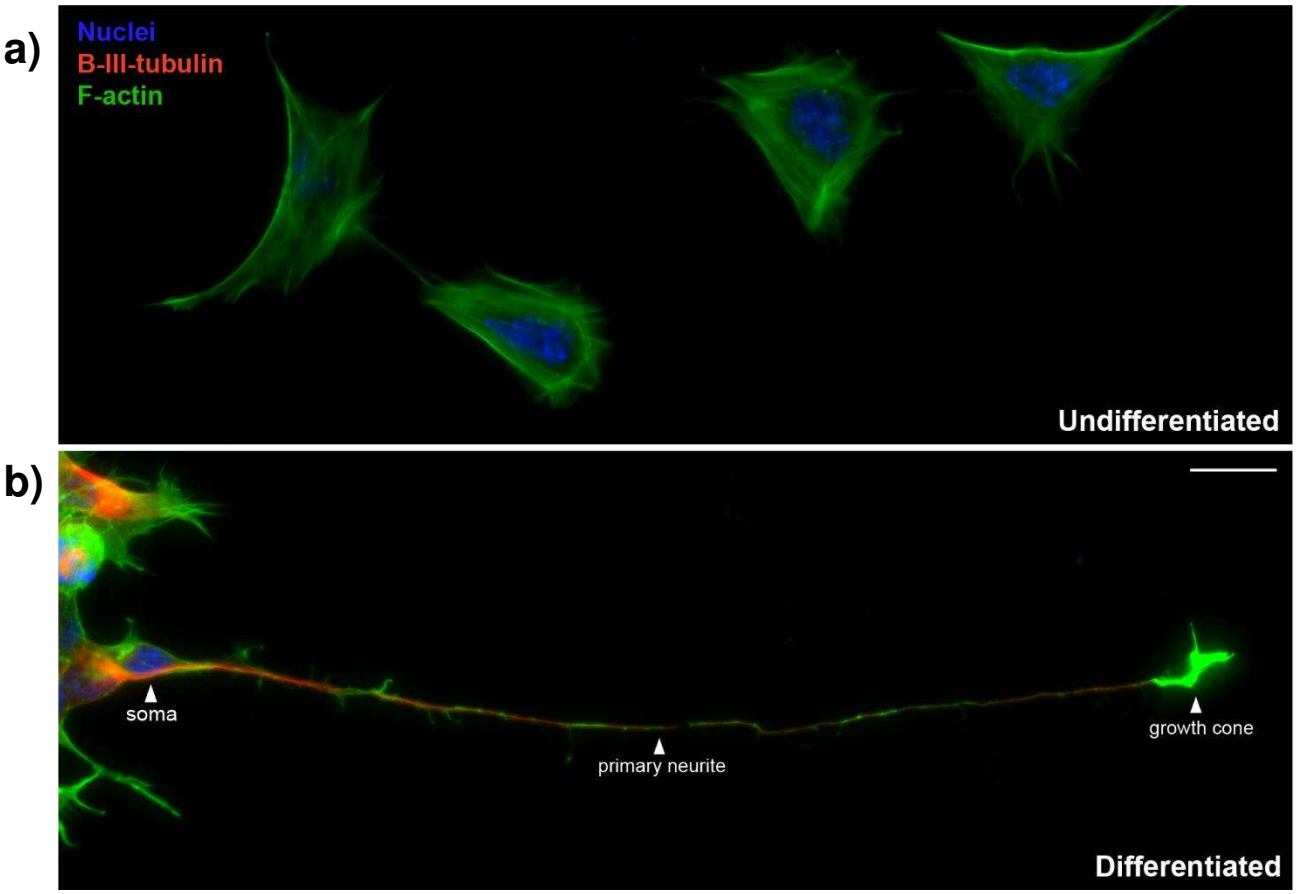

Figure 98: F-actin and B-III-tubulin distribution distinguishes differentiated and undifferentiated cells

Wild-type SH-SY5Y cells were subject to a 14-day differentiation protocol before being fixed and stained by immunocytochemistry. Cells were labelled with an antibody against B-III-tubulin (red), with Phalloidin to indicate F-actin (green) and with Hoechst to show nuclei (blue). Images shown are cells from the same coverslip, with cells defined as "undifferentiated" (a) or "differentiated" (b) dependent on morphology and distribution of cytoskeletal proteins. Images were taken using widefield immunofluorescence microscopy with a 40X objective. Scale bar = 20µm.

B-III-tubulin staining was also used to quantify the number of "differentiated" cells in a given field of view and the average length of the primary neurite in differentiated cells (**Figure 99**). From this, an average of approximately 87% of all cells in a given field of view were considered "differentiated" (**Figure 100a**). Tracing and measurement of neurites revealed that the average length of the longest neurite in a differentiated cell was approximately 100nm (**Figure 100b**). Both the average percentage of "differentiated" cells and the average length of the primary neurite was relatively uniform across the 3 biological repeats, suggesting that the impact of the differentiation protocol was consistent from one population of cells to the next. This established confidence that any differences in these characteristics in experimental cell lines would likely not be the result of variation across biological replicates.

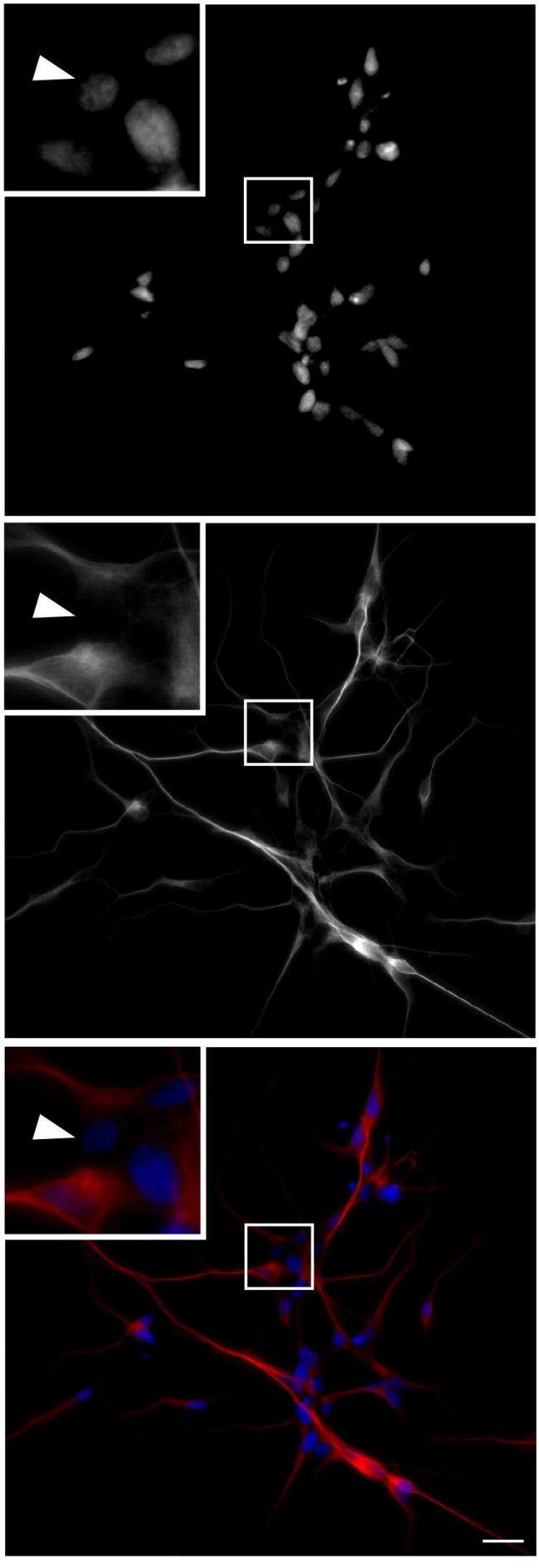
DAPI
B-III-tubulin
Nuclei
B-III-tubulin

Figure 99: B-III-tubulin staining enables identification of the percentage of differentiated cells in a given population and quantification of neurite length

Wild-type SH-SY5Y cells were subject to a 14-day differentiation protocol before being fixed and stained by immunocytochemistry. Cells were labelled with an antibody against B-III-tubulin (red) and nuclei were labelled with Hoechst (blue). Images are representative and from 1 biological repeat. An example of a cell without B-III-tubulin staining considered "undifferentiated" is highlighted by a white arrow. Images were taken using widefield immunofluorescence microscopy with a 40X objective. Scale bar = 20µm.

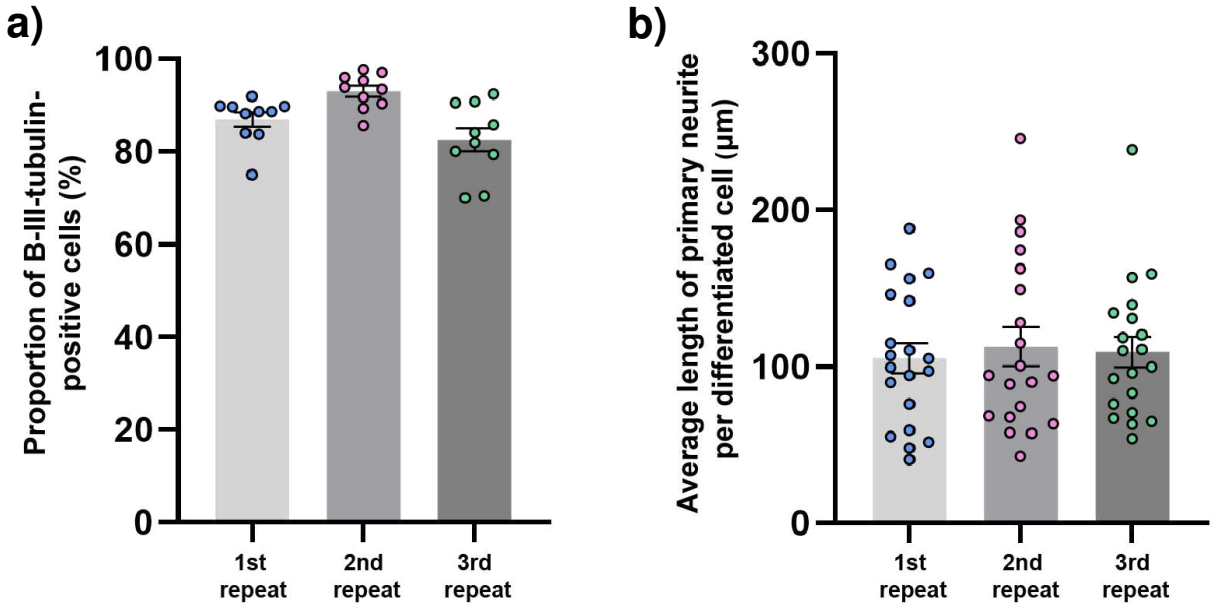

Figure 100: The proportion of differentiated cells and length of longest neurite in differentiated cells is consistent between biological repeats

a) The number of cells expressing B-III-tubulin in at least one neurite was counted and expressed as a percentage of total cells in a given field of view, identified by nuclei. This was measured in 10 fields of view per biological repeat from images taken on a 40X objective. Percentages for each field of view are represented by circles, with the average of each repeat indicated by the bar and SEM shown by black lines. (**n=3**).

b) The length of the primary B-III-tubulin-positive neurite was measured in 20 cells considered differentiated per biological repeat. Individual measurements are represented by circles, with the average of each repeat indicated by the bar and SEM shown by black lines. (**n=3**).

5.2.2 Differentiation of wild-type SH-SY5Y cells induces expression of neuronal and dopaminergic markers

After confirming that this adapted differentiation protocol could generate cells with consistent neuronal morphology, I evaluated whether these cells expressed any neuron-specific markers by Western blotting (**Figure 101**). Biochemical confirmation of neuronal phenotype in differentiated SH-SY5Y cells is standard practice throughout the literature, with B-III-tubulin and GAP43 considered reliable indicators of neuronal phenotype (Kovalevich & Langford, 2013; Kume et al., 2008).

The first of these proteins assessed was B-III-tubulin, which I had already confirmed expression of via immunocytochemistry. Western blotting affirmed that cells subject to differentiation expressed significantly higher B-III-tubulin than undifferentiated cells (**Figure 101b**, p=0.0074). Next, I measured expression of growth-associated protein (GAP43), a component of axonal growth cones involved in the formation of neurites (Meiri et al., 1986). GAP43 was also significantly increased in cells subject to differentiation compared to undifferentiated cells (**Figure 101c**, p=0.0274). The upregulation of these neuron-specific markers alongside the visible neuron-like morphology led me to conclude that differentiation of SH-SY5Y cells with the RA/BDNF protocol adapted from Shipley et al. (2016) was successful in creating neuron-like cells.

In addition to characterising differentiated cells as neuron-like, many papers define these cells as a specific neuronal subtype. Research has suggested that protocols can be tailored to develop dopaminergic neurons from undifferentiated SH-SY5Y cells, but there is no consensus on exactly which differentiation-inducing compounds lead to this neuronal subtype (de Medeiros et al., 2019; Xie et al., 2010). For example, several papers have used the same approach of combining RA and BDNF, but some have reported a dopaminergic phenotype while others claim a cholinergic phenotype (de Medeiros et al., 2019; Jauhari et al., 2017; Shipley et al., 2016). To investigate whether the differentiated cells I generated exhibited any signs of dopaminergic machinery, I assessed expression of tyrosine hydroxylase (TH), an enzyme involved in the conversion of L-tyrosine to L-DOPA prior to dopamine synthesis that is primarily expressed in the CNS (Nagatsu et al., 1964). Western blotting showed that differentiated cells expressed significantly more TH than undifferentiated cells (**Figure 101d**, p=0.0142). Though I cannot characterise these differentiated cells as fully dopaminergic from this finding alone, I conclude that they have dopaminergic characteristics.

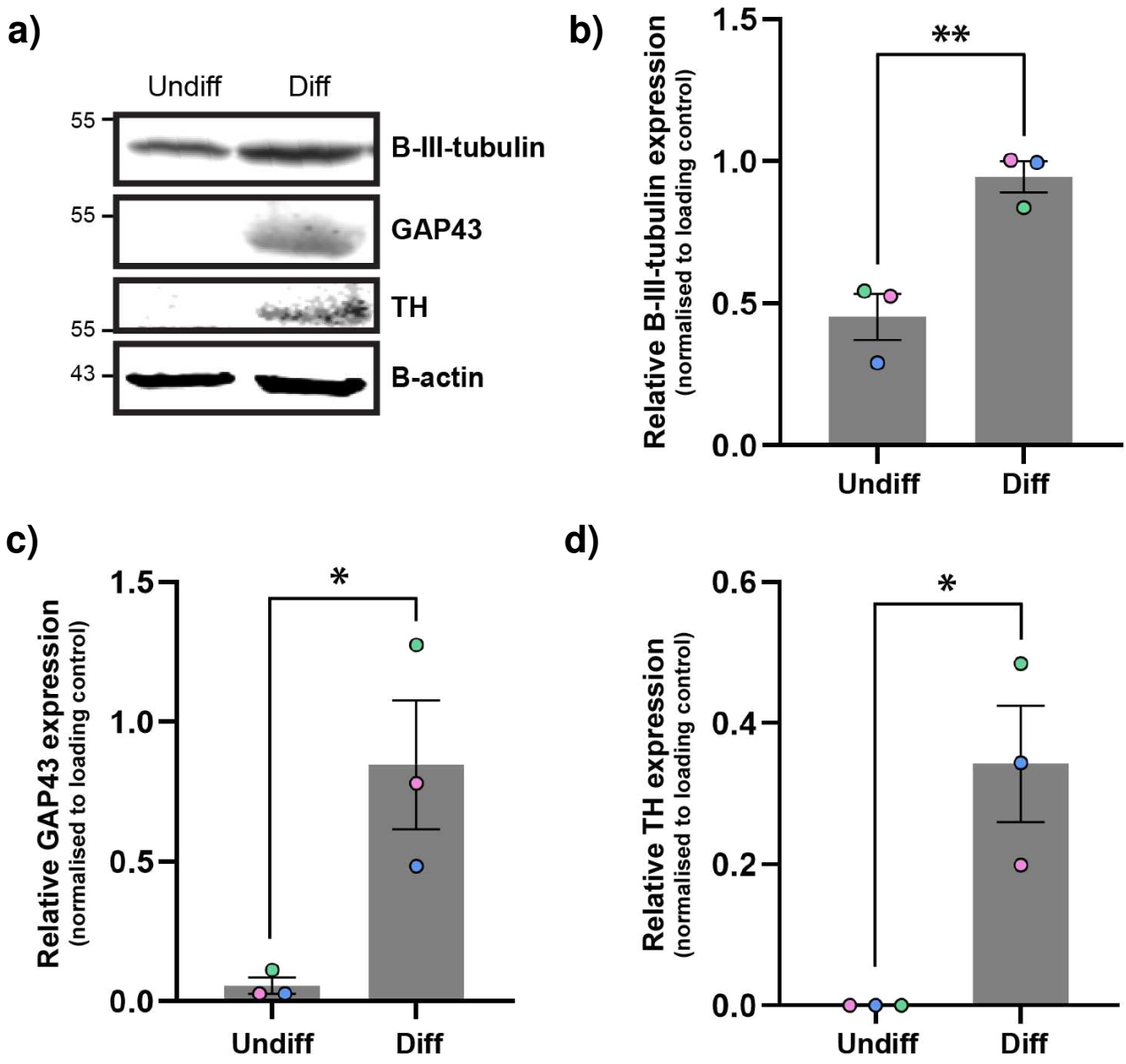

Figure 101: SH-SY5Y cells exhibit increased expression of neuronal and dopaminergic markers after a 14-day differentiation protocol

Wild-type SH-SY5Y cells were either left undifferentiated or subject to a 14-day differentiation protocol before being lysed. Lysates were processed by Western blot with antibodies against B-III-tubulin, GAP43 and TH, alongside B-actin as a protein loading control. a) is a representative blot from 1 biological repeat. Graphs show expression of b) B-III-tubulin, c) GAP43 and d) TH. Expression of each was normalised to B-actin to account for differences in protein loading, with relative expression shown by the raw values of these calculations. Biological replicates are colour coded, with circles representing the means of each repeat, the mean of the 3 repeats indicated by a bar and black lines showing SEM. Statistical analysis was performed by an unpaired t-test. Between undifferentiated and differentiated cells, there was a significant increase in B-III-tubulin (p=0.0074, **), GAP43 (p=0.0274, *) and TH (p=0.0142, *). (**n=3**).

5.2.3 Loss of α-synuclein negatively impacts the ability of SH-SY5Y cells to undergo neuronal differentiation

The physiological functions of α-synuclein are most clearly defined in mature neurons, in synaptic transmission and plasticity (Burré, 2015). The role of α-synuclein throughout neuronal development and differentiation is not well understood. However, recent work has suggested a potential role for α-synuclein in regulation of gene transcription during these processes (T. Nakamura et al., 2024). α-synuclein was shown to functionally interact with key chromatin remodelling proteins involved in neuronal maturation, representing a potential developmental role for α-synuclein (T. Nakamura et al., 2024). Interestingly, a role in regulation of developmental gene expression was also implied by Prahl et al., 2022 who found that human dopaminergic cells lacking α-synuclein appeared to differentiate normally but had a downregulation in expression of genes linked to the cell cycle and differentiation.

As such, I first investigated whether α-synuclein loss-of-function had any impact on the ability of SH-SY5Y cells to differentiate into neuronal-like cells. Immunofluorescence microscopy analysis revealed that SNCA KO cells were still able to differentiate, with many cells extending B-III-tubulin-rich projections (**Figure 102**). However, a significantly lower percentage of cells were differentiated in a given field of view compared to EV controls ($p=0.0179$) (**Figure 103**). This suggests that a lack of α-synuclein does impact the capacity of SH-SY5Y cells to undergo differentiation.

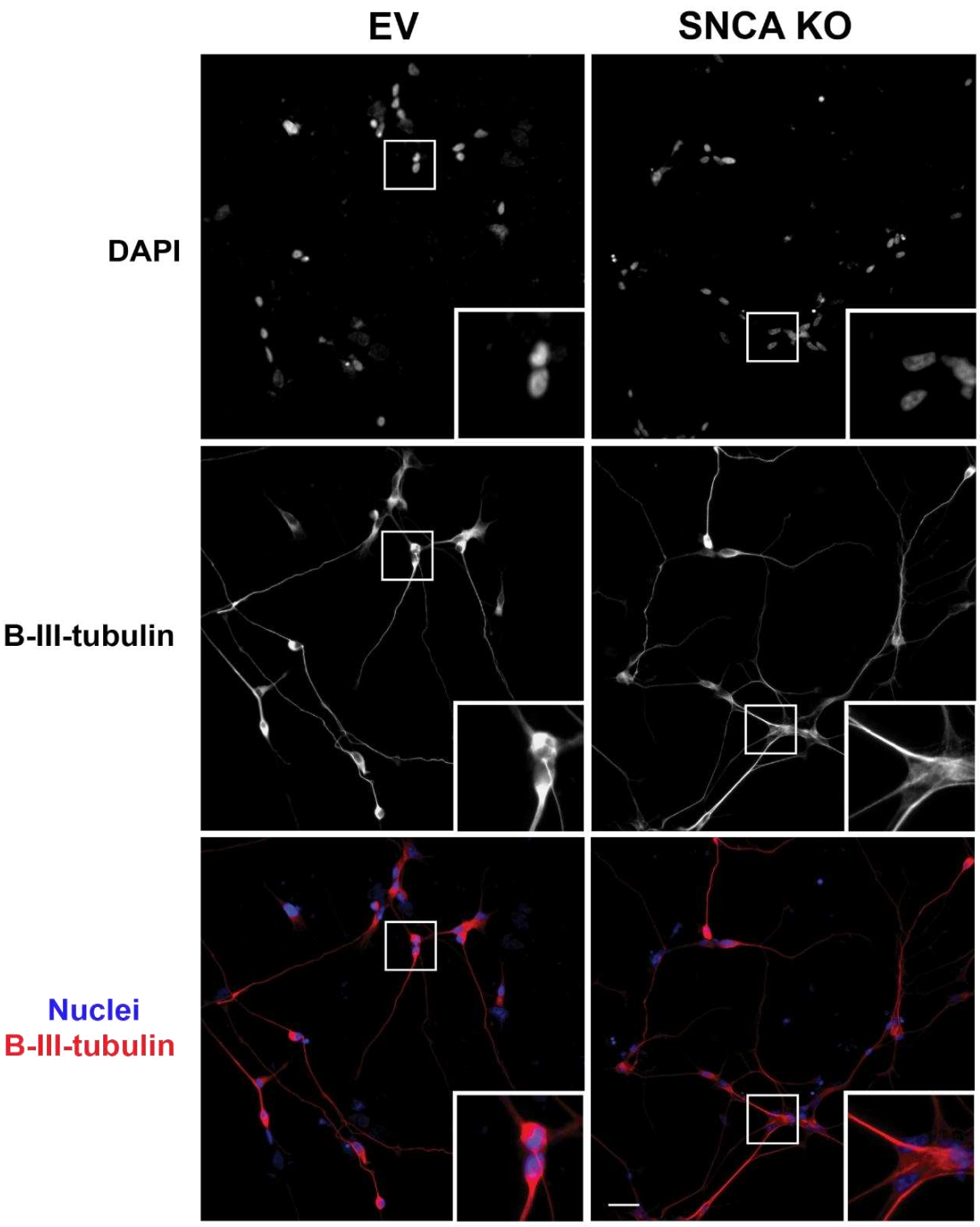

Figure 102: Lack of α-synuclein reduces the proportion of cells exhibiting B-III-tubulin staining

EV and SNCA KO cells were subject to a 14-day differentiation protocol before being fixed and stained by immunocytochemistry. Cells were labelled with an antibody against B-III-tubulin (red) and nuclei were labelled with Hoechst (blue). Images are representative and from 1 biological repeat. Images were taken by widefield immunofluorescence microscopy with a 40X objective. Scale bar = 20µm.

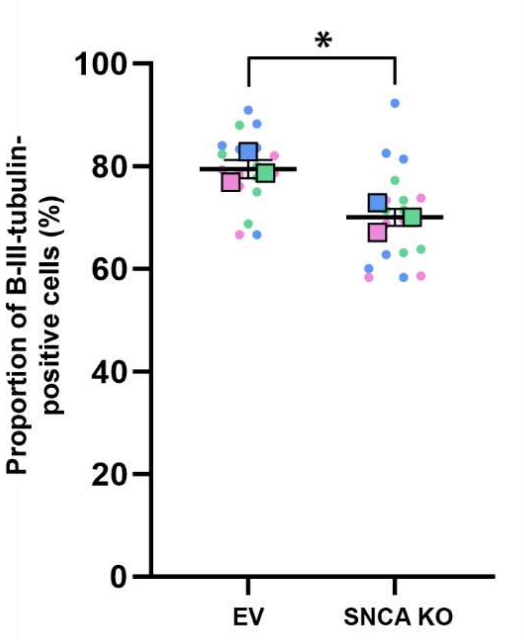

Figure 103: Lack of α-synuclein reduces the proportion of differentiated cells in a field of view

The number of cells expressing B-III-tubulin in at least one neurite was counted and expressed as a percentage of total cells in a given field of view, identified by nuclei, in EV and SNCA KO cells. This was measured in 6 fields of view per biological repeat from images taken on a 40X objective. Across the 3 repeats, the average number of nuclei per field of view was 32.64. Data points are colour coded by biological repeat, with the percentage for each field of view represented by a circle, the average of each repeat shown by a square and the average of all 3 biological repeats shown by a black line. SEM is shown by vertical black lines. Statistical analysis was performed by an unpaired t-test, showing a significant difference between the cell lines (p=0.0179, *). (**n=3**).

5.2.4 Differentiated cells lacking α-synuclein have no differences in neuronal nuclear morphology compared to EV controls

In cells that were classified as differentiated, the same B-III-tubulin staining was used to take morphological measurements to assess whether α-synuclein loss-of-function had any impact on neurite outgrowth.

Neurite sprouting is the foundation of axon generation in human neurons and is thought to be driven by the action of the cytoskeleton (Da Silva & Dotti, 2002). As such, the number of B-III-tubulin-positive neurites were counted per differentiated cell as a readout of a cell's ability to generate new neurites. In addition, the length of a differentiated cell's primary neurite was measured. Neurite length is a common readout of differentiation in SH-SY5Y cells and is considered to be a direct correlate of neuronal phenotype (J. Chen et al., 1990; Dwane et al., 2013). There were no significant differences between EV control and SNCA KO cells in either

number of neurites or primary neurite length (**Figure 104a, b**). This suggests that α-synuclein loss-of-function does not significantly impact the capacity of a cell to create or extend neurites.

Following this, I investigated whether there were any alterations to nuclear morphology. During neuronal development, nuclear reorganisation takes place to facilitate changes in gene expression (Ito & Takizawa, 2018). As such, nuclear architecture changes during neuronal differentiation. I observed that in control cells, nuclei became smaller and more elongated in response to differentiation, as indicated in **Figure 98**. Given this, nuclear area was measured along with nuclear aspect ratio, a readout of nuclear shape, to further characterise differentiated cells. Analysis of nuclear area showed that cells lacking α-synuclein had slightly larger nuclei than controls, though this was not significantly different (**Figure 104c**). There was no difference in nuclear aspect ratio between the cell lines (**Figure 104d**). This suggests that α-synuclein loss-of-function may have a subtle impact on nuclear size, but not shape.

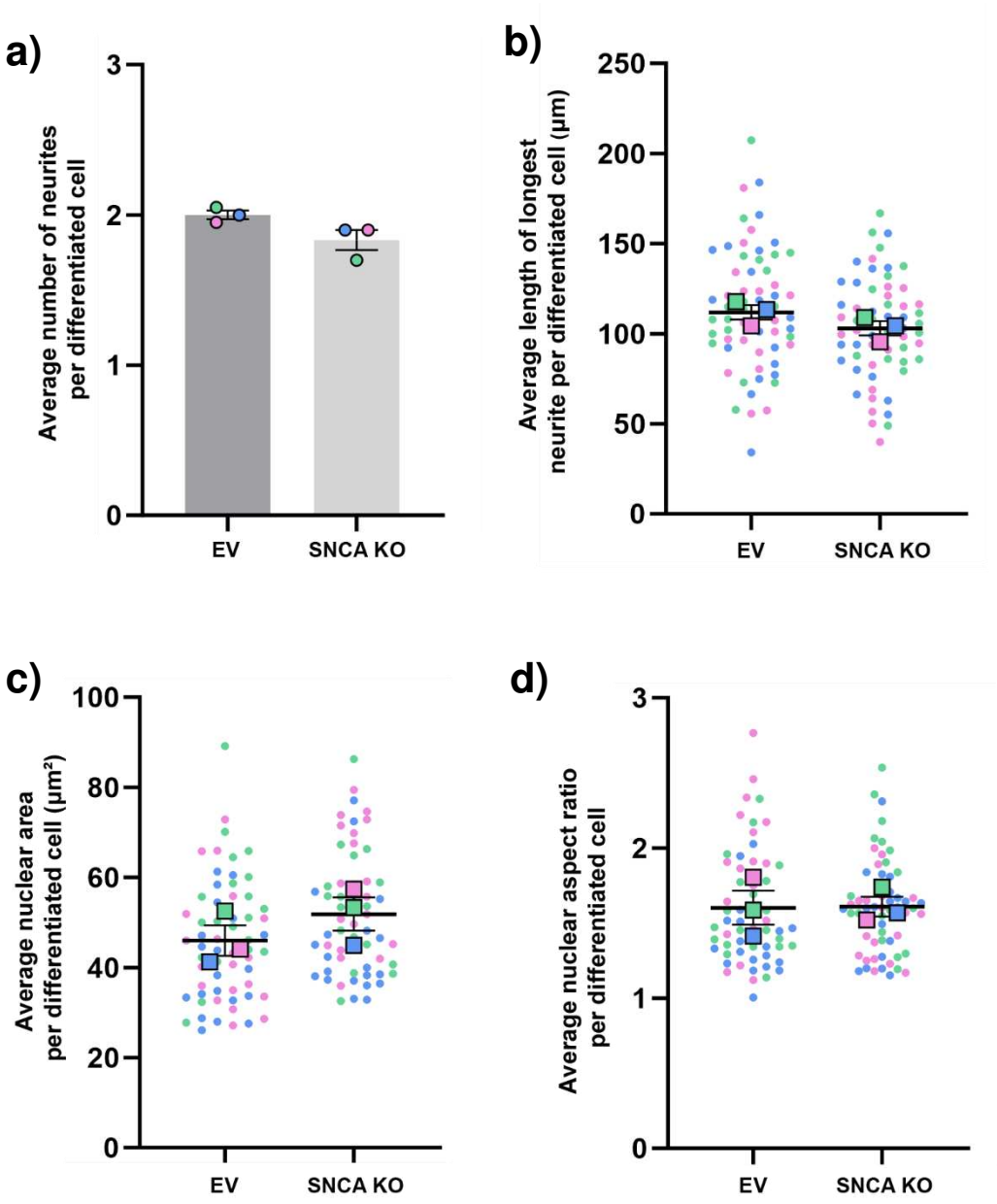

Figure 104: Lack of α-synuclein has no significant impact on neurite morphology or nuclear area in differentiated cells

EV and SNCA KO cells were subject to a 14-day differentiation protocol and stained for B-III-tubulin and for nuclei with DAPI. Images were subsequently analysed to measure neuronal and nuclear morphology. Only differentiated cells were included in this analysis, selected for by the expression of B-III-tubulin and the presence of at least one neurite. For all parameters, 20 cells per cell line were assessed across 3 biological repeats, shown by colour-coding. a) Shows the average number of neurites per cell. The mean of each repeat is shown by a circle, with the mean of all 3 repeats shown by a bar and the SEM shown by vertical black lines. Individual data points are not shown for clarity since data is discrete. The remaining graphs show b) average length of the primary neurite per differentiated cell, measured with NeuronJ, c) average nuclear area per cell and d) average nuclear aspect ratio per cell. In b), c) and d), individual data points are shown by circles, with the mean of each repeat represented by a square and the mean of all 3 repeats shown by a black line. SEM is shown by vertical black lines. Statistical analyses were performed using unpaired t-tests, but no significance was reported. (**n=3**).

5.2.5 Lack of α-synuclein results in subtle changes in the expression of neuronal and dopaminergic markers in differentiated cells

Next, I verified the neuronal phenotype of differentiated SNCA KO cells biochemically and assessed whether α-synuclein loss-of-function resulted in any differences in the expression of neuronal and dopaminergic markers (**Figure 105**). Firstly, SNCA KO cells exhibited lower levels of B-III-tubulin than EV cells (**Figure 105b**). Though cells lacking α-synuclein were able to increase B-III-tubulin in response to differentiation, this was less pronounced than in EV controls. The same pattern was reflected for a second neuronal marker, GAP43, which was also increased in response to differentiation in SNCA KO cells but to a lesser extent than in EV controls (**Figure 105c**). Though these differences were not significant, these findings suggest that lack of α-synuclein does slightly reduce the expression of neuronal markers, consistent with **Figure 103** which illustrated a decreased proportion of differentiated cells.

As seen in EV controls, lysates from differentiated SNCA KO cell populations showed increased expression of the dopamine precursor, TH, compared to undifferentiated cells (**Figure 105d**). Interestingly, TH expression was higher in differentiated SNCA KO cells compared to EV controls, suggesting that a lack of α-synuclein may enhance the expression of dopaminergic markers.

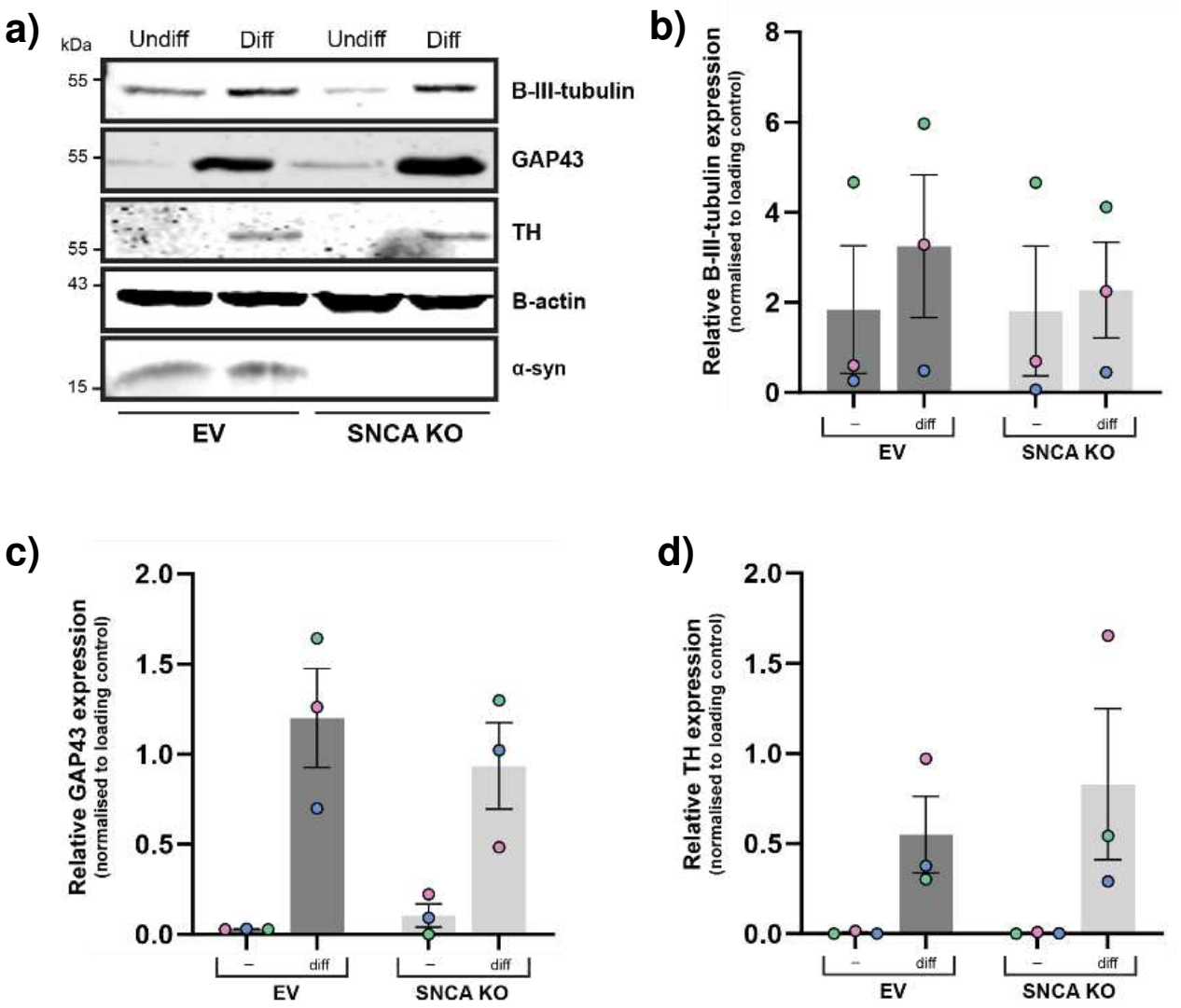

Figure 105: Loss of α-synuclein results in subtle decreases in expression of neuronal markers in cells subject to differentiation

EV and SNCA KO cells were subject to a 14-day differentiation protocol. Lysates from undifferentiated and differentiated cells were processed for Western blot with antibodies against B-III-tubulin, GAP43 and TH, with B-actin as a loading control and α-synuclein to confirm knockout in SNCA KO cells. a) is a representative blot from 1 biological repeat. Graphs show protein expression of b) B-III-tubulin, c) GAP43 and d) TH. Expression of each was normalised to B-actin to account for differences in protein loading, with relative expression shown by the raw values of these calculations. Biological replicates are colour coded with circles representing the means of each repeat, bars representing the mean of the 3repeats and black lines showing SEM. Statistical analyses were performed by unpaired t-tests but did not report any significant differences between the cell lines. (**n=3**).

5.2.6 Overexpression of GFP-α-syn has no impact on the ability of SH-SY5Y cells to undergo neuronal differentiation

Due to the adult-onset nature of PD, the impact of pathological α-synuclein has been well characterised in mature neurons. Though the exact mechanisms behind its toxicity are still undefined, aggregation of α-synuclein is known to cause neuronal damage and eventual cell death in adult dopaminergic neurons (Calabresi et al., 2023). However, in PD patients with mutations in the SNCA gene, pathological α-synuclein is present throughout the neuronal development process, prior to clinical PD onset (Olgiati et al., 2015; Polymeropoulos et al., 1997). For example, rare triplications in the SNCA gene are causative for a severe early-onset form of PD, causing a two-fold upregulation of α-synuclein expression (Olgiati et al., 2015; Zafar et al., 2018). The implications of the developing nervous system being exposed to higher, more aggregation-prone levels of α-synuclein are largely unknown (Afitska et al., 2019).

One study investigated this in iPSC neuronal progenitors from patients with an SNCA gene triplication, observing that these cells had impairments in neuronal differentiation and maturation (Oliveira et al., 2015). This led me to hypothesise that overexpression of α-synuclein may hinder the differentiation process in SH-SY5Y cells. Previous research has suggested this, with α-synuclein overexpression seen to attenuate a dopaminergic phenotype in differentiating SH-SY5Y cells (Kim et al., 2018). However, the differentiation protocol used in this study was only 4 days long and used RA alone, which arguably only captures cells at a very early stage where I see neuronal characteristics still developing (**Figure 97**) (Kim et al., 2018). As such, I aimed to investigate the impact of α-synuclein gain-of-function on the differentiation process in my model with a validated 14-day differentiation protocol (Shipley et al., 2016).

We first evaluated whether α-synuclein gain-of-function impacted SH-SY5Y differentiation by assessing neuronal morphology. By immunofluorescence microscopy, I observed that cells overexpressing GFP-α-syn WT and GFP-α-syn A53T were both able to differentiate into neuronal-like cells exhibiting B-III-tubulin-positive projections (**Figure 106**). There was no difference in the percentage of cells that were successfully differentiated in a given field of view between GFP only controls and both GFP-α-syn cell lines (**Figure 107**). Approximately 80% of cells were considered differentiated in all 3 cell lines, implying that overexpression of GFP-α-syn-WT and GFP-α-syn A53T does not impact the differentiation capacity of SH-SY5Y cells.

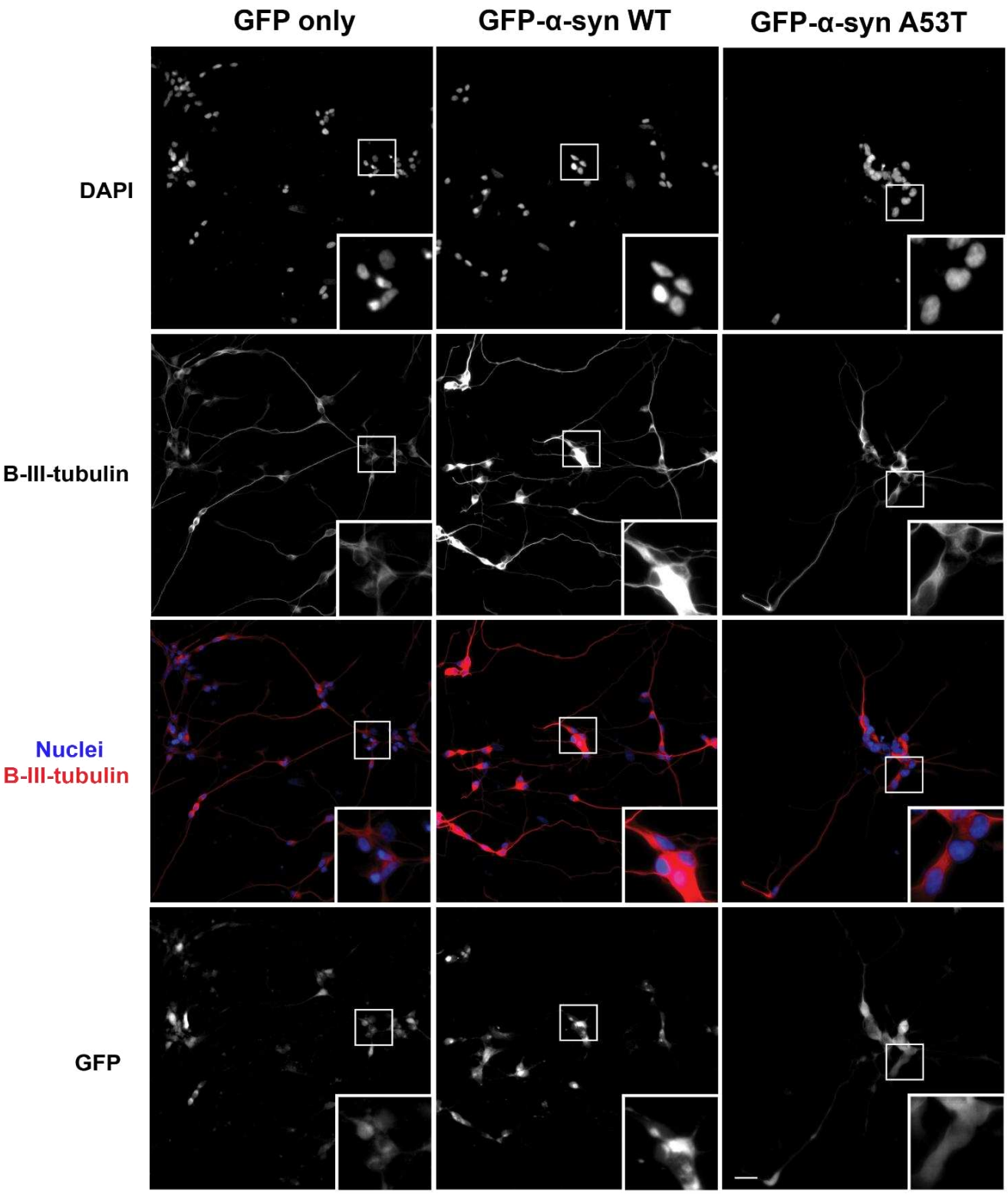

Figure 106: Overexpression of GFP-α-syn-WT or GFP-α-syn-A53T has no impact on the proportion of cells exhibiting B-III-tubulin staining

GFP only, GFP-α-syn WT and GFP-α-syn A53T overexpressing cells were subject to a 14-day differentiation protocol before being fixed and stained by immunocytochemistry. Cells were labelled with antibodies against B-III-tubulin (red) and GFP (green) with nuclei labelled by Hoechst (blue). Images are representative and from 1 biological repeat. Images were taken by widefield immunofluorescence microscopy on a 40X objective. Scale bar = 20µm.

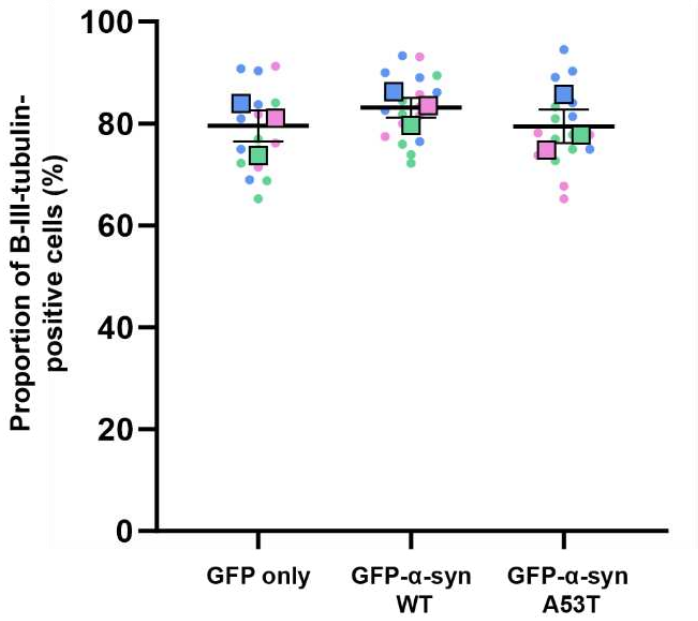

Figure 107: Overexpression of GFP-α-syn-WT or GFP-α-syn-A53T has no impact on the proportion of differentiated cells in a given field of view

The number of cells expressing B-III-tubulin in at least one neurite was counted and expressed as a percentage of total GFP-positive cells in a given field of view in GFP only, GFP-α-syn WT and GFP-α-syn A53T overexpressing cells. This was measured in 6 fields of view per biological repeat from images taken on a 40X objective. Across the 3 repeats, the average number of nuclei per field of view was 33.94. Data points are colour coded by biological repeat, with the percentage for each field of view represented by a circle, the average of each repeat shown by a square and the average of all 3 repeats shown by a black line. SEM is shown by black vertical lines. Statistical analysis was performed by an unpaired t-test and reported no significant differences between the cell lines. (**n=3**).

5.2.7 Differentiated cells overexpressing GFP-α-syn-A53T, but not GFP-α-syn-WT, have alterations in neuronal morphology compared to GFP only controls

To identify whether differentiated cells overexpressing GFP-α-syn WT or GFP-α-syn-A53T exhibited any differences in neuronal morphology, measurements were taken from immunofluorescence images. Firstly, quantification of B-III-tubulin-positive neurites revealed that cells overexpressing GFP-α-syn A53T had a lower average number of neurites per cell than both GFP only control and GFP-α-syn WT cells (p=0.0337) (**Figure 108a**). GFP-α-syn A53T cells also had the lowest average primary neurite length compared to GFP only control (p=0.0489) and GFP-α-syn WT cells (p=0.0335) (**Figure 108b**). This suggests that overexpression of GFP-α-syn A53T, but not GFP-α-syn WT, impacts the ability of cells to generate and extend neurites.

I then expanded my analysis to nuclear morphology. As previously mentioned, I observed smaller and more elongated nuclei in differentiated wild-type cells compared to undifferentiated, as seen in **Figure 98**. Though there were no significant differences in nuclear measurements between the cell lines, cells overexpressing GFP-α-syn A53T exhibited both a larger average nuclear area and a lower average nuclear aspect ratio, corresponding to larger, rounder nuclei than both GFP only control and GFP-α-syn WT cells (**Figure 108c, d**). This implies that overexpression of GFP-α-syn A53T, but not GFP-α-syn WT, may impact nuclear morphology in differentiated cells.

Interestingly, I also observed that GFP was mostly seen localised to the cell bodies of cells overexpressing GFP only and GFP-α-syn-WT (**Figure 109, pink**), but GFP was present both in the cell body and in neurite projections in cells overexpressing GFP-α-syn-A53T (**Figure 109, yellow**). Together, these observations demonstrate that overexpression of GFP-α-syn A53T causes impairments in neuronal-like morphology in differentiated cells. These defects are not caused by overexpression of GFP-α-syn-WT and thus appear to be exclusive to GFP-α-syn-A53T.

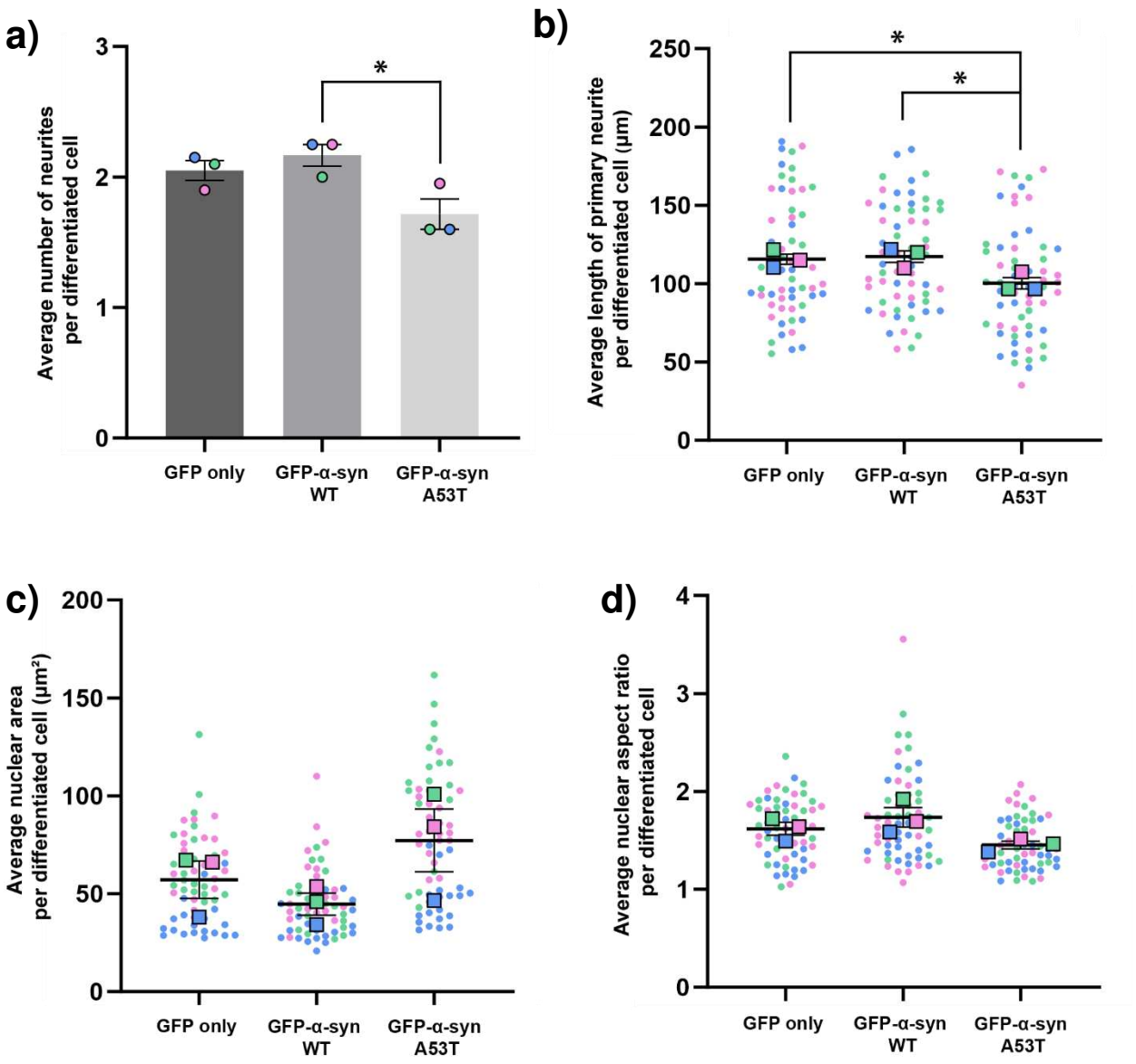

Figure 108: Overexpression of GFP-α-syn A53T reduces neurite number and primary neurite length in differentiated cells

GFP only, GFP-α-syn WT and GFP-α-syn A53T overexpressing cells were subject to a 14-day differentiation protocol and stained for B-III-tubulin and for nuclei with DAPI. Images were analysed to measure neuronal and nuclear morphology. Only GFP-positive, differentiated cells were included in this analysis, selected for by the expression of B-III-tubulin and the presence of at least one neurite as well as positive GFP staining. For all parameters, 20 cells per cell line were assessed across 3 biological repeats, shown by colour-coding. a) Shows the average number of neurites per cell. The mean of each repeat is shown by a circle, with the mean of all 3 repeats shown by a bar and the SEM shown by vertical black lines. Individual data points are not shown for clarity since data is discrete. The remaining graphs show b) average length of the primary neurite per differentiated cell, measured with NeuronJ, c) average nuclear area per cell and d) average nuclear aspect ratio per cell. In b), c) and d), individual data points are shown by circles, with the mean of each repeat represented by a square and the mean of all 3 repeats shown by a black line. SEM is shown by vertical black lines. Statistical analyses were performed using one-way ANOVAs with Tukey's multiple comparisons tests. A significant difference was seen in the average number of neurites per cell between GFP-α-syn WT and GFP-α-syn A53T cells (p=0.0337, *). GFP-α-syn A53T also exhibited a significantly shorter average primary neurite length than GFP only cells (p=0.0489, *) and GFP-α-syn WT cells (p=0.0335, *). GFP-α-syn A53T cells showed reduced nuclear aspect ratio compared to GFP-α-syn-WT but this did not reach significance (p=0.0750) (**n=3**).

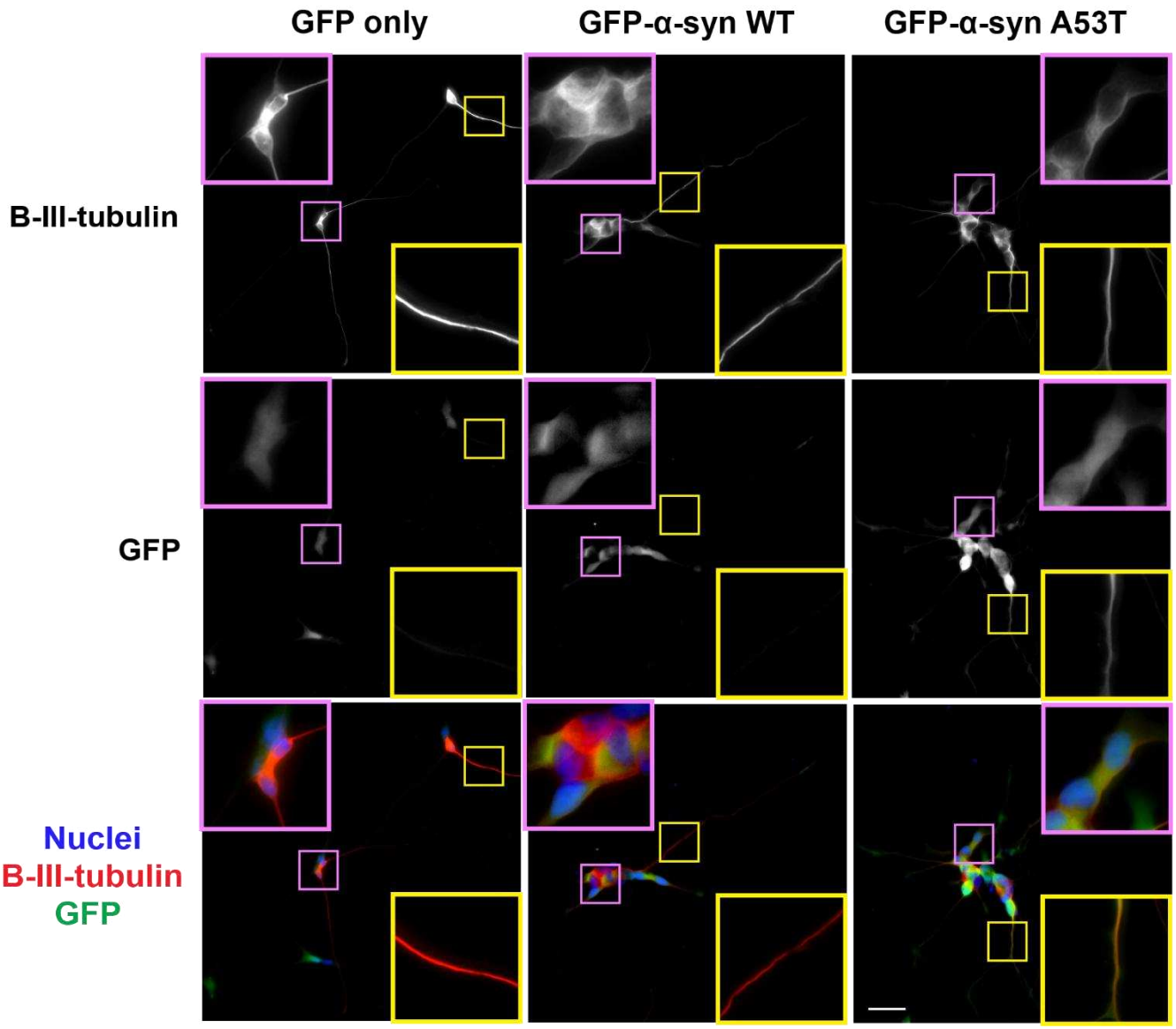

Figure 109: GFP is expressed in neurites in cells overexpressing GFP-α-syn-A53T, but not in cells overexpressing GFP only or GFP-α-syn-WT

GFP only, GFP-α-syn WT and GFP-α-syn A53T overexpressing cells were subject to a 14-day differentiation protocol before being fixed and stained by immunocytochemistry. Cells were labelled with antibodies against B-III-tubulin (red) and GFP (green) with nuclei labelled by Hoechst (blue). Examples of cell bodies (pink) and neurites (yellow) are highlighted. Images are representative and from 1 biological repeat. Images were taken by widefield immunofluorescence microscopy on a 60X objective. Scale bar = 20µm.

5.2.8 Overexpression of GFP-α-syn-A53T decreases the expression of dopaminergic markers in differentiated cells

We then investigated whether α-synuclein overexpression had any impact on the expression of neuronal and dopaminergic markers by Western blotting (**Figure 110**). Firstly, cells overexpressing GFP-α-syn WT and GFP-α-syn A53T were both able to upregulate expression of the neuronal cytoskeletal proteins B-III-tubulin and GAP43 in response to differentiation. However, differentiated cells overexpressing GFP-α-syn A53T displayed lower expression of both markers than the other cell lines (**Figure 110b, c**). Though this was not significant, this supports my morphological data which suggests that GFP-α-syn A53T overexpressing cells show less pronounced neuronal phenotypes.

Assessment of TH expression was used as a readout of dopaminergic phenotype, with the level of TH in differentiated cells overexpressing GFP-α-syn A53T significantly lower than both GFP only control ($p=0.0206$) and GFP-α-syn WT differentiated cells ($p=0.0024$) (**Figure 110d**). As such, I conclude that overexpression of GFP-α-syn A53T attenuated the dopaminergic phenotype of differentiated cells.

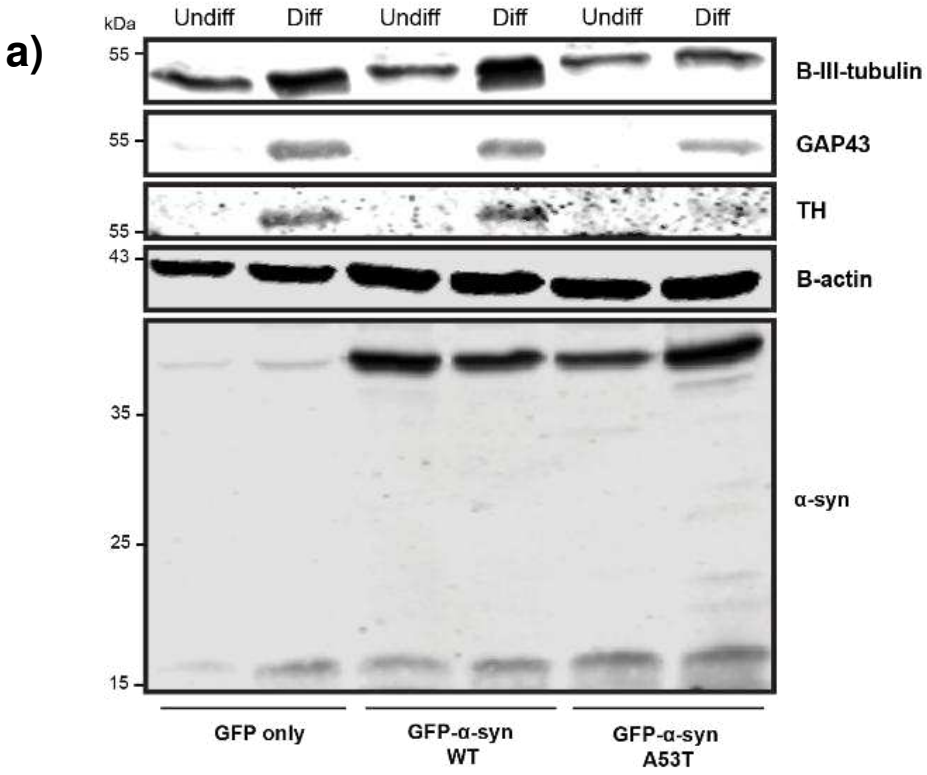
a)
kDa
Undiff
Diff
Undiff
Diff
Undiff
Diff
55
55
55
43
35
25
15
B-III-tubulin
GAP43
TH
B-actin
α-syn
GFP only
GFP-α-syn WT
GFP-α-syn A53T

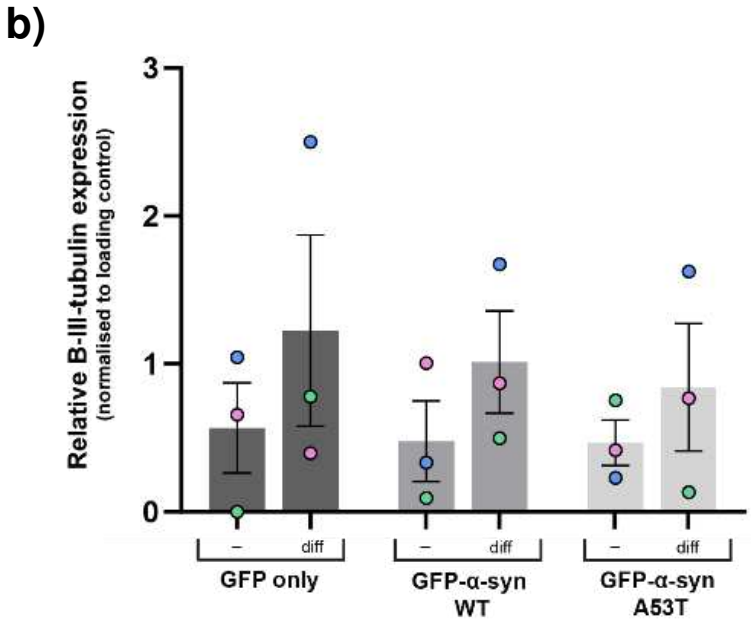
b)
Relative B-III-tubulin expression
(normalised to loading control)
3
2
1
0
–
diff
GFP only
GFP-α-syn WT
GFP-α-syn A53T

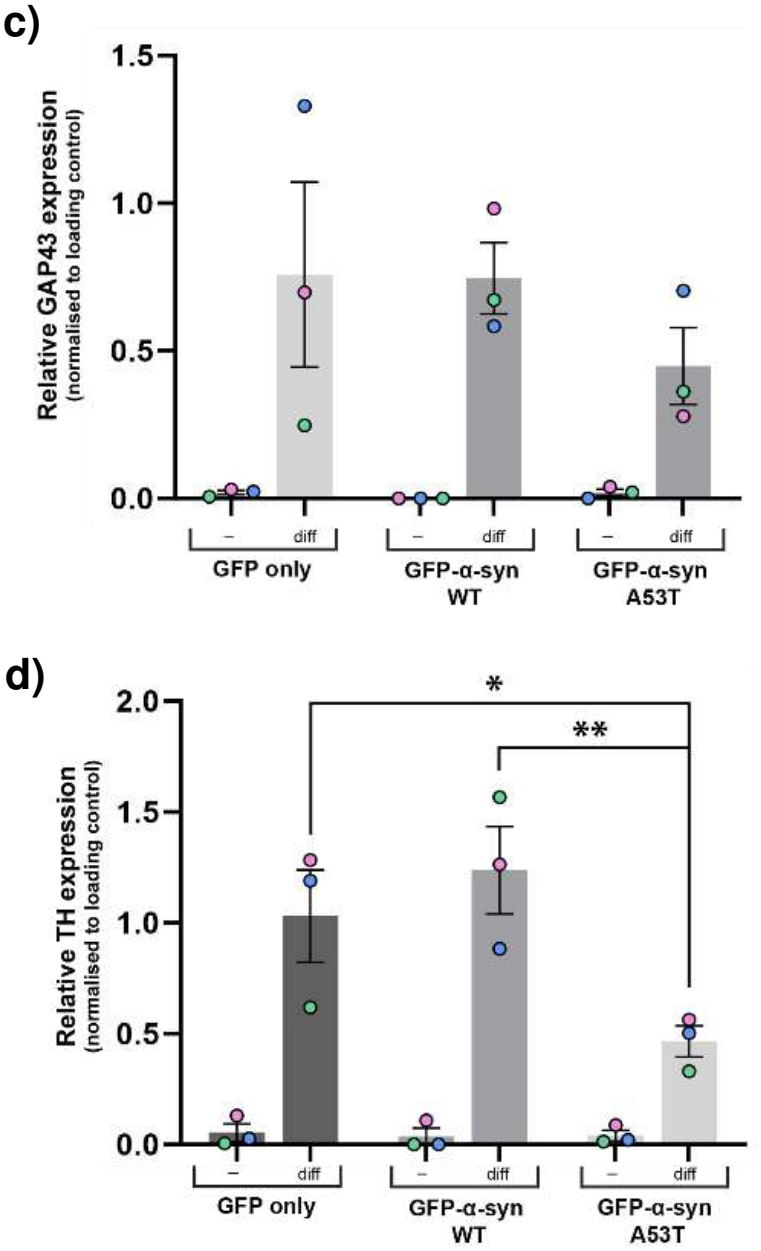

Figure 110: Overexpression of GFP-α-syn A53T reduces expression of neuronal and dopaminergic markers

GFP only, GFP-α-syn WT and GFP-α-syn A53T cells were subject to a 14-day differentiation protocol. Lysates from undifferentiated and differentiated cells were processed for Western blot with antibodies against B-III-tubulin, GAP43 and TH, with B-actin as a loading control and α-synuclein to verify overexpression of the GFP-α-syn constructs. a) is a representative blot from 1 biological repeat. Graphs show protein expression of b) B-III-tubulin, c) GAP43 and d) TH. Expression of each was normalised to B-actin to account for differences in protein loading, with relative expression shown by the raw values of these calculations. Biological replicates are colour coded with circles representing the means of each repeat, bars representing the mean of the 3 repeats and black lines showing SEM. Statistical analyses were performed by 2-way ANOVAs with Sídák's multiple comparisons tests. Significant differences were indicated for TH expression, with differentiated GFP-α-syn A53T cells expressing significantly less TH than differentiated GFP only cells (p=0.0206, *) and GFP-α-syn WT cells (p=0.0024, **). (**n=3**).

5.2.9 Organisation of the mitochondrial network changes in response to differentiation SH-SY5Y cells

Once I had established how differentiation was impacted by α-synuclein loss- and gain-of-function, I began to investigate mitochondria in neuronal-type cells. I investigated this in differentiated wild-type cells as a basis using immunofluorescence staining with B-III-tubulin alongside the mitochondrial marker, cytochrome c, enabled qualitative observations to be made. Since not every cell in a given field of view was differentiated, this enabled a direct comparison between mitochondria in undifferentiated and differentiated cells. Undifferentiated cells exhibited filamentous mitochondrial networks with well-connected organelles in the perinuclear region (**Figure 111, yellow**). In differentiated cells, mitochondria localised close to the nucleus displayed extremely bright cytochrome c signal, implying that mitochondria were condensed. This made observations about the filamentous nature of the network extremely difficult to make, though mitochondria were not obviously fragmented. In addition to this mitochondrial population, mitochondria were also present within neurites. B-III-tubulin-rich projections from the cell body often contained mitochondria, which were enriched at the very tips of neurites (**Figure 111, pink**). This suggested that differentiated SH-SY5Y cells exhibit a switch in mitochondrial organisation to metabolically support the cells' neuronal architecture. This further confirms that differentiated SH-SY5Y cells are more representative of human dopaminergic neurons.

Unfortunately, the nature of the cytochrome c signal in differentiated cells, even at higher magnification, meant that it was not possible to quantify changes to the mitochondrial network. The analysis workflow used previously (chapters 1 and 2) was unable discriminate between mitochondrial fragments in differentiated cells, meaning that only qualitative observations could be made (**Appendix B**, **Figure 128**).

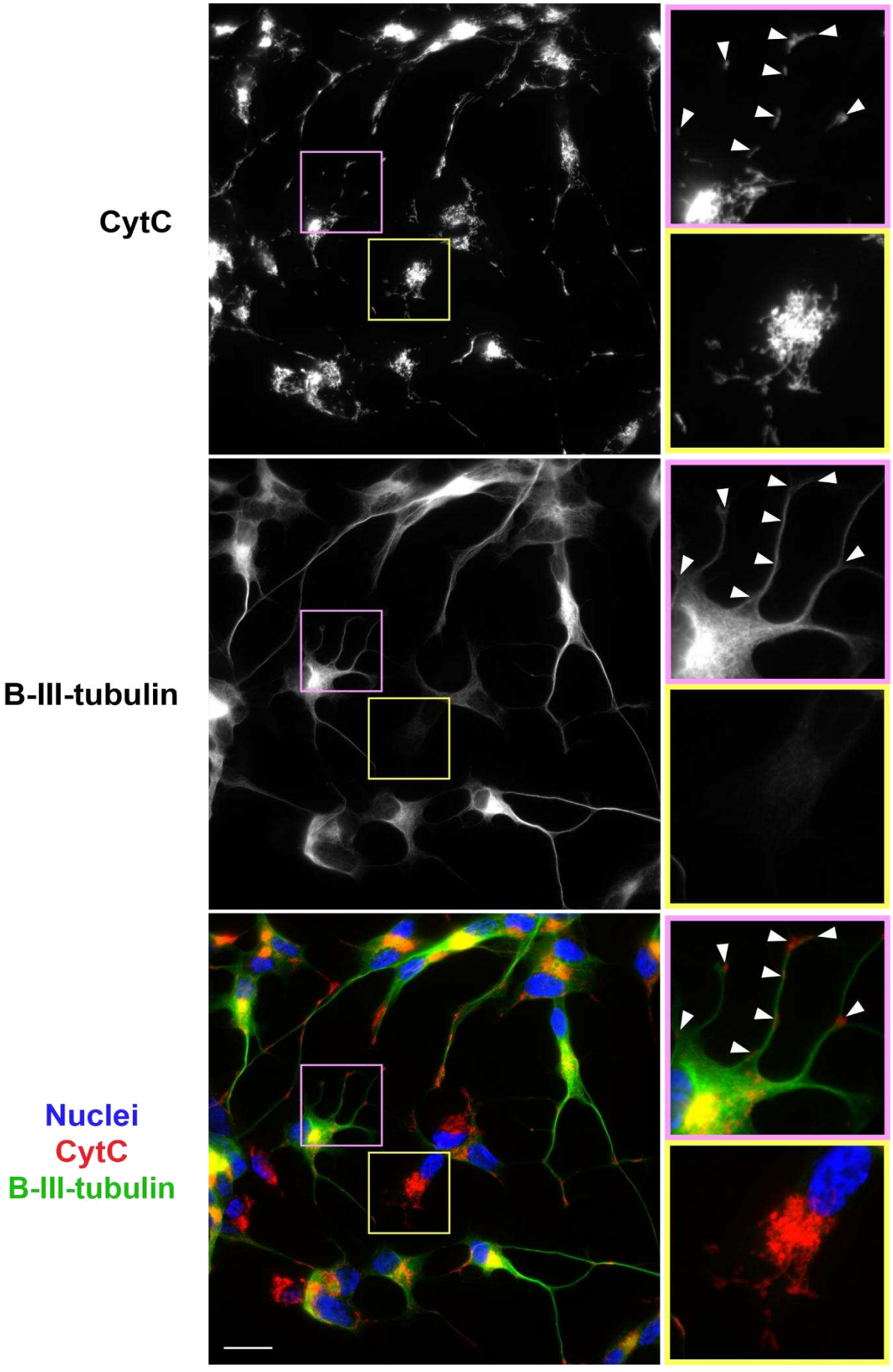
CytC
B-III-tubulin
Nuclei
CytC
B-III-tubulin

Figure 111: Differentiated SH-SY5Y cells have mitochondria localised in both the soma and neurites

Wild-type SH-SY5Y cells were subject to a 14-day differentiation protocol before being fixed and stained by immunocytochemistry. Cells were labelled with antibodies against B-III-tubulin (green) and cytochrome c (red), with nuclei labelled by Hoechst (blue). An example of a differentiated cell, identified by neurites with positive B-III-tubulin staining, is highlighted in pink. White arrow heads signify mitochondria present within neurites. An example of an undifferentiated cell, identified by negative B-III-tubulin staining, is highlighted in yellow. Representative images were taken using widefield immunofluorescence microscopy with a 60X objective. Scale bar = 20µm.

5.2.10 SH-SY5Y cells are more susceptible to mitochondrial damage when differentiated

Literature suggests that an increased energy burden makes human dopaminergic neurons more susceptible to oxidative stress in PD (Bolam & Pissadaki, 2012). Given that the altered distribution of mitochondria observed in differentiated cells implied a switch in the metabolic pressure experienced by mitochondria, I aimed to investigate whether this impacted responses to mitochondrial damage in my model. In previous work, we have shown that A/O can be used to induce a mitochondrial damage response. In undifferentiated SH-SY5Y cells, treatment with 5µm antimycin A and 10µm oligomycin triggers mitophagy, measurable by a reduction in CoxII that reflects whole mitochondrial clearance. When the same concentrations of A/O were applied to differentiated cells for 24 hours, visualisation with brightfield microscopy revealed that the cells were mostly dead and thus, their mitochondrial damage response could not be assessed by Western blotting (**Figure 112**). However, the observation that the level of A/O that induces mitophagy in undifferentiated cells causes death in differentiated cells did allow me to conclude that differentiated cells are more susceptible to mitochondrial damage.

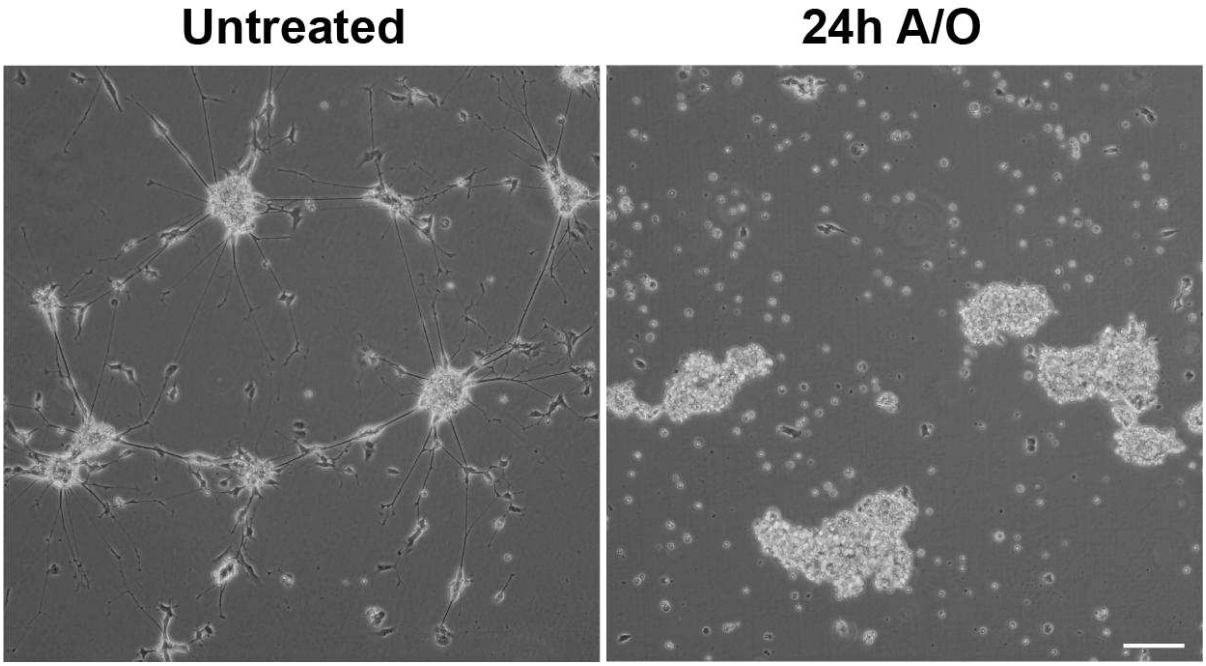

Figure 112: SH-SY5Y cells are more susceptible to mitochondrial damage when differentiated

Wild-type SH-SY5Y cells were subject to a 14-day differentiation protocol. On day 14, cells were treated for 24 hours with A/O at a concentration known to induce mitophagy in undifferentiated cells: 5µm antimycin A and 10µm oligomycin. Images are representative and from one biological repeat. Images were captured using a light microscope with a 10X objective. Scale bar = 100µm. (**n=2**).

5.3 Discussion

In this chapter, I aimed to optimise and validate a protocol for differentiating SH-SY5Y cells and investigate how neuronal phenotypes were affected by perturbations in α-synuclein. Though the impacts of α-synuclein have been well-investigated in mature adult neurons, its influence on immature neurons and the process of neuronal development is less known (Burré, 2015; Murphy et al., 2000; Raghavan et al., 2004). To explore this, I subjected SNCA KO cells and cells overexpressing GFP-α-syn-WT and GFP-α-syn-A53T to my differentiation protocol and assessed whether these exhibited measurable changes in neuronal morphology and expression of neuronal and dopaminergic markers compared to controls. I reported that loss of α-synuclein reduces the number of cells with a neuronal phenotype, but subtly increases expression of the dopamine precursor, TH. Alongside this, I show that overexpression of GFP-α-syn-A53T attenuates neuronal morphology and reduces expression of TH in differentiated cells.

Firstly, I validated a differentiation protocol using wild-type SH-SY5Y cells and established quantifiable measures that could be used to indicate neuronal phenotype. A range of SH-SY5Y differentiation methods have been published, describing the exposure of cells to various combinations of growth factors over a period of 3 days to 3 weeks (Encinas et al., 2000; Kovalevich & Langford, 2013; Presgraves et al., 2004; Shipley et al., 2016; Simões et al., 2021). I optimised a protocol based on Shipley et al (2016), utilising a combination of RA and BDNF across a 14-day period to ensure enough time for cells to exhibit clear neuronal architecture. I found that this method induced measurable changes in morphology, with differentiated cells exhibiting reduced nuclear size and long neurites rich in the neuronal marker, B-III-tubulin. Alongside this, cells upregulated expression of B-III-tubulin and the growth cone marker, GAP43, measured biochemically by Western blot. I also reported an increase in TH, suggesting that differentiated cells have dopaminergic characteristics. Though I cannot confirm whether cells created active synapses, this does indicate that differentiated cells upregulate machinery involved in dopaminergic transmission. Once I had established a reliable protocol for generating SH-SY5Y cells of a consistent neuronal phenotype, I applied this to my α-synuclein cell models: SNCA KO cells and cells overexpressing either GFP-α-syn-WT or GFP-α-syn-A53T. I considered that differentiated SH-SY5Y cells provide an environment in which α-synuclein may have a more physiologically relevant role compared to undifferentiated cells, since its primary functions have been characterised in the regulation of neuronal transmission and plasticity (Burré, 2015; Cheng et al., 2011; Gao et al., 2023; Lautenschläger et al., 2018). A key advantage of the differentiation system is that it not only better represents a neuronal system, but it provides a window into neuronal development and thus the opportunity to investigate how genetic manipulation of α-synuclein may impact this process.

Next, I assessed whether α-synuclein loss-of-function altered neuronal phenotypes in differentiated SH-SY5Y cells. Studies investigating α-synuclein expression throughout human and murine lifetimes have revealed that peak α-synuclein expression occurs early on in development during gestation, leading to suggestions that it may have a physiological role in neuronal differentiation and maturation (Alejandra Morato Torres et al., 2020; Raghavan et al., 2004). I found that the majority of SNCA KO cells expressed neuronal B-III-tubulin and exhibited neuronal morphology after undergoing the 14-day protocol, indicating that α-synuclein is not required for generation of a neuronal phenotype. However, approximately 70% of cells were considered differentiated in SNCA KO populations compared to 80% in EV controls, implying that a lack of α-synuclein did impact the differentiation capacity in a subset of cells. Interestingly, α-synuclein has been suggested to have a role in the regulation of developmental gene expression and chromatin remodelling (Nakamura et al., 2024; Prahl et al., 2022). For example, interactome analysis recently revealed an association between α-synuclein and the BRG-1 associated factor (BAF) complex, a neuron-specific chromatin remodelling complex important for regulating expression of genes important for neuronal development (Choi et al., 2015; Nakamura et al., 2024). This study suggested that α-synuclein is able to co-operate in neuronal differentiation of SH-SY5Y cells by this interaction, so loss of this interaction may explain the impact on differentiation seen in my model (Nakamura et al., 2024). In support of this nuclear role, studies have suggested that α-synuclein is able to bind RA, translocate to the nucleus and enhance the transcription of early neuronal genes (Davidi et al., 2020). Lack of this nuclear function in the absence of α-synuclein could explain the reduced differentiation capacity seen in these cells.

Studies have shown that α-synuclein is redistributed from the nucleus to the neurites over the course of neuronal development (Courte et al., 2020). This suggests that α-synuclein may reside in the nucleus to carry out regulation of developmental genes in immature neurons and then traffic to the neurites as neurons become more mature, primed for its synaptic role in mature neurons. Localisation of α-synuclein in differentiating neurons could not be assessed due to the limited specificity of antibodies against endogenous α-synuclein, but this would be important to investigate using other methods. It is not clear why the lack of α-synuclein only impacts differentiation in a small subset of cells, though it could be due to compensation of α-synuclein function by β-synuclein, which has similar properties to α-synuclein and has also been linked to neuronal development (Hayashi & Carver, 2022; Sriwimol & Limprasert, 2018). Alternatively, differentiation capacity may have been impacted by other characteristics that differ throughout populations of undifferentiated SH-SY5Y cells, including morphology, health, cell-cell contacts and cell cycle stage.

In cells subject to differentiation, I observed a subtle reduction in the expression of neuronal markers, B-III-tubulin and GAP43, in SNCA KO cells compared to EV controls. Since this was measured biochemically by Western blotting, lysates captured the entire cellular population, encompassing cells that remained undifferentiated. As such, the reduction in neuronal markers can be explained by the reduced proportion of differentiated cells in the SNCA KO population. Despite having approximately 10% less cells of a neuronal phenotype, SNCA KO cells expressed higher expression of the dopamine precursor, TH, than EV controls. This suggested that in differentiated cells, α-synuclein may have a role in regulation of dopamine synthesis. Previous literature has demonstrated that α-synuclein can act as a downregulator of TH, stimulating protein phosphatase 2A (PP2A) which in turn dephosphorylates TH and reduces its activity (Hua et al., 2015; X. M. Peng et al., 2005; Perez et al., 2002a). This has been shown to be exaggerated in the context of gain-of-function, but these studies only observe differences in TH activity rather than expression. Based on data from my loss-of-function environment, I suggest that physiological α-synuclein may be able to modulate TH expression as well as activity.

A relationship between α-synuclein and PP2A may also explain some phenotypes observed in the context of α-synuclein overexpression. Differentiated cells overexpressing GFP-α-syn-A53T exhibit less pronounced neuronal morphology, with less, shorter neurites and larger nuclei compared to GFP only and GFP-α-syn-WT overexpressing cells. Accordingly, differentiated cells overexpressing α-synuclein-A53T also expressed a slightly lower level of the growth cone marker GAP43, likely reflecting the lower number of neurites. Previous research has shown that primary neurons from mouse models of α-synuclein A53T overexpression also had less, shorter neurites, which was demonstrated to be the result of an impact on GSK3β and β-catenin facilitated by an α-synuclein-PP2A interaction (Kim et al., 2018). This mechanism was confirmed by the fact that the decrease in neurite length was rescued by the PP2A inhibitor, okadaic acid (S. Kim et al., 2018). Upon differentiation with RA, GSK3β is rendered inactive and unable to phosphorylate proteins to target them for degradation by the UPS (Castelo-Branco et al., 2004). One of its substrates, β-catenin, is able to accumulate in the cytoplasm, enter the nucleus and upregulate expression of neuronal genes (Castelo-Branco et al., 2004; Kim et al., 2018). However, in cells overexpressing α-synuclein A53T, this process was shown to be impaired due to α-synuclein-induced increase in PP2A (Kim et al., 2018). PP2A can activate GSK3β, enabling it to phosphorylate and signal the degradation of β-catenin (Il Lee et al., 2005; Zhou et al., 2009). The authors suggest the lack of β-catenin available to upregulate neuronal genes is a result of the association between α-synuclein and PP2A (Kim et al., 2018). The excess of α-synuclein in my model may have upregulated PP2A in this way, explaining the reduction in neurite length. Interestingly, I only observed this phenotype in cells overexpressing GFP-α-syn-

A53T and not GFP-α-syn-WT, suggesting that the two forms of α-synuclein may not modulate PP2A in the same way. Another factor that influences the PP2A system is oxidative stress, with increasing evidence suggesting that PP2A signalling can be influenced and mediated by ROS (Elgenaidi & Spiers, 2019). It is possible that overexpression of GFP-α-syn-A53T causes more oxidative stress in the system compared to overexpression of GFP-α-syn-WT due to differences in aggregated species, which differentially impact the regulation of PP2A and therefore neuronal characteristics.

In line with the hypothesis that GFP-α-syn-A53T may induce more oxidative stress, studies investigating neuronal development in primary human progenitor cells have shown that α-synuclein A53T is acutely toxic, with higher rates of cell death than cells overexpressing wild-type α-synuclein or controls (Schneider et al., 2007). Reduced viability of cells overexpressing α-synuclein has been shown to be recovered by use of antioxidant drugs, suggesting that α-synuclein-induced oxidative stress may be directly responsible for this (B. Kumar et al., 2005). It would be important to measure cellular ROS alongside cytotoxicity throughout the differentiation process in future, to establish whether α-synuclein overexpression is impacting levels of oxidative stress, and to identify whether this appears to correlate with both neuronal phenotypes and cell survival. Since I did not quantify cell death during the differentiation process, it is possible that the most pathogenic cells with the highest levels of α-synuclein overexpression, aggregation and oxidative stress were killed during the differentiation process and therefore only less pathogenic cells were left behind to reach a neuronal phenotype. Interestingly, one study has suggested using an inducible α-synuclein overexpression system to circumvent this potential problem (Vasquez et al., 2018). The authors describe a doxycycline-induced tetracycline-controlled transcriptional activation system (Tet-On) which enables wild-type SH-SY5Y cells to be terminally differentiated into neurons prior to the induction of α-synuclein overexpression (Vasquez et al., 2018). This has been suggested as an advantageous method for the study of PD, since it enables the impact of pathological α-synuclein on healthy neuronal cells to be assessed. Arguably, considering how perturbations in α-synuclein impact the differentiation process is an important aspect of neuronal phenotype that should not be completely discounted, since many patients with familial PD experience changes or mutations to the SNCA gene that start from birth, and thus are present throughout neuronal development (Byers et al., 2011; Oliveira et al., 2015; Siddiqui et al., 2016; Zafar et al., 2018). Induced pluripotent stem cell (iPSC) models have shown this, with cells from patients with a triplication of the SNCA gene resulting in excess α-synuclein expression shown to have impaired neuronal differentiation and maturation that may impact cell health throughout the patients' life (Oliveira et al., 2015).

An alternative explanation for the disparity in neuronal morphology between cells overexpressing GFP-α-syn-WT and GFP-α-syn-A53T could be that the two proteins have different structural preferences which can impact their interaction with other cellular components. It has been suggested that α-synuclein harbouring the A53T mutation prefers to generate a β-sheet conformation rather than an α-helix, resulting in reduced membrane binding (Jo et al., 2000). Since less α-synuclein A53T may be bound to membranes, more may be available in the cytosol to be intracellularly trafficked. Indeed, I did observe GFP-α-syn in the neurites of cells overexpressing GFP-α-syn-A53T, which was not seen in GFP only controls or GFP-α-syn-WT cells. It could be that due to structural differences, GFP-α-syn-A53T is less readily sequestered in the nucleus and thus is less able to bind RA and regulate transcription of neurodevelopmental genes, resulting in an attenuated neuronal phenotype (Nakamura et al., 2024; Prahl et al., 2022). Alternatively, the differences in morphology could relate to the relationship between α-synuclein and cytoskeletal proteins. Reorganisation of the cytoskeleton is a key stage required for differentiation of SH-SY5Y cells that directly facilitates growth cone formation and neurite outgrowth, and it has been suggested that α-synuclein has a physiological association with microtubules that may impact this (Mazzetti et al., 2023). It has been suggested that mutant forms of α-synuclein have a compromised ability to bind microtubules in neuronal cells, so an altered cytoskeletal network as a result of this may explain the difference in neurite length between cells overexpressing GFP-α-syn-WT and GFP-α-syn-A53T.

In terms of dopaminergic phenotype, GFP-α-syn-A53T overexpressing cells also expressed significantly lower levels of TH compared to both GFP only controls and cells overexpressing GFP-α-syn-WT. Though this could again relate to a relationship between α-synuclein and PP2A, pathological α-synuclein has also been shown to directly interfere with CREB signalling – a key pathway of transcription factors that increase expression of neuronal genes, including TH (Kim et al., 2011). It was found that α-synuclein overexpression did not impact baseline levels of TH in these cells, it suppressed upregulation of TH in response to the cAMP signalling activator, forskolin (Kim et al., 2011). Though this study was performed in human neuroblastoma cells, it was not in the context of neuronal differentiation (Kim et al., 2011). As such, I cannot be sure whether the same signalling pathways that upregulated TH in response to forskolin would be activated in response to differentiation. In addition, structural analysis of α-synuclein has recently revealed that it can directly enfold both TH and dopamine-β-hydroxylase, suggesting it is able to reduce synthesis of dopamine and noradrenaline (Lehrer & Rheinstein, 2022). This was investigated in the context of monomeric α-synuclein rather than aggregated species, making this study more relevant to my overexpression model which likely results in an excess of monomers with a smaller pool of aggregated α-synuclein (Lehrer & Rheinstein, 2022). However, the most likely conformations described in this study all suggest

that TH docks at the N-terminus of α-synuclein, which in my overexpression models has a GFP tag attached that may interfere with binding (Lehrer & Rheinstein, 2022). The impacts on TH level seen in both of my loss- and gain-of-function models provide good support for the relationship between α-synuclein and dopamine regulation that has been suggested in the literature (Kim et al., 2014; Kim et al., 2011; Perez et al., 2002; Yu et al., 2004).

Once I had established differentiation of SH-SY5Y cells as a neuronal model in our lab and investigated the impact of perturbations in α-synuclein, I started to characterise how mitochondria in wild-type differentiated cells were impacted by neuronal phenotype as a foundation for future investigations in mito-QC. In undifferentiated cells mitochondria appear flat, spread out in a clear network and take up at least 50% of the cell. I found that mitochondrial distribution was visibly altered in differentiated cells, with the majority concentrated in the small cell body forming a tight bundle. Interestingly, some mitochondria were seen localised to neurites, particularly at the tips of growing projections. Unfortunately, the nature of the mitochondrial network could not be quantified in differentiated cells, due to the extremely dense nature of mitochondria throughout shrunken cell bodies that could not be defined into individual segments with current image analysis workflows. Despite this, qualitative observations indicated that the morphological change experienced as cells take on a neuronal phenotype is accompanied by a switch in metabolic requirements (Bolam & Pissadaki, 2012). Mitochondria in differentiated cells are not only responsible for producing ATP to facilitate cellular reactions, but also to fuel the extension of projections and the trafficking of cellular components along these neurites. This indicated that, as in the human neurons degenerated in PD, these mitochondria may be experiencing more metabolic pressure and thus may be more sensitive to oxidative stress (Bolam & Pissadaki, 2012). This vulnerability was confirmed when differentiated cells were exposed to mitochondrial damage, since the concentration of A/O used to evoke mitophagy in undifferentiated cells resulted in death. As such, I considered that differentiated SH-SY5Y cells would provide a useful neuronal background in which to investigate mito-QC. However, assessment of mitochondrial phenotypes proved difficult. As well as difficulty with imaging mitochondria in differentiated cells by immunofluorescence microscopy, functional analysis of differentiated cells by an ATP assay or Seahorse mito-stress test was not possible due to the mismatch between the cell plating densities required for the experiments and for cells to successfully differentiate. Investigations into mito-QC in these cells would be valuable, but would require careful optimisation of imaging protocols, development of new image analysis workflows and the employment of alternative techniques such as qPCR.

Summary

To summarise, this work optimises and validates a protocol for the differentiation of SH-SY5Y cells into those of a neuronal, dopaminergic phenotype and investigates how this process is impacted by perturbations in α-synuclein. It also sets up this system as a suitable neuronal model in which to investigate the impacts of altered α-synuclein expression on mitochondrial function and quality control. Firstly, loss of α-synuclein reduced the proportion of cells that differentiated but did not impact the neuronal morphology of those which did exhibit a neuronal phenotype. However, lack of α-synuclein did subtly increase overall expression of the dopamine precursor TH in differentiated cells, which I suggest could be the result of the loss of an interaction between α-synuclein and PP2A. In terms of investigating the potential toxic gain-of-function of α-synuclein on neuronal differentiation, I found that cells overexpressing GFP-α-syn-WT had no observable phenotypes. On the other hand, cells overexpressing GFP-α-syn-A53T did still differentiate, but had less exaggerated neuronal morphology. I suggest that this could also be the result of an association between α-synuclein A53T and PP2A, which may be further modulated by oxidative stress. In addition, cells overexpressing α-synuclein A53T exhibited a significant reduction in TH, which I propose may be due to the direct ability for α-synuclein to regulate upregulation of TH gene expression in the nucleus. I also find that in wild-type cells, mitochondrial distribution is altered upon differentiation and that differentiated cells are more susceptible to mitochondrial damage. These findings support the model of differentiated SH-SY5Y cells as being valuable to investigate mitochondrial health and quality control, though considerable optimisation is needed to enable the same thorough level of investigation undertaken in undifferentiated cells.

Chapter 6 General discussion

Table 19: Summary of key phenotypes found in α-synuclein loss- and gain-of-function models over the course of this study

	SNCA KO	GFP-α-syn-WT	GFP-α-syn-A53T
Mitochondrial function	No phenotype	No phenotype	No phenotype
Mitochondrial dynamics	No phenotype	Increased fragmentation at steady state	Increased fragmentation at steady state
OMM-derived MDVs	No phenotype	More MDVs at steady state	More MDVs at steady state
IMM-derived MDVs	No phenotype	No damage-induced upregulation of MDVs	No damage-induced upregulation of MDVs
Whole mitochondrial clearance	No phenotype	No phenotype	No phenotype
Autophagosomes	Increased autophagic flux	No phenotype	Less autophagosomes
Lysosomes	No phenotype	No phenotype	No phenotype
Neuronal phenotype	No phenotype	No phenotype	Reduced neuronal morphology
Dopaminergic phenotype	No phenotype	No phenotype	Reduced TH

Both α-synuclein pathology and dysfunctional mito-QC have been well-established as key drivers of PD, but there is a lack of research on the relationship between them. Though α-synuclein has been shown to localise to mitochondria, bind membranes and incite mitochondrial dysfunction in a pathological context, limited work has investigated the association between α-synuclein and mitochondria under physiological conditions (M. L. Choi et al., 2022; Devi et al., 2008; Hegde et al., 2024; Ludtmann et al., 2018; X. Wang et al., 2019). Better understanding of this physiological relationship would provide valuable insight into PD pathogenesis (Thorne & Tumbarello, 2022). In particular, it would enable us to elucidate whether dysfunctional mito-QC in PD could result from loss-of-function of physiological α-synuclein rather than exclusively attributed to gain-of-function of pathological α-synuclein. Development of an α-synuclein loss-of-function model in mammalian cells enabled me to address this question. I found that lack of α-synuclein had limited impact on both mitochondrial respiratory function and responses to mitochondrial damage, indicating that α-synuclein does not have physiological roles in ATP production or in regulating mito-QC. Therefore, I propose that dysfunctional mitochondrial phenotypes in PD are likely not due to α-synuclein loss-of-function. These findings provide novel insight into α-synuclein's function and suggest that α-synuclein does not readily associate with mitochondria in a regulatory capacity. The primary study that has previously defined a potential functional relationship between monomeric α-synuclein and mitochondria in modulation of the ATP synthase pump did not investigate this in the context of endogenous α-synuclein; knockout models were exposed to exogenous α-synuclein species (Ludtmann et al., 2016). Though an association between α-synuclein and mitochondria may be possible, my data leads me to consider that it may not occur at physiological α-synuclein concentrations. Instead, I provide evidence that α-synuclein may modulate some elements of mito-QC through its activity in the cytosol. For example, I observe that loss of α-synuclein evokes an increase in Parkin expression at steady state, suggesting that α-synuclein may have a physiological role in Parkin regulation. This has been proposed to occur in pathological circumstances through α-synuclein-induced Parkin PTMs that result in its proteasomal degradation (Wilkaniec et al., 2019, 2021; Yao et al., 2004). In addition, lack of α-synuclein was seen to increase autophagic flux but did not impact whole mitochondrial clearance. This suggests that α-synuclein's ability to influence autophagosomes is not specific to mitochondrial degradation. Together, these data indicate that α-synuclein is not required for mito-QC, but its ability to modulate mito-QC mechanisms likely occurs outside of a direct interaction with mitochondria. To rule out a physiological association between α-synuclein and mitochondria, it would be important to specifically investigate interactions between them. Unfortunately, I was unable to explore this in my model due to antibody limitations. Though improved detection of endogenous α-synuclein by immunofluorescence microscopy would enable us to establish whether α-synuclein localises to mitochondrial networks under

physiological conditions, alternative methods such as protein-protein interaction assays may provide more detailed insight. Though many of these assays require exogenous application of a bait protein or artificial overexpression of a protein of interest, a recently developed system called Endobind circumvents these issues by using CRISPR knockin to tag endogenously expressed proteins (Bill et al., 2021; Rao et al., 2014). Accordingly, a system such as this would aid in characterising the relationship between α-synuclein and mitochondria in a physiological context.

Though the disease relevance of pathological α-synuclein has meant that it is better characterised than physiological α-synuclein, how it induces cytotoxicity and neuronal death is still poorly understood. Associations between aggregated α-synuclein and mitochondrial membranes have been shown to cause mitochondrial dysfunction and are suggested to be a potential driver of PD pathology (M. L. Choi et al., 2022; Hegde et al., 2024; Ludtmann et al., 2016; K. Nakamura et al., 2008; X. Wang et al., 2019). Recent work has even demonstrated that mitochondria represent a site of pathological structural conversion for α-synuclein, with formation of toxic oligomeric species at mitochondria shown to act as a seed for further aggregation (M. L. Choi et al., 2022). My study investigated this in the context of mito-QC, providing novel insight into how pathological α-synuclein impacts responses to mitochondrial damage. I found that overexpression of either GFP-α-syn-WT or GFP-α-syn-A53T did not impact mitochondrial function or whole mitochondrial clearance. This is in contrast to previous data showing that α-synuclein impacts both ATP production and mitophagy. However, there is no general consensus on the directionality of the relationship between α-synuclein and mitophagy. Several studies report that pathological α-synuclein causes a delay in mitophagy (Hsieh et al., 2016; Kinnart et al., 2024; Shaltouki et al., 2018; Wilkaniec et al., 2019), while others describe an increase in mitophagy (Chinta et al., 2010; Hui et al., 2024; Krzystek et al., 2021; Lurette et al., 2023).

In my study, the comparative lack of α-synuclein-induced changes compared to those reported in the literature led me to consider that α-synuclein's capacity to impact mitochondrial health may be conformation- and aggregation-dependent. Using super-resolution microscopy, it has been estimated that α-synuclein forms stable fibrils at a size of approximately 70 monomers (Sanchez et al., 2021). In SH-SY5Y cells overexpressing α-synuclein, the doubling time of α-synuclein has been calculated as 5 hours, meaning it would take approximately 32 hours for a single monomer to reach this stable fibrillar state (Sanchez et al., 2021; J. C. Sang et al., 2021). However, this was calculated upon triggering of aggregation by an external factor: the addition of exogenous α-synuclein species. The schema of α-synuclein misfolding in the absence of such a trigger has not been described in SH-SY5Y cells, suggesting that overexpression alone of α-synuclein does not induce detectable aggregates within an

experimental time window of 24-72 hours. This is supported by the fact that studies which do use an external trigger of aggregation often use overexpression of α-synuclein alone as a non-aggregatory control (Hasegawa et al., 2004; Lurette et al., 2023; Vasquez et al., 2018). Though I visualised potential aggregates in my models by immunofluorescence, I was unable to confirm their size or compostion and thus cannot be sure of their structural nature or how much of the total α-synuclein pool they represented. As such, my model cannot be said to be aggregatory. Several studies that have described direct interactions between α-synuclein and mitochondria have confirmed measurable α-synuclein aggregation, leading me to suggest that alterations in mitophagy and energy production may only occur in response to aggregated α-synuclein species (M. L. Choi et al., 2022; Ludtmann et al., 2018). Further work is needed to establish the specific conditions under which pathological α-synuclein localises to mitochondria. Elucidating whether this association is dependent specific structural characteristics of α-synuclein would be important to better define this. One method that could help clarify this is the use of inducible aggregation models; an optogenetic system where α-synuclein is overexpressed and can be artificially triggered to aggregate (Lurette et al., 2023; Vasquez et al., 2018). This would enable discrimination between mitochondrial phenotypes caused by excess α-synuclein regardless of aggregation, and phenotypes that occur as a direct result of aggregated species.

Interestingly, I did observe pathological impacts of α-synuclein on the mitochondrial network. Since α-synuclein overexpression was shown to induce mitochondrial fragmentation and increase the number of OMM-derived MDVs at steady state, I propose that pathological α-synuclein does have an impact on mitochondrial health. Specifically, I suggest that α-synuclein overexpression alters baseline mito-QC rather than responses to accumulated mitochondrial damage. Since α-synuclein loss-of-function did not impact organisation of the mitochondrial network or OMM-derived MDVs in my study, I confirm that these effects are due to a gain-of-function effect due to α-synuclein overexpression. A range of studies have shown that pathological α-synuclein can influence mitochondrial dynamics, with some suggesting this occurs through direct binding between α-synuclein and the mitochondrial membrane (Kamp et al., 2010; K. Nakamura et al., 2011). Alternatively, several papers have described interactions between pathological α-synuclein and key molecular players involved in co-ordinating fission/fusion activity, such as Drp1 and Miro (Gui et al., 2012; Hsieh et al., 2016; Krzystek et al., 2021). However, since I only see an impact of pathological α-synuclein on steady state mito-QC, I suggest that α-synuclein may act in a more indirect way. Previous research has shown that α-synuclein overexpression augments oxidative stress in human neuroblastoma cells, measured by greater levels of ROS (Parihar et al., 2009). I consider that increased ROS induced by α-synuclein may explain the increase in mitochondrial fragmentation and OMM-derived MDV generation in my model as mitochondria attempt to respond to this increase in oxidative stress.

This could be confirmed using one of several tools that have been developed to enable visualisation of ROS in real-time using live imaging, such as CellROX™ for cellular oxidative stress and MitoSOX™ for mitochondrial superoxide species (Habibalahi et al., 2020; Kauffman et al., 2016). In addition to these impacts at steady state, I also see that overexpression of α-synuclein prevents upregulation of IMM-derived MDVs in response to short exposure to mitochondrial damage inducers. Since no impact on MDVs was observed in my loss-of-function model, I again suggest that this is due to pathological α-synuclein gain-of-function. As a recently described phenomenon, the mechanisms of MDV biogenesis and trafficking are not well understood (Soubannier et al., 2012a; Sugiura et al., 2014). For example, though MDVs were originally described to be completely independent of Drp1, this has recently been reevaluated and they are now thought to be Drp1-dependent (König et al., 2021; Sugiura et al., 2014). Further characterisation of this pathway and the molecular players that facilitate it will aid understanding of how α-synuclein may interfere with damage-induced IMM-derived MDVs.

Interestingly, both α-synuclein loss-of-function and α-synuclein overexpression resulted in changes in autophagosome number. Lack of α-synuclein resulted in an early increase in autophagic flux, which suggested that α-synuclein may have a physiological role in regulating this. However, overexpression of GFP-α-syn-A53T caused a reduction in autophagosomes in response to accumulated damage. Since this phenotype was opposite to the one induced by loss-of-function, I suggest that this reduction in autophagosomes was due to α-synuclein gain-of-function. Since whole mitochondrial clearance was unaffected in both loss-of-function and α-synuclein overexpression models, the relationship between α-synuclein and autophagy does not appear to be intrinsically linked to the mitochondrial damage response. To test this, it would be useful to expose cells to cellular stressors that do not specifically target mitochondria and assess how α-synuclein impacts autophagic mechanisms.

The next step in investigating the relationship between α-synuclein and mito-QC would be to extend the work from this study into a neuronal model, since this would better recapitulate the dopaminergic neurons that are degenerated in PD (Bolam & Pissadaki, 2012). In this study, I set up a suitable neuronal model through differentiating SH-SY5Y cells which could be used in future studies. However, I faced significant challenges in assessing mitochondrial phenotypes in differentiated cells as discussed in **Chapter 5** (**5.3**). In future, use of advanced imaging techniques such as stochastic optical reconstruction microscopy (STORM), a form of super-resolution microscopy that achieves a spatial resolution of 20-30nm may alleviate these issues. This would enable visualisation of individual mitochondrial fragments to be considerably improved, permitting analysis of mitochondrial network organisation and identification of MDVs. Since the neurons targeted in PD have been shown to be more vulnerable to mitochondrial dysfunction and oxidative stress than other cells, it would be interesting to also assess ROS in

these cells both to see how this differs from undifferentiated cells and to see how oxidative stress is impacted by changes in α-synuclein. Though using alternative imaging methods would help overcome challenges in resolving mitochondrial features in neuronal-like cells, problems with functional assays would remain due to technical issues in maintaining neuronal morphology to enable analysis. As such, I consider that alternative neuronal models may aid investigations into mito-QC, such as primary neurons or iPSCs. Primary neurons already have a directed cell fate and so do not require the same complex steps to promote neurite outgrowth, making them more suitable for metabolic assays (Clerc & Polster, 2012). Neurons grown from iPSCs have also been shown to be suitable for functional assays, so could be an alternative to differentiated SH-SY5Y cells (Roy-Choudhury & Daadi, 2019). Alternatively, methods have been developed to functionally analyse isolated mitochondria from animal brain, which could provide better insight into neuronal respiration while circumventing the requirement for plating and maintaining individual neurons (Sperling et al., 2019).

Development of this neuronal model enabled me to assess how neuronal differentiation was impacted by genetic manipulation of α-synuclein expression, providing important initial characterisation prior to further use in investigating mitochondrial function and mito-QC pathways. Interestingly, I suggest that though physiological α-synuclein plays a limited role in mito-QC, it does influence the differentiation of SH-SY5Y cells. I observe that cells lacking α-synuclein have a reduction in differentiation capacity but increased TH expression, demonstrating that physiological α-synuclein has a role in influencing neuronal and dopaminergic phenotypes. Though the association of α-synuclein with neuronal development has been suggested due to its expression in early human developmental stages, its function has not been well defined (Alejandra Morato Torres et al., 2020; Raghavan et al., 2004). However, α-synucleins activity as a molecular chaperone with structural and functional homology to 14-3-3 proteins may explain its physiological role in immature neurons (Ostrerova et al., 1999). Recent work has described the importance of 14-3-3 proteins in development of the nervous system, including control of the cell cycle, transcription and differentiation (Berg et al., 2003; Cornell & Toyo-oka, 2017). This includes the synthesis of catecholamines such as dopamine through binding and activating TH (Halskau et al., 2009). Interestingly, it is α-synuclein's similarity to 14-3-3 proteins which may also explain the increase in autophagic flux and lysosome number observed in undifferentiated SNCA KO cells. Thus, I suggest that further investigation into α-synuclein's potential function as a molecular chaperone may help to define its potential physiological functions in both mito-QC and neuronal differentiation.

Limited research has focused on the pathological impact of α-synuclein in neuronal development, likely since PD pathology does not emerge until later life. However, previous research has shown that α-synuclein can reduce differentiated phenotypes in PD patient-

derived iPSCs and primary neurons from mouse models of PD (S. S. Kim et al., 2011; Oliveira et al., 2015). This was suggested to occur through α-synuclein's ability to induce degradation of β-catenin which has a key role in the upregulation of neuronal gene expression (S. S. Kim et al., 2011). My data support the idea that α-synuclein pathology can negatively impact neuronal differentiation and shows that in SH-SY5Y cells, overexpression of α-synuclein A53T reduced expression of neuronal and dopaminergic markers alongside causing morphological defects. This was specific to the A53T mutant form of the protein since cells overexpressing wild-type α-synuclein had no measurable changes in neuronal differentiation. This is interesting since in undifferentiated cells there were very limited differences in mitochondrial phenotypes between cells overexpressing wild-type or A53T α-synuclein. This suggests that though α-synuclein wild-type and A53T affect mito-QC in a similar way, they seem to function distinctly in differentiated cells. The main characteristic that differs between these two proteins is that despite being intrinsically disordered like the wild-type protein, α-synuclein A53T has an increased aggregation propensity (Kang et al., 2011). As well as exhibiting increased levels of aggregation, α-synuclein A53T has been shown to aggregate into different structural species to the wild-type protein (Lashuel et al., 2002). While wild-type α-synuclein has been shown to form annular, pore-like structures after long incubation periods, α-synuclein A53T also forms tubular structures (Kayed et al., 2009; Lashuel et al., 2002). Assessment of aggregated protein levels and structures would be a good starting point in identifying what causes the disparate impacts of wild-type and A53T α-synuclein on differentiation. Interestingly, differentiated SNCA KO cells have a similar but less exaggerated phenotype to cells overexpressing GFP-α-syn-A53T. This suggests the possibility that both cell lines could be behaving similarly in this context due to loss-of-function or related dominant negative phenotype. This is distinct from impacts on mitochondrial organisation and mito-QC, which appear to purely be driven by a gain-of-function effect. I suggest that further research on α-synuclein's physiological role in neuronal differentiation would be important to better characterise α-synuclein's capacity to influence neuronal biology in PD.

Appendix A

A.1 Materials & methods

A.1.1 Molecular cloning

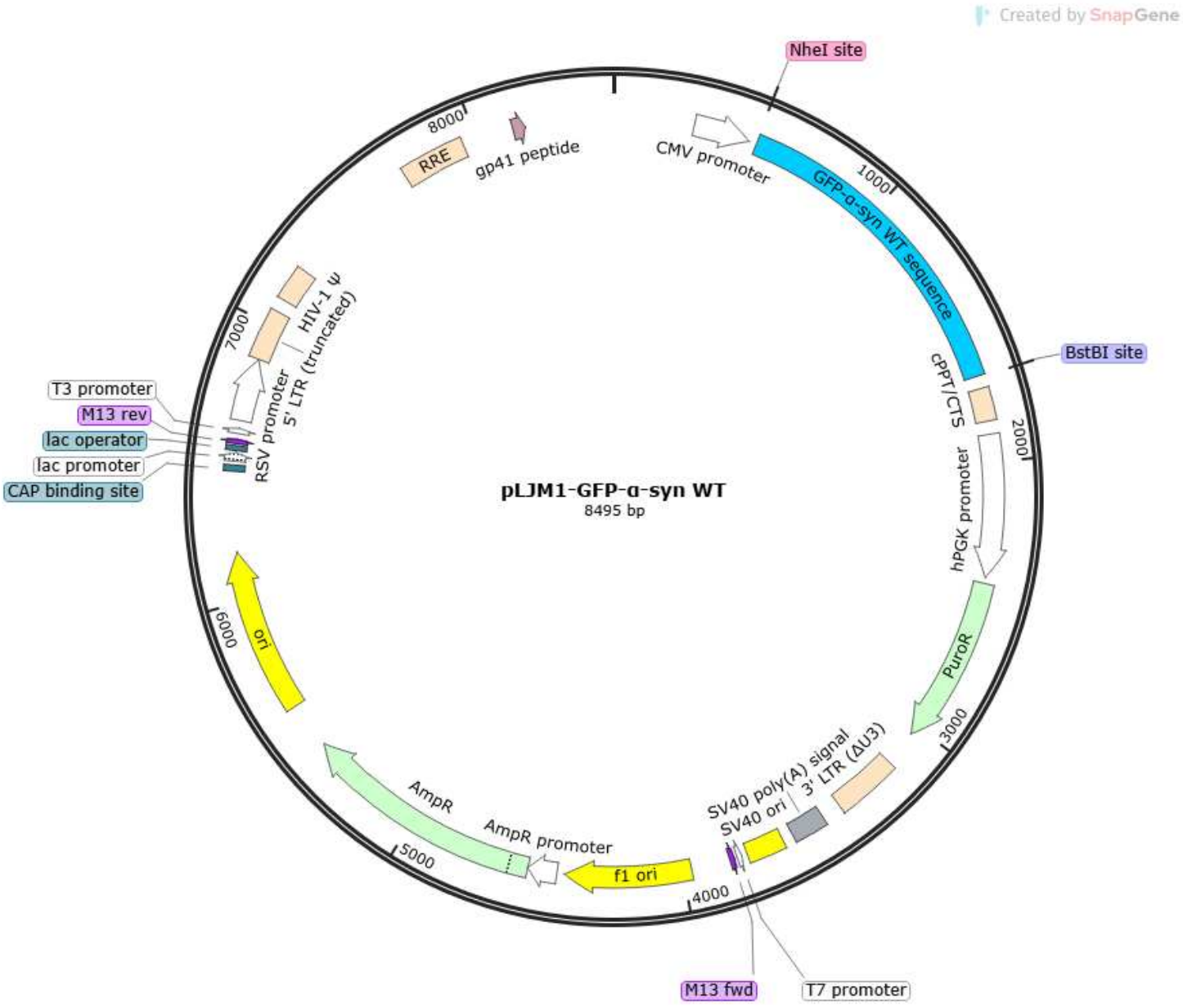

Figure 113: pLJM1-EGFP-α-syn-WT

Map of the lentiviral plasmid created to enable stable overexpression of GFP-α-syn-WT. The GFP-α-syn-WT sequence was subcloned from the EGFP-alphasynuclein-WT plasmid into the pLJM1 backbone that had been digested with NheI and BstBI restriction enzymes (shown in Methods).

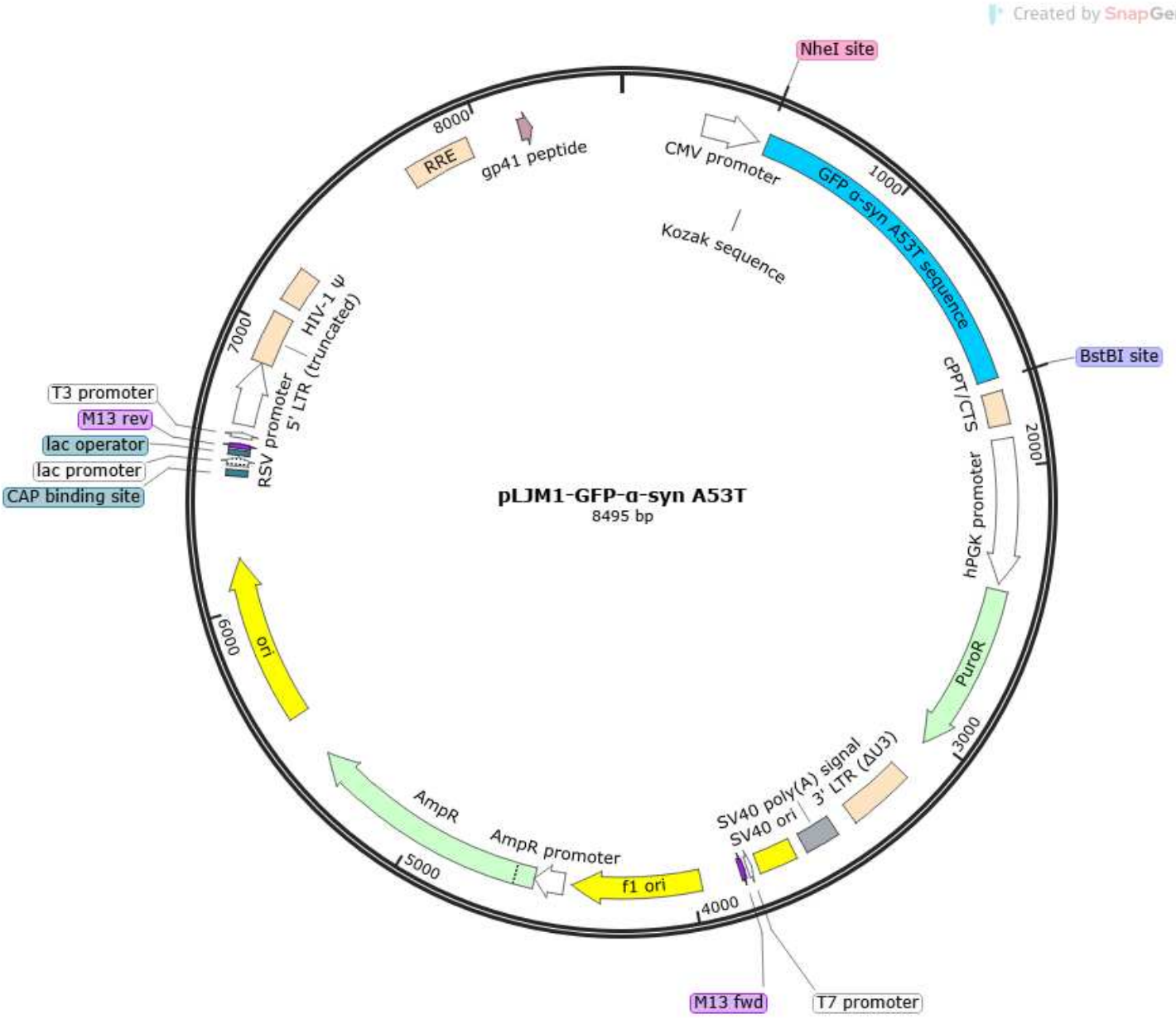

Figure 114: pLJM1-EGFP-α-syn-A53T

Map of the lentiviral plasmid created to enable stable overexpression of GFP-α-syn-A53T. The GFP-α-syn-WT sequence was subcloned from the EGFP-alphasynuclein-A53T plasmid into the pLJM1 backbone that had been digested with NheI and BstBI restriction enzymes (shown in Methods).

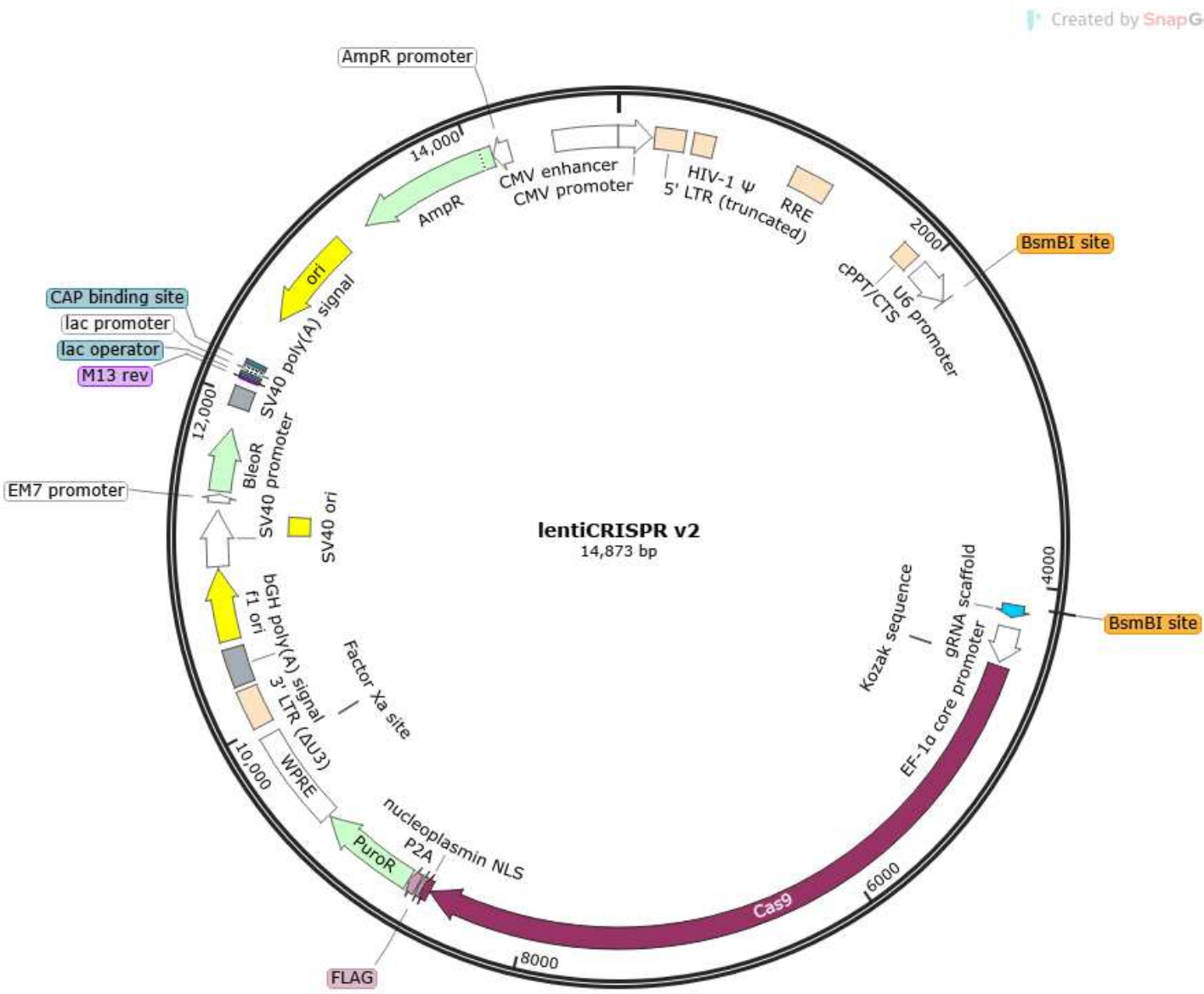

Figure 115: pLentiCRISPRv2

Map of the pLentiCRISPRv2 plasmid used to create CRISPR/Cas9 knockouts. This had been predigested by Professor Nullin Divecha with BsmBI, a dual cutter, to leave a site next to the scaffold for gRNAs. The original plasmid was Addgene #52961, a gift from Feng Zhang https://www.addgene.org/52961/; RRID: Addgene_52961.

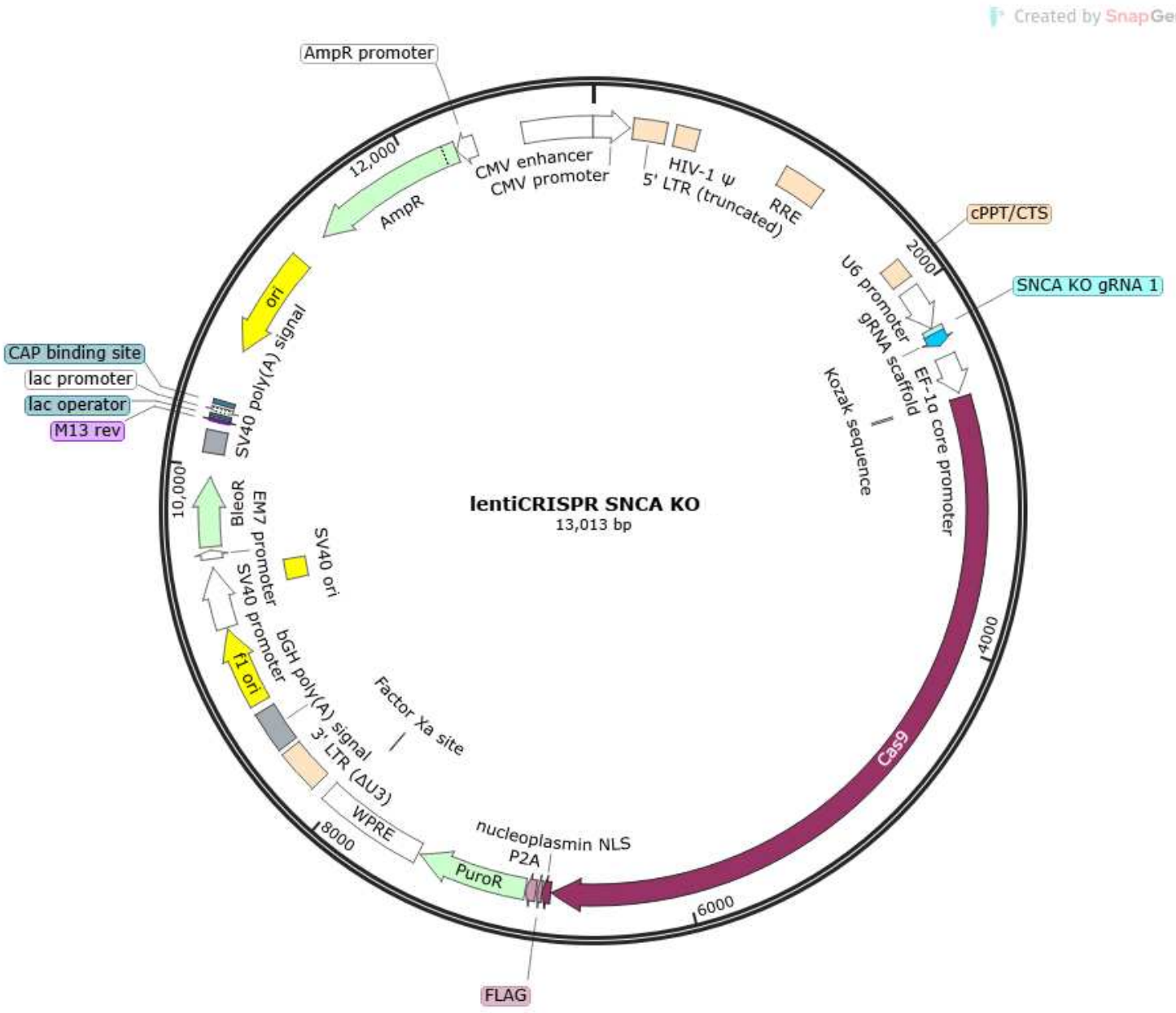

Figure 116: pLentiCRISPR SNCA KO

Map of the pLentiCRISPR plasmid with a SNCA KO gRNA sequence inserted, used to generate the SNCA KO cell line.

A.1.2 Western blot

Table 20: Western blot buffer compositions

Buffer	Composition
RIPA buffer	50mM Tris-HCl pH 7.4, 150mM NaCl, 0.1% SDS, 0.5% sodium deoxycholate, 1% Triton-X-100, protein inhibitor cocktail tablet (Roche, 04693159001)
1X running buffer	10% Laemmli buffer in dH_20
1X transfer buffer	10% 10X transfer buffer, 10% methanol in dH_20
10X Laemmli buffer	5mM Tris-HCl pH 8.3, 192mM glycine, 0.1% SDS
10X transfer buffer	60.4g Tris (Fisher Bioreagents™, BP152-500), 299g glycine (Fisher Bioreagents™, G/0800/60), dH_20
TBS wash buffer	Tris-HCl pH 7.4, 0.5M NaCl in dH_20
TBS-T wash buffer	TBS + 0.1% Tween®-20 (Sigma Aldrich, P7949)

Table 21: Western blot reagent compositions

Reagent	Composition
6X loading dye	12% SDS, 47% glycerol, 0.45M DTT, 60mM Tris pH 6.8, 0.0006% Bromophenol blue (Sigma Aldrich, B8026)
1X PBS	137mM NaCl, 2.7mM KCl, 10mM Na_2HPO_4, 2mM K_2HPO_4
10X PBS (Fisher BioReagents™, BP399-500)	1.37M NaCl, 27mM KCl, 100mM Na_2HPO_4, 20mM K_2HPO_4
Tris-HCl pH 6.8	60.57g Tris, approx. 40ml conc. HCl, dH_20
Tris-HCl pH 7.4	60.57g Tris, approx. 35ml conc. HCl, dH_20
Tris-HCl pH 8.8	60.57g Tris, approx. 7ml conc. HCl, dH_20
5 X TBE	54g Tris, 27.5g boric acid, 20ml 0.5M EDTA (pH 8), dH_20

Table 22: SDS-Page gel compositions

Reagents	15% Resolving gel	Stacking gel
Acrylamide (Severn Biotech, 20-2100-05)	3.8ml	834µl
1M Tris-HCl	1.875µl (pH 8.8)	625µl (pH 6.8)
dH_20	1.81ml	3.52ml
SDS	38µl	25µl
10% APS (Acros Organics, 327081000)	50µl	50µl
TEMED (Sigma Aldrich, T22500)	8µl	5µl

A.1.3 ATP assay

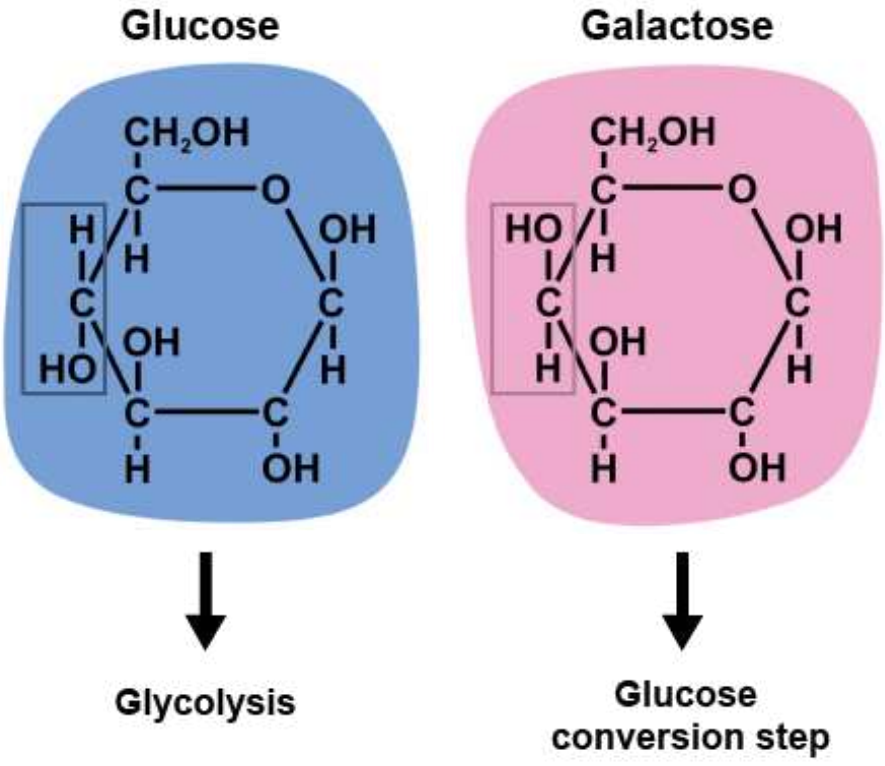

	Glucose	Glucose + O	Galactose	Galactose + O
Glycolysis	✓	✓	✗	✗
Ox phos	✓	✗	✓	✗

Figure 117: ATP assay rationale

In the ATP assay, manipulating glucose availability in growth media pushes cells to produce ATP through specific pathways which can be measured by luminescence:

1) Glucose: cells can produce ATP by **glycolysis** because of glucose in the media and by **oxidative phosphorylation** because the ETC is fully functioning
2) Glucose + oligomycin: cells can produce ATP by **glycolysis** because of glucose in the media, but not by oxidative phosphorylation because the ETC is inhibited by oligomycin
3) Galactose: cells cannot produce ATP by glycolysis because glucose is not present in the media, but can by **oxidative phosphorylation** because the ETC is fully functioning
4) Galactose + oligomycin: cells cannot produce ATP by glycolysis because glucose is not present in the media, and also cannot by oxidative phosphorylation because the ETC is inhibited by oligomycin

A.1.4 Seahorse mito-stress test

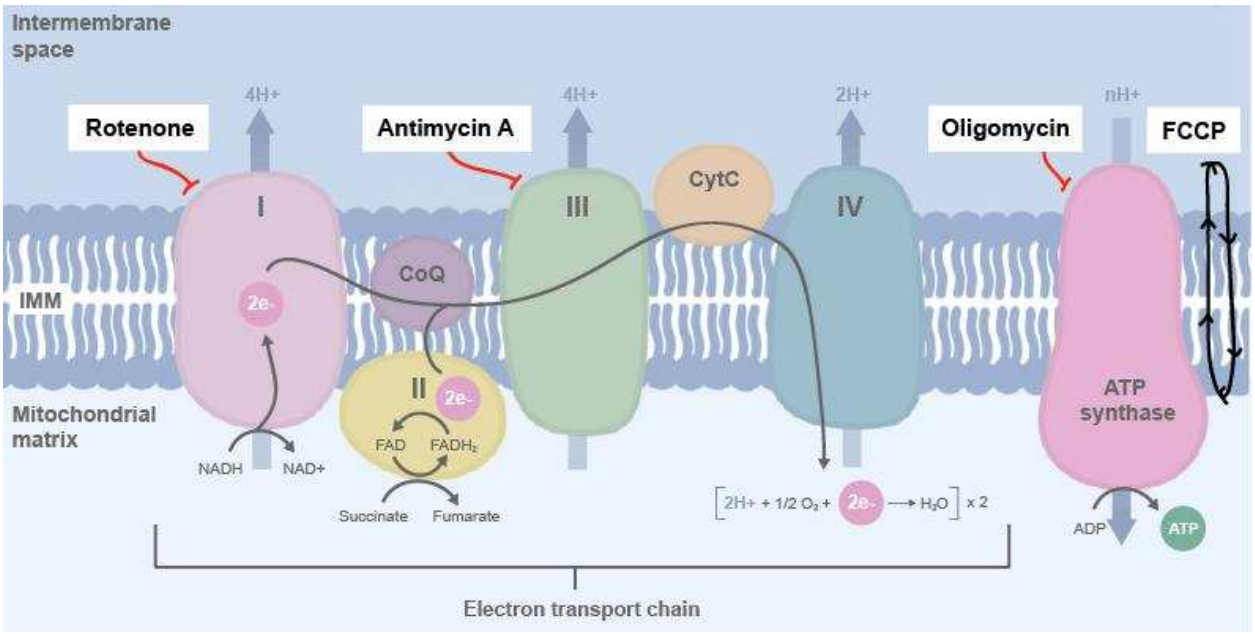

Figure 118: Inhibitors used in the Seahorse mito stress test and their targets in the ETC

In the Seahorse mito stress test, inhibitors are employed to selectively impact specific parts of the ETC. Oligomycin inhibits ATP synthase, FCCP disrupts the proton gradient across the IMM, rotenone inhibits complex I and antimycin A inhibits complex III.

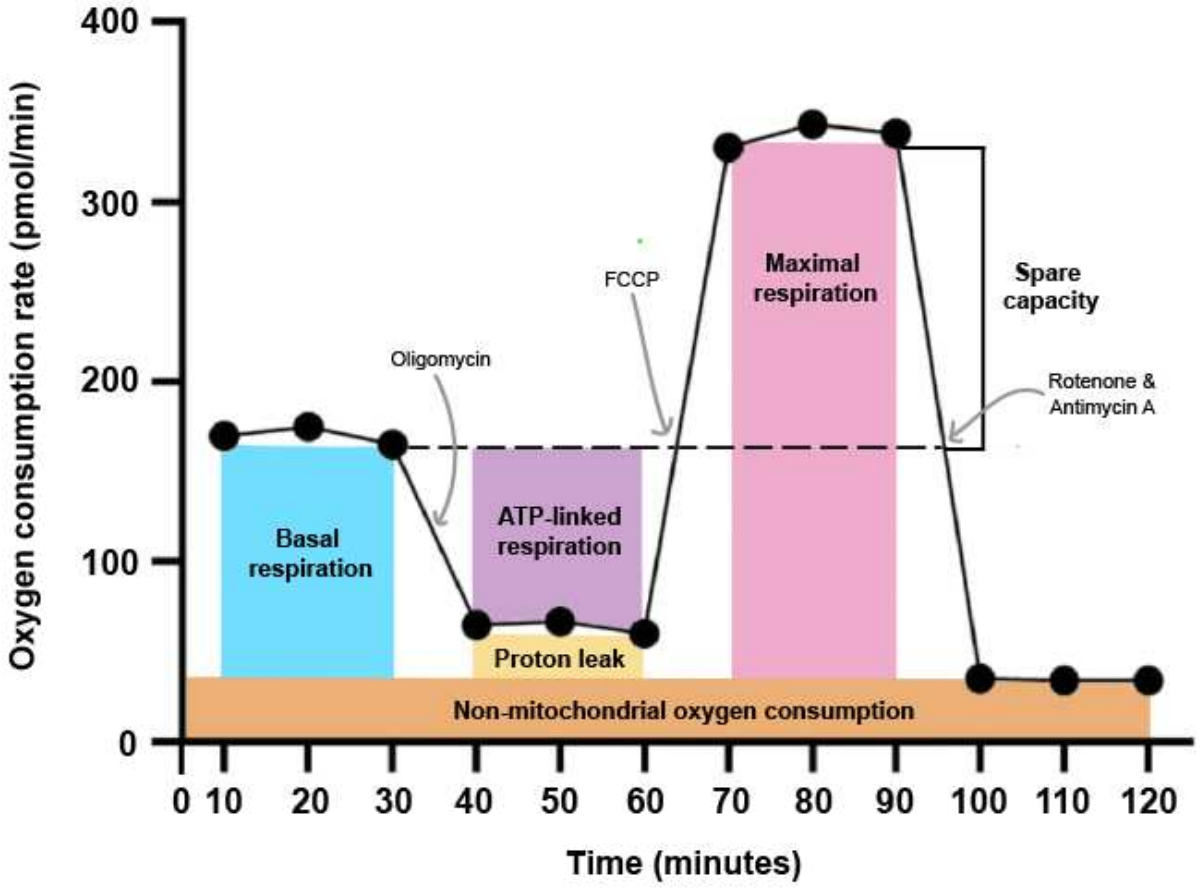

Figure 119: Example graph generated from the mito stress test showing respiratory parameters

The mito stress test measures oxygen consumption rate (OCR) in live cells over 120 minutes. Different mitochondrial inhibitors are injected at specific times to allow measurements of specific respiratory parameters. After basal readings (blue) oligomycin is injected to inhibit mitochondrial ATP synthase. As such, the difference between the OCR at baseline and with oligomycin is considered to be ATP-linked respiration (purple). Below this is considered proton leak as the result of uncoupled respiration (yellow). FCCP is injected to collapse the proton gradient, uninhibiting the ETC and driving maximal respiration (pink). Finally, rotenone and antimycin A are injected together to completely shut down mitochondrial respiration. Any oxygen consumption remaining after this is considered to be non-mitochondrial (orange), and thus is subtracted from all other measures of mitochondrial OCR. This graph and these measurements are automatically calculated by Agilent Wave Pro software.

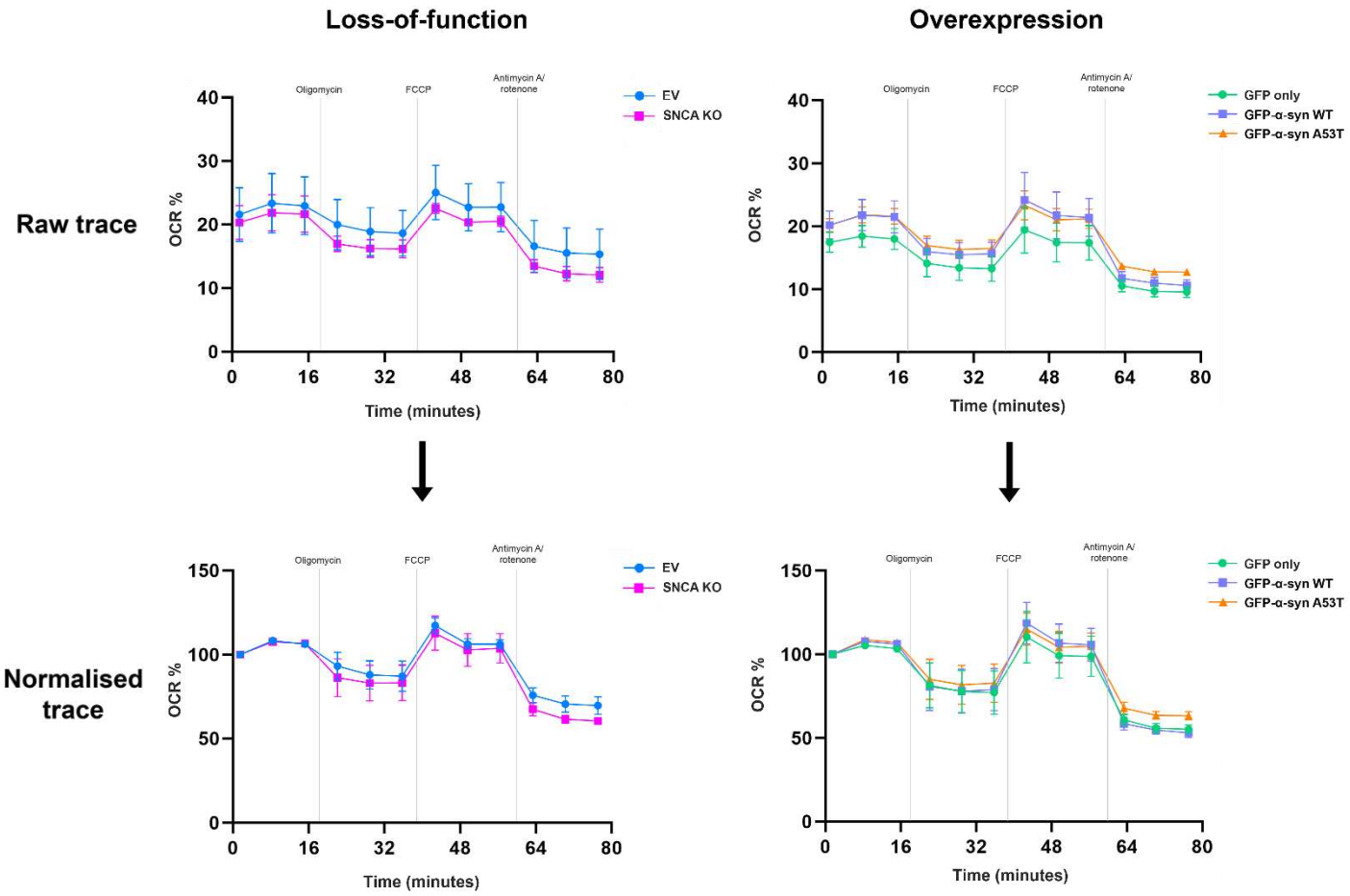

Figure 120: Normalisation of Seahorse mito stress test traces

The Seahorse mito stress test generates a trace corresponding to oxygen consumption rate (%) over time. Cell lines have different baseline OCR, but differences between groups are not measured by the raw OCR, but rather the differences between particular parts of the trace, as described in **Figure 119.** Differences in baseline can make comparisons between cell lines difficult to visualise, so I normalised traces to the first baseline reading. This reading is placed at 100%, and all other data points are shown relative to this. This enables differences between parts of the trace to be better visualised. As such, normalised traces are presented in the results chapters and traces showing the means of the raw values from all 3 repeats are shown here **(n=3)**.

A.1.5 Live imaging ΔΨm with TMRM

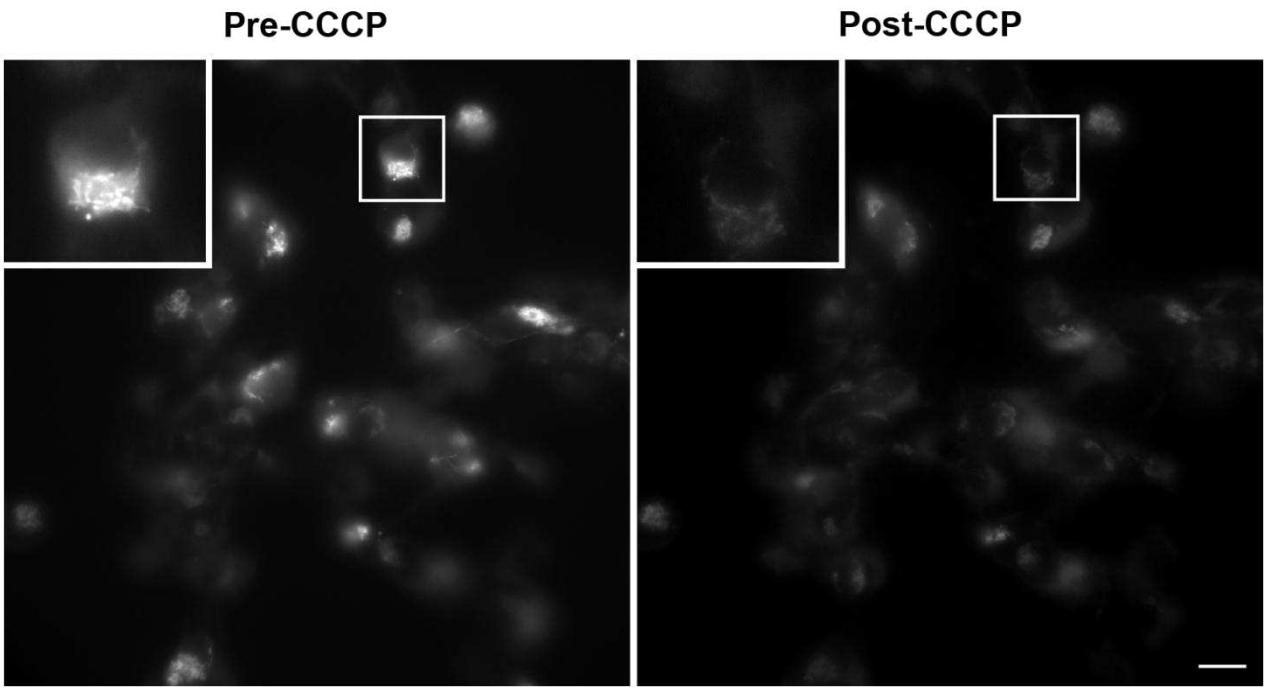

Figure 121: TMRM fluorescence intensity decreases upon depolarisation of the mitochondrial membrane with 10µM CCCP

Wild-type SH-SY5Y cells were incubated with TMRM at 37°C for 30 minutes and imaged. 10µM CCCP was added and cells were imaged over a further 10 minutes. Images show the same field of cells prior to the addition of CCCP and 10 minutes after CCCP was added. Live cell fluorescence microscopy was used to observed cells with a 63X objective and image Z-stacks. Scale = 20µm.

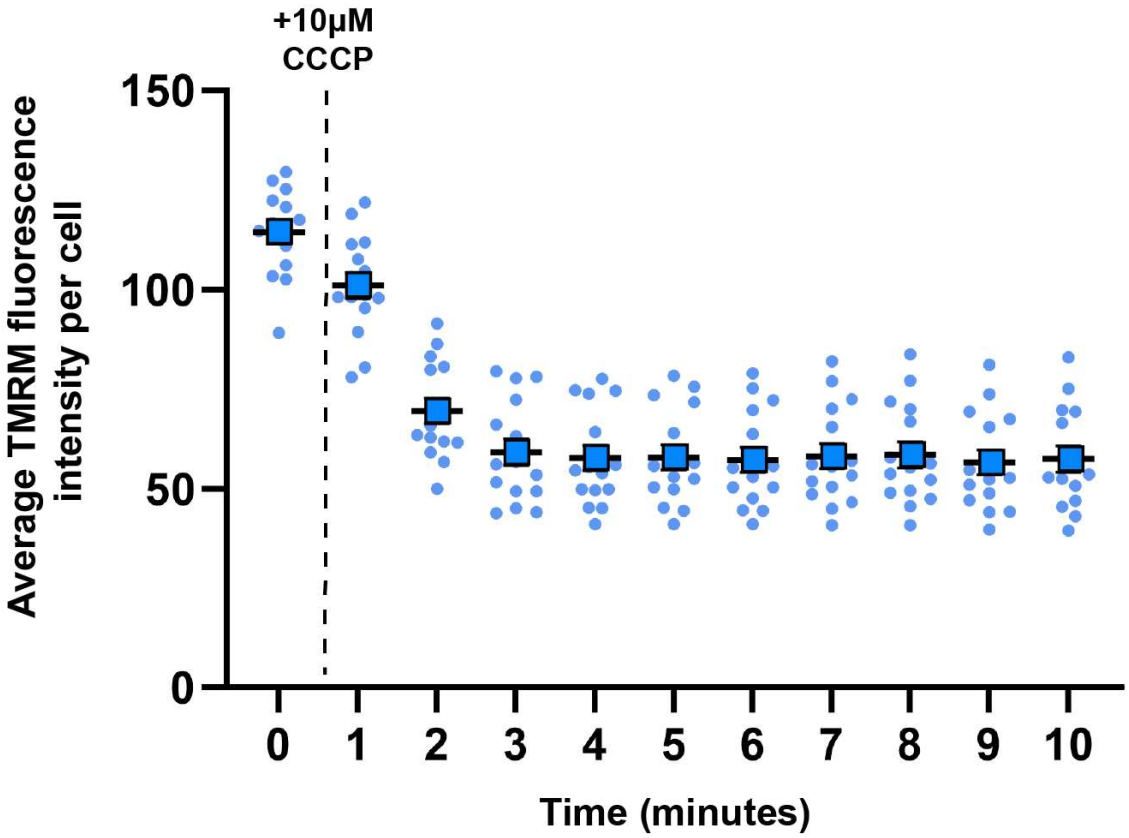

Figure 122: Quantitation confirms that fluorescence intensity of TMRM decreases upon depolarisation of the mitochondrial membrane with 10µM CCCP

Wild-type SH-SY5Y cells were incubated with TMRM at 37°C for 30 minutes and imaged. After 30 seconds, 10µM CCCP was added and images were taken once per minute for 10 minutes. 15 individual cells were selected and the fluorescence intensity of their TMRM signal was recorded at each time point. Individual data points are shown by dots, with the average of these 15 cells shown by a square. SEM is shown shown by vertical black lines. (**n=1**).

Appendix B

B.1 Data chapter 1: Investigating the role of endogenous α-synuclein in mitochondrial health and mito-QC

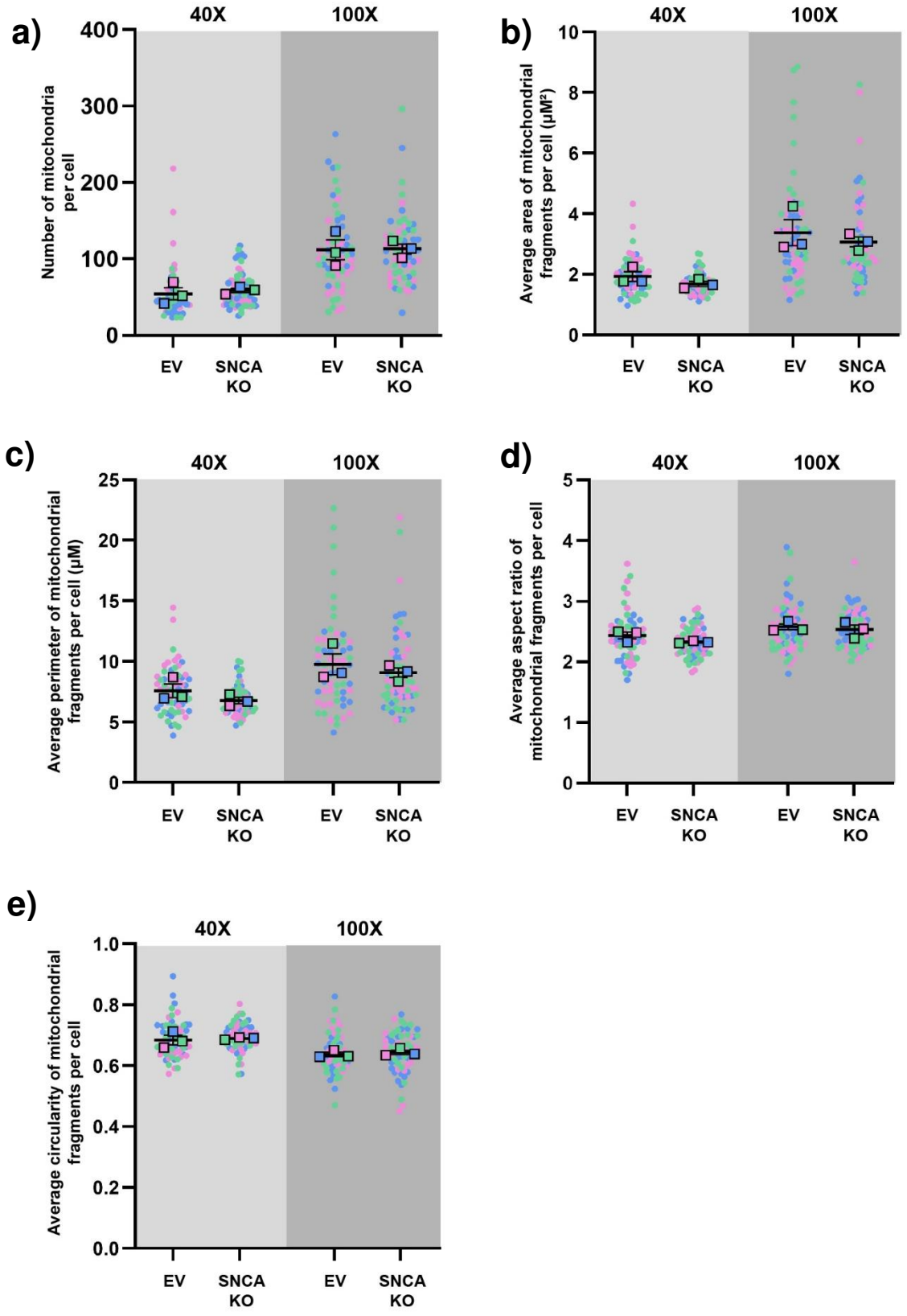

Figure 123: Comparison of mitochondrial morphology measurements in images taken at 40X and 100X magnification

Graphs show morphological measurements of mitochondria from untreated EV and SNCA KO cells imaged at both 40X (pale grey background) and 100X (medium grey background). This was to assess whether images of better resolution may be better suited to this analysis in future. Parameters measured were a) number of mitochondria per cell; b) average area of mitochondrial fragments per cell; c) average perimeter of mitochondrial fragments per cell; d) average aspect ratio of mitochondrial fragments per cell and e) average circularity of mitochondrial fragments per cell. Statistical analysis was carried out on the 100X data by a paired t-test. As with the analysis carried out at 40X, no significant differences were found between the cell lines. (**n=3**).

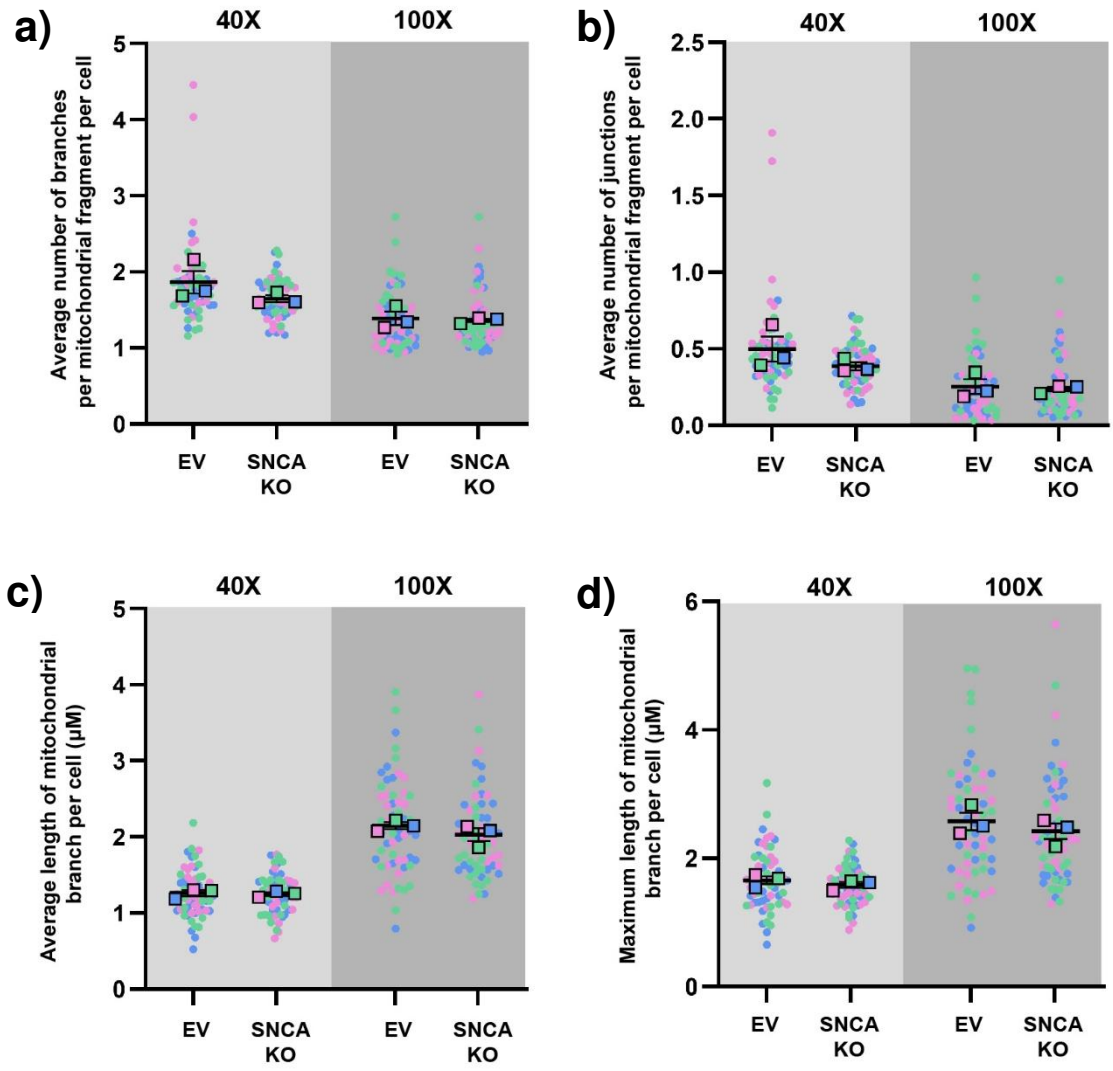

Figure 124: Comparison of mitochondrial connectivity measurements in images taken at 40X and 100X magnification

Graphs show connectivity measurements of mitochondria from untreated EV and SNCA KO cells imaged at both 40X (pale grey background) and 100X (medium grey background). This was to assess whether images of better resolution may be better suited to this analysis in future. Parameters measured were a) average number of branches per mitochondrial fragment per cell; b) average number of junctions per mitochondrial fragment per cell; c) average length of mitochondrial branch per cell and d) maximum length of mitochondrial branch per cell. Statistical analysis was carried out on the 100X data by a paired t-test. As with the analysis carried out at 40X, no significant differences were found between the cell lines. (**n=3**).

B.2 Data chapter 2: Investigating the impact of pathological α-synuclein overexpression on mitochondrial health and mito-QC

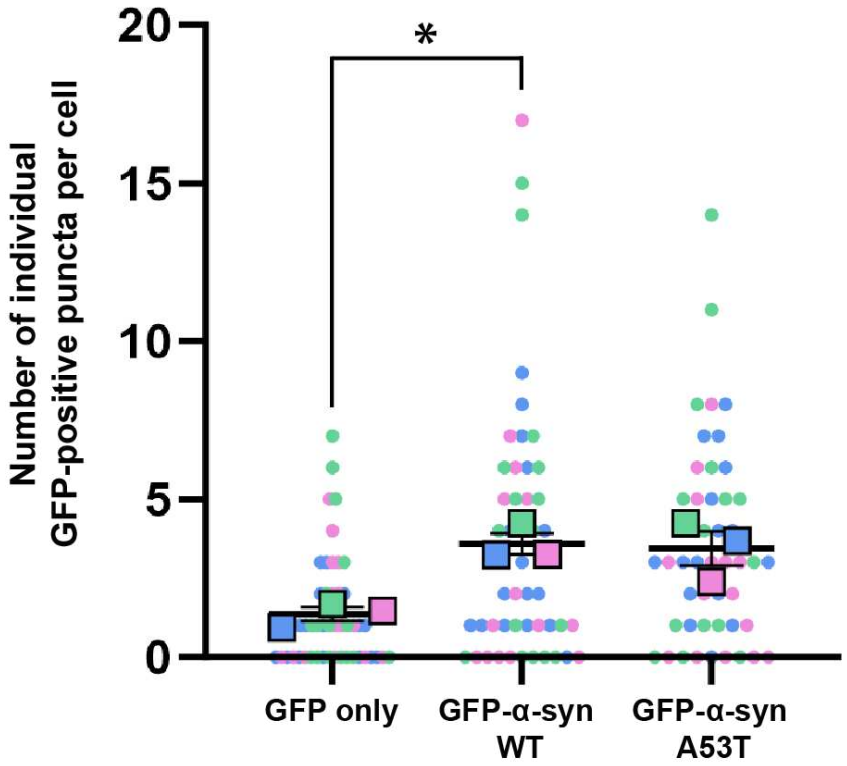

Figure 125: GFP-α-syn-WT and GFP-α-syn-A53T expressing cells have more individual clearly identifiable GFP-positive puncta than GFP only cells

GFP only, GFP-α-syn-WT and GFP-α-syn-A53T cells were fixed and permeabilised with saponin to clear out the cytoplasm. The number of bright GFP-positive puncta clearly distinguishable from background GFP was counted in 16 cells per cell line, per biological repeat. Individual data points are shown by circles, with the mean of each repeat shown by a square, the mean of all 3 repeats shown by a black bar and the SEM shown by vertical black lines. Statistical analysis was performed by a repeated measures one-way ANOVA with Tukey's multiple comparisons test. GFP-α-syn-WT cells had a significantly higher number of individual GFP puncta than GFP only cells (p=0.0182, *). (**n=3**).

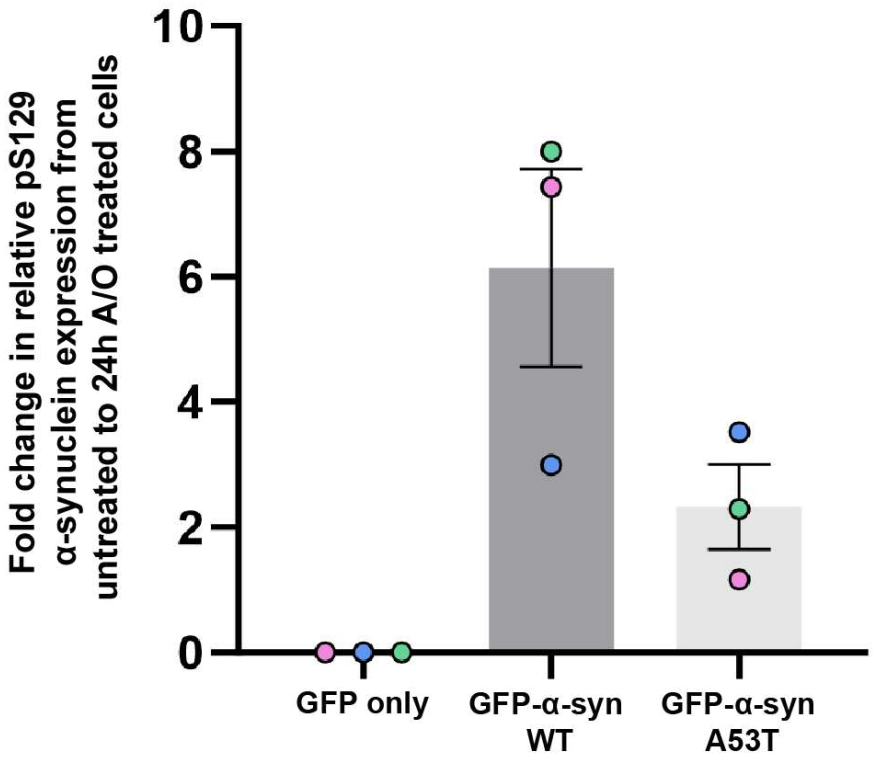

Figure 126: GFP-α-syn-WT expressing cells have a higher fold-change in pS129 α-synuclein expression from untreated to 24-hour A/O treated cells

For each of the GFP only, GFP-α-syn-WT and GFP-α-syn-A53T expressing cell lines, the fold change in relative phospho-S129 α-synuclein expression (shown in Chapter X, fig X) from untreated cells to 24-hour A/O treated cells was calculated. Relative phospho-S129 α-synuclein expression was normalised to the expression when cells were untreated for each cell line. Biological replicates are colour coded, with circles representing the fold change in each repeat, bars representing the mean of 3 repeats and black lines showing the SEM. GFP only cells are shown in dark grey, GFP α-syn-WT cells are shown in medium grey and GFP-α-syn-A53T cells are shown in pale grey. (**n=3).**

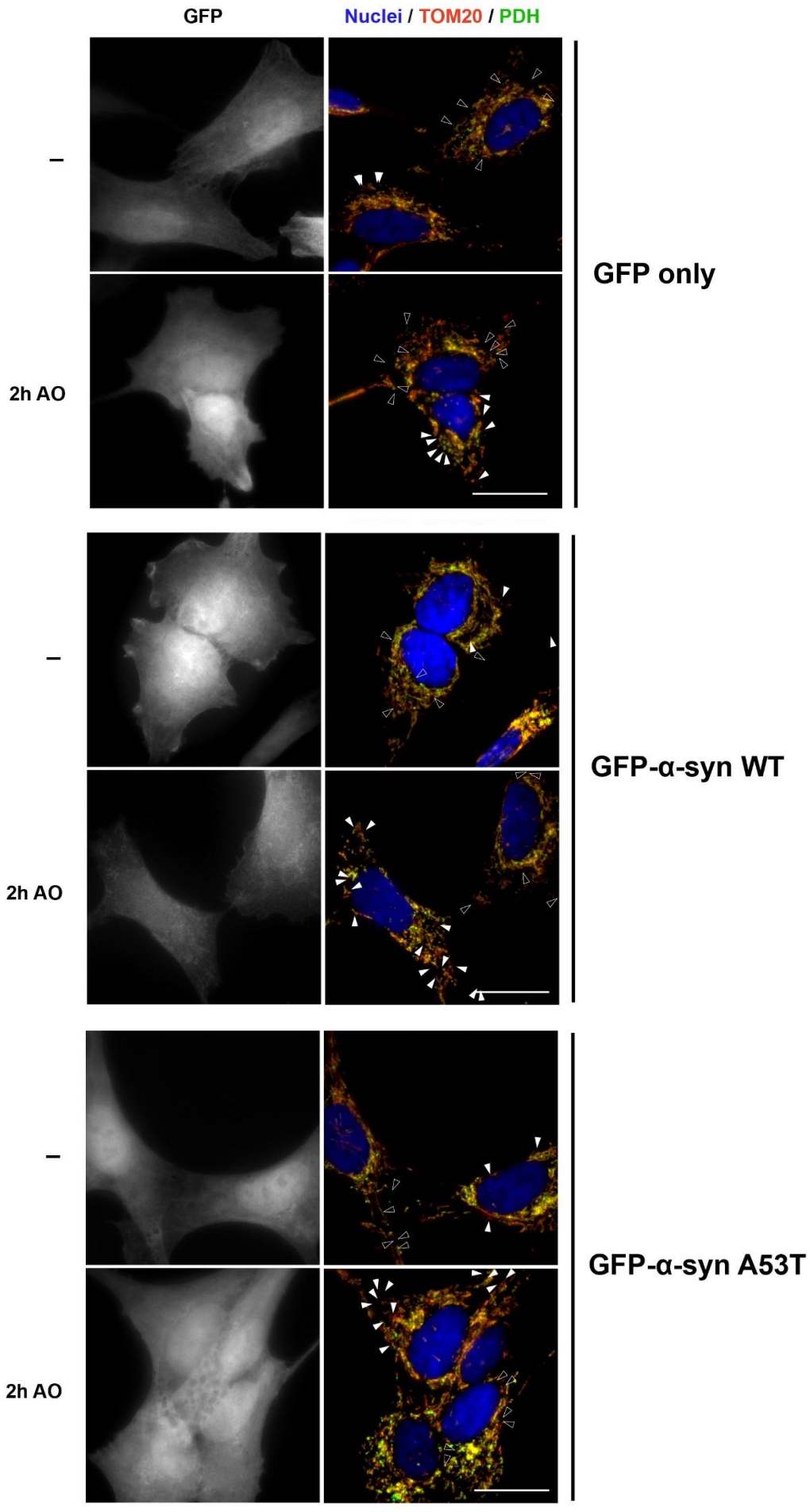
GFP
Nuclei / TOM20 / PDH
–
2h AO
GFP only
–
2h AO
GFP-α-syn WT
–
2h AO
GFP-α-syn A53T

Figure 127: Confirmation of GFP expression in cells used for MDV analysis

GFP only, GFP-α-syn-WT and GFP-α-syn-A53T cells were left untreated (-) or treated for 2 hours with A/O to induce mitochondrial damage. GFP was imaged to allow selection of only GFP-positive cells for subsequent analysis. Confirmation of GFP expression is shown here.

B.3 Data chapter 3: Investigating the impact of alterations in α-synuclein on neuronal differentiation of SH-SY5Y cells

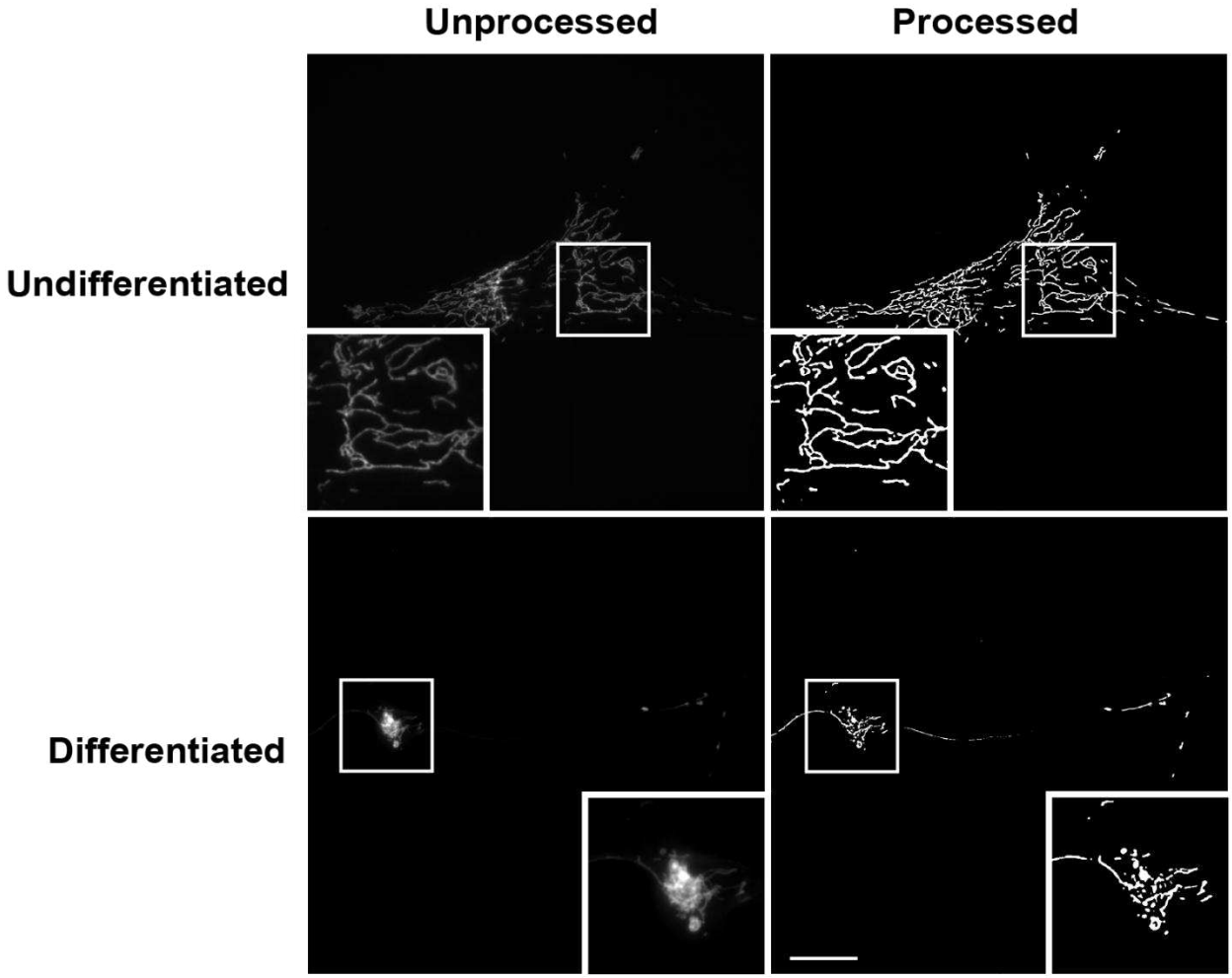

Figure 128: Mitochondrial network analysis cannot resolve mitochondrial morphology and connectivity in differentiated SH-SY5Y cells

Mitochondrial network analysis was carried out on undifferentiated and differentiated cells using the ImageJ® analysis workflow developed for SH-SY5Y cells. Thresholding was carried out to capture shape and structure of the mitochondrial network prior to measurement of mitochondrial morphology and connectivity.

List of References

Abramov, A. Y., Smulders-Srinivasan, T. K., Kirby, D. M., Acin-Perez, R., Enriquez, J. A., Lightowlers, R. N., Duchen, M. R., & Turnbull, D. M. (2010). Mechanism of neurodegeneration of neurons with mitochondrial DNA mutations. *Brain*, *133*(3), 797–807. https://doi.org/10.1093/brain/awq015

Acheson, A., Conover, J. C., Fandl, J. P., Dechiara, T. M., Russell, M., Thadani, A., Squintot, S. P., Yancopoulos, G. D., & Lindsay, R. M. (1995). A BDNF autocrine loop in adult sensory neurons prevents cell death. *Nature*, *374*, 450–453.

Afitska, K., Fucikova, A., Shvadchak, V. V., & Yushchenko, D. A. (2019). α-Synuclein aggregation at low concentrations. *Biochimica et Biophysica Acta - Proteins and Proteomics*, *1867*(7–8), 701–709. https://doi.org/10.1016/j.bbapap.2019.05.003

Aharon-Peretz, J., Rosenbaum, H., & Gershoni-Baruch, R. (2004). Mutations in the Glucocerebrosidase Gene and Parkinson's Disease in Ashkenazi Jews. *The New England Journal of Medicine*, *4*(351), 1972–1977. www.nejm.org

Alam, M. M., Yang, D., Li, X. Q., Liu, J., Back, T. C., Trivett, A., Karim, B., Barbut, D., Zasloff, M., & Oppenheim, J. J. (2022). Alpha synuclein, the culprit in Parkinson disease, is required for normal immune function. *Cell Reports*, *38*(2). https://doi.org/10.1016/j.celrep.2021.110090

Alberts, B., Johnson A, Lewis J, & et al. (2002). *Molecular Biology of the Cell* (4th ed.). Garland Science.

Alcalay, R. N., Mallett, V., Vanderperre, B., Tavassoly, O., Dauvilliers, Y., Wu, R. Y. J., Ruskey, J. A., Leblond, C. S., Ambalavanan, A., Laurent, S. B., Spiegelman, D., Dionne-Laporte, A., Liong, C., Levy, O. A., Fahn, S., Waters, C., Kuo, S. H., Chung, W. K., Ford, B., … Gan-Or, Z. (2019). SMPD1 mutations, activity, and α-synuclein accumulation in Parkinson's disease. *Movement Disorders*, *34*(4), 526–535. https://doi.org/10.1002/mds.27642

Alejandra Morato Torres, C., Wassouf, Z., Zafar, F., Sastre, D., Outeiro, T. F., & Schüle, B. (2020). The role of alpha-synuclein and other parkinson's genes in neurodevelopmental and neurodegenerative disorders. In *International Journal of Molecular Sciences* (Vol. 21, Issue 16, pp. 1–32). MDPI AG. https://doi.org/10.3390/ijms21165724

Alim, M. A., Ma, Q., Takeda, K., Aizawa, T., Matsubara, M., Nakamura, M., Asada, A., Saito, T., Kaji, M., Yoshii, M., Hinsanaga, S., & Ueda, K. (2004). Demonstration of a role for a-

synuclein as a functional microtubule-associated protein. *Journal of Alzheimer's Disease*, *6*(4), 435–442.

Allen, G. F. G., Toth, R., James, J., & Ganley, I. G. (2013). Loss of iron triggers PINK1/Parkin-independent mitophagy. *EMBO Reports*, *14*(12), 1127–1135. https://doi.org/10.1038/embor.2013.168

Anderson, J. P., Walker, D. E., Goldstein, J. M., De Laat, R., Banducci, K., Caccavello, R. J., Barbour, R., Huang, J., Kling, K., Lee, M., Diep, L., Keim, P. S., Shen, X., Chataway, T., Schlossmacher, M. G., Seubert, P., Schenk, D., Sinha, S., Gai, W. P., & Chilcote, T. J. (2006). Phosphorylation of Ser-129 is the dominant pathological modification of α-synuclein in familial and sporadic lewy body disease. *Journal of Biological Chemistry*, *281*(40), 29739–29752. https://doi.org/10.1074/jbc.M600933200

Anglade, P., Vyas, S., Javoy-Agid, F., Herrero, M. T., Michel, P. P., Marquez, J., Mouatt-Prigent, A., Ruberg, M., Hirsch, E. C., & Agid, Y. (1997). Histology and Histopathology Apoptosis and autophagy in nigral neurons of patients with Parkinson's disease. *Histol Histopathol*, *12*, 25–31.

Arcangeli, A., Rosati, B., Crociani, O., Cherubini, A., Fontana, L., Passani, B., Wanke, E., & Olivotto, M. (1999). Modulation of HERG current and herg gene expression during retinoic acid treatment of human neuroblastoma cells: Potentiating effects of BDNF. *Journal of Neurobiology*, *40*(2), 214–225. https://doi.org/10.1002/(SICI)1097-4695(199908)40:2<214::AID-NEU7>3.0.CO;2-0

Arnoult, D., Petit, F., Lelièvre, J. D., & Estaquier, J. (2003). Mitochondria in HIV-1-induced apoptosis. *Biochemical and Biophysical Research Communications*, *304*(3), 561–574. https://doi.org/10.1016/S0006-291X(03)00629-6

Auluck, P. K., Caraveo, G., & Lindquist, S. (2010). α-synuclein: Membrane interactions and toxicity in parkinson's disease. In *Annual Review of Cell and Developmental Biology* (Vol. 26, pp. 211–233). https://doi.org/10.1146/annurev.cellbio.042308.113313

Avwenagha, O., Campbell, G., & Bird, M. M. (2003). Distribution of GAP-43, β-III tubulin and F-actin in developing and regenerating axons and their growth cones in vitro, following neurotrophin treatment. *Journal of Neurocytology*, *32*, 1077–1089.

Bagkos, G., Koufopoulos, K., & Piperi, C. (2014). A new model for mitochondrial membrane potential production and storage. *Medical Hypotheses*, *83*(2), 175–181. https://doi.org/10.1016/j.mehy.2014.05.001

Balaban, R. S., Nemoto, S., & Finkel, T. (2005). Mitochondria, oxidants, and aging. In *Cell* (Vol. 120, Issue 4, pp. 483–495). Cell Press. https://doi.org/10.1016/j.cell.2005.02.001

Banerjee, K., Sinha, M., Pham, C. L. L., Jana, S., Chanda, D., Cappai, R., & Chakrabarti, S. (2010). α-Synuclein induced membrane depolarization and loss of phosphorylation capacity of isolated rat brain mitochondria: Implications in Parkinson's disease. *FEBS Letters*, *584*(8), 1571–1576. https://doi.org/10.1016/j.febslet.2010.03.012

Barba, L., Paolini Paoletti, F., Bellomo, G., Gaetani, L., Halbgebauer, S., Oeckl, P., Otto, M., & Parnetti, L. (2022). Alpha and Beta Synucleins: From Pathophysiology to Clinical Application as Biomarkers. In *Movement Disorders* (Vol. 37, Issue 4, pp. 669–683). John Wiley and Sons Inc. https://doi.org/10.1002/mds.28941

Basu, K., Lajoie, D., Aumentado-Armstrong, T., Chen, J., Koning, R. I., Bossy, B., Bostina, M., Sik, A., Bossy-Wetzel, E., & Rouiller, I. (2017). Molecular mechanism of DRP1 assembly studied in vitro by cryo-electron microscopy. *PLoS ONE*, *12*(6). https://doi.org/10.1371/journal.pone.0179397

Beilina, A., Rudenko, I. N., Kaganovich, A., Civiero, L., Chau, H., Kalia, S. K., Kalia, L. V., Lobbestael, E., Chia, R., Ndukwe, K., Ding, J., Nalls, M. A., Olszewski, M., Hauser, D. N., Kumaran, R., Lozano, A. M., Baekelandt, V., Greene, L. E., Taymans, J. M., … Cookson, M. R. (2014). Unbiased screen for interactors of leucine-rich repeat kinase 2 supports a common pathway for sporadic and familial Parkinson disease. *Proceedings of the National Academy of Sciences of the United States of America*, *111*(7), 2626–2631. https://doi.org/10.1073/pnas.1318306111

Benador, I. Y., Veliova, M., Mahdaviani, K., Petcherski, A., Wikstrom, J. D., Assali, E. A., Acín-Pérez, R., Shum, M., Oliveira, M. F., Cinti, S., Sztalryd, C., Barshop, W. D., Wohlschlegel, J. A., Corkey, B. E., Liesa, M., & Shirihai, O. S. (2018). Mitochondria Bound to Lipid Droplets Have Unique Bioenergetics, Composition, and Dynamics that Support Lipid Droplet Expansion. *Cell Metabolism*, *27*(4), 869-885.e6. https://doi.org/10.1016/j.cmet.2018.03.003

Bender, A., Desplats, P., Spencer, B., Rockenstein, E., Adame, A., Elstner, M., Laub, C., Mueller, S., Koob, A. O., Mante, M., Pham, E., Klopstock, T., & Masliah, E. (2013). TOM40 Mediates Mitochondrial Dysfunction Induced by α-Synuclein Accumulation in Parkinson's Disease. *PLoS ONE*, *8*(4). https://doi.org/10.1371/journal.pone.0062277

Bender, A., Krishnan, K. J., Morris, C. M., Taylor, G. A., Reeve, A. K., Perry, R. H., Jaros, E., Hersheson, J. S., Betts, J., Klopstock, T., Taylor, R. W., & Turnbull, D. M. (2006). High levels

of mitochondrial DNA deletions in substantia nigra neurons in aging and Parkinson disease. *Nature Genetics*, *38*(5), 515–517. https://doi.org/10.1038/ng1769

Benes, P., Vetvicka, V., & Fusek, M. (2008). Cathepsin D - Many functions of one aspartic protease. *Critical Reviews in Oncology/Hematology*, *68*(1), 12–28. https://doi.org/10.1016/j.critrevonc.2008.02.008

Bennett, M. C., Bishop, J. F., Leng, Y., Chock, P. B., Chase, T. N., & Mouradian, M. M. (1999). Degradation of α-synuclein by proteasome. *Journal of Biological Chemistry*, *274*(48), 33855–33858. https://doi.org/10.1074/jbc.274.48.33855

Bereiter-Hahn, J., & Voth, M. (1994). Dynamics of mitochondria in living cells: Shape changes, dislocations, fusion, and fission of mitochondria. *Microscopy Research and Technique*, *27*(3), 198–219.

Berg, D., Holzmann, C., & Riess, O. (2003). 14-3-3 proteins in the nervous system. *Nature Reviews Neuroscience*, *4*, 752–762.

Bernal-Conde, L. D., Ramos-Acevedo, R., Reyes-Hernández, M. A., Balbuena-Olvera, A. J., Morales-Moreno, I. D., Argüero-Sánchez, R., Schüle, B., & Guerra-Crespo, M. (2020). Alpha-Synuclein Physiology and Pathology: A Perspective on Cellular Structures and Organelles. In *Frontiers in Neuroscience* (Vol. 13). Frontiers Media S.A. https://doi.org/10.3389/fnins.2019.01399

Bernardini, J. P., Lazarou, M., & Dewson, G. (2017). Parkin and mitophagy in cancer. In *Oncogene* (Vol. 36, Issue 10, pp. 1315–1327). Nature Publishing Group. https://doi.org/10.1038/onc.2016.302

Betarbet, R., Sherer, T. B., MacKenzie, G., Garcia-Osuna, M., Panov, A. V, & Greenamyre, J. T. (2000). Chronic systemic pesticide exposure reproduces features of Parkinson's disease. *Nature America*, *3*(12), 1301–1306.

Betzer, C., Lassen, L. B., Olsen, A., Kofoed, R. H., Reimer, L., Gregersen, E., Zheng, J., Calì, T., Gai, W., Chen, T., Moeller, A., Brini, M., Fu, Y., Halliday, G., Brudek, T., Aznar, S., Pakkenberg, B., Andersen, J. P., & Jensen, P. H. (2018). Alpha-synuclein aggregates activate calcium pump SERCA leading to calcium dysregulation. *EMBO Reports*, *19*(5). https://doi.org/10.15252/embr.201744617

Biedler, J. L., Helson, L., & Spengler, B. A. (1973). Morphology and Growth, Tumorigenicity, and Cytogenetics of Human Neuroblastoma Cells in Continuous Culture1. *Cancer Res*, *33*(11),

2643–2652. http://aacrjournals.org/cancerres/article-pdf/33/11/2643/2390476/cr0330112643.pdf

Biedler, J. L., Roffler-Tarlov, S., Schachner, M., & Freedman, L. S. (1978). Multiple Neurotransmitter Synthesis by Human Neuroblastoma Cell Lines and Clones. *Cancer Res*, *38*(11), 3751–3757. http://aacrjournals.org/cancerres/article-pdf/38/11_Part_1/3751/2400538/cr03811p13751.pdf

Bill, A., Espinola, S., Guthy, D., Haling, J. R., Lanter, M., Lu, M., Marelli, A., Mendiola, A., Miraglia, L., Taylor, B. L., Vargas, L., Orth, A. P., & King, F. J. (2021). EndoBind detects endogenous protein-protein interactions in real time. *Communications Biology*, *4*(1). https://doi.org/10.1038/s42003-021-02600-5

Billingsley, K. J., Barbosa, I. A., Bandrés-Ciga, S., Quinn, J. P., Bubb, V. J., Deshpande, C., Botia, J. A., Reynolds, R. H., Zhang, D., Simpson, M. A., Blauwendraat, C., Gan-Or, Z., Gibbs, J. R., Nalls, M. A., Singleton, A., Noyce, A., Tucci, A., Middlehurst, B., Kia, D., … Koks, S. (2019). Mitochondria function associated genes contribute to Parkinson's Disease risk and later age at onset. *NPJ Parkinson's Disease*, *5*. https://doi.org/10.1038/s41531-019-0080-x

Billman, G. E. (2020). Homeostasis: The Underappreciated and Far Too Often Ignored Central Organizing Principle of Physiology. In *Frontiers in Physiology* (Vol. 11). Frontiers Media S.A. https://doi.org/10.3389/fphys.2020.00200

Binder, D. K., & Scharfman, H. E. (2004). Brain-derived Neurotrophic Factor. *Growth Factors*, *22*(3), 123–131.

Bleazard, W., McCaffery, J. M., King, E. J., Bale, S., Mozdy, A., Tieu, Q., Nunnari, J., & Shaw, J. M. (1999). The dynamin-related GTPase Dnm1 regulates mitochondrial fission in yeast. *Nature Cell Biology*, *1*(5), 298–304. https://doi.org/10.1038/13014

Bolam, J. P., & Pissadaki, E. K. (2012). Living on the edge with too many mouths to feed: Why dopamine neurons die. *Movement Disorders*, *27*(12), 1478–1483. https://doi.org/10.1002/mds.25135

Bonet-Ponce, L., Beilina, A., Williamson, C. D., Lindberg, E., Kluss, J. H., Saez-Atienzar, S., Landeck, N., Kumaran, R., Mamais, A., Bleck, C. K. E., Li, Y., & Cookson, M. R. (2020). LRRK2 mediates tubulation and vesicle sorting from lysosomes. *Science Advances*, *6*(46).

Bonifati, V., Rizzu, P., van Baren, M. J., Schaap, O., Breedveld, G. J., Krieger, E., J Dekker, M. C., Squitieri, F., Ibanez, P., Joosse, M., van Dongen, J. W., Vanacore, N., van Swieten, J. C., Brice, A., Meco, G., van Duijn, C. M., Oostra, B. A., & Heutink, P. (2002). Mutations in the

DJ-1 Gene Associated with Autosomal Recessive Early-Onset Parkinsonism. *Science*, *299*(5604), 256–259. https://www.science.org

Boveris, A., & Cadenas, E. (1975). *Mitochondrial production of superoxide and its relationship to the antimycin insensitive respiration*. *54*.

Bragoszewski, P., Gornicka, A., Sztolsztener, M. E., & Chacinska, A. (2013). The Ubiquitin-Proteasome System Regulates Mitochondrial Intermembrane Space Proteins. *Molecular and Cellular Biology*, *33*(11), 2136–2148. https://doi.org/10.1128/mcb.01579-12

Braun, A. R., Lacy, M. M., Ducas, V. C., Rhoades, E., & Sachs, J. N. (2017). α-Synuclein's Uniquely Long Amphipathic Helix Enhances its Membrane Binding and Remodeling Capacity. *Journal of Membrane Biology*, *250*(2), 183–193. https://doi.org/10.1007/s00232-017-9946-1

Brembati, V., Faustini, G., Longhena, F., & Bellucci, A. (2023). Alpha synuclein post translational modifications: potential targets for Parkinson's disease therapy? In *Frontiers in Molecular Neuroscience* (Vol. 16). Frontiers Media S.A. https://doi.org/10.3389/fnmol.2023.1197853

Brillo, V., Chieregato, L., Leanza, L., Muccioli, S., & Costa, R. (2021). Mitochondrial dynamics, ros, and cell signaling: A blended overview. *Life*, *11*(4). https://doi.org/10.3390/life11040332

Brontesi, L., Imberdis, T., Ramalingam, N., & Dettmer, U. (2023). The effects of KTKEGV repeat motif and intervening ATVA sequence on α-synuclein solubility and assembly. *Journal of Neurochemistry*, *165*(2), 246–258. https://doi.org/10.1111/jnc.15763

Bunker, E. N., Le Guerroué, F., Wang, C., Strub, M., Werner, A., Tjandra, N., & Youle, R. J. (2023). Nix interacts with WIPI2 to induce mitophagy . *The EMBO Journal*, *42*(22). https://doi.org/10.15252/embj.2023113491

Burchell, V. S., Nelson, D. E., Sanchez-Martinez, A., Delgado-Camprubi, M., Ivatt, R. M., Pogson, J. H., Randle, S. J., Wray, S., Lewis, P. A., Houlden, H., Abramov, A. Y., Hardy, J., Wood, N. W., Whitworth, A. J., Laman, H., & Plun-Favreau, H. (2013). The Parkinson's disease-linked proteins Fbxo7 and Parkin interact to mediate mitophagy. *Nature Neuroscience*, *16*(9), 1257–1265. https://doi.org/10.1038/nn.3489

Burman, J. L., Pickles, S., Wang, C., Sekine, S., Vargas, J. N. S., Zhang, Z., Youle, A. M., Nezich, C. L., Wu, X., Hammer, J. A., & Youle, R. J. (2017). Mitochondrial fission facilitates the selective mitophagy of protein aggregates. *Journal of Cell Biology*, *216*(10), 3231–3247. https://doi.org/10.1083/jcb.201612106

Burré, J. (2015). The synaptic function of α-synuclein. In *Journal of Parkinson's Disease* (Vol. 5, Issue 4, pp. 699–713). IOS Press. https://doi.org/10.3233/JPD-150642

Burré, J., Sharma, M., Tsetsenis, T., Buchman, V., Etherton, M., & Südhof, T. C. (2010). *α-Synuclein Promotes SNARE-Complex Assembly in vivo and in vitro*. *329*(5999), 1663–1667.

Butler, E. K., Voigt, A., Lutz, A. K., Toegel, J. P., Gerhardt, E., Karsten, P., Falkenburger, B., Reinartz, A., Winklhofer, K. F., & Schulz, J. B. (2012). The mitochondrial chaperone protein TRAP1 mitigates α-synuclein toxicity. *PLoS Genetics*, *8*(2). https://doi.org/10.1371/journal.pgen.1002488

Byers, B., Cord, B., Nguyen, H. N., Schüle, B., Fenno, L., Lee, P. C., Deisseroth, K., Langston, J. W., Pera, R. R., & Palmer, T. D. (2011). SNCA triplication parkinson's patient's iPSC-Derived DA neurons accumulate α-Synuclein and are susceptible to oxidative stress. *PLoS ONE*, *6*(11). https://doi.org/10.1371/journal.pone.0026159

Caccamo, D. V, Herman, M. M., Frankfurter, A., Katsetos, C. D., Collins, V. P., & Rubinstein, L. J. (1989). An Immunohistochemical Study of Neuropeptides and Neuronal Cytoskeletal Proteins in the Neuroepithelial Component of a Spontaneous Murine Ovarian Teratoma Primitive Neuroepithelium Displays Immunoreactivity for Neuropeptides and Neuron-Associated f-Tubulin Isotype. In *AmericanJournal ofPathology* (Vol. 135, Issue 5).

Cadete, V. J. J., Deschênes, S., Cuillerier, A., Brisebois, F., Sugiura, A., Vincent, A., Turnbull, D., Picard, M., McBride, H. M., & Burelle, Y. (2016). Formation of mitochondrial-derived vesicles is an active and physiologically relevant mitochondrial quality control process in the cardiac system. *Journal of Physiology*, *594*(18), 5343–5362. https://doi.org/10.1113/JP272703

Calabresi, P., Mechelli, A., Natale, G., Volpicelli-Daley, L., Di Lazzaro, G., & Ghiglieri, V. (2023). Alpha-synuclein in Parkinson's disease and other synucleinopathies: from overt neurodegeneration back to early synaptic dysfunction. In *Cell Death and Disease* (Vol. 14, Issue 3). Springer Nature. https://doi.org/10.1038/s41419-023-05672-9

Campioni, S., Mannini, B., Zampagni, M., Pensalfini, A., Parrini, C., Evangelisti, E., Relini, A., Stefani, M., Dobson, C. M., Cecchi, C., & Chiti, F. (2010). A causative link between the structure of aberrant protein oligomers and their toxicity. *Nature Chemical Biology*, *6*, 140–147.

Castelo-Branco, G., Rawal, N., & Arenas, E. (2004). GSK-3β inhibition/β-catenin stabilization in ventral midbrain precursors increases differentiation into dopamine neurons. *Journal of Cell Science*, *117*(24), 5731–5737. https://doi.org/10.1242/jcs.01505

Catterall, W. A. (2011). Voltage-gated calcium channels. *Cold Spring Harbor Perspectives in Biology*, *3*(8), 1–23. https://doi.org/10.1101/cshperspect.a003947

Cenini, G., Rub, C., Bruderek, M., & Voos, W. (2016). Amyloid β-peptides interfere with mitochondrial preprotein import competence by a coaggregation process. *Molecular Biology of the Cell*, *27*(21), 3257–3272. https://doi.org/10.1091/mbc.E16-05-0313

Chang, D., Nalls, M. A., Hallgrímsdóttir, I. B., Hunkapiller, J., Brug, M. van der, Cai, F., Kerchner, G. A., Ayalon, G., Bingol, B., Sheng, M., Hinds, D., Behrens, T. W., Singleton, A. B., Bhangale, T. R., & Graham, R. R. (2017). A meta-analysis of genome-wide association studies identifies 17 new Parkinson's disease risk loci. *Nature Genetics*, *49*(10), 1511–1516. https://doi.org/10.1038/ng.3955

Chaudhry, A., Shi, R., & Luciani, D. S. (2020). A pipeline for multidimensional confocal analysis of mitochondrial morphology, function, and dynamics in pancreatic-cells Chaudhry A, Shi R, Luciani DS. A pipeline for multidimensional confocal analysis of mitochondrial morphology, function, and dynam-ics in pancreatic-cells. *American Journal of Physiology Endocrinology and Metabolism*, *318*, 87–101. https://doi.org/10.1152/ajpendo.00457.2019.-Live-cell

Cheignon, C., Tomas, M., Bonnefont-Rousselot, D., Faller, P., Hureau, C., & Collin, F. (2018). Oxidative stress and the amyloid beta peptide in Alzheimer's disease. In *Redox Biology* (Vol. 14, pp. 450–464). Elsevier B.V. https://doi.org/10.1016/j.redox.2017.10.014

Chen, C., McDonald, D., Blain, A., Mossman, E., Atkin, K., Marusich, M. F., Capaldi, R., Bone, L., Smith, A., Filby, A., Erskine, D., Russell, O., Hudson, G., Vincent, A. E., & Reeve, A. K. (2023). Parkinson's disease neurons exhibit alterations in mitochondrial quality control proteins. *Npj Parkinson's Disease*, *9*(1). https://doi.org/10.1038/s41531-023-00564-3

Chen, H., & Chan, D. C. (2004). Mitochondrial Dynamics in Mammals. In *Current Topics in Developmental Biology* (Vol. 59, pp. 119–144). http://www.jcb.org/cgi/content/full/

Chen, J., Chattopadhyay, B., Venkatakrishnan, G., & Ross2, A. H. (1990). Nerve Growth Factor-induced Differentiation of Human Neuroblastoma and Neuroepithelioma Cell Lines. *Cell Growth Differ*, *1*(2), 79–85. http://aacrjournals.org/cgd/article-pdf/1/2/79/3173892/79.pdf

Chen, L., Xie, Z., Turkson, S., & Zhuang, X. (2015). A53T human α-synuclein overexpression in transgenic mice induces pervasive mitochondria macroautophagy defects preceding dopamine neuron degeneration. *Journal of Neuroscience*, *35*(3), 890–905. https://doi.org/10.1523/JNEUROSCI.0089-14.2015

Chen, W., Zhao, H., & Li, Y. (2023). Mitochondrial dynamics in health and disease: mechanisms and potential targets. In *Signal Transduction and Targeted Therapy* (Vol. 8, Issue 1). Springer Nature. https://doi.org/10.1038/s41392-023-01547-9

Chen, Y., & Dorn, G. W. (2013). PINK1-phosphorylated mitofusin 2 is a parkin receptor for culling damaged mitochondria. *Science*, *340*(6131), 471–475. https://doi.org/10.1126/science.1231031

Cheng, F., Vivacqua, G., & Yu, S. (2011). The role of alpha-synuclein in neurotransmission and synaptic plasticity. In *Journal of Chemical Neuroanatomy* (Vol. 42, Issue 4, pp. 242–248). https://doi.org/10.1016/j.jchemneu.2010.12.001

Chinta, S. J., Mallajosyula, J. K., Rane, A., & Andersen, J. K. (2010). Mitochondrial alpha-synuclein accumulation impairs complex I function in dopaminergic neurons and results in increased mitophagy in vivo. *Neuroscience Letters*, *486*(3), 235–239. https://doi.org/10.1016/j.neulet.2010.09.061

Chmielarz, P., & Domanskyi, A. (2021). Alpha-synuclein preformed fibrils: A tool to understand Parkinson's disease and develop disease modifying therapy. In *Neural Regeneration Research* (Vol. 16, Issue 11, pp. 2219–2221). Wolters Kluwer Medknow Publications. https://doi.org/10.4103/1673-5374.310686

Choi, K. Y., Yoo, M., & Han, J. H. (2015). Toward understanding the role of the neuron-specific BAF chromatin remodeling complex in memory formation. In *Experimental and Molecular Medicine* (Vol. 47, Issue 4). Springer Nature. https://doi.org/10.1038/EMM.2014.129

Choi, M. L., Chappard, A., Singh, B. P., Maclachlan, C., Rodrigues, M., Fedotova, E. I., Berezhnov, A. V., De, S., Peddie, C. J., Athauda, D., Virdi, G. S., Zhang, W., Evans, J. R., Wernick, A. I., Zanjani, Z. S., Angelova, P. R., Esteras, N., Vinokurov, A. Y., Morris, K., … Gandhi, S. (2022). Pathological structural conversion of α-synuclein at the mitochondria induces neuronal toxicity. *Nature Neuroscience*, *25*(9), 1134–1148. https://doi.org/10.1038/s41593-022-01140-3

Choubey, V., Safiulina, D., Vaarmann, A., Cagalinec, M., Wareski, P., Kuum, M., Zharkovsky, A., & Kaasik, A. (2011). Mutant A53T α-Synuclein induces neuronal death by increasing mitochondrial autophagy. *Journal of Biological Chemistry*, *286*(12), 10814–10824. https://doi.org/10.1074/jbc.M110.132514

Chu, C. T., Bayir, H., & Kagan, V. E. (2014). LC3 binds externalized cardiolipin on injured mitochondria to signal mitophagy in neurons: Implications for Parkinson disease. In

Autophagy (Vol. 10, Issue 2, pp. 376–378). Taylor and Francis Inc. https://doi.org/10.4161/auto.27191

Chu, C. T., Ji, J., Dagda, R. K., Jiang, J. F., Tyurina, Y. Y., Kapralov, A. A., Tyurin, V. A., Yanamala, N., Shrivastava, I. H., Mohammadyani, D., Qiang Wang, K. Z., Zhu, J., Klein-Seetharaman, J., Balasubramanian, K., Amoscato, A. A., Borisenko, G., Huang, Z., Gusdon, A. M., Cheikhi, A., … Kagan, V. E. (2013). Cardiolipin externalization to the outer mitochondrial membrane acts as an elimination signal for mitophagy in neuronal cells. *Nature Cell Biology*, *15*(10), 1197–1205. https://doi.org/10.1038/ncb2837

Clerc, P., & Polster, B. M. (2012). Investigation of mitochondrial dysfunction by sequential microplate-based respiration measurements from intact and permeabilized neurons. *PLoS ONE*, *7*(4). https://doi.org/10.1371/journal.pone.0034465

Collier, T. J., Eugene Redmond, D., Steece-Collier, K., Lipton, J. W., & Manfredsson, F. P. (2016). Is alpha-synuclein loss-of-function a contributor to parkinsonian pathology? Evidence from non-human primates. *Frontiers in Neuroscience*, *10*(JAN). https://doi.org/10.3389/fnins.2016.00012

Conley, K. E., Jubrias, S. A., & Esselman, P. C. (2000). Oxidative capacity and ageing in human muscle. *J Physiol*, *526*(Pt 1), 203–210.

Cooper, A., Gitler, A. D., Cashikar, A., Haynes, C. M., Hill, K. K., Bhullar, B., Liu, K., Strathearn, K. E., Liu, F., Cao, S., Caldwell, K. A., Caldwell, G. A., Marsischky, G., Kolodner, R. D., LaBaer, J., Rochet, J., Bonini, M., & Lindquist, S. (2006). Alpha-synuclein blocks ER-Golgi traffic and Rab1 rescues neuron loss in Parkinson's models. *Science*, *313*(5785), 324–328. https://doi.org/10.1126/science.1125694

Cooper, G. M. (2000). *The Cell: A Molecular Approach* (2nd edition). Sinauer Associates.

Cornell, B., & Toyo-oka, K. (2017). 14-3-3 proteins in brain development: Neurogenesis, neuronal migration and neuromorphogenesis. In *Frontiers in Molecular Neuroscience* (Vol. 10). Frontiers Media S.A. https://doi.org/10.3389/fnmol.2017.00318

Cortes, C. J., & La Spada, A. R. (2019). TFEB dysregulation as a driver of autophagy dysfunction in neurodegenerative disease: Molecular mechanisms, cellular processes, and emerging therapeutic opportunities. In *Neurobiology of Disease* (Vol. 122, pp. 83–93). Academic Press Inc. https://doi.org/10.1016/j.nbd.2018.05.012

Courte, J., Bousset, L., Boxberg, Y. Von, Villard, C., Melki, R., & Peyrin, J. M. (2020). The expression level of alpha-synuclein in different neuronal populations is the primary

determinant of its prion-like seeding. *Scientific Reports*, *10*(1). https://doi.org/10.1038/s41598-020-61757-x

Cremades, N., & Dobson, C. M. (2018). The contribution of biophysical and structural studies of protein self-assembly to the design of therapeutic strategies for amyloid diseases. *Neurobiology of Disease*, *109*(Part B), 178–190. https://doi.org/10.1016/j.nbd.2017.07.009

Cuervo, A. M., Stefanis, L., Fredenburg, R., Lansbury, P. T., & Sulzer, D. (2004). Impaired degradation of mutant alpha-synuclein by chaperone-mediated autophagy. *Science*, *305*(5688), 1289–1292. https://doi.org/10.1126/science.1101372

Da Silva, J. S., & Dotti, C. G. (2002). Breaking the neuronal sphere: regulation of the actin cytoskeleton in neuritogenesis. *Nature Reviews Neuroscience*, *3*, 694–704.

Dauer, W., & Przedborski, S. (2003). Parkinson's Disease: Mechanisms and Models. *Neuron*, *39*, 889–909.

Davis, G. C., Williams, A. C., Markey, S. P., Ebert, M. H., Caine, E. D., Reichert, C. M., & Kopin, I. J. (1979). Chronic Parkinsonism Secondary to Intravenous Injection of Meperidine Analogues Case Report. *Psychiatry Research*, *1*(3), 249–254.

de Araujo, M. E. G., Liebscher, G., Hess, M. W., & Huber, L. A. (2020). Lysosomal size matters. In *Traffic* (Vol. 21, Issue 1, pp. 60–75). Blackwell Munksgaard. https://doi.org/10.1111/tra.12714

de Medeiros, L. M., De Bastiani, M. A., Rico, E. P., Schonhofen, P., Pfaffenseller, B., Wollenhaupt-Aguiar, B., Grun, L., Barbé-Tuana, F., Zimmer, E. R., Castro, M. A. A., Parsons, R. B., & Klamt, F. (2019). Cholinergic Differentiation of Human Neuroblastoma SH-SY5Y Cell Line and Its Potential Use as an In vitro Model for Alzheimer's Disease Studies. *Molecular Neurobiology*, *56*(11), 7355–7367. https://doi.org/10.1007/s12035-019-1605-3

Decressac, M., Mattsson, B., Weikop, P., Lundblad, M., Jakobsson, J., & Björklund, A. (2013). TFEB-mediated autophagy rescues midbrain dopamine neurons from α-synuclein toxicity. *Proceedings of the National Academy of Sciences of the United States of America*, *110*(19). https://doi.org/10.1073/pnas.1305623110

Deng, H., Gao, K., & Jankovic, J. (2013). The VPS35 gene and Parkinson's disease. *Movement Disorders*, *28*(5), 569–575. https://doi.org/10.1002/mds.25430

Deshwal, S., Fiedler, K. U., & Langer, T. (2024). Mitochondrial Proteases: Multifaceted Regulators of Mitochondrial Plasticity. *Annual Review of Biochemistry*, *20*(89), 501–528. https://doi.org/10.1146/annurev-biochem-062917

Detmer, S. A., & Chan, D. C. (2007). Functions and dysfunctions of mitochondrial dynamics. *Nature Reviews Molecular Cell Biology*, *8*, 870–879.

Devi, L., Raghavendran, V., Prabhu, B. M., Avadhani, N. G., & Anandatheerthavarada, H. K. (2008). Mitochondrial import and accumulation of α-synuclein impair complex I in human dopaminergic neuronal cultures and Parkinson disease brain. *Journal of Biological Chemistry*, *283*(14), 9089–9100. https://doi.org/10.1074/jbc.M710012200

Di Maio, R., Barrett, P. J., Hoffman, E. K., Barrett, C. W., Zharikov, A., Borah, A., Hu, X., McCoy, J., Chu, C. T., Burton, E. A., Hastings, T. G., & Greenamyre, J. T. (2016). α-synuclein binds to TOM20 and inhibits mitochondrial protein import in Parkinson's disease. In *Science Translational Medicine* (Vol. 8, Issue 342). American Association for the Advancement of Science. https://doi.org/10.1126/scitranslmed.aaf3634

Diao, J., Burré, J., Vivona, S., Cipriano, D. J., Sharma, M., Kyoung, M., Südhof, T. C., & Brunger, A. T. (2013). Native α-synuclein induces clustering of synaptic-vesicle mimics via binding to phospholipids and synaptobrevin-2/VAMP2. *ELife*, *2013*(2). https://doi.org/10.7554/eLife.00592

Dias, V., Junn, E., & Mouradian, M. M. (2013). The role of oxidative stress in parkinson's disease. In *Journal of Parkinson's Disease* (Vol. 3, Issue 4, pp. 461–491). I O S Press. https://doi.org/10.3233/JPD-130230

Divakaruni, A. S., & Jastroch, M. (2022). A practical guide for the analysis, standardization and interpretation of oxygen consumption measurements. In *Nature Metabolism* (Vol. 4, Issue 8, pp. 978–994). Nature Research. https://doi.org/10.1038/s42255-022-00619-4

Do, C. B., Tung, J. Y., Dorfman, E., Kiefer, A. K., Drabant, E. M., Francke, U., Mountain, J. L., Goldman, S. M., Tanner, C. M., Langston, J. W., Wojcicki, A., & Eriksson, N. (2011). Web-based genome-wide association study identifies two novel loci and a substantial genetic component for parkinson's disease. *PLoS Genetics*, *7*(6). https://doi.org/10.1371/journal.pgen.1002141

Dolman, N. J., Gerasimenko, J. V., Gerasimenko, O. V., Voronina, S. G., Petersen, O. H., & Tepikin, A. V. (2005). Stable Golgi-mitochondria complexes and formation of Golgi Ca2+ gradients in pancreatic acinar cells. *Journal of Biological Chemistry*, *280*(16), 15794–15799. https://doi.org/10.1074/jbc.M412694200

Drin, G., & Antonny, B. (2010). Amphipathic helices and membrane curvature. *FEBS Letters*, *584*(9), 1840–1847. https://doi.org/10.1016/j.febslet.2009.10.022

Duan, C., Kuang, L., Xiang, X., Zhang, J., Zhu, Y., Wu, Y., Yan, Q., Liu, L., & Li, T. (2020). Drp1 regulates mitochondrial dysfunction and dysregulated metabolism in ischemic injury via Clec16a-, BAX-, and GSH- pathways. *Cell Death and Disease*, *11*(4). https://doi.org/10.1038/s41419-020-2461-9

DuBoff, B., Götz, J., & Feany, M. B. (2012). Tau Promotes Neurodegeneration via DRP1 Mislocalization In Vivo. *Neuron*, *75*(4), 618–632. https://doi.org/10.1016/j.neuron.2012.06.026

Dunlop, E. A., Hunt, D. K., Acosta-Jaquez, H. A., Fingar, D. C., & Tee, A. R. (2011). ULK1 inhibits mTORC1 signaling, promotes multisite Raptor phosphorylation and hinders substrate binding. *Autophagy*, *7*(7), 737–747. https://doi.org/10.4161/auto.7.7.15491

Durcan, T. M., Tang, M. Y., Pérusse, J. R., Dashti, E. A., Aguileta, M. A., McLelland, G., Gros, P., Shaler, T. A., Faubert, D., Coulombe, B., & Fon, E. A. (2014). USP 8 regulates mitophagy by removing K 6-linked ubiquitin conjugates from parkin . *The EMBO Journal*, *33*(21), 2473–2491. https://doi.org/10.15252/embj.201489729

Dwane, S., Durack, E., & Kiely, P. A. (2013). Optimising parameters for the differentiation of SH-SY5Y cells to study cell adhesion and cell migration. *BMC Research Notes*, *6*(1). https://doi.org/10.1186/1756-0500-6-366

Ebrahimi-Fakhari, D., Cantuti-Castelvetri, I., Fan, Z., Rockenstein, E., Masliah, E., Hyman, B. T., McLean, P. J., & Unni, V. K. (2011). Distinct roles in vivo for the Ubiquitin-Proteasome system and the Autophagy-Lysosomal Pathway in the Degradation of α-Synuclein. *Journal of Neuroscience*, *31*(41), 14508–14520. https://doi.org/10.1523/JNEUROSCI.1560-11.2011

Eisner, V., Picard, M., & Hajnóczky, G. (2018). Mitochondrial dynamics in adaptive and maladaptive cellular stress responses. *Nature Cell Biology*, *20*(7), 755–765. https://doi.org/10.1038/s41556-018-0133-0

Eldeeb, M. A., Thomas, R. A., Ragheb, M. A., Fallahi, A., & Fon, E. A. (2022). Mitochondrial quality control in health and in Parkinson's disease. *Physiological Reviews*.

Elgenaidi, I. S., & Spiers, J. P. (2019). Regulation of the phosphoprotein phosphatase 2A system and its modulation during oxidative stress: A potential therapeutic target? In *Pharmacology and Therapeutics* (Vol. 198, pp. 68–89). Elsevier Inc. https://doi.org/10.1016/j.pharmthera.2019.02.011

Ellis, C. E., Murphy, E. J., Mitchell, D. C., Golovko, M. Y., Scaglia, F., Barceló-Coblijn, G. C., & Nussbaum, R. L. (2005). Mitochondrial Lipid Abnormality and Electron Transport Chain

Impairment in Mice Lacking α-Synuclein. *Molecular and Cellular Biology*, *25*(22), 10190–10201. https://doi.org/10.1128/mcb.25.22.10190-10201.2005

Emamzadeh, F. N. (2016). Alpha-synuclein structure, functions, and interactions. *Journal of Research in Medical Sciences*, *21*(2). https://doi.org/10.4103/1735-1995.181989

Emanuele, M., & Chieregatti, E. (2015). Mechanisms of alpha-synuclein action on neurotransmission: Cell-autonomous and non-cell autonomous role. *Biomolecules*, *5*(2), 865–892. https://doi.org/10.3390/biom5020865

Emin, D., Zhang, Y. P., Lobanova, E., Miller, A., Li, X., Xia, Z., Dakin, H., Sideris, D. I., Lam, J. Y. L., Ranasinghe, R. T., Kouli, A., Zhao, Y., De, S., Knowles, T. P. J., Vendruscolo, M., Ruggeri, F. S., Aigbirhio, F. I., Williams-Gray, C. H., & Klenerman, D. (2022). Small soluble α-synuclein aggregates are the toxic species in Parkinson's disease. *Nature Communications*, *13*(1). https://doi.org/10.1038/s41467-022-33252-6

Encinas, M., Iglesias, M., Liu, Y., Wang, H., Muhaisen, A., Ceña, V., Gallego, C., & Comella, J. X. (2000). Sequential treatment of SH-SY5Y cells with retinoic acid and brain-derived neurotrophic factor gives rise to fully differentiated, neurotrophic factor-dependent, human neuron-like cells. *Journal of Neurochemistry*, *75*(3), 991–1003. https://doi.org/10.1046/j.1471-4159.2000.0750991.x

Farzadfard, A., Pedersen, J. N., Meisl, G., Somavarapu, A. K., Alam, P., Goksøyr, L., Nielsen, M. A., Sander, A. F., Knowles, T. P. J., Pedersen, J. S., & Otzen, D. E. (2022). The C-terminal tail of α-synuclein protects against aggregate replication but is critical for oligomerization. *Communications Biology*, *5*(1). https://doi.org/10.1038/s42003-022-03059-8

Faustini, G., Marchesan, E., Zonta, L., Bono, F., Bottani, E., Longhena, F., Ziviani, E., Valerio, A., & Bellucci, A. (2019). Alpha-Synuclein Preserves Mitochondrial Fusion and Function in Neuronal Cells. *Oxidative Medicine and Cellular Longevity*, *2019*. https://doi.org/10.1155/2019/4246350

Feng, Y., & Klionsky, D. J. (2017). Autophagic membrane delivery through ATG9. *Cell Research*, *27*(2), 161–162. https://doi.org/10.1038/cr.2017.4

Ferreira, P. S., Nogueira, T. B., Costa, V. M., Branco, P. S., Ferreira, L. M., Fernandes, E., Bastos, M. L., Meisel, A., Carvalho, F., & Capela, J. P. (2013). Neurotoxicity of "ecstasy" and its metabolites in human dopaminergic differentiated SH-SY5Y cells. *Toxicology Letters*, *216*(2–3), 159–170. https://doi.org/10.1016/j.toxlet.2012.11.015

Février, M., Dorgham, K., & Rebollo, A. (2011). CD4 +T cell depletion in human immunodeficiency virus (HIV) infection: Role of apoptosis. In *Viruses* (Vol. 3, Issue 5, pp. 586–612). https://doi.org/10.3390/v3050586

Fields, J. A., Serger, E., Campos, S., Divakaruni, A. S., Kim, C., Smith, K., Trejo, M., Adame, A., Spencer, B., Rockenstein, E., Murphy, A. N., Ellis, R. J., Letendre, S., Grant, I., & Masliah, E. (2016). HIV alters neuronal mitochondrial fission/fusion in the brain during HIV-associated neurocognitive disorders. *Neurobiology of Disease*, *86*, 154–169. https://doi.org/10.1016/j.nbd.2015.11.015

Filograna, R., Civiero, L., Ferrari, V., Codolo, G., Greggio, E., Bubacco, L., Beltramini, M., & Bisaglia, M. (2015). Analysis of the catecholaminergic phenotype in human SH-SY5Y and BE(2)-M17 neuroblastoma cell lines upon differentiation. *PLoS ONE*, *10*(8). https://doi.org/10.1371/journal.pone.0136769

Fonzo, A. D., Dekker, M. C. J., Montagna, P., Baruzzi, A., Yonova, E. H., Guedes, L. C., Szczerbinska, A., Zhao, T., Dubbel-Hulsman, L. O. M., Wouters, C. H., De Graaff, E., Oyen, W. J. G., Simons, E. J., Breedveld, G. J., Oostra, B. A., Horstink, M. W., & Bonifati, V. (2009). FBXO7 mutations cause autosomal recessive, early-onset parkinsonian- pyramidal syndrome. *Neurology*, *72*(3), 240–245. https://doi.org/10.1212/01.wnl.0000338144.10967.2b

Fountaine, T. M., & Wade-Martins, R. (2007). RNA interference-mediated knockdown of α-synuclein protects human dopaminergic neuroblastoma cells from MPP+ toxicity and reduces dopamine transport. *Journal of Neuroscience Research*, *85*(2), 351–363. https://doi.org/10.1002/jnr.21125

Franchino, C. A., Motori, E., & Bergami, M. (2024). Janus-faced Mitofusin 2 (MFN2): mitochondria-endoplasmic reticulum shaping and tethering functions unveiled. *Signal Transduction and Targeted Therapy*, *9*(1). https://doi.org/10.1038/s41392-023-01730-y

Frank, S., Gaume, B., Bergmann-Leitner, E. S., Leitner, W. W., Robert, E. G., Dé Ric Catez, F., Smith, C. L., & Youle, R. J. (2001). The Role of Dynamin-Related Protein 1, a Mediator of Mitochondrial Fission, in Apoptosis. *Developmental Cell*, *1*(4), 515–525. http://www.developmentalcell.

Fransen, M., Lismont, C., & Walton, P. (2017). The peroxisome-mitochondria connection: How and why? In *International Journal of Molecular Sciences* (Vol. 18, Issue 6). MDPI AG. https://doi.org/10.3390/ijms18061126

Freyer, C., Stranneheim, H., Naess, K., Mourier, A., Felser, A., Maffezzini, C., Lesko, N., Bruhn, H., Engvall, M., Wibom, R., Barbaro, M., Hinze, Y., Magnusson, M., Andeer, R., Zetterström, R. H., Von Döbeln, U., Wredenberg, A., & Wedell, A. (2015). Rescue of primary ubiquinone deficiency due to a novel COQ7 defect using 2,4-dihydroxybensoic acid. *Journal of Medical Genetics*, *52*(11), 779–783. https://doi.org/10.1136/jmedgenet-2015-102986

Friedman, J. R., & Nunnari, J. (2014). Mitochondrial form and function. In *Nature* (Vol. 505, Issue 7483, pp. 335–343). https://doi.org/10.1038/nature12985

Fu, H., Subramanian, R. R., & Masters, S. C. (2024). 4-3-3 PROTEINS: Structure, Function, and Regulation. In *Annu. Rev. Pharmacol. Toxicol* (Vol. 40). www.AnnualReviews.org,

Fujiwara, H., Hasegawa, M., Dohmae, N., Kawashima, A., Masliah, E., Goldberg, M. S., Shen, J., Takio, K., & Iwatsubo, T. (2002). α-synuclein is phosphorylated in synucleinopathy lesions. *Nature Cell Biology*, *4*(2), 160–164. https://doi.org/10.1038/ncb748

Fujiwara, I., Takahashi, S., Tadakuma, H., Funatsu, T., & Ishiwata, S. (2002). Microscopic analysis of polymerization dynamics with individual actin filaments. *Nature Cell Biology*, *4*(9), 666–673. https://doi.org/10.1038/ncb841

Fukuda, T., Furukawa, K., Maruyama, T., Yamashita, S. ichi, Noshiro, D., Song, C., Ogasawara, Y., Okuyama, K., Alam, J. M., Hayatsu, M., Saigusa, T., Inoue, K., Ikeda, K., Takai, A., Chen, L., Lahiri, V., Okada, Y., Shibata, S., Murata, K., … Kanki, T. (2023). The mitochondrial intermembrane space protein mitofissin drives mitochondrial fission required for mitophagy. *Molecular Cell*, *83*(12), 2045-2058.e9. https://doi.org/10.1016/j.molcel.2023.04.022

Funayama, M., Ohe, K., Amo, T., Furuya, N., Yamaguchi, J., Saiki, S., Li, Y., Ogaki, K., Ando, M., Yoshino, H., Tomiyama, H., Nishioka, K., Hasegawa, K., Saiki, H., Satake, W., Mogushi, K., Sasaki, R., Kokubo, Y., Kuzuhara, S., … Hattori, N. (2015). CHCHD2 mutations in autosomal dominant late-onset Parkinson's disease: A genome-wide linkage and sequencing study. *The Lancet Neurology*, *14*(3), 274–282. https://doi.org/10.1016/S1474-4422(14)70266-2

Furlong, R. M., O'Keeffe, G. W., O'Neill, C., & Sullivan, A. M. (2020). Alterations in α-synuclein and PINK1 expression reduce neurite length and induce mitochondrial fission and Golgi fragmentation in midbrain neurons. *Neuroscience Letters*, *720*. https://doi.org/10.1016/j.neulet.2020.134777

Ganjam, G. K., Bolte, K., Matschke, L. A., Neitemeier, S., Dolga, A. M., Höllerhage, M., Höglinger, G. U., Adamczyk, A., Decher, N., Oertel, W. H., & Culmsee, C. (2019). Mitochondrial

damage by α-synuclein causes cell death in human dopaminergic neurons. *Cell Death and Disease*, *10*(11). https://doi.org/10.1038/s41419-019-2091-2

Gao, N., Li, Y.-H., Li, X., Yu, S., Fu, G.-L., & Chen, B. (2007). Effect of α-synuclein on the promoter activity of tyrosine hydroxylase gene. In *Neuroscience Bulletin* (Vol. 23, Issue 1). http://www.neurosci.cn

Gao, V., Briano, J. A., Komer, L. E., & Burré, J. (2023). Functional and Pathological Effects of α-Synuclein on Synaptic SNARE Complexes. In *Journal of Molecular Biology* (Vol. 435, Issue 1). Academic Press. https://doi.org/10.1016/j.jmb.2022.167714

Ge, P., Dawson, V. L., & Dawson, T. M. (2020). PINK1 and Parkin mitochondrial quality control: A source of regional vulnerability in Parkinson's disease. In *Molecular Neurodegeneration* (Vol. 15, Issue 1). BioMed Central Ltd. https://doi.org/10.1186/s13024-020-00367-7

Gegg, M. E., Cooper, J. M., Chau, K. Y., Rojo, M., Schapira, A. H. V., & Taanman, J. W. (2010). Mitofusin 1 and mitofusin 2 are ubiquitinated in a PINK1/parkin-dependent manner upon induction of mitophagy. *Human Molecular Genetics*, *19*(24), 4861–4870. https://doi.org/10.1093/hmg/ddq419

George, J. M. (2001). The synucleins. *Genome Biology*, *3*(1). http://genomebiology.com/2001/3/1/reviews/3002.1http://genomebiology.com/2001/3/1/reviews/3002

Ghanem, S. S., Majbour, N. K., Vaikath, N. N., Ardah, M. T., Erskine, D., Jensen, N. M., Fayyad, M., Sudhakaran, I. P., Vasili, E., Melachroinou, K., Abdi, I. Y., Poggiolini, I., Santos, P., Dorn, A., Carloni, P., Vekrellis, K., Attems, J., Mckeith, I., Outeiro, T. F., … El-Agnaf, O. M. A. (2022). α-Synuclein phosphorylation at serine 129 occurs after initial protein deposition and inhibits seeded fibril formation and toxicity. *PNAS*, *119*(e2109617119). https://doi.org/10.1073/pnas

Ghio, S., Kamp, F., Cauchi, R., Giese, A., & Vassallo, N. (2016). Interaction of α-synuclein with biomembranes in Parkinson's disease - Role of cardiolipin. In *Progress in Lipid Research* (Vol. 61, pp. 73–82). Elsevier Ltd. https://doi.org/10.1016/j.plipres.2015.10.005

Giasson, B. I., Duda, J. E., Quinn, S. M., Zhang, B., Trojanowski, J. Q., & M-Y Lee, V. (2002). Neuronal-Synucleinopathy with Severe Movement Disorder in Mice Expressing A53T Human-Synuclein. In *Neuron* (Vol. 34). Golbe. http://www.

Giasson, B. I., Murray, I. V. J., Trojanowski, J. Q., & Lee, V. M. Y. (2001). A Hydrophobic Stretch of 12 Amino Acid Residues in the Middle of α-Synuclein Is Essential for Filament Assembly.

Journal of Biological Chemistry, *276*(4), 2380–2386. https://doi.org/10.1074/jbc.M008919200

Gidalevitz, T., Ben-Zvi, A., Ho, K. H., Brignull, H. R., & Morimoto, R. I. (2006). Progressive disruption of cellular protein folding in models of polyglutamine diseases. *Science*, *311*(5766), 1468–1471. https://doi.org/10.1126/science.1122125

Gilmozzi, V., Gentile, G., Castelo Rueda, M. P., Hicks, A. A., Pramstaller, P. P., Zanon, A., Lévesque, M., & Pichler, I. (2020). Interaction of Alpha-Synuclein With Lipids: Mitochondrial Cardiolipin as a Critical Player in the Pathogenesis of Parkinson's Disease. In *Frontiers in Neuroscience* (Vol. 14). Frontiers Media S.A. https://doi.org/10.3389/fnins.2020.578993

Glaser, C. B., Yamin, G., Uversky, V. N., & Fink, A. L. (2005). Methionine oxidation, α-synuclein and Parkinson's disease. In *Biochimica et Biophysica Acta - Proteins and Proteomics* (Vol. 1703, Issue 2, pp. 157–169). https://doi.org/10.1016/j.bbapap.2004.10.008

Goedert, M. (2001). Alpha-synuclein and neurodegenerative diseases. *Nature Reviews Neuroscience*, *2*, 492–501.

Gonzalez, A., Valeiras, M., Sidransky, E., & Tayebi, N. (2014). Lysosomal integral membrane protein-2: A new player in lysosome-related pathology. *Molecular Genetics and Metabolism*, *111*(2), 84–91. https://doi.org/10.1016/j.ymgme.2013.12.005

Gosavi, N., Lee, H. J., Lee, J. S., Patel, S., & Lee, S. J. (2002). Golgi fragmentation occurs in the cells with prefibrillar α-synuclein aggregates and precedes the formation of fibrillar inclusion. *Journal of Biological Chemistry*, *277*(50), 48984–48992. https://doi.org/10.1074/jbc.M208194200

Gottschalk, W. K., Lutz, M. W., He, Y. T., Saunders, A. M., Burns, D. K., Roses, A. D., & Chiba-Falek, O. (2014). The broad impact of TOM40 on neurodegenerative diseases in aging. *Journal of Parkinson's Disease and Alzheimer's Disease*, *1*(1). https://doi.org/10.13188/2376-922x.1000003

Grey, M., Linse, S., Nilsson, H., Brundin, P., & Sparr, E. (2011). Membrane interaction of α-synuclein in different aggregation states. *Journal of Parkinson's Disease*, *1*(4), 359–371. https://doi.org/10.3233/JPD-2011-11067

Gu, X., Ma, Y., Liu, Y., & Wan, Q. (2021). Measurement of mitochondrial respiration in adherent cells by Seahorse XF96 Cell Mito Stress Test. *STAR Protocols*, *2*(1). https://doi.org/10.1016/j.xpro.2020.100245

Guardia-Laguarta, C., Area-Gomez, E., Rüb, C., Liu, Y., Magrané, J., Becker, D., Voos, W., Schon, E. A., & Przedborski, S. (2014). α-synuclein is localized to mitochondria-associated ER membranes. *Journal of Neuroscience*, *34*(1), 249–259. https://doi.org/10.1523/JNEUROSCI.2507-13.2014

Gui, Y. X., Wang, X. Y., Kang, W. Y., Zhang, Y. J., Zhang, Y., Zhou, Y., Quinn, T. J., Liu, J., & Chen, S. Di. (2012). Extracellular signal-regulated kinase is involved in alpha-synuclein-induced mitochondrial dynamic disorders by regulating dynamin-like protein 1. *Neurobiology of Aging*, *33*(12), 2841–2854. https://doi.org/10.1016/j.neurobiolaging.2012.02.001

Guo, B., Liang, Q., Li, L., Hu, Z., Wu, F., Zhang, P., Ma, Y., Zhao, B., Kovács, A. L., Zhang, Z., Feng, D., Chen, S., & Zhang, H. (2014). O-GlcNAc-modification of SNAP-29 regulates autophagosome maturation. *Nature Cell Biology*, *16*(12), 1215–1226. https://doi.org/10.1038/ncb3066

Habibalahi, A., Moghari, M. D., Campbell, J. M., Anwer, A. G., Mahbub, S. B., Gosnell, M., Saad, S., Pollock, C., & Goldys, E. M. (2020). Non-invasive real-time imaging of reactive oxygen species (ROS) using auto-fluorescence multispectral imaging technique: A novel tool for redox biology. *Redox Biology*, *34*. https://doi.org/10.1016/j.redox.2020.101561

Halskau, Ø., Ying, M., Baumann, A., Kleppe, R., Rodriguez-Larrea, D., Almås, B., Haavik, J., & Martinez, A. (2009). Three-way interaction between 14-3-3 proteins, the N-terminal region of tyrosine hydroxylase, and negatively charged membranes. *Journal of Biological Chemistry*, *284*(47), 32758–32769. https://doi.org/10.1074/jbc.M109.027706

Hansen, C., Björklund, T., Petit, G. H., Lundblad, M., Murmu, R. P., Brundin, P., & Li, J. Y. (2013). A novel α-synuclein-GFP mouse model displays progressive motor impairment, olfactory dysfunction and accumulation of α-synuclein-GFP. *Neurobiology of Disease*, *56*, 145–155. https://doi.org/10.1016/j.nbd.2013.04.017

Hashimoto, M., Hsu, L. J., Xia, Y., Takeda, A., Sisk, A., Sundsmo, M., & Masliah, E. (1999). Oxidative stress induces amyloid-like aggregate formation of NACP/a-synuclein in vitro. *Neurochemistry*, *10*(4), 717–721. http://journals.lww.com/neuroreport

Hayashi, J., & Carver, J. A. (2022). β-Synuclein: An Enigmatic Protein with Diverse Functionality. In *Biomolecules* (Vol. 12, Issue 1). MDPI. https://doi.org/10.3390/biom12010142

Hegde, M., Vendula, I., & Rao, K. S. (2024). Mitochondria-Targeted Oligomeric α-Synuclein Induces TOM40 Degradation and Mitochondrial Dysfunction in Parkinson's Disease and Parkinsonism-Dementia of Guam. *Biorxiv*. https://doi.org/10.21203/rs.3.rs-3970470/v1

Henderson, M. X., Trojanowski, J. Q., & Lee, V. M. Y. (2019). α-Synuclein pathology in Parkinson's disease and related α-synucleinopathies. *Neuroscience Letters*, *709*. https://doi.org/10.1016/j.neulet.2019.134316

Hershko, A., & Ciechanover, A. (1998). THE UBIQUITIN SYSTEM. In *Annu. Rev. Biochem* (Vol. 67).

Hijioka, M., Inden, M., Yanagisawa, D., & Kitamura, Y. (2017). DJ-1/PARK7: A New Therapeutic Target for Neurodegenerative Disorders. *Biological and Pharmaceutical Bulletin*, *548*(5), 548–552.

Hinton, A., Claypool, S. M., Neikirk, K., Senoo, N., Wanjalla, C. N., Kirabo, A., & Williams, C. R. (2024). Mitochondrial Structure and Function in Human Heart Failure. In *Circulation Research* (Vol. 135, Issue 2, pp. 372–396). Lippincott Williams and Wilkins. https://doi.org/10.1161/CIRCRESAHA.124.323800

Hoffmann, A. C., Minakaki, G., Menges, S., Salvi, R., Savitskiy, S., Kazman, A., Vicente Miranda, H., Mielenz, D., Klucken, J., Winkler, J., & Xiang, W. (2019). Extracellular aggregated alpha synuclein primarily triggers lysosomal dysfunction in neural cells prevented by trehalose. *Scientific Reports*, *9*(544). https://doi.org/10.1038/s41598-018-35811-8

Hong, W. J., & Lev, S. (2014). Tethering the assembly of SNARE complexes. In *Trends in Cell Biology* (Vol. 24, Issue 1, pp. 35–43). https://doi.org/10.1016/j.tcb.2013.09.006

Hong, W. L., Huang, H., Zeng, X., & Duan, C. Y. (2024). Targeting mitochondrial quality control: new therapeutic strategies for major diseases. In *Military Medical Research* (Vol. 11, Issue 1). BioMed Central Ltd. https://doi.org/10.1186/s40779-024-00556-1

Hoogerheide, D. P., Gurnev, P. A., Rostovtseva, T. K., & Bezrukov, S. M. (2017). Mechanism of α-synuclein translocation through a VDAC nanopore revealed by energy landscape modeling of escape time distributions. *Nanoscale*, *9*(1), 183–192. https://doi.org/10.1039/c6nr08145b

Horvath, S. E., & Daum, G. (2013). Lipids of mitochondria. In *Progress in Lipid Research* (Vol. 52, Issue 4, pp. 590–614). Elsevier Ltd. https://doi.org/10.1016/j.plipres.2013.07.002

Hosokawa, N., Hara, T., Kaizuka, T., Kishi, C., Takamura, A., Miura, Y., Iemura, S.-I., Natsume, T., Takehana, K., Yamada, N., Guan, J.-L., Oshiro, N., Mizushima, N., & Schmid, S. L. (2009). Nutrient-dependent mTORC1 Association with the ULK1-Atg13-FIP200 Complex Required for Autophagy. *Molecular Biology of the Cell*, *20*(7), 1981–1991. https://doi.org/10.1091/mbc.E08

Hou, X., Fiesel, F. C., Truban, D., Castanedes Casey, M., Lin, W. lang, Soto, A. I., Tacik, P., Rousseau, L. G., Diehl, N. N., Heckman, M. G., Lorenzo-Betancor, O., Ferrer, I., Arbelo, J. M., Steele, J. C., Farrer, M. J., Cornejo-Olivas, M., Torres, L., Mata, I. F., Graff-Radford, N. R., … Springer, W. (2018). Age- and disease-dependent increase of the mitophagy marker phospho-ubiquitin in normal aging and Lewy body disease. *Autophagy*, *14*(8), 1404–1418. https://doi.org/10.1080/15548627.2018.1461294

Hsieh, C. H., Li, L., Vanhauwaert, R., Nguyen, K. T., Davis, M. D., Bu, G., Wszolek, Z. K., & Wang, X. (2019). Miro1 Marks Parkinson's Disease Subset and Miro1 Reducer Rescues Neuron Loss in Parkinson's Models. *Cell Metabolism*, *30*(6), 1131–1140. https://doi.org/10.1016/j.cmet.2019.08.023

Hsieh, C. H., Shaltouki, A., Gonzalez, A. E., Bettencourt da Cruz, A., Burbulla, L. F., St. Lawrence, E., Schüle, B., Krainc, D., Palmer, T. D., & Wang, X. (2016). Functional Impairment in Miro Degradation and Mitophagy Is a Shared Feature in Familial and Sporadic Parkinson's Disease. *Cell Stem Cell*, *19*(6), 709–724. https://doi.org/10.1016/j.stem.2016.08.002

Hsu, L. J., Sagara, Y., Arroyo, A., Rockenstein, E., Sisk, A., Mallory, M., Wong, J., Takenouchi, T., Hashimoto, M., & Masliah, E. (2000). Synuclein Promotes Mitochondrial Deficit and Oxidative Stress. *Am J Pathol.*, *157*(2), 401–410.

Hu, M., Zhou, N., Cai, W., & Xu, H. (2022). Lysosomal solute and water transport. In *Journal of Cell Biology* (Vol. 221, Issue 11). Rockefeller University Press. https://doi.org/10.1083/jcb.202109133

Hua, G., Xiaolei, L., Weiwei, Y., Hao, W., Yuangang, Z., Dongmei, L., Yazhuo, Z., & Hui, Y. (2015). Protein Phosphatase 2A is Involved in the Tyrosine Hydroxylase Phosphorylation Regulated by α-Synuclein. *Neurochemical Research*, *40*(3), 428–437. https://doi.org/10.1007/s11064-014-1477-x

Huang, C., Ren, G., Zhou, H., & Wang, C. C. (2005). A new method for purification of recombinant human α-synuclein in Escherichia coli. *Protein Expression and Purification*, *42*(1), 173–177. https://doi.org/10.1016/j.pep.2005.02.014

Huang, D., Chen, S., Xiong, D., Wang, H., Zhu, L., Wei, Y., Li, Y., & Zou, S. (2023). Mitochondrial Dynamics: Working with the Cytoskeleton and Intracellular Organelles to Mediate Mechanotransduction. In *Aging and Disease* (Vol. 14, Issue 5, pp. 1511–1532). International Society on Aging and Disease. https://doi.org/10.14336/AD.2023.0201

Huang, M., Wang, B., Li, X., Fu, C., Wang, C., & Kang, X. (2019). A-Synuclein: A multifunctional player in exocytosis, endocytosis, and vesicle recycling. In *Frontiers in Neuroscience* (Vol. 13, Issue JAN). Frontiers Media S.A. https://doi.org/10.3389/fnins.2019.00028

Huang, W., Choi, W., Hu, W., Mi, N., Guo, Q., Ma, M., Liu, M., Tian, Y., Lu, P., Wang, F. L., Deng, H., Liu, L., Gao, N., Yu, L., & Shi, Y. (2012). Crystal structure and biochemical analyses reveal Beclin 1 as a novel membrane binding protein. *Cell Research*, *22*(3), 473–489. https://doi.org/10.1038/cr.2012.24

Hui, S., George, J., Kapadia, M., Chau, H., Bariring, Z., Earnshaw, R., Shafiq, K., Kalia, L. V., & Kalia, S. K. (2024). Mitophagy Upregulation Occurs Early in the Neurodegenerative Process Mediated by α-Synuclein. *Molecular Neurobiology*. https://doi.org/10.1007/s12035-024-04131-6

Iljina, M., Garcia, G. A., Horrocks, M. H., Tosatto, L., Choi, M. L., Ganzinger, K. A., Abramov, A. Y., Gandhi, S., Wood, N. W., Cremades, N., Dobson, C. M., Knowles, T. P. J., & Klenerman, D. (2016). Kinetic model of the aggregation of alpha-synuclein provides insights into prion-like spreading. *Proceedings of the National Academy of Sciences of the United States of America*, *113*(9), E1206–E1215. https://doi.org/10.1073/pnas.1524128113

Inigo, J. R., & Chandra, D. (2022). The mitochondrial unfolded protein response (UPRmt): shielding against toxicity to mitochondria in cancer. In *Journal of Hematology and Oncology* (Vol. 15, Issue 1). BioMed Central Ltd. https://doi.org/10.1186/s13045-022-01317-0

Ishii, A., Furusho, M., Dupree, J. L., & Bansal, R. (2014). Role of ERK1/2 MAPK signaling in the maintenance of myelin and axonal integrity in the adult CNS. *Journal of Neuroscience*, *34*(48), 16031–16045. https://doi.org/10.1523/JNEUROSCI.3360-14.2014

Itakura, E., Kishi-Itakura, C., & Mizushima, N. (2012). The hairpin-type tail-anchored SNARE syntaxin 17 targets to autophagosomes for fusion with endosomes/lysosomes. *Cell*, *151*(6), 1256–1269. https://doi.org/10.1016/j.cell.2012.11.001

Ito, K., & Takizawa, T. (2018). Nuclear architecture in the nervous system: Development, function, and neurodevelopmental diseases. In *Frontiers in Genetics* (Vol. 9, Issue AUG). Frontiers Media S.A. https://doi.org/10.3389/fgene.2018.00308

Jauhari, A., Singh, T., Pandey, A., Singh, P., Singh, N., Srivastava, A. K., Pant, A. B., Parmar, D., & Yadav, S. (2017). Differentiation Induces Dramatic Changes in miRNA Profile, Where Loss of Dicer Diverts Differentiating SH-SY5Y Cells Toward Senescence. *Molecular Neurobiology*, *54*(7), 4986–4995. https://doi.org/10.1007/s12035-016-0042-9

Jęśko, H., Lenkiewicz, A. M., Wilkaniec, A., & Adamczyk, A. (2019). The interplay between parkin and alpha-synuclein; possible implications for the pathogenesis of parkinson's disease. *Acta Neurobiologiae Experimentalis*, *79*(3), 279–289. https://doi.org/10.21307/ane-2019-026

Ježek, P., & Hlavatá, L. (2005). Mitochondria in homeostasis of reactive oxygen species in cell, tissues, and organism. *International Journal of Biochemistry and Cell Biology*, *37*(12), 2478–2503. https://doi.org/10.1016/j.biocel.2005.05.013

Jin, H., Kanthasamy, A., Ghosh, A., Yang, Y., Anantharam, V., & Kanthasamy, A. G. (2011). α-synuclein negatively regulates protein kinase Cδ expression to suppress apoptosis in dopaminergic neurons by reducing p300 histone acetyltransferase activity. *Journal of Neuroscience*, *31*(6), 2035–2051. https://doi.org/10.1523/JNEUROSCI.5634-10.2011

Jin, S. M., & Youle, R. J. (2013). The accumulation of misfolded proteins in the mitochondrial matrix is sensed by PINK1 to induce PARK2/Parkin-mediated mitophagy of polarized mitochondria. *Autophagy*, *9*(11), 1750–1757. https://doi.org/10.4161/auto.26122

Jinek, M., Chylinski, K., Fonfara, I., Hauer, M., Doudna, J. A., & Charpentier, E. (2012). A Programmable Dual-RNA-Guided DNA Endonuclease in Adaptive Bacterial Immunity. *Science*, *337*, 816–821. https://www.science.org

Jo, E., Fuller, N., Rand, R. P., St George-Hyslop, P., & Fraser, P. E. (2002). Defective membrane interactions of familial Parkinson's disease mutant A30P α-Synuclein. *Journal of Molecular Biology*, *315*(4), 799–807. https://doi.org/10.1006/jmbi.2001.5269

Jo, E., McLaurin, J. A., Yip, C. M., St. George-Hyslop, P., & Fraser, P. E. (2000). α-Synuclein membrane interactions and lipid specificity. *Journal of Biological Chemistry*, *275*(44), 34328–34334. https://doi.org/10.1074/jbc.M004345200

Juhasz, K., Lipp, A. M., Nimmervoll, B., Sonnleitner, A., Hesse, J., Haselgruebler, T., & Balogi, Z. (2014). The complex function of Hsp70 in metastatic cancer. In *Cancers* (Vol. 6, Issue 1, pp. 42–66). https://doi.org/10.3390/cancers6010042

K Chung, K. K., Thomas, B., Li, X., Pletnikova, O., Troncoso, J. C., Marsh, L., Dawson, V. L., & Dawson, T. M. (2001). S-Nitrosylation of Parkin Regulates Ubiquitination and Compromises Parkin's Protective Function. In *Exp. Clin. Endocrinol. Diabetes* (Vol. 15). www.sciencemag.org/cgi/content/full/304/5675/1325/VOL304SCIENCEwww.sciencemag.org

Kabeya, Y., Mizushima, N., Ueno, T., Yamamoto, A., Kominami, E., Ohsumi, O., & Yoshimori, T. (2000). LC3, a mammalian homologue of yeast Apg8p, is localized in autophagosome membranes after processing. *The EMBO Journal*, *19*(21), 5720–5728.

Kahle, P. J., Neumann, M., Ozmen, L., & Haass, C. (2000). Physiology and pathophysiology of α-synuclein cell culture and transgenic animal models based on a Parkinson's disease-associated protein. *Annals of the New York Academy of Sciences*, *920*, 33–41. https://doi.org/10.1111/j.1749-6632.2000.tb06902.x

Kamano, S., Ozawa, D., Ikenaka, K., & Nagai, Y. (2024). Role of Lipids in the Pathogenesis of Parkinson's Disease. In *International Journal of Molecular Sciences* (Vol. 25, Issue 16). Multidisciplinary Digital Publishing Institute (MDPI). https://doi.org/10.3390/ijms25168935

Kamp, F., Exner, N., Lutz, A. K., Wender, N., Hegermann, J., Brunner, B., Nuscher, B., Bartels, T., Giese, A., Beyer, K., Eimer, S., Winklhofer, K. F., & Haass, C. (2010). Inhibition of mitochondrial fusion by α-synuclein is rescued by PINK1, Parkin and DJ-1. *EMBO Journal*, *29*(20), 3571–3589. https://doi.org/10.1038/emboj.2010.223

Kanaan, N. M., & Manfredsson, F. P. (2012). Loss of functional alpha-synuclein: A toxic event in Parkinson's disease? In *Journal of Parkinson's Disease* (Vol. 2, Issue 4, pp. 249–267). https://doi.org/10.3233/JPD-012138

Kane, L. A., Lazarou, M., Fogel, A. I., Li, Y., Yamano, K., Sarraf, S. A., Banerjee, S., & Youle, R. J. (2014). PINK1 phosphorylates ubiquitin to activate parkin E3 ubiquitin ligase activity. *Journal of Cell Biology*, *205*(2), 143–153. https://doi.org/10.1083/jcb.201402104

Kang, L., Wu, K. P., Vendruscolo, M., & Baum, J. (2011). The A53T mutation is key in defining the differences in the aggregation kinetics of human and mouse α-synuclein. *Journal of the American Chemical Society*, *133*(34), 13465–13470. https://doi.org/10.1021/ja203979j

Kauffman, M., Kauffman, M., Traore, K., Zhu, H., Trush, M., Jia, Z., & Li, Y. (2016). MitoSOX-Based Flow Cytometry for Detecting Mitochondrial ROS. *Reactive Oxygen Species*. https://doi.org/10.20455/ros.2016.865

Kayed, R., Pensalfini, A., Margol, L., Sokolov, Y., Sarsoza, F., Head, E., Hall, J., & Glabe, C. (2009). Annular protofibrils area structurally and functionally distinct type of amyloid oligomer. *Journal of Biological Chemistry*, *284*(7), 4230–4237. https://doi.org/10.1074/jbc.M808591200

Kazmierczak, A., Strosznajder, J. B., & Adamczyk, A. (2008). α-Synuclein enhances secretion and toxicity of amyloid beta peptides in PC12 cells. *Neurochemistry International*, *53*(6–8), 263–269. https://doi.org/10.1016/j.neuint.2008.08.004

Ke, P. Y. (2020). Mitophagy in the Pathogenesis of Liver Diseases. *Cells*, *9*(4). https://doi.org/10.3390/cells9040831

Kee, T. R., Espinoza Gonzalez, P., Wehinger, J. L., Bukhari, M. Z., Ermekbaeva, A., Sista, A., Kotsiviras, P., Liu, T., Kang, D. E., & Woo, J. A. A. (2021). Mitochondrial CHCHD2: Disease-Associated Mutations, Physiological Functions, and Current Animal Models. *Frontiers in Aging Neuroscience*, *13*. https://doi.org/10.3389/fnagi.2021.660843

Khandelwal, P. J., Dumanis, S. B., Feng, L. R., Maguire-Zeiss, K., Rebeck, G., Lashuel, H. A., & Moussa, C. E. (2010). Parkinson-related parkin reduces α-Synuclein phosphorylation in a gene transfer model. *Molecular Neurodegeneration*, *5*(1). https://doi.org/10.1186/1750-1326-5-47

Kidd, J. F., Pilkington, M. F., Schell, M. J., Fogarty, K. E., Skepper, J. N., Taylor, C. W., & Thorn, P. (2002). Paclitaxel affects cytosolic calcium signals by opening the mitochondrial permeability transition pore. *Journal of Biological Chemistry*, *277*(8), 6504–6510. https://doi.org/10.1074/jbc.M106802200

Kim, S., Lim, J., Bang, Y., Moon, J., Kwon, M. S., Hong, J. T., Jeon, J., Seo, H., & Choi, H. J. (2018). Alpha-Synuclein Suppresses Retinoic Acid-Induced Neuronal Differentiation by Targeting the Glycogen Synthase Kinase-3β/β-Catenin Signaling Pathway. *Molecular Neurobiology*, *55*(2), 1607–1619. https://doi.org/10.1007/s12035-016-0370-9

Kim, S., Park, J. M., Moon, J., & Choi, H. J. (2014). Alpha-synuclein interferes with cAMP/PKA-dependent upregulation of dopamine β-hydroxylase and is associated with abnormal adaptive responses to immobilization stress. *Experimental Neurology*, *252*, 63–74. https://doi.org/10.1016/j.expneurol.2013.11.009

Kim, S. S., Moon, K. R., & Choi, H. J. (2011). Interference of alpha-synuclein with cAMP/PKA-dependent CREB signaling for tyrosine hydroxylase gene expression in SK-N-BE(2)C cells. *Archives of Pharmacal Research*, *34*(5), 837–845. https://doi.org/10.1007/s12272-011-0518-0

Kinnart, I., Manders, L., Heyninck, T., Imberechts, D., Praschberger, R., Schoovaerts, N., Verfaillie, C., Verstreken, P., & Vandenberghe, W. (2024). Elevated α-synuclein levels inhibit mitophagic flux. *Npj Parkinson's Disease*, *10*(1). https://doi.org/10.1038/s41531-024-00696-0

Kirik, D., Rosenblad, C., Burger, C., Lundberg, C., Johansen, T. E., Muzyczka, N., Mandel, R. J., & Bjö, A. (2002). Parkinson-Like Neurodegeneration Induced by Targeted Overexpression of-Synuclein in the Nigrostriatal System. *Journal of Neuroscience*, *22*(7), 2780–2791.

Kitada, T., Asakawa, S., Hattori, N., Matsumine, H., Yamamura, Y., Minoshima, S., Yokochi, M., Mizuno, Y., & Shimizu, N. (1998). Mutations in the parkin gene cause autosomal recessive juvenile parkinsonism. *Nature*, *392*(6676), 605–608.

Kleele, T., Rey, T., Winter, J., Zaganelli, S., Mahecic, D., Perreten Lambert, H., Ruberto, F. P., Nemir, M., Wai, T., Pedrazzini, T., & Manley, S. (2021). Distinct fission signatures predict mitochondrial degradation or biogenesis. *Nature*, *593*(7859), 435–439. https://doi.org/10.1038/s41586-021-03510-6

Kondapalli, C., Kazlauskaite, A., Zhang, N., Woodroof, H. I., Campbell, D. G., Gourlay, R., Burchell, L., Walden, H., MacArtney, T. J., Deak, M., Knebel, A., Alessi, D. R., & Muqit, M. M. K. (2012). PINK1 is activated by mitochondrial membrane potential depolarization and stimulates Parkin E3 ligase activity by phosphorylating Serine 65. *Open Biology*, *2*(MAY). https://doi.org/10.1098/rsob.120080

Kondrikov, D., Fulton, D., Dong, Z., & Su, Y. (2015). Heat shock protein 70 prevents hyperoxia-induced disruption of lung endothelial barrier via caspase-dependent and AIF-dependent pathways. *PLoS ONE*, *10*(6). https://doi.org/10.1371/journal.pone.0129343

König, T., Nolte, H., Aaltonen, M. J., Tatsuta, T., Krols, M., Stroh, T., Langer, T., & McBride, H. M. (2021). MIROs and DRP1 drive mitochondrial-derived vesicle biogenesis and promote quality control. *Nature Cell Biology*, *23*(12), 1271–1286. https://doi.org/10.1038/s41556-021-00798-4

Korobova, F., Ramabhadran, V., & Higgs, H. N. (2013). An actin-dependent step in mitochondrial fission mediated by the ER-associated formin INF2. *Science*, *339*(6118), 464–467. https://doi.org/10.1126/science.1228360

Kovalevich, J., & Langford, D. (2013). Considerations for the use of SH-SY5Y neuroblastoma cells in neurobiology. *Methods in Molecular Biology*, *1078*, 9–21. https://doi.org/10.1007/978-1-62703-640-5_2

Koyano, F., Okatsu, K., Kosako, H., Tamura, Y., Go, E., Kimura, M., Kimura, Y., Tsuchiya, H., Yoshihara, H., Hirokawa, T., Endo, T., Fon, E. A., Trempe, J. F., Saeki, Y., Tanaka, K., & Matsuda, N. (2014). Ubiquitin is phosphorylated by PINK1 to activate parkin. *Nature*, *510*(7503), 162–166. https://doi.org/10.1038/nature13392

Krebs, H. A., & Johnson, W. A. (1937). Metabolism of ketonic acids in animal tissues. *Biochemical Journal*, *31*(4), 645–660.

Krebs, H. A., & Johnson, W. A. (1980). The role of citric acid in intermediate metabolism in animal tissues. *FEBS Letters*, *117*, 148–156.

Krzystek, T. J., Banerjee, R., Thurston, L., Huang, J. Q., Swinter, K., Rahman, S. N., Falzone, T. L., & Gunawardena, S. (2021). Differential mitochondrial roles for α-synuclein in DRP1-dependent fission and PINK1/Parkin-mediated oxidation. *Cell Death and Disease*, *12*(9). https://doi.org/10.1038/s41419-021-04046-3

Kühlbrandt, W. (2015). Structure and function of mitochondrial membrane protein complexes. In *BMC Biology* (Vol. 13, Issue 1). BioMed Central Ltd. https://doi.org/10.1186/s12915-015-0201-x

Kulkarni, P. G., Mohire, V. M., Waghmare, P. P., & Banerjee, T. (2024). Interplay of mitochondria-associated membrane proteins and autophagy: Implications in neurodegeneration. In *Mitochondrion* (Vol. 76). Elsevier B.V. https://doi.org/10.1016/j.mito.2024.101874

Kumar, B., Nahreini, P., Hanson, A. J., Andreatta, C., Prasad, J. E., & Prasad, K. N. (2005). Selenomethionine Prevents Degeneration Induced by Overexpression of Wild-Type Human α-Synuclein during Differentiation of Neuroblastoma Cells. *Journal of the American College of Nutrition*, *24*(6), 516–523. https://doi.org/10.1080/07315724.2005.10719498

Kumar, S., Sarkar, A., & Sundar, D. (2009). Controlling aggregation propensity in A53T mutant of alpha-synuclein causing Parkinson's disease. *Biochemical and Biophysical Research Communications*, *387*(2), 305–309. https://doi.org/10.1016/j.bbrc.2009.07.008

Kume, T., Kawato, Y., Osakada, F., Izumi, Y., Katsuki, H., Nakagawa, T., Kaneko, S., Niidome, T., Takada-Takatori, Y., & Akaike, A. (2008). Dibutyryl cyclic AMP induces differentiation of human neuroblastoma SH-SY5Y cells into a noradrenergic phenotype. *Neuroscience Letters*, *443*(3), 199–203. https://doi.org/10.1016/j.neulet.2008.07.079

Lane, N., & Martin, W. (2010). The energetics of genome complexity. *Nature*, *467*(7318), 929–934. https://doi.org/10.1038/nature09486

Lardy, H. A., Johnson, D., & McMurray, W. C. (1958). Antibiotics as tools for metabolic studies. I. A survey of toxic antibiotics in respiratory, phosphorylative and glycolytic systems. *Archives of Biochemistry and Biophysics*, *78*(2), 587–597.

Lashuel, H. A., Mahul-Mellier, A. L., Novello, S., Hegde, R. N., Jasiqi, Y., Altay, M. F., Donzelli, S., DeGuire, S. M., Burai, R., Magalhães, P., Chiki, A., Ricci, J., Boussouf, M., Sadek, A.,

Stoops, E., Iseli, C., & Guex, N. (2022). Revisiting the specificity and ability of phospho-S129 antibodies to capture alpha-synuclein biochemical and pathological diversity. *Npj Parkinson's Disease*, *8*(1). https://doi.org/10.1038/s41531-022-00388-7

Lashuel, H. A., Petre, B. M., Wall, J., Simon, M., Nowak, R. J., Walz, T., & Lansbury, P. T. (2002). α-synuclein, especially the parkinson's disease-associated mutants, forms pore-like annular and tubular protofibrils. *Journal of Molecular Biology*, *322*(5), 1089–1102. https://doi.org/10.1016/S0022-2836(02)00735-0

Lautenschläger, J., Stephens, A. D., Fusco, G., Ströhl, F., Curry, N., Zacharopoulou, M., Michel, C. H., Laine, R., Nespovitaya, N., Fantham, M., Pinotsi, D., Zago, W., Fraser, P., Tandon, A., St George-Hyslop, P., Rees, E., Phillips, J. J., De Simone, A., Kaminski, C. F., & Schierle, G. S. K. (2018). C-terminal calcium binding of α-synuclein modulates synaptic vesicle interaction. *Nature Communications*, *9*(712). https://doi.org/10.1038/s41467-018-03111-4

Lazarou, M., Sliter, D. A., Kane, L. A., Sarraf, S. A., Wang, C., Burman, J. L., Sideris, D. P., Fogel, A. I., & Youle, R. J. (2015). The ubiquitin kinase PINK1 recruits autophagy receptors to induce mitophagy. *Nature*, *524*(7565), 309–314. https://doi.org/10.1038/nature14893

Lee, F. J. S., Liu, F., Pristupa, Z. B., & Niznik, H. B. (2001). Direct binding and functional coupling of α-synuclein to the dopamine transporters accelerate dopamine-induced apoptosis. *The FASEB Journal*, *15*(6), 916–926. https://doi.org/10.1096/fsb2fj000334com

Lee, H. J., Kang, S. J., Lee, K., & Im, H. (2011). Human α-synuclein modulates vesicle trafficking through its interaction with prenylated Rab acceptor protein 1. *Biochemical and Biophysical Research Communications*, *412*(4), 526–531. https://doi.org/10.1016/j.bbrc.2011.07.028

Lee, Y. Il, Seo, M. R., Kim, Y., Kim, S. Y., Kang, U. G., Kim, Y. S., & Juhnn, Y. S. (2005). Membrane depolarization induces the undulating phosphorylation/ dephosphorylation of glycogen synthase kinase 3β, and this dephosphorylation involves protein phosphatases 2A and 2B in SH-SY5Y human neuroblastoma cells. *Journal of Biological Chemistry*, *280*(23), 22044–22052. https://doi.org/10.1074/jbc.M413987200

Legesse-Miller, A., Massol, R. H., & Kirchhausen, T. (1953). Constriction and Dnm1p Recruitment Are Distinct Processes in Mitochondrial Fission □ V. *Molecular Biology of the Cell*, *14*. https://doi.org/10.1091/mbc.E02-10

Lehrer, S., & Rheinstein, P. H. (2022). α-synuclein enfolds tyrosine hydroxylase and dopamine ß-hydroxylase, potentially reducing dopamine and norepinephrine synthesis. *Journal of Proteins and Proteomics*, *13*(2), 109–115. https://doi.org/10.1007/s42485-022-00088-z

Lenzen, S. (2014). A fresh view of glycolysis and glucokinase regulation: History and current status. In *Journal of Biological Chemistry* (Vol. 289, Issue 18, pp. 12189–12194). American Society for Biochemistry and Molecular Biology Inc. https://doi.org/10.1074/jbc.R114.557314

Lin, K. J., Lin, K. L., Chen, S. Der, Liou, C. W., Chuang, Y. C., Lin, H. Y., & Lin, T. K. (2019). The overcrowded crossroads: Mitochondria, alpha-synuclein, and the endo-lysosomal system interaction in Parkinson's disease. In *International Journal of Molecular Sciences* (Vol. 20, Issue 21). MDPI AG. https://doi.org/10.3390/ijms20215312

Ling, Y.-H., Liebes, L., Ng, B., Buckley, M., Elliott, P. J., Adams, J., Jiang, J.-D., Muggia, F. M., Perez-Soler, R., & Martell, T. J. (2002). PS-341, a Novel Proteasome Inhibitor, Induces Bcl-2 Phosphorylation and Cleavage in Association with G 2-M Phase Arrest and Apoptosis 1. *Mol Cancer Ther*, *1*(10), 841–849. http://aacrjournals.org/mct/article-pdf/1/10/841/2221507/gd1002000841.pdf

Liu, H., Liu, W., Wu, Y., Zhou, Y., Xue, R., Luo, C., Wang, L., Zhao, W., Jiang, J. D., & Liu, J. (2005). Loss of epigenetic control of synuclein-γ gene as a molecular indicator of metastasis in a wide range of human cancers. *Cancer Research*, *65*(17), 7635–7643. https://doi.org/10.1158/0008-5472.CAN-05-1089

Liu, J., Wang, X., Lu, Y., Duan, C., Gao, G., Lu, L., & Yang, H. (2017). Pink1 interacts with α-synuclein and abrogates α-synuclein-induced neurotoxicity by activating autophagy. *Cell Death and Disease*, *8*(9). https://doi.org/10.1038/cddis.2017.427

Liu, L., Feng, D., Chen, G., Chen, M., Zheng, Q., Song, P., Ma, Q., Zhu, C., Wang, R., Qi, W., Huang, L., Xue, P., Li, B., Wang, X., Jin, H., Wang, J., Yang, F., Liu, P., Zhu, Y., … Chen, Q. (2012). Mitochondrial outer-membrane protein FUNDC1 mediates hypoxia-induced mitophagy in mammalian cells. *Nature Cell Biology*, *14*(2), 177–185. https://doi.org/10.1038/ncb2422

Liu, W., Vives-Bauza, C., Acín-Peréz, R., Yamamoto, A., Tan, Y., Li, Y., Magrané, J., Stavarache, M. A., Shaffer, S., Chang, S., Kaplitt, M. G., Huang, X. Y., Beal, M. F., Manfredi, G., & Li, C. (2009). PINK1 Defect Causes Mitochondrial Dysfunction, Proteasomal Deficit and a-Synuclein Aggregation in Cell Culture Models of Parkinson's Disease. *PLoS ONE*, *4*(2). https://doi.org/10.1371/journal.pone.0004597

Lo Bianco, C., Ridet, J.-L., Schneider, B. L., Dé, N., & Aebischer, P. (2002). Synucleinopathy and selective dopaminergic neuron loss in a rat lentiviral-based model of Parkinson's disease.

Proc. Natl. Acad. Sci. USA, *99*(16), 10813–10818. www.pnas.orgcgidoi10.1073pnas.152339799

Lonskaya, I., Desforges, N. M., Hebron, M. L., & Moussa, C. E. H. (2013). Ubiquitination increases parkin activity to promote autophagic a-synuclein clearance. *PLoS ONE*, *8*(12). https://doi.org/10.1371/journal.pone.0083914

López-Carballo, G., Moreno, L., Masiá, S., Pérez, P., & Barettino, D. (2002). Activation of the phosphatidylinositol 3-kinase/Akt signaling pathway by retinoic acid is required for neural differentiation of SH-SY5Y human neuroblastoma cells. *Journal of Biological Chemistry*, *277*(28), 25297–25304. https://doi.org/10.1074/jbc.M201869200

Lord, S. J., Velle, K. B., Dyche Mullins, R., & Fritz-Laylin, L. K. (2020). SuperPlots: Communicating reproducibility and variability in cell biology. In *Journal of Cell Biology* (Vol. 219, Issue 6). Rockefeller University Press. https://doi.org/10.1083/JCB.202001064

Luchtman, D. W., & Song, C. (2010). Why SH-SY5Y cells should be differentiated. *NeuroToxicology*, *31*, 164–166. https://doi.org/10.1016/j.neuro.2009.10.016

Ludtmann, M. H. R., Angelova, P. R., Horrocks, M. H., Choi, M. L., Rodrigues, M., Baev, A. Y., Berezhnov, A. V., Yao, Z., Little, D., Banushi, B., Al-Menhali, A. S., Ranasinghe, R. T., Whiten, D. R., Yapom, R., Dolt, K. S., Devine, M. J., Gissen, P., Kunath, T., Jaganjac, M., … Gandhi, S. (2018). α-synuclein oligomers interact with ATP synthase and open the permeability transition pore in Parkinson's disease. *Nature Communications*, *9*(1). https://doi.org/10.1038/s41467-018-04422-2

Ludtmann, M. H. R., Angelova, P. R., Ninkina, N. N., Gandhi, S., Buchman, V. L., & Abramov, A. Y. (2016). Monomeric alpha-synuclein exerts a physiological role on brain ATP synthase. *Journal of Neuroscience*, *36*(41), 10510–10521. https://doi.org/10.1523/JNEUROSCI.1659-16.2016

Lurette, O., Martín-Jiménez, R., Khan, M., Sheta, R., Jean, S., Schofield, M., Teixeira, M., Rodriguez-Aller, R., Perron, I., Oueslati, A., & Hebert-Chatelain, E. (2023). Aggregation of alpha-synuclein disrupts mitochondrial metabolism and induce mitophagy via cardiolipin externalization. *Cell Death & Disease*, *14*(11), 729. https://doi.org/10.1038/s41419-023-06251-8

MacHnicka, B., Grochowalska, R., Bogusławska, D. M., Sikorski, A. F., & Lecomte, M. C. (2012). Spectrin-based skeleton as an actor in cell signaling. *Cellular and Molecular Life Sciences*, *69*(2), 191–201. https://doi.org/10.1007/s00018-011-0804-5

Madsen, D. A., Schmidt, S. I., Blaabjerg, M., & Meyer, M. (2021). Interaction between parkin and α-synuclein in park2-mediated parkinson's disease. In *Cells* (Vol. 10, Issue 2, pp. 1–30). MDPI. https://doi.org/10.3390/cells10020283

Maechler, P., & Wollheim, C. B. (2001). Mitochondrial function in normal and diabetic beta-cells. *Nature*, *414*, 807–812. www.nature.com

Magalhaes, J., Gegg, M. E., Migdalska-Richards, A., Doherty, M. K., Whitfield, P. D., & Schapira, A. H. V. (2016). Autophagic lysosome reformation dysfunction in glucocerebrosidase deficient cells: Relevance to Parkinson disease. *Human Molecular Genetics*, *25*(16), 3432–3445. https://doi.org/10.1093/hmg/ddw185

Mailloux, R. J. (2018). Mitochondrial antioxidants and the maintenance of cellular hydrogen peroxide levels. *Oxidative Medicine and Cellular Longevity*, *2018*. https://doi.org/10.1155/2018/7857251

Mak, S. K., McCormack, A. L., Manning-Bog, A. B., Cuervo, A. M., & Di Monte, D. A. (2010). Lysosomal degradation of α-synuclein in vivo. *Journal of Biological Chemistry*, *285*(18), 13621–13629. https://doi.org/10.1074/jbc.M109.074617

Manganelli, V., Capozzi, A., Recalchi, S., Riitano, G., Mattei, V., Longo, A., Misasi, R., Garofalo, T., & Sorice, M. (2021). The role of cardiolipin as a scaffold mitochondrial phospholipid in autophagosome formation: In vitro evidence. *Biomolecules*, *11*(2), 1–14. https://doi.org/10.3390/biom11020222

Maroteaux, L., Campanelli, J. T., & Scheller, R. H. (1988). Synuclein: A Neuron-Specific Protein Localized to the Nucleus and Presynaptic Nerve Terminal. In *The Journal of Neuroscience* (Vol. 8, Issue 8).

Mårtensson, C. U., Priesnitz, C., Song, J., Ellenrieder, L., Doan, K. N., Boos, F., Floerchinger, A., Zufall, N., Oeljeklaus, S., Warscheid, B., & Becker, T. (2019). Mitochondrial protein translocation-associated degradation. *Nature*, *569*(7758), 679–683. https://doi.org/10.1038/s41586-019-1227-y

Martin, L. J., Pan, Y., Price, A. C., Sterling, W., Copeland, N. G., Jenkins, N. A., Price, D. L., & Lee, M. K. (2006). Parkinson's disease α-synuclein transgenic mice develop neuronal mitochondrial degeneration and cell death. *Journal of Neuroscience*, *26*(1), 41–50. https://doi.org/10.1523/JNEUROSCI.4308-05.2006

Martina, J. A., Diab, H. I., Lishu, L., Jeong-A, L., Patange, S., Raben, N., & Puertollano, R. (2014). The Nutrient-Responsive Transcription Factor TFE3 Promotes Autophagy, Lysosomal

Biogenesis, and Clearance of Cellular Debris. *Science Signaling*, *7*(309). www.SCIENCESIGNALING.org

Martínez, J. H., Fuentes, F., Vanasco, V., Alvarez, S., Alaimo, A., Cassina, A., Coluccio Leskow, F., & Velazquez, F. (2018). Alpha-synuclein mitochondrial interaction leads to irreversible translocation and complex I impairment. *Archives of Biochemistry and Biophysics*, *651*, 1–12. https://doi.org/10.1016/j.abb.2018.04.018

Martín-Jiménez, R., Lurette, O., & Hebert-Chatelain, E. (2024). Alpha-synuclein aggregates trigger cardiolipin externalization and mitophagy. *Autophagy Reports*, *3*(1). https://doi.org/10.1080/27694127.2024.2314361

Martinou, J.-C., Desagher, S., & Antonsson, B. (2000). Cytochrome c release from mitochondria: all or nothing. *Nature Cell Biology*, *2*(E41-43).

Masliah, E., Rockenstein, E., Veinbergs, I., Mallory, M., Hashimoto, M., Takeda, A., Sagara, Y., Sisk, A., & Mucke, L. (2000). Dopaminergic loss and inclusion body formation in a-synuclein mice: implications for neurodegenerative disorders. *Science*, *287*(5456), 1265–1269. https://www.science.org

Matés J. (1999). Antioxidant Enzymes and Human Diseases. *Clinical Biochemistry*, *32*(8), 595–603.

Matsuda, S., Kitagishi, Y., & Kobayashi, M. (2013). Function and characteristics of PINK1 in mitochondria. In *Oxidative Medicine and Cellular Longevity*. Hindawi Limited. https://doi.org/10.1155/2013/601587

Matsui, T., Jiang, P., Nakano, S., Sakamaki, Y., Yamamoto, H., & Mizushima, N. (2018). Autophagosomal YKT6 is required for fusion with lysosomes independently of syntaxin 17. *Journal of Cell Biology*, *217*(8), 2633–2645. https://doi.org/10.1083/jcb.201712058

Mazzulli, J. R., Xu, Y. H., Sun, Y., Knight, A. L., McLean, P. J., Caldwell, G. A., Sidransky, E., Grabowski, G. A., & Krainc, D. (2011). Gaucher disease glucocerebrosidase and α-synuclein form a bidirectional pathogenic loop in synucleinopathies. *Cell*, *146*(1), 37–52. https://doi.org/10.1016/j.cell.2011.06.001

McCarron, J. G., Wilson, C., Sandison, M. E., Olson, M. L., Girkin, J. M., Saunter, C., & Chalmers, S. (2013). From structure to function: Mitochondrial morphology, motion and shaping in vascular smooth muscle. In *Journal of Vascular Research* (Vol. 50, Issue 5, pp. 357–371). https://doi.org/10.1159/000353883

Mccormack, J. G., & Denton, R. M. (1989). The role of Ca z+ ions in the regulation of intramitochondrial metabolism and energy production in rat heart. In *Molecular and Cellular Biochemistry* (Vol. 89).

McLelland, G. L., Lee, S. A., McBride, H. M., & Fon, E. A. (2016). Syntaxin-17 delivers PINK1/parkin-dependent mitochondrial vesicles to the endolysosomal system. *Journal of Cell Biology*, *214*(3), 275–291. https://doi.org/10.1083/jcb.201603105

McLelland, G. L., Soubannier, V., Chen, C. X., McBride, H. M., & Fon, E. A. (2014). Parkin and PINK1 function in a vesicular trafficking pathway regulating mitochondrial quality control. *EMBO Journal*, *33*(4), 282–295. https://doi.org/10.1002/embj.201385902

McWilliams, T. G., Barini, E., Pohjolan-Pirhonen, R., Brooks, S. P., Singh, F., Burel, S., Balk, K., Kumar, A., Montava-Garriga, L., Prescott, A. R., Hassoun, S. M., Mouton-Liger, F., Ball, G., Hills, R., Knebel, A., Ulusoy, A., Di Monte, D. A., Tamjar, J., Antico, O., … Muqit, M. M. K. (2018). Phosphorylation of Parkin at serine 65 is essential for its activation in vivo. *Open Biology*, *8*(11). https://doi.org/10.1098/rsob.180108

Meeusen, S., Mccaffery, J. M., & Nunnari, J. (2004). Mitochondrial Fusion Intermediates Revealed in Vitro. *Science*, *305*(5691), 1747–1752. https://www.science.org

Meiri, K. F., Pfenninger, K. H., & Willard, M. B. (1986). Growth-associated protein, GAP-43, a polypeptide that is induced when neurons extend axons, is a component of growth cones and corresponds to pp46, a major polypeptide of a subcellular fraction enriched in growth cones. *Proc. Natl. Acad. Sci. USA*, *83*, 3537–3541.

Melnikova, A., Pozdyshev, D., Barinova, K., Kudryavtseva, S., & Muronetz, V. I. (2020). α-Synuclein Overexpression in SH-SY5Y Human Neuroblastoma Cells Leads to the Accumulation of Thioflavin S-positive Aggregates and Impairment of Glycolysis. *Biochemistry (Moscow)*, *85*(5), 604–613. https://doi.org/10.1134/S0006297920050090

Melo, T. Q., Copray, S. J. C. V. M., & Ferrari, M. F. R. (2018). Alpha-Synuclein Toxicity on Protein Quality Control, Mitochondria and Endoplasmic Reticulum. In *Neurochemical Research* (Vol. 43, Issue 12, pp. 2212–2223). Springer New York LLC. https://doi.org/10.1007/s11064-018-2673-x

Melo, T. Q., van Zomeren, K. C., Ferrari, M. F. R., Boddeke, H. W. G. M., & Copray, J. C. V. M. (2017). Impairment of mitochondria dynamics by human A53T α-synuclein and rescue by NAP (davunetide) in a cell model for Parkinson's disease. *Experimental Brain Research*, *235*(3), 731–742. https://doi.org/10.1007/s00221-016-4836-9

Middleton, E. R., & Rhoades, E. (2010). Effects of curvature and composition on α-synuclein binding to lipid vesicles. *Biophysical Journal*, *99*(7), 2279–2288. https://doi.org/10.1016/j.bpj.2010.07.056

Montava-Garriga, L., & Ganley, I. G. (2020). Outstanding Questions in Mitophagy: What We Do and Do Not Know. In *Journal of Molecular Biology* (Vol. 432, Issue 1, pp. 206–230). Academic Press. https://doi.org/10.1016/j.jmb.2019.06.032

Morel, N. (2003). Neurotransmitter disease: The dark side of the vacuolar-H+ATPase. *Biology of the Cell*, *95*(7), 453–457. https://doi.org/10.1016/S0248-4900(03)00075-3

Mortiboys, H., Thomas, K. J., Koopman, W. J. H., Klaffke, S., Abou-Sleiman, P., Olpin, S., Wood, N. W., Willems, P. H. G. M., Smeitink, J. A. M., Cookson, M. R., & Bandmann, O. (2008). Mitochondrial function and morphology are impaired in parkin-mutant fibroblasts. *Annals of Neurology*, *64*(5), 555–565. https://doi.org/10.1002/ana.21492

Murphy, D. D., Rueter, S. M., Trojanowski, J. Q., & M-Y Lee, V. (2000). *Synucleins Are Developmentally Expressed, and-Synuclein Regulates the Size of the Presynaptic Vesicular Pool in Primary Hippocampal Neurons*.

Nagatsu, T., Levitt, M., & Udenfriend, S. (1964). Tyrosine Hydroxylase THE INITIAL STEP IN NOREPINEPHRINE BIOSYNTHESIS. *THE JOURNAL OF BIOLOQICAL CHEMISTRY*, *239*(S). http://www.jbc.org/

Nakamura, K., Nemani, V. M., Azarbal, F., Skibinski, G., Levy, J. M., Egami, K., Munishkina, L., Zhang, J., Gardner, B., Wakabayashi, J., Sesaki, H., Cheng, Y., Finkbeiner, S., Nussbaum, R. L., Masliah, E., & Edwards, R. H. (2011). Direct membrane association drives mitochondrial fission by the Parkinson disease-associated protein α-synuclein. *Journal of Biological Chemistry*, *286*(23), 20710–20726. https://doi.org/10.1074/jbc.M110.213538

Nakamura, K., Nemani, V. M., Wallender, E. K., Kaehlcke, K., Ott, M., & Edwards, R. H. (2008). Optical reporters for the conformation of α-synuclein reveal a specific interaction with mitochondria. *Journal of Neuroscience*, *28*(47), 12305–12317. https://doi.org/10.1523/JNEUROSCI.3088-08.2008

Nakamura, T., Sugeno, N., Hasegawa, T., Ikeda, K., Yoshida, S., Ishiyama, S., Sato, K., Takeda, A., & Aoki, M. (2024). Alpha-synuclein promotes PRMT5-mediated H4R3me2s histone methylation by interacting with the BAF complex. *FEBS Journal*, *291*(9), 1892–1908. https://doi.org/10.1111/febs.17037

Nakatogawa, H. (2020). Mechanisms governing autophagosome biogenesis. In *Nature Reviews Molecular Cell Biology* (Vol. 21, Issue 8, pp. 439–458). Nature Research. https://doi.org/10.1038/s41580-020-0241-0

Nalls, M. A., Pankratz, N., Lill, C. M., Do, C. B., Hernandez, D. G., Saad, M., Destefano, A. L., Kara, E., Bras, J., Sharma, M., Schulte, C., Keller, M. F., Arepalli, S., Letson, C., Edsall, C., Stefansson, H., Liu, X., Pliner, H., Lee, J. H., … Ansorge, O. (2014). Large-scale meta-analysis of genome-wide association data identifies six new risk loci for Parkinson's disease. *Nature Genetics*, *46*(9), 989–993. https://doi.org/10.1038/ng.3043

Narendra, D. P., Jin, S. M., Tanaka, A., Suen, D. F., Gautier, C. A., Shen, J., Cookson, M. R., & Youle, R. J. (2010). PINK1 is selectively stabilized on impaired mitochondria to activate Parkin. *PLoS Biology*, *8*(1). https://doi.org/10.1371/journal.pbio.1000298

Narendra, D., Tanaka, A., Suen, D. F., & Youle, R. J. (2008). Parkin is recruited selectively to impaired mitochondria and promotes their autophagy. *Journal of Cell Biology*, *183*(5), 795–803. https://doi.org/10.1083/jcb.200809125

Narhi, L., Wood, S. J., Steavenson, S., Jiang, Y., Wu, G. M., Anafi, D., Kaufman, S. A., Martin, F., Sitney, K., Denis, P., Louis, J.-C., Wypych, J., Biere, A. L., & Citron, M. (1999). Both Familial Parkinson's Disease Mutations Accelerate-Synuclein Aggregation. *The Journal of Biological Chemistry*, *274*(14), 9843–9846. http://www.jbc.org

Nascimento, A. C., Erustes, A. G., Reckziegel, P., Bincoletto, C., Ureshino, R. P., Pereira, G. J. S., & Smaili, S. S. (2020). α-Synuclein Overexpression Induces Lysosomal Dysfunction and Autophagy Impairment in Human Neuroblastoma SH-SY5Y. *Neurochemical Research*, *45*(11), 2749–2761. https://doi.org/10.1007/s11064-020-03126-8

Neuspiel, M., Schauss, A. C., Braschi, E., Zunino, R., Rippstein, P., Rachubinski, R. A., Andrade-Navarro, M. A., & McBride, H. M. (2008). Cargo-Selected Transport from the Mitochondria to Peroxisomes Is Mediated by Vesicular Carriers. *Current Biology*, *18*(2), 102–108. https://doi.org/10.1016/j.cub.2007.12.038

Ninkina, N., Millership, S. J., Peters, O. M., Connor-Robson, N., Chaprov, K., Kopylov, A. T., Montoya, A., Kramer, H., Withers, D. J., & Buchman, V. L. (2021). β-synuclein potentiates synaptic vesicle dopamine uptake and rescues dopaminergic neurons from MPTP-induced death in the absence of other synucleins. *Journal of Biological Chemistry*, *297*(6). https://doi.org/10.1016/j.jbc.2021.101375

Nita, M., & Grzybowski, A. (2016). The Role of the Reactive Oxygen Species and Oxidative Stress in the Pathomechanism of the Age-Related Ocular Diseases and Other Pathologies of the

Anterior and Posterior Eye Segments in Adults. In *Oxidative Medicine and Cellular Longevity* (Vol. 2016). Hindawi Limited. https://doi.org/10.1155/2016/3164734

Nolfi-Donegan, D., Braganza, A., & Shiva, S. (2020). Mitochondrial electron transport chain: Oxidative phosphorylation, oxidant production, and methods of measurement. In *Redox Biology* (Vol. 37). Elsevier B.V. https://doi.org/10.1016/j.redox.2020.101674

Nunnari, J., & Suomalainen, A. (2012). Mitochondria: In sickness and in health. In *Cell* (Vol. 148, Issue 6, pp. 1145–1159). Elsevier B.V. https://doi.org/10.1016/j.cell.2012.02.035

Ohgita, T., Namba, N., Kono, H., Shimanouchi, T., & Saito, H. (2022). Mechanisms of enhanced aggregation and fibril formation of Parkinson's disease-related variants of α-synuclein. *Scientific Reports*, *12*(1). https://doi.org/10.1038/s41598-022-10789-6

Okochi, M., Walter, J., Koyama, A., Nakajo, S., Baba, M., Iwatsubo, T., Meijer, L., Kahle, P. J., & Haass, C. (2000). Constitutive phosphorylation of the Parkinson's disease associated α-synuclein. *Journal of Biological Chemistry*, *275*(1), 390–397. https://doi.org/10.1074/jbc.275.1.390

Olgiati, S., Thomas, A., Quadri, M., Breedveld, G. J., Graafland, J., Eussen, H., Douben, H., de Klein, A., Onofrj, M., & Bonifati, V. (2015). Early-onset parkinsonism caused by alpha-synuclein gene triplication: Clinical and genetic findings in a novel family. *Parkinsonism and Related Disorders*, *21*(8), 981–986. https://doi.org/10.1016/j.parkreldis.2015.06.005

Olichon, A., Baricault, L., Gas, N., Guillou, E., Valette, A., Belenguer, P., & Lenaers, G. (2003). Loss of OPA1 perturbates the mitochondrial inner membrane structure and integrity, leading to cytochrome c release and apoptosis. *Journal of Biological Chemistry*, *278*(10), 7743–7746. https://doi.org/10.1074/jbc.C200677200

Oliveira da Silva, M. I., & Liz, M. A. (2020). Linking Alpha-Synuclein to the Actin Cytoskeleton: Consequences to Neuronal Function. *Frontiers in Cell and Developmental Biology*, *8*. https://doi.org/10.3389/fcell.2020.00787

Oliveira, L. M. A., Falomir-Lockhart, L. J., Botelho, M. G., Lin, K. H., Wales, P., Koch, J. C., Gerhardt, E., Taschenberger, H., Outeiro, T. F., Lingor, P., Schüle, B., Arndt-Jovin, D. J., & Jovin, T. M. (2015). Elevated α-synuclein caused by SNCA gene triplication impairs neuronal differentiation and maturation in Parkinson's patient-derived induced pluripotent stem cells. *Cell Death and Disease*, *6*(11). https://doi.org/10.1038/cddis.2015.318

Olzmann, J. A., & Carvalho, P. (2019). Dynamics and functions of lipid droplets. In *Nature Reviews Molecular Cell Biology* (Vol. 20, Issue 3, pp. 137–155). Nature Publishing Group. https://doi.org/10.1038/s41580-018-0085-z

Opara, J. A., Małecki, A., Małecka, E., & Socha, T. (2017). Motor assessment in parkinson's disease. In *Annals of Agricultural and Environmental Medicine* (Vol. 24, Issue 3, pp. 411–415). Institute of Agricultural Medicine. https://doi.org/10.5604/12321966.1232774

Ordonez, D. G., Lee, M. K., & Feany, M. B. (2018). α-synuclein Induces Mitochondrial Dysfunction through Spectrin and the Actin Cytoskeleton. *Neuron*, *97*(1), 108–124. https://doi.org/10.1016/j.neuron.2017.11.036

Ostrerova, N., Petrucelli, L., Farrer, M., Mehta, N., Choi, P., Hardy, J., & Wolozin, B. (1999). Synuclein Shares Physical and Functional Homology with 14-3-3 Proteins. *Journal of Neuroscience*, *19*(14), 5782–5791.

Pacelli, C., Giguère, N., Bourque, M. J., Lévesque, M., Slack, R. S., & Trudeau, L. É. (2015). Elevated Mitochondrial Bioenergetics and Axonal Arborization Size Are Key Contributors to the Vulnerability of Dopamine Neurons. *Current Biology*, *25*(18), 2349–2360. https://doi.org/10.1016/j.cub.2015.07.050

Pahlman, S., Hoehner, J. C., Ndnberg, E., Hedborg, F., Fagerstrom, S., Gestblom, C., Johansson, I., Larsson, U., Lavenius, E., Ortoft, E., & Sgderholm, H. (1995). Differentiation and Survival Influences of Growth Fa.ctors in Human Neuroblastoma. *EurJ Cancer*, *31*(4), 453–458.

Paisán-Ruíz, C., Jain, S., Evans, E. W., Gilks, W. P., Simó, J., Van Der Brug, M., Ló Pez De Munain, A., Aparicio, S., Gil, A. M., Khan, N., Johnson, J., Ruiz Martinez, J., & Nicholl, D. (2004). Cloning of the Gene Containing Mutations that Cause PARK8-Linked Parkinson's Disease. *Neuron*, *44*(4), 595–600.

Palikaras, K., Lionaki, E., & Tavernarakis, N. (2018). Mechanisms of mitophagy in cellular homeostasis, physiology and pathology. In *Nature Cell Biology* (Vol. 20, Issue 9, pp. 1013–1022). Nature Publishing Group. https://doi.org/10.1038/s41556-018-0176-2

Panduri, V., Weitzman, S. A., Chandel, N. S., & Kamp, D. W. (2004). Mitochondrial-derived free radicals mediate asbestos-induced alveolar epithelial cell apoptosis. *Am J Physiol Lung Cell Mol Physiol*, *286*, 1220–1227. https://doi.org/10.1152/ajplung.00371.2003.-Asbestos

Paradies, G., Paradies, V., Ruggiero, F. M., & Petrosillo, G. (2019). Role of cardiolipin in mitochondrial function and dynamics in health and disease: Molecular and

pharmacological aspects. In *Cells* (Vol. 8, Issue 7). MDPI. https://doi.org/10.3390/cells8070728

Parihar, M. S., Parihar, A., Fujita, M., Hashimoto, M., & Ghafourifar, P. (2009). Alpha-synuclein overexpression and aggregation exacerbates impairment of mitochondrial functions by augmenting oxidative stress in human neuroblastoma cells. *International Journal of Biochemistry and Cell Biology*, *41*(10), 2015–2024. https://doi.org/10.1016/j.biocel.2009.05.008

Park, J. H., Burgess, J. D., Faroqi, A. H., Demeo, N. N., Fiesel, F. C., Springer, W., Delenclos, M., & McLean, P. J. (2020). Alpha-synuclein-induced mitochondrial dysfunction is mediated via a sirtuin 3-dependent pathway. *Molecular Neurodegeneration*, *15*(1). https://doi.org/10.1186/s13024-019-0349-x

Pawlyk, A. C., Giasson, B. I., Sampathu, D. M., Perez, F. A., Lim, K. L., Dawson, V. L., Dawson, T. M., Palmiter, R. D., Trojanowski, J. Q., & Lee, V. M. Y. (2003). Novel Monoclonal Antibodies Demonstrate Biochemical Variation of Brain Parkin with Age. *Journal of Biological Chemistry*, *278*(48), 48120–48128. https://doi.org/10.1074/jbc.M306889200

Paxinou, E., Chen, Q., Weisse, M., Giasson, B. I., Norris, E. H., Rueter, S. M., Trojanowski, J. Q., M-Y Lee, V., & Ischiropoulos, H. (2001). Induction of-Synuclein Aggregation by Intracellular Nitrative Insult. *The Journal of Neuroscience*, *21*(20), 8053–8061.

Pellegrino, M. W., Nargund, A. M., Kirienko, N. V., Gillis, R., Fiorese, C. J., & Haynes, C. M. (2014). Mitochondrial UPR-regulated innate immunity provides resistance to pathogen infection. *Nature*, *516*(7531), 414–417. https://doi.org/10.1038/nature13818

Peng, T., Xie, Y., Sheng, H., Wang, C., Lian, Y., & Xie, N. (2022). Mitochondrial-derived vesicles: Gatekeepers of mitochondrial response to oxidative stress. In *Free Radical Biology and Medicine* (Vol. 188, pp. 185–193). Elsevier Inc. https://doi.org/10.1016/j.freeradbiomed.2022.06.233

Peng, X. M., Tehranian, R., Dietrich, P., Stefanis, L., & Perez, R. G. (2005). α-synuclein activation of protein phosphatase 2A reduces tyrosine hydroxylase phosphorylation in dopaminergic cells. *Journal of Cell Science*, *118*(15), 3523–3530. https://doi.org/10.1242/jcs.02481

Perez, R. G., Waymire, J. C., Lin, E., Liu, J. J., Guo, F., & Zigmond, M. J. (2002a). A Role for-Synuclein in the Regulation of Dopamine Biosynthesis. *Journal of Neuroscience*, *22*(8), 3090–3099.

Perez, R. G., Waymire, J. C., Lin, E., Liu, J. J., Guo, F., & Zigmond, M. J. (2002b). A Role for-Synuclein in the Regulation of Dopamine Biosynthesis. *The Journal of Neuroscience*, *22*(8), 3090–3099.

Pfefferkorn, C. M., Jiang, Z., & Lee, J. C. (2012). Biophysics of α-synuclein membrane interactions. *Biochimica et Biophysica Acta - Biomembranes*, *1818*(2), 162–171. https://doi.org/10.1016/j.bbamem.2011.07.032

Pickart, C. M., & Eddins, M. J. (2004). Ubiquitin: Structures, functions, mechanisms. In *Biochimica et Biophysica Acta - Molecular Cell Research* (Vol. 1695, Issues 1–3, pp. 55–72). https://doi.org/10.1016/j.bbamcr.2004.09.019

Pickrell, A. M., Pinto, M., & Moraes, C. T. (2013). Mouse models of Parkinson's disease associated with mitochondrial dysfunction. In *Molecular and Cellular Neuroscience* (Vol. 55, pp. 87–94). https://doi.org/10.1016/j.mcn.2012.08.002

Pickrell, A. M., & Youle, R. J. (2015). The roles of PINK1, Parkin, and mitochondrial fidelity in parkinson's disease. *Neuron*, *85*(2), 257–273. https://doi.org/10.1016/j.neuron.2014.12.007

Pitt, A. S., & Buchanan, S. K. (2021). A biochemical and structural understanding of tom complex interactions and implications for human health and disease. *Cells*, *10*(5). https://doi.org/10.3390/cells10051164

Polymeropoulos, M. H., Lavedan, C., Leroy, E., Ide, S. E., Dehejia, A., Dutra, A., Pike, B., Root, H., Rubenstein, J., Boyer, R., Stenroos, E. S., Chandrasekharappa, S., Athanassiadou, A., Papapetropoulos, T., Johnson, W. G., Lazzarini, A. M., Duvoisin, R. C., Di Iorio, G., Golbe, L. I., & Nussbaum, R. L. (1997). Mutation in the α-synuclein gene identified in families with Parkinson's disease. *Science*, *276*(5321), 2045–2047. https://doi.org/10.1126/science.276.5321.2045

Portz, P., & Lee, M. K. (2021). Changes in drp1 function and mitochondrial morphology are associated with the α-synuclein pathology in a transgenic mouse model of parkinson's disease. *Cells*, *10*(4). https://doi.org/10.3390/cells10040885

Prahl, J., Pierce, S. E., Coetzee, G. A., & Tyson, T. (2022). Alpha-synuclein negatively controls cell proliferation in dopaminergic neurons. *Molecular and Cellular Neuroscience*, *119*. https://doi.org/10.1016/j.mcn.2022.103702

Preminger, N., & Schuldiner, M. (2024). Beyond fission and fusion—Diving into the mysteries of mitochondrial shape. *PLOS Biology*, *22*(7), e3002671. https://doi.org/10.1371/journal.pbio.3002671

Presgraves, S. P., Ahmed, T., Borwege, S., & Joyce, J. N. (2004). Terminally Differentiated SH-SY5Y Cells Provide a Model System for Studying Neuroprotective Effects of Dopamine Agonists. *Neurotoxicity Research*, *5*(8), 579–598. https://doi.org/10.1007/BF03033178

Quinsay, M. N., Thomas, R. L., Lee, Y., & Gustafsson, Å. B. (2010). Bnip3-mediated mitochondrial autophagy is independent of the mitochondrial permeability transition pore. *Autophagy*, *6*(7), 855–862. https://doi.org/10.4161/auto.6.7.13005

Raben, N., & Puertollano, R. (2016). TFEB and TFE3: Linking Lysosomes to Cellular Adaptation to Stress∗. In *Annual Review of Cell and Developmental Biology* (Vol. 32, pp. 255–278). Annual Reviews Inc. https://doi.org/10.1146/annurev-cellbio-111315-125407

Raghavan, R., Kruijff, L. de, Sterrenburg, M. D., Rogers, B. B., Hladik, C. L., & White, C. L. (2004). Alpha-synuclein expression in the developing human brain. *Pediatric and Developmental Pathology : The Official Journal of the Society for Pediatric Pathology and the Paediatric Pathology Society*, *7*(5), 506–516. https://doi.org/10.1007/s10024-003-7080-9

Rakovic, A., Grünewald, A., Seibler, P., Ramirez, A., Kock, N., Orolicki, S., Lohmann, K., & Klein, C. (2010). Effect of endogenous mutant and wild-type PINK1 on Parkin in fibroblasts from Parkinson disease patients. *Human Molecular Genetics*, *19*(16), 3124–3137. https://doi.org/10.1093/hmg/ddq215

Ramakrishnan, M., Jensen, P. H., & Marsh, D. (2003). α-Synuclein Association with Phosphatidylglycerol Probed by Lipid Spin Labels. *Biochemistry*, *42*(44), 12919–12926. https://doi.org/10.1021/bi035048e

Ramalingam, N., Jin, S. X., Moors, T. E., Fonseca-Ornelas, L., Shimanaka, K., Lei, S., Cam, H. P., Watson, A. H., Brontesi, L., Ding, L., Hacibaloglu, D. Y., Jiang, H., Choi, S. J., Kanter, E., Liu, L., Bartels, T., Nuber, S., Sulzer, D., Mosharov, E. V., … Dettmer, U. (2023). Dynamic physiological α-synuclein S129 phosphorylation is driven by neuronal activity. *Npj Parkinson's Disease*, *9*(1). https://doi.org/10.1038/s41531-023-00444-w

Ramirez, A., Heimbach, A., Gründemann, J., Stiller, B., Hampshire, D., Cid, L. P., Goebel, I., Mubaidin, A. F., Wriekat, A. L., Roeper, J., Al-Din, A., Hillmer, A. M., Karsak, M., Liss, B., Woods, C. G., Behrens, M. I., & Kubisch, C. (2006). Hereditary parkinsonism with dementia is caused by mutations in ATP13A2, encoding a lysosomal type 5 P-type ATPase. *Nature Genetics*, *38*(10), 1184–1191. https://doi.org/10.1038/ng1884

Ran, F. A., Hsu, P. D., Wright, J., Agarwala, V., Scott, D. A., & Zhang, F. (2013). Genome engineering using the CRISPR-Cas9 system. *Nature Protocols*, *8*(11), 2281–2308. https://doi.org/10.1038/nprot.2013.143

Rangaraju, V., Lewis, T. L., Hirabayashi, Y., Bergami, M., Motori, E., Cartoni, R., Kwon, S. K., & Courchet, J. (2019). Pleiotropic mitochondria: The influence of mitochondria on neuronal development and disease. *Journal of Neuroscience*, *39*(42), 8200–8208. https://doi.org/10.1523/JNEUROSCI.1157-19.2019

Rao, V. S., Srinivas, K., Sujini, G. N., & Kumar, G. N. S. (2014). Protein-Protein Interaction Detection: Methods and Analysis. *International Journal of Proteomics*, *2014*, 1–12. https://doi.org/10.1155/2014/147648

Reeve, A. K., Ludtmann, M. H. R., Angelova, P. R., Simcox, E. M., Horrocks, M. H., Klenerman, D., Gandhi, S., Turnbull, D. M., & Abramov, A. Y. (2015). Aggregated α-synuclein and complex I deficiency: Exploration of their relationship in differentiated neurons. *Cell Death and Disease*, *6*(7). https://doi.org/10.1038/cddis.2015.166

Rhodes, C. J. (2005). Type 2 diabetes - A matter of β-cell life and death? In *Science* (Vol. 307, Issue 5708, pp. 380–384). https://doi.org/10.1126/science.1104345

Rizzuto, R., Bernardi, P., & Pozzan, T. (2000). Mitochondria as all-round players of the calcium game. In *Journal of Physiology* (Vol. 529, Issue 1, pp. 37–47). Cambridge University Press. https://doi.org/10.1111/j.1469-7793.2000.00037.x

Robak, L. A., Jansen, I. E., Rooij, J. van, Uitterlinden, A. G., Kraaij, R., Jankovic, J., Heutink, P., Shulman, J. M., Nalls, M. A., Plagnol, V., Hernandez, D. G., Sharma, M., Sheerin, U. M., Saad, M., Simón-Sánchez, J., Schulte, C., Lesage, S., Sveinbjörnsdóttir, S., Arepalli, S., … Singleton, A. B. (2017). Excessive burden of lysosomal storage disorder gene variants in Parkinson's disease. *Brain*, *140*(12), 3191–3203. https://doi.org/10.1093/brain/awx285

Roberts, H. L., & Brown, D. R. (2015). Seeking a mechanism for the toxicity of oligomeric α-synuclein. In *Biomolecules* (Vol. 5, Issue 2, pp. 282–305). MDPI AG. https://doi.org/10.3390/biom5020282

Roberts, R. F., Bayne, A. N., Goiran, T., Lévesque, D., Boisvert, F. M., Trempe, J. F., & Fon, E. A. (2021). Proteomic Profiling of Mitochondrial-Derived Vesicles in Brain Reveals Enrichment of Respiratory Complex Sub-assemblies and Small TIM Chaperones. *Journal of Proteome Research*, *20*(1), 506–517. https://doi.org/10.1021/acs.jproteome.0c00506

Robertson, D. C., Schmidt, O., Ninkina, N., Jones, P. A., Sharkey, J., & Buchman, V. L. (2004). Developmental loss and resistance to MPTP toxicity of dopaminergic neurones in substantia nigra pars compacta of γ-synuclein, α-synuclein and double α/γ-synuclein null mutant mice. *Journal of Neurochemistry*, *89*(5), 1126–1136. https://doi.org/10.1111/j.1471-4159.2004.02378.x

Robotta, M., Gerding, H. R., Vogel, A., Hauser, K., Schildknecht, S., Karreman, C., Leist, M., Subramaniam, V., & Drescher, M. (2014). Alpha-synuclein binds to the inner membrane of mitochondria in an a-helical conformation. *ChemBioChem*, *15*(17), 2499–2502. https://doi.org/10.1002/cbic.201402281

Robustelli, P., Piana, S., & Shaw, D. E. (2018). Developing a molecular dynamics force field for both folded and disordered protein states. *Proceedings of the National Academy of Sciences of the United States of America*, *115*(21), E4758–E4766. https://doi.org/10.1073/pnas.1800690115

Roca-Portoles, A., & Tait, S. W. G. (2021). Mitochondrial quality control: from molecule to organelle. In *Cellular and Molecular Life Sciences* (Vol. 78, Issue 8, pp. 3853–3866). Springer Science and Business Media Deutschland GmbH. https://doi.org/10.1007/s00018-021-03775-0

Rödl, S., & Herrmann, J. M. (2023). The role of the proteasome in mitochondrial protein quality control. In *IUBMB Life* (Vol. 75, Issue 10, pp. 868–879). John Wiley and Sons Inc. https://doi.org/10.1002/iub.2734

Ronayne, C. T., & Latorre-Muro, P. (2024). Navigating the landscape of mitochondrial-ER communication in health and disease. In *Frontiers in Molecular Biosciences* (Vol. 11). Frontiers Media SA. https://doi.org/10.3389/fmolb.2024.1356500

Rossignol, R., Gilkerson, R., Aggeler, R., Yamagata, K., Remington, S. J., & Capaldi, R. A. (2004). Energy Substrate Modulates Mitochondrial Structure and Oxidative Capacity in Cancer Cells. In *CANCER RESEARCH* (Vol. 64). http://aacrjournals.org/cancerres/article-pdf/64/3/985/2521841/zch00304000985.pdf

Rostovtseva, T., & Colombini, M. (1997). Vdac channels mediate and gate the flow of ATP: Implications for the regulation of mitochondrial function. *Biophysical Journal*, *72*(5), 1954–1962. https://doi.org/10.1016/S0006-3495(97)78841-6

Rostovtseva, T. K., Gurnev, P. A., Protchenko, O., Hoogerheide, D. P., Yap, T. L., Philpott, C. C., Lee, J. C., & Bezrukov, S. M. (2015). α-synuclein shows high affinity interaction with voltage-dependent anion channel, suggesting mechanisms of mitochondrial regulation and toxicity

in Parkinson disease. *Journal of Biological Chemistry*, *290*(30), 18467–18477. https://doi.org/10.1074/jbc.M115.641746

Roy-Choudhury, G., & Daadi, M. M. (2019). Assay for assessing mitochondrial function in iPSC-derived neural stem cells and dopaminergic neurons. In M. M. Daadi (Ed.), *Neural Stem Cells. Methods in Molecular Biology* (Vol. 1919). Human Press. http://www.springer.com/series/7651

Ruan, L., Zhou, C., Jin, E., Kucharavy, A., Zhang, Y., Wen, Z., Florens, L., & Li, R. (2017). Cytosolic proteostasis through importing of misfolded proteins into mitochondria. *Nature*, *543*(7645), 443–446. https://doi.org/10.1038/nature21695

Rüb, C., Wilkening, A., & Voos, W. (2017). Mitochondrial quality control by the Pink1/Parkin system. *Cell and Tissue Research*, *367*(1), 111–123. https://doi.org/10.1007/s00441-016-2485-8

Ruprecht, J. J., King, M. S., Zögg, T., Aleksandrova, A. A., Pardon, E., Crichton, P. G., Steyaert, J., & Kunji, E. R. S. (2019). The Molecular Mechanism of Transport by the Mitochondrial ADP/ATP Carrier. *Cell*, *176*(3), 435-447.e15. https://doi.org/10.1016/j.cell.2018.11.025

Ryan, M. T., & Stojanovski, D. (2012). Mitofusins “bridge” the gap between oxidative stress and mitochondrial hyperfusion. *EMBO Reports*, *13*(10), 870–871.

Ryan, T. A., Phillips, E. O., Collier, C. L., JB Robinson, A., Routledge, D., Wood, R. E., Assar, E. A., & Tumbarello, D. A. (2020). Tollip coordinates Parkin-dependent trafficking of mitochondrial-derived vesicles. *The EMBO Journal*, *39*(11). https://doi.org/10.15252/embj.2019102539

Ryan, T. A., & Tumbarello, D. A. (2018). Optineurin: A coordinator of membrane-associated cargo trafficking and autophagy. *Frontiers in Immunology*, *9*. https://doi.org/10.3389/fimmu.2018.01024

Ryan, T., Bamm, V. V., Stykel, M. G., Coackley, C. L., Humphries, K. M., Jamieson-Williams, R., Ambasudhan, R., Mosser, D. D., Lipton, S. A., Harauz, G., & Ryan, S. D. (2018). Cardiolipin exposure on the outer mitochondrial membrane modulates α-synuclein. *Nature Communications*, *9*(1). https://doi.org/10.1038/s41467-018-03241-9

Sabbah, H. N., Gupta, R. C., Singh-Gupta, V., Zhang, K., & Lanfear, D. E. (2018). Abnormalities of Mitochondrial Dynamics in the Failing Heart: Normalization Following Long-Term Therapy with Elamipretide. *Cardiovascular Drugs and Therapy*, *32*(4), 319–328. https://doi.org/10.1007/s10557-018-6805-y

Sang, M. P., Han, Y. J., Kim, T. D., Jeon, H. P., Yang, C. H., & Kim, J. (2002). Distinct roles of the N-terminal-binding domain and the C-terminal-solubilizing domain of α-synuclein, a molecular chaperone. *Journal of Biological Chemistry*, *277*(32), 28512–28520. https://doi.org/10.1074/jbc.M111971200

San-Millán, I. (2023). The Key Role of Mitochondrial Function in Health and Disease. In *Antioxidants* (Vol. 12, Issue 4). MDPI. https://doi.org/10.3390/antiox12040782

Santanasto, A. J., Glynn, N. W., Jubrias, S. A., Conley, K. E., Boudreau, R. M., Amati, F., Mackey, D. C., Simonsick, E. M., Strotmeyer, E. S., Coen, P. M., Goodpaster, B. H., & Newman, A. B. (2015). Skeletal Muscle Mitochondrial Function and Fatigability in Older Adults. *Journals of Gerontology - Series A Biological Sciences and Medical Sciences*, *70*(11), 1379–1385. https://doi.org/10.1093/gerona/glu134

Santo-Domingo, J., & Demaurex, N. (2010). Calcium uptake mechanisms of mitochondria. In *Biochimica et Biophysica Acta - Bioenergetics* (Vol. 1797, Issues 6–7, pp. 907–912). https://doi.org/10.1016/j.bbabio.2010.01.005

Sarkar, S., Olsen, A. L., Sygnecka, K., Lohr, K. M., & Feany, M. B. (2021). α-synuclein impairs autophagosome maturation through abnormal actin stabilization. *PLoS Genetics*, *17*(2). https://doi.org/10.1371/JOURNAL.PGEN.1009359

Schapira, A. H. (2006). Mitochondrial disease. *The Lancet*, *368*(9529), 70–82.

Schapira, A. H. V, Cooper, J. M., Dexter, D., Jenner, P., Clark, J. B., & Marsden, C. D. (1989). Mitochondrial complex I deficiency in Parkinson's disease. *The Lancet*, *333*(8649), 1269.

Schildknecht, S., Gerding, H. R., Karreman, C., Drescher, M., Lashuel, H. A., Outeiro, T. F., Di Monte, D. A., & Leist, M. (2013). Oxidative and nitrative alpha-synuclein modifications and proteostatic stress: Implications for disease mechanisms and interventions in synucleinopathies. In *Journal of Neurochemistry* (Vol. 125, Issue 4, pp. 491–511). https://doi.org/10.1111/jnc.12226

Schneider, B. L., Seehus, C. R., Capowski, E. E., Aebischer, P., Zhang, S. C., & Svendsen, C. N. (2007). Over-expression of alpha-synuclein in human neural progenitors leads to specific changes in fate and differentiation. *Human Molecular Genetics*, *16*(6), 651–666. https://doi.org/10.1093/hmg/ddm008

Schuchman, E. H. (2010). Acid sphingomyelinase, cell membranes and human disease: Lessons from Niemann-Pick disease. *FEBS Letters*, *584*(9), 1895–1900. https://doi.org/10.1016/j.febslet.2009.11.083

Serrao, E., & Engelman, A. N. (2016). Sites of retroviral DNA integration: From basic research to clinical applications. In *Critical Reviews in Biochemistry and Molecular Biology* (Vol. 51, Issue 1, pp. 26–42). Taylor and Francis Ltd. https://doi.org/10.3109/10409238.2015.1102859

Shah, S. I., Paine, J. G., Perez, C., & Ullah, G. (2019). Mitochondrial fragmentation and network architecture in degenerative diseases. *PLoS ONE*, *14*(9). https://doi.org/10.1371/journal.pone.0223014

Shaltouki, A., Hsieh, C. H., Kim, M. J., & Wang, X. (2018). Alpha-synuclein delays mitophagy and targeting Miro rescues neuron loss in Parkinson's models. *Acta Neuropathologica*, *136*(4), 607–620. https://doi.org/10.1007/s00401-018-1873-4

Sheng, Z. H., & Cai, Q. (2012). Mitochondrial transport in neurons: Impact on synaptic homeostasis and neurodegeneration. In *Nature Reviews Neuroscience* (Vol. 13, Issue 2, pp. 77–93). https://doi.org/10.1038/nrn3156

Shimura, H., Hattori, N., Kubo, S.-I., Mizuno, Y., Asakawa, S., Minoshima, S., Shimizu, N., Iwai, K., Chiba, T., Tanaka, K., & Suzuki, T. (2000). Familial Parkinson disease gene product, parkin, is a ubiquitin-protein ligase. *Nature Genetics*, *25*(3), 302–305. http://genetics.nature.com

Shipley, M. M., Mangold, C. A., & Szpara, M. L. (2016). Differentiation of the SH-SY5Y human neuroblastoma cell line. *Journal of Visualized Experiments*, *2016*(108). https://doi.org/10.3791/53193

Shteinfer-Kuzmine, A., Verma, A., Arif, T., Aizenberg, O., Paul, A., & Shoshan-Barmaz, V. (2021). Mitochondria and nucleus cross-talk: Signaling in metabolism, apoptosis, and differentiation, and function in cancer. *IUBMB Life*, *73*(3), 492–510. https://doi.org/10.1002/iub.2407

Siddiqui, I. J., Pervaiz, N., & Abbasi, A. A. (2016). The Parkinson Disease gene SNCA: Evolutionary and structural insights with pathological implication. *Scientific Reports*, *6*(24475). https://doi.org/10.1038/srep24475

Sidransky, E., Nalls, M. A., Aasly, J. O., Aharon-Peretz, J., Annesi, G., Barbosa, E. R., Bar-Shira, A., Berg, D., Bras, J., Brice, A., Chen, C. M., Clark, L. N., Condroyer, C., De Marco, E. V, Durr, A., Eblan, M. J., Fahn, S., Farrer, M. J., Fung, H.-C., … Ziegler, S. G. (2009). Multicenter Analysis of Glucocerebrosidase Mutations in Parkinson's Disease. *New England Journal of Medicine*, *361*(17), 1651–1661.

Simões, R. F., Ferrão, R., Silva, M. R., Pinho, S. L. C., Ferreira, L., Oliveira, P. J., & Cunha-Oliveira, T. (2021). Refinement of a differentiation protocol using neuroblastoma SH-SY5Y cells for use in neurotoxicology research. *Food and Chemical Toxicology*, *149*. https://doi.org/10.1016/j.fct.2021.111967

Singh, R., Letai, A., & Sarosiek, K. (2019). Regulation of apoptosis in health and disease: the balancing act of BCL-2 family proteins. In *Nature Reviews Molecular Cell Biology* (Vol. 20, Issue 3, pp. 175–193). Nature Publishing Group. https://doi.org/10.1038/s41580-018-0089-8

Smith, W. W., Jiang, H., Pei, Z., Tanaka, Y., Morita, H., Sawa, A., Dawson, V. L., Dawson, T. M., & Ross, C. A. (2005). Endoplasmic reticulum stress and mitochondrial cell death pathways mediate A53T mutant alpha-synuclein-induced toxicity. *Human Molecular Genetics*, *14*(24), 3801–3811. https://doi.org/10.1093/hmg/ddi396

Snead, D., & Eliezer, D. (2014). Alpha-Synuclein Function and Dysfunction on Cellular Membranes. *Experimental Neurobiology*, *23*(4), 292–313. https://doi.org/10.5607/en.2014.23.4.292

Soubannier, V., McLelland, G. L., Zunino, R., Braschi, E., Rippstein, P., Fon, E. A., & McBride, H. M. (2012). A vesicular transport pathway shuttles cargo from mitochondria to lysosomes. *Current Biology*, *22*(2), 135–141. https://doi.org/10.1016/j.cub.2011.11.057

Soubannier, V., Rippstein, P., Kaufman, B. A., Shoubridge, E. A., & McBride, H. M. (2012). Reconstitution of Mitochondria Derived Vesicle Formation Demonstrates Selective Enrichment of Oxidized Cargo. *PLoS ONE*, *7*(12). https://doi.org/10.1371/journal.pone.0052830

Sousa, V. L., Bellani, S., Giannandrea, M., Yousuf, M., Valtorta, F., Meldolesi, J., & Chieregatti, E. (2009). α-Synuclein and its A30P mutant affect actin cytoskeletal structure and dynamics. *Molecular Biology of the Cell*, *20*(16), 3725–3739. https://doi.org/10.1091/mbc.E08-03-0302

Sperling, J. A., Sakamuri, S. S. V. P., Albuck, A. L., Sure, V. N., Evans, W. R., Peterson, N. R., Rutkai, I., Mostany, R., Satou, R., & Katakam, P. V. G. (2019). Measuring Respiration in Isolated Murine Brain Mitochondria: Implications for Mechanistic Stroke Studies. *NeuroMolecular Medicine*, *21*(4), 493–504. https://doi.org/10.1007/s12017-019-08552-8

Spillantini, M. G., Schmidt, M. L., Lee, V. M.-Y., Trojanowski, J. Q., Jakes, R., & Goedert, M. (1997). Alpha-synuclein in Lewy bodies. *Nature*, *388*, 839–840.

Sriwimol, W., & Limprasert, P. (2018). Significant Changes in Plasma Alpha-Synuclein and Beta-Synuclein Levels in Male Children with Autism Spectrum Disorder. *BioMed Research International*, *2018*. https://doi.org/10.1155/2018/4503871

Stefanis, L., Larsen, K. E., Rideout, H. J., Sulzer, D., & Greene, L. A. (2001). *Expression of A53T Mutant But Not Wild-Type-Synuclein in PC12 Cells Induces Alterations of the Ubiquitin-Dependent Degradation System, Loss of Dopamine Release, and Autophagic Cell Death*.

Stefanovic, A. N. D., Stöckl, M. T., Claessens, M. M. A. E., & Subramaniam, V. (2014). α-Synuclein oligomers distinctively permeabilize complex model membranes. *FEBS Journal*, *281*(12), 2838–2850. https://doi.org/10.1111/febs.12824

Sudhof, T. (1999). Composition of Synaptic Vesicles. In G. J. Siegel, B. W. Agranoff, & B. W. Albers (Eds.), *Basic Neurochemistry: Molecular, Cellular and Medical Aspects* (6th ed.). Lippincott-Raven.

Südhof, T. C. (2012). Calcium control of neurotransmitter release. *Cold Spring Harbor Perspectives in Biology*, *4*(1). https://doi.org/10.1101/cshperspect.a011353

Sugiura, A., McLelland, G., Fon, E. A., & McBride, H. M. (2014). A new pathway for mitochondrial quality control: mitochondrial-derived vesicles. *The EMBO Journal*, *33*(19), 2142–2156. https://doi.org/10.15252/embj.201488104

Sukumaran, P., Da Conceicao, V. N., Sun, Y., Ahamad, N., Saraiva, L. R., Selvaraj, S., & Singh, B. B. (2021). Calcium signaling regulates autophagy and apoptosis. In *Cells* (Vol. 10, Issue 8). MDPI. https://doi.org/10.3390/cells10082125

Sulzer, D., & Edwards, R. H. (2019). The physiological role of α-synuclein and its relationship to Parkinson's Disease. In *Journal of Neurochemistry* (Vol. 150, Issue 5, pp. 475–486). Blackwell Publishing Ltd. https://doi.org/10.1111/jnc.14810

Taanman, J.-W. (1999). The mitochondrial genome: structure, transcription, translation and replication. *BBA - Bioenergetics*, *1410*(2), 103–123.

Tafani, M., Sansone, L., Limana, F., Arcangeli, T., De Santis, E., Polese, M., Fini, M., & Russo, M. A. (2016). The Interplay of Reactive Oxygen Species, Hypoxia, Inflammation, and Sirtuins in Cancer Initiation and Progression. In *Oxidative Medicine and Cellular Longevity* (Vol. 2016). Hindawi Limited. https://doi.org/10.1155/2016/3907147

Tait, S. W. G., & Green, D. R. (2010). Mitochondria and cell death: Outer membrane permeabilization and beyond. *Nature Reviews Molecular Cell Biology*, *11*(9), 621–632. https://doi.org/10.1038/nrm2952

Talari, N. K., Mattam, U., Meher, N. K., Paripati, A. K., Mahadev, K., Krishnamoorthy, T., & Sepuri, N. B. V. (2023). Lipid-droplet associated mitochondria promote fatty-acid oxidation through a distinct bioenergetic pattern in male Wistar rats. *Nature Communications*, *14*(1). https://doi.org/10.1038/s41467-023-36432-0

Tang, Q., Gao, P., Arzberger, T., Höllerhage, M., Herms, J., Höglinger, G., & Koeglsperger, T. (2021). Alpha-Synuclein defects autophagy by impairing SNAP29-mediated autophagosome-lysosome fusion. *Cell Death and Disease*, *12*(10). https://doi.org/10.1038/s41419-021-04138-0

Taylor, E. B., & Rutter, J. (2011). Mitochondrial quality control by the ubiquitin-proteasome system. *Biochemical Society Transactions*, *39*(5), 1509–1513. https://doi.org/10.1042/BST0391509

Thorne, N. J., & Tumbarello, D. A. (2022). The relationship of alpha-synuclein to mitochondrial dynamics and quality control. *Frontiers in Molecular Neuroscience*, *15*. https://doi.org/10.3389/fnmol.2022.947191

Thul, P. J., Akesson, L., Wiking, M., Mahdessian, D., Geladaki, A., Ait Blal, H., Alm, T., Asplund, A., Björk, L., Breckels, L. M., Bäckström, A., Danielsson, F., Fagerberg, L., Fall, J., Gatto, L., Gnann, C., Hober, S., Hjelmare, M., Johansson, F., … Lundberg, E. (2017). A subcellular map of the human proteome. *Science*, *356*(6340). https://doi.org/10.1126/science.aal3321

Tofaris, G. K., Layfield, R., & Spillantini, M. G. (2001). α-Synuclein metabolism and aggregation is linked to ubiquitin-independent degradation by the proteasome. *FEBS Letters*, *509*(1), 22–26. https://doi.org/10.1016/S0014-5793(01)03115-5

Tripathi, T., & Chattopadhyay, K. (2019). Interaction of α-Synuclein with ATP Synthase: Switching Role from Physiological to Pathological. In *ACS Chemical Neuroscience* (Vol. 10, Issue 1, pp. 16–17). American Chemical Society. https://doi.org/10.1021/acschemneuro.8b00407

Twig, G., Elorza, A., Molina, A. J. A., Mohamed, H., Wikstrom, J. D., Walzer, G., Stiles, L., Haigh, S. E., Katz, S., Las, G., Alroy, J., Wu, M., Py, B. F., Yuan, J., Deeney, J. T., Corkey, B. E., & Shirihai, O. S. (2008). Fission and selective fusion govern mitochondrial segregation and elimination by autophagy. *EMBO Journal*, *27*(2), 433–446. https://doi.org/10.1038/sj.emboj.7601963

Ugarte-Uribe, B., Müller, H. M., Otsuki, M., Nickel, W., & García-Sáez, A. J. (2014). Dynamin-related protein 1 (Drp1) promotes structural intermediates of membrane division. *Journal of Biological Chemistry*, *289*(44), 30645–30656. https://doi.org/10.1074/jbc.M114.575779

Ungerstedt, U. (1971). Postsynaptic supersensitivity after 6-hydroxy-dopamine induced degeneration of the nigrostriatal dopamine system. *Acta Physiologica Scandinavica Supplements*, *367*, 69–93.

Uversky, V. N., Li, J., Souillac, P., Millett, I. S., Doniach, S., Jakes, R., Goedert, M., & Fink, A. L. (2002). Biophysical properties of the synucleins and their propensities to fibrillate: Inhibition of α-synuclein assembly by β- and γ-synucleins. *Journal of Biological Chemistry*, *277*(14), 11970–11978. https://doi.org/10.1074/jbc.M109541200

Valente, E. M., Abou-Sleiman, P. M., Caputo, V., Muqit, M. M. K., Harvey, K., Gispert, S., Ali, Z., Del Turco, D., Bentivoglio, A. R., Healy, D. G., Albanese, A., Nussbaum, R., González-Maldonado, R., Deller, T., Salvi, S., Cortelli, P., Gilks, W. P., Latchman, D. S., Harvey, R. J., … Wood, N. W. (2004). Hereditary early-onset Parkinson's disease caused by mutations in PINK1. *Science*, *304*(5674), 1158–1160. https://doi.org/10.1126/science.1096284

Varughese, J. T., Buchanan, S. K., & Pitt, A. S. (2021). The role of voltage-dependent anion channel in mitochondrial dysfunction and human disease. In *Cells* (Vol. 10, Issue 7). MDPI. https://doi.org/10.3390/cells10071737

Vasquez, V., Mitra, J., Perry, G., Rao, K. S., & Hegde, M. L. (2018). An inducible alpha-synuclein expressing neuronal cell line model for Parkinson's disease. *Journal of Alzheimer's Disease*, *66*(2), 453–460. https://doi.org/10.3233/JAD-180610

Venda, L. L., Cragg, S. J., Buchman, V. L., & Wade-Martins, R. (2010). α-Synuclein and dopamine at the crossroads of Parkinson's disease. In *Trends in Neurosciences* (Vol. 33, Issue 12, pp. 559–568). https://doi.org/10.1016/j.tins.2010.09.004

Vives-Bauza, C., Zhou, C., Huang, Y., Cui, M., De Vries, R. L. A., Kim, J., May, J., Tocilescu, M. A., Liu, W., Ko, H. S., Magrané, J., Moore, D. J., Dawson, V. L., Grailhe, R., Dawson, T. M., Li, C., Tieu, K., & Przedborski, S. (2010). PINK1-dependent recruitment of Parkin to mitochondria in mitophagy. *Proceedings of the National Academy of Sciences of the United States of America*, *107*(1), 378–383. https://doi.org/10.1073/pnas.0911187107

von der Malsburg, A., Sapp, G. M., Zuccaro, K. E., von Appen, A., Moss, F. R., Kalia, R., Bennett, J. A., Abriata, L. A., Dal Peraro, M., van der Laan, M., Frost, A., & Aydin, H. (2023). Structural mechanism of mitochondrial membrane remodelling by human OPA1. *Nature*, *620*(7976), 1101–1108. https://doi.org/10.1038/s41586-023-06441-6

Wai, T., García-Prieto, J., Baker, M. J., Merkwirth, C., Benit, P., Rustin, P., Rupérez, F. J., Barbas, C., Ibañez, B., & Langer, T. (2015). Imbalanced OPA1 processing and mitochondrial

fragmentation cause heart failure in mice. *Science*, *350*(6265). https://doi.org/10.1126/science.aad0116

Wang, G. F., Li, C., & Pielak, G. J. (2010). 19F NMR studies of α-synuclein-membrane interactions. *Protein Science*, *19*(9), 1686–1691. https://doi.org/10.1002/pro.449

Wang, X., Becker, K., Levine, N., Zhang, M., Lieberman, A. P., Moore, D. J., & Ma, J. (2019). Pathogenic alpha-synuclein aggregates preferentially bind to mitochondria and affect cellular respiration. *Acta Neuropathologica Communications*, *7*(1), 41. https://doi.org/10.1186/s40478-019-0696-4

Wang, X., Su, B., Siedlak, S. L., Moreira, P. I., Fujioka, H., Wang, Y., Casadesus, G., & Zhu, X. (2008). Amyloid-overproduction causes abnormal mitochondrial dynamics via differential modulation of mitochondrial fission/fusion proteins. *Proc Natl Acad Sci USA*, *105*(49), 19318–19323. www.pnas.org/cgi/content/full/

Wang, X., Winter, D., Ashrafi, G., Schlehe, J., Wong, Y. L., Selkoe, D., Rice, S., Steen, J., Lavoie, M. J., & Schwarz, T. L. (2011). PINK1 and Parkin target miro for phosphorylation and degradation to arrest mitochondrial motility. *Cell*, *147*(4), 893–906. https://doi.org/10.1016/j.cell.2011.10.018

Wang, Y., Li, L., Hou, C., Lai, Y., Long, J., Liu, J., Zhong, Q., & Diao, J. (2016). SNARE-mediated membrane fusion in autophagy. In *Seminars in Cell and Developmental Biology* (Vol. 60, pp. 97–104). Academic Press. https://doi.org/10.1016/j.semcdb.2016.07.009

Warburg, O. (1956). On respiratory impairment in cancer cells. *Science*, *124*(3215).

Wauer, T., Simicek, M., Schubert, A., & Komander, D. (2015). Mechanism of phospho-ubiquitin-induced PARKIN activation. *Nature*, *524*(7565), 370–374. https://doi.org/10.1038/nature14879

Wersinger, C., & Sidhu, A. (2003). Attenuation of dopamine transporter activity by α-synuclein. *Neuroscience Letters*, *340*(3), 189–192. https://doi.org/10.1016/S0304-3940(03)00097-1

Westermann, B. (2012). Bioenergetic role of mitochondrial fusion and fission. *Biochimica et Biophysica Acta - Bioenergetics*, *1817*(10), 1833–1838. https://doi.org/10.1016/j.bbabio.2012.02.033

Westphal, C. H., & Chandra, S. S. (2013). Monomeric synucleins generate membrane curvature. *Journal of Biological Chemistry*, *288*(3), 1829–1840. https://doi.org/10.1074/jbc.M112.418871

Wilkaniec, A., Lenkiewicz, A. M., Babiec, L., Murawska, E., Jęśko, H. M., Cieślik, M., Culmsee, C., & Adamczyk, A. (2021). Exogenous Alpha-Synuclein Evoked Parkin Downregulation Promotes Mitochondrial Dysfunction in Neuronal Cells. Implications for Parkinson's Disease Pathology. *Frontiers in Aging Neuroscience*, *13*. https://doi.org/10.3389/fnagi.2021.591475

Wilkaniec, A., Lenkiewicz, A. M., Czapski, G. A., Jęśko, H. M., Hilgier, W., Brodzik, R., Gąssowska-Dobrowolska, M., Culmsee, C., & Adamczyk, A. (2019). Extracellular Alpha-Synuclein Oligomers Induce Parkin S-Nitrosylation: Relevance to Sporadic Parkinson's Disease Etiopathology. *Molecular Neurobiology*, *56*(1), 125–140. https://doi.org/10.1007/s12035-018-1082-0

William Langston, J., Ballard, P., Tetrud, J. W., & Irwin, I. (1983). Chronic parkinsonism in humans due to a product of meperidine-analog synthesis. *Science*, *219*(4587), 979–980. https://doi.org/10.1126/science.6823561

Williams, J. K., Yang, X., & Baum, J. (2018). Interactions between the Intrinsically Disordered Proteins β-Synuclein and α-Synuclein. In *Proteomics* (Vol. 18, Issues 21–22). Wiley-VCH Verlag. https://doi.org/10.1002/pmic.201800109

Winner, B., Jappelli, R., Maji, S. K., Desplats, P. A., Boyer, L., Aigner, S., Hetzer, C., Loher, T., Vilar, M., Campioni, S., Tzitzilonis, C., Soragni, A., Jessberger, S., Mira, H., Consiglio, A., Pham, E., Masliah, E., Gage, F. H., & Riek, R. (2011). In vivo demonstration that α-synuclein oligomers are toxic. *Proceedings of the National Academy of Sciences of the United States of America*, *108*(10), 4194–4199. https://doi.org/10.1073/pnas.1100976108

Winslow, A. R., Chen, C. W., Corrochano, S., Acevedo-Arozena, A., Gordon, D. E., Peden, A. A., Lichtenberg, M., Menzies, F. M., Ravikumar, B., Imarisio, S., Brown, S., O'Kane, C. J., & Rubinsztein, D. C. (2010). α-Synuclein impairs macroautophagy: Implications for Parkinson's disease. *Journal of Cell Biology*, *190*(6), 1023–1037. https://doi.org/10.1083/jcb.201003122

Won, S. J., Fong, R., Butler, N., Sanchez, J., Zhang, Y., Wong, C., Tambou Nzoutchoum, O., Huynh, A., Pan, J., & Swanson, R. A. (2022). Neuronal Oxidative Stress Promotes α-Synuclein Aggregation In Vivo. *Antioxidants*, *11*(12). https://doi.org/10.3390/antiox11122466

Wong, Y. C., Kim, S., Peng, W., & Krainc, D. (2019). Regulation and Function of Mitochondria–Lysosome Membrane Contact Sites in Cellular Homeostasis. In *Trends in Cell Biology* (Vol. 29, Issue 6, pp. 500–513). Elsevier Ltd. https://doi.org/10.1016/j.tcb.2019.02.004

Wördehoff, M., & Hoyer, W. (2018). α-Synuclein Aggregation Monitored by Thioflavin T Fluorescence Assay. *BIO-PROTOCOL*, *8*(14). https://doi.org/10.21769/bioprotoc.2941

Xiang, W., Schlachetzki, J. C. M., Helling, S., Bussmann, J. C., Berlinghof, M., Schäffer, T. E., Marcus, K., Winkler, J., Klucken, J., & Becker, C. M. (2013). Oxidative stress-induced posttranslational modifications of alpha-synuclein: Specific modification of alpha-synuclein by 4-hydroxy-2-nonenal increases dopaminergic toxicity. *Molecular and Cellular Neuroscience*, *54*, 71–83. https://doi.org/10.1016/j.mcn.2013.01.004

Xicoy, H., Wieringa, B., & Martens, G. J. M. (2017). The SH-SY5Y cell line in Parkinson's disease research: a systematic review. In *Molecular Neurodegeneration* (Vol. 12, Issue 1, pp. 1–11). BioMed Central Ltd. https://doi.org/10.1186/s13024-017-0149-0

Xie, H. R., Hu, L. Sen, & Li, G. Y. (2010). SH-SY5Y human neuroblastoma cell line: In vitro cell model of dopaminergic neurons in Parkinson's disease. In *Chinese Medical Journal* (Vol. 123, Issue 8, pp. 1086–1092). https://doi.org/10.3760/cma.j.issn.0366-6999.2010.08.021

Yadati, T., Houben, T., Bitorina, A., & Shiri-Sverdlov, R. (2020). The Ins and Outs of Cathepsins: Physiological Function and Role in Disease Management. *Cells*, *9*(7). https://doi.org/10.3390/cells9071679

Yamamoto1, A., Tagawa1, Y., Yoshimori2, T., Moriyama3, Y., Masaki1, R., & Tashiro1, Y. (1998). Bafilomycin Ai Prevents Maturation of Autophagic Vacuoles by Inhibiting Fusion between Autophagosomesand Lysosomesin Rat HepatomaCell Line, H-4-II-E Cells. In *CELL STRUCTURE AND FUNCTION* (Vol. 23).

Yamazaki, T., & Galluzzi, L. (2022). BAX and BAK dynamics control mitochondrial DNA release during apoptosis. In *Cell Death and Differentiation* (Vol. 29, Issue 6, pp. 1296–1298). Springer Nature. https://doi.org/10.1038/s41418-022-00985-2

Yang, S., & Lian, G. (2020). ROS and diseases: role in metabolism and energy supply. *Molecular and Cellular Biochemistry*, *467*(1–2). https://doi.org/10.1007/s11010-019-03667-9

Yang, Z., & Klionsky, D. J. (2010). Mammalian autophagy: Core molecular machinery and signaling regulation. In *Current Opinion in Cell Biology* (Vol. 22, Issue 2, pp. 124–131). https://doi.org/10.1016/j.ceb.2009.11.014

Yao, D., Gu, Z., Nakamura, T., Shi, Z.-Q., Ma, Y., Gaston, B., Palmer, L. A., Rockenstein, E. M., Zhang, Z., Uehara, T., & Lipton, S. A. (2004). Nitrosative stress linked to sporadic Parkinson's disease: S-nitrosylation of parkin regulates its E3 ubiquitin ligase activity.

Proceedings of the National Academy of Sciences of the United States of America, *101*(9), 10810–10814. https://www.pnas.org

Yin, Z., Pascual, C., & Klionsky, D. J. (2016). Autophagy: Machinery and regulation. In *Microbial Cell* (Vol. 3, Issue 12, pp. 588–596). Shared Science Publishers OG. https://doi.org/10.15698/mic2016.12.546

Youle, R. J., & Van Der Bliek, A. M. (2012). Mitochondrial Fission, Fusion, and Stress. *Science*, *337*(6098), 1062–1065. https://www.science.org

Yu, S., Zuo, X., Li, Y., Zhang, C., Zhou, M., Zhang, Y. A., Uéda, K., & Chan, P. (2004). Inhibition of tyrosine hydroxylase expression in α-synuclein- transfected dopaminergic neuronal cells. *Neuroscience Letters*, *367*(1), 34–39. https://doi.org/10.1016/j.neulet.2004.05.118

Yuan, J., & Ofengeim, D. (2024). A guide to cell death pathways. In *Nature Reviews Molecular Cell Biology* (Vol. 25, Issue 5, pp. 379–395). Nature Research. https://doi.org/10.1038/s41580-023-00689-6

Zachari, M., & Ganley, I. G. (2017). The mammalian ULK1 complex and autophagy initiation. In *Essays in Biochemistry* (Vol. 61, Issue 6, pp. 585–596). Portland Press Ltd. https://doi.org/10.1042/EBC20170021

Zafar, F., Valappil, R. A., Kim, S., Johansen, K. K., Chang, A. L. S., Tetrud, J. W., Eis, P. S., Hatchwell, E., Langston, J. W., Dickson, D. W., & Schüle, B. (2018). Genetic fine-mapping of the Iowan SNCA gene triplication in a patient with Parkinson's disease. *Npj Parkinson's Disease*, *4*(1). https://doi.org/10.1038/s41531-018-0054-4

Zampagni, M., Cascella, R., Casamenti, F., Grossi, C., Evangelisti, E., Wright, D., Becatti, M., Liguri, G., Mannini, B., Campioni, S., Chiti, F., & Cecchi, C. (2011). A comparison of the biochemical modifications caused by toxic and non-toxic protein oligomers in cells. *Journal of Cellular and Molecular Medicine*, *15*(10), 2106–2116. https://doi.org/10.1111/j.1582-4934.2010.01239.x

Zamzami, N., Marchetti, P., Castedo, M., Decaudin, D., Macho, A., Hirsch, T., Susin, S. A., Petit, P. X., Mignotte, B., & Kroemer, G. (1995). Sequential Reduction of Mitochondrial Transmembrane Potential and Generation of Reactive Oxygen Species in Early Programmed Cell Death. *J Exp Med*, *182*(2), 367–377.

Zhang, M., Lu, H., Xie, X., Shen, H., Li, X., Zhang, Y., Wu, J., Ni, J., Li, H., & Chen, G. (2020). TMEM175 mediates Lysosomal function and participates in neuronal injury induced by

cerebral ischemia-reperfusion. *Molecular Brain*, *13*(1). https://doi.org/10.1186/s13041-020-00651-z

Zheng, X., & Gallot, G. (2020). Dynamics of Cell Membrane Permeabilization by Saponins Using Terahertz Attenuated Total Reflection. *Biophysical Journal*, *119*(4), 749–755. https://doi.org/10.1016/j.bpj.2020.05.040

Zheng, Y. R., Zhang, X. N., & Chen, Z. (2019). Mitochondrial transport serves as a mitochondrial quality control strategy in axons: Implications for central nervous system disorders. In *CNS Neuroscience and Therapeutics* (Vol. 25, Issue 7, pp. 876–886). Blackwell Publishing Ltd. https://doi.org/10.1111/cns.13122

Zhong, S. C., Luo, X., Chen, X. S., Cai, Q. Y., Liu, J., Chen, X. H., & Yao, Z. X. (2010). Expression and subcellular location of alpha-synuclein during mouse-embryonic development. *Cellular and Molecular Neurobiology*, *30*(3), 469–482. https://doi.org/10.1007/s10571-009-9473-4

Zhou, X., Winblad, B., Guan, Z., & Pei, J. (2009). Interactions between glycogen synthase kinase 3B, protein kinase B, and protein phosphatase 2A in tau phosphorylation in mouse N2a neuroblastoma cells. *Journal of Alzheimer's Disease*, *17*(4), 929–937.

Zigoneanu, I. G., Yang, Y. J., Krois, A. S., Haque, M. E., & Pielak, G. J. (2012). Interaction of α-synuclein with vesicles that mimic mitochondrial membranes. *Biochimica et Biophysica Acta - Biomembranes*, *1818*(3), 512–519. https://doi.org/10.1016/j.bbamem.2011.11.024

Zimprich, A., Benet-Pagès, A., Struhal, W., Graf, E., Eck, S. H., Offman, M. N., Haubenberger, D., Spielberger, S., Schulte, E. C., Lichtner, P., Rossle, S. C., Klopp, N., Wolf, E., Seppi, K., Pirker, W., Presslauer, S., Mollenhauer, B., Katzenschlager, R., Foki, T., … Strom, T. M. (2011). A mutation in VPS35, encoding a subunit of the retromer complex, causes late-onset parkinson disease. *American Journal of Human Genetics*, *89*(1), 168–175. https://doi.org/10.1016/j.ajhg.2011.06.008

Ziviani, E., Tao, R. N., & Whitworth, A. J. (2010). Drosophila Parkin requires PINK1 for mitochondrial translocation and ubiquitinates Mitofusin. *Proceedings of the National Academy of Sciences of the United States of America*, *107*(11), 5018–5023. https://doi.org/10.1073/pnas.0913485107

Zorova, L. D., Popkov, V. A., Plotnikov, E. Y., Silachev, D. N., Pevzner, I. B., Jankauskas, S. S., Babenko, V. A., Zorov, S. D., Balakireva, A. V., Juhaszova, M., Sollott, S. J., & Zorov, D. B. (2018). Mitochondrial membrane potential. *Analytical Biochemistry*, *552*, 50–59. https://doi.org/10.1016/j.ab.2017.07.009

Zü, G., & Reiser, G. (2011). Calcium Dysregulation and Homeostasis of Neural Calcium in the Molecular Mechanisms of Neurodegenerative Diseases Provide Multiple Targets for Neuroprotection. *Antioxid Redox Signal*, *14*(7), 1275–1288. www.liebertonline.com=ars